ECSS-E-HB-32-25A
14 July 2015

Space engineering

Mechanical shock design and verification handbook

ECSS Secretariat
ESA-ESTEC
Requirements & Standards Division
Noordwijk, The Netherlands

Foreword

This Handbook is one document of the series of ECSS Documents intended to be used as supporting material for ECSS Standards in space projects and applications. ECSS is a cooperative effort of the European Space Agency, national space agencies and European industry associations for the purpose of developing and maintaining common standards.

The material in this Handbook is defined in terms of description and recommendation how to organize and perform mechanical load analyses of spacecraft and payloads.

This handbook has been prepared by the ECSS-E-HB-32-25A Working Group, reviewed by the ECSS Executive Secretariat and approved by the ECSS Technical Authority.

Disclaimer

Published by: ESA Requirements and Standards Division
ESTEC, P.O. Box 299,
2200 AG Noordwijk
The Netherlands

Change log

ECSS-E-HB-32-25A 14 July 2015	First issue

Table of contents

Acknowledgements

The key idea of the Handbook is to document the current know-how on mechanical shock design and verification. This was implemented in steps by an ECSS working group, leading to the present ECSS Handbook.

For this continuous effort, ECSS would like to thanks the following experts:

Sonia AITZAID	CNES	Daniel KEIL	Jena Optronik
Stéphanie BEHAR-LAFENETRE	Thalès Alenia Space	Andy KILEY	ASTRIUM
Michele BERNASCONI	RUAG	Stéfan KIRYENKO (Convenor)	ESA/ESTEC
Jean-Baptiste BERNAUDIN	ASTRIUM	Sébastien LABORDE	ASTRIUM
Gérard BORELLO	InterAC	Grégory LADURÉE	ESA/ESTEC
Benjamin BRAUN	Space Structures GmbH	Michel LATHUILIERE	01dB-Metravib
Bertrand BREVART	Thalès Alenia Space	Simon LEWIS	ESTL
Didier BURTIN	Arianespace	Pietro MARUCCHI-CHIERRO †	Thalès Alenia Space
Giacomo CALVISI	Thalès Alenia Space	Stéphane MARY	CNES
Patrick CAMARASA	ASTRIUM	Gérard NADALIN	ASTRIUM
Carlo COLOMBO	Thalès Alenia Space	Alexandre PIQUEREAU	CNES
Christophe DEFRUYTIER	Thalès Alenia Space	Jean POLOME	Thalès Alenia Space
Tony DEMERVILLE	SMAC	Michel RANCHOUX	ASTRIUM
Denis DILHAN	CNES	Philippe ROUX	CNES
Stefan EBERL	IABG	Florian RUESS	Space Structures GmbH
Domenico FOTINO	AVIO	Roberto ULLIO	Thalès Alenia Space
Henri GRZESKOWIAK	HG Consultant	Jean-Baptiste VERGNIAUD	ASTRIUM
Jan KASPER	ASTRIUM	Mark WAGNER	ESA/ESTEC

The completion and the harmonization of the handbook was a complex undertaking, this was made possible thanks to the dedication of all, under technical management by S. Kiryenko (ECSS WG convenor).

Comments concerning the technical content of this handbook are welcomed by the European Cooperation for Space Standardization, Noordwijk, the Netherlands, www.ecss.nl.

Introduction

In recent years, discussions concerning "what to do about shock" in relation to spacecraft have taken more importance. During launch and deployment operations, a spacecraft can be exposed to energetic shock environments. As spacecraft have become more capable, more equipment can be flown, and components are closer together. In addition, more sophisticated and delicate instruments are flown to maximize mission results.

As such, the shock environment has become a source of concern for spacecraft and payload developers. However, not only the definition of the environment, but also the analysis and test verification is complex.

In the same way than for other mechanical environment, it is important to properly address the shock early in the development phase until the final verification of the shock environment, to ensure a successful qualification.

The experience, gained over the past years by Agencies and industries, greatly improves the state of the art in this domain and has helped clear a large number of equipment and spacecraft for launch.

However, one of the problems with respect to mechanical shock design and verification is the fact that relevant information is spread over ESA and industry documents and specialists. To improve this, the current know-how on mechanical shock design and verification is documented in the present handbook in order to make this expertise available to all European spacecraft and payload developers.

The handbook is divided into four parts:

- Part 1 Overview
- Part 2 Shock input derivation to space segment elements and equipment
- Part 3 Shock verification approach
- Part 4 Shock damage risk assessment

1
Scope

The intended users of the "Mechanical shock design and verification handbook" are engineers involved in design, analysis and verification in relation to shock environment in spacecraft. The current know-how relevant to mechanical shock design and verification is documented in this handbook in order to make this expertise available to all European spacecraft and payload developers.

The handbook provides adequate guidelines for shock design and verification; therefore it includes advisory information, recommendations and good practices, rather than requirements.

The handbook covers the shock in its globally, from the derivation of shock input to equipment and sub-systems inside a satellite structure, until its verification to ensure a successful qualification, and including its consequences on equipment and sub-systems. However the following aspects are not treated herein:

- No internal launcher shock is treated in the frame of this handbook even if some aspects are common to those presented hereafter. They are just considered as a shock source (after propagation in the launcher structure) at launcher/spacecraft interface.
- Shocks due to fall of structure or equipment are not taken into account as they are not in the frame of normal development of a spacecraft.

2
References

2.1 References of Part 1

[RD-01] Guide de spécification d'essais et de conception d'équipements, Grzeskowiak, MBDA, Jan. 2003

[RD-02] Mechanical Vibration and Shock – Mechanical Shock, Volume 2, C. Lalanne

[RD-03] Harris' Shock and Vibration Handbook, CM Harris, AG Piersol, Fifth edition

[RD-04] Pyroshock Test Criteria, NASA Technical Standard, NASA-STD-7003, May 1999

[RD-05] Environmental Engineering considerations and laboratory tests, MIL Technical Standard, MIL-STD-810F, Jan. 2000

[RD-06] Pyrotechnic Shock Loads, Test evaluation, equipment protection, E. Hornung, Daimler-Benz Aerospace AG, Space infrastructure, Bremen, Germany, H. Öery, University Aaschen, Germany – 48th Congress of the International Astronautical Federation – Turin, Oct. 1997

[RD-07] Susceptibility of equipment to pyroshocks – Return of experience from ESA programmes, Kiryenko, Parquet, Grzeskowiak, ESA/ESTEC and MBDA, Dec. 2002

[RD-08] An introduction to the shock response spectrum, Tom Irvine, May 2002.

[RD-09] The shock response spectrum at low frequencies, D. O. Smallwood, Sandia National Laboratories, Albuquerque, NM

2.2 References of Part 2

[RD-010] Report on alternative devices to pyrotechnics on spacecraft, M. Lucy, R. Hardy, E. Kist, J. Watson, S. Wise, National Aeronautics and Space Administration, Langley Research Center

[RD-011] Very low shock release pyromechanisms, Geachter, Tarkhani, LACROIX PYROTECHNOLOGIES, Dec. 2002

[RD-012] Dynamics simulation of pyro actuated "ball lock" separation system for micro-satellites to evaluate release shock, S. Somanath, E.J. Francis, Vikram Sarabhai Space Centre (India) – ESA - 9th European Space Mechanisms and Tribology Symposium – Liege Belgium 19-21th September 2001

[RD-013] TO5 - Shock Measurement:- Exploitation des essais de chocs réalisés sur les composants pyrotechniques, Valerio Cippola, CNES, 2002

[RD-014] Shock predictions for aerospace applications - return of experience from ESA programmes, Kiryenko, Kasper, Ngan, 6th International Symposium on Launcher Technologies, Munich, 2005

[RD-015] Shock environment in spacecraft from an early definition to a final verification, Kiryenko, Parquet, ESA/ESTEC, Dec. 2002

[RD-016] Guide de specification d'essais et de conception d'equipements, H. Grzeskowiak, MBDA, Jan. 2003

[RD-017] Aerospace Systems Pyrotechnic Shock Data (Ground Test and Flight), Martin Marietta Corporation, Mars 1970

[RD-018] A Comparison of the Normal Tolerance Limit and Bootstrap Methods With Application to Spacecraft Acoustic Environments, William O. Hughes, July 2005

[RD-019] Factors for One-Sided Tolerance Limits and for Variables Sampling Plans, Owen, D.B., Sandia Monograph SC-R-607, Sandia Corporation,1963

[RD-020] Pyroshock Test Criteria, NASA Technical Standard, NASA-STD-7003, May 1999

[RD-021] Dynamic Environmental Criteria, NASA Technical Standard NASA-STD-7005, March 2001

[RD-022] Harris' Shock and Vibration Handbook, CM Harris, AG Piersol, Fifth edition

[RD-023] Pyroshock Test Criteria, NASA Technical Standard, NASA-STD-7003, May 1999

[RD-024] Environmental Engineering considerations and laboratory tests, MIL Technical Standard, MIL-STD-810F, Jan. 2000

[RD-025] Survey of pyroshock prediction methodology, D.L. Van Ert

[RD-026] R&D Propagation de choc – Rapport final, Pichon, EADS-Astrium, July 2002

[RD-027] Simulation de la transmission de chocs avec le logiciel PAMSHOCK, B. Laine, Alcatel Alenia Space, April 2002

[RD-028] Pyroshock modelling using mechanical shock sources, J.B. Bernaudin, EADS-Astrium, Dec. 2002

[RD-029] Shock propagation prediction in satellite structures, Pichon, EADS-Astrium, Dec. 2002

[RD-030] Shock propagation simulation using FEM software, S. Mary, V. Cipolla, CNES, May 2005

[RD-031] Ariane 5 shock environment qualification for an earth observation satellite, E. Courau, May 2005

[RD-032] W. Westphall, "Ausbreitung vor Körperschall in Gebäuden", Acustica, Vol 7, 1957, p.335-348

[RD-033] Richard H. Lyon, Gideon Maidanik, "Power Flow between Linearly Coupled Oscillators", Acoust. Soc. Am. 34, 623 (1962)

[RD-034] R. H. Lyon and Dejong, "Statistical Energy Analysis", Sd Edition 1995 Butterworth-Heinemann

[RD-035] L. Gagliardini, L. Houillon, L. Petrinelli, G. Borello, "Virtual SEA: mid-frequency structure-borne noise modeling based on Finite Element Analysis", SAE - NVC 2003-01-1555, Traverse City, MI, USA

[RD-036] N. Lalor, "The Experimental Determination of Vibrational Energy Balance in Complex Structures", Paper 108429 Proc. SIRA Conference on Stress & Vibration, 1989, London

[RD-037] G. Borello, " Influence sur le niveau de bruit sous coiffe Ariane 4 de l'interaction satellite-cavité acoustique », Intespace report D090.152.EIA/GB, 20 Août 1990

[RD-038] D. Lednik, «Prediction of high frequency vibrations induced by pyrotechnic shock sources of separation-Part1: transient power flow between two coupled oscillators", ESA report 89/26, March 1989

[RD-039] G. Borello(InterAC), V. Cipolla (CNES Toulouse), "Prediction of high frequency shock response of a satellite using SEA" European Conference on Spacecraft Structures, Materials & Mechanical Testing – December 11–13, 2002 – Toulouse, France

[RD-040] 01dB-METRAVIB, Shock attenuators, Application Note IVA 18

[RD-041] R. J. Schaefer, "Chapter 33 – Mechanical properties of rubber"

[RD-042] Société de Technologie Michelin, "Le pneu – L'adhérence", Janvier 2001

[RD-043] A. Klembczyk (Taylor device, INC), "Presentation to European Space Agency", Taylor device, February 4, 2010

[RD-044] Barry Control "Isolator Selection Guide"

[RD-045] ECSS-E-ST-35C Rev 1 "Space engineering – Propulsion general requirements", 6 March 2009

[RD-046] S. Mary (CNES), Shock Environment Qualification for Small Satellite, Shock workshop ESTEC, May 2008

[RD-047] ESA/ESTEC shock bench presentation, Kiryenko, Piret, Kasper, European Conference on Spacecraft Structures, Material and Mechanical Testing, Noordwijk, 2005

2.3 References of Part 3

[RD-048] Shock predictions for aerospace applications - return of experience from ESA programmes, S. Kiryenko, J. Kasper, Ngan, ESA/ESTEC, Oct 2005

[RD-049] ECSS-E-ST-10-03C, Space engineering-Testing

[RD-050] ECSS-E-ST-10-02C, Space engineering-Verification, 6 March 2009

[RD-051] Test requirements for launch, upper stages and space vehicles, MIL Technical Standard, MIL-HDBK-340A, April 1999

[RD-052] Environmental Engineering Considerations and Laboratory Tests, MIL Technical Standard, MIL-STD-810F, January 2000

[RD-053] Pyroshock Test Criteria, NASA Technical Standard, NASA-STD-7003, May 1999

[RD-054] Pyroshock Testing Techniques, Institute of Environmental Sciences and Technology, IEST-RP-DT032.1

[RD-055] ESA/ESTEC shock bench presentation, S. Kiryenko, Kasper, ESA/ESTEC, May 2005

[RD-056] Zeroshift of piezoelectric accelerometers in pyroshock measurements, Endevco Corporation

[RD-057] Selecting Accelerometers for and Assessing Data from Mechanical Shock Measurements, PCB Piezotronics

[RD-058] Selecting Accelerometers for Mechanical Shock Measurements, PCB Piezotronics

[RD-059] Explosive,Gun&ImpactTesting, PCB Piezotronics

[RD-060] Brüel & Kjær product data

[RD-061] Isotron and charge mode piezoelectric accelerometers pros and cons, Endevco

[RD-062] Survivability and linearity of the high-survivability high-shock 60000g accelerometer, Endevco

[RD-063] Problems in high-shock measurement, Endevco

[RD-064] Steps to selecting the right accelerometer, Endevco

[RD-065] An introduction to the shock response spectrum, T. Irvine, May 2002

[RD-066] The shock response spectrum at low frequencies, D. O. Smallwood, Sandia National Laboratories, Albuquerque, NM

[RD-067] Digital calculation of shock response spectra from strong-motion earthquake records, Navin C. Nigam, Paul C. Jennings, California Institute Of Technology, June 1968

[RD-068] The Scientist and Engineer's Guide to Digital Signal Processing, Second Edition, Steven W. Smith, California Technical Publishing, San Diego, California, 1999

[RD-069] Time-Frequency Toolbox – For use with Matlab, François Auger, P. Flandrin, P. Gonçalvès, O. Lemoine, CNRS France, 1996

[RD-070] Les représentations temps-fréquence en traitement du signal, Sciences de l'ingénieur

[RD-071] Analyses temps-fréquence linéaires et quadratiques, Sciences de l'ingénieur

[RD-072] Shock qualification methods for equipment, J.B. Bernaudin, EADS-Astrium, May 2005

[RD-073] Handbook for Dynamic Data Acquisition and Analysis, Himelblau, H., Piersol, A.G., Wise, J.H., and Grundvig, M.R., Institute of Environmental Sciences-Reference Publication-DTE012.1, Inst. Envir. Sc., Mt Prospect, IL, Mar. 1994.

[RD-074] Pyroshock Data Acquisition and Analysis, A. G. Piersol, Piersol Engineering Company, Woodland Hills, California

[RD-075] A shock amplifier evaluation, Anthony S. Chu Endevco Corporation, San Juan Capistrano, CA 92675

[RD-076] The effects of digitizing rate and phase distortion errors on the shock response spectrum, James H. Wise, Jet Propulsion Laboratory, California Institute of Technology

[RD-077] Experimental contribution to the modelling of shock propagation induced by linear pyrotechnical source, C. Boutry, H. Grzeskowiak, P. Chabin

[RD-078] Practical Measurement Analyze, 2.2 Reconstruction of the digitalized signal, C. Lalanne, TOME 6

[RD-079] Techniques For The Normalization of Shock Data, S. Smith and W. Hollowell, 62nd Shock and Vibration Symposium, October 1991

[RD-080] Shock Response Spectrum Synthesis via Wavelets, T. Irvine, www.vibrationdata.com

[RD-081] Demonstration de la tenue aux environnements – Conception et realisation des essais en environnement – Part 3, AFNOR norm, AFNOR NF X 50144-3

[RD-082] Shock Analysis Using The Pseudo Velocity Shock Spectrum, Part 1, Part 2, Part 3, H. Gaberson

[RD-083] Pyro Shock mount investigation for Ariane 5 Components, E. Hornung (ERNO Deutsche Aerospace) et H.Ory (Aachen University – Germany) - 1992

[RD-084] Pyrotechnic Shock Loads; Test evaluation, Equipment protection - E. Hornung (ERNO Deutsche Aerospace) et H.Ory (Aachen University – Germany)

[RD-085] Modal Velocity as a criterion of Shock Severity – H. Gaberson et D. Chalmers

[RD-086] Relation contrainte – vitesse et interet du SRC des pseudo vitesses, Christian Lalanne, XVIII symposium Vibrations Chocs et Bruit & ASTELAB, July 2012

[RD-087] Relation between strain and velocity in resonant vibration - S. Crandall

[RD-088] Stress and Strain limits on the attainable velocity in mechanical vibration, Hunt Journal of acoustics Society of America, 32,1123-1128 (1960)

[RD-089] An introduction to the vibration response spectrum, T. Irvine, June 2000

[RD-090] Flight Unit Qualification Guidelines, John W. Welch, June 2010

[RD-091] Smallwood, David: “An Improved Recursive Formula for Calculating Shock Response Spectra” 51st Shock and Vibration Bulletin, 1980

[RD-092] Kelly, R.D. and Richman, G., “Principals and Techniques of Shock Analysis”, SVM-5, Sec. 6.7, Shock and Vibration Information Center. 1969

2.4 References of Part 4

[RD-093] Shock predictions for aerospace applications - return of experience from ESA programmes, S. Kiryenko, J. Kasper, Ngan, ESA/ESTEC, Oct 2005

[RD-094] Shock environment in spacecraft from an early definition to a final verification, S. Kiryenko, J.L. Parquet, ESA/ESTEC, Dec. 2002

[RD-095] ESCC Generic Specification n°3602 Issue 3 – Relays, Electromagnetic, Latching

[RD-096] ESCC Generic Specification n°3601 Issue 3 – Relays, Electromagnetic, Non-latching

[RD-097] Shock Test Report for ENVISAT P/L Relays, Test N° 2229 doc n° YTO/REP/VIB/1070 issue 1 dated 13/8/1996 issued by ESA/ESTEC

[RD-098] ENVISAT Relay Report Shock Test – Facility Data Report, Test n°3526" doc. N° MTT/REP/VIB/2299 ISSUE 1 DATED 15/01/2000

[RD-099] Test requirements for launch, upper stages and space vehicles, MIL Technical Standard, MIL-HDBK-340A, April 1999

[RD-0100] Equipment Design - Chapter 41 Harris and Crede Shock and Vibration Handbook – A. Piersol

[RD-0101] MIL-STD-883E NOTICE 3 Method 2020.7 22 March 1989 Method 2020.7 "Particle Impact Noise Detection Test"

[RD-0102] CARES (Ceramics Analysis and Reliability Evaluation of Structures) Theory Guide, September 13, 2007

[RD-0103] Design Strength of Optical Glass, Keith B. Doyle, Mark A. Kahan

[RD-0104] TIE-33: Design strength of optical glass and ZERODUR®, Technical Information, Oct 2004

[RD-0105] ZERODUR® Glass Ceramics - Strength Data for the Design of Structures with High Mechanical Stresses, Peter Hartmann, Kurt Nattermann, Thorsten Döhring, Markus Kuhr, Peter Thomas, Guenther Kling, Peter Gath, Stefano Lucarelli

[RD-0106] Pyrotechnic shock response predictions combining statistical energy analysis and local random phase reconstruction, Bodin E., Brévart B., Wagstaff P., Borello G., Journal of the Acoustical Society of America, 112 (1), July 2002

[RD-0107] Simulation des niveaux vibratoires générés par les chocs pyrotechniques en vue de prédire les dysfonctionnements électriques des équipements embarqués, D. Wattiaux, PhD dissertation, Faculté Polytechnique de Mons, Belgium, 2009.

[RD-0108] Shock analysis philosophy for electronic units, B. Brévart, V. Cipolla, Proceedings of the European Conference on Spacecraft Structures, Materials & Mechanical Testing, ESTEC, NL, 2005

[RD-0109] Comportement dynamique d'un équipement électronique soumis à des chocs mécaniques ou pyrotechniques, E. Bodin, PhD dissertation, Université de Technologie de Compiègne, 2001

[RD-0110] Shock response predictions on electronic units, B. Brévart., E. Bodin., M. Blanquet., Proceedings of the European Conference on Spacecraft Structures, Materials & Mechanical Testing, Toulouse, France, 2002.

[RD-0111] Prediction of an electronic equipment response to a pyrotechnic shock excitation, E. Bodin, B. Brevart, T. Youssefi, Lauch Vehicle Vibration Proceedings, Toulouse, 14-16 December 1999.

[RD-0112] Shock Analysis of the Sentinel-3 SLSTR Parabolic Mirror Assembly, B. Braun, D. Keil, D, European Conference on Spacecraft Structures Materials & Environmental Testing, 1-4 April 2014, Braunschweig, Germany.

[RD-0113] Vibration Analysis for electronic equipment, 2nd EDITION, D. S. Steinberg, JOHN WILEY, 1988, vol. 1.

[RD-0114] Elastohydrodynamic Lubrication, D. Dowson., & G.R. Higginson, Pub. Pergammon, 1977

[RD-0115] Simplified solution for elliptical-contact deformation between two elastic solids, D.E. Brewe & B.J. Hamrock, Jnl. Of Lubrication Technology Trans ASME, 1977, Series F, Vol. 99 p 485.

[RD-0116] ECSS-E-ST-32-10C, Space engineering – Structural factors of safety for spaceflight hardware

[RD-0117] Effects of Axial Vibration on Ball Bearings & Draft Design Guidelines for Vibration-Induced Gapping, S.D. Lewis, ESA-ESTL-TM-0019

[RD-0118] Test Method Standard, Electronic and Electrical Component Parts, MIL-STD-202G, 2002

[RD-0119] ROARKS's Formulas for Stress and Strain, 6th edition, Chapter 13, Bodies under Direct Bearing and Shear Stress

[RD-0120] ECSS-E-ST-33-01C, Space engineering – Mechanisms, 6 March 2009

[RD-0121] ECSS-Q-ST-70-08C, Space product assurance - Manual soldering of high-reliability electrical connections, 6 March 2009

[RD-0122] ECSS-Q-ST-70-38C, Space product assurance – High-reliability soldering for surface-mount and mixed technology, 31 July 2008

3
Terms, definitions and abbreviated terms

3.1 Terms and definitions from other documents

For the purpose of the present document, the terms and definitions from ECSS-S-ST-00-01 and ECSS-E-ST-32 apply.

3.2 Terms and definitions specific to the present document

3.2.1 shock

local transient mechanical loading of short duration, high frequency and high amplitude, with substantial initial rise time

NOTE For additional details, see 4.1.1.

3.2.2 shock response spectrum (SRS)

calculated function based on an input transient, allowing characterizing the shock effect on a dynamical standardized system in order to estimate its severity or its damaging potential

NOTE For additional details, see 4.1.4.2.

3.2.3 similarity

degree to which different specimens show the same behaviour when exposed to the same shock condition.

NOTE See para 12.6.2, for an example of process for verification by similarity. Verification by similarity is part of the verification by analysis.

3.3 Abbreviated terms

For the purpose of this document, the following abbreviations apply:

Abbreviation	Meaning
CoG	centre of gravity
CDF	cumulative distribution function
CLF	coupling loss factors
DLAT	destructive lot acceptance testing
DLF	damping loss factors
ESEA	experimental statistical energy analysis
FEA	finite element analysis
FEM	finite element model
FFT	fast fourier transform
FRF	frequency response function
HDRM	hold-down and release mechanism
HF	high frequency
HSRSF	highest shock response spectrum frequency
IEPE	integrated electronics piezolectric
I/F	interface
IP	in plane
ISM	iso-static mount
LFA	lowest frequency analysis
LMPR	local modal phase reconstruction
LV	launch vehicle
MAC	modal assurance criteria
MAF	maximal analysed frequency
MEE	maximum expected environment
MF	medium frequency
NRL	naval research laboratories
NTL	normal tolerance limit
OOP	out of plane
PCB	printed circuit board
PDF	probability distribution function
PIND	particle impact noise detection
PLF	payload fairing
ppm	parts per million (10^{-6})
PSD	power spectral density
PV	pyrovalve

Abbreviation	Meaning
QL	qualification level
R&D	research and development
RRS	random response spectrum
S/C	spacecraft
SDRA	shock damage risk analysis
SEA	statistical energy analysis
Shogun	shock generator unit
SASSA	shock attenuator system for spacecraft and adaptor
SRS	shock response spectrum
STFT	short time fourier transform
TFA	time frequency analysis
TFT	time frequency transform
TWT	travelling wave tube
VEB	vehicle equipment bay
VSEA	virtual statistical energy analysis
WT	wavelet transform

Part 1
General

4
Background – Shock environment description

4.1 Shock definition and main characteristics

4.1.1 Shock definition

A shock is a local **transient mechanical loading** characterised by its **short duration** (order of magnitude from 50 μs to 20 ms), its high frequency (>1 kHz up to 1 MHz in case of pyroshock) and **high amplitude** with substantial initial rise time (approaching 10 μs).

It is usually very difficult to precisely measure or characterise the loading itself. Therefore a shock is classically observed through acceleration measurements which constitute the system response to the shock loading. These measurements are characterised in terms of time history by:

- Highly oscillatory response with large positive and negative peak amplitudes with the same order of magnitude;
- An envelope by a decreasing form of exponential function.

In terms of frequency, typical acceleration response to a shock loading are characterised by:

- Forced response at frequencies contained in the external shock loading (usually at high frequency);
- System natural frequencies (usually at lower frequency).

As an example, Figure 4-1 presents the typical acceleration profile resulting from a pyroshock.

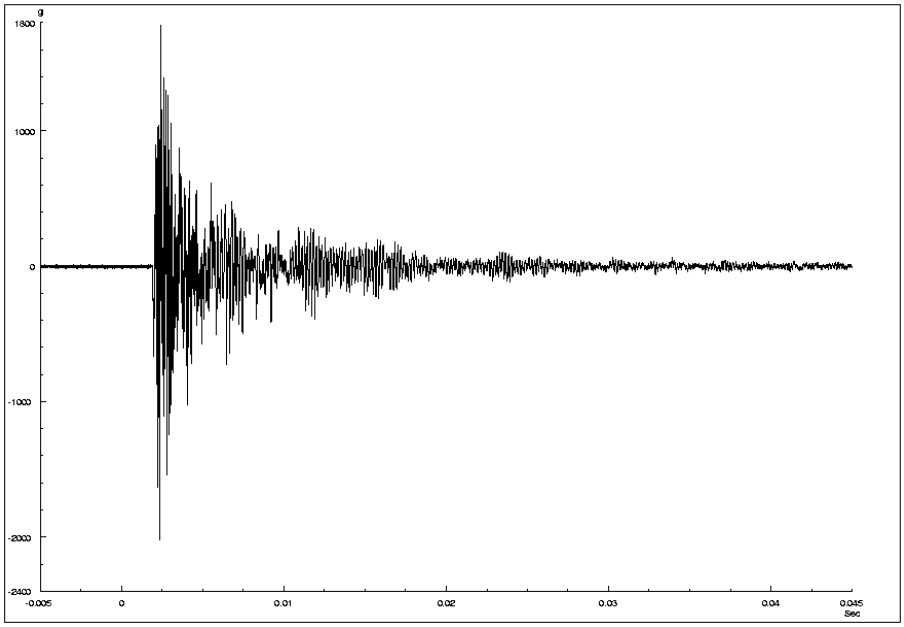

Figure 4-1: Example of shock acceleration measurements resulting from a pyroshock

4.1.2 Physical aspects of shocks

A shock **propagates** throughout the considered system as tension-compression, flexural or shear **waves** with **complex phenomena of reflection, dissipation and diffraction** at boundary conditions or mechanical discontinuities (bolted and riveted joints for instance). The flexural waves are dispersive whereas tension-compression and shear waves are not dispersive.

High frequency waves quickly vanish both in time and space, reducing the sharpness of the wave front, because of damping in materials and attenuation in joints: therefore it is more observable at the beginning of the shock measurement time history and at the vicinity of the shock source. Waves reflect on boundary conditions and internal interfaces, initiating a modal response of the system: this produces longer wavelength responses which can be found wherever in the structure even far from the shock source.

Such a shock environment is completely different from standard vibration. On one side a shock has an excitation duration which is significantly shorter than the response time of the equipment, and then the system responds freely. On the other side a vibration environment has an excitation duration which is long compared the response time of the equipment.

4.1.3 Main shock effects

The shock environment is an important matter of interest as it can induce **major failure** resulting in the total or partial loss of a space mission [RD-01][RD-07].

A non-exhaustive list of problems that can be caused by shocks at equipment level is given hereafter:

- Impact on electronics: material electronic card malfunction due to failure or degradation of electronic components such as for example relay, quartz, transformer, and self.
- Structural impact on materials: cracks and fractures in brittle materials (ceramics, crystals, epoxies or glass envelopes), local plastic deformation, or accelerated fatigue of materials for repeated shocks;

- Impacts on mechanisms: the components used in the mechanisms, which are reputed sensitive are the bearings, gears, worm gears; their degradation mode is an excessive marking. The life duration impacts on the selection and the severity of the damage criteria. In this way, the residual marking is practically forbidden for long life duration mechanisms. In the opposite, for the mechanisms which are activated only a few times during their life, the residual marking size allowed are limited by their functionalities.
- Impacts on valves: the valve degradation modes are a limited leakage in quantity and time, a significant or permanent leakage and a structural degradation, which involves a malfunction of the valve mechanism.

4.1.4 Shock response spectra (SRS)

4.1.4.1 Overview

Time history constitutes the primary (and the most natural) accessible data since almost all physical signals are obtained by receivers recording variations with time. It contains obviously all the pertinent information and it is essential to save any time history in order not to lose any information.

However, a shock measurement in the form of a time-history is not directly useful for engineering purposes, e.g. comparing shocks severities and frequency contents, or understanding its effect on components. A reduction to a different form is widely used to deal with shocks: the Shock Response Spectrum (SRS).

4.1.4.2 Shock response spectra definition

The shock response spectrum (SRS) is a calculated function based on an input transient. It allows characterizing the shock effect on a **dynamical standardized system** in order to estimate its **severity or its damaging potential**. Thus it allows to compare shocks with each other or to establish equivalence criterion between a measured transient environment and a laboratory simulation of that transient environment.

The method consists in applying a time history as a base excitation to **an array of single-degree-of-freedom (SDOF) systems** and then calculating for each of them the **temporal maximum of their response**. The SRS can be defined for any input or response parameters of interest (displacement, velocity, or acceleration). For aerospace structures, it is common to define the input transient in terms of an **acceleration**. See Figure 4-2 and Figure 4-3.

The natural frequency of each SDOF is an independent variable. Thus, the calculation is performed for a number of independent SDOF systems, each with a unique quality factor Q=10, assuming conventionally the same damping (5 %) for each SDOF.

The choice of damping should be carried out according the structure subjected to the shock under consideration. When this is not known, or studies are being carried out with a view to comparison with already calculated spectra, a Q factor Q=10 is conventionally chosen.

Any arbitrary set of unique natural frequencies can be used for the shock response spectrum calculation. A typical scheme, however, is based on a proportional bandwidth, such as 1/24 octave. This means that each successive natural frequency is $2^{1/24}$ times the previous natural frequency. The SRS resolution is determined by this bandwidth and is independent of the transient duration. There are several SRS values that can be of interest for different applications, namely, the maximum absolute response of the SDOF versus frequency that occurs:

- during the application of the transient, called the **primary** SRS,
- after the transient is over, called the **residual** SRS,
- in the positive direction, called the **positive** SRS or SRS+,

- in the negative direction, called the **negative** SRS or SRS-,
- at any time in either direction, called the **maximax** SRS (most usually used).

A typical maximax SRS is shown hereafter. The SRS acceleration is also called the maximum or peak absolute response.

NOTE 1 Primary and maximax SRS can differ when time signal has a non-negligible zero shift (also called DC-offset). See Paragraph 14 of the Part 3.

NOTE 2 SRS are often presented on a log-log graph. It is important to take care with this representation because of the real gap between two curves are visually minimized at high frequencies. A lin-lin representation allows sometimes to clearly visualise gaps.

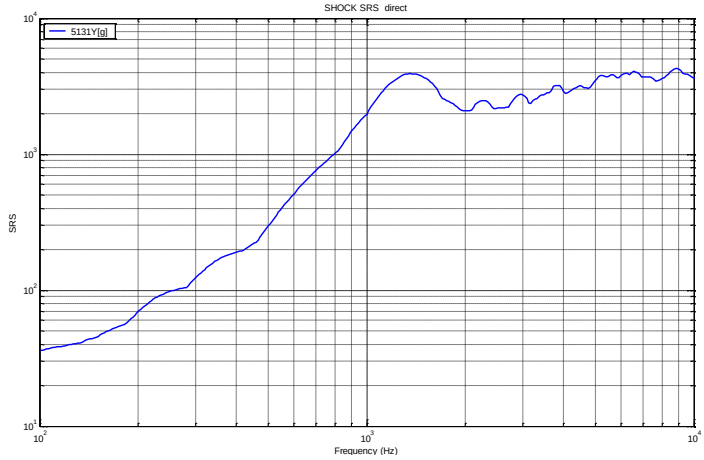

Figure 4-2: SRS example

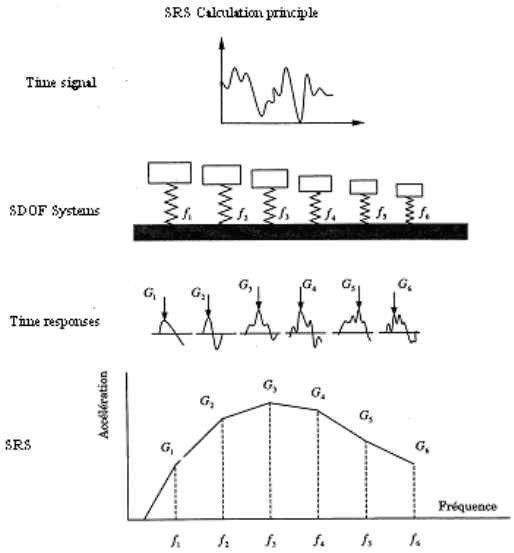

Figure 4-3: Shock response spectra principle

4.1.4.3 SRS properties

SRS main properties are given hereafter:

- If the velocity change is zero between the beginning and the end of the transient, the shock response spectra should have an initial slope of 12 dB/octave or a slope which changes in a smooth manner between 6 dB/octave and 12 dB/octave. SRS should be globally increasing (i.e. without taking into account local maxima) in low frequency range up to a maximum value. If the curve is decreasing or flat at the beginning, it could indicate a problem of zero offset or a truncation error. One of the dangers of these errors is they can propagate when specification are derived from incorrect measured SRS [RD-09]. See Figure 4-4.

NOTE The slope N of a line on a log-log graph is defined as

$$N = \frac{\log_{10} \frac{A_2}{A_1}}{\log_{10} \frac{f_2}{f_1}}$$

Therefore:

N=1 corresponds to a 6dB/octave line.

N=2 corresponds to a 12dB/octave line

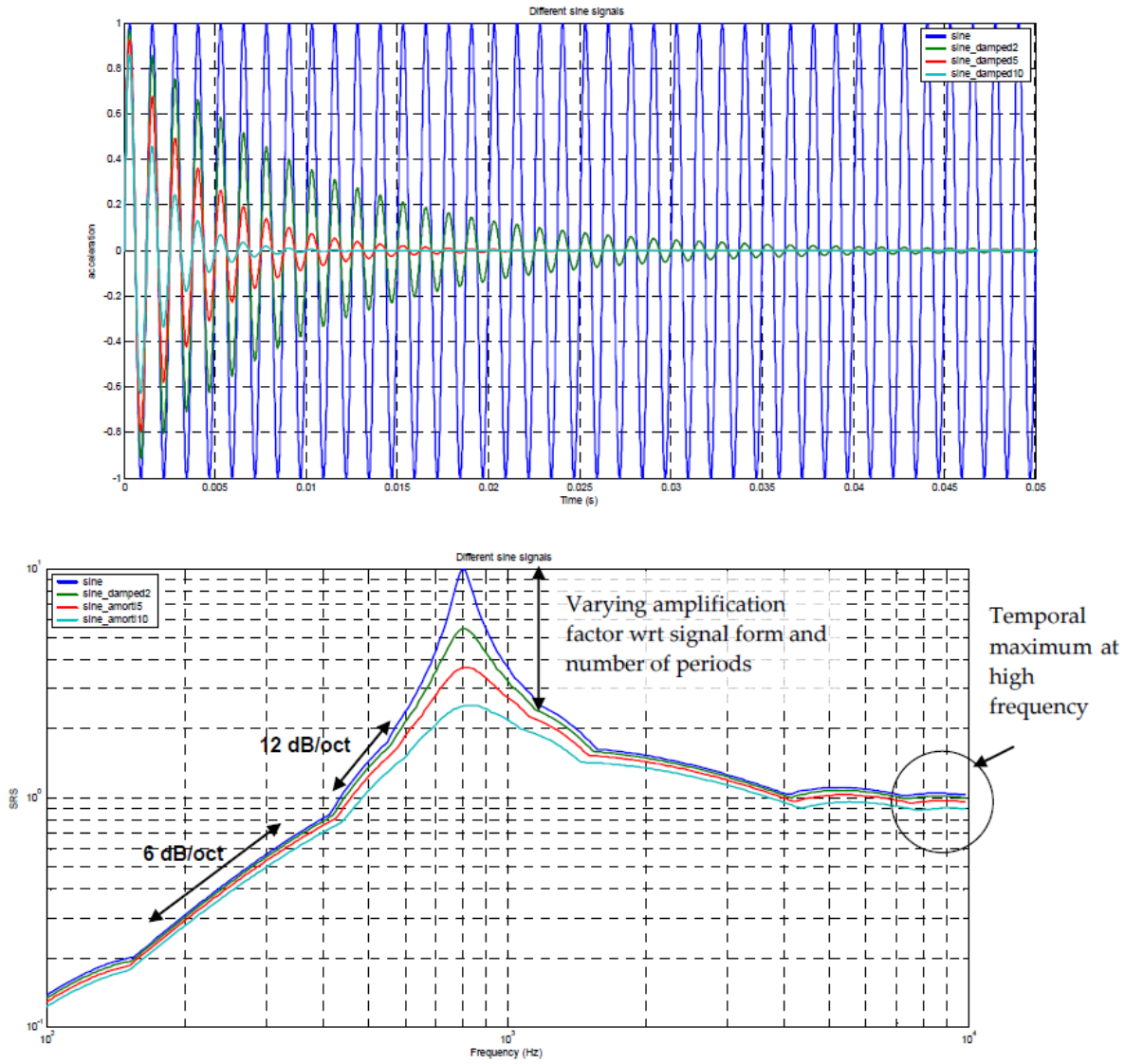

Figure 4-4: Example of SRS calculations, as function of transient signal characteristics

- The value of the SRS approaches the absolute maximum value of the transient acceleration as the natural frequency of the SDOF exceeds the lesser of the highest frequency in the Fourier spectrum of the transient, or the upper frequency limit of the data acquisition system. The time history at the base of the considered SDOF acts indeed as a quasi-static excitation at this frequency. The SDOF's response follows consequently the time history oscillations. (see Figure 4-4)
- The amplification factor of a component in a signal depends on the signal form (see Figure 4-5). Considering a Q-factor of 10 for SRS calculation, it is comprised between 1,6 , corresponding to a half-sine time signal, up to 10, corresponding to a perfect sine signal with a sufficient number of periods. SRS of real signals have generally an amplification comprised between 3 and 4. In other words, a shock spectrum response (Q=10) performed on a shock signal has an amplitude about **3 to 4 times** higher than the maximum of the time history due to the transient (non-harmonic) nature of the signal. **This order of magnitude is useful to determine accelerometers calibration during a test campaign.**

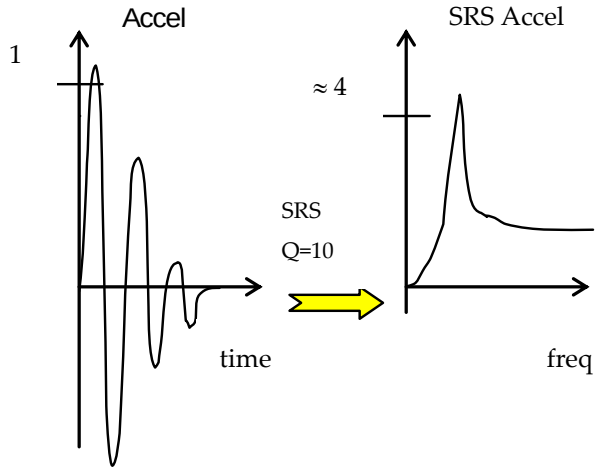

Figure 4-5: SRS peak amplitude derived from typical transient shock signal

- The SRS is **not linear with regard to the addition** of time signals. That is to say that the SRS of time signals sum is not equal to the sum of the individual time signals SRS.
- The SRS **is, in return, linear with regard to a scalar multiplication**. That is to say that the SRS of a time signal multiplied by a scalar α is equal to α times the SRS of the time signal.
- The SRS calculation is **not a bijective calculation**. Some information is definitively lost (like the phase or the effective duration information). It is thus essential to save any time history in order not to lose any information. Both the transient time history and resulting spectrum are critical to the environmental definition and test verification.

4.1.4.4 Recommendations on SRS calculation

It is recommended to adhere to the following general guidelines:

a. The sampling rate for the input time history should be 8 times greater than the highest shock response spectrum calculation frequency and at least superior to 5 times.

b. The recommended frequency range for a SRS of a near-field time source is 100 Hz-100 kHz.

c. The recommended frequency range for a SRS of a medium or far-field time source is 100 Hz - 10 kHz.

d. The minimum sampling rate should be 12 points per octave, with an optimum number of 24 points per octave. Note that the higher the used Q-factor is the higher the frequency sampling should be.

e. For measurements on structures that experience no net velocity change due to the transient event, **the signal should be forced to yield a net velocity change of zero from the beginning to the end of the transient** event before the SRS computation. This condition is achieved by calculating the mean value of the acceleration signal, and subtracting this mean value from all data values.

4.1.4.5 SRS limitations

The notion of severity is relative to the considered dynamical system. Thus, real systems do never correspond to the standardized system: they do not have the same natural frequencies, and the real damping can be very different from 5 % (Q = 10).

Damage can be caused by amplification on an eigenmode. A source time signal with a frequency component near this eigenfrequency can be very severe, whereas another time signal with a high but different frequency component can be less severe for the considered unit. The difficulty comes generally from a very approximate knowledge of the mid and high frequency eigenmodes of real systems.

The SRS tool allows to compare shocks transients with each other, to consider envelopes and then specify shocks levels. This is today the universal tool for describing shocks, specify them or pronouncing qualification. However, it is not a perfect tool:

- The SRS **does not have a unique relationship with the transient signal** from which it is computed; i.e., it is possible for different transients to have the same SRS. These shocks have consequently the same effect on any of the SDOF with a Q-factor of 10 but can have a different effect on the considered system. In particular, it is often possible to at least coarsely approximate the maximax SRS for a complex, multi-cycle transient environment by an appropriately shaped single pulse transient in the laboratory. Of course, the required single pulse used for the simulation can have a much higher maximum level and a different effective duration than the actual environment, raising serious questions about the real severity of the simulation.
- The SRS does not allow to describe completely the frequency content of a signal. Some frequencies can be hidden by others peaks. Changing the Q-factor is the method to reveal these hidden peaks.
- The SRS is based on the response of a 1-DOF system which is not representative of real multi-DOF systems. This limitation is all the more important that the studied system has eigenmodes at close frequencies.

5
Shock events

5.1 Shock occurrence

Spacecraft can sustain various types of shock during their development and mission.

From the launch to its mission end, a spacecraft can for instance sustain the following shocks:

- Launcher induced shocks such as fairing or stage separation. They propagate in the launcher structure, reach the launcher-spacecraft interface and then propagate in the spacecraft structure. These shocks are usually comprised in the launcher specification.
- Spacecraft release shock. They are directly generated at the launcher-spacecraft interface by the separation system (clampband release or other system). These shocks are also usually comprised in the launcher specification.
- Appendage release shocks or subsystem actuating shocks. Some appendages which are clamped for launch are released when in function (solar arrays, antenna reflectors, instruments). In the same way some subsystems can be actuated by devices producing shocks, such as pyrovalves or mechanisms. These shocks occur generally during stationing or at the beginning of mission, but can occur even later after an interplanetary travel for instance.

These shocks can sometimes be generated by low shock devices, which significantly reduces their criticality.

During spacecraft development, some shocks can also occur: they are usually qualification or acceptance shock tests at system (spacecraft release shock) or subsystem level (equipment qualification on shock machine or test bench); they can also be characterisation tests (SHOck Generator UNit or Shogun to evaluate propagation w.r.t. launcher induced shocks).

5.2 Shock environmental categories

Shock environment is usually divided into three categories, basically near-field, medium-field and far-field. The distinction between these categories is based on the magnitude and the spectral content of the environment. There is however neither formal separation nor precise limit value, especially in terms of distance from the source: such a classification depends on the type and strength of the considered device and the detailed configuration of the structure (that drives the shock propagation path). However these categories can have a strong influence on the hardware design or selection.

These categories are generally described as follows:

- The **near-field** environment is dominated by **direct wave propagation** from the source with very high peak accelerations (that can exceed 5000 g) and a very high frequency content (well above 10 kHz for pyrotechnic sources). Depending of the source such a near-field environment is located from several to a dozen centimetres from the source.

- The **mid-field** environment is characterised by a **combination of the propagating waves and the structural resonances**, issued from recombination of reflecting waves on the boundary conditions. The maximum acceleration peak is weaker than in near-field (down to a fifth of the near-field peak values) and the frequency content still presents high frequency components (up to 10 kHz). Depending on the source, mid-field environment is located from a dozen to several dozen centimetres from the source.
- The **far-field** environment is dominated by the **structural resonances** issued from recombination of reflecting waves on the boundary conditions. The resulting peak accelerations are really weaker (up to a fifth of the near-field peak values) as compared to those in near- or medium-field and most of the frequency content is below 10 kHz. The far-field environment is located outside the mid-field environment.

As illustrated in Figure 5-1, the severity (characterised here by its Shock Response Spectrum, see 4.1.4) of a far-field environment is not necessarily decreasing when the distance from the source to the response point of interest is increasing. This is especially true in the frequency range dominated by high structural resonances (typically below 2 kHz).

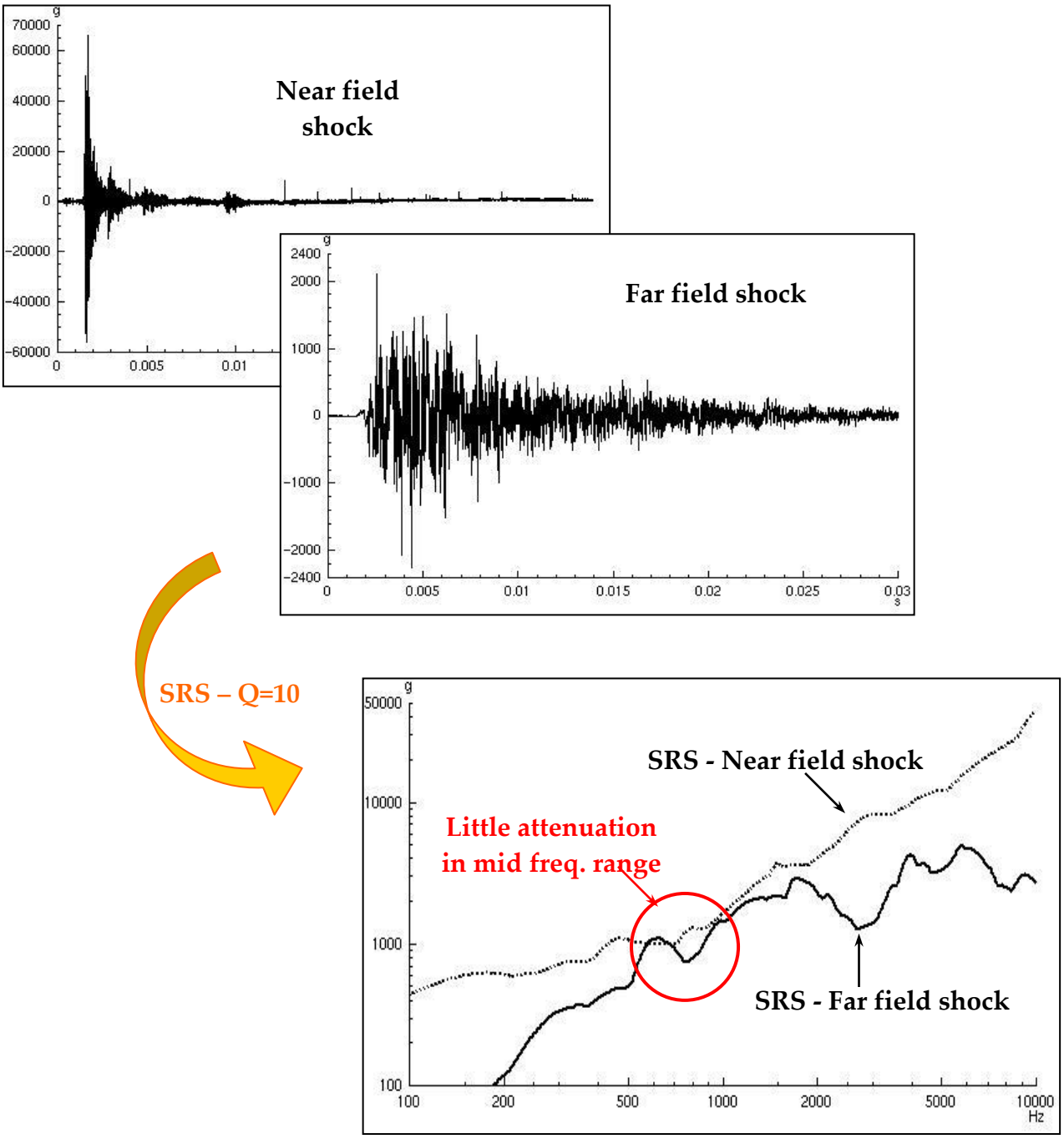

Figure 5-1: Comparison of shock severity of two signals, one close to the shock source (near field) and the other several meters from the source (far field)

6
Introduction to shock design and verification process

6.1 Presentation of the global process

The process of shock design and verification is illustrated in Figure 6-1.

The structure of this Handbook is built with respect to this process.

The first part is the current one, presenting the basis of shock design and verification.

The second part is dealing with the derivation of spacecraft shock environment to units and subsystems. The main inputs are information on shock sources such as shock specification from the launcher and spacecraft internal shocks environments and the spacecraft architecture. The objective is to determine the shock environment for each unit of the spacecraft and use it to derive a specification using a given margin policy. The main methods to do it are similarity and heritage methods and numerical FEM calculations. Additional inputs are required depending on the method: a test database for the first one and a Finite Element Model or SEA model for the second. Additional outputs can be attenuation rules related to the studied structure or Maximum Expected Flight Environment (MEFE) when using statistical methods.

The third part focuses on the shock verification approach. The objective of the verification is to prove that the specimen (at unit or system level) can sustain the required shock environment. This can be done either by analysis or by testing. In case of testing, specific inputs are needed: a shock test facility adequate with the specification and the unit hardware depending on the testing philosophy (e.g. PFM and QM). The test results should be used to feed shock databases as these are inputs for derivation of spacecraft shock environment to units or for unit qualification by analysis. In this part, methods and tools to have a proper assessment of shock data and thus evaluate the shock test are also given. In the ideal case, the capability of the spacecraft to withstand or, if appropriate, to operate in the induced shock environments is demonstrated after this operation. And the shock qualification is achieved.

However, in some cases, the shock qualification cannot be directly achieved (shock environment not completely validated by system level and unit level testing). In general, this problem is discovered too late to perform a delta qualification at unit level. This can lead to a Shock and Damage Risk Analysis (SDRA) which is the topic of the **fourth part**. This part focuses on shock consequences on equipment and needs many engineering or functional data on the concerned unit. Equipment sensitivity and failure modes are particularly focused on. The main output is a risk analysis which concludes on the ability to flight of the concerned unit.

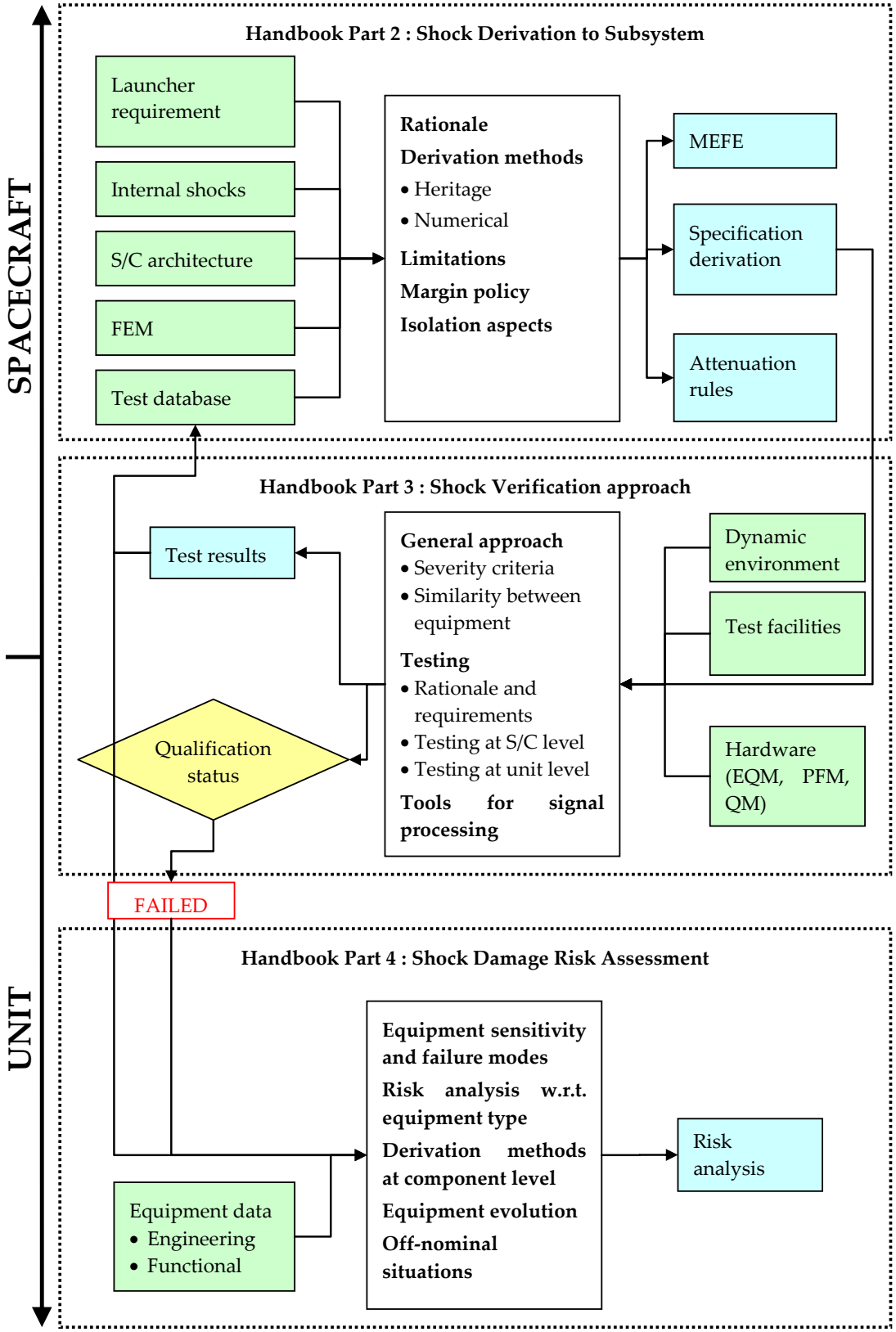

Figure 6-1: Overall logic of shock handbook w.r.t. shock design and verification process

6.2 Means to conduct an evaluation of shock environment and criticality

To follow this global process of shock design and verification, several means are available and can be explained and detailed in the further parts of the handbook: e.g. numerical analyses and extrapolation methods.

The objective of this paragraph 6.2 is to present what is recommended in term of tasks to be performed with respect to the workflow of a standard programme. Table 6-1 thus shows the hypotheses, objectives, recommended method and requirements of this shock evaluation at 3 main stages of a programme: Early phase (SRR level), Intermediate phase (PDR/CDR level) and Final verification phase (QR level).

Table 6-1: Shock evaluation methods w.r.t. project status

	Early phase (SRR level)	**Intermediate phase (PDR/CDR level)**	**Final verification phase (QR level)**
Hypothesis	• Overall configuration defined but structural details not fixed. • Shock events known but sources and inputs only roughly defined.	• S/C structure already defined but layout subject to changes. • Shock events, sources and inputs known.	• System and subsystems shock tests already performed. • Qualification status not achieved.
Objective	To derive preliminary conservative specification within each zone of the spacecraft, and better understand/anticipate the shock severity within each zone	To derive consolidated and conservative specification within each zone of the spacecraft.	To have a critical review of test results and specifications (doubt on representativeness of test configuration,…) in order to consolidate the qualification status.
Method	Identify dimensioning shock environment and apply relevant similarity-heritage-extrapolation methods.	Combination of similarity-heritage-extrapolation methods and numerical analyses (several restitution points within each zone).	Verification of analysis robustness followed by detailed numerical analyses (restitution points at sensors location).

Part 2
Shock input derivation to space segment elements and equipment

7 Shocks in spacecraft

7.1 Overview

This chapter lists the different shock events and associated devices. Its aim is to remind that the use of certain devices should always make shock a matter of concern.

7.2 Potential shock sources for spacecraft

The different shock events are separated in two different categories: shocks during service life and shocks related to testing as described in Figure 7-1.

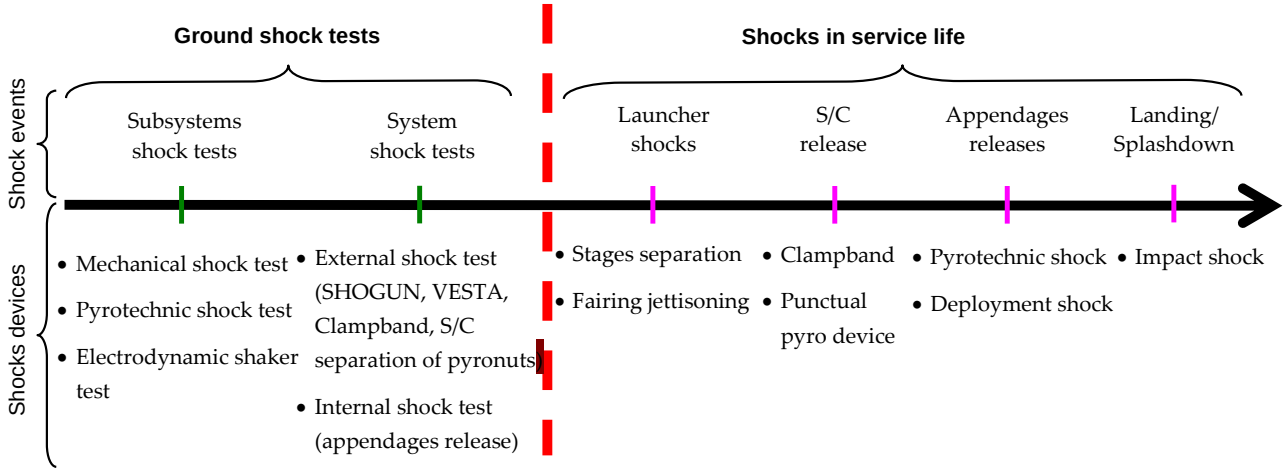

Figure 7-1: Shocks in a spacecraft project

7.3 Shocks devices description

Shock devices used for these different shock events are quickly presented in Table 7-1 for ground shock tests and in Table 7-2 for shocks in service life, for which indication of shock origin (external/internal with respect to spacecraft) is given.

Table 7-1: List of potential shock sources for ground shock tests

Ground shock tests	
Subsystem shock test	Mechanical and pyrotechnic shock machine used for equipment testing: several kinds of shock machines have been developed to qualify equipment to shocks. They can be either mechanical (usually by the mean of a hammer hitting a dedicated shock table) or pyrotechnic. See Part 3 of this handbook for further information. Electrodynamic means (shaker): shakers can be used to qualify equipment to shock with short excitation pulses. They are however relatively limited in terms of level and frequency band capacities.
Specific shock tests at system level (i.e. not on-ground tests of flight devices)	SHOGUN: this device is intended to represent Ariane 5 launcher shocks, especially fairing separation. It is composed of a pyrotechnic linear cord charge inside a weakened aluminium structure. The shock wave is generated by the expansion of the tube causing a controlled rupture of the lower flange screw section. VESTA: this device is intended to represent VEGA launcher shocks, especially fairing separation. It is represented by a full scale mock-up of the VEGA upper composite and the shock is generated by the release of the HSS belt achieved through the activation of bolt cutters. Pyrotechnic Ariane 5 ASAP kit: such a device is intended to be representative of an ASAP 5 microsatellite separation system shock. See 7.4.4 for further information.

Table 7-2: List of potential shock sources for shocks in service life

Shocks in service life		
Shock	**Description**	**Origin (w.r.t. S/C)**
Launcher induced shock before spacecraft release	This category gathers all shock sources inside the launcher, such as stages separations or fairing jettisoning. Different systems exist: for instance separation by pyrojets, symmetric or asymmetric tight barrier.	External
Spacecraft release from launcher	Clampband release: the clampband is a structural piece usually used to link the spacecraft to the launcher interface. This clampband is preloaded and is released by different means, usually using pyrotechnics. Other separation systems (see 7.4.4 for further information): Rockot Mechanical Lock Systems: used for spacecraft attached to the launch vehicle through discrete points. PSLV spacecraft separation system: separation system based on ball locks. ASAP 5 microsatellite separation system: this device is used on Ariane 5 structure for microsatellites ASAP5. Classical pyronut separation systems	External
Appendages release (during stationing or mission)	Bolt-cutter: a pyrotechnic device actuates a cutter which cuts a pre-loaded bolt that maintains a subsystem in its clamped configuration. Wire-cutter: a pyrotechnic device actuates a cutter which cuts a pre-loaded wire that maintains a subsystem in its clamped configuration. Pin-puller: a pyrotechnic device generates gases which drive the pin through pressure effect from its initial clamping position to its end position, releasing a mechanism. Explosive bolts (including for separation system): bolts loaded by a pyrotechnic device that explode to release the subsystem they were maintaining. "Low shock" devices with a mechanical pre-load which is released by other means than a pyrotechnic system: these devices can be used as pin pullers, separation nuts or bolts, release mechanisms, actuators, switches, powered hinges and valves. See below.	Internal
Other shock sources during mission	Mechanical stop in mechanisms: Such shocks can occur in mechanisms such as stepper, or at the end of an appendage deployment due to stop end. Pyrotechnic valves: a pyrotechnic device produces gases under high pressure, which has the effect of suddenly deforming a membrane equipped with a rigid weight. The latter projects a punch, which shears a tight end fitting, thus freeing the fluid passage.	Internal

Low shock devices are used for internal appendages release, in order to protect very sensitive equipment or instruments which are implemented in direct vicinity of the release device (shock source). This allows facilitating or even making possible the spacecraft or sub-system architecture, e.g. on optical instruments where systems are installed close to the secondary mirror for opening a protection cap.

The implementation of such devices is very complex, as most of the time a lot of electrical energy is needed to actuate them the routing of adequate cables can, in some cases, be complex, and therefore it is very important to take this into account as early as possible in the design process.

It is also noticeable that "low-shock" can be an abusive term where it consists only in replacing the pyrotechnic actuator (thus reducing a primary shock) without changing the released mechanical element. For instance, when a low-shock device is used to release a highly preloaded tie-rod, high shock loads can still be generated by the relaxation of the stored energy into the tie-rod.

A specific list of current low shock technologies is shown hereafter to sum up the currently available shock devices technologies ([RD-010][RD-011]):

- Electro-mechanical spool: a spring is loaded by a sectioned spool, overwrapped by a retaining wire, the latter held in-place by a linkwire. Current passing through the linkwire causes it to fail, thereby releasing the retainer wire and allowing separation of the spool halves.
- Paraffin actuator: High Output Paraffin (HOP) actuator uses constrained volumetric expansion of highly refined polymer at a given transition temperature to produce large hydrostatic pressure that is translated to actuator through a hermetic seal.
- Shape Memory Alloy (SMA): such system uses the shape memory effect which is based on a transformation which is reversible upon heating. Thus SMAs can undergo deformation which is retained until they are heated above a transition temperature at which point a reverse transformation occurs and the original non-deformed shape is restored.
- Pyrosoft: the Pyrosoft is a low shock device. The release of the screw is initiated by the melting of a thermite composition. Those thermite allow the debasing of a threaded ring which releases the piston and the threaded segment. The duration of the process, at least 0,5 second allows a progressive release of the screw in two phases; first the release of the tension and in a second part the liberation of the screw.
- Thermal knife: this kind of device is based on thermal degradation of a pre-tensioned cable (for instance Kevlar/Aramid). An electrically heated knife gradually melts through the cable causing degraded fibres to fail reducing cable cross section until the cable to fail under the residual tension.

7.4 Detailed information on specific shock events

7.4.1 Overview

This paragraph 7.4 describes the different shock events and their main characteristics (notably in terms of frequency content with an SRS representation). A distinction is made between external shocks originating from payload fairing jettison, launcher stage separation or spacecraft release and internal shocks occurring in the spacecraft, typically for appendage release.

7.4.2 Launcher induced shocks

Launcher induced shocks gather all shocks occurring in the launcher structure that propagate through the launcher structure and the payload adaptor up to the spacecraft interface. Such shocks are mainly due to stage separation and fairing jettisoning. Clampband release is not considered, in this handbook, as a launcher induced shock and is specifically addressed in the paragraph 7.4.3.

The severity of the launcher induced shock seen by the spacecraft, mainly depends on:

- The type of separation devices used for the stage separation or fairing jettisoning, with a lower severity for bi-rupture (symmetric) separation or punctual separation systems compared to mono-rupture or pyrojet separation systems.
- The overall architecture of the launcher, and especially distance and loadpath characteristics between the shock sources and the spacecraft interface.

There is therefore no absolute rule valid for all launchers, each of them having its own specificities:

- **ARIANE 5**: Owing to continuous improvements of the launch vehicle, the severity of the launcher induced shocks has been significantly reduced, through the introduction of a bi-rupture separation system for the upper stage separation (replacing mono-rupture separation system), and of a quasi-symmetric separation device for the fairing (so-called HSS3+, with recurring production target in mid 2015).

  NOTE With the introduction of the HSS3+, the fairing separation shock level is equivalent to the upper stage separation shock and below 0.2 x f. The dimensioning shock event for the spacecraft becomes the clamp-band release.

  NOTE The handbook currently presents the shock environment of the earlier and current launch vehicle definition (excluding HSS3+) and associated verification method (i.e. Shogun test method, see Para. 7.4.2.1, and Part 3).

- **VEGA:** Dimensioning shock is induced by the fairing separation especially for frequencies up to about 3kHz. For higher frequencies, the upper stage separation is dimensioning.

In general these specificities are presented and continuously updated in user manuals. For other launcher, user manuals should be consulted.

The launch induced shocks have specific characteristics depending on the type of separation.

- Frequency content of the excitation: There can be important **low frequency components** in launcher induced shock, typically from 300 Hz to 1kHz. These components are due to modal response of some elements of the launcher that are well transmitted to the spacecraft-launcher interface. An important parameter driving these low frequency components is the stiffness and the diameter of the interface where the separation occurs.

  Figure 7-2 here below presents the envelope spectrum for stage and fairing separations (HSS1) and for clampband release. The existence of specific modal responses between 400 and 700 Hz is here indicated through the particular shape of the stage/fairing spectrum at these frequencies. Thus level is higher in this band in comparison with a continuously increasing slope (of 12 dB or 9dB per octave) up to the elbow point at 1000 Hz. This is not seen for clampband release for which response is driven by interface ring mode around 1000 Hz, depending from the spacecraft ring diameter.

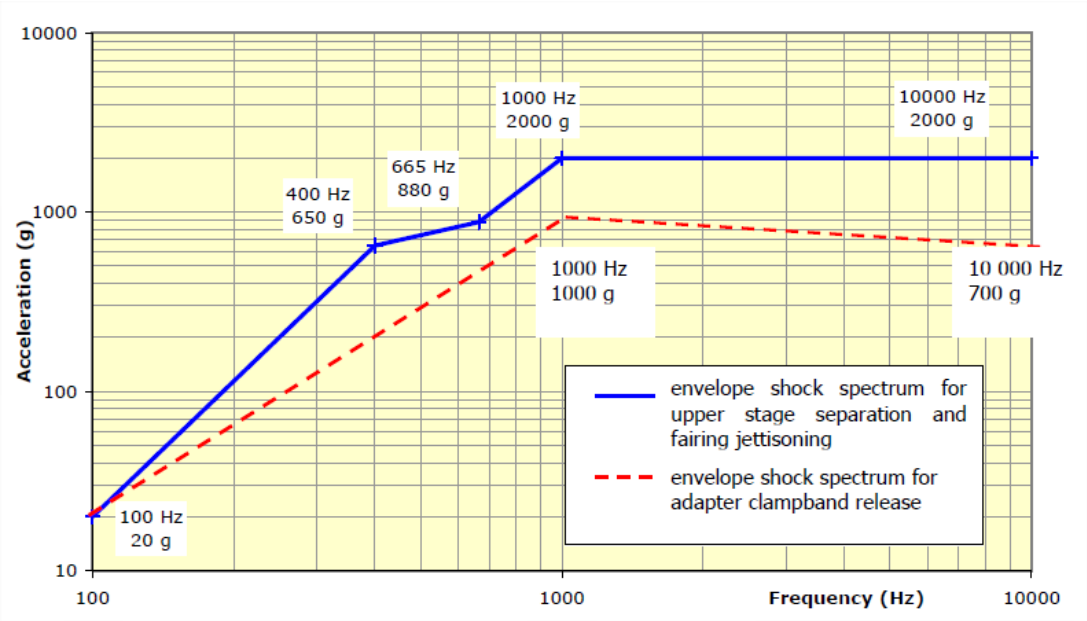

Figure 7-2: Envelope shock spectrum for the upper stage separation and fairing jettisoning and envelope shock spectrum for clampband release at spacecraft interface – From Ariane 5 User's Manual Issue 5

- Due to dissipation and diffraction effects, the further the separation occurs from the spacecraft-launcher interface, the greater is the attenuation of the high frequency levels. This notion of distance is based on both the physical distance and the complexity of the propagation path (number of structural joints). This is usually not true for low or medium frequency levels. An example of the dependency of high frequencies shock levels with respect to the distance is shown in Figure 7-3, with the comparison of shock levels along the primary loadpath and for increasing distances with respect to the shock source. As such, the excitation of lower frequency modes are well transmitted to the spacecraft-launcher interface and beyond, whereas the high frequencies shock levels are more quickly attenuated.

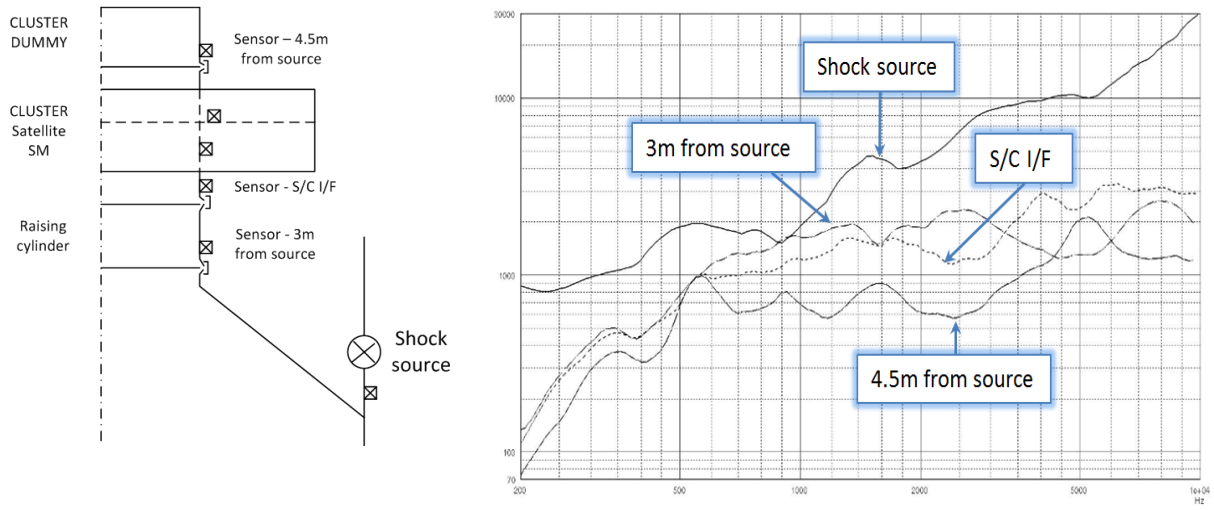

Figure 7-3: Comparison of shock levels with increasing distances from the shock source (system level shock test performed on CLUSTER satellite)

- Severity: A mono-rupture separation creates more levels at low and medium frequencies up to 6000Hz than a bi-rupture separation. An example of such an impact of the separation type is shown in Figure 7-4.

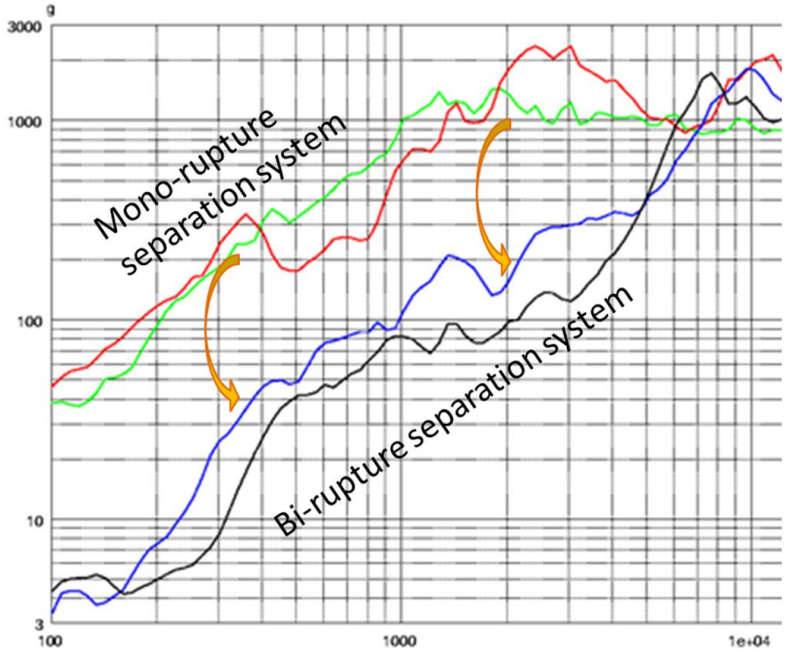

Figure 7-4: Comparison of shock levels at spacecraft interface for a mono-rupture and a bi-rupture separation system

- The best way to have a representative characterisation of such a launcher induced environment is to conduct a test at system level with launcher structures and a payload dummy, with a flight representative separation system being fired. In this case a particular attention should be paid to boundary conditions.
- As the pyrotechnic separation device is very well controlled, if the mechanical characteristic on the propagation path toward the spacecraft are identical, a good repeatability is achieved.
- The launcher induced shock specification is derived from flight measurement and statistics made on a spacecraft family using a given launcher position and a given adaptor. An illustration of consistency between launcher induced specification and the shock flight measurement for two spacecraft within the same family (same platform in same launcher position with same adaptor) on Ariane 5 is presented on Figure 7-5. It shows the good repeatability of launcher induced shock and the adequacy of the specification at spacecraft interface.

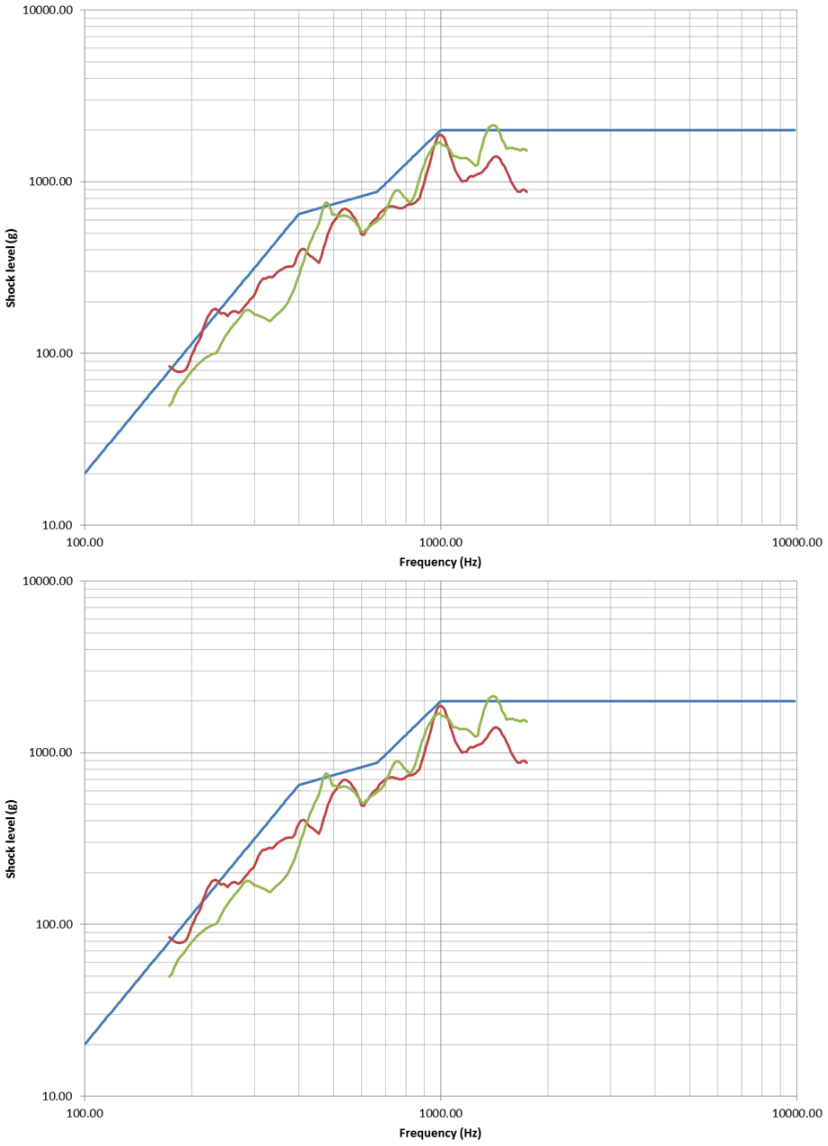

Figure 7-5: Consistency between flight shock measurement and launcher induced specification for Ariane 5 at spacecraft interface in launcher Axial direction.

7.4.2.1 Example of spacecraft/LV shock compatibility test – SHOGUN

Shogun stands for SHock Generator UNit: it is a **characterisation mean** designed for dealing with the specificity of shocks generated by the Ariane 5 launcher. It is a pyrotechnic device based on the expansion of a pyrotechnic tube that breaks a weakened section (Figure 7-6). In this way the principle is similar to the of a launcher stage separation, which it is intended to represent.

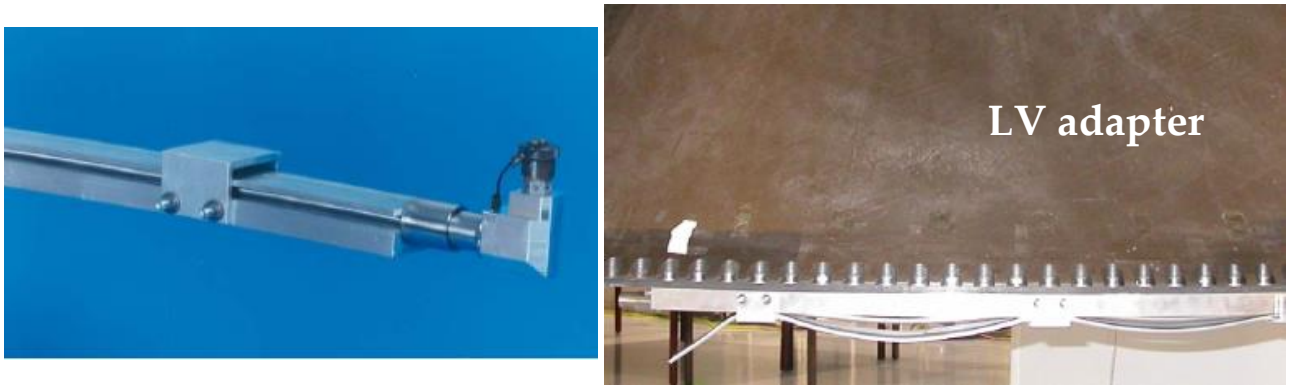

Figure 7-6: Views of a Shogun device (Dassault / Courtesy)

The main characteristics of such a shock are given hereafter:

- Even if the shock source is achieved by adopting the same principle of a launcher stage separation, this shock occurs with different boundary conditions (LV adapter is free at its base) in comparison to those of a real launcher induced shock. Thus the Shogun low frequency content can be quite different from the one of a launcher induced shock. This can be seen in Figure 7-7.

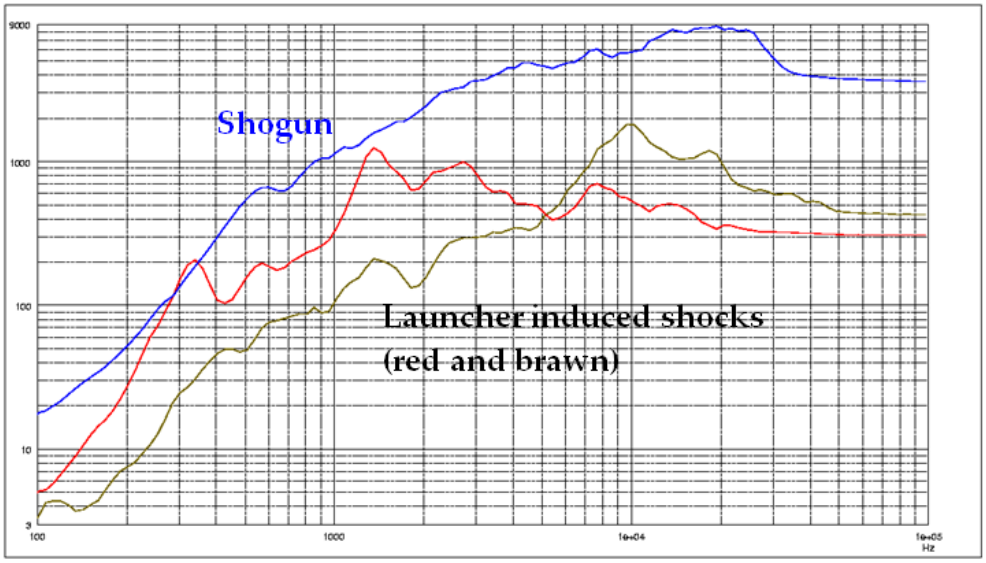

Figure 7-7: Comparison between Shogun and launcher induced shocks levels at the spacecraft interface

- A Shogun test occurs immediately at the base of the payload adapter, which is far closer to the spacecraft interface than for a real launcher shock. As a consequence high frequency levels are less attenuated than for a real launcher shock event. This can also be seen in Figure 7-7.

Therefore the use of such a test is limited to the characterisation of the transfer function between spacecraft launcher interface and an equipment inside the spacecraft. As a matter of fact the Shogun test is considered representative of the shock propagation inside the structure for launcher induced shocks type of source.

Details on the associated extrapolation method to derive qualifying environment at unit levels, can be found in paragraph 13.3.2.2.2.

7.4.2.2 Example of spacecraft/LV shock compatibility test – VESTA

VESTA is the acronym for VEga Shock Test Apparatus. It is a test method designed and developed in order to support the qualification of spacecraft to be flown on the VEGA launcher. It aims at reproducing the shock generated during the VEGA fairing jettisoning phase.

The test method (see Figure 7-8) is built from several stage/component full scale mock-ups used during the VEGA development and consists in a flight representative model of the VEGA upper composite. VESTA simulates the release of the fairing belt at the base of the payload adapter using the same hardware available during a typical VEGA flight (fairing belt and bolt cutters), then the shock generated is fully representative with respect to the one experienced in flight.

Figure 7-8: VESTA test method including the AGILE STM

The main characteristics of the shock generated by VESTA are given hereafter:

- The shock level at the spacecraft base is driven by the tension applied in the HSS belt. The SRS is mainly dominated by the response of the adapter ring mode at about 800 Hz
- The shock levels can be tuned by adjusting the tension of the HSS belt (from typically 20kN up to the HSS tension foreseen at the time of the Fairing separation).

Several tests have already been performed in order to characterize and validate this test tool. Some results in terms of shock at spacecraft interface are shown in Figure 7-9.

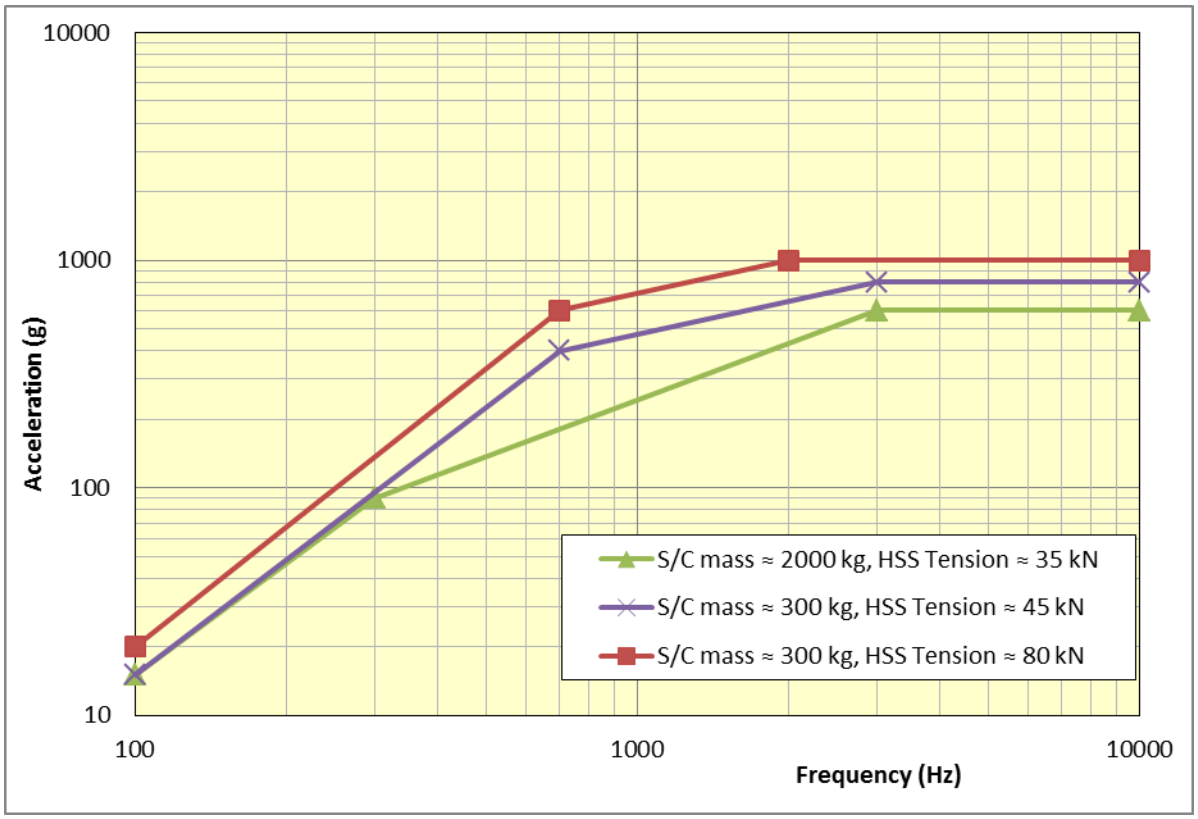

Figure 7-9: Results from VESTA test method for different configurations (shock at S/C interface, on the LV side)

Details on the associated extrapolation method to derive qualifying environment at unit levels, can be found in paragraph 13.3.2.2.2.

7.4.3 Clampband release

7.4.3.1 Overview

Two kinds of Clampband devices are treated here: standard one and low shock. These two kinds of devices are treated separately due to their differences in terms of generated shocks.

7.4.3.2 Standard clampband device

This usual kind of separation system consists of a Clampband set, release mechanism, and separation springs (see Figure 7-10). The Clampband usually includes clamp segments that hold the payload adapter and spacecraft rings together and a retaining band that applies the clamping forces to the clamp segments. The ends of the retaining band are held together by tension bolts. For separation, a pyrotechnically activated system (bolt-cutters for instance) cuts the tension bolts, allowing the end of the clamp segments to move apart and release the payload adapter and spacecraft mating rings.

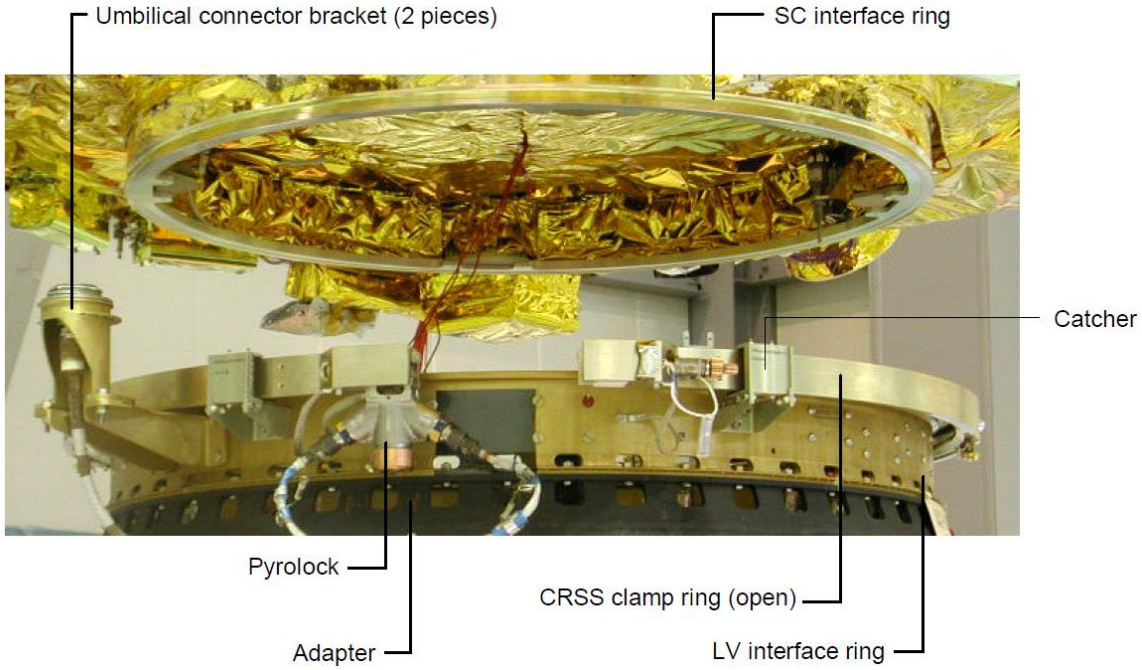

Figure 7-10: Example of a clampband mounted at a LV/SC interface (CASA CRSS with KSRC pyrolock)

Therefore the shock has two main physical origins:

- The **pyrotechnic part** due to the pyromechanism used to cut the tensioning part of the Clampband. This induces mostly the **high frequency components** of the shock (especially in the vicinity of the pyrotechnic device).
- The **pre-tension** in the Clampband is relaxed at a very high speed which induces a **low-damping medium frequency component**. It should be noticed that the effect of the pre-tension is local: the deformed area is rather small. This has some consequence on the Clampband release shock propagation (see 8.3.2.2).

As a consequence, several general characteristics of Clampband shocks can be put forward.

For homogeneous, uniform and unsupported circular rings, the pre-tension release induces an excitation of the first breathing mode (n=0) corresponding radial expansion and contraction of the ring. This is not exactly true if for some reasons the cylindrical symmetry is lost but this remains a meaningful hypothesis which provides correct approximation. The frequency of this mode is directly linked to the interface diameter and to the material used for the pre-loaded structure.

Frequency and the maximum associated acceleration (corresponding to SRS plateau) of the first breathing mode can be analytically approached by the following formulas:

$$\omega^2 = \frac{E}{\rho.R^2} \qquad a = \frac{\beta T_b}{\rho A R}$$

Where:

— E is the Young Modulus of the spacecraft lower ring material;

— ρ is the material density of the spacecraft lower ring material;

— R is the spacecraft ring radius;

— β is the tensile load distribution factor between the spacecraft lower ring and the adaptor upper ring. It is recommended to use $\beta = ½$;

— T_b is the total band tensile load acting on both spacecraft lower ring and the adaptor upper ring;

— A is the cross-section area of the spacecraft lower ring. It is recommended to consider an effective ring area up to an height h=5cm along the spacecraft lower cylindrical shell. Examples of such calculated cross-section area are given hereafter.

The use of such formula is illustrated in Table 7-3 and Figure 7-11 to Figure 7-14.

Table 7-3: Frequency of the first main radial mode – comparison between theory and test measurements

Diameter of spacecraft interface (mm)	937	1194	1666	2624	3936
Theoretical frequency (Hz)	1699	1333	955	607	404
Measured frequency (Hz)	1600	1350	920	580	350-600

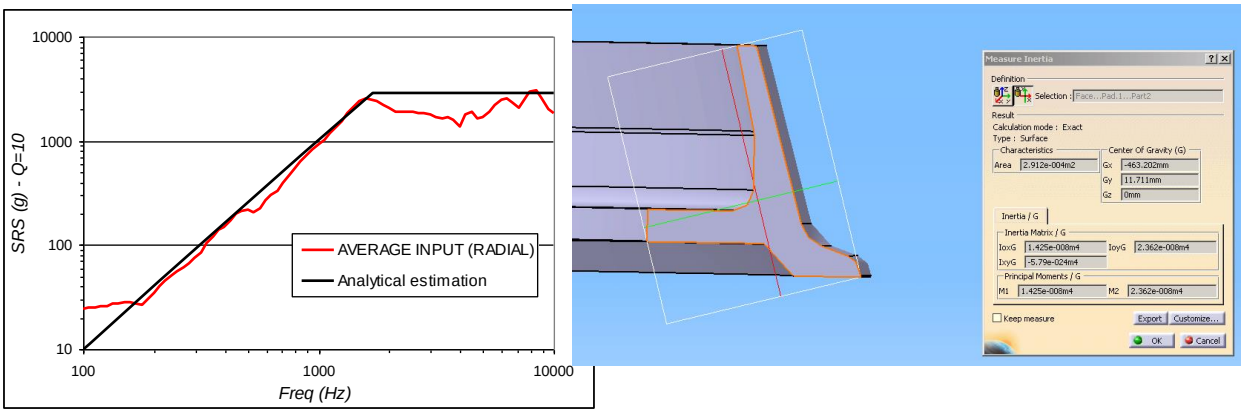

Figure 7-11: Comparison between theory and test measurements for Clampband radial SRS levels (I/F diameter 937 mm – SMART-1 interface ring)

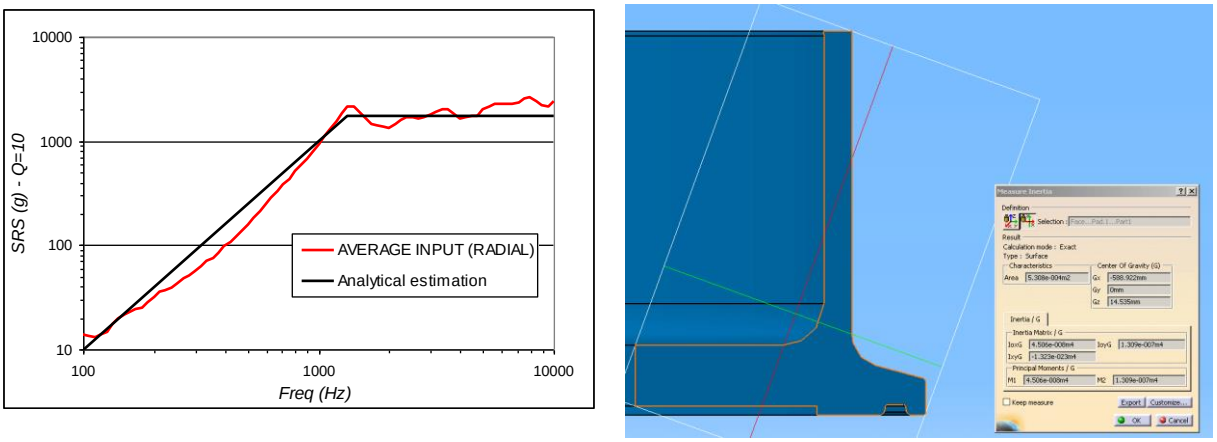

Figure 7-12: Comparison between theory and test measurements for Clampband radial SRS levels (I/F diameter 1194 mm – ROSETTA interface ring)

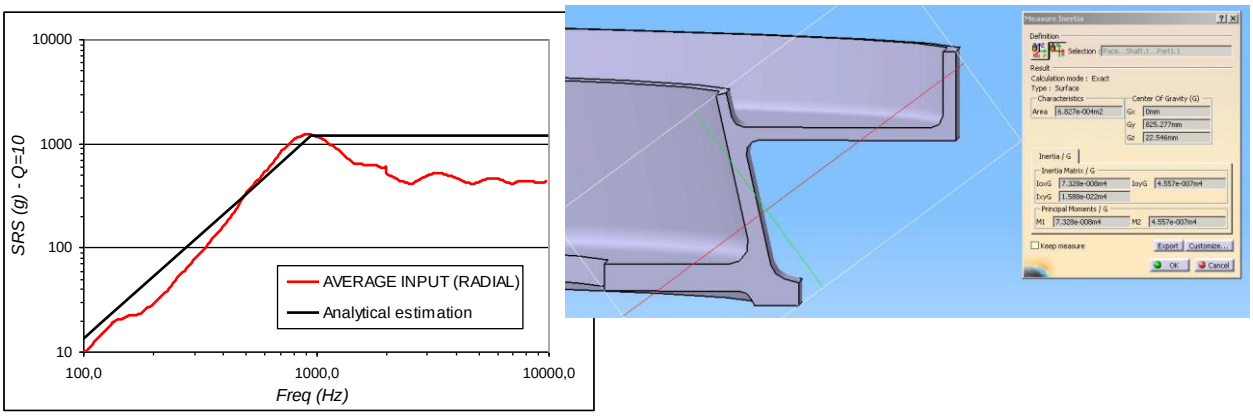

Figure 7-13: Comparison between theory and test measurements for Clampband radial SRS levels (I/F diameter 1666 mm – MSG interface ring)

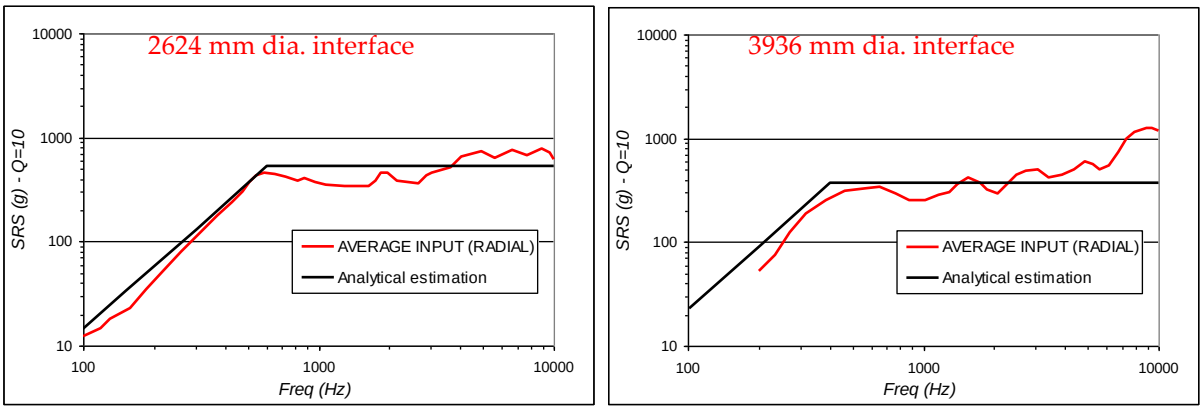

Figure 7-14: Comparison between theory and test measurements for Clampband radial SRS levels (I/F diameter 2624 mm (INTEGRAL) and I/F diameter 3936 mm (ATV))

As it has been explained, if for some reasons the cylindrical symmetry is lost, some in-plane flexural modes can be excited. It is important to emphasize that flexural modes have fundamental natural frequencies lower than the fundamental natural frequencies of the extensional or breathing mode. On the Figure 7-15, the first two flexural modes are illustrated. Frequencies of in-plane flexural modes can be analytically approached by the following formula:

$$\omega = \frac{n(n^2-1)}{R^2\sqrt{n^2+1}}\sqrt{\frac{EI_y}{\mu}} \quad \text{with n=2,3 …}$$

Where:

— E is the Young Modulus of the spacecraft lower ring material

— μ is the mass per unit length of ring

— R is the spacecraft ring radius

— I_y area moments of inertia about y axis (see Figure 7-15 for corresponding axis)

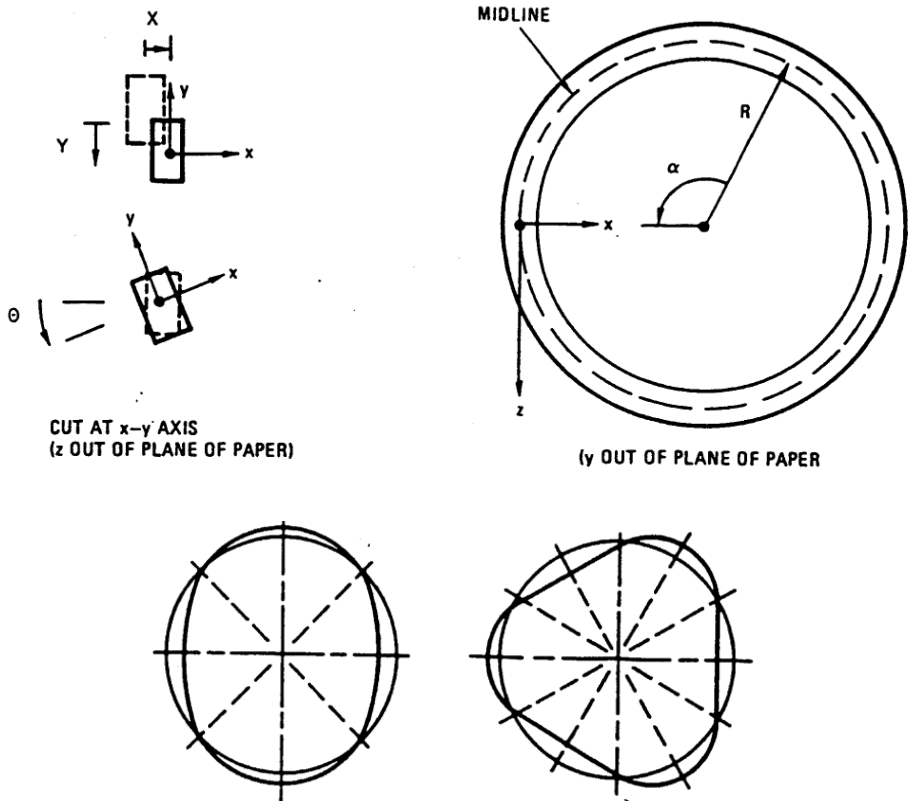

Figure 7-15: Example of ring in-plane flexural modes n=2 and n=3

If no flexural modes are excited, there is no important frequency content below the main breathing mode at medium frequency. Therefore the SRS is characterised in this frequency range (~100 Hz - 800 Hz) by a **constant slope of 12 dB/octave**.

Another point is the important difference in the acceleration levels at the spacecraft interface between longitudinal and radial components. General rules based on experience are given below and illustrated in Figure 7-16:

- The **radial component** is always **higher** than the **longitudinal** one, in low and medium frequencies;
- This difference generally rises from about 6 dB in low frequency (~100 Hz) to about 12 dB at the frequency of the main breathing mode.
- The lower the frequency of the first main breathing mode, the larger is the difference between radial and longitudinal levels.
- This difference then decreases at very high frequency: the levels are resulting from three-dimensional—pyrotechnic—effects in this frequency range. The radial and longitudinal components have equivalent levels from about 5 kHz.

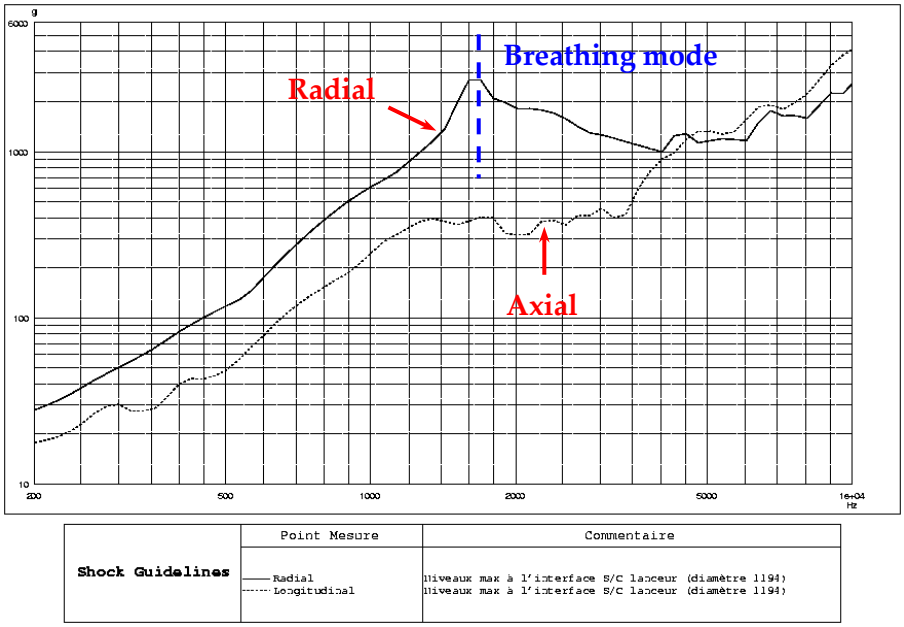

	Point Mesure	Commentaire
Shock Guidelines	Radial Longitudinal	niveaux max à l'interface S/C lanceur (diamètre 1194) niveaux max à l'interface S/C lanceur (diamètre 1194)

Figure 7-16: Difference between radial and longitudinal clampband levels at launcher-spacecraft interface – Example for a 1194 mm I/F diameter

Beyond the frequency of the main breathing mode, high frequency components are usually measured. These components are mainly due to pyrotechnic parts of the Clampband releases mechanism. Therefore the SRS magnitude and frequency content depend on the specific case.

Clampband release shock has a good reproducibility at least in low and medium frequency because of its predominant mechanical component (i.e. release of stored energy in the ring and adjacent structure).

7.4.3.3 Low shock clampband device

Low shock clampband device are designed to reduce shock level at spacecraft interface compared to clampband including pyro actuation. The overall concept of low shock device is to introduce constrain relaxation mechanisms in order to distribute energy over a longer period of time (compared to short spike introduce by pyro actuation) in order to reduce global levels (as illustrated in Figure 7-17). Several types of low shock device are proposed by launcher with different concepts and designs. The main ones used by European launchers are:

- CASA LPSS
- RUAG CBOD

Low shock device can be dissymmetric. Thus, with some low shock clampband design, the levels measured at the spacecraft interface can be inhomogeneous in both radial and longitudinal response directions. This could be the case when the pre-load release is made in a single point in a progressive way. As a matter of fact some examples have already shown a large discrepancy of level around the interface (up to factor 5)

It is important to notice that all the rules and remarks made in the previous sections to characterise a Clampband release shock source do not strictly apply to low shock Clampband devices especially if the distribution of level along the circular interface is not axisymmetric on spacecraft side.

Similarly, for the shock input derivation in various location inside the spacecraft (as described in paragraph 8.3), a distinction should be made between:

- the shock environment induced by the release of the pretension (excitation of spacecraft ring breathing mode) – See method 8.3.2
- the shock environment induced by the actuation device (point source excitation) – See method 8.3.1

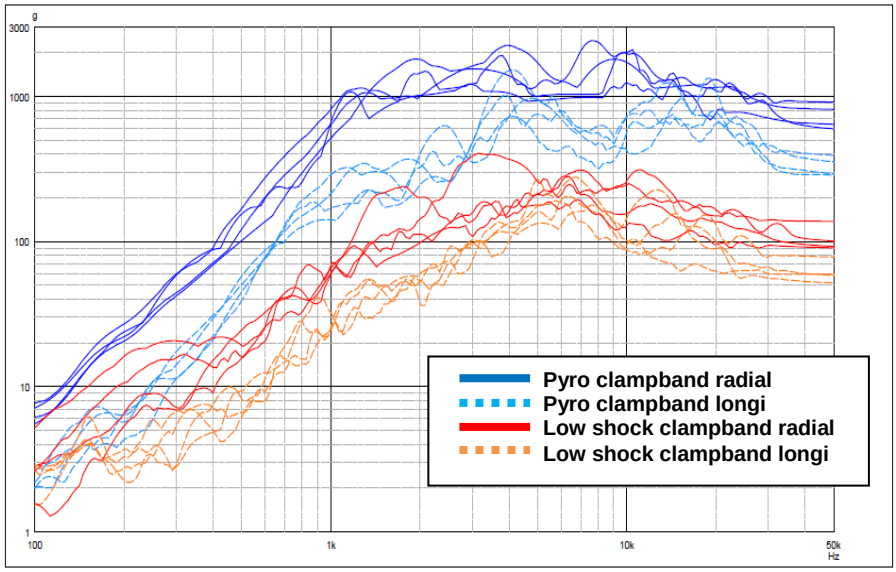

Figure 7-17: Example of spacecraft shock level induced by pyro clampband (blue curves) and low shock clampband (red curves) on similar telecom spacecraft with similar clampband tension (35kN)

7.4.4 Other S/C separation systems

7.4.4.1 Mechanical lock systems by EUROCKOT

Mechanical Lock Systems are offered by EUROCKOT for use with spacecraft that are attached to the launch vehicle at discrete points, rather than via a ring as in a standard Clampband system. The adapter system developed for CRYOSAT launch is shown in Figure 7-18 to Figure 7-19 as an example for single satellite adapter using mechanical lock system. It incorporates the mechanical lock separation components including pyroactuator, rods, spring pushers, connectors and bonding provisions. The satellite is fastened to the launch vehicle payload adapter via four (or three) mechanical locks using four (or three) brackets at the base of each satellite. The number of attachment points depends on the satellite shape and mass. Separation is achieved by igniting the pyroactuator which in turn rotates the mechanical locks via the mechanism rods releasing the spacecraft adapter frame. The spacecraft is then pushed away by spring pushers. Shock is not exerted directly on the spacecraft interfaces but on the parts of the mechanical drive, thus significantly attenuating the pyrotechnic shock levels at spacecraft level.

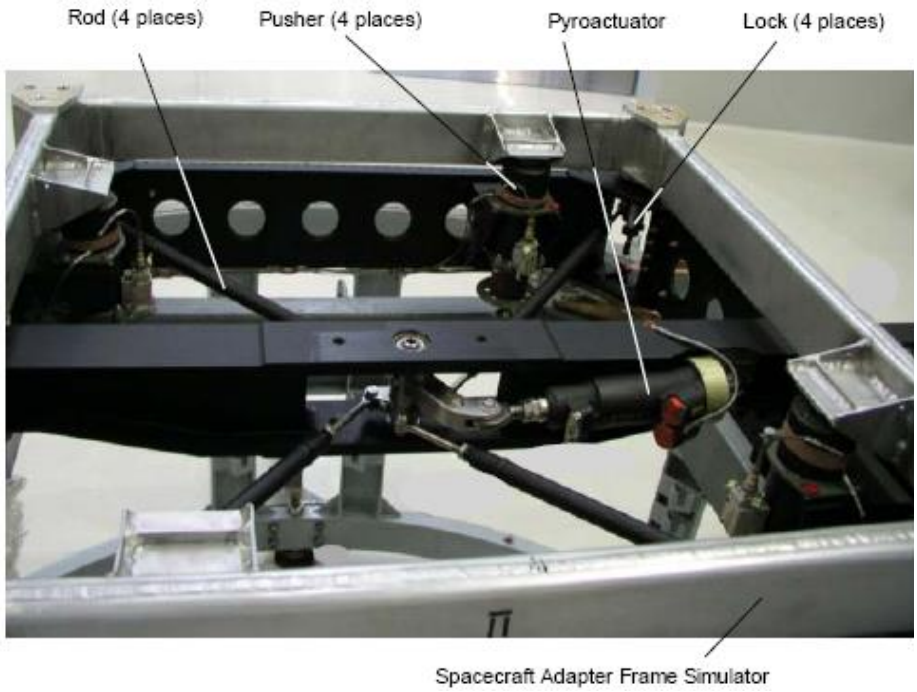

Figure 7-18: Adapter system for single satellite accommodation (KSRC / Courtesy)

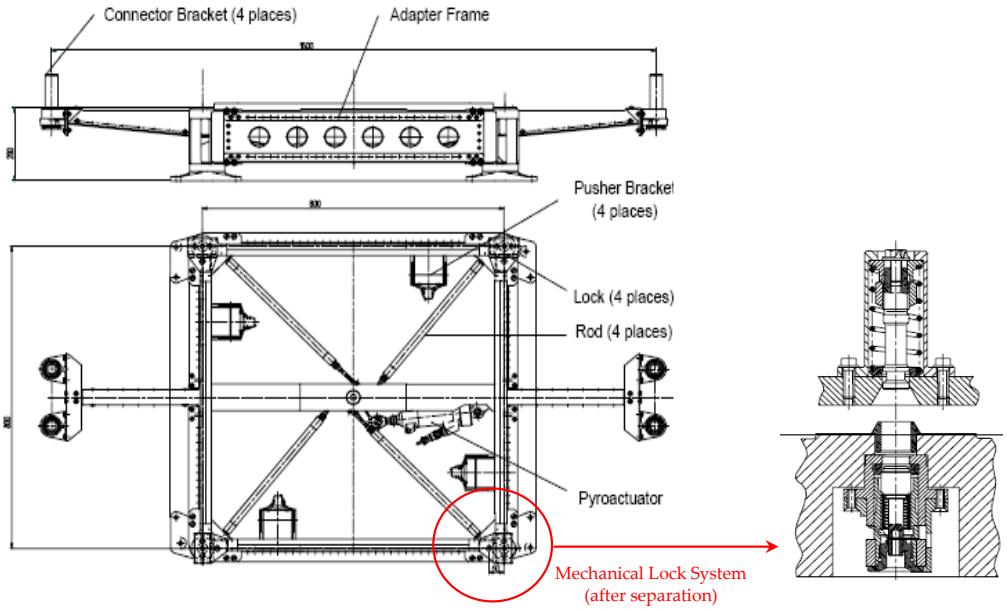

Figure 7-19: Adapter system for single satellite accommodation using the mechanical lock system (KSRC / Courtesy)

Figure 7-20 provides a typical shock specification for the Mechanical Lock System [MLS] (generic specification with typical pre-tension of 40 kN), and the maximum recorded shock during the CRYOSAT MLS release test (specific application of the MLS).

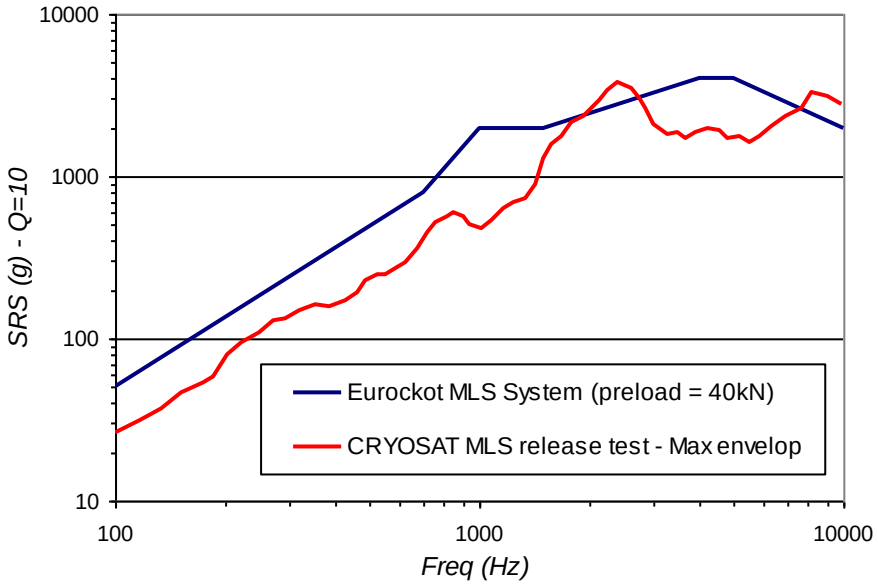

Figure 7-20: Typical shock specification for the Rockot mechanical lock system

7.4.4.2 PSLV separation system

The PSLV separation system [RD-012] consists in three rings. The fore end ring interfaces with the satellite. The aft end ring is attached to the launch vehicle deck. These rings are held together using a ball lock which is radially pre-loaded using a retainer ring providing the required joint stiffness. The retainer ring is locked in position using two shear screws. The system is released by rotating the retainer ring. The holes on the retainer align with the balls in the aft ring and jettisoning springs cause the separation of the fore end ring. The rotation is achieved by two pyrothrusters.

The configuration of the separation system is shown in Figure 7-21.

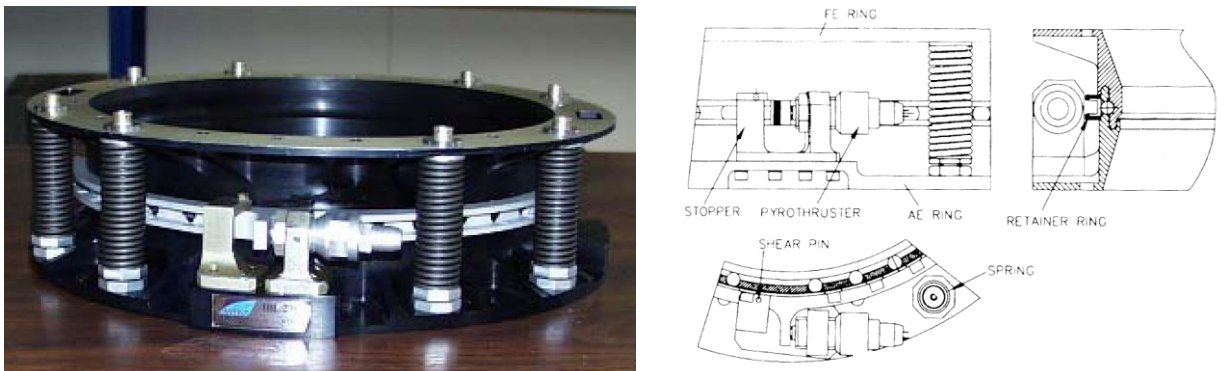

Figure 7-21: Configuration of the IBL 298 system

A typical SRS at the satellite interface is shown in Figure 7-22.

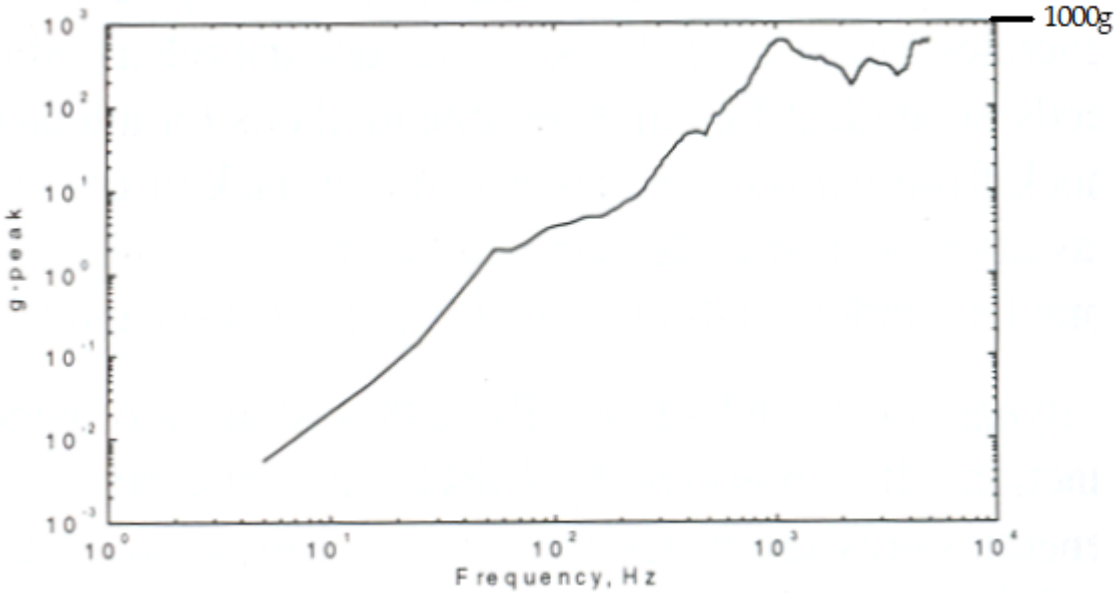

Figure 7-22: Typical SRS at the satellite interface

7.4.4.3 Dnepr explosive bolts

The micro satellites in the 120 kg class are fixed on the Dnepr launcher using 3 pyrotechnic devices, operating like pyrotechnic bolts. A view of the bracket at the satellite interface, and a view of the pyrotechnic device are shown in Figure 7-23.

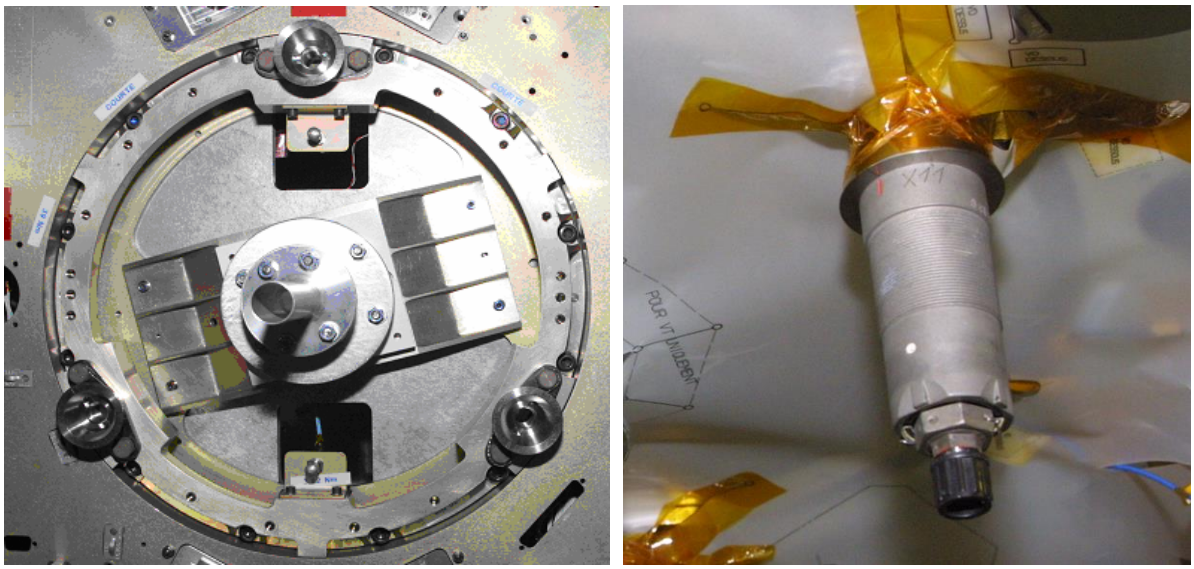

View of the bracket at the satellite interface on the left; view of the pyrotechnic device on the right

Figure 7-23: Dnepr separation system

Figure 7-24 illustrate SRS at satellite / launcher interface (excitation dominated by axial component).

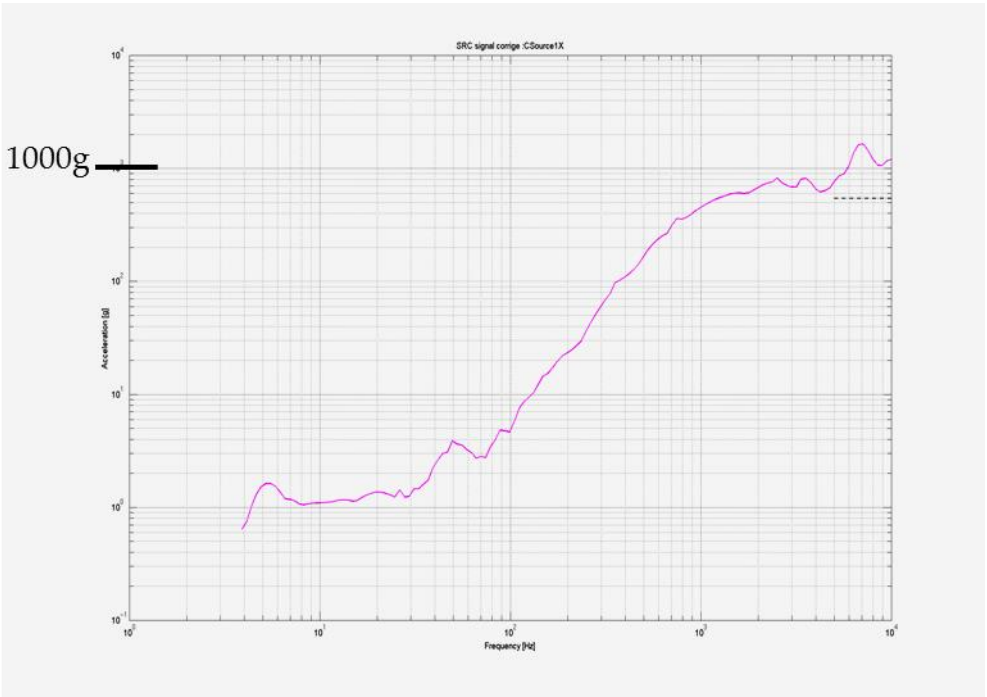

Figure 7-24: Shock level at spacecraft interface in longitudinal direction

7.4.4.4 Ariane 5 micro satellite separation system

The Ariane 5 micro satellite separation system (officially referenced as 5SSASAP 5S) is intended to fasten a micro satellite to the Ariane 5 ASAP 5 structure and to separate it (Figure 7-25). It is a pyrotechnic device based on the expansion of a pyrotechnic tube that breaks a weakened section. Several springs are released and push the micro satellite.

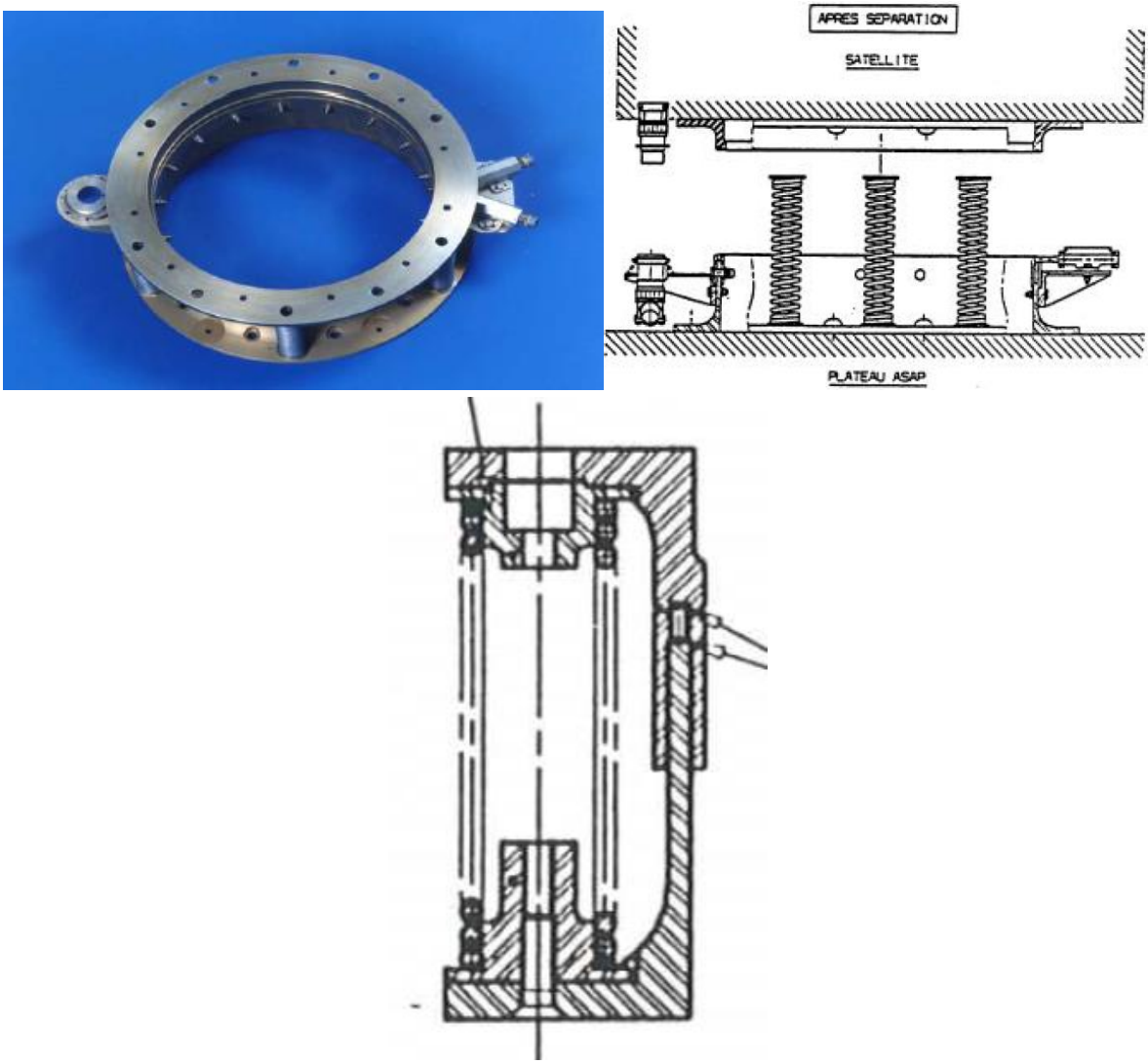

Figure 7-25: Ariane 5 micro satellite separation system

A qualification kit (officially referenced as 5SSASAP 5SCH) exists to qualify small payloads, whose mass does not exceed 150 kg, to be set up on ASAP 5 structure (Figure 7-26). The shock is generated by both a pyrotechnic device and a projectile.

Figure 7-26: ASAP 5 micro satellite qualification system

The pyrotechnic device is composed of three parts (see Figure 7-27):

- the mechanical assembly (2 parts);
- the mechanical impactor; a limited section is designed to break during the explosion and the impactor is ejected;
- the explosive charge.

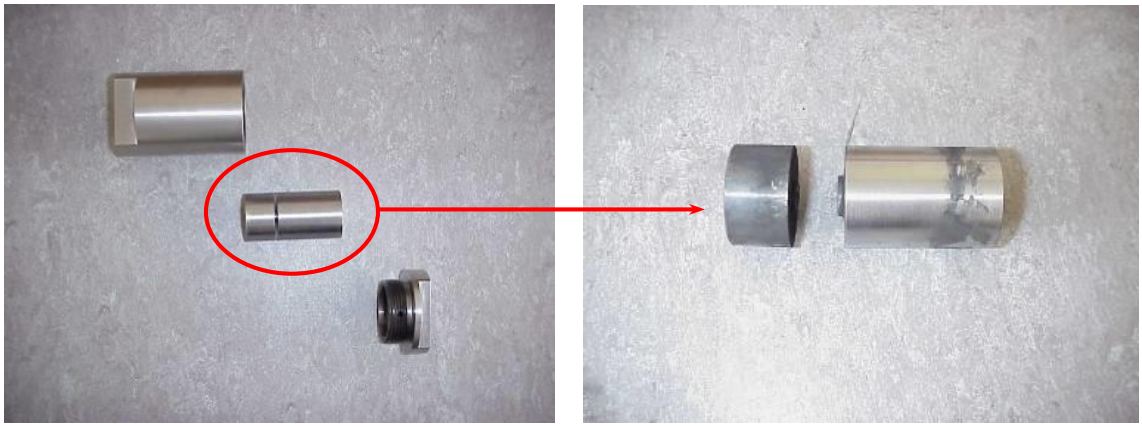

Mechanical assembly on the left and impactor after use on the right

Figure 7-27: Dassault impactor description

A typical SRS at 10 cm from the ASAP5 qualification system is shown in Figure 7-28.

It should be noticed that the measured environment generated by this device proved to be relatively dispersive. The shock source at launcher interface is extremely difficult to measure due to the extreme level at high frequency, typically above 100 kHz.

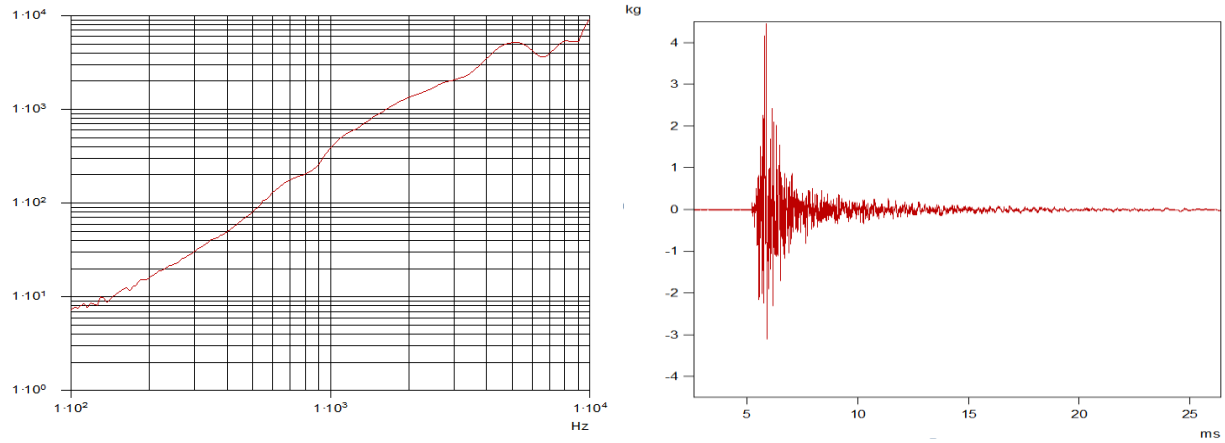

Figure 7-28: Temporal data of acceleration and the linked SRS at 10 cm from the ASAP5 qualification system

The repeatability of the ASAP 5 pyroshock qualification kit is rather satisfactory. A 3 dB scattering on the SRS is usually recorded. This variation comes from the scattering of the pyrotechnic charge and the shearing section of the pyroshock hammers. A special attention should be paid to the selection of an appropriate firing unit to guarantee the synchronisation of the "N" firing current pulses (better than 0,5ms) .

The repeatability is evidenced in Figure 7-30, where SRS of two consecutive tests are superimposed. To cover this variability, and satisfy the purpose of qualification, a least two tests are executed.

Figure 7-29: Myriade Platform structural model with PICARD Payload Flight model

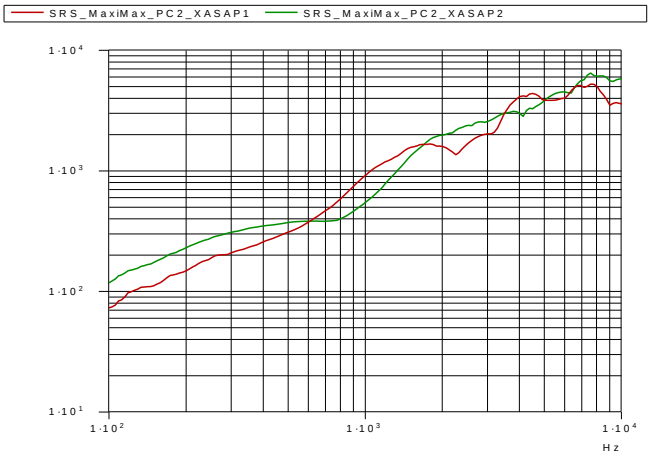

Figure 7-30: SRS of two identical tests using the ASAP 5 qualification kit

7.4.4.5 Soyouz Dispenser

The Soyuz launcher enables multiple launches using mission specific dispensers. These mission specific dispensers have been purposely developed in the frame of Globalstar, Galileo and O3b constellation deployment missions. As an example of the dispenser that has been used for the Galileo launches; it primarily comprises of an aluminium sandwich panel "box" structure that allows the structural support to the 2 integrated Galileo Spacecraft and an arrangement of struts that allow the interconnection to the FREGAT upper stage for load transfer. Figure 7-31 depicts the unloaded Dispenser, and the dispenser loaded with the Galileo satellites during final integration.

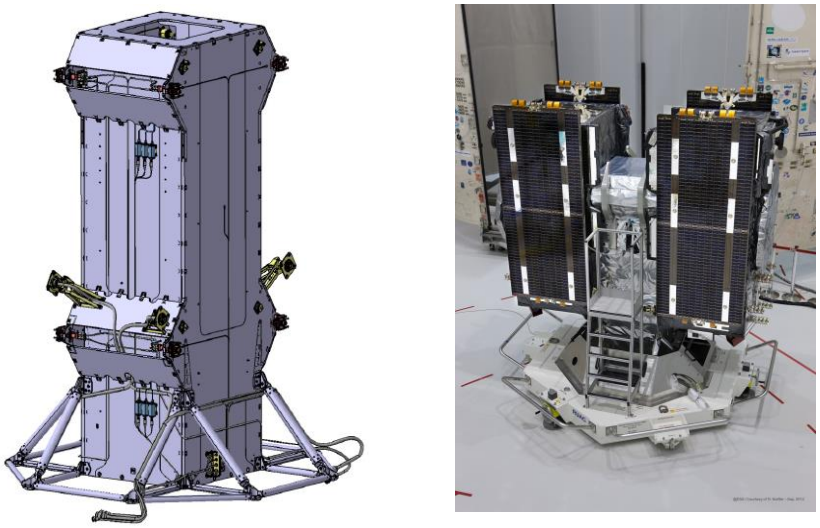

Figure 7-31: General view of Galileo Soyuz dispenser (ESA / Courtesy)

Each spacecraft has four dedicated interface points with the dispenser. The Dispenser System Separation subsystem consists of four dedicated Hold and Release Separation Units (HRS Units) that attach the spacecraft to the Dispenser and four separation and distancing spring actuators. Each of the 4 HRS units comprise of a pyro-nut/bolt and the corresponding pyrotechnic initiation (or charge) unit.

The induced shock environment during the spacecraft release depends on the selection of the pyro-nut/bolt, and typical levels dispenser/spacecraft interface are shown in Figure 7-32.

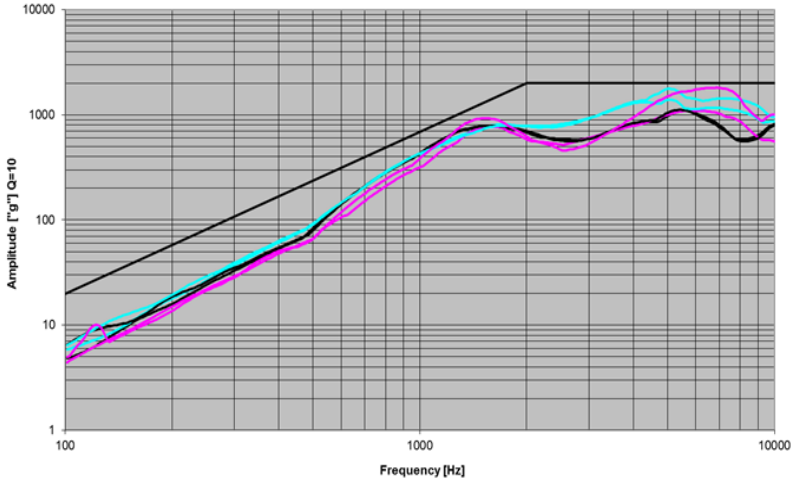

Figure 7-32: SRS levels at Soyouz dispenser / spacecraft interface

7.4.5 Internal shock sources

Release devices are extensively used inside satellites, covering various functions, such as:

- Solar array release
- Antenna deployment
- Radiator deployment
- Release of sub-spacecraft

Depending on the application and on the type of release system selected, high shock loads can be experienced and propagated through the satellite structure. Among the family of release devices commonly used inside satellites, the ones actuated by pyrotechnic cutter or pyrotechnic nut are inducing higher shock loads.

In addition to release devices, another stringent shock source is the pyrovalve. The function of a pyrovalve is to definitely shut down or open a fluid circuit. The energy needed for actuation is supplied by a pyrotechnic system, and as most of the other propulsion units are accommodated in direct vicinity to the pyrovalve(s), they are exposed to very high shock levels. The pyrovalves are specifically addressed in the paragraph 12.7.2

Each shock source has a **particular signature**, but their comparison is often not straightforward, as their signatures are identified using different test configurations and methods. In order to allow the comparison of the induced shock environment by different release devices and to generate a test database, a specific test bench has been developed through an ESA and CNES contract ([RD-013], [RD-046]). The configuration of this test bench, together with the list of tested devices is presented in Figure 7-33.

The main interest in such test bench (and its associated test database), lies in the possibility to compare in the same test configuration, the induced shocks for different release devices. It allows in particular:

- to bench mark new release devices,
- to identify the parameters having an influence on the induced shocks.

With respect to the latter point, it has been observed that the diameter and the preload (for pyronut or pyrocutter) are directly influencing the induced shocks (the higher the diameter or preload, the higher the induced shocks).

The signatures of each of the tested devices are provided in Figure 7-34.

The presented signatures give qualitative and relative information, for comparison of severities between different devices, and therefore to support the selection of a release device. However, it cannot be used to define a shock specification due to the influence of the supporting structure itself in the shock levels (mounting conditions, bracketry). Additional characterization testing is therefore recommended at that stage.

	Tested components	Bolt/Preload
Cutter	7CCD45 PWH 90°	7kN
	HSTC SL1056	7kN
	ML036	4.5kN
	7CCD15W	1.5kN
	7CC45 PWH90° 80mg	7kN
	7CC45 PWH90° 100mg	7kN
	7CC60DPWH3-90°	140kN
Sep. Nut	ME 016/ME 045	13kN
	ME 038 AA	30kN
	HS 9422-33	30kN
	HS 9364610-1	21kN
	Pyrosoft 12400 HN	12kN
	NEA 9102C	12kN
	ME044	30kN
	ME047	12kN
	Pyrosoft 12400 LE	12kN

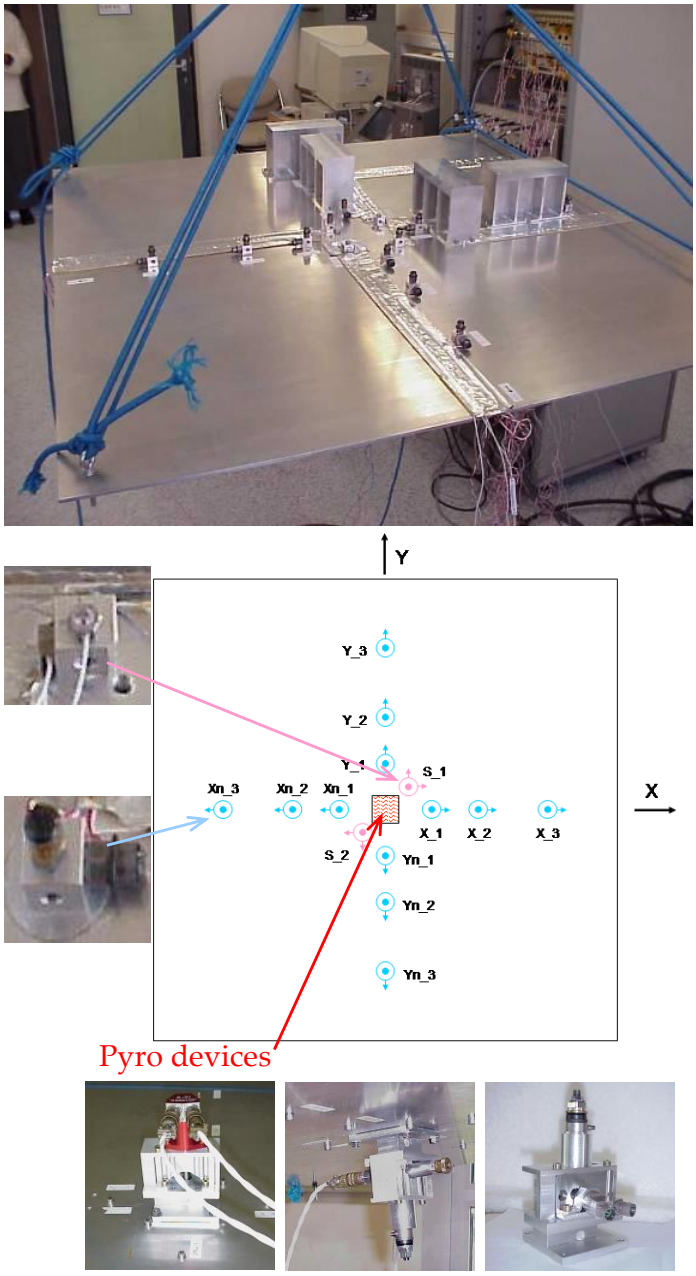

Figure 7-33: Test bench configuration

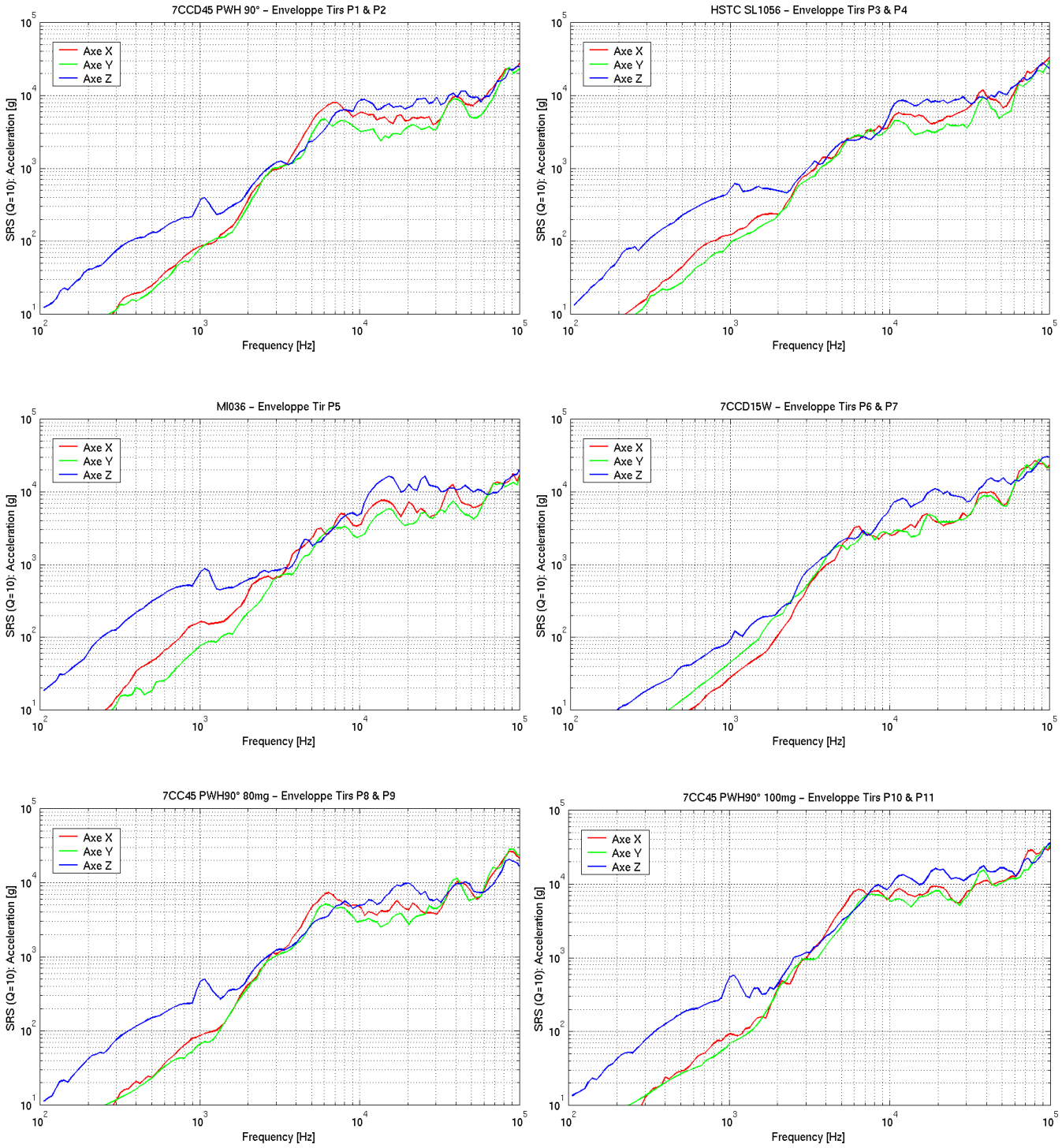

Figure 7-34: Components signatures

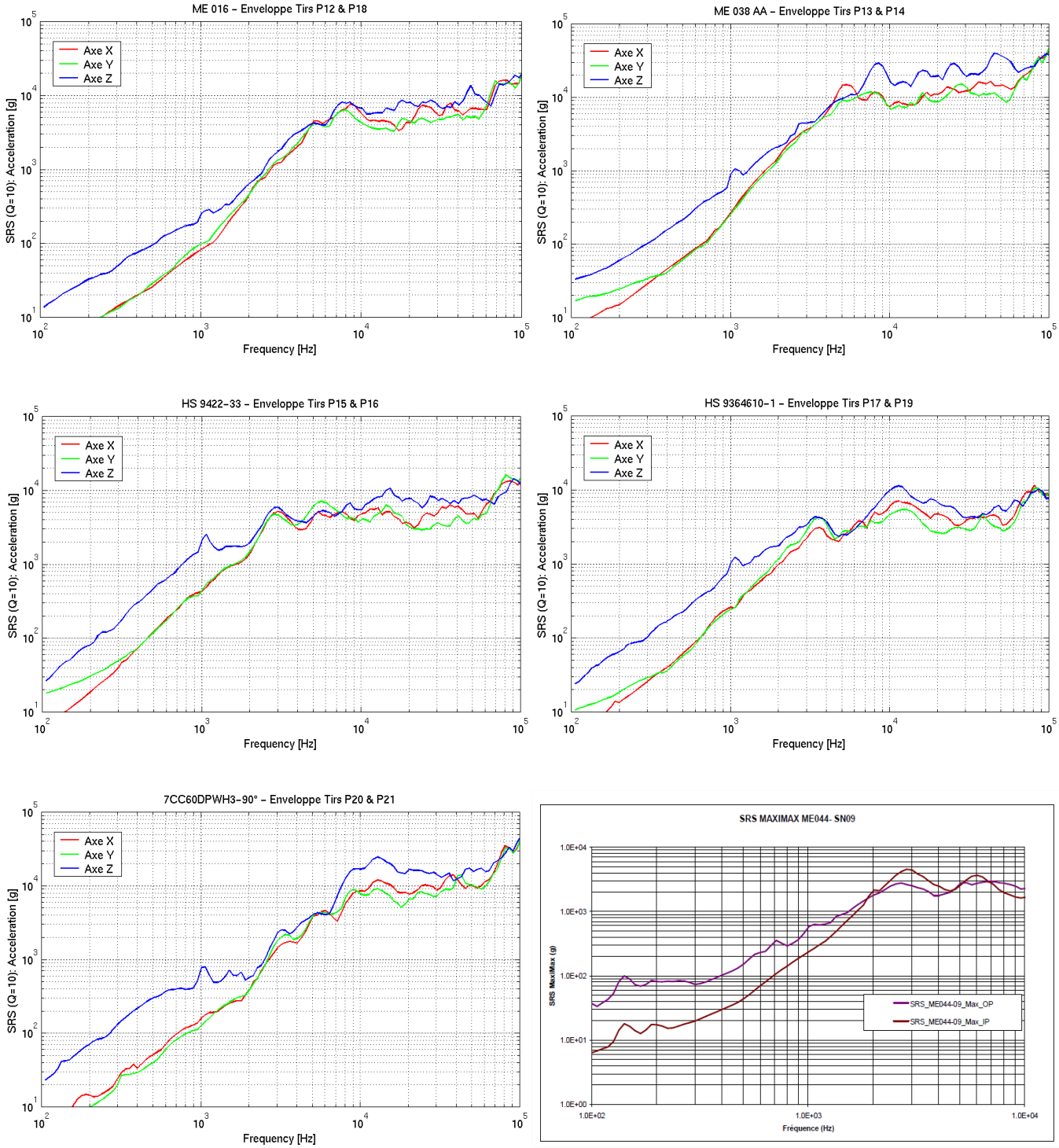

Figure 7-34: Components signatures (continued)

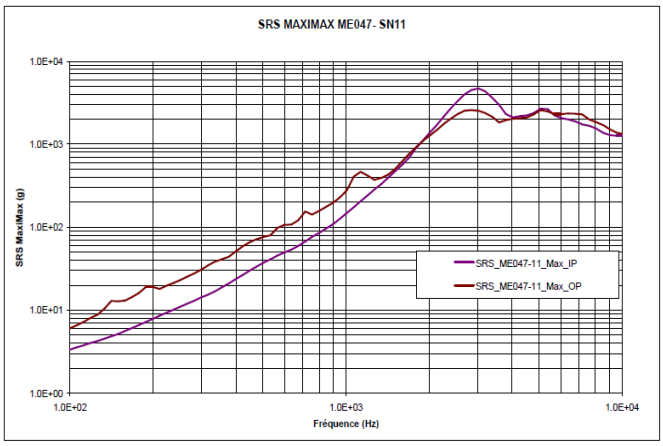

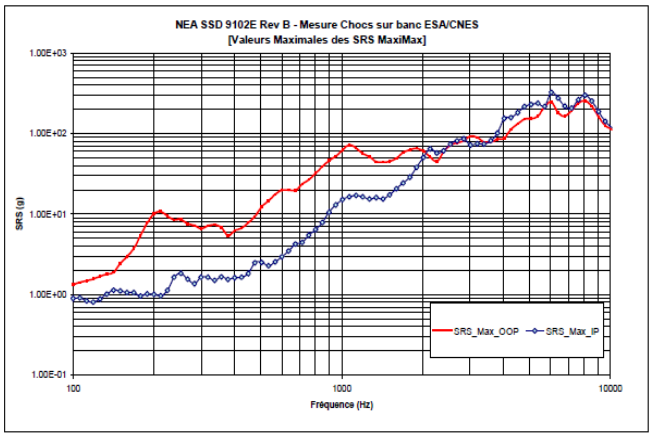

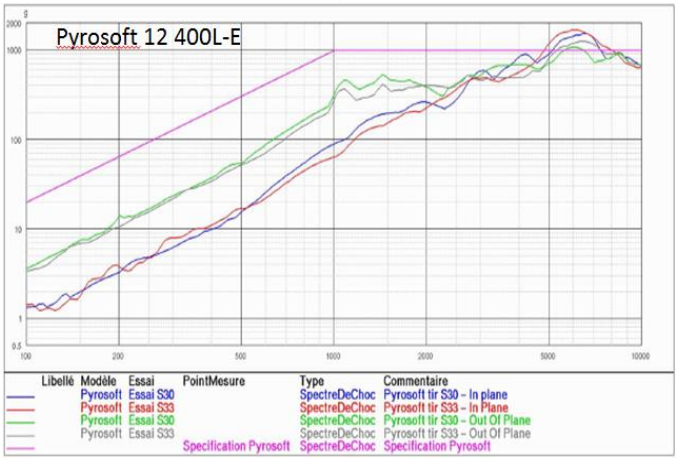

Figure 7-34: Components signatures (continued)

7.4.6 Landing and splashdown

In several ESA space programs, it is planned to develop space systems in which it is expected the landing on asteroids, on Moon and Mars and also the return of space system on Earth's surface and/or on water.

In order to ensure a successful final landing phase on asteroids, Moon or Mars surface, a landing crushable or airbag system is needed, capable of absorbing the residual velocities (vertical, horizontal and angular) at touch-down, limiting the landing loads and insuring stability.

While for an Earth-Entry vehicle it is necessary to design a reliable capsule that can use an energy absorber or parachute system to safely return a payload to the Earth's or water surface.

In the final seconds before touchdown phase, after parachute deceleration, the purpose of all energy absorbing systems is to limit the maximum acceleration of the payload. The energy absorbing systems can be subdivided into the following two main categories:

- Passive
  - Air-bag system (vented or no-vented)
  - Crushable system (legs or platform)
- Active
  - Skycrane system
  - Leg with active (i.e. electromagnetic) damper system

Loading scenarios include a wide range of different initial impact parameters as:

- Impact velocity
  - Vertical velocity
  - Clocking horizontal velocity
  - Clocking angular velocity (roll, pitch and yaw)
- Lander orientation (roll, pitch and yaw attitude) and clocking
- Impacting surface
  - from rigid to soft soil and its friction
  - water
- Surfaces slope
- Rock height, position and numbers
- Wave slopes and clocking
- Lander mass, stiffness and damping

Although the landing/splashdown event can be basically associated to a shock event, differently from the behaviour of the most common spacecraft shock sources, the landing/splashdown load has also significant low-frequency content that induces a quasi-static load. Therefore this load can be considered as additional design load case to the stress verification. Nevertheless a contribution at the medium-high frequency contest is also present. For this reason the general approach to the touchdown (landing/splashdown) is to consider both the design loads and shock effects derivations.

The approach to the design loads derivation and stability verification analysis can be described as follows:

a) Take into account conservative touchdown conditions,

b) Derive limit loads in terms of acceleration and/or pressure levels at vehicle CoG and at equipment locations from the worst case loads by exploiting a wide matrix of touchdown load cases,

c) Consider case-consistent (i.e. assuming that the peaks occur simultaneously) but not time-consistent loads,

d) Apply a load uncertainty factor to account the model uncertainty and unpredicted load cases.

The approach to the shock environment derivation can be described as follows

a) Take into account conservative touchdown conditions,

b) Derive SRS environment in terms of acceleration at vehicle CoG and at equipment locations and/or pressure at the impacted area generated by the vehicle in the worst load case by exploring a wide matrix of touchdown condition load cases,

c) Consider different time-consistent loads and envelop them,

d) Apply a load uncertainty factor to account the model uncertainty and unpredicted load cases.

During a crash event, the structure experiences high impact loads which produce localized plastic hinges and buckling. This can ultimately lead to large deformations and rotations with contact and stacking among the various components.

In the past, this kind of mechanical engineering problems were always verified by experimental drop test campaign because they were too complicated to be solved in a closed form (analytically) but recent advancement in the high-speed computing technology for large-scale analyses and the development of the advanced explicit nonlinear dynamic finite element techniques provide a powerful capability for solving the fluid and flexible structure interaction problems.

The numerical method, which can be used for solving this touchdown impact problem, is usually based on the Finite Element Method (FEM). There are two general schemes for calculating an approximate solution: explicit and implicit methods. Between the two methods, the explicit one is the most suitable.

The explicit finite element code is able to analyse non-linear dynamic problems in three dimensions including the computation of explicit dynamic relaxations and static implicit solutions. Also interaction between fluid and structures can be analysed. Some specialized capabilities allow an easily modelling of airbags and sensors.

In the current available commercial codes, such as Altair-Radioss, LS-DYNA and MSC.Dytran, different algorithms are implemented to treat this explicit non-linear dynamic problem as:

- Pure Lagrangian algorithm
- Pure Eulerian algorithm
- Coupled Arbitrary Lagrange Euler (ALE) algorithm
- Smooth Particle Hydrodynamics (SPH) algorithm

Lagrangian solution techniques are usually preferred for speed and accuracy, but fail in case of large deformations and rotations; consequently, the Eulerian approach becomes a necessity.

Explicit nonlinear dynamic finite element codes based on an Arbitrary Lagrangian Eulerian (ALE) solver are recommended especially to analyze the interaction between Lagrangian (structures) and Eulerian (air/water) meshes. An example of the application of this algorithm is represented by the IXV splashdown simulation (Figure 7-35).

The Smooth-Particle Hydrodynamics (SPH) technique is a meshless numerical method based on interpolation theory and it can be used to model the motion of a fluid and its interaction with the structure.

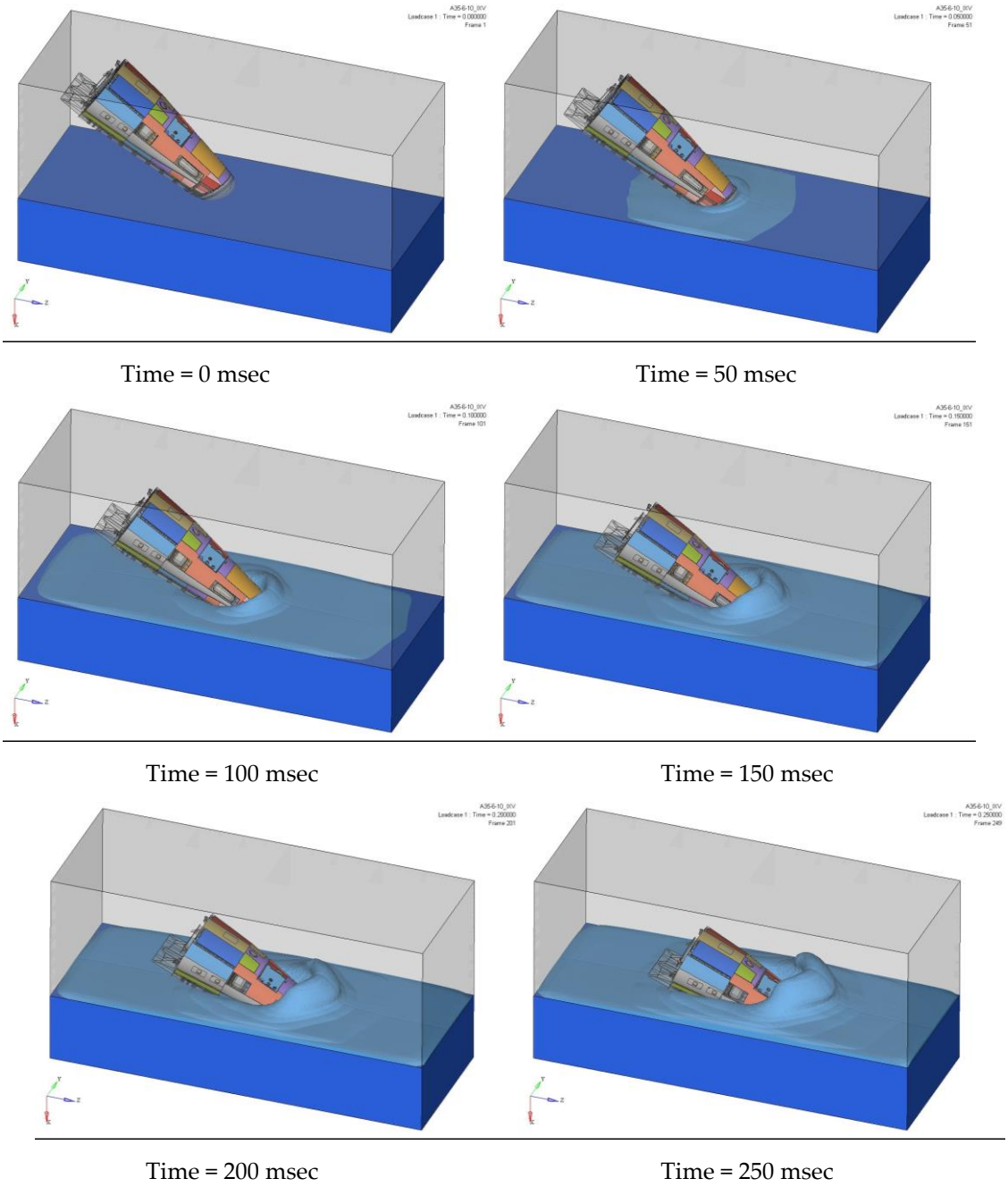

Figure 7-35: Time evolution of the motion during IXV Water Landing simulation

It is important to pay attention during the post-processing phase of the analysis results because the correctness of the outputs depends on correct application of the following post-processing conditions:

- Aliasing prevention
  Due to the presence of high frequency content of landing impact event in crash analysis, it is important to prevent aliasing errors by using a time-step sufficiently small for writing out the output time histories. This is done by considering a minimum sampling frequency sufficiently high, however this value is in any case superseded by the computational time step if it is smaller.

- Energy considerations
  To validate the model some quality checks on the output results are needed, such as carefully observing the system and component energies for growth or instabilities.
  The laws of physics cannot be violated in the model thus the total energy should not grow as the model progress in time. The time histories of the various forms of energy (i.e. kinetic energy, internal strain energy, hourglass energy and interface energy) should be examined individually as well as the total energy.

- Filtering of crash data
  For the design load derivation purpose, due to the high frequency content typically seen in analytical acceleration time-histories, it is necessary to filter the acceleration data obtained as output from the simulation (Figure 7-36).
  In order to post-process acceleration data it is possible to refer to filter standards. Present practice is to use a low-pass filter based on a 4th-order Butterworth low pass with forwards and backwards linear phase processing. Engineering judgment is required in the choice of the filtering frequency in order to extract the important physical information such as rise time and peak acceleration.
  Often the choice of the filtering frequency is usually driven by the need to correlate the numerical results with experimental data, in this case the filtering rule used for the numerical data is recommended to be the same as for the experimental ones.

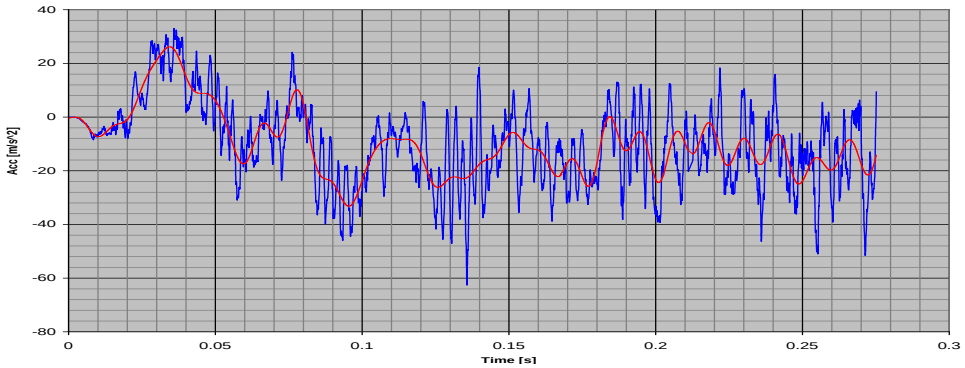

Figure 7-36: Acceleration time history unfiltered vs. 100 Hz low pass filter

7.5 Conclusion

As a conclusion there are many different shock sources acting on satellites. Some induce high shock levels, at spacecraft-launcher interface or at discrete locations inside the satellites. A specification based only on a SRS is not sufficient piece of information to precisely know how to deal with this specification, and therefore it should be completed by the description of the shock origin.

8
Shock inputs derivation by similarity-heritage-extrapolation

8.1 Overview

Although the state of the art for shock environment prediction in spacecraft have not yet reached the maturity of other environmental disciplines due to the high-frequency nature of pyroshocks, recent advances in prediction techniques bring more confidence and a better understanding of this environment.

The derivation of a consolidated shock environment is an achievable goal, under the condition that a consistent approach is strictly followed. This goal can be achieved through similarity-heritage-extrapolation, based on past experiences, and through good engineering practices in shock FEA [RD-014][RD-015].

In this respect, the shock inputs derivation to sub-systems by similarity-heritage-extrapolation is discussed herein.

Early definition or consolidation of the shock environment is an essential aspect, in order to avoid facing spacecraft and equipment qualification problems later in the qualification phase. The derived shock environment is finally used to establish shock specification for equipment or subsystems.

Similarity-heritage-extrapolation methods are widely used because of the lack of good predictive methods of shock levels inside a spacecraft in contrast to what exists for other mechanical environment (e.g. static and sine). The aim of such methods is to compare the studied spacecraft structure with already tested spacecraft structures presenting similar architecture, design and/or configuration. This is always a tough job requiring experience as the similarity between spacecraft is a rather subjective evaluation that thus requires a justification.

A more precise definition of these methods is given hereafter:

- **Similarity-heritage methods** aim at **evaluating shock levels using data from different structures** considered as similar for possibly different (but physically similar) shock sources. Such methods are usually used early in a programme when no data on the studied structure is available. The main question, which drives the analysis validity, is about the degree of similarity between the studied structure and the reference structure(s).
- **Extrapolation methods** aim at **evaluating shock levels using data for the same structure** (typically from a structural model to a protoflight model) for possibly different (but physically similar, typically Shogun to launcher induced shock) shock sources. Such methods are usually used later in a programme when some shock tests have been performed on structural model or representative structures.

8.2 Similarity-heritage-extrapolation methods principle

8.2.1 Overview

The spectra of the responses measured on one system during its operation or ground simulation can often be used to predict the spectra in another spacecraft, assuming the old and new systems are of broadly similar design. In such cases, the shock responses of the new system can be predicted, at least coarsely, by scaling the measurements made on the previous system. This philosophy based on similarity and heritage is often the most reliable way to derive shock levels at equipment interface. Since shock transient analysis cannot be considered mature enough to predict accurately the shock propagation in a complex structure like a satellite or a launcher, empirical derivation is often a good manner to estimate, even coarsely, sub-system levels.

As a result, engineers have established some relevant shock databases containing test results from various spacecraft or R&D projects, even if the availability of a meaningful shock database is difficult to obtain.

8.2.2 Use of database

8.2.2.1 Characterization database

These databases collect results from **standardised shock tests** to get an evaluation of shock levels in precise conditions which can be described with a few parameters. These test results are usually **not suitable for direct derivation of shock levels** as the standardised conditions of the tests are generally idealisation of real spacecraft conditions. However they can be used as a **comparison tool** in order to derive some extrapolation rules (extrapolation from a local configuration to another). These rules can be used at spacecraft level to represent the local configuration change.

Two examples of such characterisation databases are given hereafter:

- Lockheed-Marietta database [RD-016][RD-017]

  The so-called “Lockheed-Marietta” database aimed at compiling representative pyroshock data in order to characterize shock sources (e.g. linear explosive sources, explosive bolts, separation nuts, pin-pullers, and bolt cutters) in terms of e.g. frequency content, amplitude, attenuation with distance, influence of structural configuration on waves propagation, compared severity, and recommendations on test simulation.

- ESA-CNES database for characterisation of internal pyrotechnic devices [RD-013]

  The database on the ESA/CNES test bench was developed more recently to characterize different shock sources corresponding to shocks produced during appendages release. Different pyrotechnic cutter and nuts (used by European companies) have been tested on two different plates (one aluminium plate and one aluminium sandwich plate). See 7.4.5.

8.2.2.2 Spacecraft test results databases

Large amount of shock tests, at system level, have been performed over the past years. Pyroshock data has been acquired and analysed on different spacecraft and for different excitations. These data can be used as reference as no better knowledge of shocks levels are available than those given by tests.

Before these data are utilized, the quality of these data should be ascertained based on the data acquisition and analysis criteria provided in 15.3.

Such a database is useful only if it collects all possible details in term of test configuration such as:

- Spacecraft configuration: e.g. presence of appendages, and dummies or real equipment;
- Type of excitation: Clampband release (with pre-load), Shogun, appendage release (pre-tension of an eventual tie rod);
- Boundaries conditions: free-free, clamped on launcher adaptor;
- Instrumentation plan and if possible photos of all accelerometers;
- Accelerometers type and characteristics;
- Acquisition chain with its limitation (filter, acquisition frequency).

This type of database permits pairing of new spacecraft with already tested spacecraft. And the possibility of cross checking the results, considering different spacecraft presenting the same characteristics, brings more confidence in the final evaluation of the shock environment.

Even though the data have been acquired for different spacecraft designs and different pyrotechnic devices, at least crude estimates for **the shock environment to be expected on a new spacecraft design can be determined by extrapolations from measurements on a previous spacecraft of similar design**, commonly referred to as the reference spacecraft. Of course, the closer the design details of the new and reference spacecraft, the more accurate the extrapolations.

This concept of similarity is a little bit subjective and usually needs experience to be used wisely. It is based on a general principle to be respected: the similarity of the compared structures in terms of shock propagation.

The notion of similarity can be derived on different topics that should be taken into account to assess the similarity between structures:

- Spacecraft class (small, medium, heavy): the size of the structure has a tremendous importance for shock propagation. It is nonsense to directly use shock propagation data achieved on a big telecommunication satellite to a micro satellite.
- Type of primary structure: the global type of structure is the main driver of the shock propagation paths. Some of the most common characteristics that define a structure type are given hereafter: general shape (e.g. box type, and cylindrical structure), presence of a central tube, presence of shear walls, presence of supporting struts, and presence of intermediate plat-forms.
- Interfaces: different types of interfaces between parts can lead to different propagation in the structure. This element has less influence than the previous one but is important when focusing on a local area. For instance the presence of interface parts (angle parts between two panels or supporting ring for a plat-form) has a role in shock propagation compared to a direct interface.
- An example of such an assessment is given below. It deals with the comparison of a new structure to two structures that have already been shock tested at system level and are potentially used as reference for shock level evaluation. See Table 8-1 and Figure 8-1.

Table 8-1: Comparison of structures for similarity evaluation in terms of shock propagation

	PLEIADES/SPOT5	STM3000
General configuration	≠: Service module is located higher in the structure	=: Same height of service module
	≠: Only a cylinder instead of a cone	=: Cone as for PLEIADES
	=: Battery plate similar to propulsion substructure	≠: No plate stiffening and loading the base of the cone
	=: link type (plate between the two parts of the tube) similar to PLEIADES	≠: Link with lower attenuation (flange)
Wheel		≠: a part of the shock energy runs to the floor directly through the tank struts
Instrument	≠: Measurement at a too high place, with a part of the shock energy running into the propulsion truss	=: Measurement at the top of the cone, as for PLEIADES

The results of such a comparison can be used differently according to the couple excitation/structure. If both structures and shock excitation are similar, the measured levels can be directly used as an evaluation of the shock environment. However, these data are usually better used to extrapolate shock levels from a couple shock excitation / structure to another using calculated attenuation between launcher I/F and different points in the spacecraft structure. This is further discussed in 8.2.4.

Finally the possibility of cross checking the results, considering different spacecraft presenting the same characteristics, brings more confidence in the final evaluation of the shock environment.

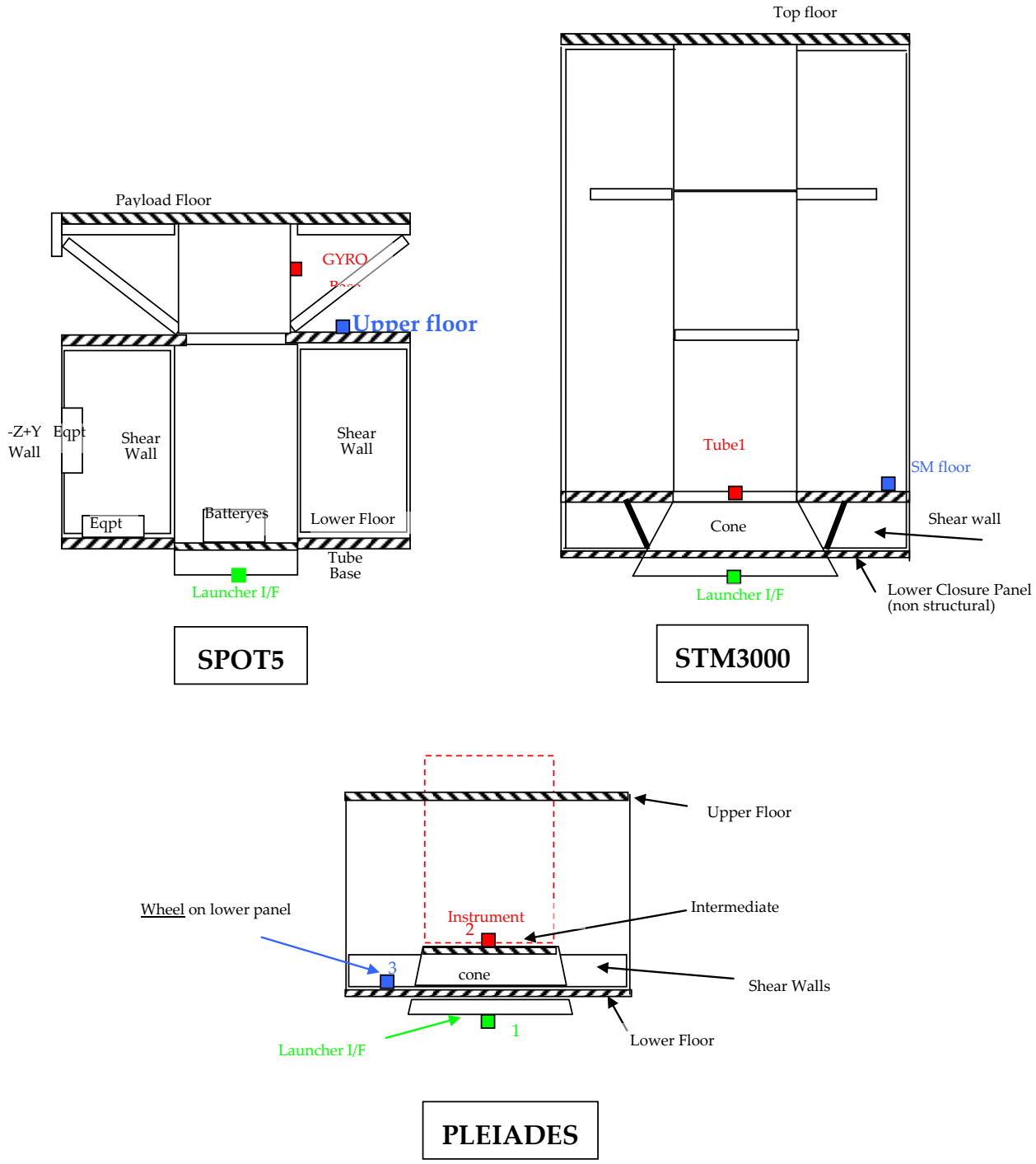

Figure 8-1: Comparison of structures for similarity evaluation in terms of shock propagation

8.2.3 Zoning procedure

In the early phase of a project, to achieve the most accurate prediction is not a goal in itself. Indeed the design of a spacecraft can be subjected to modifications. The most important is to have a better understanding of the **shock severity in different zones of the spacecraft**. Therefore the spacecraft is divided into different parts with respect to their supposed shock environment: this is the zoning procedure.

The objective of zoning is to divide the spacecraft structure into regions or zones such that the **responses at all points within each zone are reasonably homogeneous**. Speaking in terms of SRS, this means that the SRS magnitudes of the responses at all points within each zone can be described by a single SRS that exceeds most or all of the SRS magnitudes at the individual points without severely exceeding the SRS magnitude at any one point. This definition has been kept relatively subjective as the zoning refinement can differ depending on the real objective of the zoning procedure: such a zoning can be either rough or somewhat precise.

Some tips are given hereafter to help building a correct zoning:

- The main concern is the importance of that the defined zones **respect the physical aspects of shock propagation**. The best way to deal with that principle is to imagine the different possible propagation paths with the idea that shock prefers stiff paths. Then the main geometry of the structure is always a main driver of zoning because physical joints and links have an important role in shock propagation physics. Thus the zoning usually results in a division based on physical substructures of the global structure. This can be considered sufficient or not, depending essentially on the size of the different substructures.
- It should be noticed that it is illusory to hope getting very homogeneous levels on a given substructures or zone. As a matter of fact, shock measurements have shown that the real shock levels are strongly depending on many parameters such as local boundary conditions, local loading or precise position of the accelerometer with respect to its direct environment. Therefore a defined zone does not necessarily group areas where the shock levels are completely similar.
- An example is given in Figure 8-2. It deals with an *a posteriori* zoning, which means that the zoning is made with measured data. The two plots concern the same substructure, an external wall of a satellite, for the same Shogun excitation in out-of-plane response (plot on the left) and in in-plane response (plot on the right). The measurements points differ by their positions but also and primarily by their local boundary conditions and loading. As shown on the left plot (out of plane responses), at least two or even three groups can be identified, whereas the right plot shows only two groups (in plane responses). Moreover the yellow curve would be in the low level group on the left plot but in the high level group on the right plot. Consequently, for a same sub-structure, two different zones can be defined: out of plane and in plane zones.

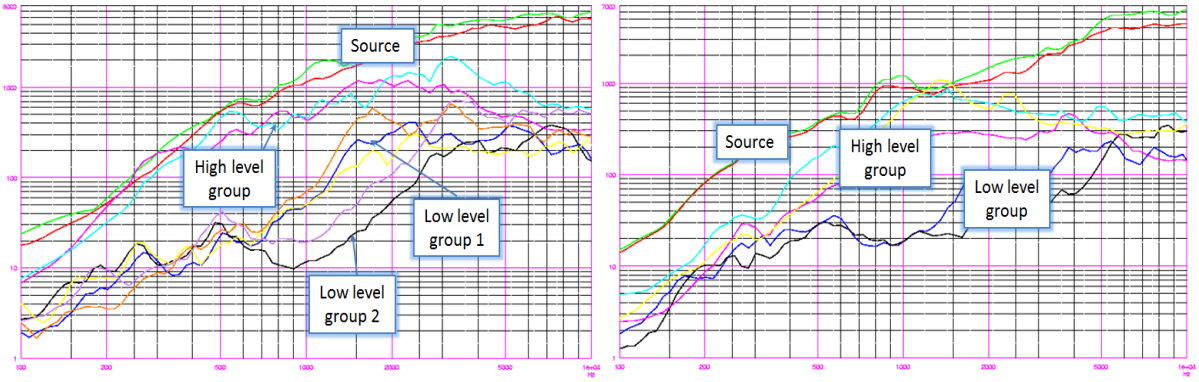

Figure 8-2: Example of zoning procedure with measured data

This illustrates that zoning is a tough job that need compromises and has intrinsic limitations even when the shock levels are known. That means that it is not useful to try to get a very precise zoning in a spacecraft structure.

8.2.4 SRS ratio as approximation of transfer functions

Evaluation of a shock environment by similarity-heritage-extrapolation methods requires transposing **a SRS level at spacecraft-launcher interface elsewhere in the spacecraft**. This evaluation is based on the fact that the shock propagation is common for the reference structure and the studied structure. This **propagation** is usually **characterised by a ratio of SRS** between a given point in the spacecraft and the spacecraft-launcher interface. Thus the assumption concerning shock propagation can be written as:

$$\frac{\gamma_{SRS\,1}^{eqpt}}{\gamma_{SRS\,1}^{IF}} = \frac{\gamma_{SRS\,2}^{eqpt}}{\gamma_{SRS\,2}^{IF}}$$

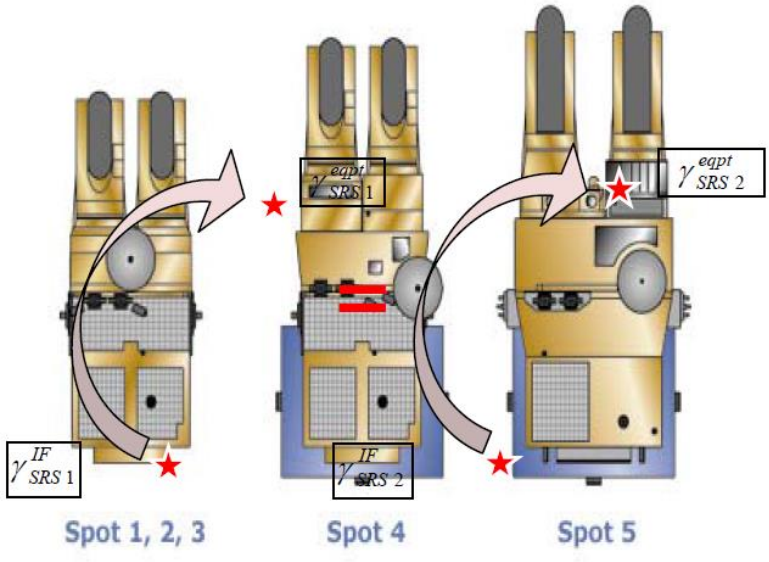

Figure 8-3: Principle SRS ratio assumption for similar structures

The above equation uses the transfer function of frequency response function terminology. It is important to note that the above equation can be considered as a strong hypothesis. It relies however on experimental observations. Approximation is rather precise in low frequency but is approximate in high frequency domain

SRS ratio is thus the direct ratio between the SRS at the studied area and the SRS at the source on the complete frequency range. The attenuation calculated by SRS ratio is sometimes called transmissibility by reference to the FRF terminology.

Several means can be used to calculate attenuation factor. Some of them are listed hereafter:

- ratio for each frequency: this is the easiest and most used way to calculate an attenuation factor

$$att\left(f\right)=\frac{\gamma_{SRS}^{eqpt}\left(f\right)}{\gamma_{SRS}^{IF}\left(f\right)}$$

- on a given frequency range around the frequency of interest, the maximum value of response is divided by the maximum value at the source. It aims at taking into account some potential frequency shifts between the excitation frequency and the response frequency (shifts due to measurement uncertainty or to particular modal behaviour). Such a method results in a smoother attenuation function.

$$att\left(f\right)=\frac{Max_{f_1\le f\le f_2}\left(\gamma_{SRS}^{eqpt}\left(f\right)\right)}{Max_{f_1\le f\le f_2}\left(\gamma_{SRS}^{IF}\left(f\right)\right)}$$

- the maximum ratio calculated at each frequency over a given frequency range around the frequency of interest is retained as the attenuation factor at the frequency of interest. This is another way to represent the dispersion in frequency that can appear between excitation and response. Such a method results in an even smoother attenuation function.

$$att\left(f\right)=Max_{f_1\le f\le f_2}\left(\frac{\gamma_{SRS}^{eqpt}\left(f\right)}{\gamma_{SRS}^{IF}\left(f\right)}\right)$$

Calling such a ratio an attenuation is a misuse of language as values higher than 0dB are amplification and values lower than 0dB are attenuation, physically speaking.

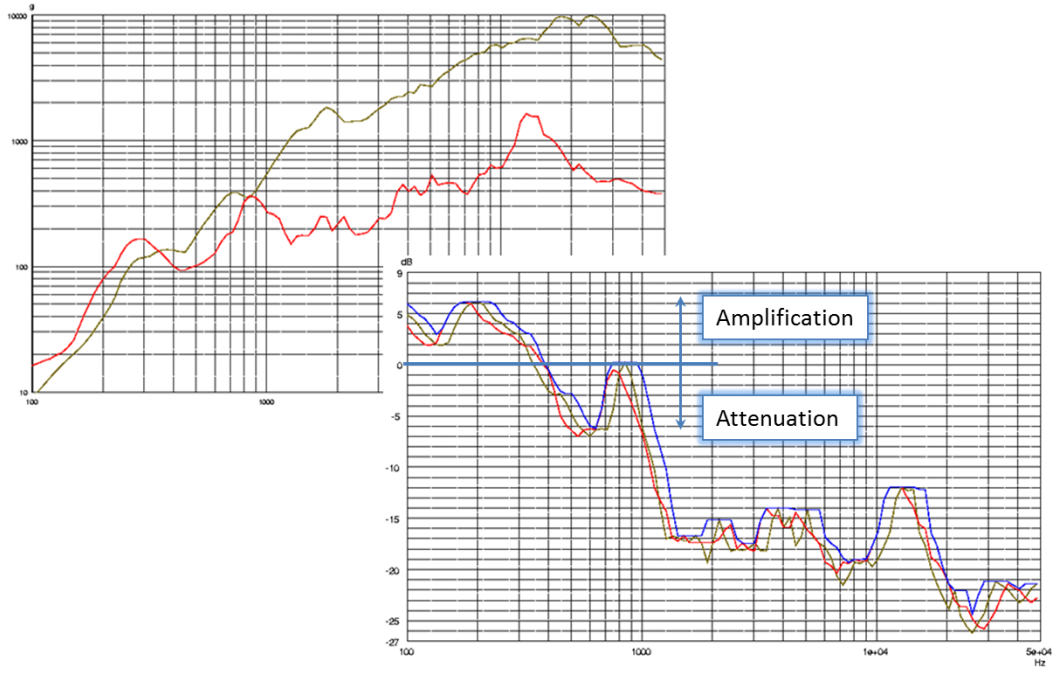

Figure 8-4: Calculation of the attenuation by SRS ratio with the three previously described methods

Several limitations of methodologies and analyses using SRS ratio should be kept in mind:

- **Attenuation is a piece of information difficult to interpret**. As a ratio it loses some information with respect to what is present in the initial data constituted by the SRS level at the shock source and the SRS level in the studied zone. A peak in the transmissibility function can be due to different causes: either a direct peak on the response with a relatively flat excitation or a peak-valley-peak configuration on the excitation with a relatively flat response. The consequence is that such SRS ratios are preferably used as order of magnitude. This remark is particularly true for SRS ratios calculated with the first method. The other methods try to minimise these difficulties.

- Another important point is that there are **many ways to calculate SRS ratios**. The Choice of reference at interface (mean average, radial/longitudinal) is a major assumption and should be consistent with the rest of derivation analysis. The main choice focuses on the reference levels used at launcher-spacecraft interface. Levels at this interface are usually composed of several measurements which implies the necessity of combining these different measurements to produce a unique reference. This combination can be based on mean value, maximum envelope or minimum envelope. Moreover the levels at launcher-spacecraft interface are three-dimensional which means that several components are measured. Usually, two components (longitudinal and radial) are measured, taking benefit from a circular interface. There are several possibilities to combine these levels in different directions, e.g. to consider their mean value, their maximum value, or to consider them separately. All of them are theoretically interesting. For instance it has been shown that considering an attenuation based only on longitudinal levels leads to attenuation for a single structure that is less dependent from the shock source than using an attenuation based on a combination of both radial and longitudinal components. This is due to the high attenuation of the high radial component in a Clampband release test in regard with launcher induced shocks. However the calculated attenuation is most of the time used directly in combination with specified levels at launcher interface. These specified levels are usually composed of a unique SRS concerning all directions of excitation (sometimes specification is composed of several curves, one for each direction of response). Therefore, the most common way to calculate SRS ratio is to use a reference based on maximum levels, taking into account all directions of response at the launcher-spacecraft interface, which is the most consistent with the specifying philosophy.

- When using a SRS ratio method, **attention has also to be paid to the excitation type**, since past experiences have shown that the attenuations are strongly dependent with regard to the configuration of the system test set-up used to identify them. In particular, the attenuation resulting from a Clampband release test can be – depending on the chosen reference – higher than the ones resulting from a Shogun or a launcher induced shock test. This is due to the fact that attenuation calculated by SRS ratio has no rigorous theoretical justification as it assumes a linear behaviour to a shock phenomenon that is well known to be highly non-linear. Therefore, when applying SRS ratio method, it is strongly recommended to use the attenuation corresponding to the right excitation type (Clampband or Shogun for instance), and to avoid the extrapolation from one excitation type to another. See paragraph 8.3.3.3, for illustration of the limitation.

8.2.5 Difference between structural model and flight model

Several types of model philosophies can be employed according to verification requirements, with the final shock verification achieved either on SM or PFM/FM (typically consisting in characterisation testing on SM early in the development programme, and/or acceptance testing on PFM/FM).

In the case where the test baseline requires the performance of shock testing on a SM satellite (for early definition of the qualification shock environment at equipment level), attention should be paid to the representativeness of the satellite Structural Model SM, and in particular to the equipment dummies definition and distribution.

The following two cases can then be encountered:

- **Case1** – Fully representative SM structure, with representative equipment dummies definition and distribution: This is typically the case for a one-off satellite (e.g. scientific or earth observation satellite), for which the SM structure can eventually be refurbished later on in PFM. The equipment dummies are usually defined to be representative at least in terms of interface/mass/CoG, and are accommodated at their correct locations. The only differences between SM and PFM satellites, are then limited to the absence of harness and omission of some light equipment or bracketry in the SM satellite.

  Under case 1, the experience shows that the shock environment is adequately captured on the SM satellite, with a sufficient agreement over the entire frequency range, and something with a beneficial effect from the presence of harness in the PFM/FM satellite above 3kHz.

- **Case 2** – SM structure representative of spacecraft family, with generic equipment dummies distribution: Falls under this case, a SM satellite representative of a spacecraft family (e.g. telecom satellite), where the equipment dummies are defined to be representative of a typical mass distribution within the satellite structure.

  Under case 2, the experience shows that the shock environment can differ significantly between SM and PFM, but usually with the trend that the environment characterised on the SM satellite is enveloping the environment seen on any spacecraft of the family, which is the primary purpose of such shock test on SM satellite.

Illustrations of these 2 cases are provided in Figure 8-5 and Figure 8-6.

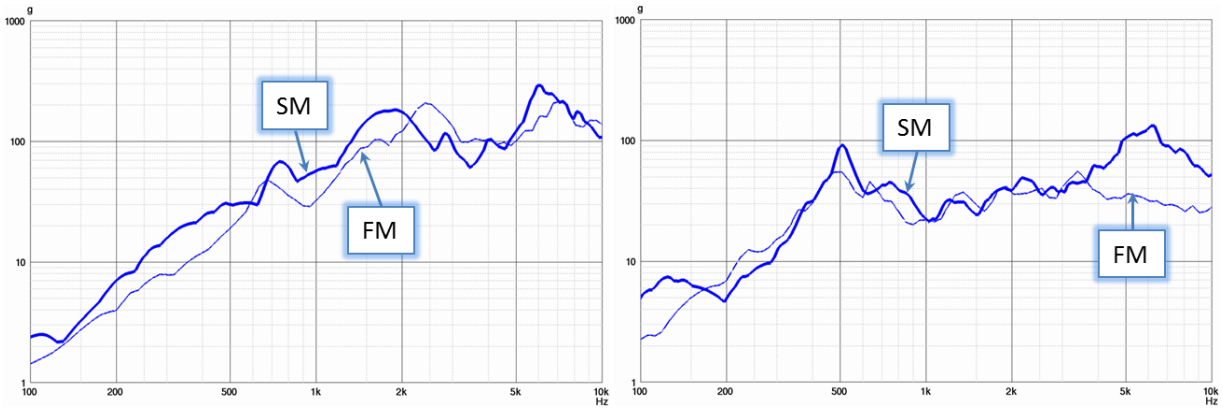

Figure 8-5: Difference between SM and FM – Case 1 – Fully representative SM structure, with representative equipment dummies distribution

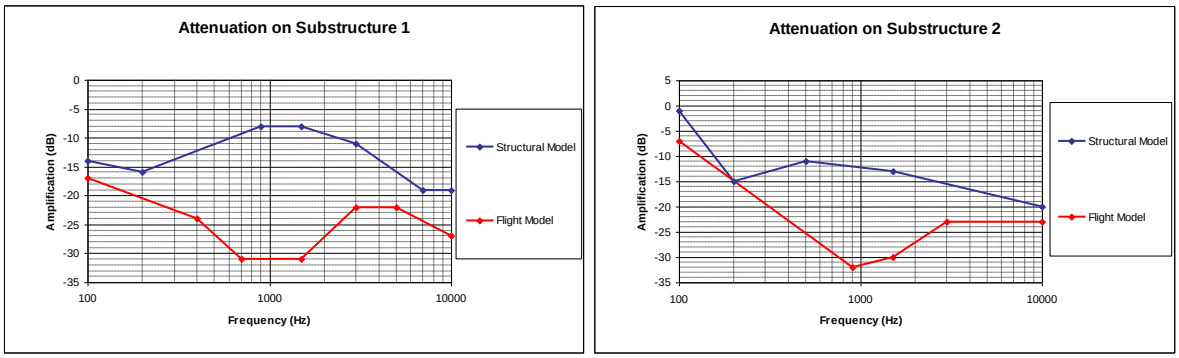

Figure 8-6: Difference between SM and FM – Case 2 – SM structure representative of spacecraft family, with generic equipment dummies distribution

8.2.6 Statistical methods to derive maximum expected environment

8.2.6.1 Overview

The documents [RD-018] and [RD-019] can be consulted for more details on statistical processing of measured data.

Statistical processing is one method to define a maximum expected environment (MEE) or to build a zoning of a spacecraft. This processing is rarely employed in the aerospace industry because relevant database are not often available. However, with spacecraft families, satellite manufacturers can more and more dispose of a shock test database allowing thus a statistical processing of the SRS in order to define or refine statistically a maximum expected shock environment.

The specification process begins by defining some zones or regions where it is expected that the shock environment within that zone is reasonably similar. Similar means that some limited scattering is expected within the particular zone, which is necessary to characterize. This phase is of paramount importance for the statistical processing because it is of no use to perform some statistical computation on very dissimilar or scattered data since the results are not meaningful.

It is well known that for a given launch or ground shock test, there are some flight-to-flight or spacecraft-to-spacecraft variability. Some of this variability can be due to unavoidable differences between the flight and payload configuration. However, some variability can also be linked to the randomness of the launch or ground test events themselves. These uncertainties should also be characterized in order to define the so-called maximum expected environment as a level that would typically not be exceeded or be exceeded exceptionally. Therefore, the MEE should account for both the expected spatial variation within a particular zone as well as the flight-to-flight changeability. This MEE is usually described in terms of spectrum of a motion parameter, commonly the acceleration.

Most frequently one uses the Normal Tolerance limit (NTL) method to compute statistically the MEE. An alternative method is also described: the Bootstrap technique. The Bootstrap is a statistical subsampling method which uses sample data to generate replicates that are utilized for parameter and confidence interval estimation. An important feature of this method is that it does not make any assumption on the underlying distribution of data.

In practice, the statistical method is only applicable when a database with similar spacecraft and shock source is available. There is no link with the level specified by launcher, as the database covers the specific launcher-spacecraft configuration, including however the effect of randomness of repeated similar events.

The obtained Maximum Expected Environment is used to derive reliable specification to equipment units based on experience and therefore avoiding over-testing at unit level. This is a tool to reduce risks for the system shock test that remains however the formal verification that the spacecraft is qualified versus the required qualification level: the satellite qualification is achieved when the qualification status of each sub-systems covers the required qualification level (derived from satellite system test, as per procedure I, described in paragraph 13.3.2), hence including a qualification margin of 3dB.

8.2.6.2 Normal Tolerance Limit method

The NTL method is described in numerous American NASA standards and military standards [RD-020] [RD-021] and is used to derive the MEE from random vibration, vibroacoustic, and shock environments [RD-018]. It consists in computing a normal tolerance limit for the predicted spectra in each frequency resolution bandwidth. NTL method should be applied only to normally distributed random variables. If this is true, then the one-sided normal tolerance limit for the set of y variables, y_i , i = 1, 2,…, n is given by:

$$NTL_y(n,p,\gamma) = \overline{Y} + K_{n,p,\gamma}.S_y$$

Where:

— $\overline{Y} = \frac{1}{n}\sum_{i=1}^{n} y_i$ is the sample mean,

— $S_y^2 = \frac{1}{n-1}\sum_{i=1}^{n}(y_i - \overline{Y})^2$ is the sample standard deviation,

— $K_{n,p,\gamma}$ the one-sided tolerance factor with p the percentile of data (e.g. 95 %) and g the confidence level (e.g. 50 %). See Table 8-2 for K values as function of the desired percentile and the chosen confidence.

Table 8-2: K factor for NTL method

n	γ=0.50			γ=0.75			γ=0.90		
	β=0.90	β=0.95	β=0.99	β=0.90	β=0.95	β=0.99	β=0.90	β=0.95	β=0.99
3	1.50	1.94	2.76	2.50	3.15	4.40	4.26	5.31	7.34
4	1.42	1.83	2.60	2.13	2.68	3.73	3.19	3.96	5.44
5	1.38	1.78	2.53	1.96	2.46	3.42	2.74	3.40	4.67
6	1.36	1.75	2.48	1.86	2.34	3.24	2.49	3.09	4.24
7	1.35	1.73	2.46	1.79	2.25	3.13	2.33	2.89	3.97
8	1.34	1.72	2.44	1.74	2.19	3.04	2.22	2.76	3.78
9	1.33	1.71	2.42	1.70	2.14	2.98	2.13	2.65	3.64
10	1.32	1.70	2.41	1.67	2.10	2.93	2.06	2.57	3.53
12	1.32	1.69	2.40	1.62	2.05	2.85	1.97	2.45	3.37
14	1.31	1.68	2.39	1.59	2.01	2.80	1.90	2.36	3.26
16	1.31	1.68	2.38	1.57	1.98	2.76	1.84	2.30	3.17
17	1.31	1.68	2.37	1.55	1.96	2.74	1.82	2.27	3.14
18	1.30	1.67	2.37	1.54	1.95	2.72	1.80	2.25	3.11
20	1.30	1.67	2.37	1.53	1.93	2.70	1.76	2.21	3.05
25	1.30	1.67	2.36	1.50	1.90	2.65	1.70	2.13	2.95
30	1.29	1.66	2.35	1.48	1.87	2.61	1.66	2.08	2.88
35	1.29	1.66	2.35	1.46	1.85	2.59	1.62	2.04	2.83
40	1.29	1.66	2.35	1.44	1.83	2.57	1.60	2.01	2.79
50	1.29	1.65	2.34	1.43	1.81	2.54	1.56	1.96	2.74
∞	1.28	1.64	2.33	1.28	1.64	2.33	1.28	1.64	2.33

A more complete K-factor table can be found in [RD-019].

The K factor is both a function of the desired percentile and the chosen confidence. This uncertainty in the confidence results from using a sample mean and sample standard deviation instead of the true or entire population's mean and standard deviation values which are by nature unknown. For the special case where n is infinite, the K one-sided normal tolerance factor becomes the percentile point of the standardized Gaussian distribution (last row of Table 8-2). It means that there is no more uncertainty in the mean and standard deviation of the population. One notices that increasing the level of confidence, particularly when n is small is very costly and can lead to over-conservative results.

Both NASA and the U.S. AFSSD have standardized their MEE to be the p=0,95, γ=0,50 level. This is commonly referred to as the P95/C50 or P95/50 level. This level can be interpreted as follows: there is a 50-50 chance of one exceeding of the P95/50 level in 20 flights or ground test.

The qualification level is not yet completely standardized as the MEE. NASA and European Agencies use generally the following definition:

$$QL=MEE + 3\ dB.$$

The return on experience using such method is that shock data set are generally not normally distributed but indeed lognormal [RD-022]. In order to apply correctly the NTL method, one should use the following transformation on the data.

$$z = \log_{10} y$$

$$NTL_y(n,p,\gamma) = 10^{NTL_z(n,p,\gamma)}$$

An illustration is given in Figure 8-7 (radial direction) and Figure 8-9 (longitudinal direction) representing the normal tolerance limits of clampband interface data for Telecom spacecraft family, computed with p = 95 % and γ = 50 %.

The P95/50 level is logically exceeded on some frequency bandwidth by some measurements. It is interesting to verify the percentage of points that exceeds the defined level. This percentage should be compliant with the chosen percentile (i.e. 95 %) with a confidence of 50 % if the main assumption of this method is valid, that is to say if the measurements follow a lognormal distribution (or equivalently if the logarithm of the data follow a normal distribution).

- For the radial direction: 7 % of the points are higher P95/50 shock level: the NTL method is slightly less conservative as expected.
- For the longitudinal direction: 5 % of the points are higher P95/50 shock level: the NTL method performs as expected.

To understand these numerical results, the best approach consists in plotting the empirical probability distribution function (PDF) and/or cumulative distribution function (CDF) of the data and compare them with the standardized normal one. Figure 8-8 and Figure 8-10 provide an example of such empirical distribution functions and the comparison with the theoretical standardized normal one (red curves). One notices that the radial direction data are not perfectly normal whereas the longitudinal ones are very close to the normal distribution.

As a general result, it is considered as very important to verify that the spectral test data (SRS for shock data) follow a lognormal distribution by computing the empirical distribution functions. The defined level can indeed be very conservative if the major hypothesis of normal distribution has a low degree of validity. If this method is used to specify a zone, then this recommended procedure should be carefully followed to avoid any over specification that can drive the structural hardware design (e.g. added mass) or alternatively, lead to late and then costly mitigation treatments as isolation systems. If the distribution of the data is not lognormal, it is then necessary to find an alternative solution, or at least to compare the NTL level with another approach to determine the degree of conservatism it has generated.

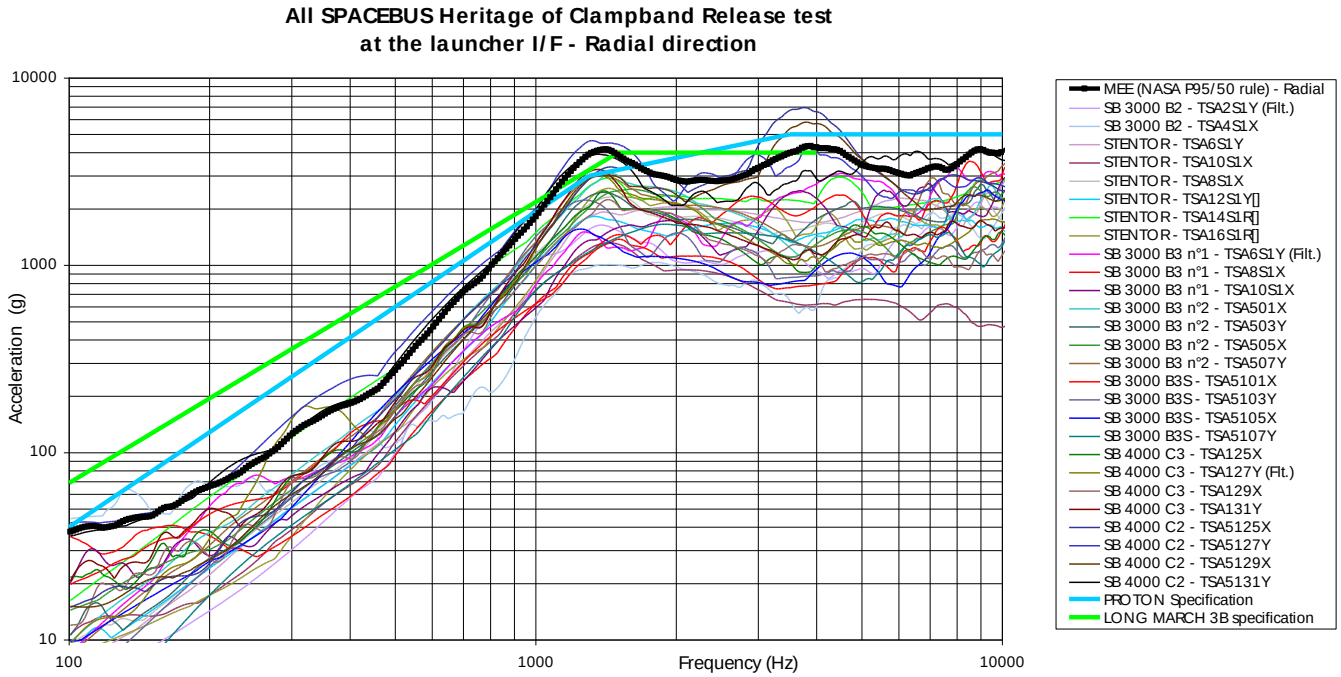

Figure 8-7: Statistical processing of clamp band test data at S/C I/F - radial direction

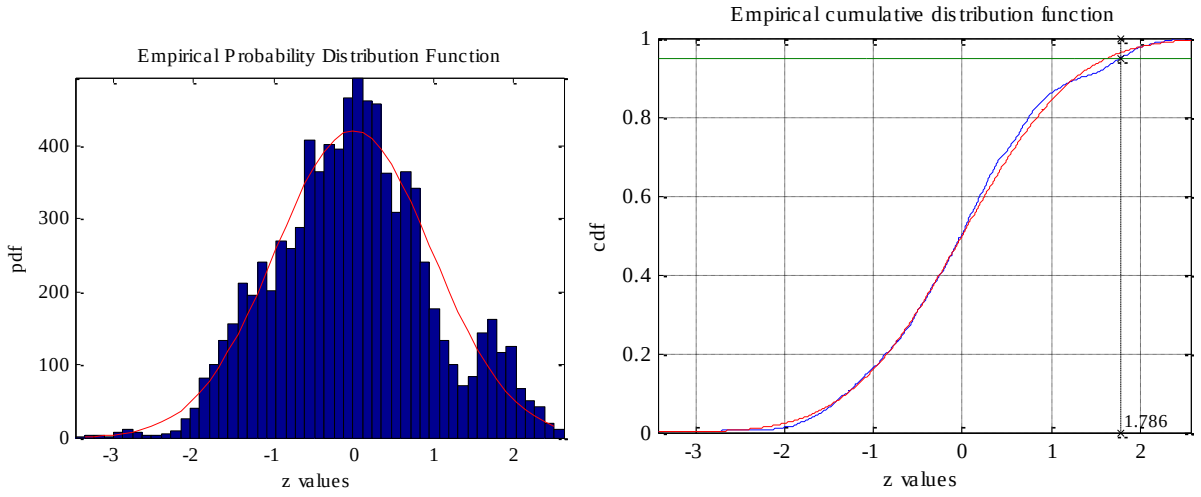

Figure 8-8: Empirical probability distribution function and cumulative distribution function – radial direction

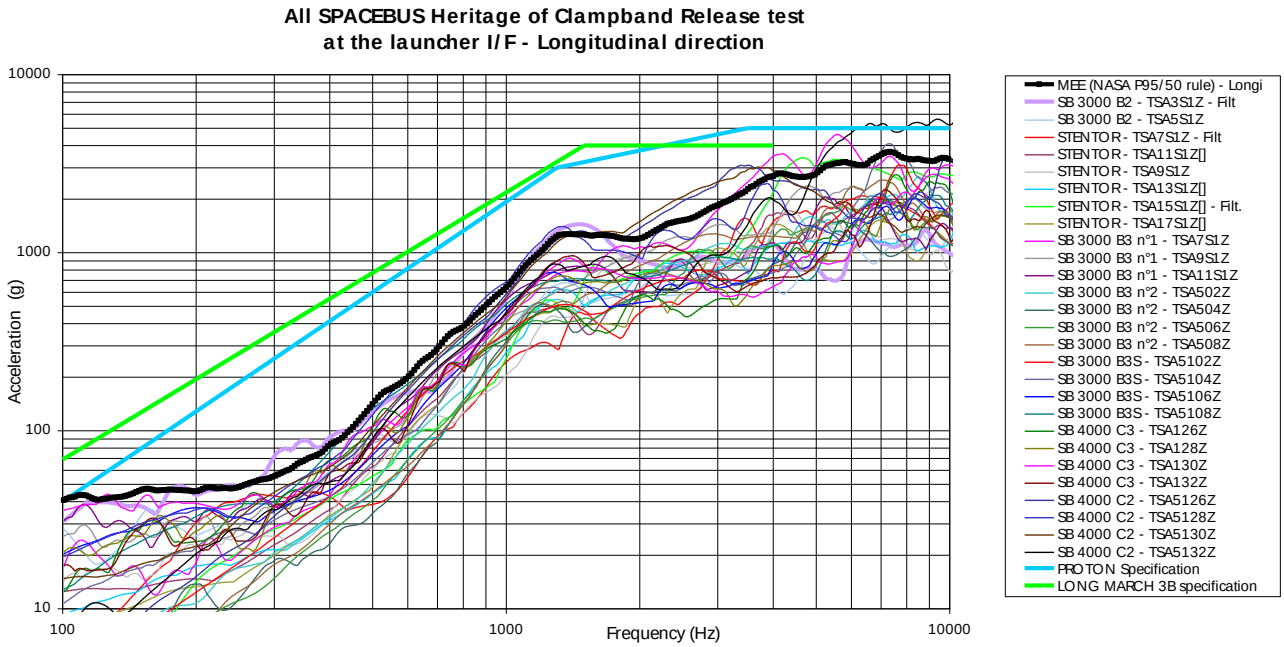

Figure 8-9: Statistical processing of clamp band test data at S/C I/F - longitudinal direction

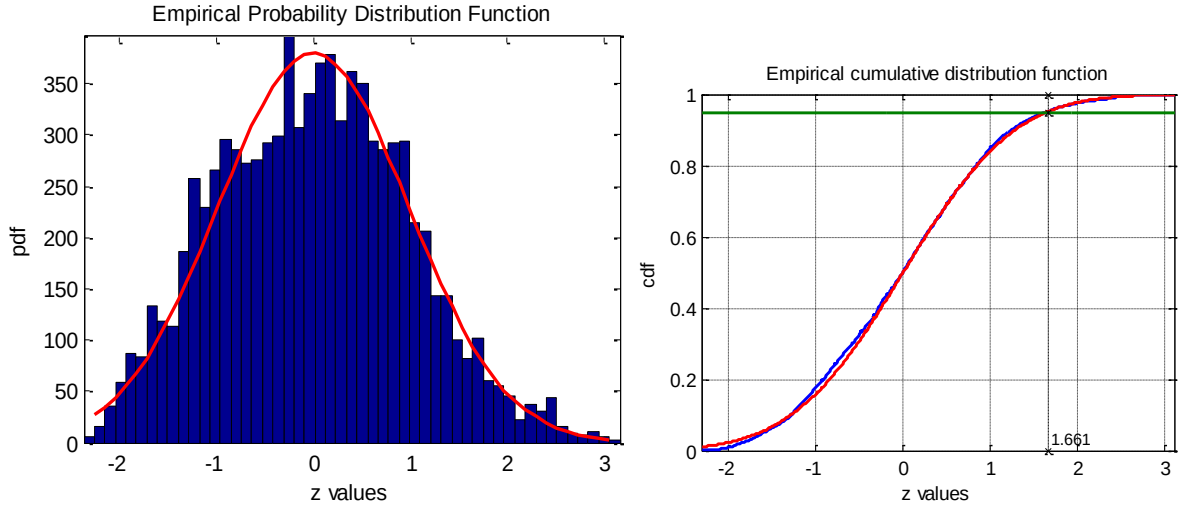

Figure 8-10: Empirical probability distribution function and cumulative distribution function– longitudinal direction

8.2.6.3 Bootstrap method

The main idea of such technique is that the data arise as a sample from some existing probability distribution, *f* (most of the time, the normal distribution is assumed). Uncertainties of our inferences can be measured if *f* can be estimated. The most fundamental idea of the Bootstrap method is that one computes measures of our inference uncertainty from that estimated sampling distribution of *f*.

The method consists of:

- Generating B Bootstrap replicate samples of the same size n as the original data sample. Each value in the original data sample is assigned an equal probability of 1/n. The elements of these Bootstrap samples are randomly chosen from the original data, with replacements. It means that a particular data can be chosen several times or not at all in a given replicate.
- Evaluating a parameter or statistic of interest for each of the B Bootstrap samples generated. Each computation produces a Bootstrap replicate of the statistic of interest (e.g. mean, standard deviation, P95, and P99).
- Estimating an empirical cumulative distribution function (CDF) for this parameter by using the numerous Bootstrap replicates of this parameter.
- Establishing confidence intervals from this distribution.

The method principle is summarized in Figure 8-11.

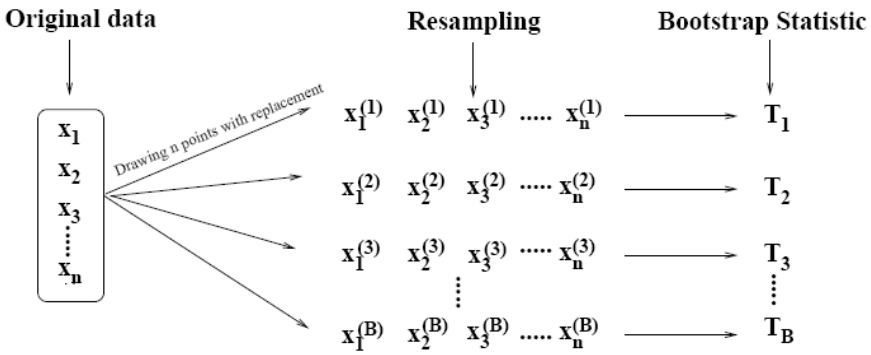

Figure 8-11: Bootstrap method principle

The set of B Bootstrap samples is a proxy for a set of B independent real samples from f (in reality we have only one actual sample of data). Properties expected from replicate real samples are inferred from the Bootstrap samples by analysing each Bootstrap sample exactly as the real data sample were first analysed. From the set of results of sample size B we measure our inference uncertainties from sample to population. In other words, the Bootstrap allows assessment of the accuracy and uncertainty of estimated parameters (even if no closed form exists) from small samples, without any prior assumptions about the underlying distribution (particularly the usual normal distribution). In that case, when no assumption or inference on the distribution f is made, the bootstrap is called non parametric. Other forms of parametric Bootstrap have been described in literature but have not been treated in the frame of this work.

As explained in [RD-018] for vibroacoustic data, the statistics of interest for the Bootstrap analysis are the P95 or P99 probability levels. This requires that the bootstrap mean and bootstrap standard deviation be used as a bootstrap pair to compute the desired probability level. In other words, the statistic of interest mentioned previously is not just the mean and standard deviation but instead the values generated by these that are associated with the P95 or P99 probability levels.

In practice, the Bootstrap mean and standard deviation are computed for each replicate. Then, in order to derive the level P95 or P99 levels which can be expressed as $P95 = \bar{x}_b + k\sigma_b$, one needs to determine the coefficient k. Several methods can be used. The k factor could be chosen as the $K_{n,p,\gamma}$ one-sided tolerance factor. However, that method would assume a normal distribution of the data which is not known, reducing consequently the generality of the problem. The k factor can be computed using the original data sample. By using the CDF of the standard normalized data $z = \frac{x - \bar{x}}{\sigma}$ (about which the underlying distribution is not known). This solution can be retained.

For SRS, the size of each sample at a given frequency is usually very small and does not allow to correctly define a CDF and its tails per frequency. It is assumed thus that the CDF can be computed by combining all the frequencies of the SRS together. This assumption introduces an error that is generally found acceptable.

The previous procedure leads to B replicate values of the P95 or P99 level. The confidence level is finally computed by sorting all the values of the statistic of interest and then selecting the percentage of the empirical sampling distribution of the P95 or P99 level. For instance, for a confidence level of 50 % with 1000 Bootstrap replicates, the 500^{th} = 0,5 x 1000 sorted value is chosen.

1000 to 2000 replicates are usually found acceptable for defining correctly a Bootstrap statistic.

The bootstrap method has been used to compute the P95/50 and P99/90 levels of the clampband SRS data shown in Figure 8-7 and Figure 8-9. For that case, the k factor can be found using the CDF of the data. The k factors for the P95 level can be read on Figure 8-8 and Figure 8-10 and are respectively 1,786 and 1,661.

The computed levels are compared with the NTL method: Figure 8-12 and Figure 8-13 show the results. The two methods gives similar results especially in the longitudinal direction where the PDF of the data are quite close to the standard distribution (see Figure 8-10). This result is quite reassuring since the Bootstrap method is quite different from the NTL one.

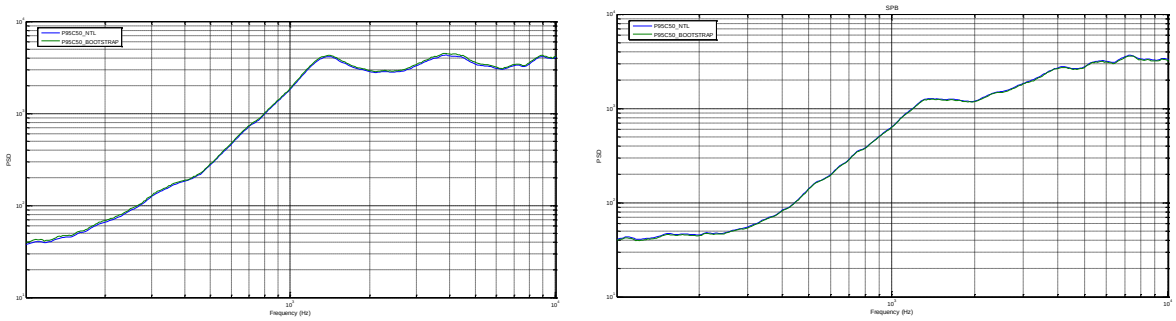

Figure 8-12: P95/50 level for clamp band test data at S/C I/F – NTL and Bootstrap – radial and longitudinal direction

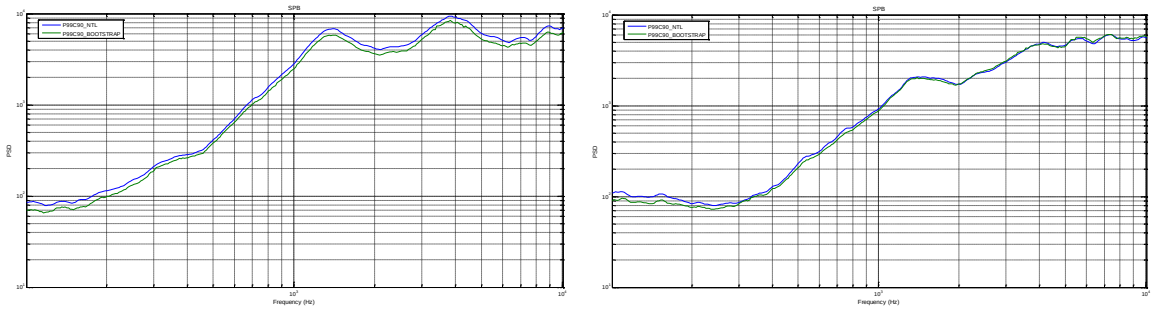

Figure 8-13: P99/90 level for clamp band test data at S/C I/F – NTL and Bootstrap – radial and longitudinal direction

Figure 8-12 and Figure 8-13 are very interesting since they provide the influence of the non-normality of the original data sample on the probability levels. They clearly show that non-normality increases the scattering of probability levels between the three methods when using high percentile/confidence values. In the radial direction, the PDF are not so close to the standard distribution than in the longitudinal direction. As a consequence, the NTL method provides more conservative results for the P99/90 level in radial direction than the Bootstrap method. For the longitudinal direction, the P99/90 levels given by the two methods are still in a good agreement because the original data sample is close to the normal distribution.

8.2.6.4 Comparison between P99/90 and P95/50+3 dB levels

This comparison aims at determining the qualification level that is defined by NASA as MEE+3 dB, i.e. P95/50+3 dB and by AFSSD and ECSS as P99/90 level. As the data in general cannot be for sure associated with the normal distribution, it was decided to compare these probability levels thanks to the Bootstrap method.

Figure 8-14 shows empirically that the P95/50+3 dB and the P99/90 level are quite equivalent and can both be utilized to define a qualification level. The usual 3 dB margin for qualification [RD-023] finds with the P99/90 level a statistical justification.

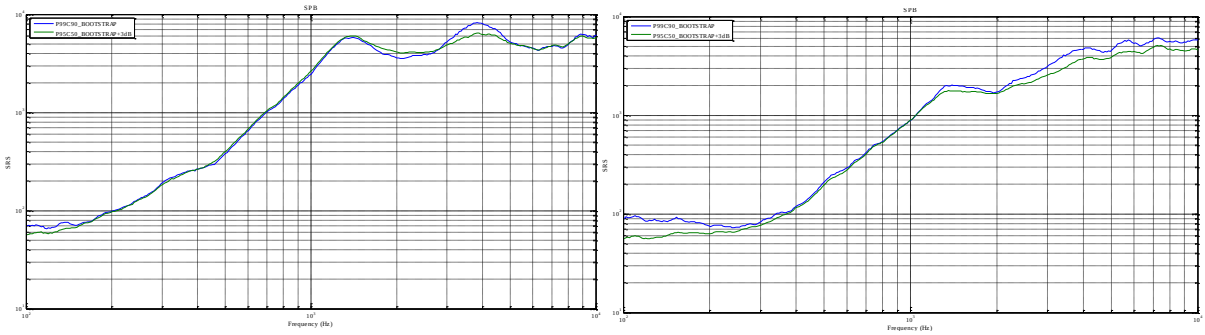

Figure 8-14: P95/50+3 dB and P99/90 levels for clamp band test data at S/C I/F – radial and longitudinal direction

The P95/50 + 3dB statistics therefore appears as a reasonable level to be used for units shock specification, in order to anticipate the results of a system test.

8.2.6.5 Conclusions

Statistical processing of shock test data constitutes one method to define the MEE with regards to the shock environment as other classical methods like extrapolation techniques or numerical analysis. The classical NTL method is widely used in the US aerospace industry with success since more than 40 years. The simplicity of the NTL method should not hide its fundamental assumption that the original data is normally distributed. If it is not the case, the NTL method can become over-conservative, especially for small samples. Another statistical technique has been presented to be used with shock test data aiming at correcting the NTL defaults.

The return of experience using these methods shows the following:

- When database is available, a statistical method is an efficient way to have a good reliability in specification derivation.
- The two methods (NTL and Bootstrap) give similar results for normally distributed data.
- Non-normality increases the scattering of evaluation between the two methods when using high percentile/confidence values (NTL seems too conservative).
- If the data are not distributed normally, the Bootstrap method seems to give the most reliable results but with an increased computation time (linked to the number of replicates).

8.3 Similarity-heritage-extrapolation methods in practice

Propagation of shock energy depends strongly on the geometry of the intervening structure. The involved energy does not propagate the same way in a 1D (struts), 2D (panels) or 3D (massive parts or panels junction) structure because the interested volume is not identical. In the same way, the notion of distance evocated in the following sections refers to the geometry and interested volume where the shock energy can propagate.

The following rules are only relevant for shock propagation along the primary load path (propagation of shock along main spacecraft structure e.g. central tube, shear-wall and lateral panel). And they should not be considered valid for bracket and supported equipment (e.g. instrument mounted on isotactic mounts), as their responses are dominated by modal behaviour (see paragraph 8.3.6 for specificities in this case).

The following rules are, a priori, defined in a conservative way: a margin policy (to cover uncertainties and to derive the Maximum Expected Environment **MEE**) should be taken when used to derive shock specification for equipment but it can be user dependant depending on the way the source specification (input specification already defined as MEE, or single test result envelope) is taken and the maturity of project definition. On the top of this, **a qualification margin of 3dB is** added(see 10.2).

A special care should be taken when using generic attenuation factors for the following reasons:

- They do not cover modal responses of the different substructures: amplification or reduction of attenuation which can occur at some specific frequencies (especially below 1000 Hz) due to modal responses in some specific cases are not taken into account.
- These attenuation factors can be used to derive shock levels from measured data on the same or very similar structure at another location or other local interface conditions.
- Attenuation at interfaces should be used with particular caution
    - Shock levels just before a mechanical link are higher than those measured without mechanical interface due to wave reflection
    - Shock levels after a mechanical link are lower but in a limited extent than those measured without mechanical interface. Such phenomenon can lead to overestimating attenuation by mechanical link in a wrong way.
- **Adding attenuation factors is always dangerous as shock is not a linear phenomenon: As a general rule, and when applying the attenuation rules described in the following paragraphs 8.3.1 and 8.3.4, no more than 3 junctions should be cumulated along the loadpath.**

8.3.1 Method A – Point source excitation

8.3.1.1 Presentation of the used method

In Europe with the advent of smaller spacecraft (earth observation and constellation types of satellites) which are usually interfaced to the launcher through discrete interface points, there is a growing interest in attenuation factors applicable for point source excitation. Furthermore, pyrodevices such as pyronut are extensively used for deployment of appendages (e.g. solar array and antenna).

A number of empirically derived shock attenuation rules have been proposed over the years (see [RD-023], [RD-024], [RD-025]). Relevance of those rules has been assessed, based on Galileo-IOV, Terrasar-X (satellite by DLR & Astrium) and Cryosat heritages. In the case of point source excitation on a conventional spacecraft structure, the attenuation rule is best represented by an attenuation of the plateau in the SRS and attenuation of the ramp in the SRS of the point sources, with distance from the source.

Illustrations of both the original attenuation rule (MIL-810-F method 517) and the ESTEC attenuation rule are illustrated in Figure 8-15.

MIL-810F attenuation rule (method 517)	**ESTEC attenuation rule for point source**
- Attenuation of SRS peak and SRS ramp with distance from the source - 40% attenuation per joint up to 3 joints (no attenuation in the ramp portion)	- Inspired by MIL method and consolidated with ESTEC shock database - Slightly more conservative than MIL method - Plateau attenuation: 40% attenuation per joint (1) up to 3 joints - Ramp attenuation: 40% attenuation per joint (1) , but counting 1 joint less than for plateau (2) - Percentage of source value remaining to be capped to 100%, for distance lower than 30cm and 15cm for SRS Ramp and SRS peak respectively
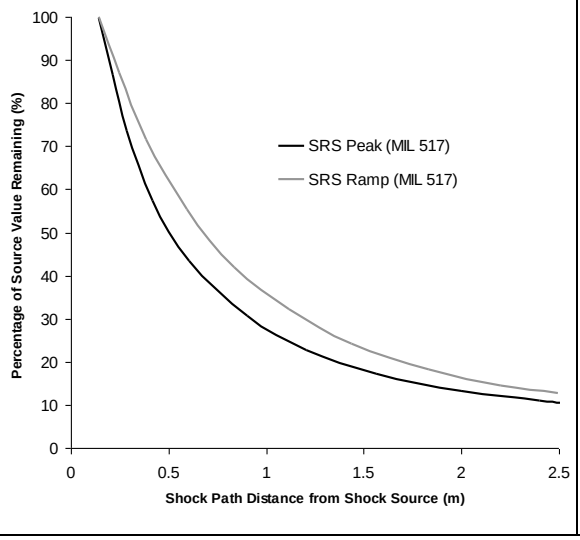	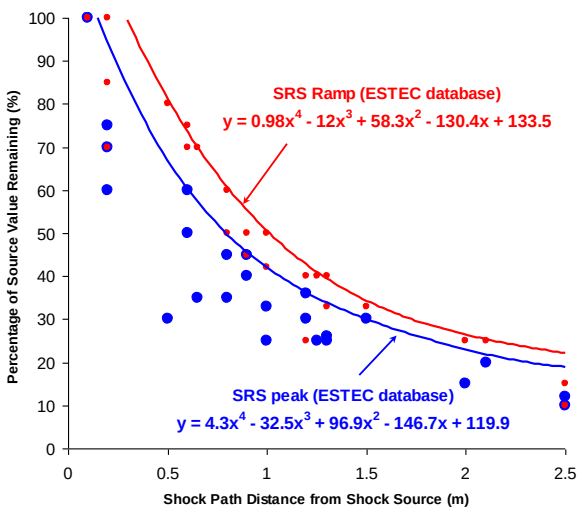

Figure 8-15: Comparison btw MIL-810-F (method 517) and ESTEC attenuation rules

(1) A joint is defined as clear change along the load path: bifurcation, change of impedance, junction between panels. For instance 2 panels connected together through screwed cleats is one junction (in this example, the bolted connection from panel to cleat should not be counted as an additional junction).

(2) For the ramp, the formula of attenuation with respect to distance is different from the one used for plateau and the number of joints to take into account is 1 less than for the plateau, this induce a drift in low frequency (as illustrated on Figure 8-17).

8.3.1.2 Example 1 – Shock mapping of the EXPERT re-entry vehicle due to separation from LV

As an example of implementation of the method, these attenuation rules have been utilized to define the shock mapping of the EXPERT re-entry vehicle.

The zoning operation consisted in dividing the EXPERT structure into zones (bottom panel – cross panel lower zone – cross panel upper zone – upper platform – TPS – nose), and the shortest load path for each zone, and in particular the number of junctions between the shock source and the zones of interest were identified (see Figure 8-16).

	Bottom panel	Cross panel - Lower zone	Cross panel - Upper zone	Upper platform	TPS	Nose
Dist. Source (m)	0.1	0.2	0.5	0.55	0.3	1
Nb joint(s)	0	1	2	2	1	2
Nb joint(s) for Ramp	0	0	1	1	0	1
SRS Ramp (%)	100	100	50	47	100	31
SRS Peak (%)	100	57	24	22	51	15

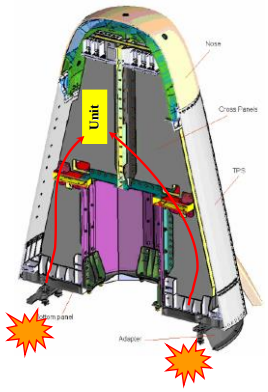

Figure 8-16: Loadpaths identification (number of junctions and distance from source)

Subsequently the attenuations have been computed for each zone according to ESTEC-rules. The responses at all points within each zone are considered to be homogeneous. Finally, these attenuations were applied to the LV shock specification (2000 g @ 1 kHz for the type of pyrodevice used for the EXPERT separation from the launch vehicle), in order to derive the shock levels in different zones of EXPERT S/C.

As a general observation for propagation of shocks induced by point sources, one can say that despite a severe shock input to the spacecraft, the shock levels are quickly attenuated with the distance from the source and with the number of joints.

This type of excitation could remain of concern at direct vicinity to the source. Therefore as a general rule, there should be no sensitive equipment installed close to the source (20 cm to 30 cm could be considered as a "safe" distance).

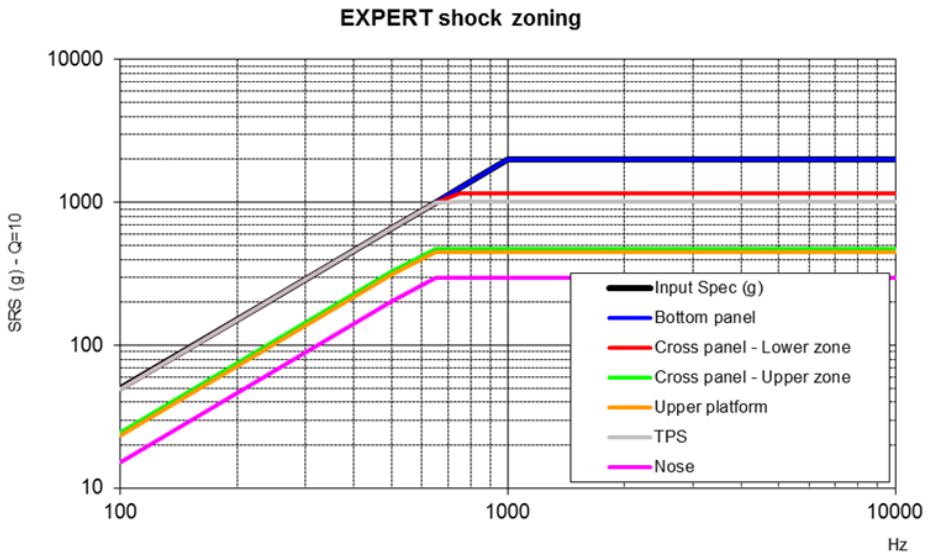

Figure 8-17: EXPERT shock mapping

8.3.1.3 Example 2 – Internal shock induced by appendages deployment

This second example could be treated using the method previously presented. But in that specific case, a number of system level tests have been performed (Deployments of Solar Array and antennas on a large telecom platform family), with the main purpose to better characterize the shock propagation.

During these tests, a large attenuation with the distance and with the number of junctions has been evidenced. The Figure 8-18 shows the SRS of eight successive shocks measured on the same accelerometer corresponding to the eight solar array Hold-Down and Release Mechanism (HDRM) releases of a telecom spacecraft. The distances from the shock source to the location of the accelerometer vary from a HDRM to another and thus explain the difference between SRS. It can be seen on the figure that high frequencies vanish quickly with the distance whereas low frequencies can propagate without practically any attenuation.

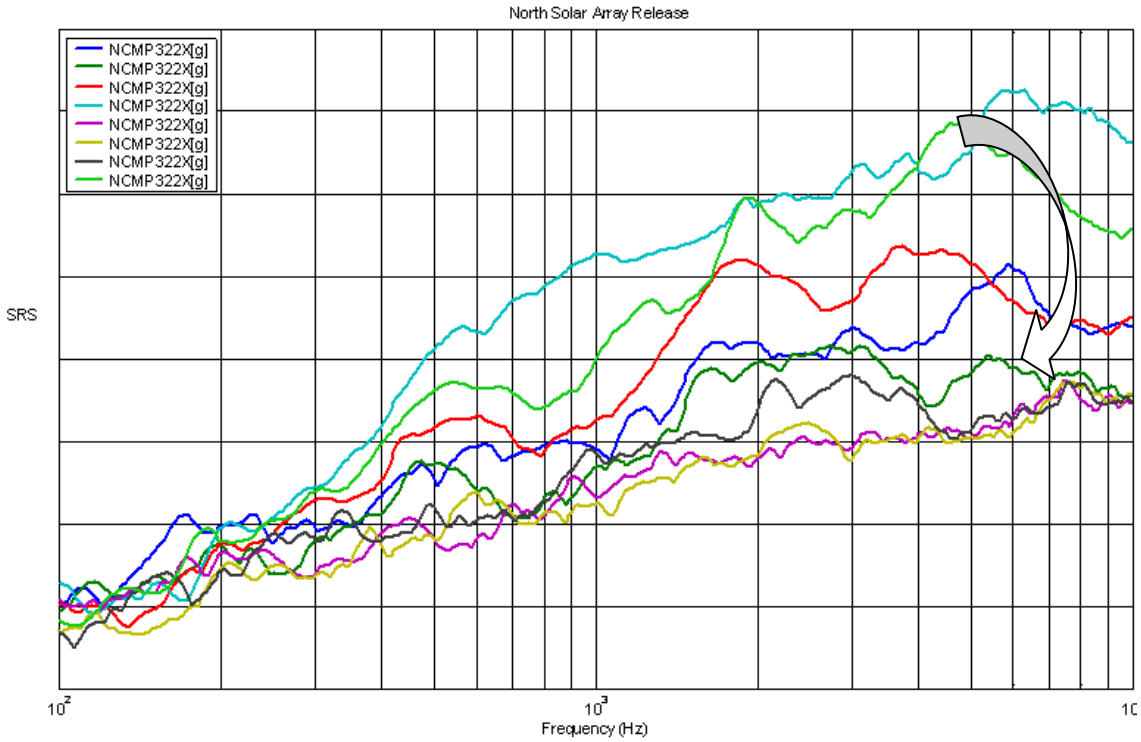

Figure 8-18: Example of attenuation with distance

The above figure clearly shows on the higher frequencies the attenuation with distance to the shock source. The absence of effect at lower frequency is due to some measurement artefact.

The shock zoning operation for internal shocks consisted in evaluating **concentric circular zones around the shock sources on external and internal faces of the panels**. The further the point of interest from the source is, the less severe the shock becomes. Hereunder is an example of shock zoning of the north communication module panel of a telecom spacecraft. eight shock sources corresponding to the eight pods of the solar array can be visualized through concentric circular zones around the bipod or tripod I/F. Several zones are considered with the distance. In the mentioned example, three zones are specified. The first one, called Spec1, is the most severe since it is near the shock source. Then the second one, called Spec2, is less severe as the distance from the source increases. Finally, the rest of the panel for the considered shock is in the Spec3 zone. Defining zones finally consists in determining a radius and an associated level.

It can be seen on the attenuation factors (Figure 8-20) that high frequencies are naturally more attenuated than low frequencies.

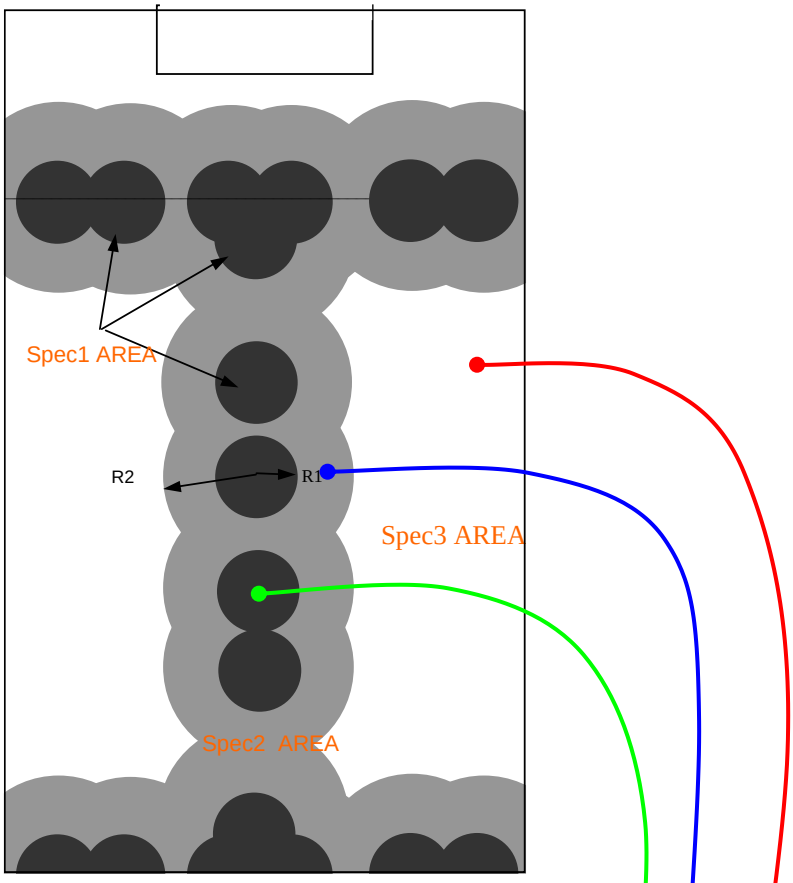

Figure 8-19: Example of shock zoning for Solar array shocks

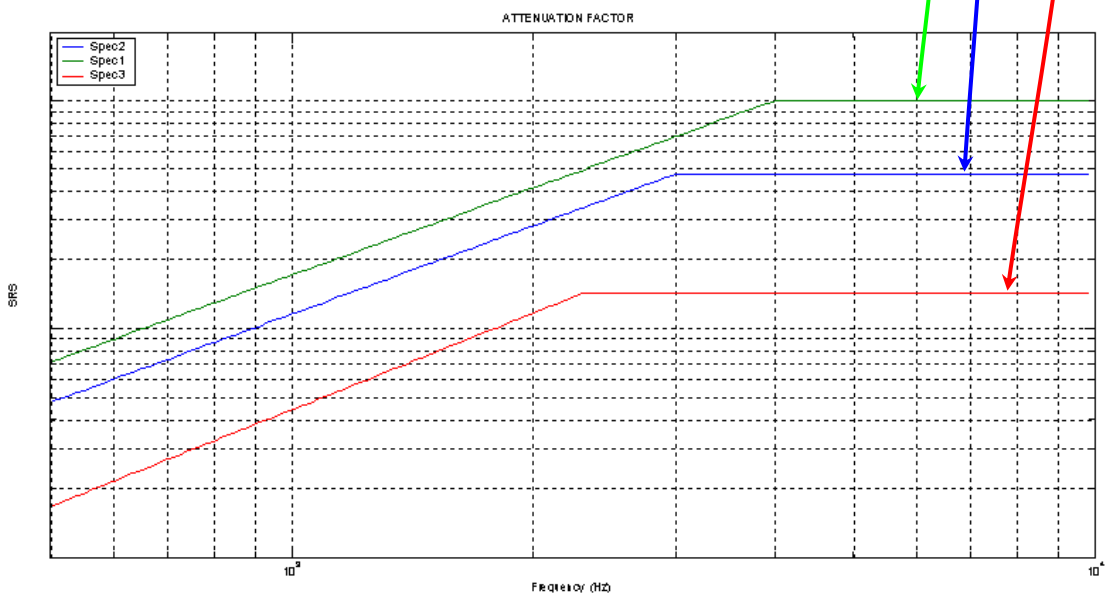

Figure 8-20: Attenuation factors between solar array zones

The next example illustrates another category of internal shocks: antenna release. Figure 8-21 shows the shock zoning of an earth panel of a telecom spacecraft. Four antenna hold down points can be visualized through four concentric circular zones. As it has been seen on the previous example, three different areas are defined corresponding to three specifications. An important point to underline is the **sensitivity of these specifications to the type of HDRM**. Specifically for antennas and reflectors where architecture constraints are relatively strong, HDRM can be of several types: single blocks or tripod following the available volume. Empirical verifications show that single block HDRM produces higher shocks or shocks that propagate further than tripod ones. Thus the different specification and areas take into account the type of mounting of the appendages.

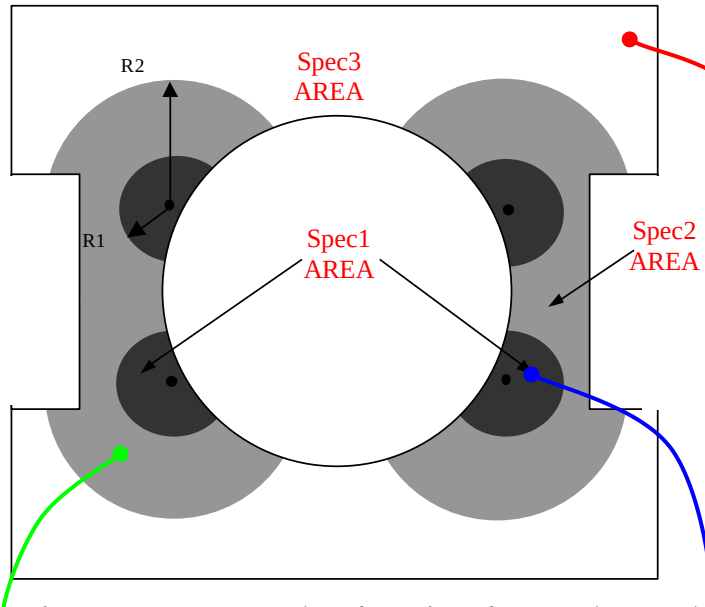

Figure 8-21: Example of zoning for Earth panel

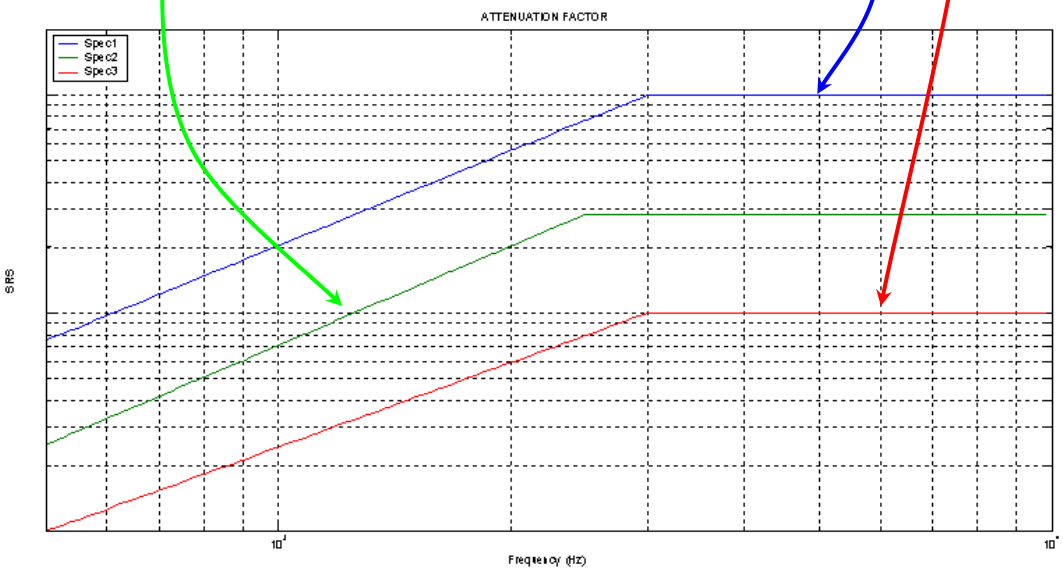

Figure 8-22: Attenuation factors between earth antennas zones

8.3.2 Method B – Clampband excitation

8.3.2.1 Presentation of the used method

As mentioned in paragraph 8.3.1.1 a number of empirically derived shock attenuation rules have been proposed over the years (see [RD-023], [RD-024], [RD-025]). They are generally known as NASA rules. Although the NASA rules are in principle limited to discrete shock sources (e.g. internal shock sources), they are sometimes used for other purposes (e.g. spacecraft separation by means of a Clampband or pyrozip system).

NASA proposes the following scaling relationship $att = \exp\left[\left(-8.10^{-4}.f^{\left(2,4.f^{-0,105}\right)}\right)d\right]$ to correct the magnitude of pyroshock environments, versus frequency and versus distance "d" from a pyrotechnic source to a response location of interest. This relationship is illustrated by the Figure 8-23

It is important to note that this equation was derived from pyroshock data produced by a point source on a complex truss structure, **hence not applicable to every case, in particular not applicable for a conventional spacecraft.**

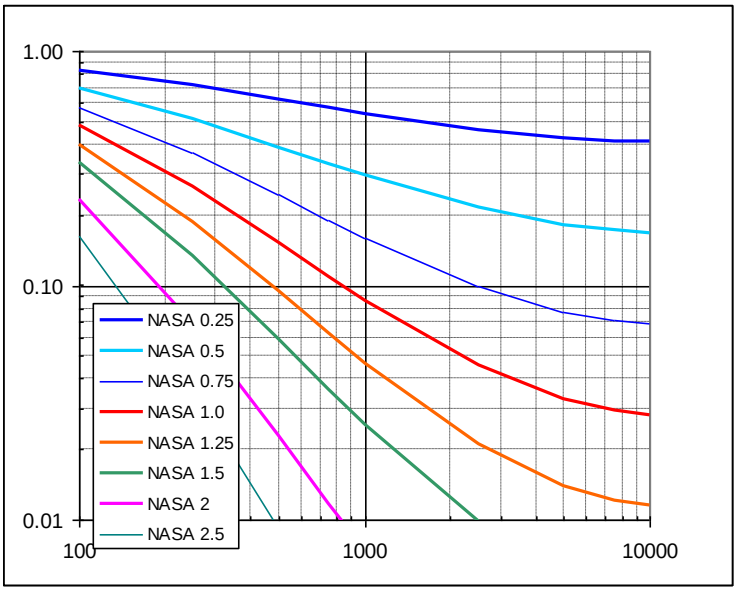

Figure 8-23: Correction of SRS for distance from pyrotechnic source – NASA rule for point source excitation on a complex truss structure

It is evident that this type of scaling relationship presents the advantage to be easily programmed and allows a quick derivation of attenuation factors. This probably explains why it has been sometimes wrongly applied to every excitation type.

However, based on the observation that for a Clampband excitation, the attenuation factor follows a similar profile, it has been assessed by ESA-ESTEC, if this equation could be adapted to derive the attenuation factors applicable for a clampband excitation.

Based on SMART-1, Cluster, ROSETTA, Spot5 and Eurostar 3000 heritages, the applicability of the NASA rules has been assessed. Some correlated rules (so-called ESTEC rules) have been derived [RD-014]. The investigations yielded in the following equation

$$att = \exp\left[\left(-8.10^{-4}.f^{\left(2{,}515.f^{-0{,}115}\right)}\right)\left(0{,}0144.d^3 - 0{,}2.d^2 + 0{,}93.d + 0{,}024\right)\right]$$, See Figure 8-24

Where "d" is the minimum distance along the load path between the shock source and the zones of interest.

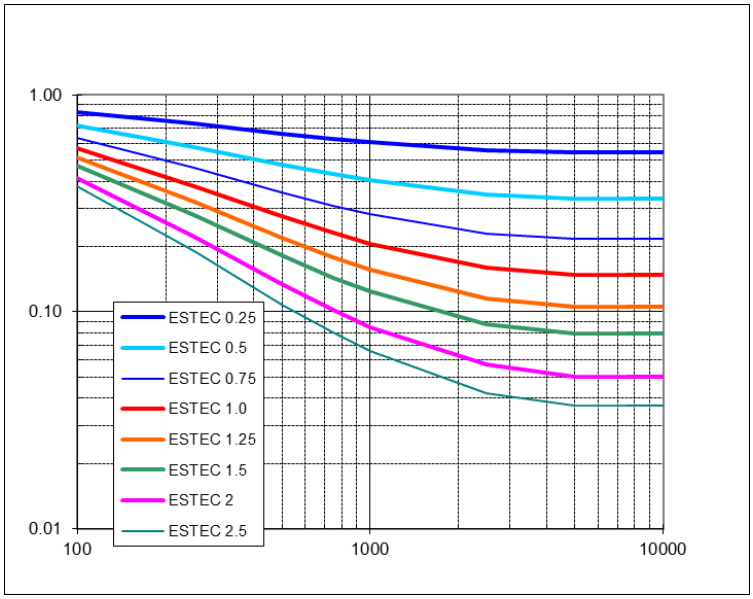

Figure 8-24: ESTEC attenuation rule for clampband excitation

It is fundamental to note that the proposed rules are only valid for prediction of shock environment induced by a clampband separation.

In this respect, the **attenuations are computed considering the radial average at the spacecraft interface** (the axial specification is usually not given in the user's manuals, therefore the derivation of attenuation rules based on the axial average at the spacecraft I/F would be of little use).

The junction effect is implicitly included in the attenuation rule; hence additional attenuation through joint should not be added.

The different steps, leading to the ESTEC rules, are not discussed in detail. In short, the NASA rules were found to be too conservative at proximity to the source (up to 0,7 m) and not conservative enough above. See Figure 8-25, using the ESTEC-rules the attenuation profile is better approximated over the whole frequency range.

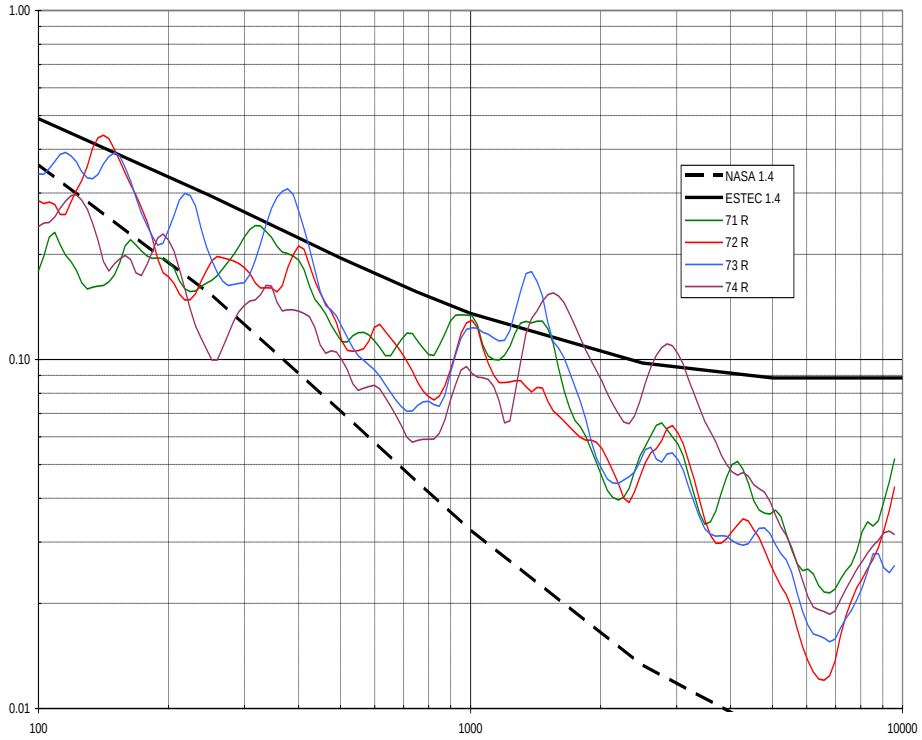

Figure 8-25: Example of validation of ESTEC attenuation rule, by comparison with actual test, and comparison against NASA rule

A special attention has been given to the low frequency range. It is important that a good correlation is achieved in the lower frequency range, whereas the prediction of the higher frequency range (above 1500 Hz) can be less accurate. Indeed the shock environment, seen around 500 Hz to 2000 Hz, is considered to be the most stringent at unit level, due to the greater energy involved and displacements associated.

As mentioned before, the procedure of shock mapping by means of attenuation rules has been verified based on SMART-1, Cluster, ROSETTA, Spot5 and Eurostar 3000 heritages.

As an example of implementation of the method, these attenuation rules have been utilized to define the shock mapping of AEOLUS spacecraft. As the level of similarity with AEOLUS was considered as adequate it provided justification for extrapolation to AEOLUS case.

The zoning operation consisted in dividing the AEOLUS structure into zones (lower deck – side wall lower half – side wall upper half – shear wall lower half – shear wall upper half – top floor), and the load paths between the shock source and the zones of interest have been identified.

Subsequently the attenuations have been computed for each zone according to ESTEC-rules. The responses at all points within each zone are considered to be homogeneous.

Finally, these attenuations were applied to the LV shock specification (radial Clampband specification (1500 g @ 1500 Hz)), in order to derive the shock mapping for AEOLUS spacecraft.

Main results are shown below.

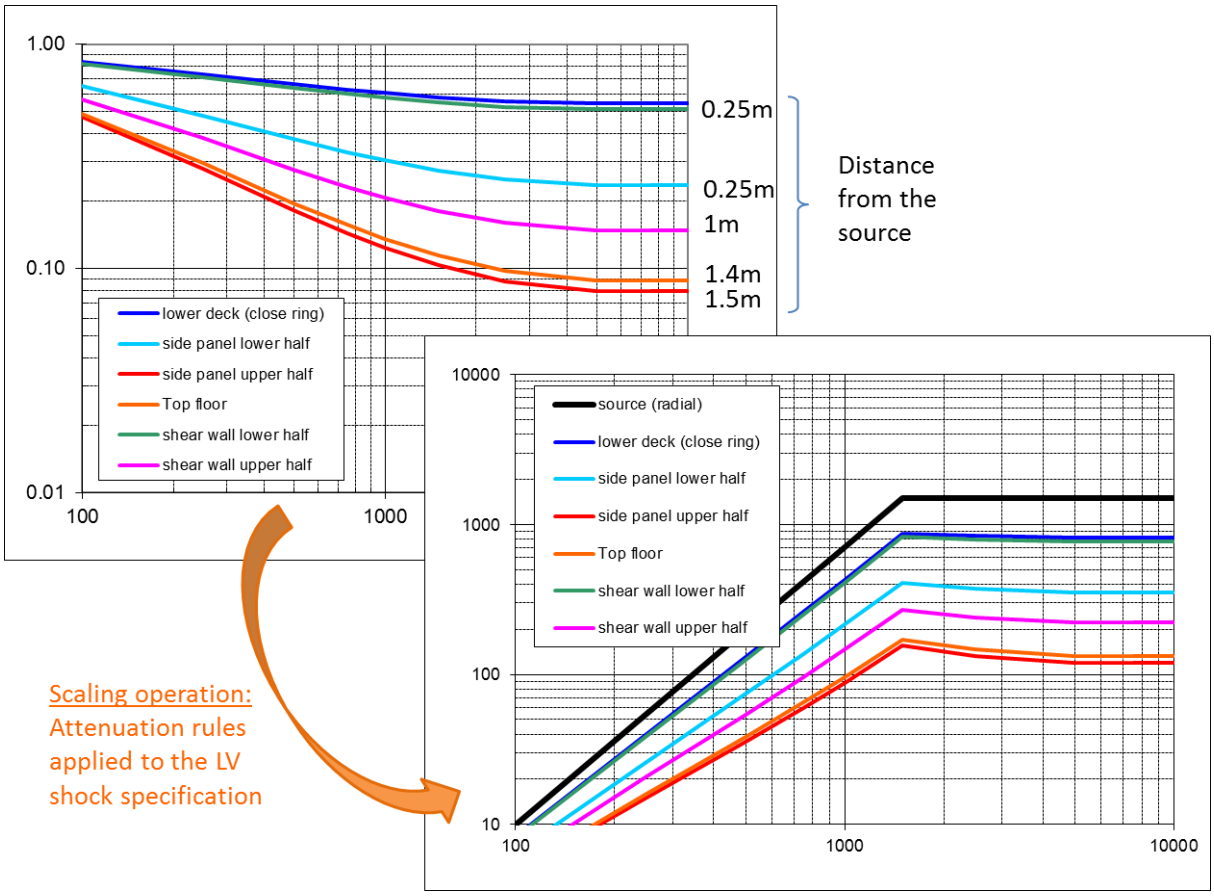

Figure 8-26: Shock mapping process on AEOLUS

The shock zoning of a spacecraft excited by a Clampband excitation can be realized by means of analytical attenuation rules, making the identification of problem areas very easy to be conducted.

It is nevertheless recommended to consolidate the shock zoning through good engineering practices in shock Finite Element Analysis (see chapter 9), in order to identify local responses, which can affect the shock levels of equipment mounted in that area.

8.3.2.2 General observations for a better understanding of Clampband release shock propagation

An important specificity of the Clampband release is its **high inhomogeneity between longitudinal and radial levels**, with significantly higher radial levels (see Figure 8-27). This is mainly due to the fact that the pre-tension, which release is the main mechanical source of the shock, is essentially a radial pre-load.

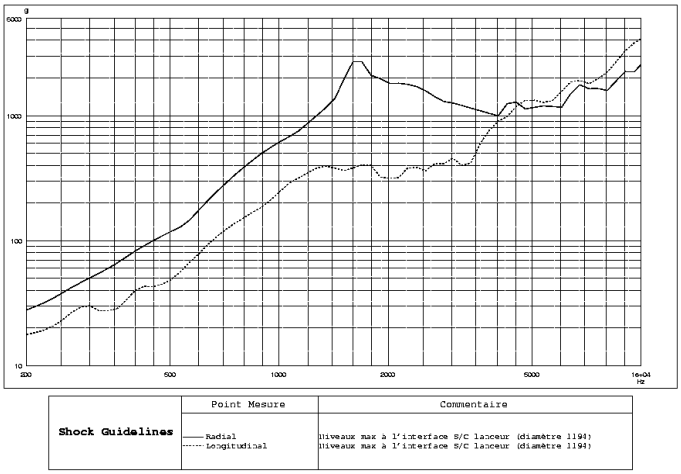

Figure 8-27: Difference between radial and longitudinal clampband levels at launcher-spacecraft interface – Example for a 1194 mm I/F diameter

The effect of this pre-tension is local as the deformed area is rather small (Figure 8-28).

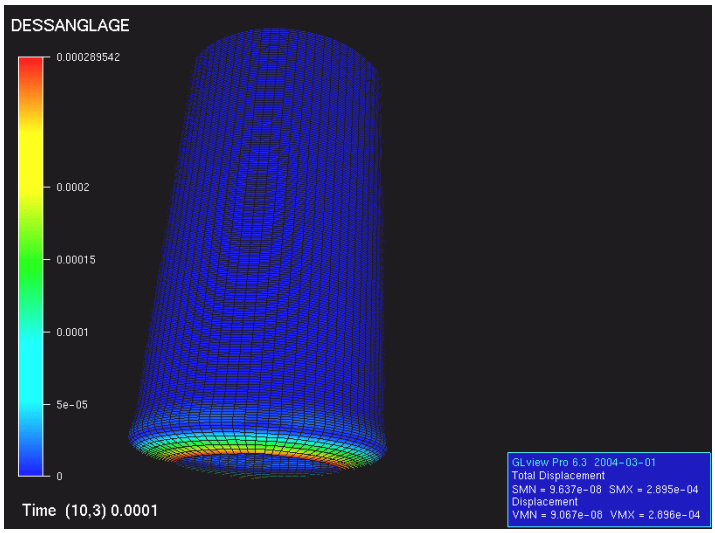

Figure 8-28: View of a radial pre-load at the base of a cylinder

A general observation made also on clampband data is that such the radial component does not propagate in an efficient way in the longitudinal direction: the deformation and thus the high acceleration levels are concentrated at the base of the structure and are fast decreasing when running up in the structure. This phenomena has been modelled using FEM, see Figure 8-29.

This effect concerns the radial component. However the longitudinal component is not affected in the same way, as its physical origin is not directly the radial pre-load.

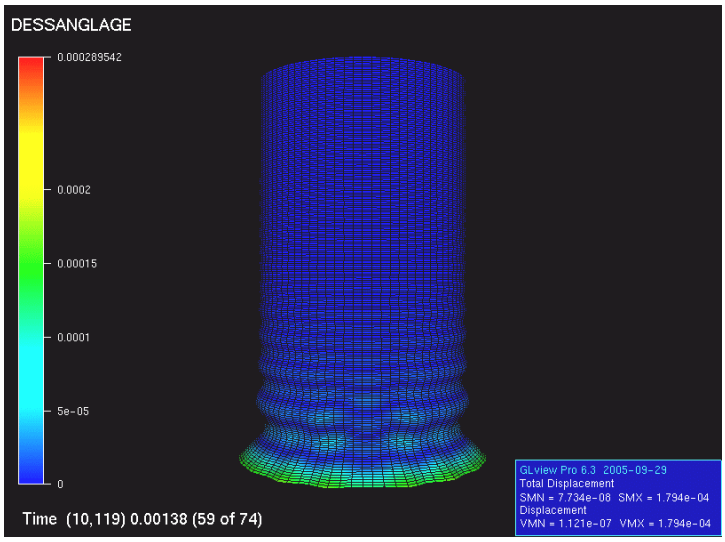

Figure 8-29: View of the deformed shape resulting from a radial pre-load release at the base of a cylinder

Such a propagation physics result in attenuation curves significantly different between a clampband test and launcher induced shocks or Shogun: There are two major reasons explaining this difference:

- The shock source components and frequency content are different
- The spacecraft boundary conditions are different: still clamped on LVA for launcher events and released after clampband release. The whispering modes of the central cylinder are thus different for the 2 types of event.

For instance attenuation curves calculated as the ratio between the SRS response at a given point in the structure and the maximum SRS at the launcher interface are presented in Figure 8-30. **This point emphasizes the fact that clampband release data should never be used directly to predict launcher induced shock levels.**

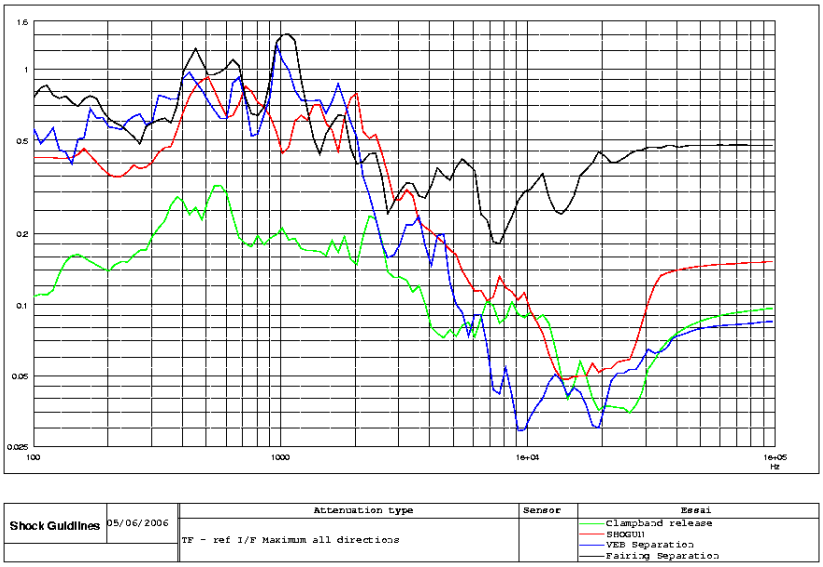

Figure 8-30: Comparison of attenuation curves between Clampband release and launcher induced shock (reference: maximum SRS at the launcher interface)

8.3.3 Method C – Launcher induced shock

8.3.3.1 Presentation of the used method

The second example presents the shock zoning of the Herschel-Planck service module [RD-014]. The launcher of Herschel and Planck is an Ariane5 ECA; the dimensioning shock event is generated by the fairing jettisoning, as the assessment was made at this time with and HSS1 fairing.

The Herschel Planck service module is closely derived from XMM. However only a clampband test has been performed on XMM, making this past heritage inadequate for the shock zoning definition of Herschel-Planck.

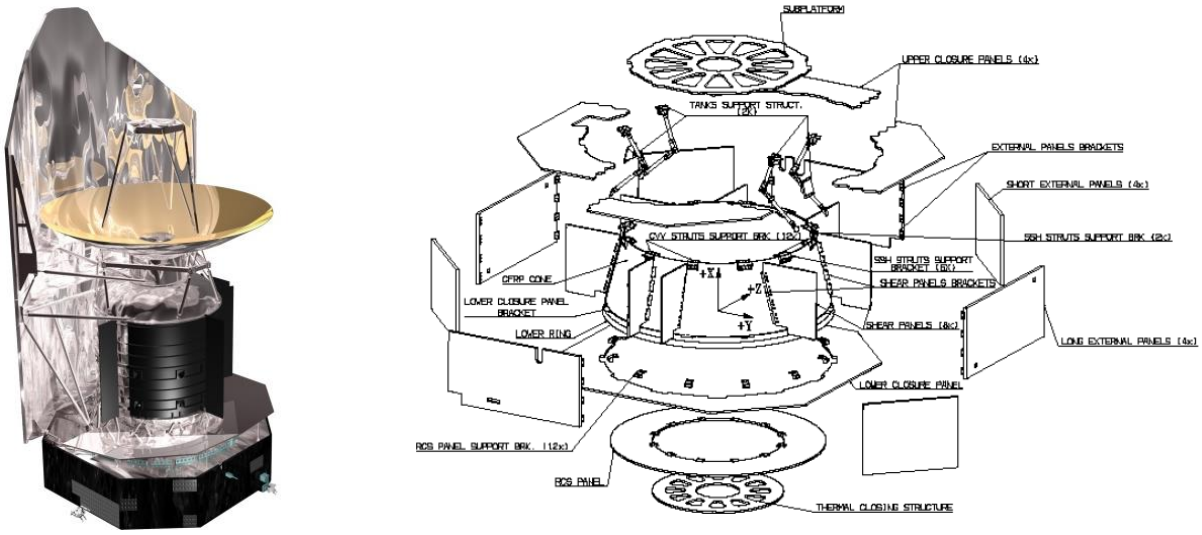

Figure 8-31: Herschel satellite – Configuration of service module

Considering the recommendation on the dependence of SRS ratios w.r.t. the experimental conditions, the extrapolation for Herschel-Planck SVM should only be based on representative shock test data (Shogun).Among the ESA satellites tested in ESTEC, Envisat/PPF was the most suitable candidate (Shogun tests both on STM and PFM). Indeed the level of similarity with HP SVM was found adequate: Both spacecraft present the same interface diameter (∅2624), the central structure consists of a cone on which are attached the shear walls, most of the equipment/units are fitted on the lateral walls/shear walls and their main structures are of sandwich type.

All these aspects are essential drivers to the shock propagation inside the spacecraft, and this adequate level of similarity brings confidence in the derived attenuation factors.

With the difference with a Clampband excitation, the propagation of shock inside the spacecraft does not follow simple attenuation rules (as the distance from the source to the point of interest, or the number of joints along the load path). In case of a launcher induced shock, the level of similarities between the new and the reference spacecraft is directly driving the accuracy of the extrapolations.

The results of this assessment are provided in the Figure 8-32. Herschel-Planck SVM has been divided into 5 zones and the load paths between the shock source and the zones of interest have been identified.

Based on the Envisat/PPF Shogun tests data, the attenuation factors have been computed for each zone:

- central cone (blue)
- shear walls (red)
- lower floor (green)
- upper floor (orange)
- side walls (grey)

The responses at all points within each zone are considered to be homogeneous.

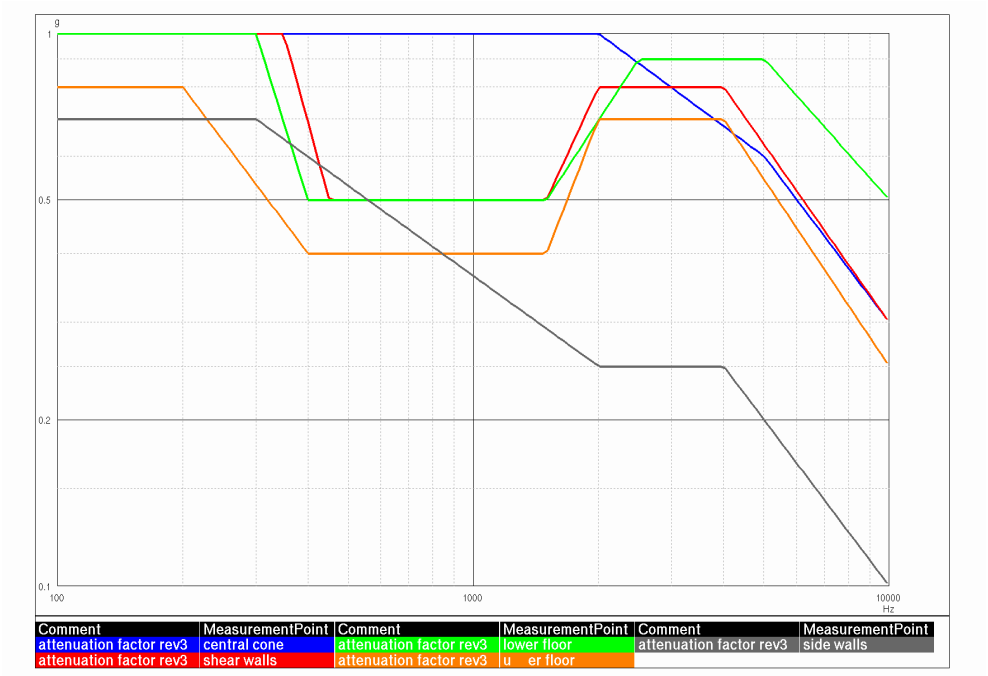

Figure 8-32: Attenuation factor defined for each zone

For each zone, an attenuation factor has been defined. It is then applied to the LV shock specification, in order to derive the estimated flight levels for equipment mounted in that area induced by the fairing jettisoning event:

$$SRS^{equipment}_{estimated.\,flight.level} = ATT\_FACTOR \cdot SHOCK\_SPEC$$

The resulting shock mapping for Herschel-Planck SVMs as upper passenger is shown in the Figure 8-33.

A qualification margin should be considered in the final derivation of shock inputs to the sub-systems.

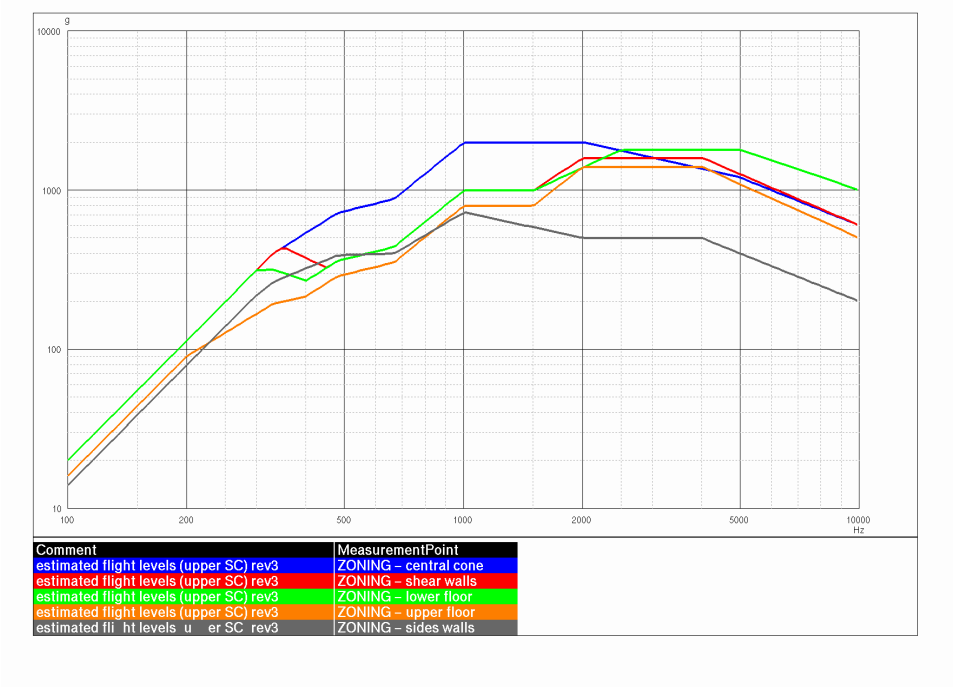

Figure 8-33: Herschel shock mapping - FLL

The closer the design details of the new and reference spacecraft, the more accurate the extrapolations are. It is nevertheless recommended to consolidate the shock zoning through good engineering practices in shock FEA (see 9), in order to identify local responses, which can affect the shock levels of equipment mounted in that area.

The adequacy of this derivation method based on past heritage for the identification of attenuation factors within each zone of interest has been demonstrated on Herschel/Planck, by comparing the test prediction (Figure 8-33) with the actual test data. An example of such comparison is shown in Figure 8-34, where the prediction for the zone of interest is depicted by the black line (defined at qualification level), and where the test data is depicted by the red curve.

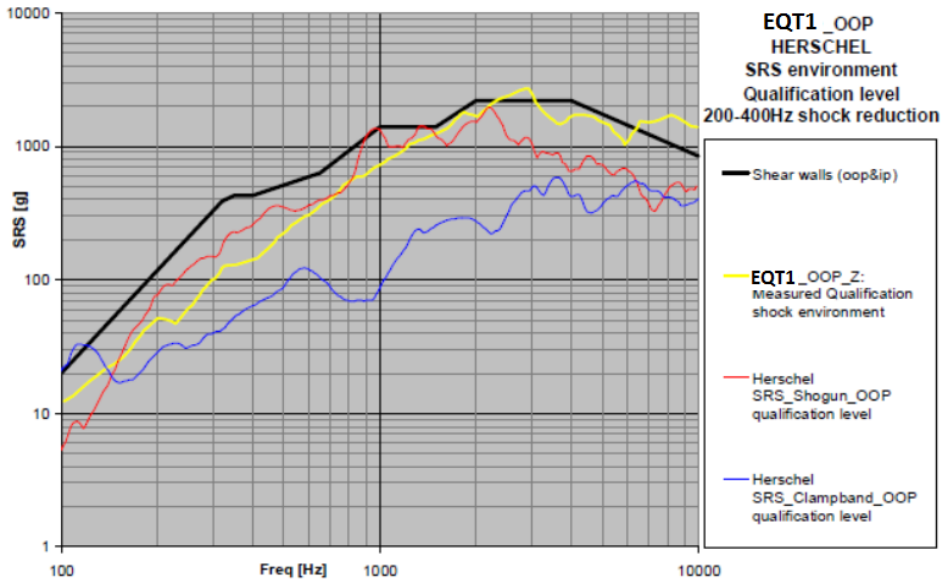

Figure 8-34: Herschel shock mapping – Post test comparison - QL

8.3.3.2 General observations for a better understanding of launcher induced shock propagation

As discussed in paragraph 8.2.3, the zoning operation is essentially based upon engineering judgment and experience. In order to improve the understanding of launcher induced shock propagation and to get a reasonable physical sense of the phenomena, an attempt has been made to **define general rules for shock transmission**. This investigation has been carried out using the ESTEC shock database; six satellites have been considered (PPF-Envisat, ROSETTA, SMART-1, METOP, CLUSTER, MSG).

Some **precautions** should be taken with respect to these observations as they are made on a limited range of spacecraft. Moreover these global phenomena are always superimposed to local phenomena due to local loading, interfaces, and stiffness, resulting in observations different from those listed here. Therefore these statements are true "on average" but can be contradicted at some locations because of local phenomena.

The following observations can be made (see illustration on general observation regarding shock propagation in spacecraft in Figure 8-35 and Figure 8-36):

- Central cone and cylinder:
  - Better shock transmission when travelling through a cone - Radial excitation quickly recombined into axial radial components
  - In contrast to a central cone, a central cylinder limits the shock transmission towards adjacent panels
  - Central cylinder is also more favourable with shock longitudinal transmission

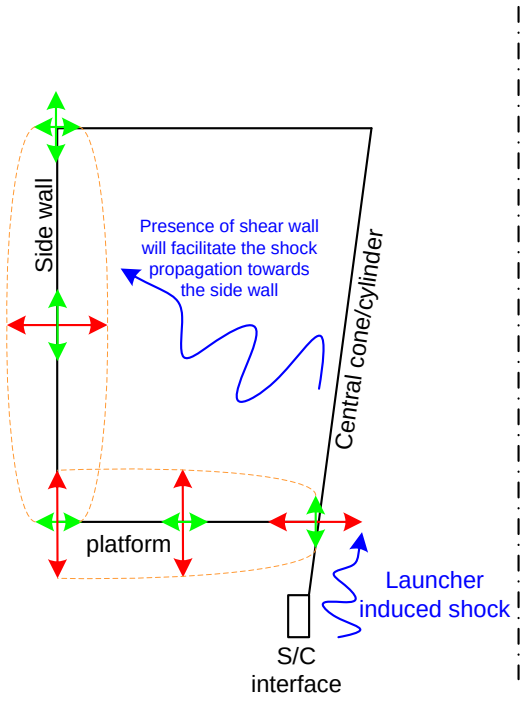

Figure 8-35: General observation on shock propagation through cone/shear walls/platform/side walls

- Horizontal platform connected to central cone/cylinder:
  - Connection to a central cone: Higher IP levels close to the junction
  - Connection to a central cylinder: Consistent IP and OOP levels (lower IP level than with a cone)
  - Higher OOP levels in the free areas of the platform (further away from junction)
- Side walls:
  - Responses generally dominated by OOP levels, this is especially true for large side walls
  - IP levels gain importance close to junctions (with horizontal platform or shear wall)
  - Boundaries conditions (connected along 3 or 4 edges) influence the repartition between IP and OOP. OOP and IP become close together in case the side wall is connected along 3 edges only.
  - Strong interaction between heavy equipment and side wall usually happen in the centre region of the panel
- Shear walls:
  - Good transmissibility through short shear wall connected to a central cone
  - Better transmissibility of IP waves (OOP at least 2 dB lower)
  - Size of shear wall influence the repartition between IP and OOP, OOP levels tend to increase with the size of the shear wall
- Influence of supporting struts (see Figure 8-36):
  - Shock transmission strongly influenced by supporting struts, this generally results in increased levels (both OOP and IP) into the supported platform (example: outer edge of cylindrical platform on MSG or CLUSTER)

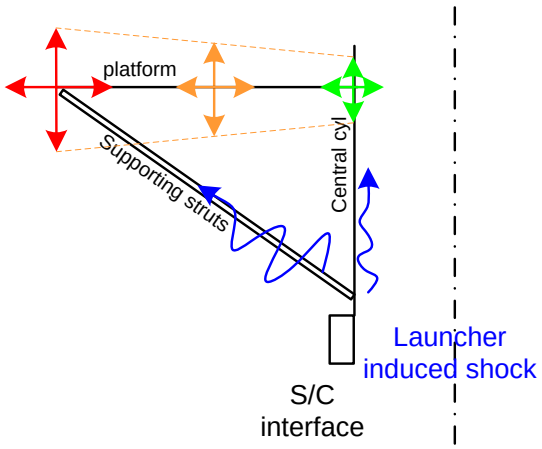

Figure 8-36: General observation on influence of supporting struts

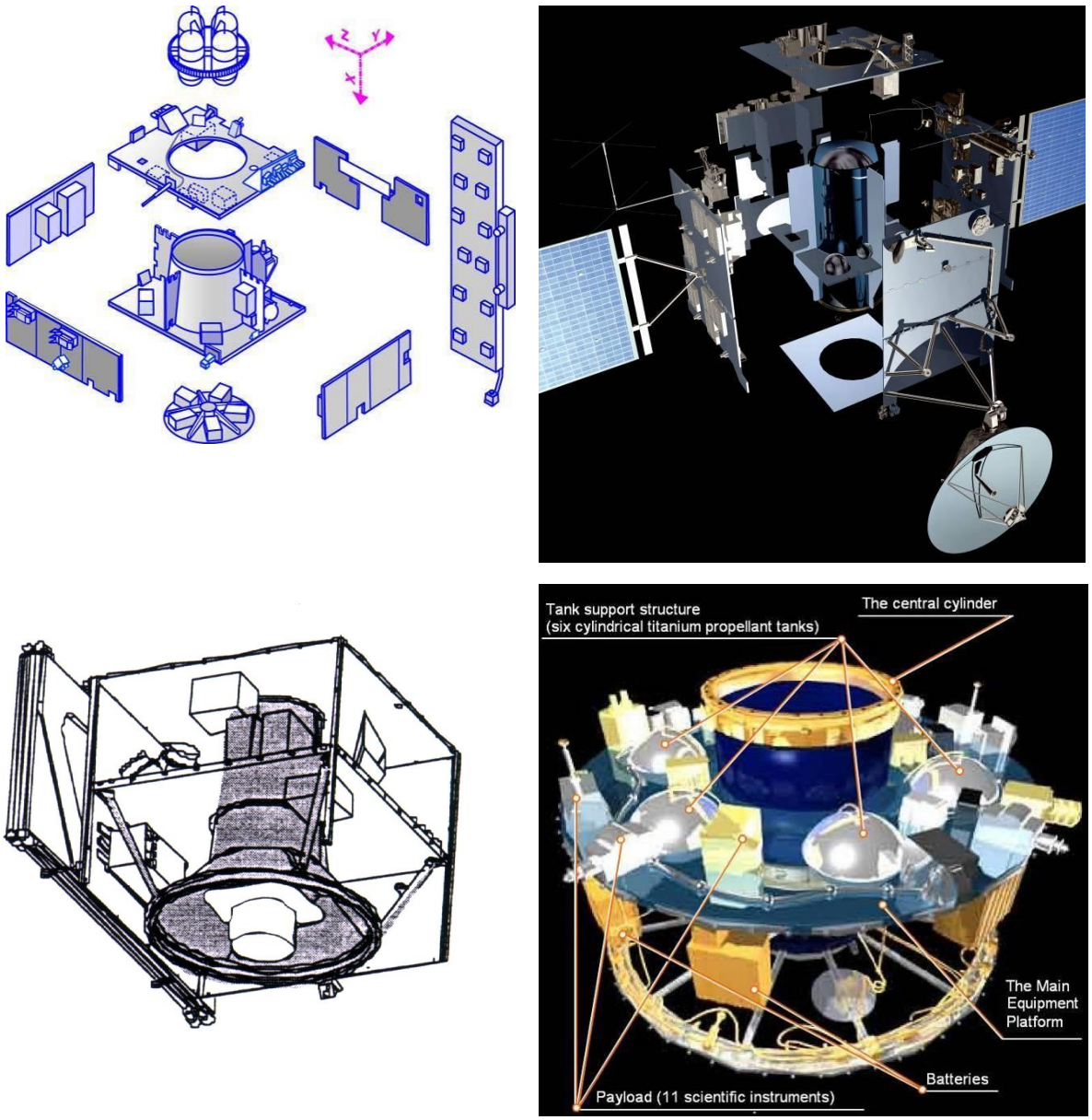

Figure 8-37: Examples of spacecraft architecture

8.3.3.3 Differences between clampband and launcher induced shock

This paragraph highlights the complexity to derive launcher event level with clampband test data, and should not be understood as a guideline for the extrapolation of one excitation type to another (for example from clampband induced shock to a launcher induced shock).

It is recommended in any case to perform a representative test to demonstrate the qualification of spacecraft even if in some cases, when a reference test in available (for instance on one specimen representative of the family in the critical areas of the spacecraft, e.g. close to S/C interface), a correction factor based on this experience can be agreed with launcher authorities and applied on clampband results.

As mentioned previously, it is important to pay dedicated attention to the excitation type in extrapolation methods, since past experiences have shown that the transfer functions are strongly dependent with regard to the configuration of the system test set-up used to identify them. In particular, the transfer functions resulting from a clampband release test are lower than the ones resulting from a Shogun test.

In a zoning procedure, it is strongly recommended to take into account the excitation type (Clampband or Shogun), and to avoid the extrapolation from one excitation type to another.

However, for some special cases, and with the agreement of the launcher authority, this recommendation can need to be re-examined/tailored. Recently this was necessary for MSG2 [RD-014], for which the recording of shock response data during Shogun test were affected by electrical pollution. Only the clampband data could be used to derive a LV "representative" shock environment.

In this frame, some correction factors have been defined based on Shogun and Clampband test data of SMART, CLUSTER, ROSETTA, SPOT5 and E3000 spacecraft. This assessment consisted in comparing SRS ratios identified using two different types of pyroshock tests, Shogun test and Clampband test.

The comparison is based on the ratio:

$$\overline{R} = \frac{R(\text{C/B release})}{R(\text{Shogun test})} \quad \text{where} \quad R = \frac{SRS\ (Q=10)\,\text{Equip}^{t}\ \text{I/F}}{SRS\ (Q=10)\,\text{Spacecraft I/F}}$$

$\overline{R}$ represents the "transfer function" from C/B to Shogun ratios.

$\overline{R}$ can be computed in different ways, as function of the considered direction for the spacecraft interface levels.

Among these combinations, the ones involving different references for the spacecraft interface levels have been rejected. Only ratios $\overline{R}$ with the same references have been retained. The main reason for this choice was to maintain the link with the standard SRS ratio approach, as proposed by the Ariane 5 Launcher Authorities.

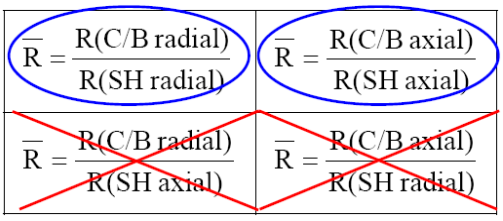

Figure 8-38: Possible combinations from comparing clampband and SHOGUN

The ratios $\overline{R}$, identified from different experiences (SMART, CLUSTER, ROSETTA, SPOT5 and E3000), allow the definition of the correction factors.

Figure 8-39 presents two results of such ratios computed for SMART-1:

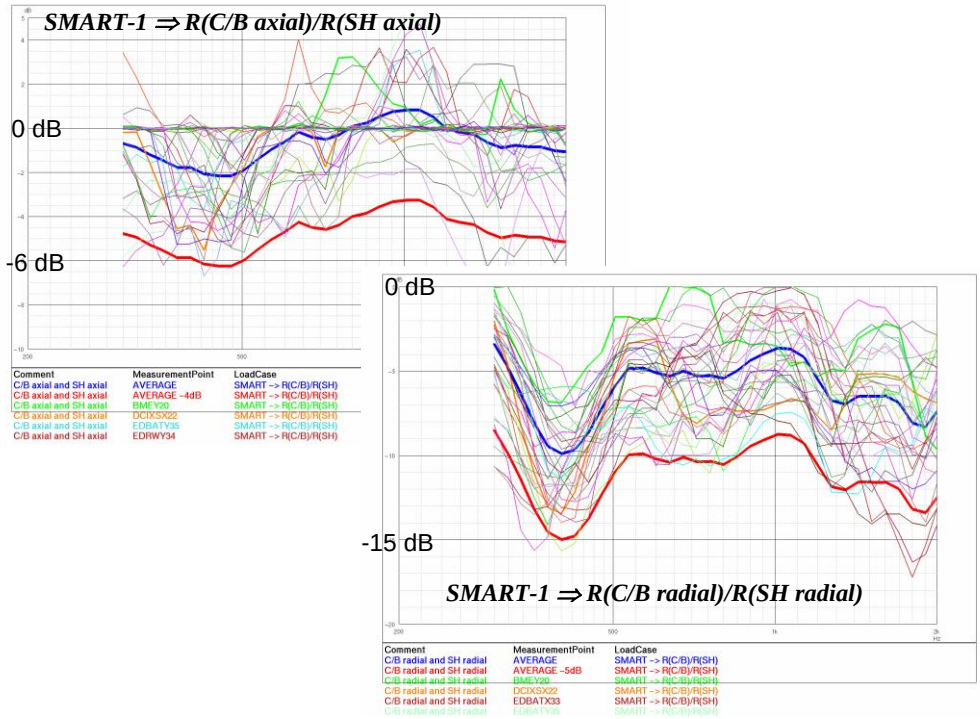

Figure 8-39: Examples of ratio calculated for clampband and SHOGUN

Some general observations can be made:

a. A large scattering of results is observed for one spacecraft (4 dB – 5 dB around average value),

b. This assessment failed to identify a unique "transfer function" from one spacecraft to another,

c. Average (bold blue) and lower envelopes (bold red) are computed. The lower envelope corresponds to the maximum observed difference between C/B and SH,

d. Similarities can be observed between different spacecraft but this is insufficient to establish a definitive trend,

e. The difference in Clampband/Shogun configurations can excite different modes, and some frequency cluster shifts between the two shock tests can explain the discrepancies observed. A small shift could cause great scatter. In order to overcome this problem, the ratios $\overline{R}$ are minimised (in absolute value) at each frequency *fn* by retaining the smallest ratio within the frequency range [0,9 x *fn*, 1,1 x *fn*]. In other words, a dispersion of ± 10 % around *fn* is allowed.

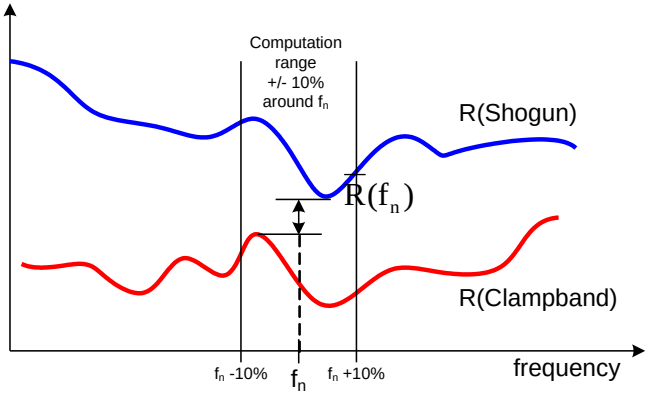

Figure 8-40: Minimisation of effect of frequency shift

f. The final correction factors (Figure 8-41) are enveloping all the considered spacecraft (including scatterings).

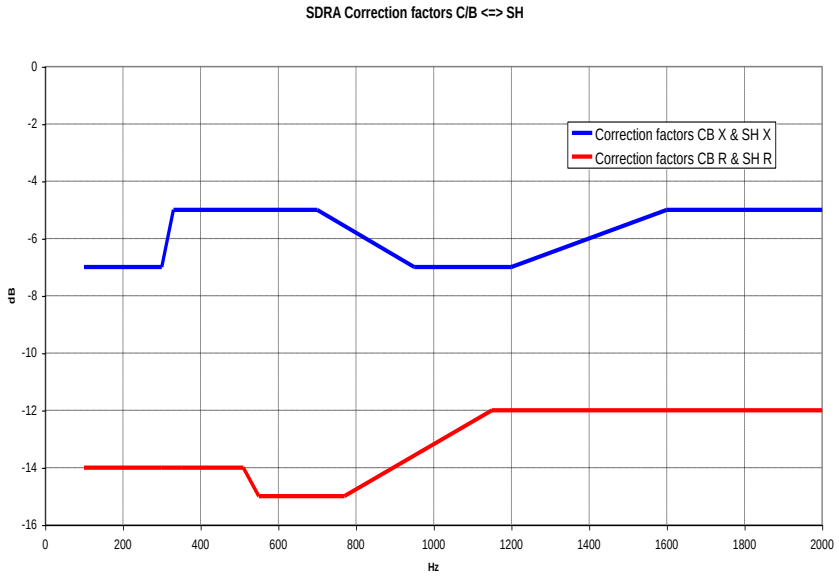

Figure 8-41: Example of final correction factor

This extrapolation method is closely linked to the standard SRS ratio method as recommended by the launcher authorities, but it has been improved taking advantage of the experience gained by ESA in this domain. Different correction factors are identified for axial and radial directions:

$$\gamma_1 = R^{C/B}_{\text{axial I/F}} . Spec_{\text{axial}} + \text{correction factor}^{C/B \Leftrightarrow SH}_{\text{SH axial}}$$

$$\gamma_2 = R^{C/B}_{\text{radial I/F}} . Spec_{\text{radial}} + \text{correction factor}^{C/B \Leftrightarrow SH}_{\text{SH radial}}$$

$$\gamma_{\text{unit}} = \text{Max}(\gamma 1, \gamma 2)$$

Where $$R^{C/B}_{\text{axial or radial I/F}} = \frac{SRS^{C/B\,\text{test}}_{\text{eqt I/F}}}{SRS^{C/B\,\text{test}}_{\text{axial or radial I/F}}}$$

8.3.4 Method D – Unified approach and practical implementation of attenuation rules for typical spacecraft shock generated environments

Major contributors to shock attenuation in spacecraft are path length, orientation (angles) between structure elements joint together and type of joints.

The physical background describes that shock waves are spread over a structure element like plate, cylinder or cone, are reflected at bends and joints and are attenuated in joints due to friction.

Therefore, as a start the attenuation can be estimated by taking into account the sections of a shock path consisting of structures (plates, cylinders, cones) with a certain length, the orientation of this structure (section) compared to its predecessor and the type of joint at the end of the structure section.

The empirical approach given below, allows the consideration of the major contributions. The attenuation effects are implemented via empirical equations and factors which can and need to be fitted to the specific cases.

> The overall attenuation factor between the shock source and the equipment/measurement point is calculated by multiplying the attenuation factors for each section of the shock propagation path. Each section along the transmission path consists in a certain distance, plus a joint. The 'load path angle' required by the attenuation estimation tool is between α=0° and 90° where α=0° typically describes the axial or longitudinal orientation and 90° the radial orientation (typical test set-up with spacecraft launching axis vertical).

Methodologies for estimating the junction attenuation factors $\boxed{Att_{Joint}(axial, radial)}$, and the distance attenuation factors $\boxed{Att_{Distance}(axial, radial)}$, as well as scaling to the input shock specification and consideration of correction factors, are discussed in the following paragraphs.

8.3.4.1 Junction attenuation factors $\boxed{Att_{Joint}(axial, radial)}$

In order to calculate the attenuation over a joint, the orientations of the sections before and after the joint should be taken into consideration. This is realized by introducing the following section orientation factors *e* and *f* (where α_j is the angle between section *i* and section *(i+1)*, see Figure 8-42, *i* referring to section number):

- Axial direction: $f_j = \dfrac{1+\cos^2(\alpha_j)}{2}$
- Radial direction: $e_j = \dfrac{1+\sin^2(\alpha_j)}{2}$

Ratios r_{ax} and r_{rad} of these factors are now calculated: $r_{ax,j} = \dfrac{e_j}{f_j}$ and $r_{rad,j} = \dfrac{f_j}{e_j}$

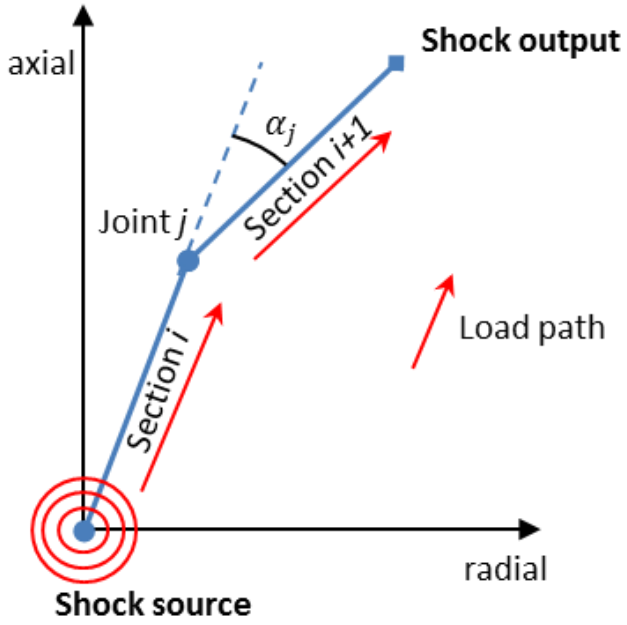

Figure 8-42: Load-path example

The axial and radial junction attenuation factors $Att^{j}_{Joint}(axial)$ and $Att^{j}_{Joint}(radial)$ of one single joint can be calculated (index *j* refers to the joint number), as follows:

- $$Att^{j}_{Joint}(axial) = 1 - r_{ax,j} * \frac{K_{joint}}{20}$$
- $$Att^{j}_{Joint}(radial) = 1 - r_{rad,j} * \frac{K_{joint}}{20}$$

K_{joint} is an additional factor that gives the opportunity to influence the junction attenuation factor by empirically considering different types of joints:

joint damping	K(joint)
1 - low	1
2 - medium	2
3 - high	5

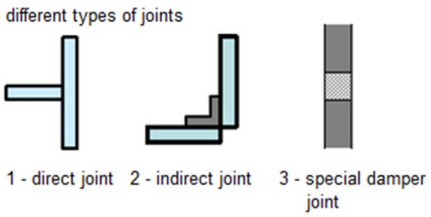

Figure 8-43: K_{joint} definition depending on joint configuration

The axial/radial total junction attenuation factors $Att_{Joint}(axial)$ and $Att_{Joint}(radial)$ are the product of all single junction attenuation factors:

$$Att_{Joint}(axial) = \prod_{j} Att^{j}_{Joint}(axial) \quad \text{and} \quad Att_{Joint}(radial) = \prod_{j} Att^{j}_{Joint}(radial)$$

The following figure provides the junction attenuation factors $Att^{j}_{Joint}(axial, radial)$, as function on the junction angle, and computed for a direct joint ($K_{joint}=1$).

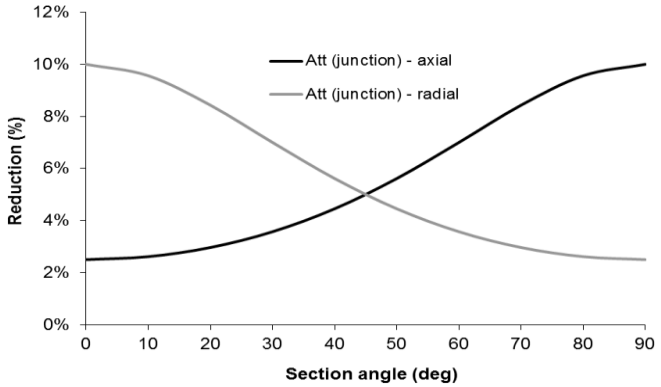

Figure 8-44: Junction attenuation factors $Att^{j}_{Joint}(axial, radial)$ depending on section angle, for $K_{joint}=1$

8.3.4.2 Distance attenuation factors $Att_{Distance}(axial, radial)$

If structures, as there are long struts or beams, are part of the shock load path, the length is of minor importance because these elements guide shock waves without significant attenuation.

At first, an "adjusted" length L_i is calculated in order to consider different types of sections influencing the section attenuation factors with the help of an additional factor K_{struct}, which depends from the structural characteristic of the section.

$L_i = l_i * K_{struct}$ where l_i is the length of the section *i* and K_{struct} defined as follows:

sect. damping	K(struct)
1 - low	0.8
2 - medium	1
3 - high	1.25

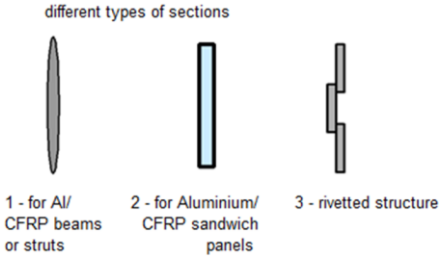

Figure 8-45: K_{struct} definition depending on section configuration

Then, it has to be taken into account that the shock attenuation along sections depends on the direction of shock propagation and the orientation of the section. For example, the axial orientated (0°) part of a shock would propagate without significant attenuation through an equal orientated section.

The resulting distance attenuation factors are derived as follows:

- $Att^{i}_{Distance}(axial) = e^{-e_i \cdot L_i}$, where $e_i = \frac{1+\sin^2(\alpha_i)}{2}$
- $Att^{i}_{Distance}(radial) = e^{-f_i \cdot L_i}$, where $f_i = \frac{1+\cos^2(\alpha_i)}{2}$

The axial/radial total distance attenuation factors $Att_{Distance}(axial)$ and $Att_{Distance}(radial)$ are the product of all single distance attenuation factors:

$$\boxed{Att_{Distance}(axial) = \prod_i Att^i_{Distance}(axial)} \text{ and } \boxed{Att_{Distance}(radial) = \prod_i Att^i_{Distance}(radial)}$$

The following figure provides the distance attenuation factors $Att^i_{Distance}(axial, radial)$, computed for a sandwich panel ($K_{struct} = 1$).

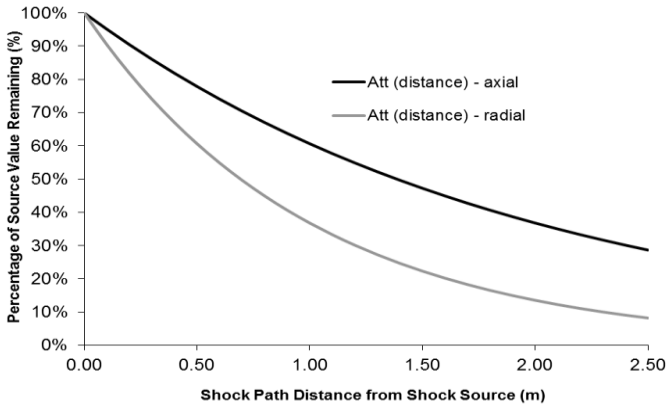

Figure 8-46: Distance attenuation factors $Att^i_{Distance}(axial, radial)$, for $K_{struct} = 1$

8.3.4.3 Calculation of total shock attenuation factors and derivation of shock output

The total shock attenuation factors result from the combination of junction and distance attenuation factors, which may need to be corrected to account for possible uncertainties such as modal responses in low frequency (up to typically around 500-800Hz), or for additional attenuation in high frequency (typically above 5kHz). Opportunity for considering a correction factor is further discussed in paragraph 8.3.4.4.

At this stage, two total attenuation factors are defined:

- $\boxed{Att(axial) = Corr.Att_{Joint}(axial).Att_{Distance}(axial)}$, where *Corr* refers to the correction factor to account for modal responses in low frequencies, or additional attenuation in high frequencies.
- $\boxed{Att(radial) = Corr.Att_{Joint}(radial).Att_{Distance}(radial)}$

Which should then be scaled to their respective input specification. **This last step requires the knowledge of the nature of shock input to the spacecraft (e.g. axial input, radial input or balanced axial/radial input):**

- Case of shock specification defined for each direction axial and radial (e.g. Ariane 5 HSS1 separation event, with 2 specifications provided by the launcher authority):

  $$\boxed{Shock\ output = MAX[SPEC(axial)\ x\ Att(axial)\ ;\ SPEC(radial)\ x\ Att(radial)]}$$

- Case of balanced input axial/radial to the spacecraft case of lack of knowledge on the nature of the shock input (e.g. typical launcher separation event):

  $$\boxed{Shock\ output = MAX[SPEC(envelope)\ x\ Att(axial)\ ;\ SPEC(enveloppe)\ x\ Att(radial)]}$$

- Case of shock specification dominated by axial input to the spacecraft (e.g. VEGA HSS separation, or point source excitation):

$$\boxed{Shock\ output = SPEC(axial).Att(axial)}$$

- Case of shock specification dominated by radial input to the spacecraft (e.g. Clampband):

$$\boxed{Shock\ output = SPEC(radial).Att(radial)}$$

8.3.4.4 Correction factors

Test evaluations have shown that correction factors are necessary in the following cases:

- **Case of launcher induced shock** (egg stage and fairing separations) – As the excitation is occurring below the spacecraft interface, the responses inside the spacecraft are influenced/promoted by the launcher modes (such as breathing modes of main interfaces or membrane modes of payload adapter). Correction factor to account for modal responses occurring at low frequency (up to typically 500-800Hz, mainly depending on the size of the spacecraft and on the type of launch vehicle) is by principle spacecraft/launcher dependent, and as such a correction factor identified on one spacecraft can become inaccurate when applied to another spacecraft.

  An attempt has been made to identified a set of correction factors from comparison between analytical predictions and system shock test results, depending on the type of launcher shock (VEGA or Ariane 5) and on the type of spacecraft structure (structure with internal cone or box structure). Those correction factors are provided as an illustration (Figure 8-47), and may change when additional system shock test results become available. Applicability of those correction factors is therefore not guaranteed for any type of spacecraft configurations and for any type of launchers.

  NOTE In the following example, correction factors are defined both in low frequency (to account for modal responses), and in higher frequency (resulting from observations made from test results).

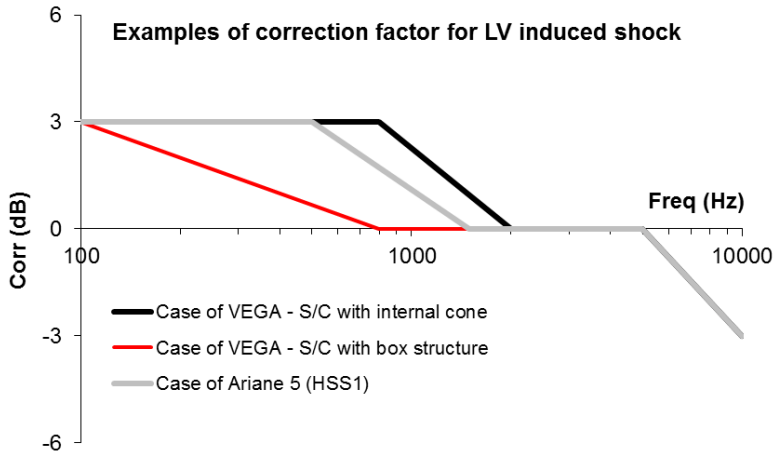

Figure 8-47: Example of correction factors for launcher induced shock

- **Case of Point source excitation** – As compared to the attenuation rules specifically identified for point source excitation (see paragraph 8.3.1), the distance attenuation factor considered herein (see Figure 8-46) overestimates the attenuation close to the shock source. A correction factor should be then considered up to 30 cm from the shock source in order to maintain the full transmissibility to 100%.

8.3.4.5 Methodology correlation with test results

Adequacy of the methodology 8.3.4 has been checked with respect to various type of shock excitation (Clampband, point source, launcher shock).

In the following Figure 8-48, the attenuations measured during tests (launcher shock – Type Shogun) have been conservatively predicted using the methodology 8.3.4 (with consideration of correction factors for launcher induced shock, in this case):

- The RED curves corresponds to the prediction using the methodology 8.3.4 (including correction factors in low and high frequency) for different zones of the considered spacecraft (Smart-1, Rosetta, Artemis, PPF, Herschel).
- The BLUE curves corresponds to the prediction using direct heritage (methodology 8.3.3).

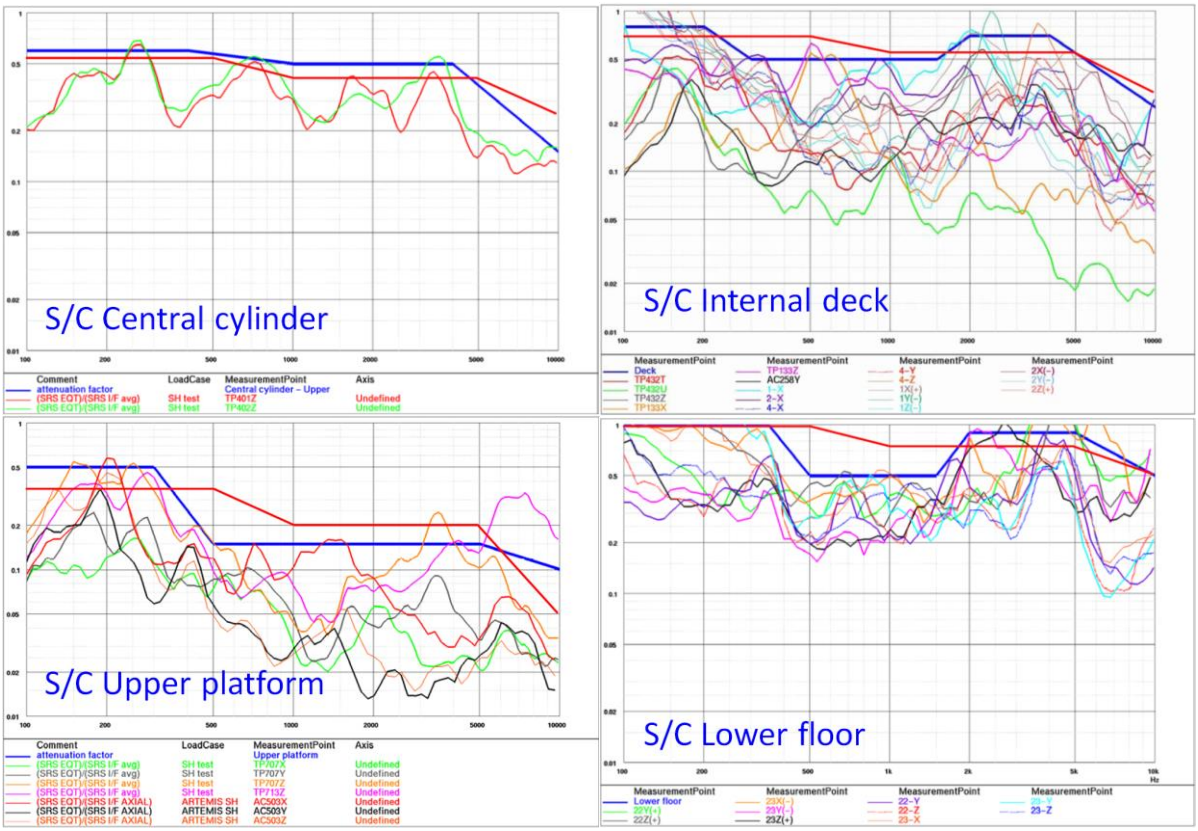

Figure 8-48: Illustration of methodology correlation on Sentinel 3 VESTA test

8.3.4.6 Example of implementation of the methodology

An example of the implementation of the methodology is provided hereafter.

The considered spacecraft presents a classical design with central cone / shear walls / lateral walls, and the prediction is made for an equipment accommodated on a lateral wall.

The most direct loadpath (and "stiffest" loadpath) goes through the central cone, then through the shear wall, and finally through the lateral wall. Each section along the loadpath is identified (including loadpath angle, distance, type of joint and type of structure), and the resulting attenuations are derived for both the axial and radial shock input directions, see Figure 8-49.

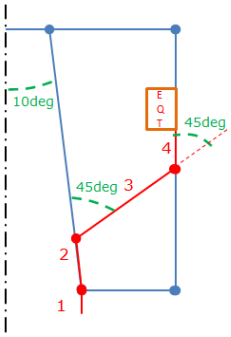

-Y panel DPU Loadpath along shear web

Input Data					Axial Shock Attenuation				Radial Shock Attenuation				
Section	Joint Factor	Structure Factor	Joint Angle	Length	e	e/f	Total Factor		f	f/e	Total Factor		
	Kjoint	Kstruct	degs	m			Att(axial)	dB			Att(radial)	dB	
1	0.0	1.0	0	0.050	0.50	0.50	**0.98**	-0.2	1.00	2.000	**0.95**	-0.4	LVA
2	0.0	1.0	-10	0.450	0.52	0.52	**0.79**	-2.0	0.98	1.912	**0.64**	-3.8	Cone
3	1.0	1.0	45	0.420	0.75	1.00	**0.69**	-3.2	0.75	1.000	**0.69**	-3.2	Shear
4	2.0	1.0	-45	0.140	0.75	1.00	**0.81**	-1.8	0.75	1.000	**0.81**	-1.8	Panel
TOTAL				1.060			**0.43**	-7.2			**0.34**	-9.3	

Figure 8-49: Example of implementation of the methodology

Once the attenuation factors are defined for each location, they should then be scaled to their respective input specification, applying the combination procedure as explained in the paragraph 8.3.4.3. At this stage, the correction factors from paragraph 8.3.4.4, should also be applied when relevant (launcher shock, and point source shock). And finally, a qualification margin of 3dB should be added to all scaled environment.

8.3.5 Additional attenuation factors

In addition of previously defined attenuation factors based on similarity-heritage-extrapolation methods, additional attenuation parameters can introduce shock attenuation and thus can be cumulated.

A list of commonly agreed attenuation factors is given hereafter:

- Effect of heatpipes: In relation to the point source excitation, an attenuation of -3 dB above 3000 Hz can be taken into account with respect to the shock environment predicted/measured on the structure at heatpipes interface.

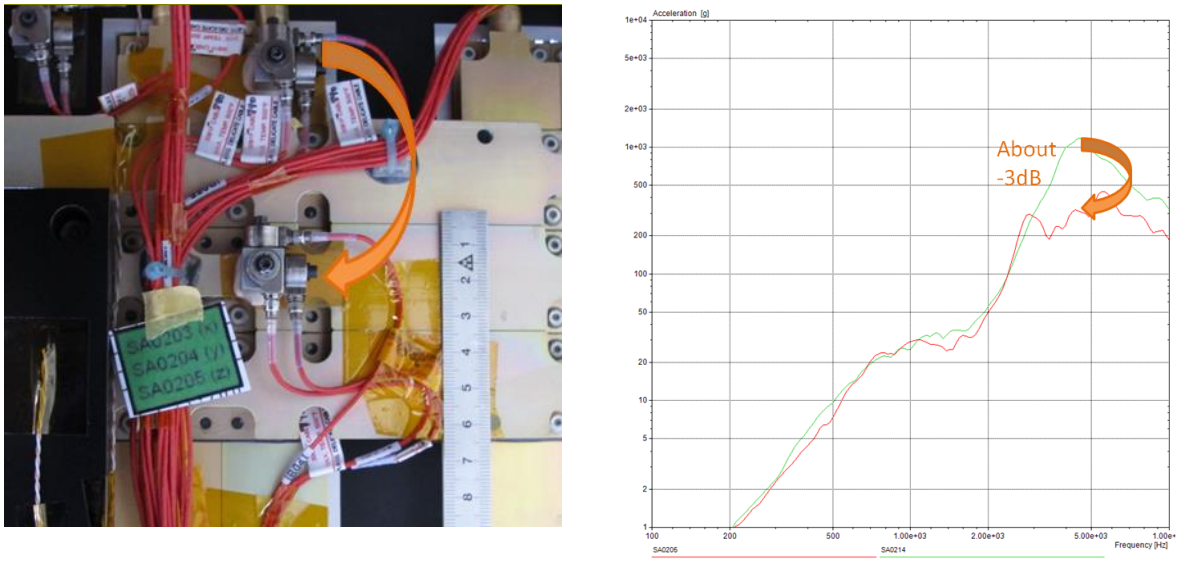

Figure 8-50: SRS attenuation in plane (blue) out of plan (red) due to Heatpipe

- Effect of equipment mass: for equipment heavier than 5 kg, an attenuation of -3 dB on the entire frequency range can be taken into account with respect to a non-loaded or very lightly loaded structure (for a given location).

8.3.6 Method E – Shock responses in instruments

The different methods presented in previous paragraphs 8.3.1 (A), 8.3.2 (B), 8.3.3 (C) and 8.3.4 (D), can only be applied along the primary load path of a satellite structure (propagation of shock along main spacecraft structure e.g. central tube, shear-wall and panels), hence valid up to the interface with equipment and instruments.

Once the shock input is derived at the equipment or instrument interface, the general approach for shock verification, as presented in paragraph 12.1 (Part 3), should be followed; covering some considerations on compliance to severity criteria (paragraph 12.4), equivalence with other mechanical environment (paragraph 12.5), or verification by similarity (paragraph 12.6). In case the capability to withstand the qualifying shock environment cannot be established, a coherent test programme is established, encompassing shock testing.

If this approach is well established for equipment shock verification, the case of instrument usually requires a specific verification logic (see paragraph 12.7).

For instruments, typically mounted on Iso-Static-Mounts, the dynamic behaviour is dominated by the main global modes, which tend to filter the higher frequency environment. The so-called isolation effect depends on the frequency decoupling between the main global modes and the frequency content of the shock excitation, depends on the effective masses of those global modes and on their associated damping.

Ideally for instruments suspended at low frequency around 100Hz (or below) with most of the mass participating on the main global mode, the isolation effect will be more efficient, as compared to instruments suspended at higher frequency than 100Hz or with complex dynamic behaviour (i.e. effective masses split in between several modes). These two cases are illustrated in the following figures:

- Case 1 – In the Figure 8-51, is illustrated the case of an instrument having a main axial mode with a large effective mass (90% in this case). A dominant axial mode with low damping, and excited in this case with an axial excitation (from a fully representative system shock test), results in the situation where the response on the Optical Bench is amplified in correspondence to the main mode, but at the same time an effective isolation can be observed in the higher frequency range.
- Case 2 – In the Figure 8-52, is illustrated the case of an instrument presenting a more complex dynamic behaviour (Optical Bench with main modes up to 200Hz, mounted on a Main Structure with modes up to 1kHz). The responses on the Main Structure and on the Optical Bench, as observed during a fully representative system level shock test, are clearly driven by the modal response of the main modes. The amplification region extends to about 300Hz, and at the same time a less effective isolation can be observed in the higher frequency range.

In a general case, the shock response inside an instrument is driven by its dynamic behaviour, in conjunction with the nature of the shock excitation (i.e. on the ability of the shock input to excite the main modes of an instrument). As such, the shock response inside an instrument cannot be derived from application of some shock attenuation rules, as function of distance and number of junctions.

NOTE The nature of the shock excitation as seen at the instrument interface, namely in terms of direction of application and spatial coherence, directly influences the response of the main modes. For example, a shock input seen as spatially coherent at the instrument interfaces, promotes the response of the main modes in the direction of the shock excitation, and may lead to a situation where the shock input is actually amplified.

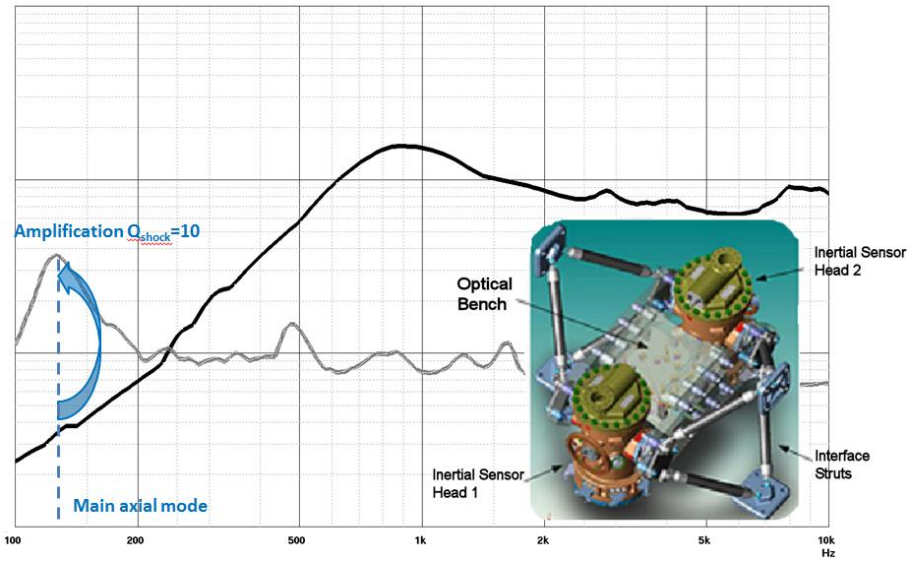

Figure 8-51: Instrument shock response – Instrument presenting main mode with large effective mass – Optical Bench on Lisa Path Finder

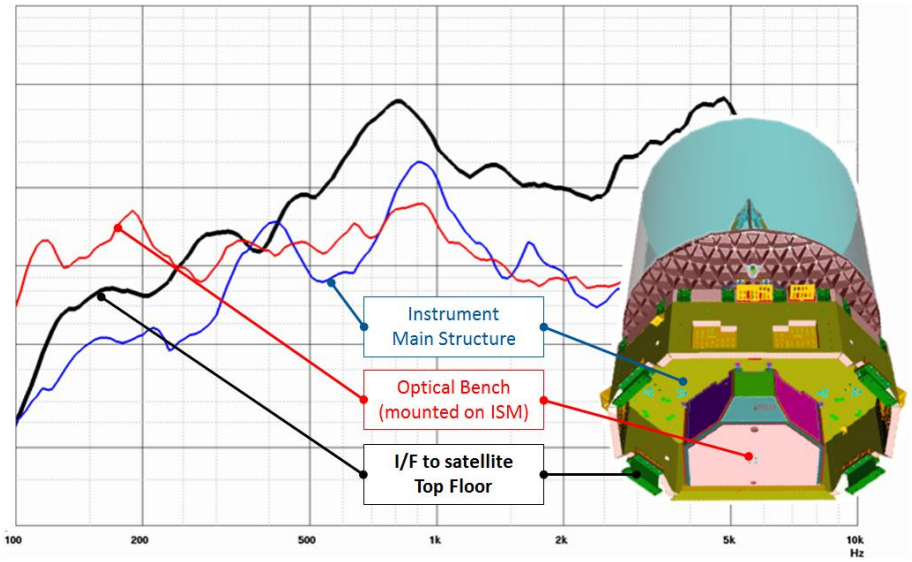

Figure 8-52: Instrument shock response – Instrument presenting a more complex dynamic behaviour – Main instrument on Aeolus

Considering the above, the prediction method for shock responses in instruments should be defined, such that the dynamic behaviour is taken into account. Some general methods are herein proposed, however they may not cover all application cases and variations around those are possible. From the proposed methods E-1 and E-2 (see paragraphs 8.3.6.1and 8.3.6.2), some analogies can be clearly established with equipment shock analysis (see paragraph 18.2.4), and therefore the related paragraph in Part 4 is a useful complement to the proposed Methods E-1 and E-2.

In all cases, the prediction should be made at qualification level (including 3dB qualification factor) and should account for an additional uncertainty factor, which depends from:

- The design maturity of the instrument – with instrument design still subject to changes or model uncorrelated, implying an uncertainty factor of at least 3dB,
- The availability of test or consolidated data – with consolidation activity of the selected method based on a representative heritage or prediction based on instrument level test data (either with correlated model or with direct usage of test data), allowing reducing the uncertainty factor accordingly.

8.3.6.1 Method E-1: Transmissibility approach – transfer function scaled to input shock specification

This method is closely derived from the one established for equipment shock response prediction based on transmissibility (see paragraphs 18.2.3 and 18.2.4.4.1), with some minor adaptations to account for a lower transition frequency in the case of an instrument mounted on Iso-Static-Mounts. The main steps are recalled hereafter:

1. Determine instrument transmissibility function $FRF_{sine}(f)$, under a sine excitation on a rigid interface (obtained from a shaker test or by analysis). In case $FRF_{sine}(f)$ is identified from analysis, attention should be drawn to the damping assumption, ideally justified from a representative heritage.
2. The transmissibility identified during sine sweep (test or analysis) considers that the full resonance is reached on each mode. In shock regime, the transmissibility is lower due to the transient type of excitation (see paragraph 18.2.2), and needs to be corrected to obtain an approximation of the shock transmissibility function $TF_{shock}(f)$ as follows:

$$TF_{shock}(f) = \sqrt{2.FRF_{sine}(f)}$$

3. The resulting shock transmissibility function should then be scaled to the input specification of the instrument, in order to derive the internal responses of the instrument.
4. Finally the response prediction resulting from the previous step needs to be corrected in higher frequency, by maintaining a constant SRS level (i.e. plateau) from the maximum SRS peak response obtained in the window [100-1000Hz].

   The reason for this correction being that the SRS in the higher frequency converges towards the maximum value of the transient acceleration, and in case of excitation of instrument main modes, the maximum temporal is usually experienced in correspondence to the response of the main modes.

The method should be applied for each axis of excitation, and resulting envelope be considered at the output location, unless a dominant direction of excitation is expected at the instrument interface.

This method has the advantage to be relatively easy to implement, from the moment a detailed FEM of the instrument is available, or better, test data or correlated FEM are available. On the other hand, the method assumed a spatially correlated input, which in turn can lead to an overestimation of the instrument responses, in case such in-phase load imposition is not representative with respect to the instrument input once integrated on the satellite.

8.3.6.2 Method E-2: Transient analysis approach – coupled analysis with platform

The second method is based on a transient analysis, performed on the complete satellite model, hence including detailed models of the platform and of the instrument. Examples of such predictions are presented in paragraph 9.5, and are repeated herein.

This method has the advantage to better represent the mechanical impedance at the instrument interface, as well as the coupling between the instrument and platform modes. On the other hand, the method assumes that a detailed model of the satellite is available, as well as knowledge on the modelling aspects (see paragraph 9.2.4) and forcing functions definition (see paragraph 9.5).

9
Shock inputs derivation by numerical analysis

9.1 Numerical simulation principles

9.1.1 Rationale and limitations

Numerical simulation (based on FEA and/or SEA approaches) is another tool that can be used to **evaluate a shock environment in a spacecraft**.

Concerning FEA approach, the aim is to use a standard FEM (i.e. the model used for dynamic analyses), to modify it (as low as possible) in order to make it suitable for shock prediction analysis and to run a transient response analysis to get the acceleration levels at desired locations in the spacecraft. Several FEA numerical methods exist to deal with these shock prediction analyses (see 9.2).

There are **many limitations** to such methods. As the physics of shock is complex, it can only be modelled by simplifying the reality. Important modelling aspects are presented hereafter to help users to have a FEM as suitable as possible for shock prediction analysis: e.g. meshing (see 9.2.4.1), damping (see 9.2.4.7), source modelling (see 9.2.4.8), equipment modelling and junctions modelling (see 9.2.4.6).

Even with a FEM as good as possible shock predictions at system level remains a tough job which does not provide perfect results. As a matter of fact such a numerical method does **not produce well-correlated results with test results at every location**. For instance, the measured levels at a given point can be very different from the measured levels at very close points just because very local conditions differ (positions with respect to local boundary conditions, local loading, even by the accelerometer itself). This is never precisely reproduced by FEM analysis.

Experience has shown that the best predictions are made in the following domains:

- Frequency range of validity: generally low or medium frequency (at the most < 2 kHz) rather than high frequency. Clampband release can be properly evaluated up to those frequencies thanks to its excitation specificity (see 7.4.3). However for more complex shock source such as Shogun, the upper limit of validity is lower: this upper limit is rather about 600 Hz - 800 Hz for an implicit code such as Nastran. Nevertheless explicit codes give usually better prediction at higher frequencies (up to several kHz) provided the Finite Element Model has been adapted to such a frequency range (especially in terms of meshing size).
- Spatial range of validity: limited to far-field. The high levels seen in near-field area are mainly driven by non-linear phenomena with especially badly known damping. That is why the shock evaluation can only be valid in far-field area where modal content, correctly modelled in the usual FEM, are important contributors to shock levels.

As a consequence **numerical analysis is a tool that should be used in conjunction with other ones** (such as similarity methods) to consolidate results or design choices. It should never be used alone.

Experience has shown that system level FEM, which are usually available at PDR/CDR, can be used to derive a conservative shock environment in the intermediate phase of a project. The simulation results allow consolidating the spacecraft zoning that has been based on similarity methods during early project phase (SRR level).

An example of such a combination between shock level evaluation at low frequency by FEM analysis and shock level evaluation by similarity methods is given hereafter (Figure 9-1): the left figure shows the result of numerical analysis and the left figure shows the test data to which the studied case has been considered similar. The essential point is to evaluate the consistency between the two approaches: here it is based on attenuation and presence of low frequency modes but not on absolute shock levels.

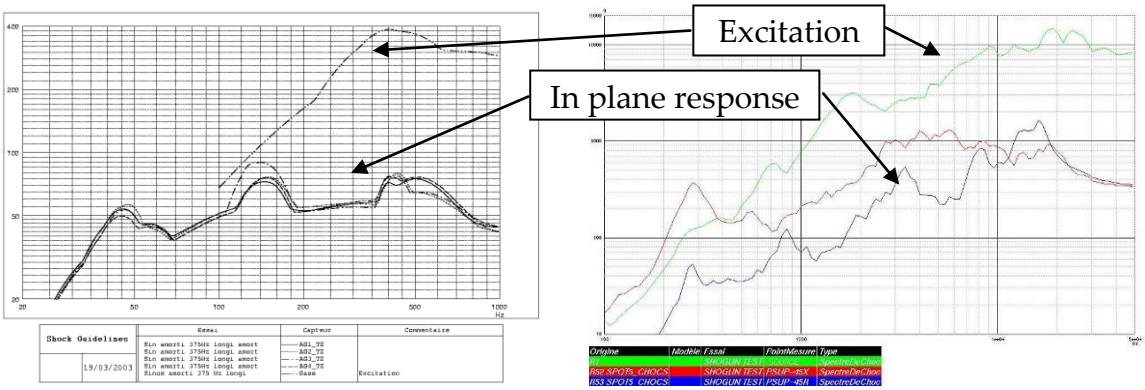

Figure 9-1: Comparison of results from numerical analysis and similarity methods

During final verification process (QR level) detailed numerical analyses can indeed be used to consolidate qualification status of certain equipment by deriving shock levels at unit interface. Special attention needs to be paid to a proper representation of equipment (according to test conditions – e.g. dummy or real equipment) and the selection of appropriate restitution points (according to sensor location during test). More detailed descriptions are given in paragraph 9.2.4.

9.2 Finite Element Analysis (FEA) Numerical methods

9.2.1 Comparison of explicit and implicit methods

Table 9-1 compares advantages and disadvantages of the transient explicit and implicit solution methods.

Table 9-1: Advantages/Drawbacks of transient implicit and explicit methods

	Explicit	Implicit
Physical phenomena	Fast dynamic transient, fast oscillating responses; fast dynamic loading	Static and ~~low~~ dynamic at low frequency range, low frequency responses Simple loading functions
Linearity of the phenomena	highly nonlinear behaviour	Linear behaviour or moderate dependent nonlinear behaviour
Stability	☹ Conditional stability $\Delta t < \Delta t_c$	☺ Always stable
Time step	☹ Small Δt (μs)	☺ Large Δt (ms)
Precision	☺ ≈ $(\Delta t)^2$	☺ ≈ $(\Delta t)^2$
Matrix inversion	☺ $[M]^{-1}$ (diagonal matrix)	☹ $([M]+\alpha[K])^{-1}$ (non diagonal matrix)
Convergence	☺ No need of global resolution → "Element-by-Element" approach	☹ Need of global convergence at each step
Software Robustness	☺ High (High and Coupled non linearities)	☹ Low (Null pivots, Divergence)
CPU requirement	☺ Low	☹ High
Memory requirement	☺ Low	☹ High

The use of explicit solution is indicated when the event is highly dynamic or dominated by wave propagation and when the event's duration is relatively short. That is the reason why **explicit solutions are recommended for shock transient calculation**. Explicit solution is more recommended to specific case where non-linear effects are dominant while implicit solution can be considered when the influence of non-linear effects is negligible.

Figure 9-2 illustrates a comparison of the fields of application for transient implicit and explicit methods.

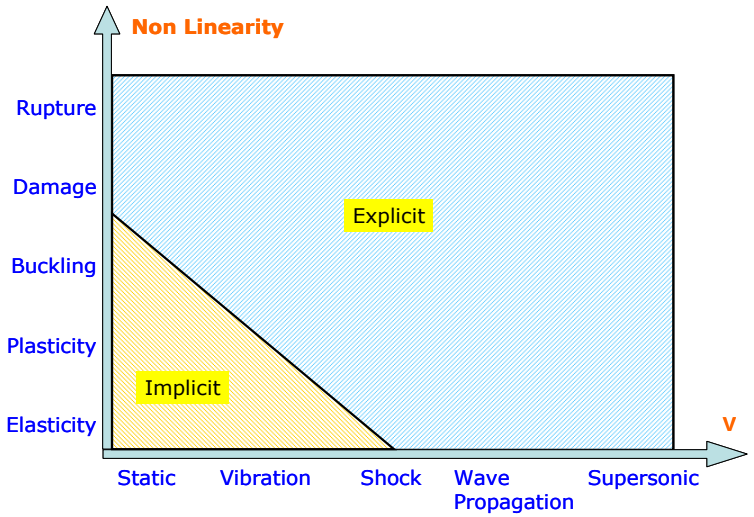

Figure 9-2: Comparison of transient implicit and explicit methods

The use of implicit solution is indicated to solve transient linear problems directly because all boundary conditions at all nodes are simultaneously satisfied, whereas with explicit methods, boundary condition or load are propagated one row of elements per time step.

9.2.2 Explicit and implicit integration schemes

The principle of both solutions can be explained on a linear spring-mass system without damping or SDOF as follows (Figure 9-3):

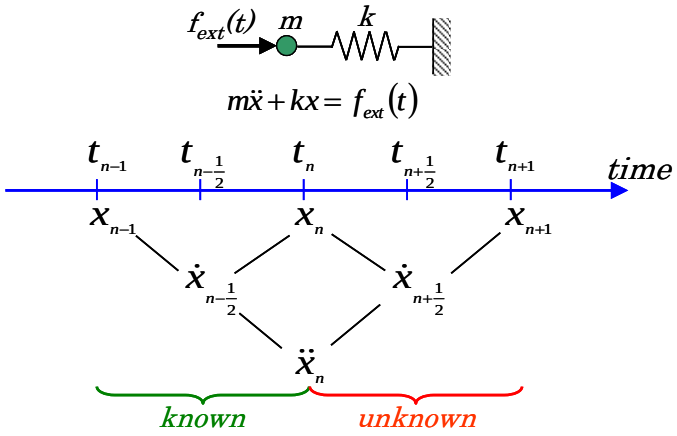

Explicit integration scheme (Central Difference Calculation)	Implicit integration scheme (Newmark-beta method β=1/4, γ=1/2)
$\ddot{x}_n = \frac{f_{Ext}(t_n)-kx_n}{m} = \frac{f_{Ext}(t_n)-f_{Int}(t_n)}{m}$	$x_{n+1} = \left(\frac{4m}{\Delta t^2}+k\right)^{-1}\left[f_{Ext}(t_{n+1})+m\left(\frac{4}{\Delta t^2}x_n+\frac{4}{\Delta t}\dot{x}_n+\ddot{x}_n\right)\right]$
$\dot{x}_{n+\frac{1}{2}} = \dot{x}_{n-\frac{1}{2}} + \ddot{x}_n\Delta t_n$	$\ddot{x}_{n+1} = \frac{4}{\Delta t^2}(x_{n+1}-x_n)-\frac{4}{\Delta t}\dot{x}_n-\ddot{x}_n$
$x_{n+1} = x_n + \dot{x}_{n+\frac{1}{2}}\Delta t_{n+\frac{1}{2}}$	$\dot{x}_{n+1} = \dot{x}_n + \frac{1}{2}\Delta t(\ddot{x}_n+\ddot{x}_{n+1})$

Figure 9-3: Principle of implicit and explicit integration scheme on a SDOF system

The advantage of the explicit method is that only the mass appears in the denominator. The main disadvantage of this solution is that the requirement on stability puts an upper limit on the time step Δt (see 9.2.4.2)

The advantage of the implicit method is that the integration scheme is independent of the value of Δt. But the main disadvantage is the need to invert that both *K* and *M* matrices.

9.2.3 Example of simulation codes (implicit and explicit)

A non-exhaustive list of commercial FE codes able to drive shock numerical simulations is given in Table 9-2.

Table 9-2: Example of FE codes

Explicit FEM codes	Implicit FEM codes
LS-DYNA	NASTRAN
PAMSHOCK	ABAQUS
RADIOSS	SAMCEF
ABAQUS	
DYTRAN	

Model adaptation from one simulation code to another is often a delicate problem. Dynamical system model are often available, but they are initially designed for low frequency analysis. They are not a priori relevant for wave propagation problem of short duration.

Guidelines to improve the FE model fidelity at higher frequency are discussed in the following paragraph 9.2.4, covering meshing size, element type, modelling of equipment/junction, restitution point, damping and time step.

The simulation code should be selected according to the effect/response which need to be identified taking into consideration advantages and drawbacks of transient implicit and explicit methods summarized in paragraph 9.2.1. For example, for system that can be approximated as linear in the frequency domain of interest, then implicit codes are well suited and easier to use. On the contrary, if non-linear effects and/or highly dynamic are expected then an explicit code becomes more suited.

Implicit simulation codes are generally well suited to address most of the shock prediction problems in spacecraft (as discussed in paragraphs 9.5.1, 9.5.2 and 9.5.3), however some problems involving non-linear and fast systems imply that an explicit simulation code should be used. In complement to the already provided examples of such explicit simulations within this handbook (see paragraphs 7.4.6 and 9.5.4), the following one presents the detailed definition of the ESA/ESTEC shock test facility, namely for the material selection of anvil plate, hammer radii and masses (see [RD-047]). The anvil plate and its plastic deformation has been taken into consideration (yield model) and multi-body motions have been modelled allowing simulating the hammer impact from different drop heights. During the test campaign, aluminium, copper and steel have been used for the anvil plates. Simulations with these different materials showed that the choice of the anvil plate material effects only frequencies above 1000Hz.This complies fully with test results.

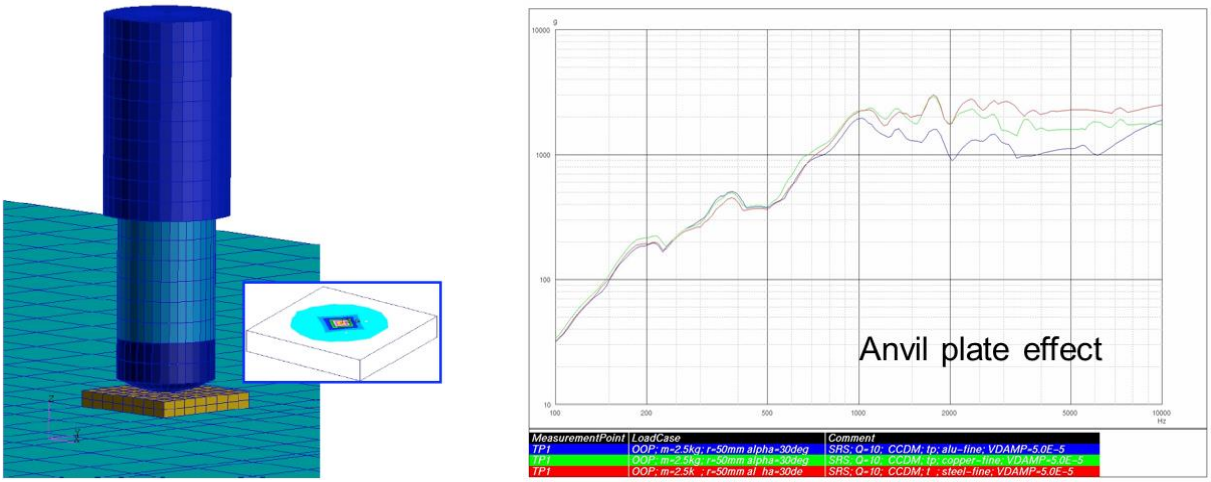

Figure 9-4: Explicit simulation in support to the definition of the ESA/ESTEC shock test facility (anvil plate material selection, hammer radii and masses)

9.2.4 Modelling aspects

This paragraph addresses the modelling aspects related to FE Analysis (implicit or explicit) needed to increase the model FE fidelity especially at high frequency.

9.2.4.1 Meshing size

Dynamic simulations consist first in meshing the considered system. If elements size should be the biggest as possible to limit the CPU time, their definition is first of all guided by minimal acceleration wavelength susceptible to propagate into the system for an observation frequency f_{max}. The mesh size is therefore guided by the shortest wavelength corresponding to a shear, flexural or traction-compression wave.

Aerospace structures are generally composed of aluminium or carbon-epoxy sandwich. Dimensioning wavelengths are thus generally:

- Flexural wave in aluminium sandwich
- Shear wave in CFRP plates.

The definition of the mesh size is a very important task in the frame of the shock FEM numerical simulation because numerical errors can be caused by the non-correct selection of the number of element per wavelength.

In the following example the influence on the results due to the choice of different mesh size is shown. A sample square aluminium plate with 2D shell elements (Figure 9-5) has been modelled with different element length to ensure diverse numbers of elements per bending wavelength up to 40 kHz (Table 9-3) and an half-sine pulse has been applied to the FE model to simulate a shock event.

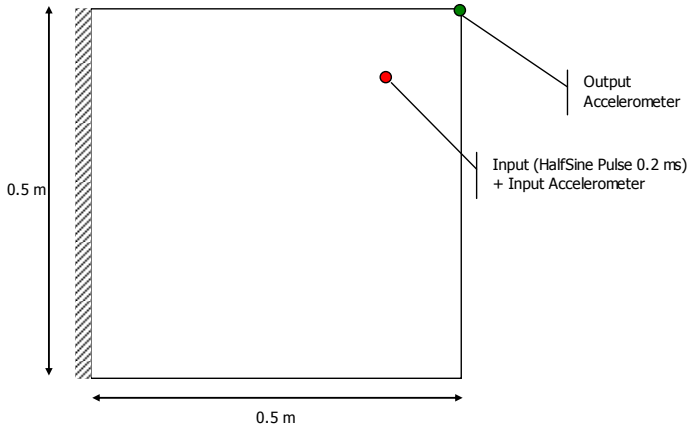

Figure 9-5: Sample square aluminium plate with 2D shell elements

Table 9-3: Element length per bending wavelength up to 40 kHz

$\lambda / \Delta x_{(40kHz)}$	$\Delta x_{(40kHz)}(mm)$
4	12.0
8	6.0
16	3.0
28	1.71

Displacement contour plots at different time step, for the different element lengths, are illustrated in Figure 9-6, Figure 9-7 and Figure 9-8. The simulation cases related to 16 and 28 numbers of elements per bending wavelength provide the same responses while the responses coming from the simulation cases related to 8 and 4 numbers of elements per bending wavelength are less accurate.

Moreover the FE numerical analysis results was also assessed with respect to the shock response spectra at different locations (i.e. at the input and output nodes). Results are plotted in Figure 9-9.

Outcome of this SRS comparison indicates that the accuracy of the FE numerical analysis is of the same order of magnitude for all simulation cases, also showing that a mesh size with 4 numbers of elements per bending wavelength can provide good enough SRS spectra.

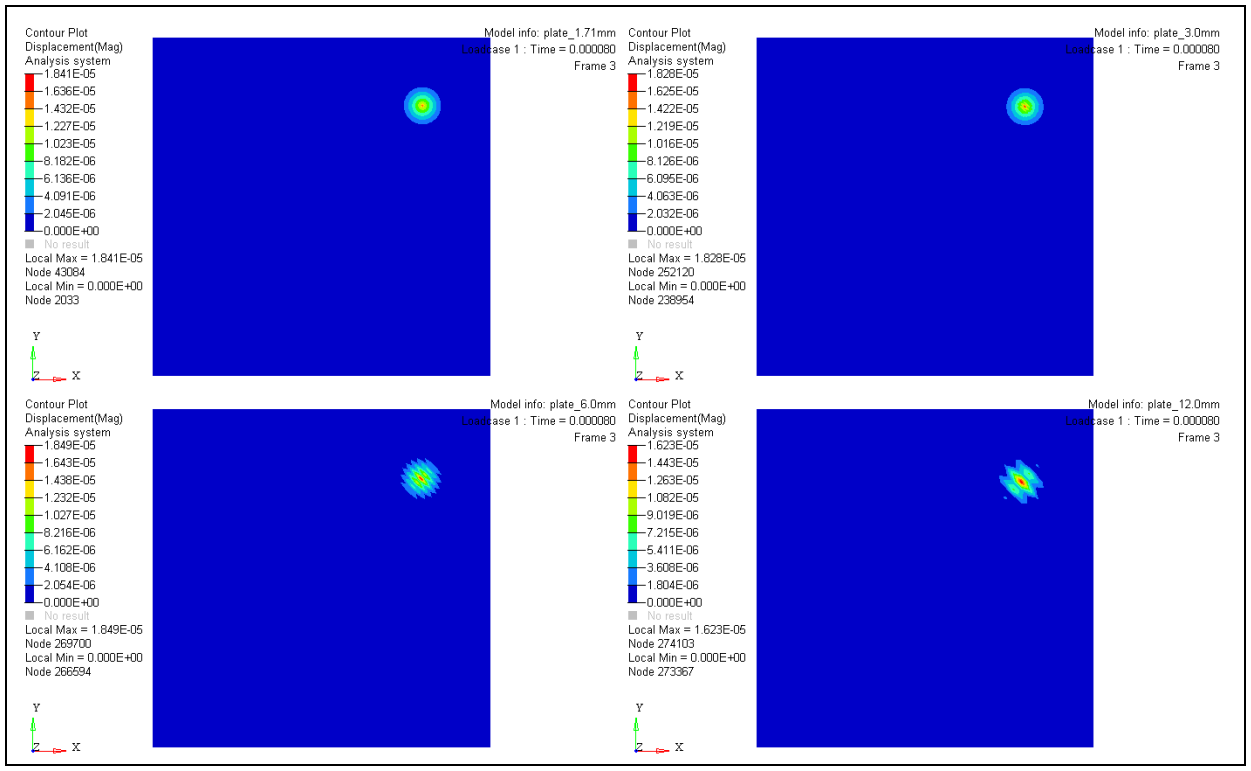

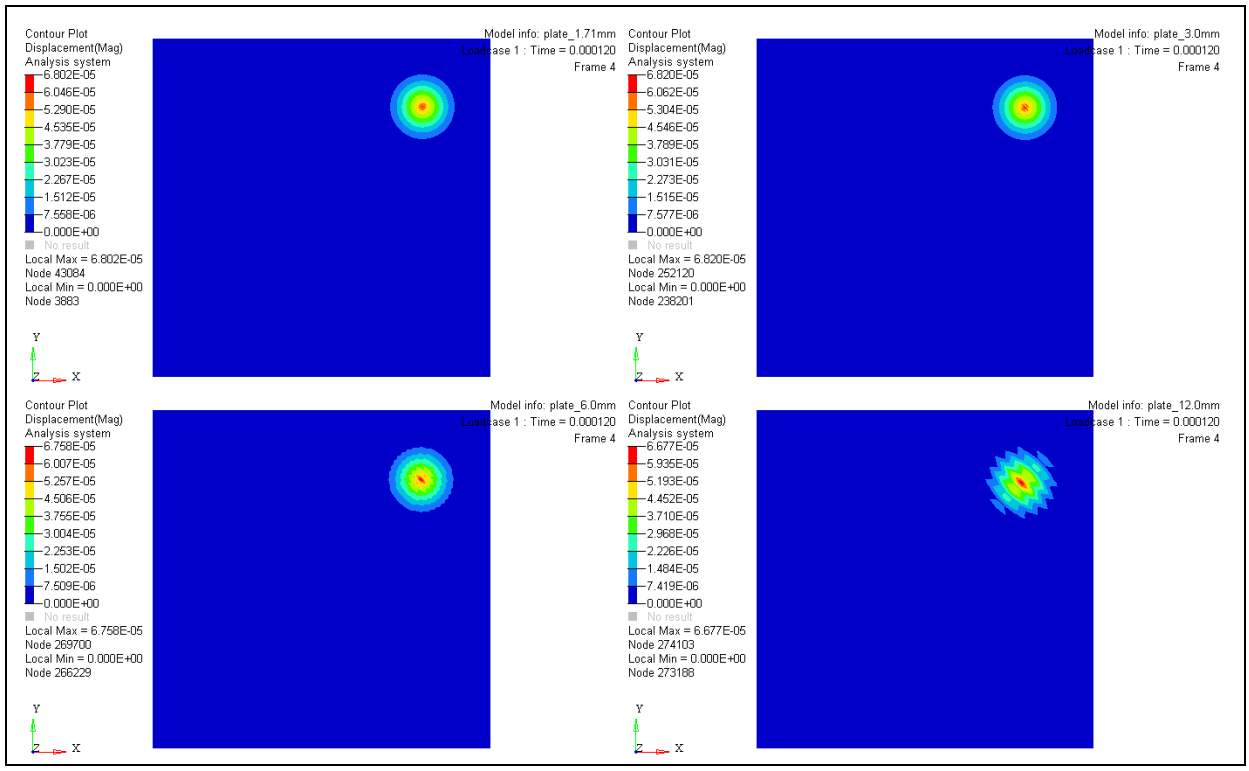

Figure 9-6: Displacement contour plot at time frame 3 &4

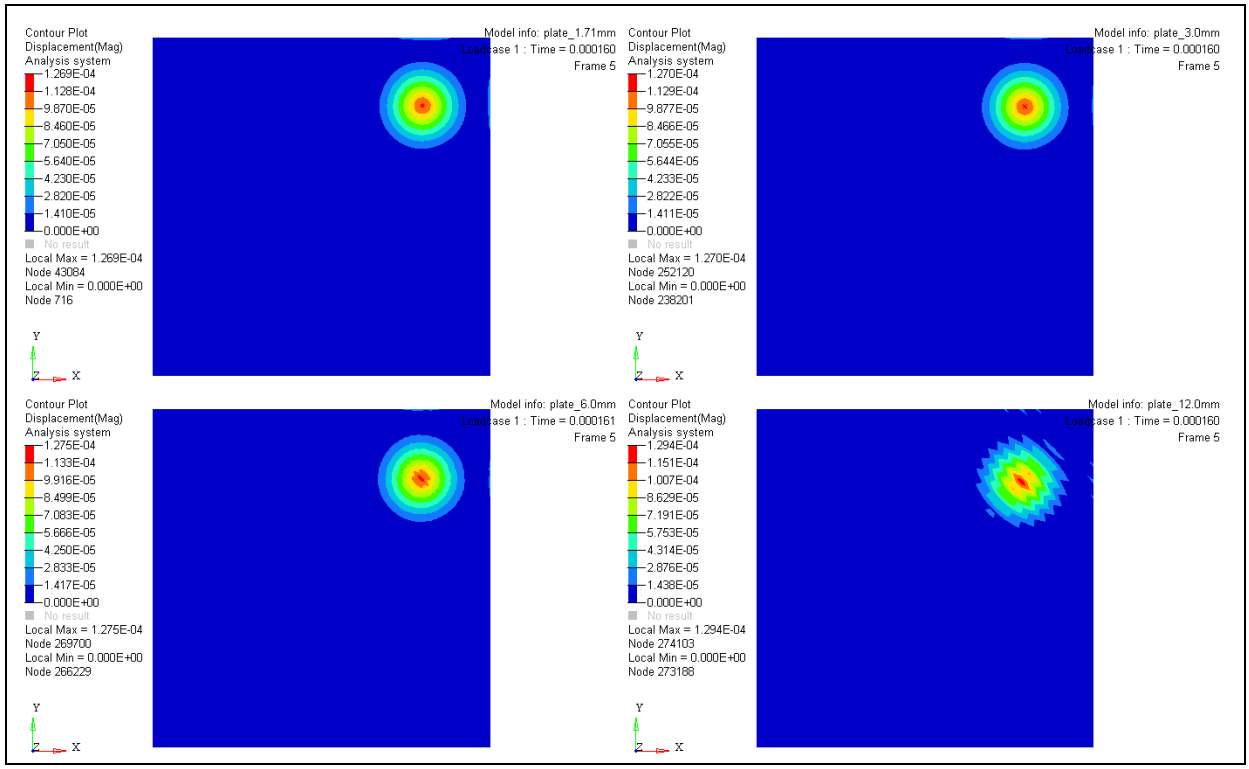

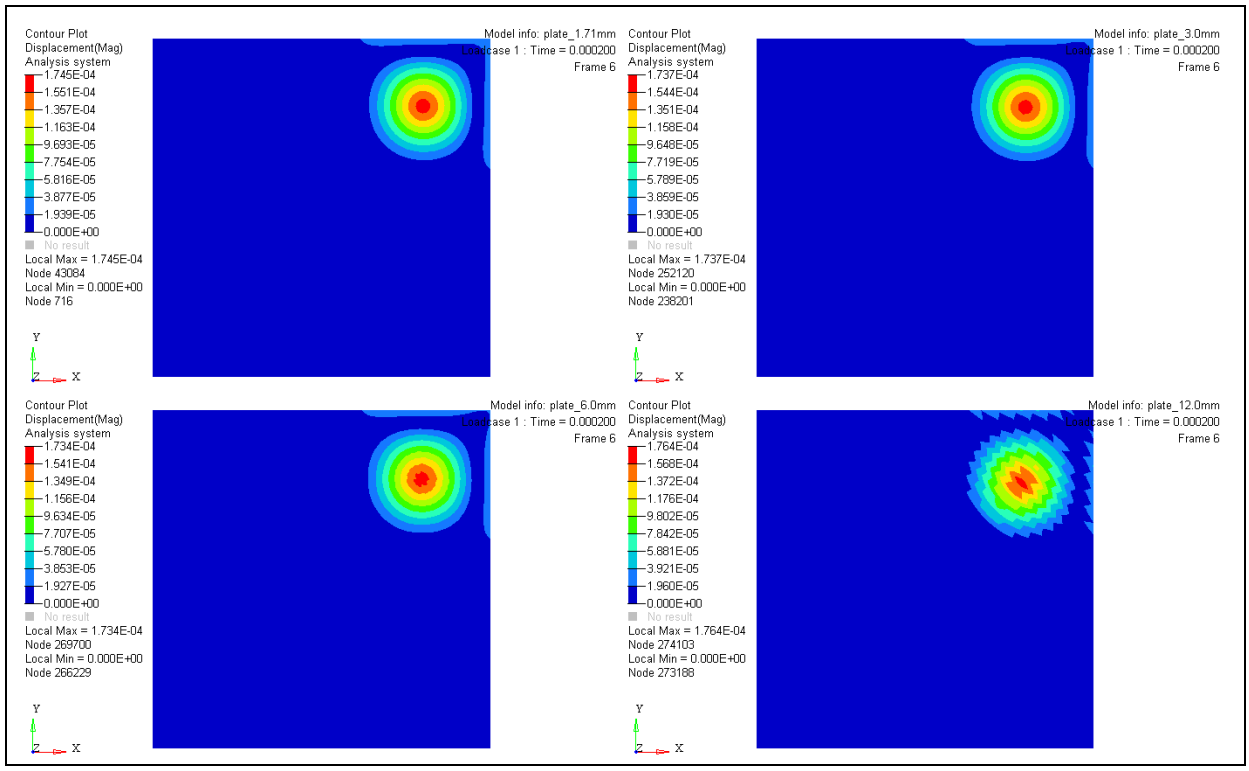

Figure 9-7: Displacement contour plot at time frame 5 &6

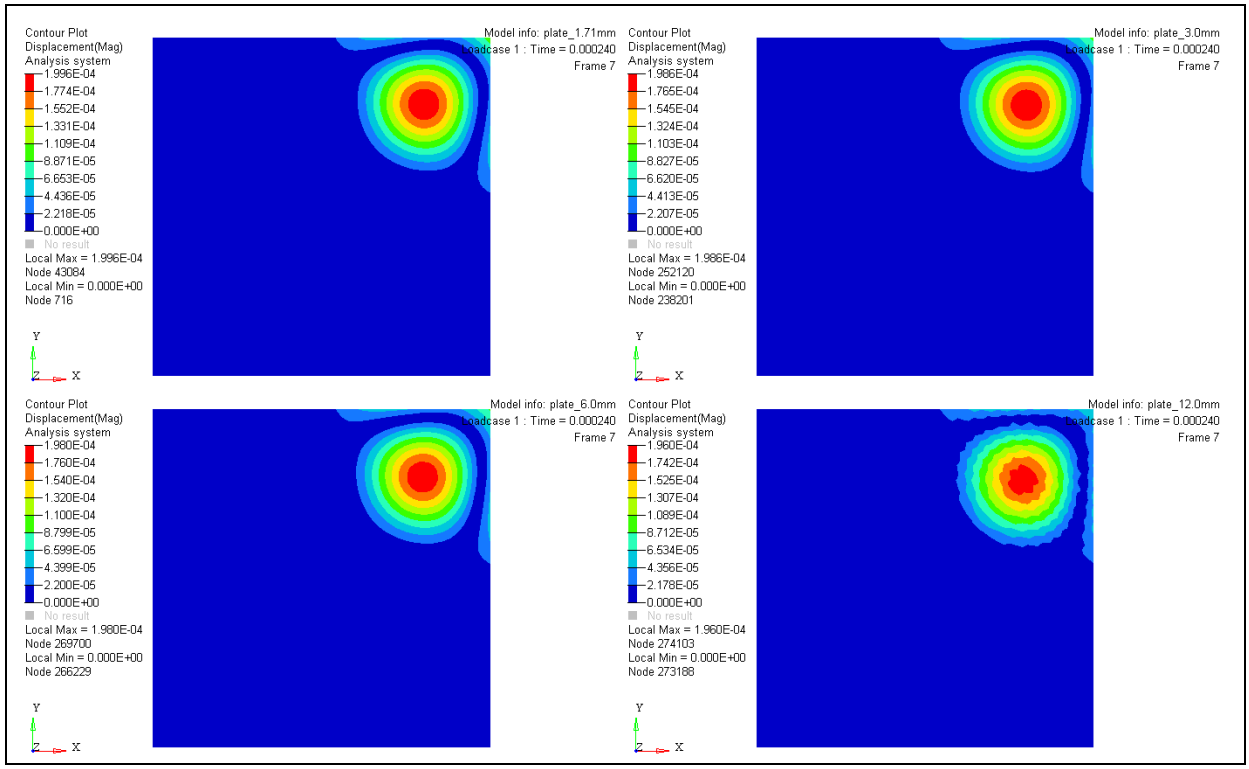

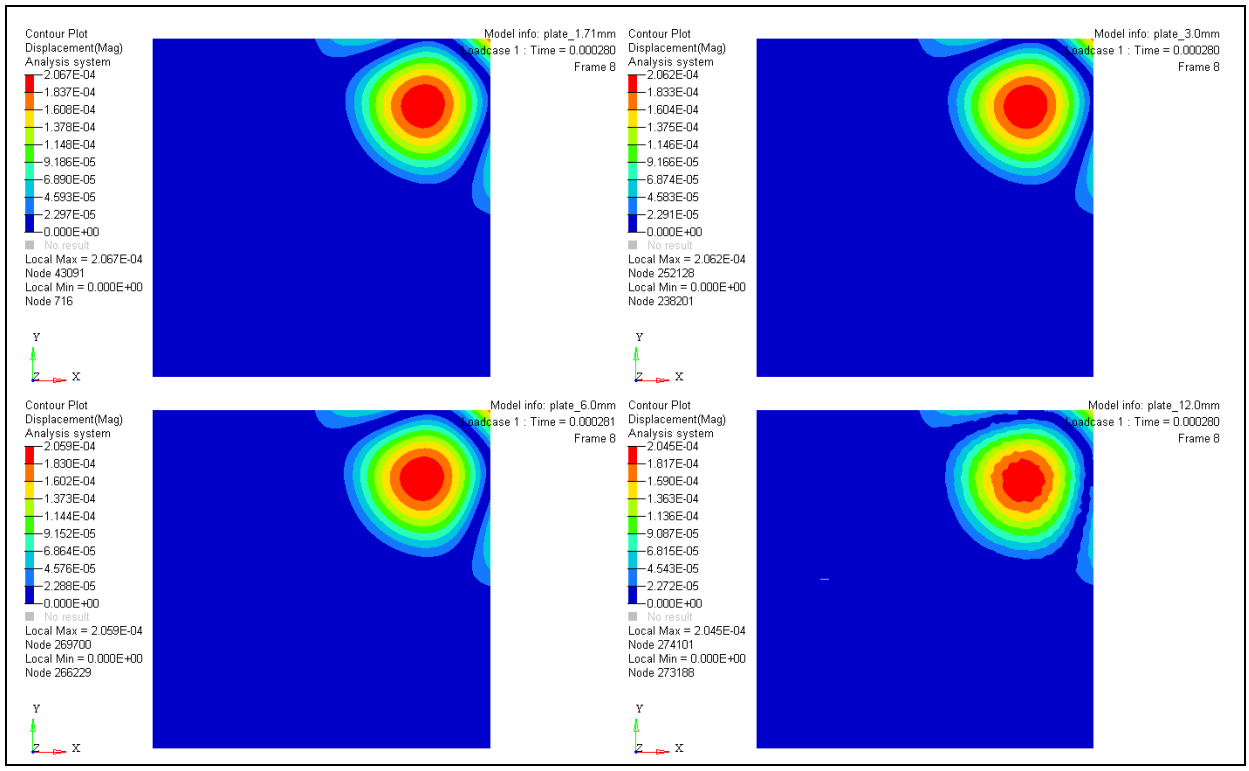

Figure 9-8: Displacement contour plot at time frame 7 &8

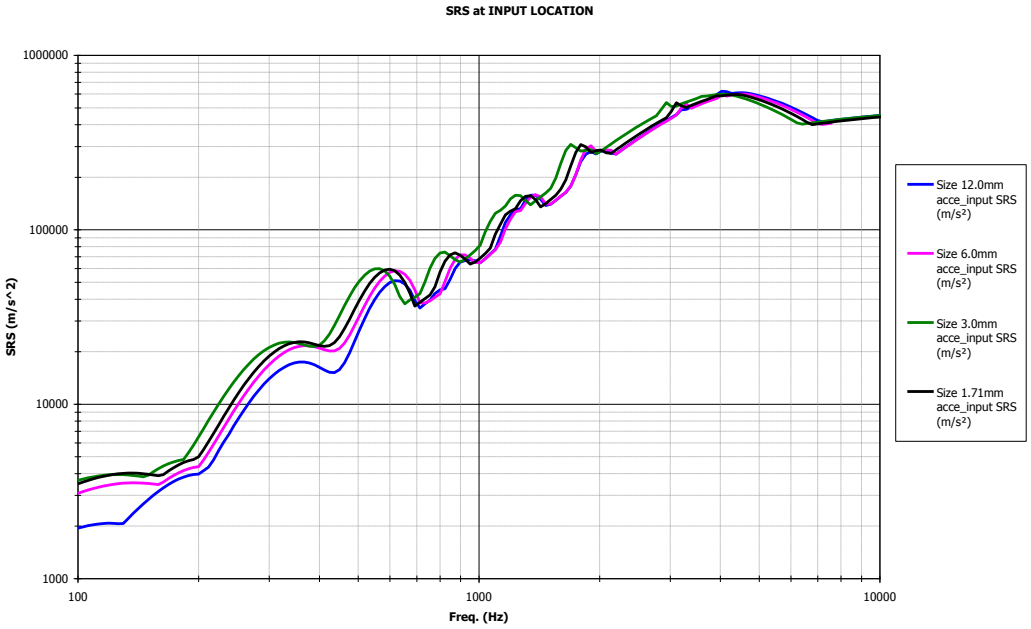

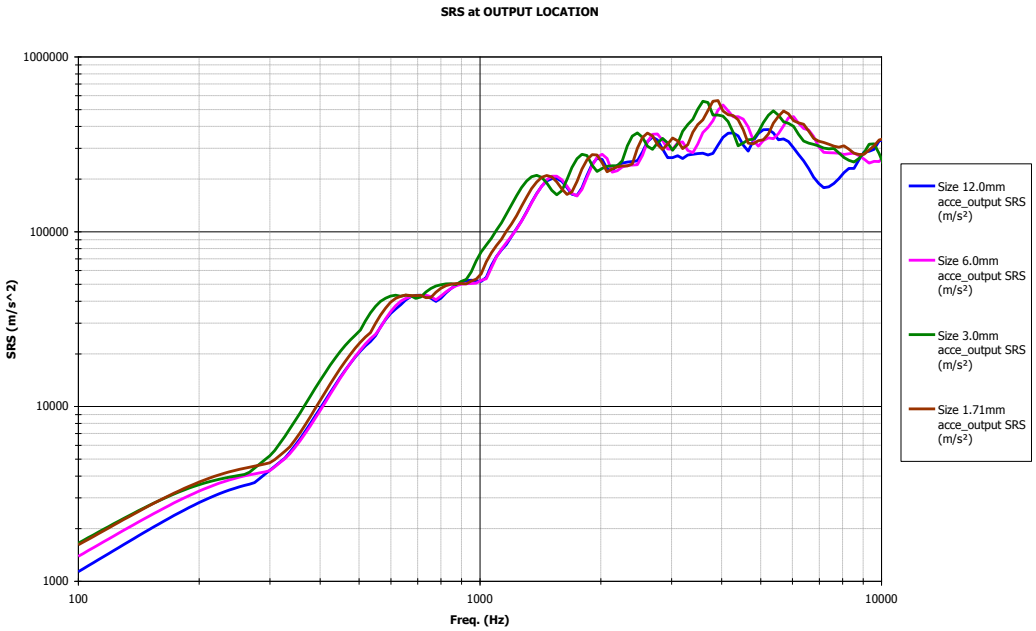

Figure 9-9: SRS at the input and output nodes.

It is generally considered that, for a mesh definition, **a wavelength should be approximated by a minimum of 4 to 6 elements**, in order to avoid numerical filtering or reflection of incident waves (Figure 9-10) but **the use of a mesh with at least 8 elements per wavelength is strongly recommended**.

More than 16 elements per wavelength do not provide significant improvement of the results while increases CPU time.

Moreover it is important to consider the meshing homogeneity and regularity in order to ensure a correct propagation in the whole structure. In a case where a wave propagates successively through a refined then coarse and finally refined meshing, high frequency waves are filtered and reflected by the second zone as it would be on a boundary condition.

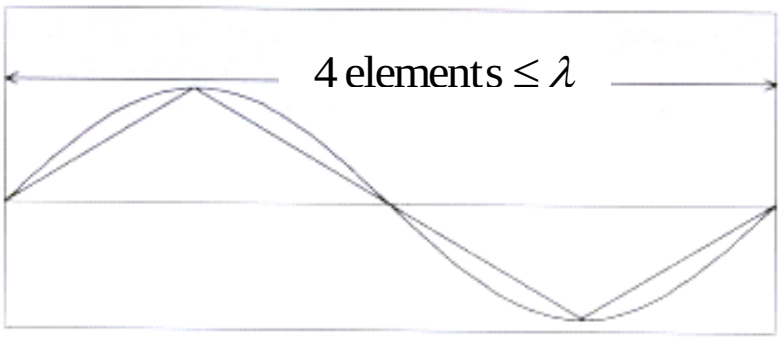

Figure 9-10: Number of elements per wavelength

Table 9-4 gives the classical expression of different kind of wavelength:

Table 9-4: Wavelength formulation for different wave types

	Wavelength	
Traction-compression	$\lambda = \frac{\sqrt{\frac{E}{\rho}}}{f}$	*E*: Young Modulus ρ: density *f*: frequency
Shear	$\lambda = \frac{\sqrt{G/\rho}}{f}$	*G*: Shear modulus
Flexural	$\lambda = \left(\frac{2.\pi}{f}\right)^{1/2}\left(\frac{D}{\mu}\right)^{1/4} = \left(\frac{2.\pi}{f}\right)^{1/2}\left(\frac{Et^2}{12\rho}\right)^{1/4}$	*D*: bending stiffness μ: mass per surface area *t*: thickness

Remark: only flexural waves are dispersive, i.e. flexural wave celerity expression depends directly from the frequency.

A common value for mesh size of aluminium structure is between 5 and 10 mm (especially true for explicit computation) on a satellite for a frequency bandwidth of interest [100-5000] Hz. This requirement can be achieved by refining the original mesh.

For flat surface, there is no critical aspect.

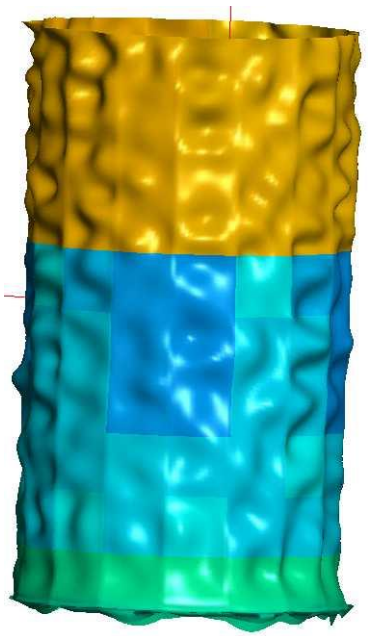

Curved surface (like central tube) can be more problematic to refine because the original mesh has already facetted the geometry. The elements ridges have a tendency to modify the high frequency behaviour of the structure. Wavelength equal to the ridges distance are indeed privileged. The figures beside show the deformed shape of central tube with geometric facets and the same deformed shape with a refined mesh based on the real geometry.

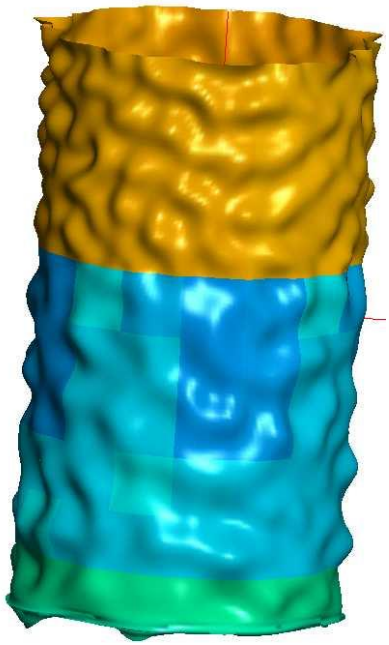

Figure 9-11: Deformed shape of a central tube with and without ridges effect

The refinement of the mesh is thus not always trivial. It is important to take cautions for the validation of the new mesh.

The **following rule for model limitation is proposed, when using an implicit code** such as NASTRAN [RD-014]:

The particularity of far-field environment lies in the fact that the response is dominated by modal structural resonances. This environment is considered to be the most stringent at unit level, due to the great energy involved and displacements associated. This fact makes possible to use implicit codes such as NASTRAN to predict the shock environment (in the frequency range where these kinds of analysis make a sense, i.e. up to 1500 Hz, where modal responses are encountered).

It is important that the mesh is fine enough to accurately represent the deformed shape of the modes of interest. In order to provide sufficient accuracy for numerical shock simulation at around 1200 Hz, a ½ octave margin has been imposed to give a good representation of modes up to 2000 Hz.

To achieve this, the following rules, extrapolated from the element per wavelength criteria used in the explicit method, are proposed:

- Model the mesh of the structural parts in a way such that the following conditions are met:
  - Longitudinal modes up to 2000 Hz limit case (4 to 6 segments per wavelength of the deformation pattern). Assuming an in plane speed of sound of typically 6000 m/s in the face sheets; at 2000 Hz, this corresponds to a wavelength of 3 m. i.e., a maximum element length between 0,75 m and 0,5 m.
  - Bending modes up to 2000 Hz limit case (4 to 6 segments per wavelength of the deformation pattern). Assuming a bending speed up to 1000 m/s in the face sheets; at 2000 Hz, this corresponds to a wavelength of 0,5 m. i.e., a maximum element length between 0,125 m and 0,083 m.
  - Local deformation of the structure due to a bending load (10 to 8 segments per wavelength).
- Assume that the propagation of a shock in plane is covered by the propagation with respect to bending (element mesh size as resulting from condition on bending modes is smaller, as compared to condition in plane shock). Hence, if a mesh is adequate to represent properly propagation of bending modes, it should provide also a good prediction for longitudinal modes.

Table 9-5 presents the element mesh sizes in meter (square mesh), taking into account the typical diameters of Ariane 5 interfaces and some typical node number at the interface (36, 72 and 144 nodes):

Table 9-5: Element mesh size for different interface diameter and different number of nodes along the circumference

	Ø 5400 mm	Ø 3936 mm	Ø 2624 mm	Ø 1666 mm	Ø 1194 mm	Ø 937 mm	Min. bending
144 nodes	0,1178	0,0859	-	-	-	-	0,125
72 nodes	-	0,1717	0,1145	0,0727	-	-	0,125
36 nodes	-	-	-	0,1454	0,1042	0,0818	0,125

Hence it can be seen that 72 nodes at Ø 5400 is capable to reach:

$$2000 \times \frac{0,125}{0,1717} = 1455 Hz$$

The upper frequency limits are shown in Table 9-6:

Table 9-6: Upper frequency limit for different interface diameter and different number of nodes along the circumference

	Ø 5400 mm	Ø 3936 mm	Ø 2624 mm	Ø 1666 mm	Ø 1194 mm	Ø 937 mm	limit case
144 nodes	2125 Hz	2910 Hz	-	-	-	-	2000 * 0,125 / element length
72 nodes	-	1455 Hz	2180 Hz	3440 Hz	-	-	
36 nodes	-	-	-	1720 Hz	2400 Hz	3055 Hz	

Based on these data, it can be concluded that 72 nodes at 5400 mm diameter interface would limit the accuracy of the model (up to 1000 Hz) and that 144 nodes would be more appropriate. For interfaces with a diameter of 3936 mm, 2624 mm or 1666 mm, a 72 nodes distribution would be adequate. For smaller diameters e.g. 1194 and 937 mm, 36 nodes would properly represent the modes up to at least 2000 Hz.

9.2.4.2 Time step

The simulation time step in transient analyses needs to be sufficiently small in order to assure a proper representation of all relevant frequencies and to capture the travelling shock wave in the structure

In **both transient explicit and implicit solution methods** the computational time step Δt is firstly based on the sampling rate of the shock input signal. It is recommended to consider a sampling rate at least 5 times per cycle to be able to fully reproduce the shock input signal.

In dynamic FE codes with **explicit integration scheme** such as Central Difference Method (CDM) the numerical stability is ensured by the verification of the Courant condition.

$$C = \frac{c \cdot \Delta t_{\max}}{\Delta x} \leq 1$$

This condition imposes that the distance travelled by the fastest sound wave inside the FE model ($c\Delta t_{\max}$) is smaller than the characteristic element size (Δx) in the mesh.

Consequently the time step Δt, which is of the order of magnitude of μs, can be obtained imposing in the analysis: the maximum frequency of interest $f_{\max}$, taking into consideration the element per wavelength criteria and the sampling rate of the shock input signal.

In dynamic FE codes with **implicit integration scheme** the time step $\Delta t = 1/f_{Sampling}$, which is of the order of magnitude of *ms* or less, can be obtained imposing in the analysis the minimum sampling frequency $f_{Sampling}$ considering the Nyquist Criterion that is stated as:

$$f_{Sampling} \geq 2 \cdot f_{Max}$$

Where the maximum frequency of interest $f_{\max} = \frac{1}{2\Delta t} = \frac{1}{2}\frac{N_T}{T}$ is obtained by the application of the Shannon's Theorem with $T = N_T \cdot \Delta t$ (having: T= total time period and N_T=number of samples).

9.2.4.3 Elements type

The choice of element type is essentially a matter of elements library, material laws and also CPU time. For aerospace structures shell elements are obviously privileged.

As a general rule, the increasing of the maximum frequency of interest f_{max} means that the selection of the element type has to be reviewed with care, for example changing the FE model from 2D to 3D elements.

For composite sandwich, the choice is not trivial. On one hand, one can use homogenisation techniques to model sandwich properties with simple shells elements but it is not possible then to recover stress and strain at ply level. On the other hand, each ply can be modelled (if the software's elements library allows it) but the properties description (shear property of the core, L-W orientation of the core, ply-by-ply orientation and material) is more complicated and the CPU time increases because of increased gauss points.

A 3D model is also possible to model accurately the core of the sandwich. Faces can then either be detailed ply-by-ply or homogenized as for shell model. The number of elements and consequently the CPU time is also increased.

With respect to the mesh quality the following recommendations should be respected:

- The shell mesh is recommended to be as homogeneous as possible.
- Triangle shell are not recommended; if the mesh includes triangle elements due to a difficult mesh or mesh transition, it is recommended to reduce its number to 5% per part.
- To realize an accurate mesh it is usually recommended to set a minimum of 5 to 10 elements in a structural characteristic length, however at least 3 elements are necessary to reproduce an elasto-plastic behaviour with a low accuracy.
- The applicability of a FE model based on a 2D mesh versus a 3D mesh schematization should be verified taking into consideration the type of the structure to be modelled.

9.2.4.4 Modelling of equipment

The equipment model is a **key problem for wave propagation calculation**. The main FEM adaptation usually concerns this point. The experience gained from Envisat/PPF and SMART-1 programmes has shown that a conventional modelling of equipment (lumped mass rigidly connected to a few points) is not appropriate for shock analysis [RD-014]. The equipment representation by lumped mass rigidly connected is valid only for low frequency response analysis (typically up to 100Hz). For shock calculation, equipment cannot be considered as infinitely rigid. This kind of modelling leads indeed to overstress the region close to the hard mounting points, making the predictions inadequate. This problem is paradoxically amplified with refined meshing because the rigid element distributes the whole equipment mass to the connecting nodes which are part of small, and consequently light, shell elements. Node dynamic is thus completely modified: a "heavy" node cannot move as a "light" one. High frequency has tendency to be filtered by the local mass effect.

The way in which equipment are represented in the spacecraft FEM strongly depends on the purpose of the investigation.

To achieve a global understanding of the shock propagation inside the spacecraft and to define critical areas, as it is intended in early and intermediate project phases, it does not require a detailed equipment modelling. Indeed equipment design and location can still be subject to changes during further development process. Hence **it is recommended to adopt a NSM (Non Structural Mass) formulation** and to distribute the equipment mass over the panel on which they are accommodated.

This formulation is of course not entirely satisfactory because the dynamic filtering of the equipment is not modelled. On the contrary, suppressing completely the equipment model leads to a substantial increase of acceleration level, notably at low frequency because the absence of equipment mass makes the supporting structures more excitable. The consequence is an appropriate prediction in areas without lightweight equipment and a conservative shock prediction in areas with heavy equipment.

In order **to explain/understand local behaviours**, which can affect the shock levels of equipment mounted in that area **the NSM formulation is not appropriate anymore.** Instead a **refined modelling of equipment** should be adopted. This can in some cases even justify a local relaxation of the unit shock specification in later project phases. (e.g. in case the local behaviour identified during test is inherent to a non-representative dummy for instance).

Experience has shown that it is advisable to use three-dimensional SOLID elements to generate refined equipment. It is evident that the refined units are representative particularly in terms of mass, footprint and centre of gravity (COG) at least in an out-of-plane direction. Figure 9-12 shows exemplarily computed transfer functions for a SMART-1 equipment dummy using different modelling techniques:

- Lumped mass rigidly connected to a few nodes – blue
- Non-structural mass formulation – green
- SOLID equipment with representative mass and footprint – red
- SOLID equipment with representative mass, footprint and CoG in out-of-plane direction – pink

in comparison with test results (black) for the out-of-plane response on the left and the in-plane response on the right.

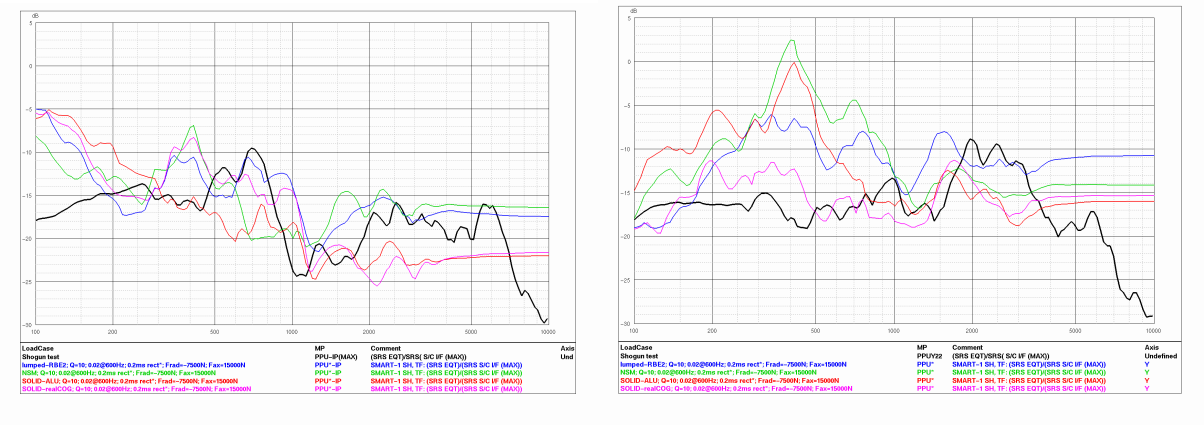

Figure 9-12: Effect of equipment modelling in terms of FEM prediction

Since a very detailed equipment modelling does not appear to be absolutely necessary this way of modelling could even be feasible for the whole spacecraft or at least for the most heavy equipment. However in a general case, a refined modelling of equipment is an exercise, which can be done once the shock test has been performed to evaluate local effects. In the early phases of a project, this is not of major interest but can be very helpful later in the project.

9.2.4.5 Restitution point

If the purpose of the numerical shock simulation is to support or consolidate a similarity based zoning of the spacecraft in an early project phase it is recommended to evaluate the response of a couple of nodes per zone. These restitution points should be chosen preferably in areas without equipment or at least far away from heavy equipment.

For more detailed analyses in later project phases, experience has shown that a proper representation of the sensor location is critical for the accuracy of the shock predictions. The following recommendations are given for the selection of the restitution point representing a sensor close to a heavy equipment. It is important to ensure that the following guidelines for the selected FEM-node are met:

- The selected FEM node is located close to the real sensor location but still a few centimetres away from the unit (one gridline next to the equipment)
- The selected FEM node does not belong to the rigid body link representing the investigated unit
- The selected FEM node is not a part of the solid element representing the unit (e.g. not be a node of the equipment edge)
- The selected FEM node is not located under the equipment in terms the unit is represented by solid elements

Another point that should not be neglected when going into detailed analysis is the sensor effect. Sensors are generally installed on cubes (

Figure 9-13). Those cubes lead to an offset on the measurement with the structure. One of the main consequences of this offset is that a part of the measured translation is in fact a rotation of the base. If this offset is not taken into account, the rotation effect is neglected and the imposed signal is thus incorrect.

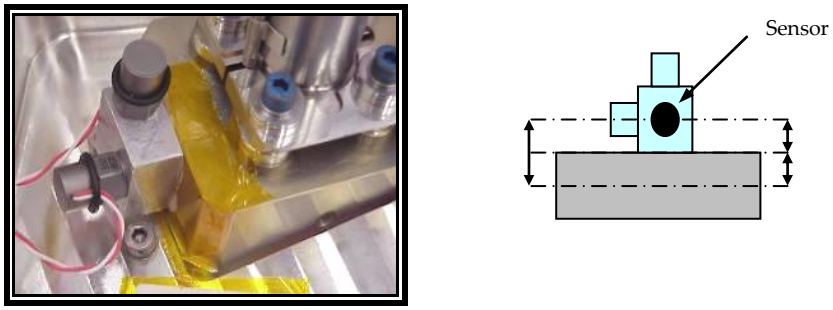

Figure 9-13: Shock sensor on cube

Taking the rotation into account modifies the imposed acceleration, and, as a consequence, alters the shock response spectrum (Figure 9-14).

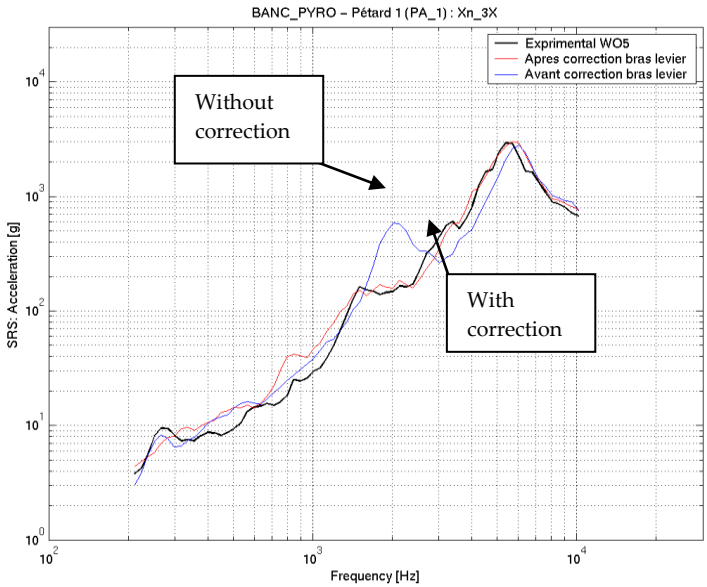

Figure 9-14: Shock sensor mounting effect on SRS

Two modifications of the SRC can be seen: a global modification of the SRS level and a modification of the frequency of the peaks, as those peaks are due to important rotation effects.

9.2.4.6 Modelling of junctions

The modelling of links or junctions between components of a spacecraft (equipment on a mounting panel or inter-panels connections) allows to represent a **local stiffness and eventually a local source of damping** generated by local complex mechanical phenomena (e.g. dissipation, global and micro-friction)

The stiffness is often given by a relation force versus displacement. This relation can be linear (constant stiffness) or not (stiffness varying with displacement, gaps, different compressive and tensile stiffness…). It depends on the characteristics of the links which can be not accurately known by the user and also from the FE software element's library. Generally, the simplest way to model links is to use a linear relation with a global stiffness value as representative as possible. If not available, the preferable way to model links is to consider them as infinitely rigid (for instance stiffness in translation of 10^8 N/m, and in 10^6 Nm/rad in rotation). Physically, an important stiffness allows bringing together the intervening sub-structures. Vibrating phenomena are better transmitted to sub-structure (e.g. from the central tube to the floors or webs…).

The number and locations of these links appear to be critical parameters to model. Transient analyses involve small wavelengths close to the inter-links distance. The propagation phenomenon to solve is thus directly impacted by the locations and number of links. The SPOT5 example has enlightened that increasing the number of links is equivalent to increasing their stiffness: vibrations are better transmitted and low frequency modes are more constrained and thus less excited.

The damping of the links is characterized by a relation damping force versus relative velocity of joined nodes. This relation can be linear (constant force) or not. When the relation is linear, it corresponds to the classical viscous damping between links extremities. The effect of damping affects essentially modes that justly involve links. The attenuation is globally proportional to the number of links between the source and the considered point.

At equipment level the link between equipment and panel is the main source of attenuation. It is often assumed that this link can lead to 3 dB of attenuation.

A parametric study on the influence of stiffness and damping of this connection has been performed on the small payload DEMETER and evolved two main phenomena:

- As presumed, the damping has an influence on the level of the SRS, but the influence is limited to the high frequency.
- A non-expected phenomenon occurred at low frequency with a frequency shift due to the high damping in the link.

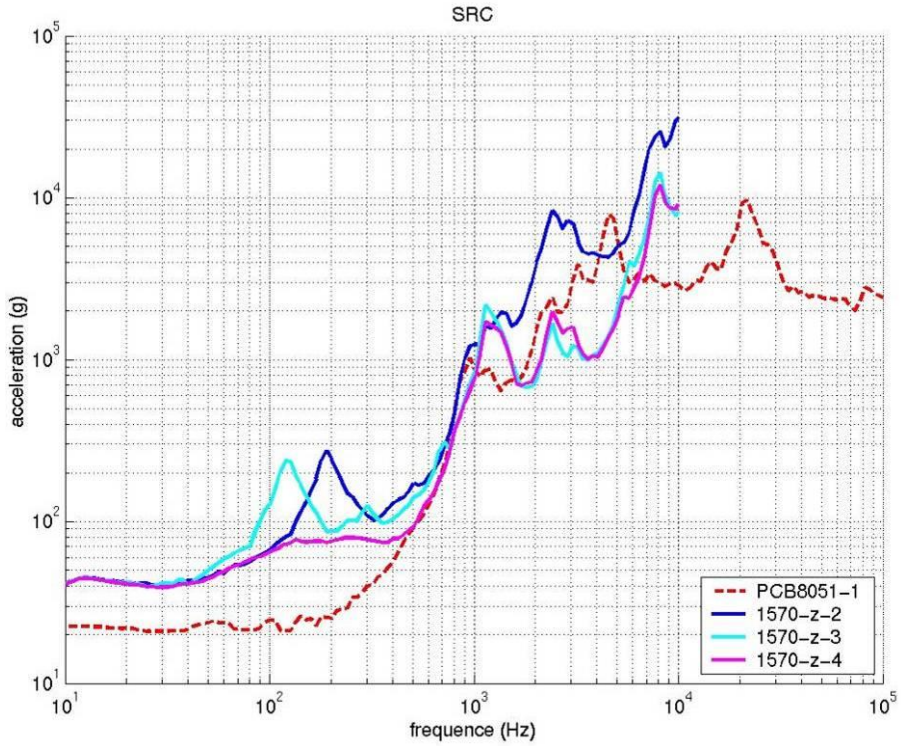

Legend: Measure Low damping High Damping

Figure 9-15: Influence of damping in joints and comparison with measurement

The links were modelled by elements including both aspects:

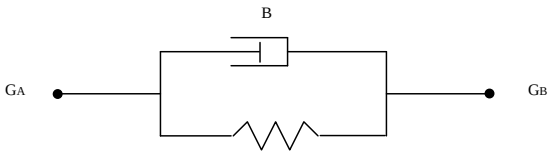

Figure 9-16: Joints modelled with stiffness and dashpot

The main difficulty lies in the fact that those parameters (stiffness and damping) need specific study and test characterization in order to have validated values. Hence, for simplicity, damping is often taken into account globally in the model by equivalent model of damping.

Another detailed study on a SMART-1 equipment showed the necessity of representing all junctions between equipment and panel. It turned out that it is not sufficient to model only joints like inserts and screws but also glued connections. The representation of the glued connection between equipment and panel particularly effects the out-of-plane response as to be seen below.

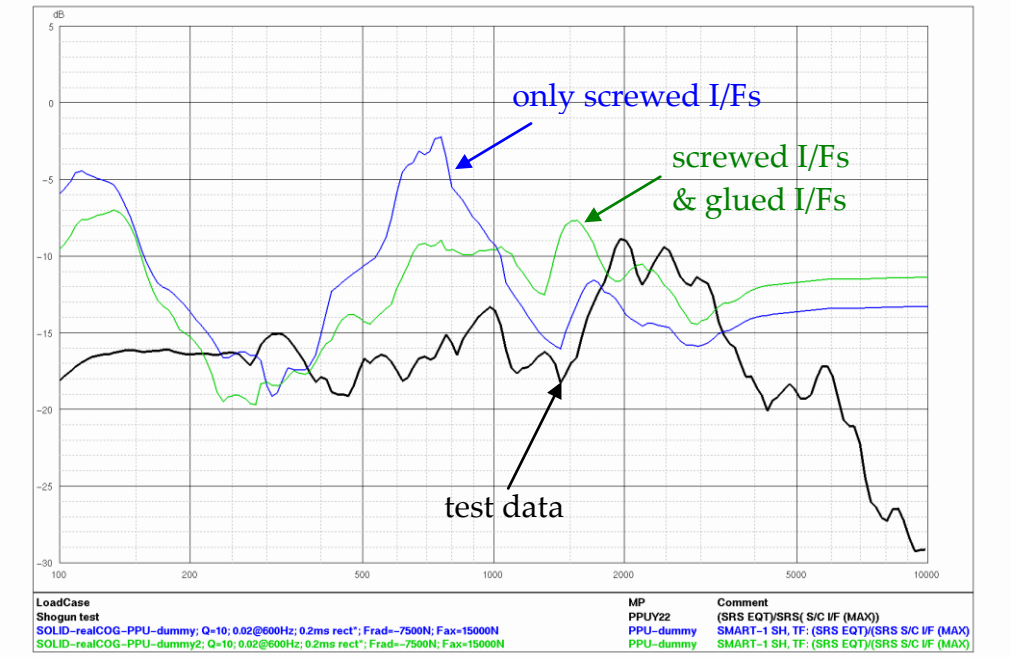

Figure 9-17: Effect of I/F representation on transfer function

9.2.4.7 Damping modelling

The understanding of damping forces in vibrating structures is not well developed. A major reason for this is that, by contrast with inertia and stiffness forces, the physics behind the damping forces is in general not clear. As a consequence, **modelling of damping appears to be difficult**.

Different formulations (only most current ones are described here) are used depending on the type of solutions used and on the FEM code used:

Table 9-7: Most current formulation for damping modelling in shock transient calculation

Types of damping	Modal transient (implicit only)	Direct transient (explicit and implicit)
Structural damping	✓	
Viscous damping	✓	✓
Modal damping	✓ (recommended)	

Direct transient response analysis does not permit the use of complex coefficients because solutions are expressed in the real plane. Therefore, structural damping and/or modal damping cannot be modelled directly. Structural damping is included by means of equivalent viscous damping. The impact of this on the solution can be appreciated by defining a relation between structural damping and equivalent viscous damping, assuming constant amplitude oscillatory response for an SDOF system.

The viscous damping force F_v is a damping force that is function of a damping coefficient c and the velocity.

$$F_v = c.i.\omega.u$$

The structural damping force F_s is a displacement u dependent damping. The structural damping force is function of a damping coefficient g and a complex component of the structural stiffness matrix.

$$F_s = i.g.k.u$$

The two damping forces are thus identical if

$$g.k = c.\omega$$

Therefore, if structural damping is modelled using equivalent viscous damping, then the equality holds at only one frequency ω_c. It is important to note that structural damping is independent of frequency whereas the equivalent viscous damping varies linearly with the frequency, namely under the frequency ω_c, the system is under-damped and over this frequency it is over-damped. Figure 9-18 illustrates this equivalence.

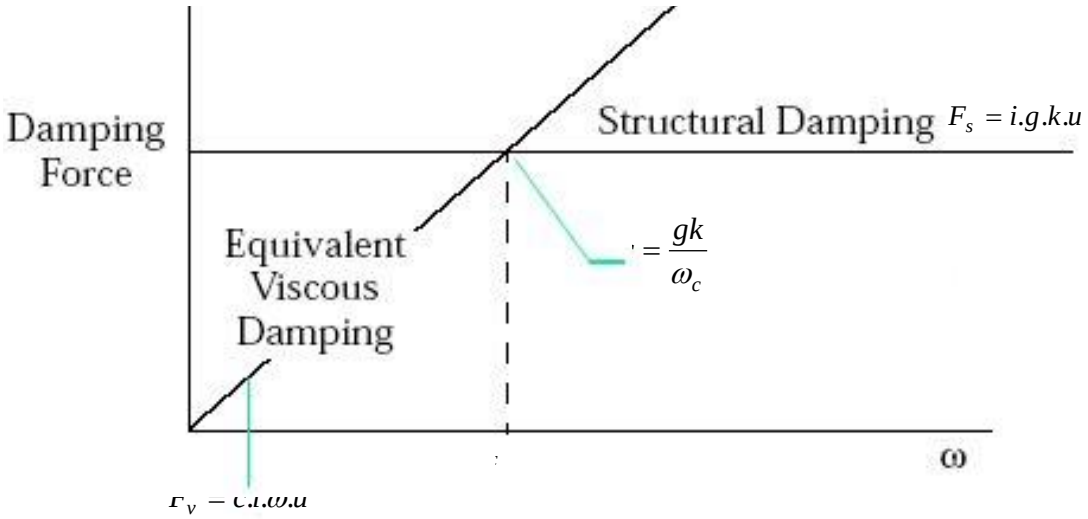

Figure 9-18: Structural Damping Versus Viscous Damping

For information only, qualitative order of magnitude of equivalent structural damping for aluminium is around 0,1 % at 10000 Hz. For aluminium sandwich, value around 2 % at 10000 Hz can be considered.

Generally, viscous damping and its derivative are the most widely used because they allow some mathematical simplifications useful to solve the mechanical equations. It is thus common to assume a special type of viscous damping: the proportional damping. This model expresses the damping matrix as a linear combination of the mass and stiffness matrices, that is:

$$C = \alpha.M + \beta.K$$

where α and β are real scalars. This damping model is also known as "Rayleigh damping" or "classical damping". Eigenmodes of systems with "Rayleigh damping" preserve the simplicity of the real normal modes as in the undamped case. It is important to note that generalization of "Rayleigh damping" expressed in terms of a series expression of the mass and stiffness matrices so that the system can be decoupled by the undamped modal matrix have also been developed. This generalization is nevertheless beyond the scope of this paragraph. The "Rayleigh damping" is a

mathematical artefact to solve more easily the mechanical equation. It is not directly linked with physical considerations.

Another source of damping in FE analysis is the numerical damping. It has no physical meaning. But it is systematically added to stabilize the numerical integration. The numerical damping dampens only the contributions in the high frequency response. Example of instability in explicit code is given by the Hourglass effect. It is a purely numerical phenomenon which implies, for under-integrated element, deformation mode without any induced strain and consequently no stress or internal forces to resist this deformation mode. It can therefore grow unboundedly. This kind of instability can be controlled notably by introducing numerical viscous damping.

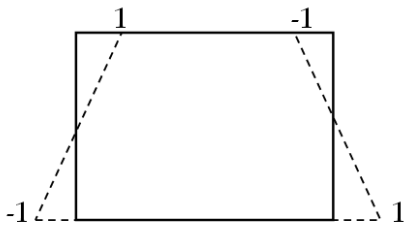

Figure 9-19: Example of hourglass mode for an under-integrated shell element

There are two ways suggested to overcome the damping limitations in direct transient analyses:

The first method requires for example 3 different simulation runs with damping adjusted at 3 different frequencies with a specific structural damping. It is considered that the structural damping is higher in the low frequency range, and decreases when the frequency increases. In a post processing procedure the results of the 3 different runs (resulting SRS or SRS-ratio) are linearly merged to compute the final solution.

Table 9-8: Structural damping versus frequency

Frequency [Hz]	ζ [%]
300	1,5
600	1,0
1000	0,5

The second method is based on a pseudo inversion of the modal damping matrix. This is a way to impose in the same time a modal damping, with in addition a viscous damping for direct transient solver.

$$\phi^T [B] \phi = \begin{bmatrix} \cdots & & \\ & \xi_i & \\ & & \cdots \end{bmatrix}$$

ϕ *Eigenvector*

ξ_i *Modal damping, frequency i*

From this we can define a pseudo inversion of the matrix [ξi].

$$[B] = [M]\Phi \begin{bmatrix} \ddots & & \\ & \xi_i & \\ & & \ddots \end{bmatrix} \Phi^T [M]$$

This equation defines the modal damping matrix [ξi] on the physical degrees of freedom of the direct damping matrix. This matrix can be used in the transient direct solution to impose a damping equivalent to modal damping [ξi].

The combination of modal damping and viscous damping allows a complete definition of the damping.

In the FEM solver, we can add the two damping to get a global damping

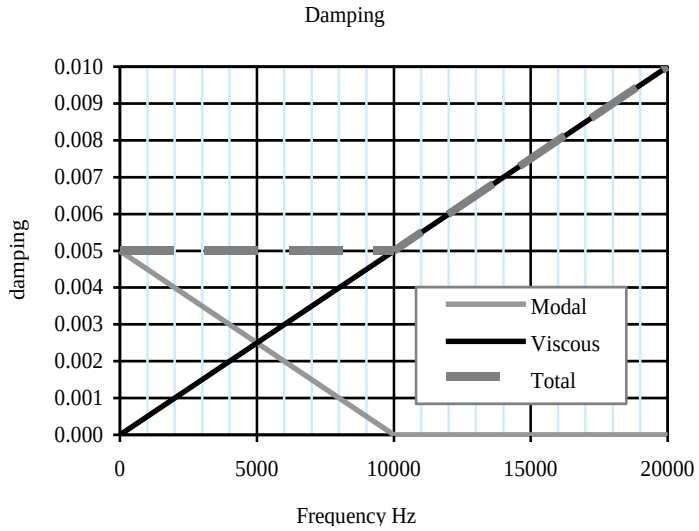

Figure 9-20: Illustration of the total damping composed of modal and viscous damping

This modelling of the damping leads to link different degrees of freedom by the damping matrix. The consequence of this coupling is that the damping does not only modify the level, but also the modes.

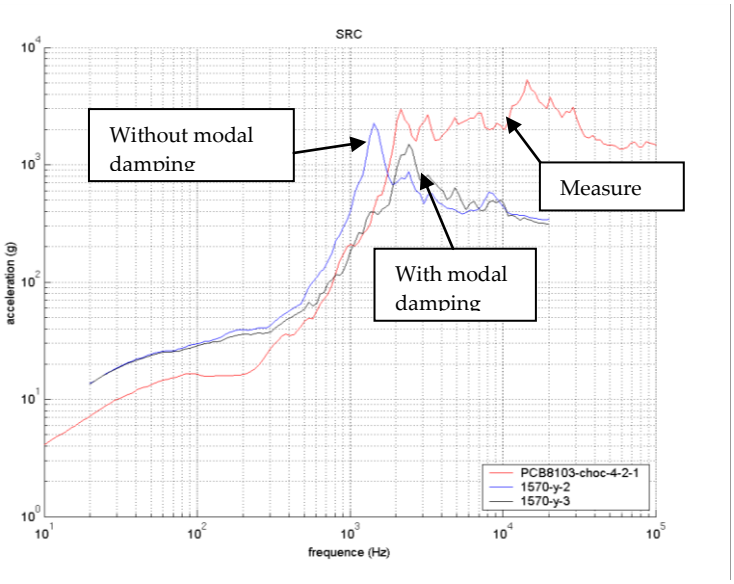

Figure 9-21: Effect of the damping on the S

The use of this type of damping modelling can improve the quality of the results.

9.2.4.8 Source modelling and boundary conditions

The shock source can be introduced in the FE model either by imposing a synthetic or measured load or by imposing locally a displacement or acceleration coming from measurements or not. It is important to note that it is very difficult to measure accurately and properly acceleration at less than 50 mm of a pyroshock and that the measurements during a long time include the response of the structure.

- **Excitation imposed by load**: the force is the origin of the shock. When feasible (hammer tests for instance), the force recording is used as input for the corresponding calculation. If it is not possible, build an approximation that respects form and duration. The purpose is not to have an input signal as close as possible of the physical reality, but only to obtain results near the measures, with a likely signal, as simple as possible. As inverse allowable methods are not well developed, the definition of the input is obtained after successive iterations. It seems possible to represent a pyrotechnic input with a superposition of triangles or other simple elementary signals (rectangular, ½ sinus, low sustained sinus, damped sinus) of different durations in the relevant directions (for instance out of plane and in plane directions or radial direction in the case of Clampband). The content of the synthetic signal can slightly differ of the real physical signal (e.g. even if the input signal has a continuous spectrum, the representation of the only frequencies generating a significant response is sufficient). It is important that all the excited points are included in the source model, and that the time structure of the source is respected. The latter implies that:
  - If it is a scrolling excitation like a linear explosive source, the time lag between each excitation node, standing for the cutting celerity, is integrated in the model.
  - If the sources are not perfectly synchronised like different pyrotechnic point sources, the delay between each node is introduced in the calculation.

  If the analysis aims at evaluating the SRS ratio or attenuations between the source and inside nodes in a linear model, it has been noticed that the knowledge of form, amplitude and

duration of the source is not mandatory. The use of simple normalised signals like ½ sine or crenel signal is thus recommended. However, if the source is not well known, it can be modelled by a high frequency simple signal like a ½ sinus which can excite a broad frequency band.

Another advantage of imposing a force at the source resides in the boundary conditions choice. They are generally chosen free (example of SHOGUN simulation) but it is not systematic. For example, the case of a clampband calculation has enlightened the fact that leaving the ACU boundary conditions free brings out important bending deformation in the axial direction. This deformation does not seem physical because of the contact between ACU and spacecraft interface during the first few milliseconds after shock. It has been considered consequently that the ACU imposes a symmetry condition at the spacecraft interface and the rotations around in-plane axes have been blocked on the interface frame.

- **Excitation imposed by displacement or acceleration**: the use of acceleration seems easier because tests data can be used. In order to minimize the structure response and consequently to avoid introducing energy in the structure after the shock end, the use of measures as near as possible from the real source is mandatory. Those near field measurements are often disturbed by measurement problems like noise, electrical contamination, static and/or dynamic offsets… Before performing a simulation with test input, it is thus mandatory to perform some digital signal processing in order to reduce unwished effects that could be amplified by the calculation. The use of punctual measured acceleration raises the problem of the other interface points where no measure is available (e.g. a clampband test where often only four measurements are available). If no validated and accurate measurement is available, a method consists in introducing displacement or acceleration in the form of synthetic signals like a combination of damped sine (e.g. Prony type) that stands a priori for the real excitation in term of frequency content and amplitude. The advantage of this synthetic input is that it does not contain any noise or zero-shift as measures do.

  One of the main disadvantages of this method is that boundary conditions are thus imposed for the source DOF.

9.3 Statistical Energy Analysis (SEA) Numerical Methods

9.3.1 The classical SEA approach

SEA method has been introduced end of fifties. Formalized in next decades ([RD-032], [RD-033], [RD-033]), SEA describes behaviour of complex systems by a set of energy-balanced equations between the various domains (subsystems) of the analyzed system. SEA assumes both perfect diffusion and weak coupling of subsystem vibrations. From these, coefficients of energy exchange driving the equations are predicted classically from analytical wave theory by decomposing modes into uncorrelated waves (diffusion of energy).

In an analysis band of central radian frequency ω and width $\omega\Delta$, the total energy (spaced and frequency integrated), of a subsystem denoted by *i*, is defined as: $E_i = \int_{\Delta\mathbf{x}} \int_{\Delta\omega} m v_i^2(\omega, \mathbf{x}) d\omega d\mathbf{x}$.

Given the intrinsic Damping Loss Factors (DLF), η_i and the Coupling Loss Factors (CLF) between connected subsystems, η_{ij}, SEA energy-balanced equations are written in a matrix form as:

$\mathbf{P}/\omega = [\eta] \cdot \mathbf{E}$ where $\mathbf{P}$ and $\mathbf{E}$ are respectively the power vector injected by external applied loads to subsystems and the subsystem total energy vector. $[\eta]$ is the loss matrix of which diagonal is given by: $\eta_i + \sum_{j \text{ coupled to } i} \eta_{ij}$ where *i* is the index of the subsystem equation and *j* the index of coupled subsystems to *i*.

By introducing modal density of subsystems, $n(\omega)$, the energy-balanced equations may also be formulated as $\mathbf{P}/\omega = [\eta n] \cdot \mathbf{E}_n$ with $\mathbf{E}_n$, vector of subsystem modal energy E_i / n_i.

As soon as injected power, P_i, provided by the external loads to subsystem is calculable, assuming DLF and CLF are known quantities and providing a reasonable estimate of subsystem modal densities, previous energy-based equations are solved with energy or modal energy as unknowns.

In practice $n(\omega)$ is derived from simple-shaped analytical dynamical system (beam, plate, shell, acoustic cavity). CLF are computed most of the time by wave theory applied to coupled plates but may also be extracted by inverse methods from finite element model or test data ([RD-034], [RD-035]).

Size of subsystems should be large enough to include several local resonant modes when analyzed in a frequency band of given width.

SEA is then not suited to low frequency and variance of SEA results is generally decreasing when frequency increases providing confident mean energies above some frequency threshold depending of both subsystem size and frequency bandwidth. SEA assumes also steady-state random excitation, but as shown in the next paragraph the theory has been extended to predict transient events.

9.3.2 The Transient SEA formulation

In the framework of transient SEA, energy and power are time-dependent quantities related by:

$$\mathbf{P}(t,\omega,\Delta t)-\frac{\mathbf{dE_i}(t,\omega,\Delta t)}{\mathbf{dt}}=\omega[\eta]\cdot\mathbf{E}(t,\omega,\Delta t)$$

$\mathbf{E}(t,\omega,\Delta t)$ represents the energy at time *t*, averaged over time-constant Δt, filtered in a frequency band centred around ω (generally 1/3rd octave band). Δt is chosen large enough for modal behaviour to be established in all subsystems.

Transient SEA formulation is in practice very effective to predict time decay rate of mean subsystem responses [RD-036] but gives biased information on instantaneous levels when dealing with short duration pyroshock transients [RD-037].

9.3.3 Prediction of shock response by Local Modal Phase Reconstruction (LMPR)

Here, instantaneous levels prediction is required involving previous SEA transient equations are no more applicable. Nevertheless, SEA still provides estimate of mean vibrational transfer over $\Delta\omega$ between two coupled subsystems. This transfer is independent of the force process as soon as the response points are far enough from the excitation, thanks to diffusion assumption.

Valid for steady-state, SEA equations need to be complemented by extra theory for predicting highly transient pyroshock events in time domain. LMPR algorithm provides fast solution to this problem. The SEA model is used to predict transfer velocity Vr/Fe between excited subsystem (emitter) and targeted subsystem (receiver). Vr/Fe is real-valued as SEA only provides power spectral density outputs. Vr/Fe is an estimate of the actual modulus of the mean complex transfer velocity between source and receiver.

A pyroshock source delivers a large amount of shear power. Thus structural SEA subsystems should incorporate energy of both flexural, extensional and shear waves. They are usually considered as three coupled separate subsystem energy entities inside the physical structural subsystem. These energies are cross coupled between subsystems at junctions due to force projection.

The full SEA transfer between emitter and receiver is then a 3 x 3 matrix relating source and wave velocity of receiver and expressed as:

$$\begin{Vmatrix} v_{iF}^2 \\ v_{iE}^2 \\ v_{iS}^2 \end{Vmatrix} = \begin{bmatrix} H^2{}_{FF} & H^2{}_{FE} & H^2{}_{FS} \\ H^2{}_{EF} & H^2{}_{EE} & H^2{}_{ES} \\ H^2{}_{SF} & H^2{}_{SE} & H^2{}_{SS} \end{bmatrix} \begin{Vmatrix} S_{jF}^2 \\ S_{jE}^2 \\ S_{jS}^2 \end{Vmatrix}$$

i is the index of receiver subsystem and *j* emitter one. *F*, *E*, *S* are respectively the flexural, extensional and shear energies, *H* is the modulus of SEA transfer between various wave-type energies. v^2 is the velocity of a given wave type in the receiver subsystem while S^2 is the PSD of the source (force or constrained velocity of emitter).

Given a time-history descriptor $f_e(t)$ of the shock source and its Fourier's transform $F_e(\omega)$, Vr/Fe and $f_e(t)$ are jointly used to deliver a mean time history profile V(t) of receiver.

Receiver response is first developed in modal series based on local mode shapes and eigenvalues, $\left\{\omega_k^2,\psi_k(\mathbf{x})\right\}$ extracted from the subsystem analytical differential equation driving its modes.

Receiver response is then expressed as: $v_{re}(\omega,\mathbf{x}) = \sum_k j\omega \cdot Q_k(\omega,\omega_k)\psi_k(\mathbf{x}_r)$ with Q_k local modal amplitude of mode k,. *r* is received index and *e* emitter. The generalized force propagated to the receiver is represented by an equivalent point force with $\beta F_e(\omega)$ amplitude where β is a force calibration coefficient assumed to be constant over $\Delta\omega$.

From this, an admissible narrow band transfer function, $\tilde{h}_{re}(\omega,\mathbf{x}_r,\mathbf{x}_e) = H_{re}(\omega,\mathbf{x}_r,\mathbf{x}_e)e^{j\alpha(\omega,\omega_k)}$ between source and receiver is built from interpolation procedures in the complex number domain.

H_{re}, when band-averaged over $\Delta\omega$, gives same level than Vr/Fr.

$e^{j\alpha(\omega,\omega_k)}$ is the phase term provided by the local modes of the receiver.

By inverse Fourier's transform the impulse response $h_{re}(t)$ of $\tilde{h}_{re}$ is processed.

For each energy type indexed *i* (flexural, shear and extensional), the response in the receiver is finally obtained by convoluting $h_{ire}(t)$ and with the source term $f_{ie}(t)$ as shown in Figure 9-22.

As v_{ire} is still dependent of an arbitrary choice of observation and response points in the receiver, location points within source and receiver are randomized and the final SRS is an average over all point-to-point SRS. The computed variance of final SRS allows some engineering judgment over sensitivity to point location which generally falls within 1 or 2 dB.

Application examples of this technique are given in [RD-038] describes early application of LMPR to SPOT payload response to SHOGUN test. [RD-038] describes joint use of LMPR and VSEA technique (see next paragraph) to the prediction of four shock tests of SMART1 payload and VEGA upper part. These latter predictions were validation procedures of the SEA-Shock module of SEA+ software implementing LMPR technique. VEGA subsystem partitioning is shown in Figure 9-23. On the emitter side, in-plane and flexural source powers are simulated by dedicated SEA+ theory and are applied on reinforced junction between annular source ring and upper part skirt cylinder. SEA+ VEGA subsystems incorporate the three wave types. In same figure, predicted flexural SRS at payload interface is compared with pyroshock related test SRS.

NOTE To predict a robust SEA mean transfer function between source and receiver, both flexural and in-plane wave energies are required as in-plane energy is generally dominant at very high frequency and cannot be neglected. At junctions the three energies carried by structural subsystems are cross-coupled and specific attention should be paid on CLF calculation by taking into account curvature effects. CLF computed using plate-to-plate coupling theory used in analytical SEA software are overestimating CLF between curved structures below their ring frequency. In these cases, CLF may be computed from FEM related model following the Virtual SEA technique.

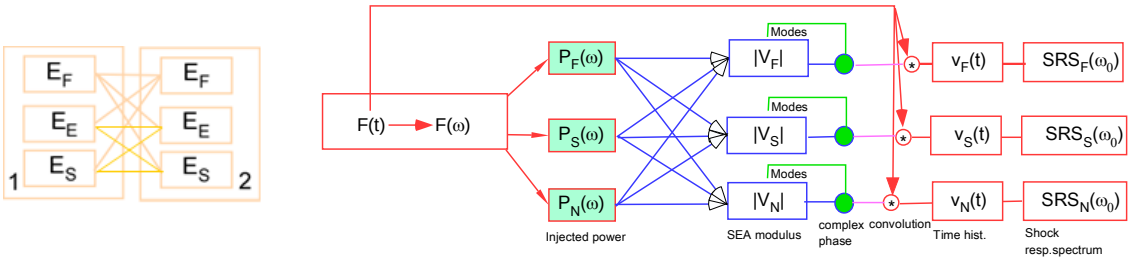

Figure 9-22: Left, coupling of wave energy between 2 subsystems due to flexural, extensional and shear waves and right, LMPR data flow

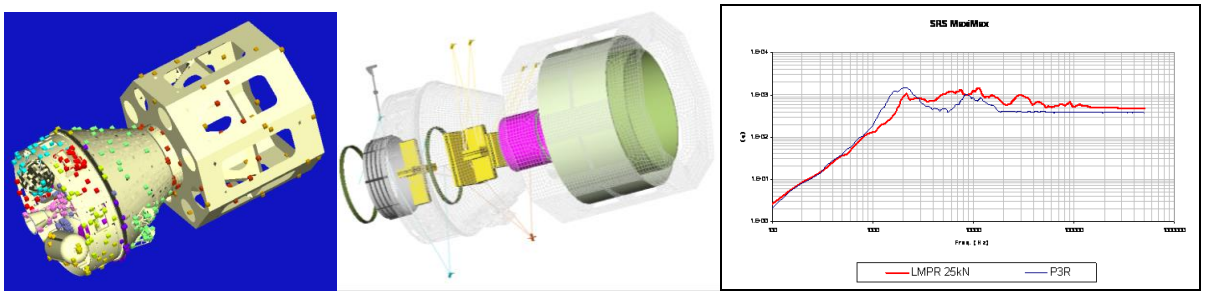

Figure 9-23: SEA model of VEGA upper part (SEA+) for pyroshock prediction

9.3.4 Virtual SEA modelling for robust SEA modelling in the mid-frequency

In MF range (200-2000 Hz), SEA transfers may be difficult to derive with accuracy with standard analytical theory for two main following reasons:

- Analytical description is not enough informative or too simple,
- Geometry is too complex and is difficult to subdivide into set of weakly coupled flat panels or cylindrical shell.

VSEA technique has been developed to override previous difficulties by relying on FEM modeling for predicting a rationale subsystem partitioning, the modal density and CLF of related subsystems. To avoid arbitrary user's choice, the FEM-to-SEA process is automated following steps sketched in Figure 9-24.

- **First**, an original FEM model is post-processed in a classic way by extracting global eigenvalues and eigenmode amplitudes on a grid of nodes which maps the system.
- **Second**, transfer functions are synthesized between all nodes.
- **Third**, the node set is sorted into groups (or subsystems) by a specific attractive algorithm that detects energy gap between groups.
- **Fourth**, the FRF matrix is compressed on this subsystem decomposition to get mean transfer velocity per subsystem (compressed FRF matrix).
- **Fifth**, this latter matrix is used to identify the SEA loss factors by inverting the compressed energy matrix as in experimental SEA.

On output, it provides modal density, CLF and wave number of the various subsystems. DLF is an input in VSEA as FRF are synthesized with given user-defined damping. The identified CLF are shown to be independent of damping as soon as they stay in a reasonable range (0,001 up to 0,1) which covers most of the vibrational problems. Actual DLF are then introduced afterwards in the VSEA model to fit to physical damping.

VSEA models are frequency-band limited due to FEM mesh size. For high frequency pyroshock applications, VSEA models are expended at high frequency using embedded analytical modeling. Time to setup a SEA model from FEM representation is drastically reduced to a few hours of processing, making any FEM developed throughout projects easily reusable for pyroshock prediction as no particular request is made by VSEA regarding FEM characteristics.

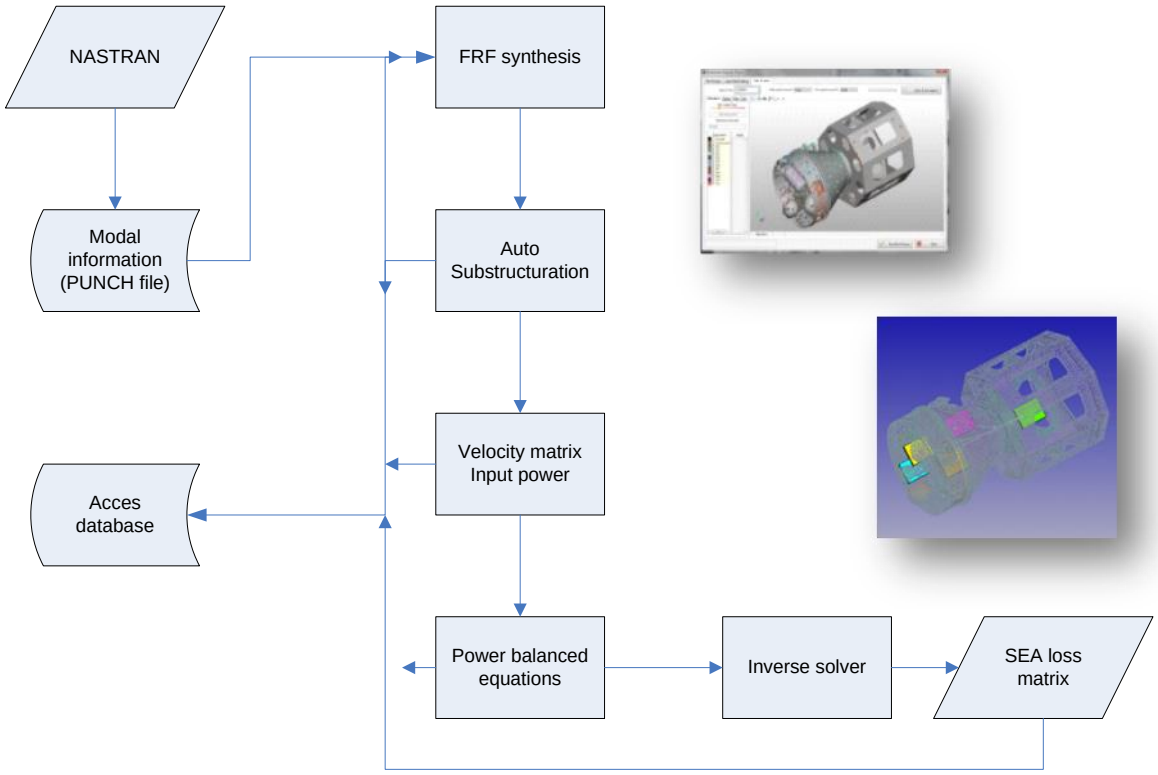

Figure 9-24: Diagram flow of VSEA processing

9.4 Best practices for shock derivation by simulation

The evaluation of the shock environment in a spacecraft can be also obtained using numerical simulations based on FEA and/or SEA approaches although these methods have many limitations.

In fact, as noted in the examples related to the numerical simulation reported in this handbook, the shock prediction remains a difficult task and does not produce well-correlated results with test results at every location.

For this reason the shock environment derivation by simulation should never be used alone but it is recommended to use it in conjunction with other ones (such as similarity / extrapolation methods).

The range of validity of the FE method shock predictions is usually limited to the shock far-field range and at generally low or medium frequency (< 2 kHz) rather than high frequency.

The simulation methods are recommended to consolidate the spacecraft zoning shock environment obtained by the similarity /extrapolation methods used, during the early project phase, and eventually to derive the shock levels at the equipment interfaces.

In the shock transient analysis based on FE method both explicit and implicit solutions are available and the explicit solution is more recommended when the shock event is highly dynamic and when the event's duration is relatively short.

9.5 Examples of methodology for numerical simulation

9.5.1 Numerical simulation for clampband release

Besides the analytical shock zoning of SMART-1 a time domain analysis has been carried out to consolidate the shock environment generated by the clampband release [RD-014].

Special attention has been given to the model limitation with regard to shock. Rules, as presented in paragraph 9.2.4.1, have been followed for the adaptation of SMART-1 FEM model to a dedicated model compatible with shock analysis (Figure 9-25). In particular, 64 nodes at 937 mm diameter interface are enough to properly represent modes up to the main breathing mode (around 1600 Hz). A Non Structural Mass formulation has also been adopted for all equipment.

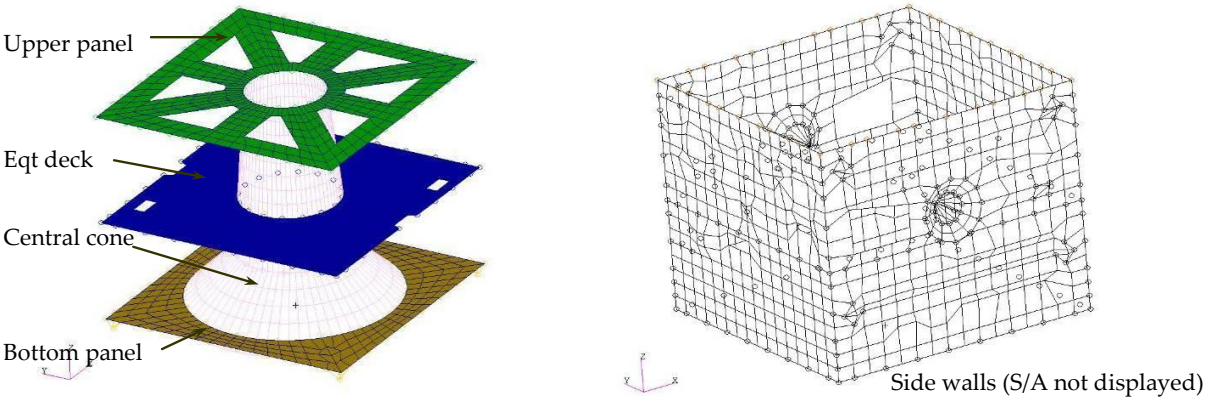

Figure 9-25: Overview of SMART-1 FEM

The Forcing function as shown below was found to be an "optimum".

It consists of 3 phases: The loading phase is bringing slowly (in order to avoid numerical instabilities) the system up to pre-separation condition. Then the preload is released in 0,2 ms, which is consistent with test data (using the ESTEC shock database). Finally, the system responds in free-free conditions. See Figure 9-26.

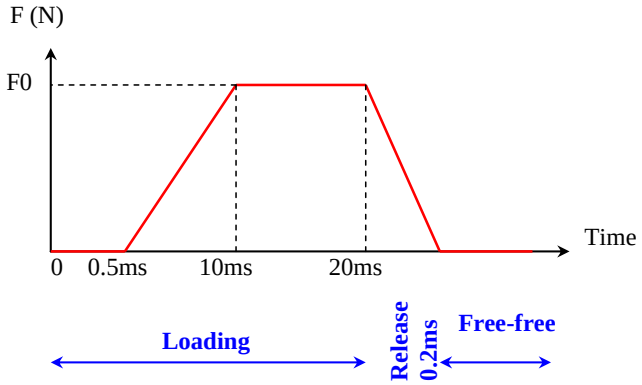

Figure 9-26: Force vs. time scheme used for source modelling

The time dependant load is applied radially at 64 equally spaced locations around the bottom of the interface ring (64 times F_0). The amplitude of the radial force F_0 (equivalent to the clampband pre-tension) can be derived from the preload, as follows (Figure 9-27):

In the test campaign, the clampband had a preload of P=21,8 kN.

$$P = \int_0^{\frac{\pi R}{2}} \varphi.\cos\theta.dl \quad \text{with} \quad \varphi = \frac{64F}{2R\pi} \quad \text{(induced flux around the ring)}$$

It comes $F = \frac{\pi P}{32} = 2140\,N$

Then, assuming the stiffness of the spacecraft ring and the ACU ring to be roughly the same, we can derive the radial force to be applied on the model:

$$F0 = \frac{F}{2} = 1070N$$

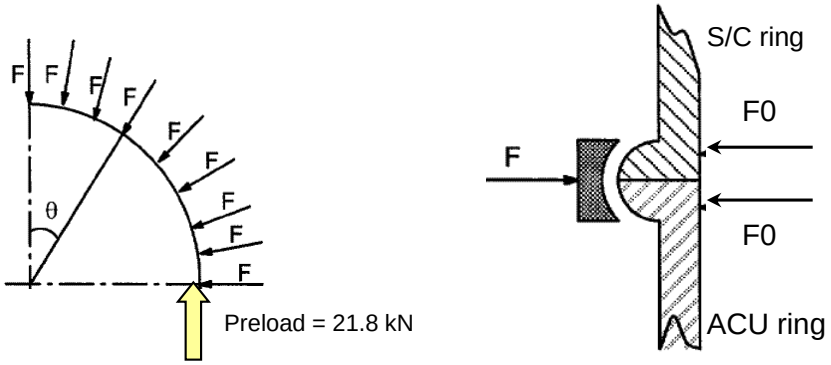

Figure 9-27: Calculation of radial load corresponding to a given clampband preload

The external load is assumed to be axially symmetrical at any time step. This leads to excite preferably the first breathing mode (n = 0). Some special techniques exist to excite other breathing modes (e.g. n = 2, 4, …), but bring more complexity than advantage. Therefore, it is expected that the SRS levels are under-estimated in the lower frequency band.

Various aspects have been studied, such as input change (different shape of forcing functions, different release time) or loads applied with delay (to take into account the relaxation in the band). Resulting outputs have been evaluated and confronted to both relevant test data and analytical SRS prediction (based on ESTEC attenuation rules – see 0).

Figure 9-28 present two examples of achieved correlations with test data. These figures also show the analytical SRS prediction based on ESTEC attenuation rules (see 8.3.2)

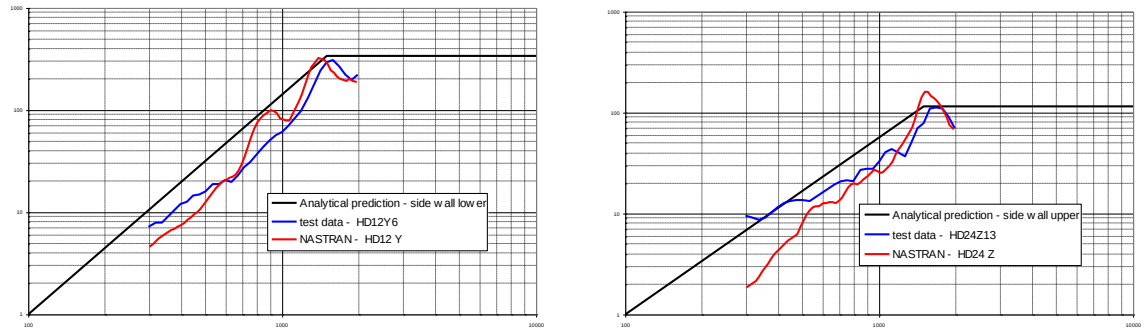

Figure 9-28: Comparison between analytical prediction, FEM prediction and test data

Generally speaking, a sufficient correlation between FEA results and test data is achieved:

- The maximum levels (at the corner frequency of 1600 Hz) are in the same order of magnitude (around 3 dB inaccuracy).
- In the lower frequency band, the FEA results are usually under-estimated. The loading condition leads to excite preferably the first breathing mode (n = 0), other contributions (e.g. n = 2, 4, …) are not excited.
- Finally, the analytical SRS predictions (correlated ESTEC rules applied to the radial shock specification at the spacecraft interface) are in agreement with both test data and FEA results. This fact allows to get more confidence in the shock zoning operation, and to consolidate the shock specification at unit interface.

9.5.2 Numerical simulation for Shogun

In addition to the C/B test SMART-1 was also subjected to a Shogun test in the frame of the qualification of SMART-1 with respect to shock.

A study has been carried out aiming first at refining and improving the forcing function representative for the Shogun shock event. Further aspects such as damping parameters, equipment modelling and selection of restitution points (effect of sensor location) have been studied to improve confidence in implicit computations and assess their robustness. Resulting outputs were evaluated in terms of SRS levels or SRS ratios (transfer function).

$$R = \frac{SRS(Q=10)EQT\_I/F}{SRS(Q=10)S/C\_I/F}$$

The test configuration was made up of SMART-1 STM connected to the payload adapter (ACU937). The simulation was conducted on a fully representative configuration, as shown in Figure 9-29.

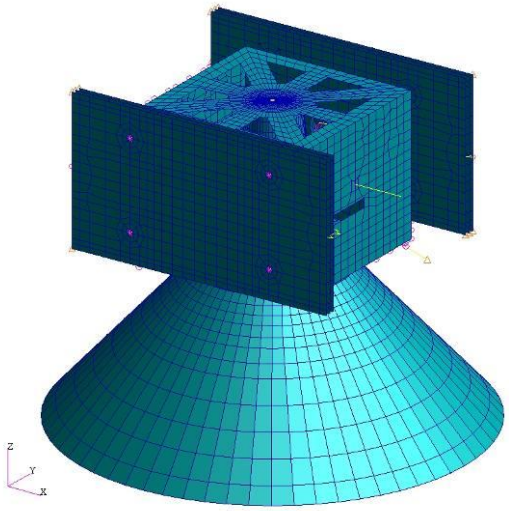

Figure 9-29: SMART-1 Shogun configuration

The shock was applied in the form of a rectangular force impulse at 64 equally spaced locations around the bottom of the payload adapter.

An impulse of 0,2 ms (-7500 N in radial direction and 15000 N in axial direction) was found as an optimum for a proper correlation of the shock response between test and simulation at S/C I/F. The figure below compares the maximum envelope (of radial and axial levels) of test and simulation for structural damping of 1 % at 600 Hz.

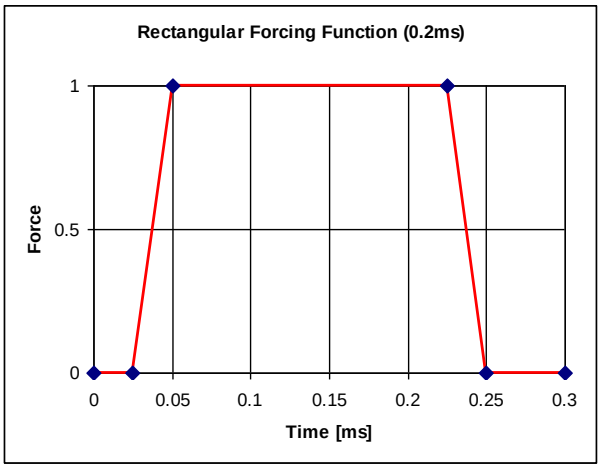

Figure 9-30: Shogun force impulse

As shown in Figure 9-31 a good correlation is achieved at the S/C I/F over the entire frequency range with only a local exceeding around 1500 Hz.

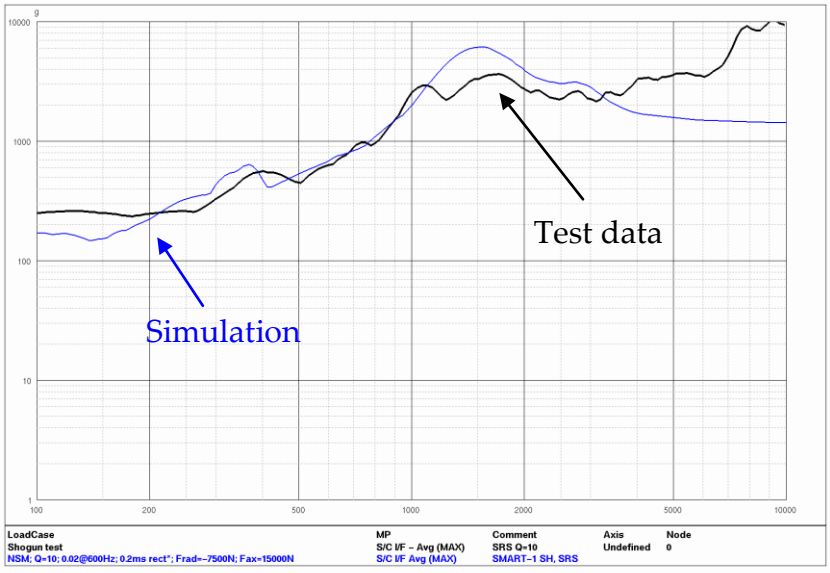

Figure 9-31: SMART-1 Shogun test correlation at S/C I/F

Subsequent to the forcing function definition and based on the above correlation the Shogun NSM-model was used to derive SRS ratios between spacecraft interface and unit interface. These ratios are independent from the energy actually introduced into the system and confronted towards system test data measured in areas without or at least lightweight equipment. In terms of definition of suitable damping parameters the method of adjusting the structural damping at 3 different frequencies (1,5 % at 300 Hz, 1% at 600 Hz and 0,5 % at 1000 Hz) was used. Examples of typical correlations which have been achieved inside the spacecraft can be seen in Figure 9-32.

The achieved correlation is considered sufficient and gives evidence that a conservative global shock environment derivation, as it is done during zoning procedure, can be supported and consolidated by numerical analysis.

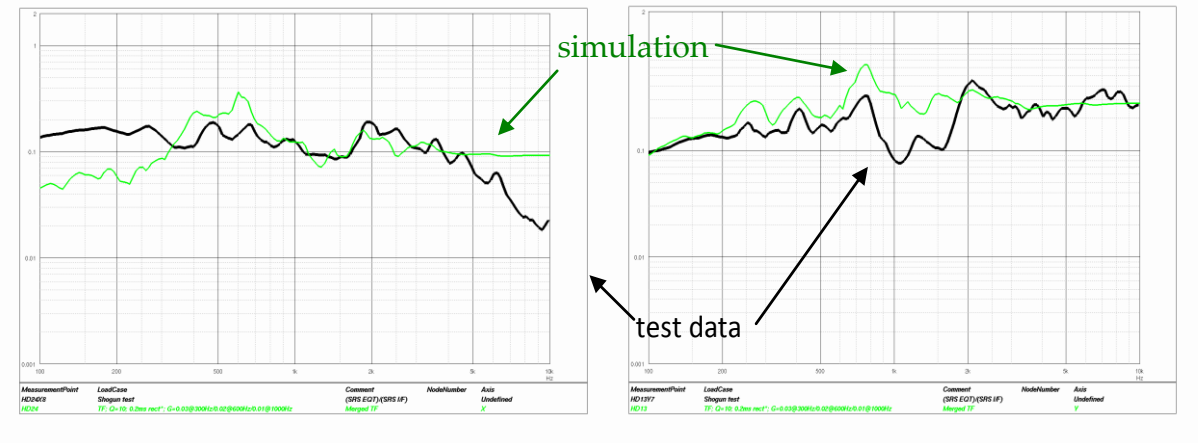

Figure 9-32: Shogun correlation in area without equipment

In order to assess the opportunities and robustness of detailed shock predictions at equipment interface using implicit codes (such as NASTRAN), the SMART-1 STM-model was modified with respect to equipment modelling. Different methods have been evaluated using lumped mass formulation, solid boxes and detailed unit modelling. To limit the effort the heaviest unit (PPU-dummy) was selected and served as example case (see Figure 9-33). As described in 9.2.4.5 special attention has been paid to the proper selection of the restitution point representing the sensor location.

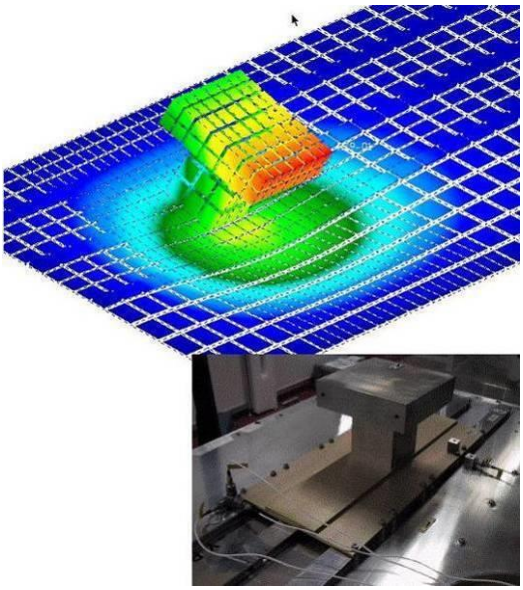

Figure 9-33: SMART-1 PPU-dummy

It turned out that already with a limited effort (equipment modelled as a box with solid elements and representative in terms of mass, footprint, CoG in out-of-plane direction) a good agreement between test and analysis is indeed feasible.

As shown in Figure 9-34, a sufficient correlation with test data is achieved in in-plane as well as out-of-plane direction. Analyses showed that the way equipment are modelled is critical particularly in terms of response in out-of-plane direction.

The investigations on SMART-1 Shogun test give confidence that numerical simulations are adequate for early prediction of far-field shock environment (shock zoning) as well as for more detailed analyses in qualification phase of projects.

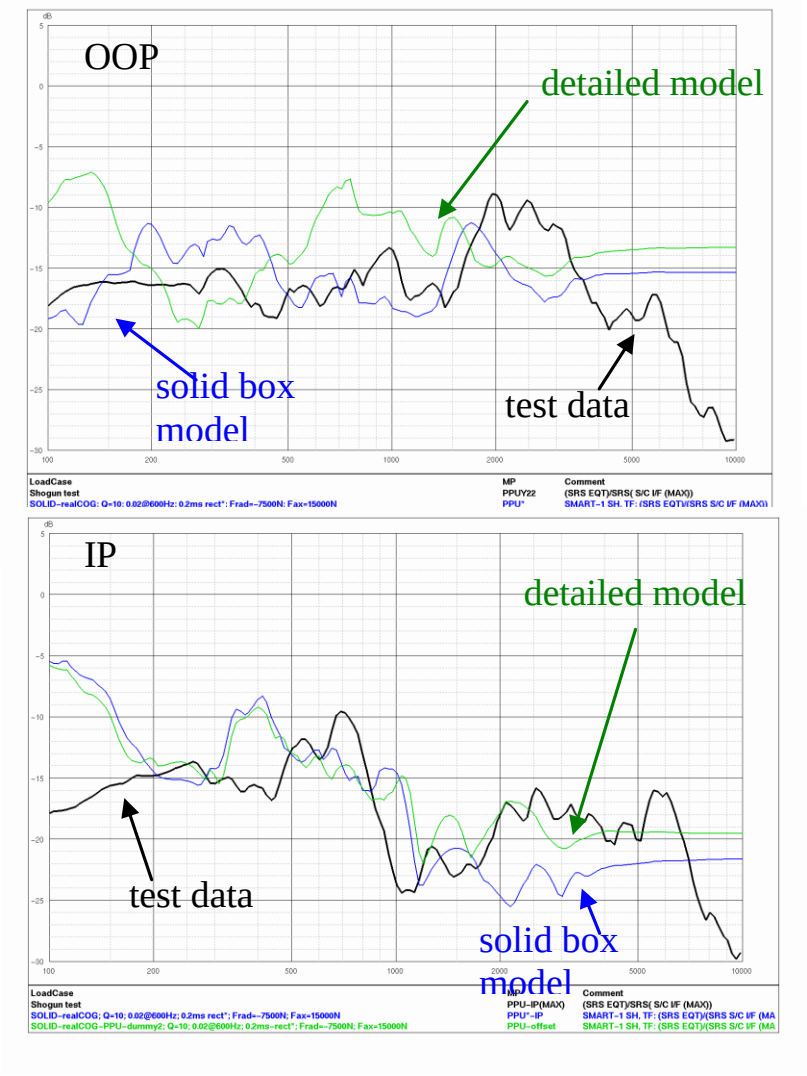

Figure 9-34: SMART-1 PPU-dummy correlation

9.5.3 Numerical simulation for launcher induced shock

9.5.3.1 Overview

Full coupled shock analysis capabilities have been developed over the past years and have been used for the consolidation of launch configuration. Such numerical analysis aims at predicting the shock level at the spacecraft interface, taking the coupling effect with the adjacent structures into account. For Ariane5, this capability is particularly used for "off-nominal" launch configurations, for which the return of experience from previous flights is limited. A5 /MSG configurations were in this situation, and dedicated analyses performed by ESA/ESTEC [RD-014] are presented in paragraph 9.3.3.2 below. Studies performed recently in the frame of the A5 Low Shock Recovery Plan aimed at limiting shock levels at payload interface were also based on a model (see paragraph 9.3.3.3).

In both cases, this capability consists in a database of dedicated shock FE Models of the Ariane 5 upper composite stage (JAV, VEBs, EPS, ECA, SYLDA, ACY, ACUs, SADs, Payloads), and it consists in a set of forcing functions (with an associated methodology) representing the main shock events (VEB and fairing).

9.5.3.2 A5 / MSG coupled shock analyses

MSG was qualified with respect to a clamp-band excitation, but due to some programmatic reasons the extrapolation/verification of the shock environment imposed by Ariane 5 was incomplete. Therefore, the shock levels at the spacecraft interface had to be reduced by means of heavy mass dummies (MFDs) and attenuation systems (PSAD, GSAD).

9.5.3.2.1 MSG1 coupled shock analysis (successfully launched by Ar5 on 29/08/2002)

9.5.3.2.1.1 Introduction

This capability was first used for the consolidation of MSG1 launch configuration. The dimensioning shock environment was generated by the VEB separation (1st generation of A5 family). A stack of attenuation systems was necessary to bring the shock environment (generated by the VEB separation) down to levels compatible with the qualification status of MSG.

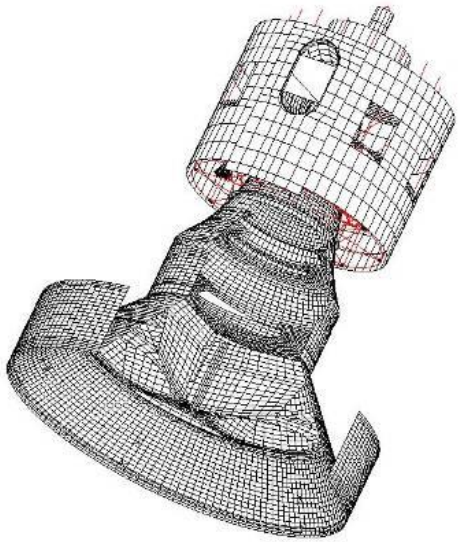

Figure 9-35: Ar5 upper composite model for MSG1 Coupled Shock Analysis (VEB sep.)

A step-by-step approach has been undertaken, aiming at deriving a consolidated prediction. Aspects such as test correlations, configuration changes, study of interactions between different LV elements, and the resulting uncertainties have been evaluated.

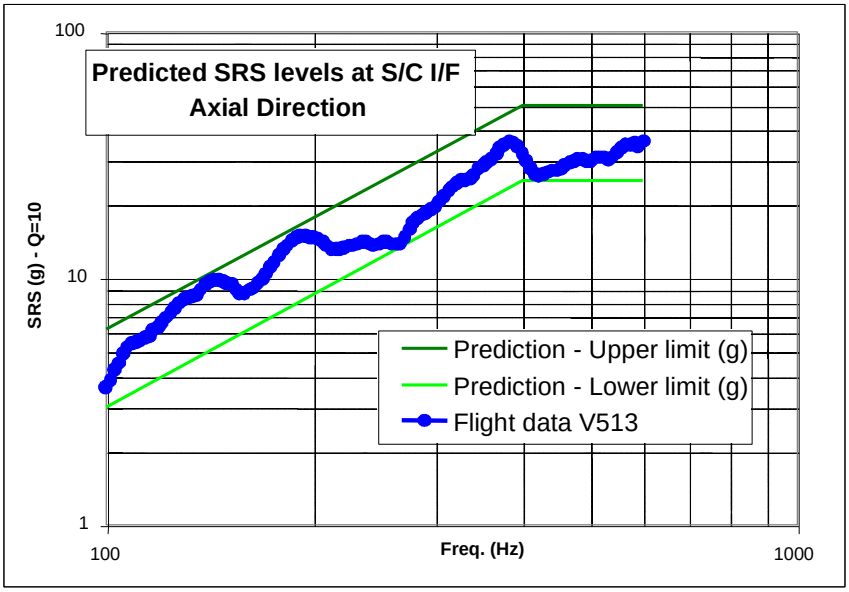

Figure 9-36: MSG1 flight prediction, compared to actual flight data

It is important to note that these predictions were performed prior the MSG1 flight V513.

The predictions, of the shock environment induced by the VEB separation event, were presented as a form of a band (in green), in which the MSG1 flight data should be contained.

As shown in Figure 9-36, the comparison between the prediction and the flight data shows a very good agreement. A sufficient correlation with flight data is achieved (flight data within predicted range of ± 3 dB).

The predictions were initially limited to the dimensioning shock event (VEB separation). In prevision of the next launch of MSG2, and in order to demonstrate the adequacy of the proposed methodology, the Coupled Shock Analysis capability has been extended to the prediction of the shock environment induced by the fairing jettisoning event.

The results of this investigation, including the correlation with flight data, are presented here below. Two methodologies, for deriving the shock environment at the spacecraft interface, have been investigated.

9.5.3.2.1.2 Method ① - Direct Computation

The shock environment at the spacecraft interface is a direct output of a direct transient analysis.

Pulse forces are introduced into the system (at fairing separation interface), propagate through the structures and excite the structure mode shapes.

Some detailed investigations have been conducted to derive a consolidated forcing function. Aspects such as repartition of amplitudes between axial and radial excitations, duration, and delay have been studied in details.

Pulse forces are applied, in axial and radial directions, at 144 equally spaced locations around the top of the ACY interface ring. The output is directly predicted at the spacecraft interface.

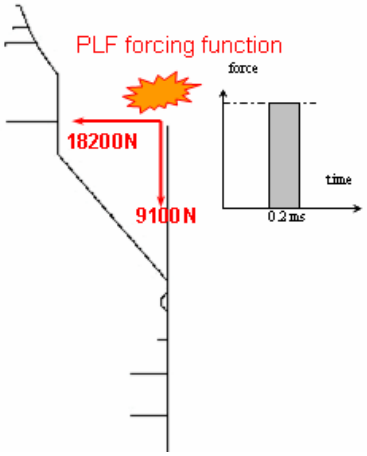

Figure 9-37: Applied forcing function for MSG2 Coupled Shock analysis

9.5.3.2.1.3 Method ② - Attenuation Identification by FEA and scaling to flight data

This second method is more in line with the previous MSG1 computation of the VEB separation event. The SADs combined attenuation is identified by analysis, and corresponds to the ratio between two systems (with and without Shock Attenuation Devices):

$$SADattenuation = \frac{SRS(configuration\_with\_SADs)}{SRS(configuration\_w/o\_SADs)}$$ (ratio of SRS at spacecraft interface)

This identified attenuation is then applied to relevant flight data (reference flight without attenuator device), in order to derive the estimated flight environment for MSG1.

This method presents the advantage to be less sensitive to the forcing function definition (the pulse force amplitude can be normalized; the ratio is independent from the energy introduced in the system).

Figure 9-38 presents the results of both predictive methods compared with V513 flight data.

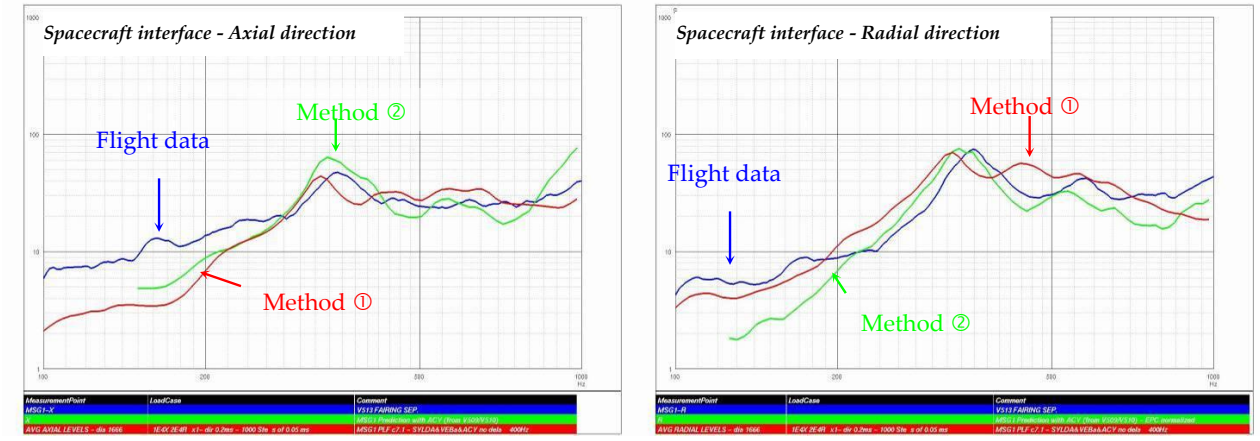

Figure 9-38: Comparison between both predictive methods and V513 flight data

It can be concluded that the first method correlates well with V513 flight data. Adequate correlation in both directions (axial and radial) has been achieved. Underestimation occurs only in axial direction below 200 Hz, but it is due to the damping assumption (centred at 400 Hz), and due to the boundary conditions of JAV-EPC.

Same quality of results is also achieved when following the 2nd method. Adequate correlation with flight data is evidenced in both directions, bringing high confidence in the adequacy of the predictive methods.

The adequacy of the Coupled Shock Analysis capability is demonstrated and builds up the basis for MSG2 predictions.

9.5.3.2.2 MSG2 coupled shock analysis (successfully launched by Ar5 on 21/12/2005)

All MSG satellites (FM1 to 4) are identical with regard to sensitivity to shock events and environmental qualification status. The launch configuration adopted for MSG1 had to be reviewed in order to be in line with the modifications implemented on the Ariane 5GS Launch Vehicle, and to become more flexible in finding a suitable co-passenger. The main modification, among others, concerns the VEB separation system, which induces a lower excitation to the spacecraft. The dimensioning shock event becomes the fairing jettisoning event.

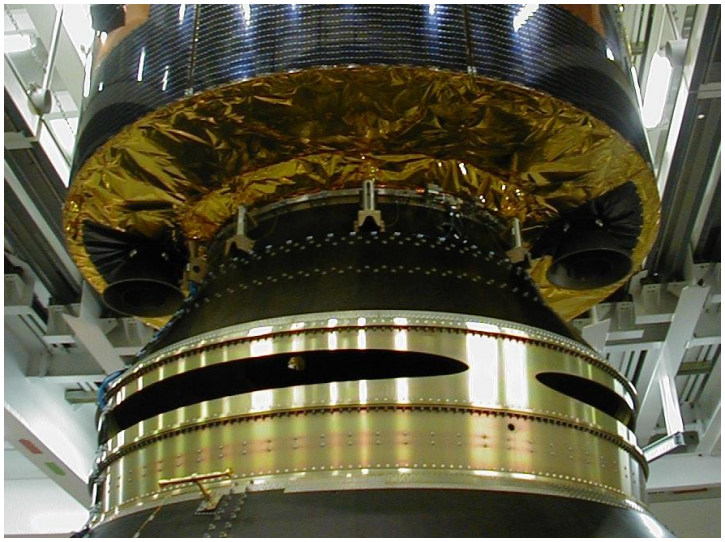

Figure 9-39: Stack of attenuation systems for MSG2

Although the severity of the shock environment has decreased, it is still outside the qualification status of MSG. Due to a lower attenuation need, the stack of attenuation systems has been adapted.

In complement to the Arianespace predictions, based on flight and experimental data, a Coupled Shock Analysis has been carried out by ESA/ESTEC to consolidate the MSG2 launch configuration.

As for MSG1, a step-by-step approach has been undertaken, aiming at deriving a consolidated prediction. Aspects such as V513 (MSG1) correlation, test correlations, configuration changes (e.g. ACY and SYLDA effects, SADs combined attenuation), Study of interactions between different LV elements, and the resulting uncertainties have been evaluated.

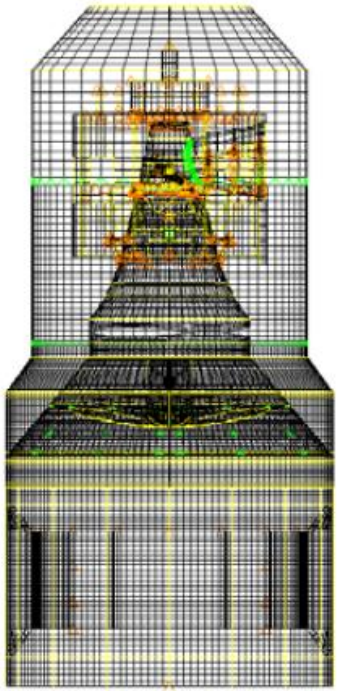

Figure 9-40: Ar5 upper composite model for MSG2 coupled shock analysis (PLF sep.)

As shown in Figure 9-41, the MSG-2 post flight evaluation evidenced the adequacy of the prediction. The comparison between the prediction and the flight data shows a very good agreement (flight data within predicted range of ± 3 dB).

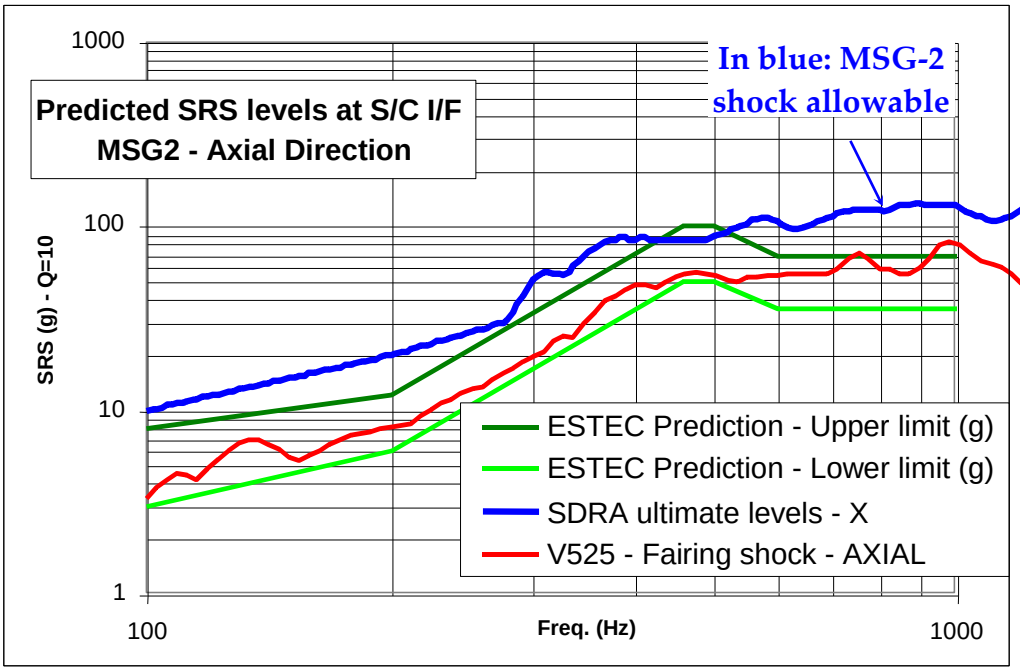

Figure 9-41: Results of Launcher Induced Shock prediction compared to flight measurement

9.5.3.3 Ariane5 Low Shock Recovery Plan Analyses

This project led between 2009 and 2013 addressed different topics among which:

- improvement of an existing shock attenuator, (with a purpose of mass reduction keeping same attenuation performances);
- development of new shock attenuators as close as possible from the payload, i.e. at I/F 1780;
- analysis of HSS1 modification in order to limit the propagation of shocks from the source;
- Improvement of flight measurement plan.

These activities require a good understanding of the physics, both for shock propagation from source to payloads, and for mechanical behaviour of the attenuators themselves under shock waves. Thus, in order to fully understand these points before implementing the attenuator concepts or modifying measurement location, a numerical model has been developed. It represents the physics of the shock induced by the fairing jettisoning in the mid frequency domain. This tool was used in parallel to flight data and ground test data analysis as well.

Major achievements have become possible thanks to this tool (see below). Anyway, due to its limitations (e.g. limitation of model validity to the frequency range [200:800] Hz) it is important to note that this tool can't be a pure prediction tool but stills a help to decision.

9.5.3.3.1 Model description

Finite Element Model has been built for NASTRAN software analyses. It represents all structural parts involved in fairing shock propagation towards payloads: HSS1 ring, SYLDA5, PAS, VEB, ECA, 3936 Cone, ESC-A and Payload (here represented by MAQSATB). Generally models are derived from

static/dynamic models available in the context of Ariane 5 Programs and provided by System or Sub-Contractor teams. In some cases meshes have been refined in order to roughly reach a 1000 Hz capability (actual capability of the global model being estimated at 800 Hz).

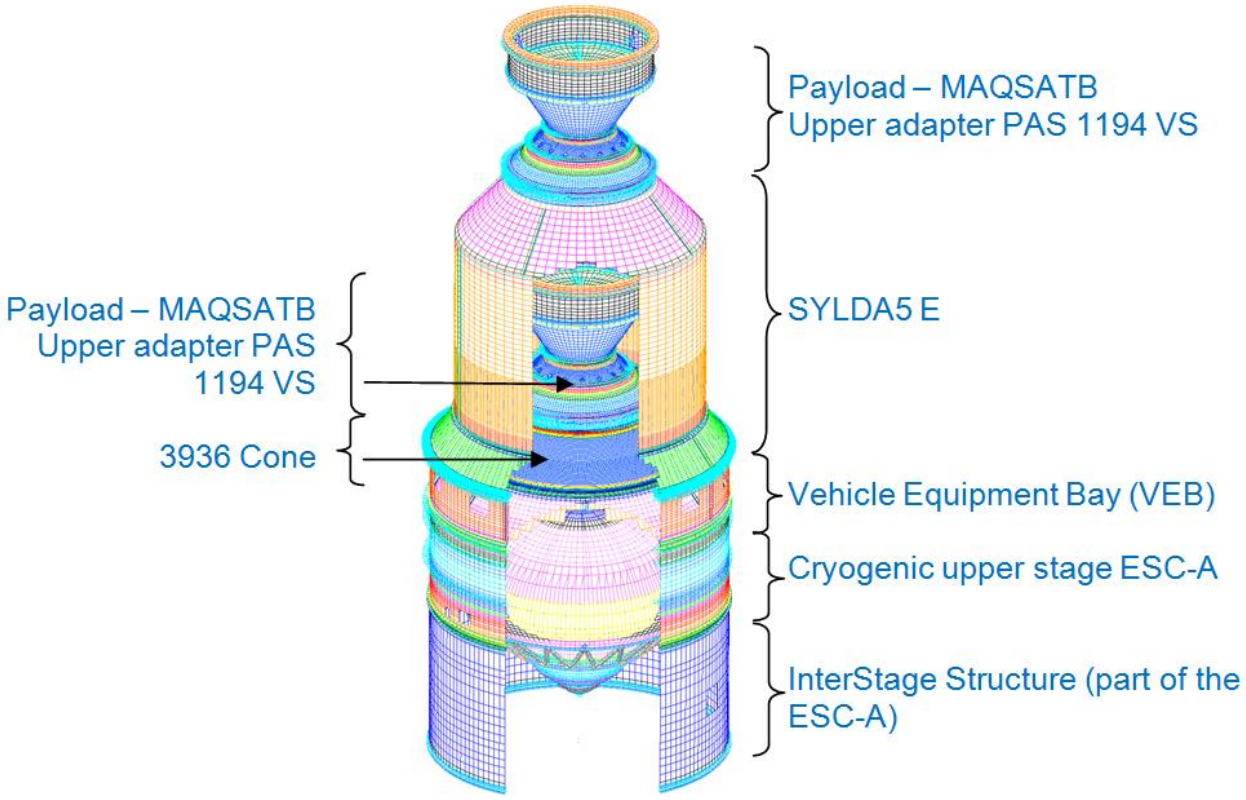

Figure 9-42: FEM of A5 Upper Part configuration

Model assembly is validated through longitudinal and lateral first modes restitution of both lower and upper branches.

It is important to pay specific attention to the mesh refinement and model assembly for good simulation results, which needs experienced people on this kind of topic.

9.5.3.3.2 Model excitation

Shock induced by HSS1 fairing separation is represented through a running force imposed in the model at the cutting location. Running forces are imposed from the initiation points of these pyrocords. Time delay between point initiations can be represented according to physical parameters of the separation device. Ratio between longitudinal and radial forces has been set to get the best correlation with flight data.

9.5.3.3.3 Main achievements

As it has been said before, this model cannot been understood as a fully predictive tool but has been very useful for analysis and comprehension of shock propagation in the Ariane 5 upper part. Main conclusions which were derived from analyses based on this model are presented hereafter:

Flight levels comparison:

Comparisons obtained with flight data are satisfactory as shown below for example in the frequency validity domain expected:

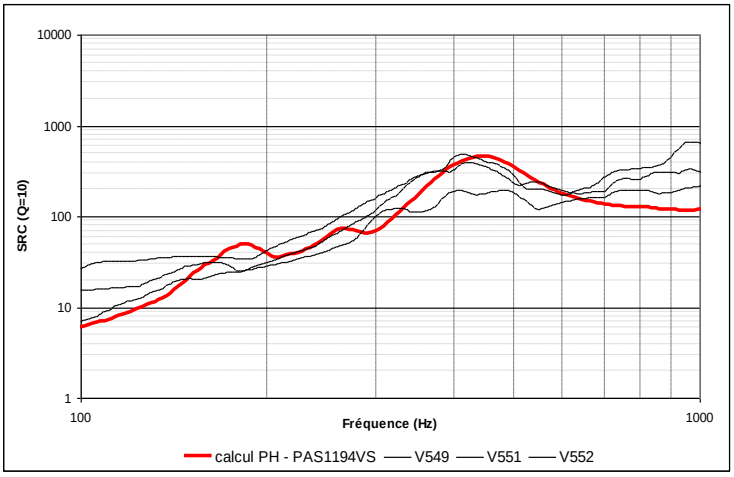

Figure 9-43: Comparison of simulation result w.r.t. flight levels

Model result is among flight measurement acquired with similar upper part configuration (A5-ECA with same PAS, but discrepancies induced by payloads are not tackled by the model).

Launcher / Payload Interface levels discrepancies:

One other outcome of the model is the demonstration of spectrum dispersion at the payload interface with regard to azimuth location. Figure below give illustrations of the difference obtained at payload interface in two different configurations:

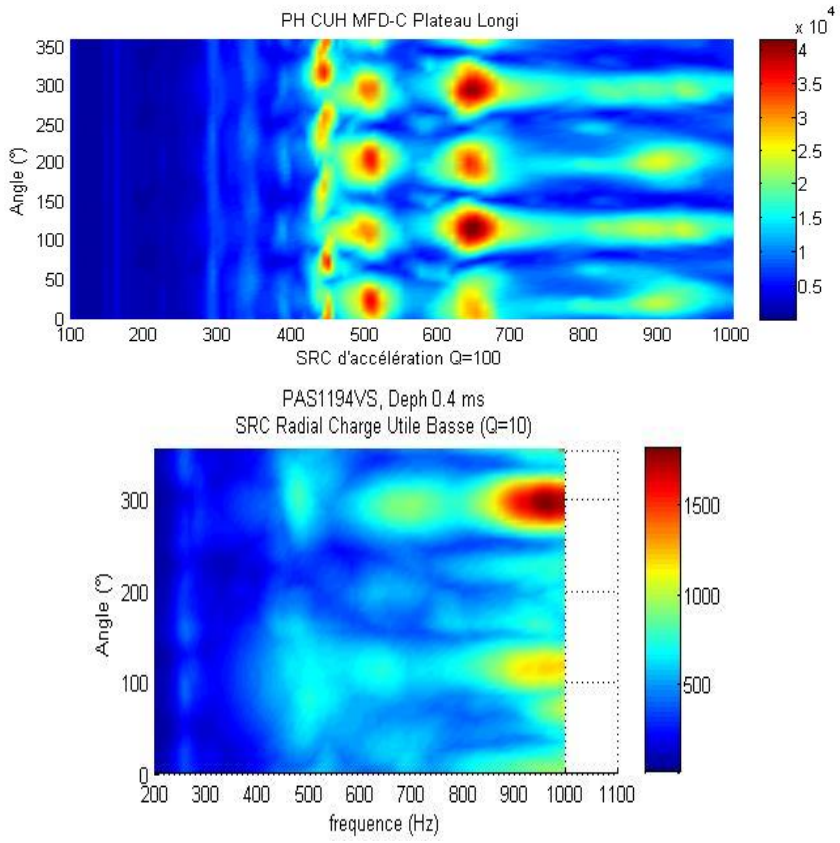

Figure 9-44: spectrum dispersion at the payload interface with regard to azimuth location

This kind of results has been used for the improvement of flight measurement plan and for the explanation of flight anomalies. (Analysis of local geometrical or mechanical details for example).

Attenuator development:

The tool has also been widely used in the frame of attenuator improvement giving a comparison between SHOGUN ground test, A5 lower position and A5 upper position configurations.

This had an impact on specifications for attenuator devices like SASSA and also helped in MFD improvement which is now achieved (light MFD has successfully flown on flight L563 with MSG3 in lower position and on L566 in upper position with attenuation performance in accordance with prevision).

9.5.3.4 Synthesis

For Ariane 5 shocks for which mid frequencies (~[200 – 1000 Hz]) is the domain of interest, numerical simulations can provide good information for shock levels at payload interface. It is recommended to pay attention to the model constitution, and excitation should be relevant with regards to actual separation device. In these conditions, numerical analyses can be very useful for the comprehension of physical phenomena involved in shock propagation towards payload and is a good tool for solution identification, classification and evaluation.

9.5.4 Implicit vs. explicit method: Example of a shock prediction on a complex structure

In the frame of a R&T CNES, different computations methods have been compared to predict the shock propagation on a satellite structure. The MSTH SPOT5/HELIOS2 model was chosen. Explicit, implicit and energetic methods have been used through commercial codes (NASTRAN, MARC, PAMSHOCK, RADIOSS and AUTOSEA2) to predict propagation inside the spacecraft with notably a SHOGUN type excitation. The initial FEM was the model designed for sine prediction, namely for low frequency study. This particular choice aimed at verifying the availability or the necessary adaptations to lead a shock propagation analysis in a complex structure until the ambitious objective of 10000 Hz. The results have been compared between codes and with SHOGUN test data. Finally, the last aspect of the study was a sensitivity analysis on important parameters (link, equipment, damping …)

The first step of this study was the adaptations of the FEM to the method, codes or type of loading. It is important to note that this step arose some serious difficulties (see 9.2.4.1) and was time consuming especially for explicit codes. The automatic gateway between commercial codes are indeed often insufficient to ensure a rapid and complete translation of the model, boundary conditions and loading (loading possibilities are often a particularity of each code). Moreover, it is important that the updated model is checked with regard to the initial one (e.g. modal behaviour, global stiffness, and stiffness matrix conditioning).

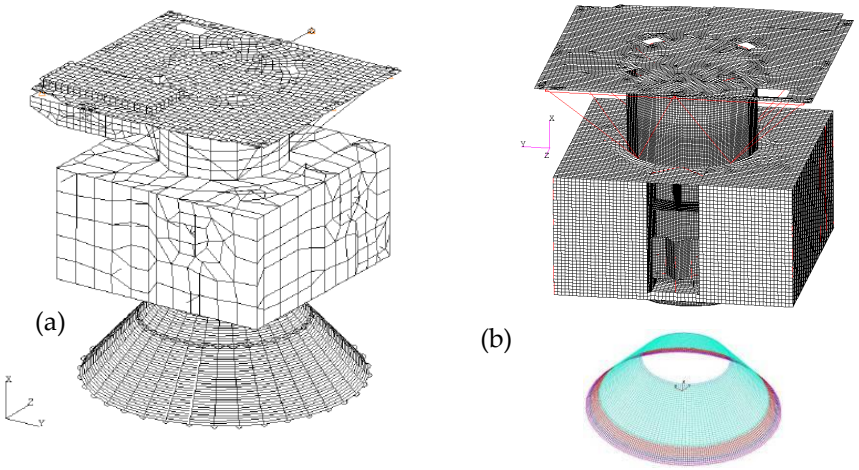

Figure 9-45: NASTRAN initial model (a) and PAMSHOCK model after adaptation for SHOGUN (b)

It can be seen on the Figure 9-45 that for explicit methods, as it is mentioned in paragraph 9.2.4.1, the mesh density and homogeneity are far above the implicit method needs. It was also necessary for this first step to refer to the plane for improving the model.

The computations results (see Figure 9-46) and sensitivity analysis have shown:

- Predictions are globally and logically better for low frequencies independently of the method (below 2000 Hz for explicit method and below 1000 Hz for implicit ones).
- Correlation quality for explicit method does not depend on the considered zone but on local effects
- Correlation quality for implicit method seems relatively homogeneous.

- The excitation is a key parameter, notably for SHOGUN test. For instance, the initiator synchronization when known, is included in the source model.
- Equipment level prediction is strongly dependent on equipment modelling, sensor and associated node.
- Position, number, stiffness and damping of links. These parameters become crucial with complex structure like spacecraft structure.

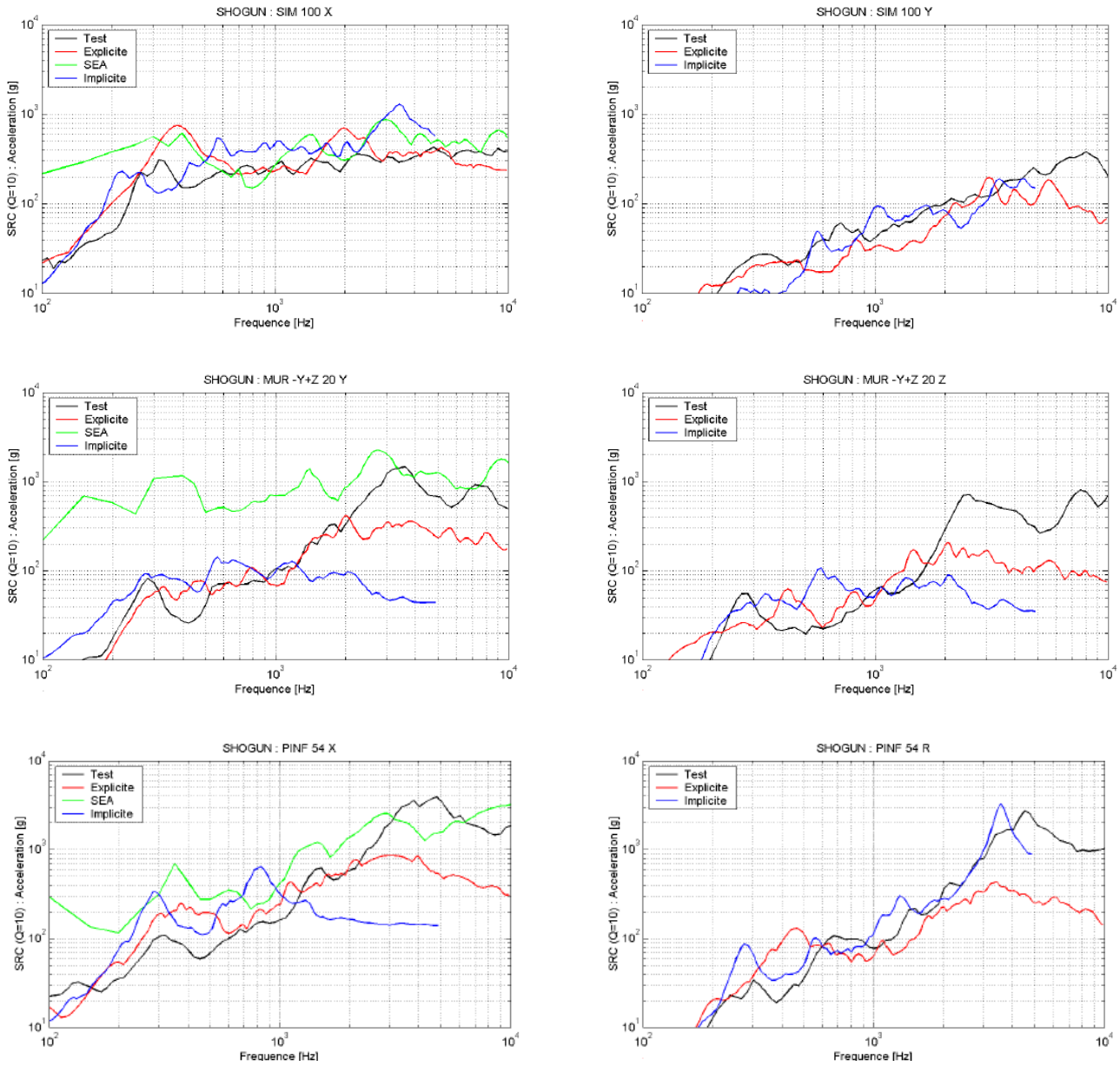

Figure 9-46: Comparison between explicit, implicit computations and SHOGUN test data

9.5.5 Shock prediction analysis examples using SEA-Shock module of SEA+ software

SEA-Shock module has been developed on the top of SEA+ software with the support of ESA by integrating SEA modelling capabilities based on analytical and virtual SEA combined with the technique of time reconstruction provided by LMPR algorithm. This integrated software was validated on realistic test cases (SMART1 clampband/Shogun tests, and VEGA stages separation / fairing separation tests).

SEA-Shock has been designed as SEA modeller with dedicated theory:

- to simulate the injected power by the shock source torque in the source subsystems
- to calculate modal densities and CLF of spacecraft structures from which the FRF are derived in a more accurate way than previously used numerical SEA software
- to transform FEM model into SEA parameters to cover MF range with more accuracy

The SRS on a receiver subsystem is thus obtained at the end from a hybrid SEA model based on FEM-derived parameters in MF band and on analytical SEA parameter in HF band.

This work has included:

- Experimental SEA (ESEA) test on a payload (SMART1) to identify SEA parameters in the MF and HF ranges such as DLF and CLF, mainly for validation purposes of the integrity of the SEA model construction,
- Software development to automate the LMPR prediction loop as explained previously,
- Validation test cases by correlating 4 different shock tests results with their simulation by SEA-Shock.
    - Test cases A & B: Prediction of SMART1 payload Shogun and clampband tests.
    - Test cases C & D: Prediction of VEGA launch vehicle stage separation test (pyrozip) and fairing separation test (clampband).

By the integration of the different steps applied separately in previous shock studies within a single user interface (shown in Figure 9-47), shock calculation accuracy has been dramatically improved. The main important causes of improvement which were brought to the fore were:

- the calculation of injected power by dedicated models for clampband and pyrozip cut,
- the possibility of applying shock force to a junction (taking into account the coupled subsystem impedance),
- the entirely new library of analytical structural CLF for coupling extensional, shear and flexural wave types,
- the VSEA modelling technique which has allowed to derive a consistent analytical set of coupled subsystems for representing the actual dynamical behaviour of both SMART1 and VEGA system with the combined advantage of getting at the end simpler SEA analytical model with better accuracy.

The modelling of power injection process is particularly efficient and, for a pyrotechnical source, takes into account the propagation speed of force profile along the cutting line. For clampband separation, it is the relaxation speed of the extensional energy of the clampband which describes the spatial evolution of the force. Figure 9-48 shows the difference in computing injected power spectra between the case a fixed location point-force is applied to the SEA model and the case where the pyrozip force is applied. The pyrozip force is moving along the cutting line at 7000 m/s contrarily to the fixed classical point-force. From this the injected power spectrum supported by flexural waves (Pwr_F_Pyro

compared to Pwr_F_rectangle) is modified compared to the one due to the fixed point force, The propagation of the pyroforce is thus boosting BF and lowering HF spectral content of the injected power. Extensional and shear wave injected powers are also modified, mainly increased at low frequencies.

Figure 9-49 shows the prediction of SRS on a wall subsystem of the SMART1 payload for the Shogun test and the comparison with some test SRS in this subsystem. Within the latter, it is possible to also describe local mass attenuation of the response due to the presence of massive equipment by introducing a local mass correction factor in the frequency range where subsystems are described by analytical theory. When there are described by VSEA and if the original FEM maps also the equipment, this correction is not necessary.

Figure 9-50 shows similar comparison between prediction and test-SRS for VEGA upper part performed with SEA-Shock.

The integrated user interface has then allowed an important gain in accuracy compared to SPOT5 prediction seen in Figure 9-23: . In SPOT 5 prediction, the source was the measured acceleration constraining the subsystem source and results were found acceptable far away from the source, mainly on the dummy payload used for the SHOGUN test. Now the model is fully theoretical. The input data from the user is a generic time domain force characterized by amplitude and duration. Both amplitude and force duration are strongly tight to the shock mechanism. Simple force profiles such as triangles have been used with success in the four shock simulations.

In clampband separation, the ring frequency of the pre-stressed source subsystem is involved in the force duration due to the liberation of its internal stored potential energy contained in n=0 mode which is transformed into vibrational energy feeding all modes of the system.

In a pyrozip separation, the duration of the force is mainly related to the time the shock device needs to reach fracture stress.

In the four simulations A, B, C and D, both force duration and amplitude were set to fit the measurement available near the source.

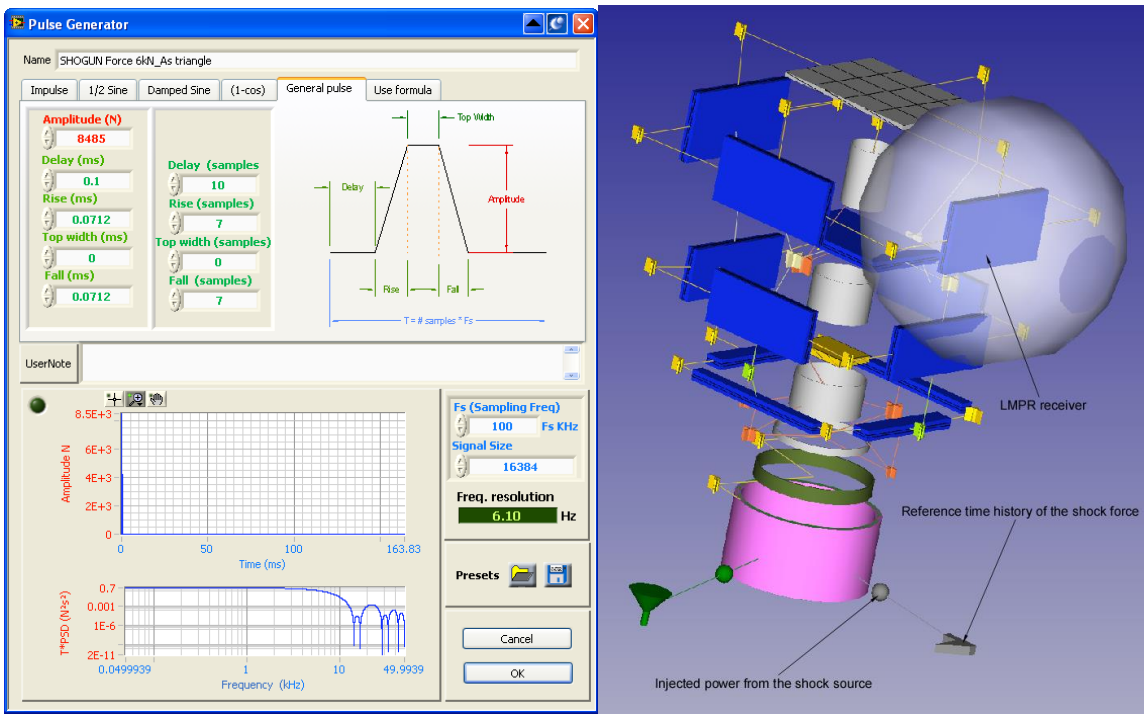

Shock interface (right) and the force profile generator (left)

Figure 9-47: Shock model of SMART1 spacecraft in SEA

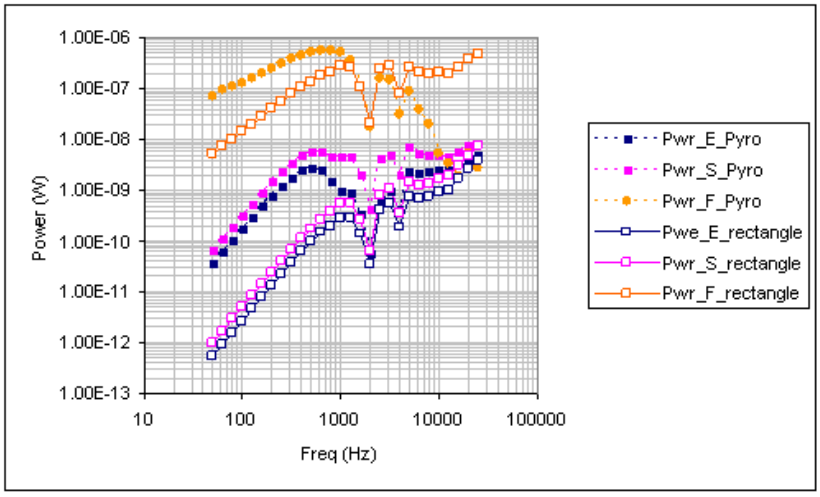

Figure 9-48: Injected power in the SMART1 ACU for a pyrozip and a "static" unit rectangular force

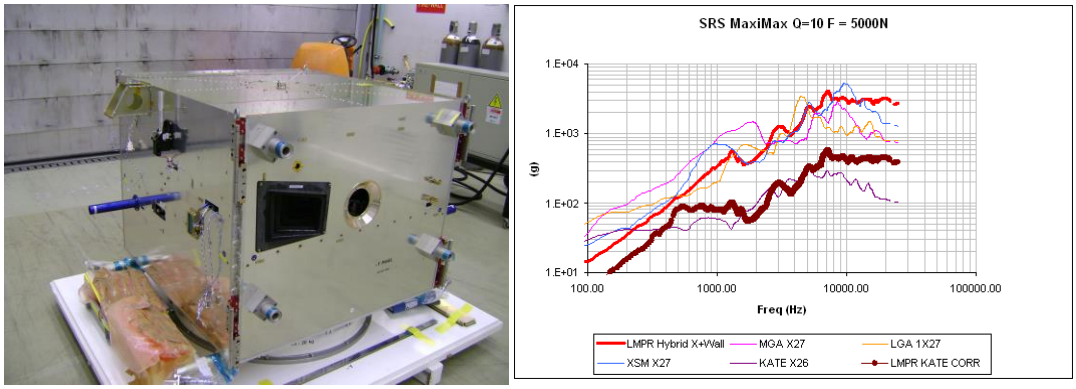

In thick red with bare panel velocity and thick brown for mass corrected bare velocity

Figure 9-49: X+Wall SRS predicted by LMPR and SRS computed from SHOGUN measured responses

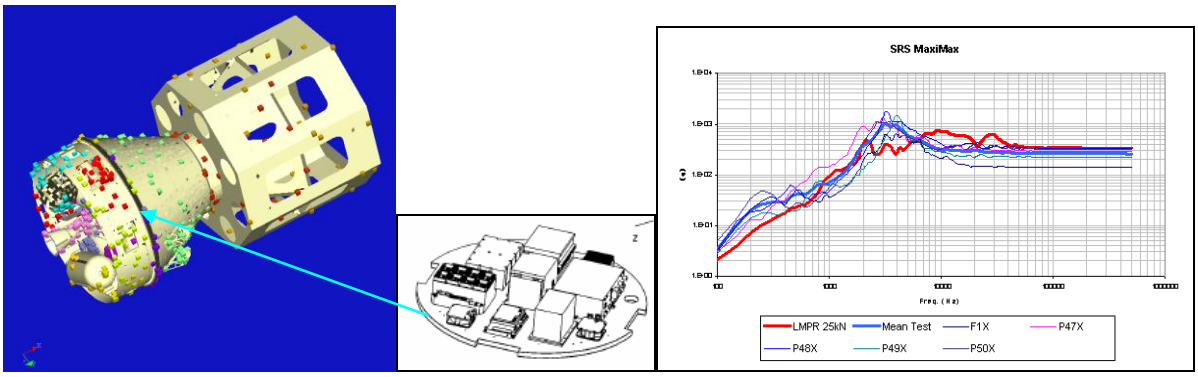

Figure 9-50: SRS prediction (red and blue)/tests results on equipment platform for AVUM stage separation for VEGA system

The degree of accuracy of LMPR-SEA technique has proven to be satisfactory for all simulations. The same SEA model can be used for predicting several loading cases by changing only the source and its location on the subsystem.

The main steps for the prediction are then shortened here below

- Building a structural SEA model from scratch using SEA+ analytical library of subsystems (plate, shell, beam) or post-processing with SEAVirt software representative FEM of the system up to its maximal limit of validity and import it in SEA+ where it is possible to expand it to HF by setting each virtual subsystem to a related asymptotic analytic subsystem,
- Generate force input using the force profile generator
- Apply it to the source subsystem and set the associated options
- Select the receiver subsystem and perform a LMPR solve for which additional options are asked such as number of reconstructed points inside subsystem and mass correction factors.

Both SRS and time histories of responses related to flexural and in-plane wave energies are provided as output of the simulation.

Main benefits of this technique is the quickness of the calculation which takes only a few minutes on a PC, diagnosing and transmission path ranking capabilities and ability to perform parametric sensitivity analysis.

10 Deriving a specification from a shock environment

10.1 Specification tool

The most popular way to specify a shock test is the use of the **maximax SRS with a standard Q-factor of 10**. The SRS is indeed the **simplest method to compare severities and damage potential** between shocks. The data reduction technique of SRS computation, whose purpose is to make the source signal more readable, has naturally a more reduced range of applicability compared to the original time history because of the loss of information (shock duration and form) generated by its calculation: whereas the Fourier spectrum defines the shock in terms of the amplitudes and phase relations of its frequency components and is completely reversible, the SRS describes only the effect of the shock upon a structure in terms of peak responses and is therefore **irreversible**. But the fact of reducing complex time history to the peak response of a SDOF damped linear system is of importance in the design of equipment and in the specification of tests because the limited number of parameters (SDOF frequency and damping) allows to **characterize simply and systematically** a shock excitation.

The SRS specification is generally composed of **line portions on a log-log graph**: for aerospace structures, far-field specification is often composed of an initial line of constant slope between 100 Hz and a cut-off frequency. Then, from this frequency up to 10000 Hz the specification follows a constant plateau. Figure 10-1 shows a typical example of this type of shock specification.

NOTE The full definition of the specification includes description of the expected time signal shape and duration, as detailed in Part 3. Otherwise infinity of time signals can give the right SRS without representing the real expected shape.

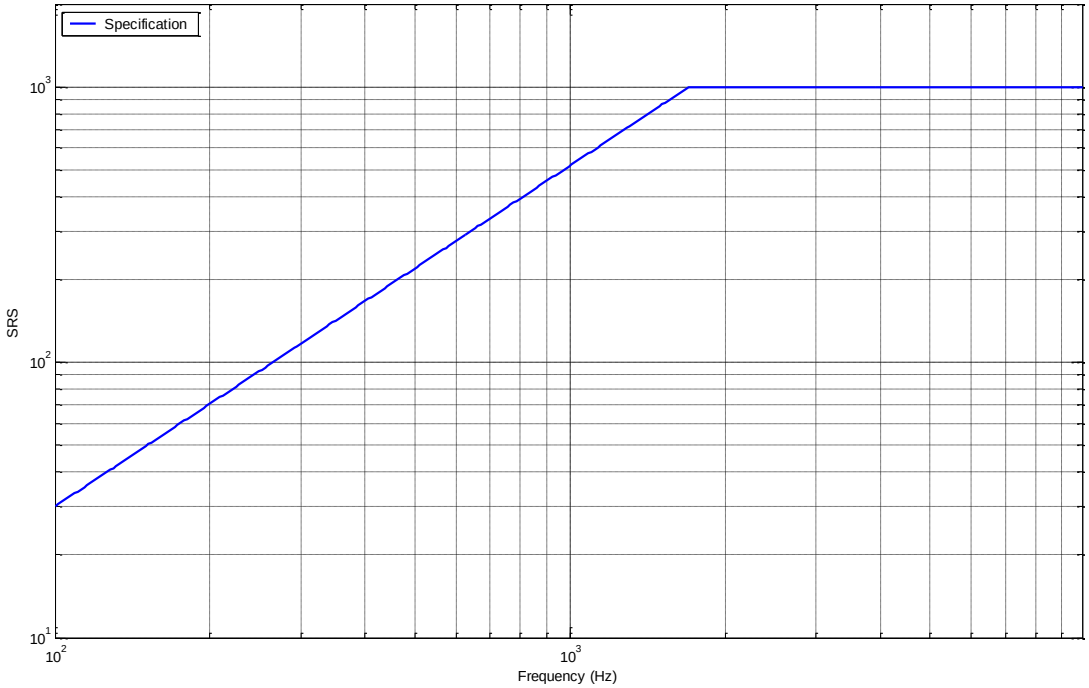

Figure 10-1: Example of SRS specification

Another way to specify a shock test is the half-sine acceleration specification. It corresponds to a half-sine pulse of acceleration roughly representative of an impact. It is specified through **two parameters only**: its magnitude $\ddot{u}_0$ and duration τ. Moreover, this kind of specification has been often used in the past because of its **simplicity and reproducibility** in laboratory tests. Impact machine, electro-dynamic shaker, drop table are indeed able to reproduce accurately this kind of specification. It is however important to notice that this type of specification become obsolete for aerospace structures where real shocks are generally complex waveform and, therefore, very different from a half-sine pulse. This particular shock **induces notably a non-zero velocity change** (Figure 10-2), counter to real pyrotechnic devices, that has a tendency to increase mainly the very low frequency leading sometimes to aberrant value at the beginning of the spectrum (i.e. at 100 Hz). High frequencies are generally less excited and consequently this type of specification cannot reproduce with fidelity pyrotechnic devices.

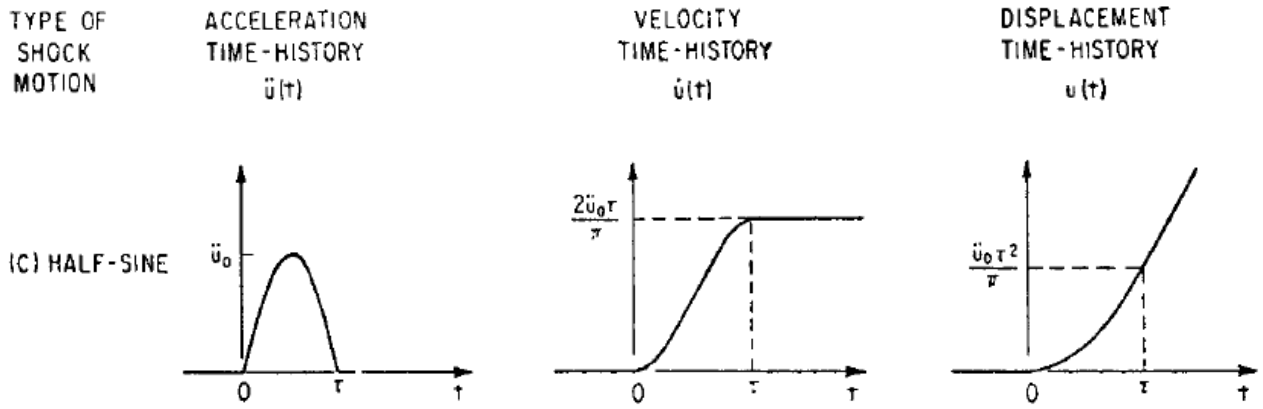

Figure 10-2: Example of half-sine acceleration, velocity and displacement

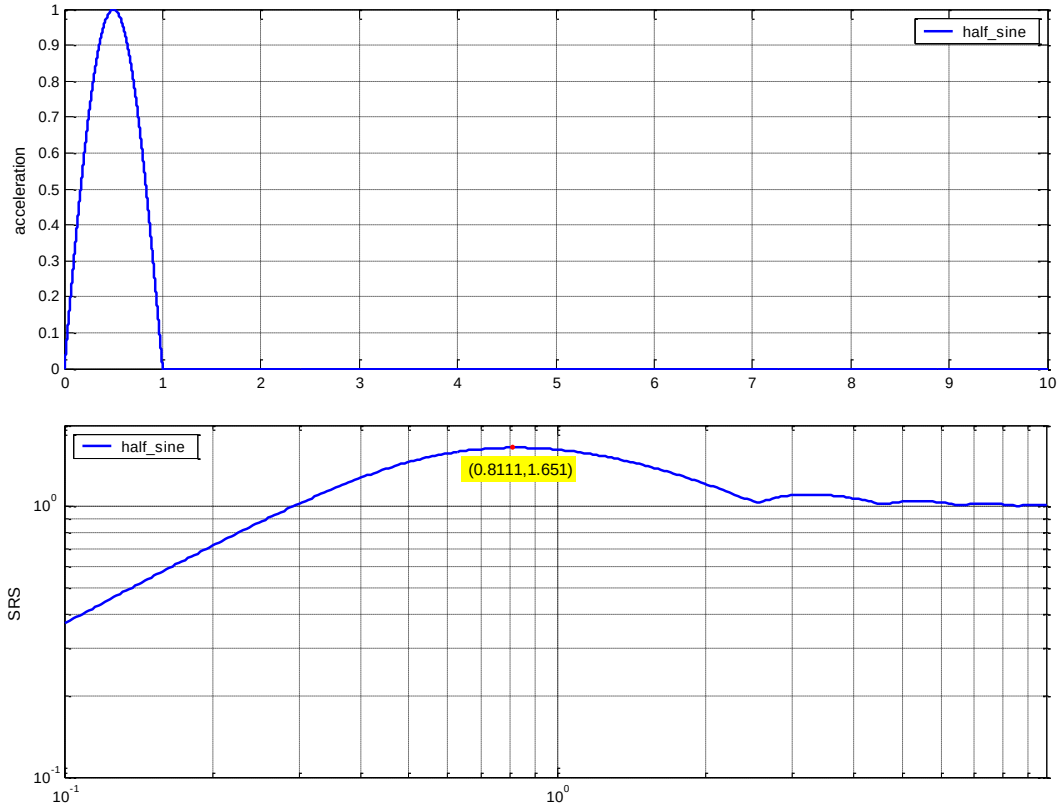

Figure 10-3: Normalised half-sine and associated SRS

The SRS of a half sine signal can be described, as follows:

- The rising portion presents a slope of 6 dB/oct. This portion of the spectrum can be approximated by $SRS(f) = 4.f.\gamma^{max}_{halfsine}.\Delta t_{halfsine}.\left(1-\frac{\pi}{40}\right)$
- The SRS peak occurs at **0,8 / $\Delta t_{half\ sine}$** (where $\Delta t_{half\ sine}$ is the duration of the half sine signal) and reaches **1,65 times the signal amplitude**.
- One can also remark on Figure 10-3 that high frequencies are not excited. The spectrum converges towards the signal maximum amplitude.

10.2 Deriving the qualification environment – MEE and qualification margin

The unit shock specification is based upon the Maximum Expected shock Environment (MEE) augmented by a qualification margin.

- The **Maximum Expected shock Environment** is a guaranteed level which is not expected to be exceeded during the operational life of the item with a certain level of confidence, accounting for randomness and inherent variability of the environment. The MEE may be estimated from (a) analytical and numerical shock analysis (see paragraphs 8 and 9), (b) envelope of system test measurements with associated scaling method where relevant (see Procedure I, in paragraph 13.3.2) , or (c) a statistical analysis based on shock test database to derive a reliable unit level shock specification (see paragraph 8.2.6).
- The **Qualification margin** that increases the environmental range to account for hardware strength variability (it is indeed possible that a test article would pass a specified test, and the flight hardware fails the same test conditions because of hardware strength variability and shock test jig variability). It ensures (with an acceptable level of confidence) that a failure does not occur during the product lifetime of the item. **A qualification margin of minimum 3 dB is added to the MEE.**

10.3 From level derivation/Measure to specification

Once the level has been measured or derived with the appropriate methodology in a particular zone or region, one needs to build a usable and correct specification by using the SRS tool (with a Q-factor of 10). This phase aims both at **enveloping and simplifying** the measures and/or predictions SRS **including the 3dB qualification margin** to create a specification that can be easily reproduced in laboratory tests with any kind of shock testing machine (mechanical, pyrotechnical device…). That is why specifications result generally into **constant slope lines and plateau on a log-log graph**. This procedure tends obviously to mask some eventual eigenmodes in the measures and/or predictions. Unlike random specification where some sharp peaks can be cut off during specification construction, it is preferable to completely envelop all the peaks due to modal behaviour in a shock specification. This rule engenders some hidden margin on certain frequency bands as it can be seen hereunder on Figure 10-4. In return, at the transition between line of constant slope and plateau, there is often no margin. **This transition band often expresses the presence of a peak in the real shock** and is consequently of great importance. Some precautions are useful to be reminded concerning the Q-factor effect. If the real Q-factor of a specified item is largely different from 10, it can engender greater amplification on some eigenmodes than it was initially forecast and can cause some damage. So before designing a specification, it is always interesting to let the Q-factor vary in the measures and/or predictions SRS computations in order to avoid this particular phenomenon.

Another key point to survey in the construction of a shock specification is the value of the initial slope and the very first value of the SRS specification (i.e. value at 100 Hz for far-field specification). **The initial slope is a priori superior to 6 dB/octave. So when enveloping the measures and/or predictions, it is important to verify that the initial slope is at least superior to this minimum slope**. Small slopes (inferior to 6 dB/octave) are sometimes encountered because SRS of time measures are not always corrected from zero-shift errors. These specifications are not correct. Moreover, an incorrect initial slope implies often a very high first value at 100 Hz (for instance, initial value superior to 200 g at 100 Hz). **It is also important to check this initial value to remain physical.**

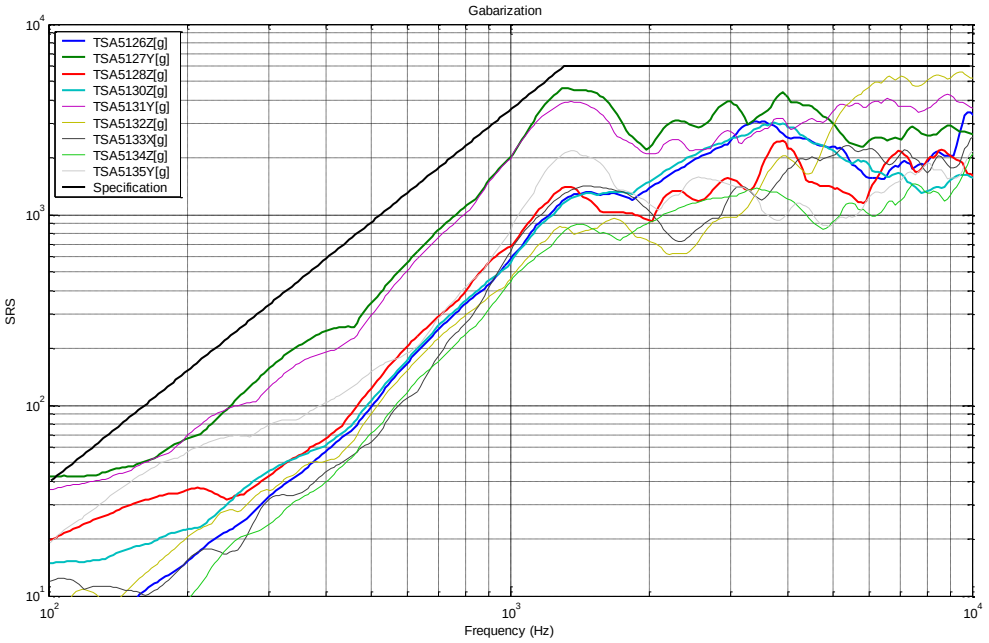

Figure 10-4: Example of specification from measurements

If the enveloping process with an initial slope of 6 dB/octave leads all the same to a very first value too high, it is then possible to add another intermediate point between the initial slope and the plateau in order to increase this initial slope and decrease the very first value until physical value. (Figure 10-5)

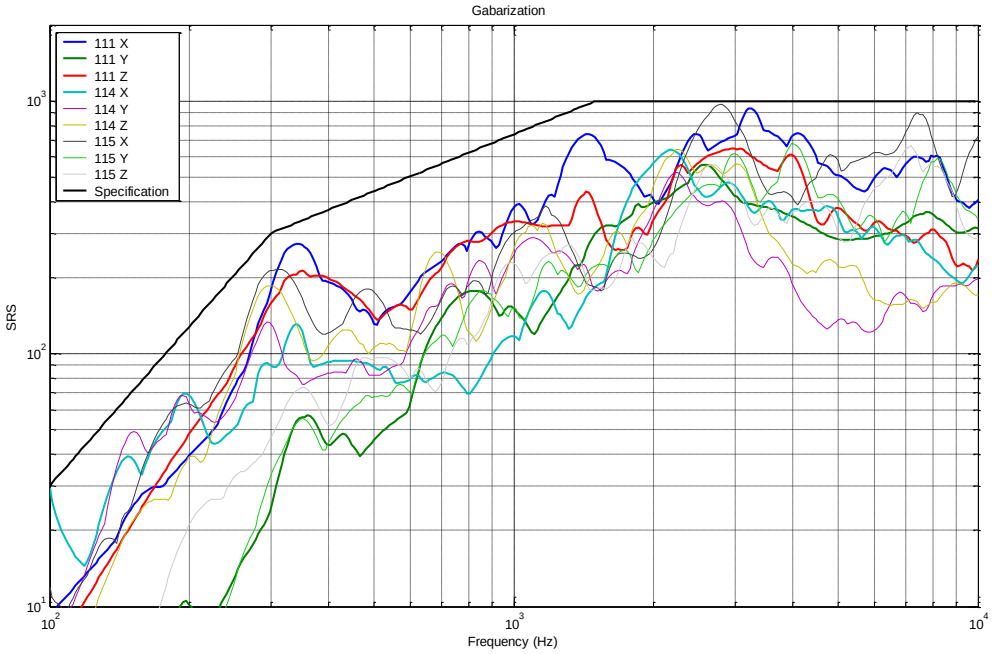

Figure 10-5: Example of specification with intermediate point

11
Shock attenuation

11.1 Definitions

11.1.1 History of shock attenuation

The need for isolation of shock first appears in Europe with the ARIANE launcher technology. In fact, most of the launcher separation events are performed with pyrotechnical cutting systems which generate shock levels significantly higher than the one encountered in satellites. As the source shock levels depend of the mass constrained by the mechanism, this is consequently higher for launcher cutting parts.

The first shock isolators developed for ARIANE were:

- Isolators for ARIANE booster release.
- Isolators for equipment of ARIANE 5 VEB (Vehicle Equipment Bay) to isolate from shock induced by case cutting. All equipment are settled on two panels linked to central cone by brackets designed with shock dampers to isolate from VEB release shock system (see Figure 11-1).

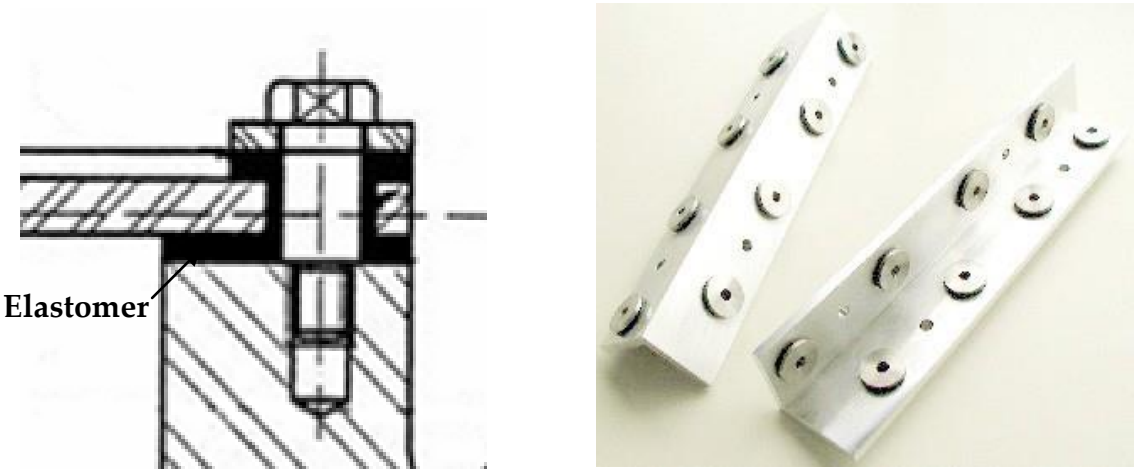

Figure 11-1: Example of Ariane 5 isolator insert

Shock sources have always been present in spacecraft for main release mechanism (e.g. spacecraft release, appendage deployment).

The design of shock isolation system for satellite has been motivated by Telecom missions which have seen the number of their equipment increasing: as a consequence the equipment density has increased leading to equipment closer to shock sources. This has induced non conformity of equipment shock qualification with respect to specified shock environment and a need to find solutions to isolate sensitive equipment from shock sources. The need of shock isolation is today motivated by another

constraint which is the introduction of more and more sensitive equipment, especially for observation missions.

There are two approaches for shock isolation of a given problem: shock is either isolated at the interface of sensitive equipment or directly at the interface of shock source. The most effective solution is the isolation at the source of the shock but it is rarely the simplest solution. Appendages releases are simpler to isolate at source as they are more confined and imply less constraint for stiffness specification.

Two families of isolation systems have been developed to answer to specific needs. The most used family is the family of passive isolators which uses specific properties of non-linear materials to isolate for high frequency excitation with a sufficient stiffness at low frequencies to sustain launcher typical dynamic loads. The other family is the family of active isolators which impose an active response to reduce shock excitation but which is not widely used in space industry due to lack of efficiency and technology maturity.

11.1.2 Impedance breakdown

The main principle used for shock attenuation is the impedance breakdown between the structure (from where the shock waves come) and the equipment to protect.

In general, especially for high frequencies, shock attenuation comes from solid wave propagation. The attenuation is achieved thanks the local stiffness difference between the mechanical structure and the relatively soft attenuator stiffness. This phenomenon can be illustrated with a simple bar with local property discontinuities. Each discontinuity of local stiffness E.S (Young modulus multiplied by the section) or of density ϱ lead to reflected and refracted shock waves. The quantity of the shock waves refracted (transmitted) depends on the value of this discontinuity called also local impedance α (See R.W Clough & J.Penzien).

$$\alpha = \frac{c_1}{c_2} * \frac{S_2 * E_2}{S_1 * E_1} = \sqrt{\frac{\rho_2 E_2 S_2}{\rho_1 E_1 S_1}}$$

The following figure presents the bar characteristics and the shock waves celerity c1 and c2:

- Incident shock wave ua
- Reflected shock wave ub
- Refracted shock wave uc

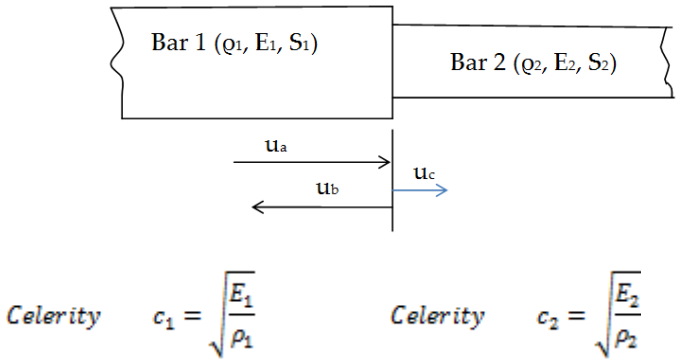

Figure 11-2: Shock wave propagation in bar discontinuity

This principle of impedance breakdown for shock attenuation is applicable for high frequency propagation; it is relatively different of sine steady state isolation for low frequency. The main difficulty for shock attenuation deals with intermediate bandwidth frequency between sine isolation and shock attenuation. In this frequency bandwidth, typically between 300 Hz and 700 Hz, modal responses are due to shock wave go back and forth in the different sub-structure. In this case, for a better efficiency the shock attenuator becomes a shock isolator for wide frequency range (see next paragraph).

The impedance breakdown principle is illustrated on the Figure 11-3. The **dark blue curve** is the input signal before the impedance breakdown whereas the **soft blue curve** is after.

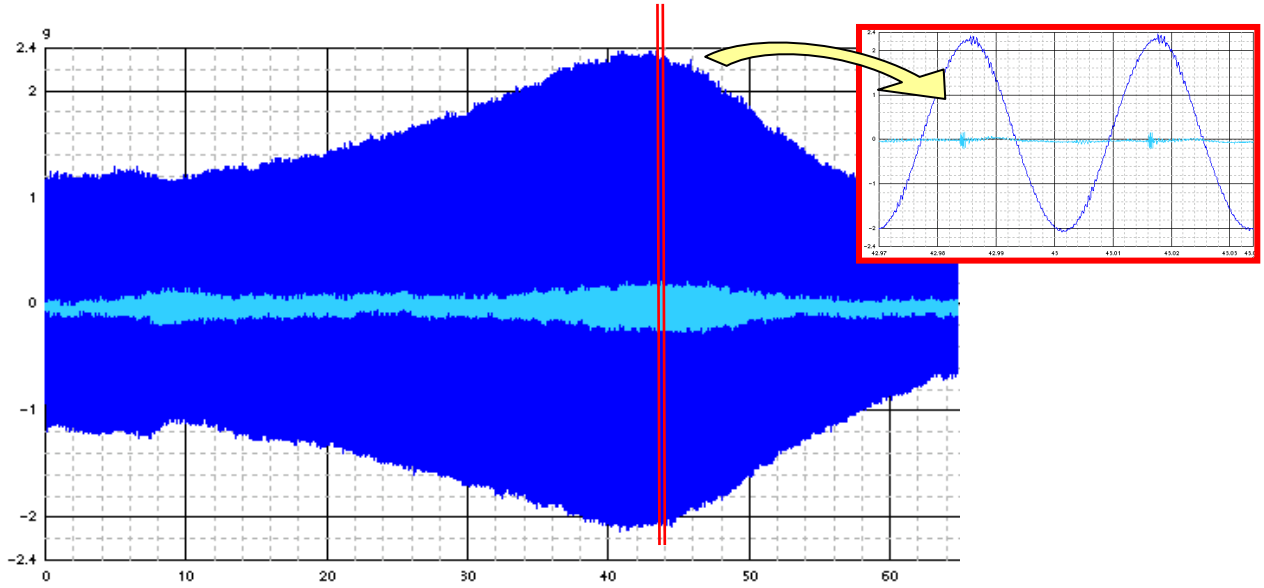

Figure 11-3: Impedance breakdown principle example

11.1.3 Shock and vibration Isolator

As explained in previous paragraph, a shock isolator is a more flexible shock attenuator, in order to cover low frequency shocks. Nevertheless, in practice, to meet the shock attenuation requirement, it is not necessary to obtain six isolation modes well decoupled of structure modes. Furthermore, a "perfect" isolator with 6 isolation modes is not recommended, because it is more challenging and difficult with the high displacements involved during resonances.

As reminder, an isolator device is defined as a device that decouples or isolates to some degree, the input energy from a protected mass or structure:

- Some energy does get through, but isolator parameters are optimized to reduce the response to acceptable levels
- Doesn't necessarily absorb a maximum amount of energy, but attempts to remove the input as much as possible.

The isolator is thus equivalent to a mechanical filter or a suspension.

The isolator principle is illustrated on the Figure 11-4.

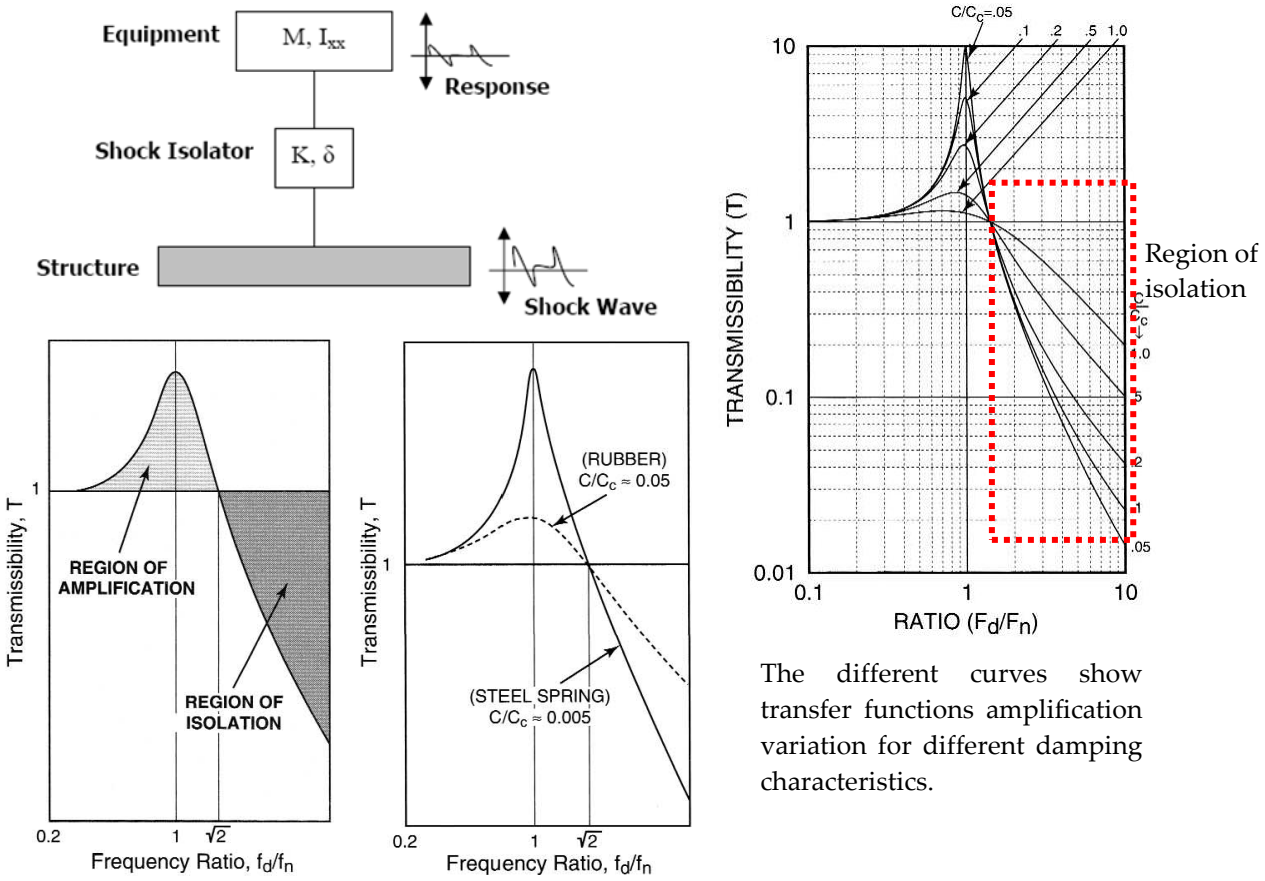

Figure 11-4: Illustration of the filtering effect of an isolator

This type of shock isolator is principally used for space application, with typical products as shown on the Figure 11-5.

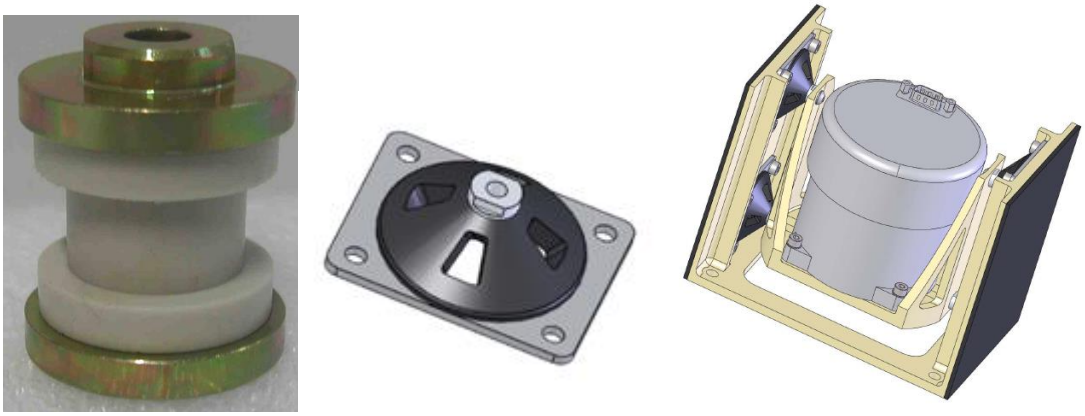

Figure 11-5: Illustration of space application of an isolator

Such type of isolator is further developed in this shock handbook.

This type of isolator can be enhanced to cover wide frequency range and commonly referred to shock and vibration isolator.

11.1.4 Damper

A damper is defined as a device that removes continuously energy from a moving system to control its response. The damper material has resilient properties allowing him absorbing energy when it is deformed elastically. Such types of device are mostly interesting for low frequency environment (type sine environment, i.e. up to 150 Hz) where the main goal is to dissipate large energy accumulated in the system. The shock amplitude is mainly defined by few highest peaks in a short time window; therefore the damping is not very efficient. It is illustrated by the SRS which is calculated with the highest peak. The damper principle is illustrated on the Figure 11-6.

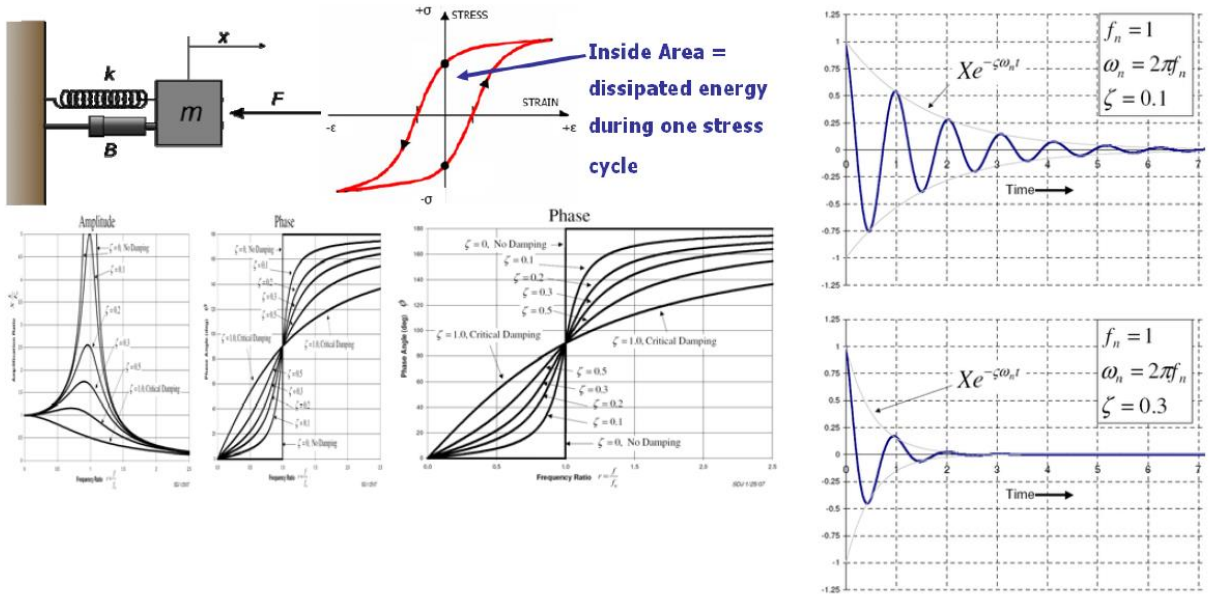

Figure 11-6: Illustration of the damper effect

Such type of device is not generally used as spacecraft flight hardware space application but for other application like Ariane 5 upper stage, ground wind damper system for launch vehicle standing on the launch pad, on the satellite container or EGSE. This is illustrated on the Figure 11-7.

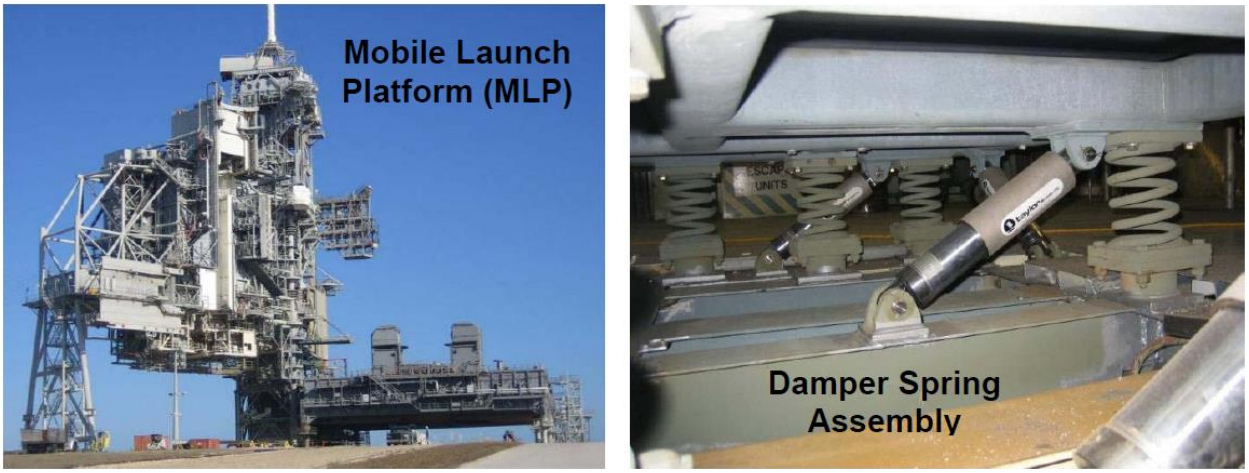

Figure 11-7: Illustration of space application of a damper

11.1.5 Shock absorber

A shock absorber is defined as a device that absorbs a maximum amount of kinetic energy, and brings a moving mass to a stop with minimal force. In space industry, the stop can be generated by a crushable material like honeycomb. Honeycomb crush absorber is an efficient solution for attenuation shock due to impact against end stop of an highly preloaded system.

Absorber design (honeycomb type, confinement, diameter) usually results from a development test campaign, and best attenuation is achieved when a large portion of the energy is absorbed by crushing the honeycomb (i.e. honeycomb completely crushed). Also in order to offer less resistance to the initiation of the collapse of the honeycomb, it has been characterised that a pre-crushing of honeycomb improves the attenuation efficiency.

The shock absorber principle is illustrated on the Figure 11-8.

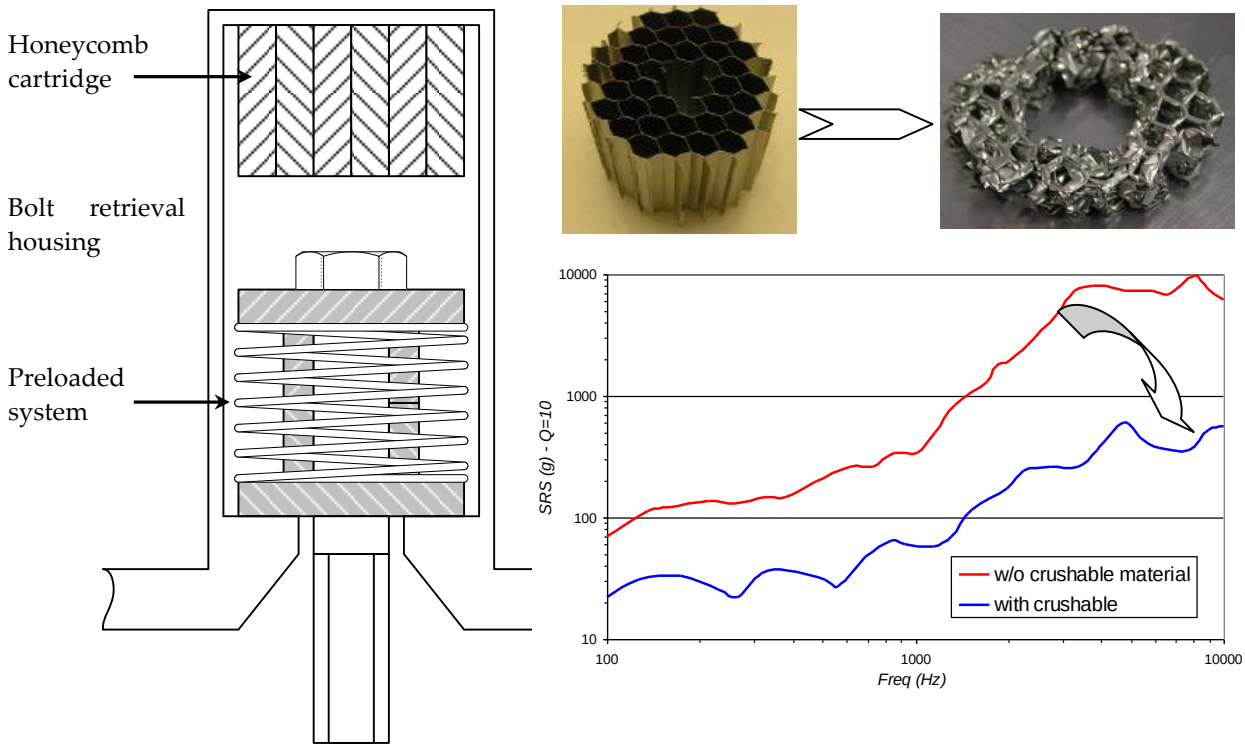

Figure 11-8: Illustration of a shock absorber

11.2 Theoretical background

11.2.1 Shock attenuation problematic approach

The shock is a complex phenomenon materialised by shock waves confined in a very short time, as illustrated on the Figure 11-9, where the shock event duration is about 20 ms.

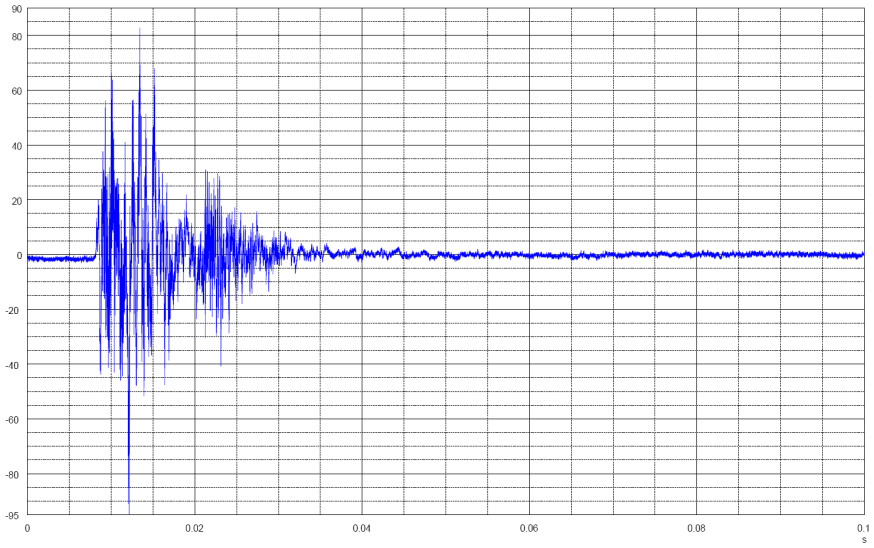

Figure 11-9: Shock event time history

Depending of the pyro shock environmental category to isolate (far field / near field) two different approaches can be highlighted here:

- **Far field:** The shocks levels are more important in low frequency (due to modal amplification of the structure and thus associated to relatively important displacement) than in high frequency. It is thus necessary to add damping in order to dissipate energy.
- **Near field:** The shock levels are more important in high frequency. It is thus better to use filtering effect to reduce the shock transmission.

The shock protection solution to be applied, varies depending of the shock environment nature (far or near field). Thus, by efficiency order, three approaches can thus be distinguished:

Approach 1 - Isolation of the source: This application aims at filtering the shock intensity induced by a pyro shock source. The maximum decoupling effect between the shock source and the rest of the structure is searched. This is achieved by placing a shock isolator between the shock source and the structure. This is the most efficient solution; on the other hand, it is not always possible to implement such solutions.

Approach 2 - Isolation of a sub-system: This application aims protecting an equipment directly at its interface. This is achieved by mounting the equipment on an isolator based on viscoelastic materials. As for the isolation of the source, this solution has the advantage of the simplicity of local device for an interface. On the other hand it is more difficult to decouple the isolation modes with the rest of the structure.

Approach 3 - Isolation applied along the load path: This application aims at limiting the shock propagation inside a structure. This is achieved by placing a shock isolator on the propagation path of the shock wave. In practice, it is very difficult, because the implementation of such

isolators modify the load path and the efficiency is not guarantee (amplifications are possible). It is more recommended to use damping along the load path.

The main principle of passive isolation is linked to the behaviour of a single-degree-of-freedom (SDOF) response system. And the effectiveness of isolators in reducing vibration is indicated by the transmissibility of the system.

When the system is excited at its natural frequency, the system is in resonance and the disturbances are amplified rather than reduced. Therefore it is very desirable to select the proper isolator so that its natural frequency is excited as little as possible and does not coincide with any critical frequencies of the supported equipment.

Referring to the Figure 11-4 and Figure 11-10, it can be seen that when the ratio of the disturbing frequency over the natural frequency is less than √2, the transmissibility is greater than one (so-called region of amplification), and opposite, when the ratio is greater than √2, the mounted unit is said to be isolated (so-called isolation region).

Those figures also illustrate the relationship between a highly damped and a lightly damped system: as damping is increasing, isolation efficiency is somewhat reduced in the isolation region. While high values of damping cause significant reduction of transmissibility at resonance, its effect in the isolation region is only a small increase in transmissibility.

Limiting the amplification at the isolation frequency often leads to the use of elastomer which has a high damping coefficient and thus low amplification.

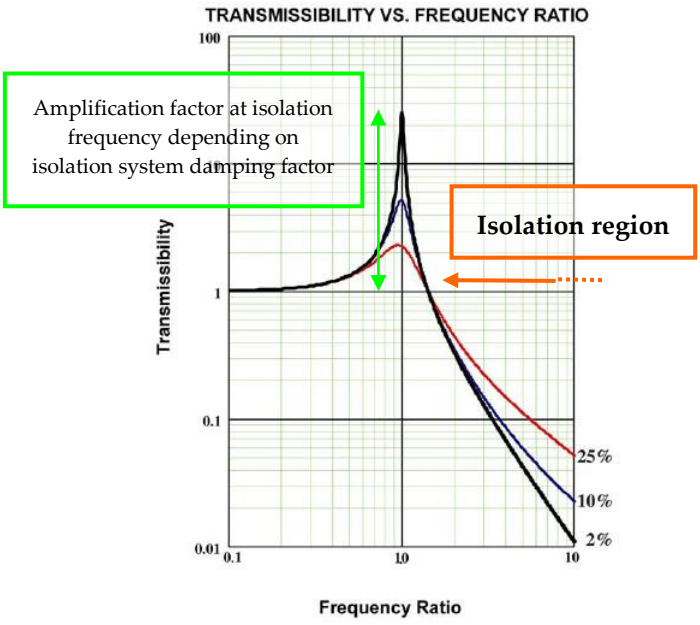

Figure 11-10: Passive isolation principle – SDOF transmissibility vs. frequency

Consequently, the definition of an isolator device is a compromise into using two effects characteristics: a mechanical filter and a damper.

11.2.2 Shock isolator device features

The shock isolation principle is to use a specific device to protect from shock events or avoid shock propagation. This requires fulfilling a complex set of constraints:

- Isolate the 6 degree of freedom, otherwise shock could propagate.
- Use a compact and relatively light solution.
- Avoid important amplification of the device on its main mode to prevent structure to protect over dimensioning at low frequency.
- Use strength solution able to sustain all the mechanical environments.

Metallic structures can be used to isolate from shock but they can't be integrated in a small volume and are heavy and complex systems to provide a complete isolation of the whole degree of freedom enabling to sustain the mechanical loads.

The needs of compactness, lightness, damping, complete isolation of 6 degree of freedom and strength lead naturally to consider the elastomer materials families as they present a lot of attractive properties:

- Important strength to sustain mechanical environments,
- Tuneable damping properties,
- Easy to use and create complex geometry allowing building a 6 degree of freedom isolation,
- Low mass density allowing creating light device,
- Good bonding on metal/organic parts thanks to primer whose strength depends on the family.

Rubbers main characteristics and damping effect are presented hereafter.

11.2.3 Rubber and damping effect

Rubbers are constituted of very long molecular chains (M_n > 10000 elements) which are entangled up the ones with the others, as shown in the Figure 11-11.

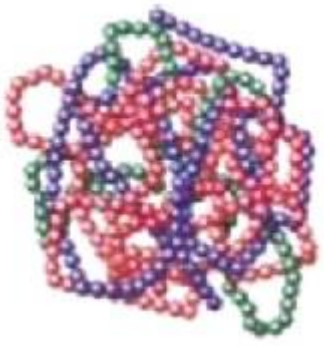

Figure 11-11: Overview of a rubber molecular chain entangled up the ones with the others

Rubbers belong to thermo-hardening materials which can be characterized by the key parameter glass temperature ($T_g << T_{Ambient}$) leading to a very different behaviour w.r.t. this critical temperature:

- Below this temperature, the behaviour is vitreous and thus the material is brittle with a high Young's modulus

- Beyond this temperature, the behaviour is rubbery and characterised by an important softness: molecular chains can be characterized by a high mobility, numerous conformations and very flexible chains.

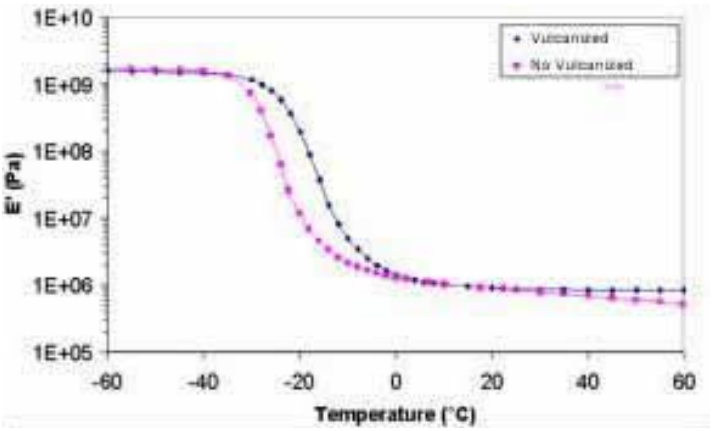

Figure 11-12: Rubber behaviour change around the T_g temperature

However, the material elasticity behaviour is only obtained after the vulcanisation phase which consists in linking all the molecular chains together thanks to sulphured bridges, as shown on the Figure 11-13.

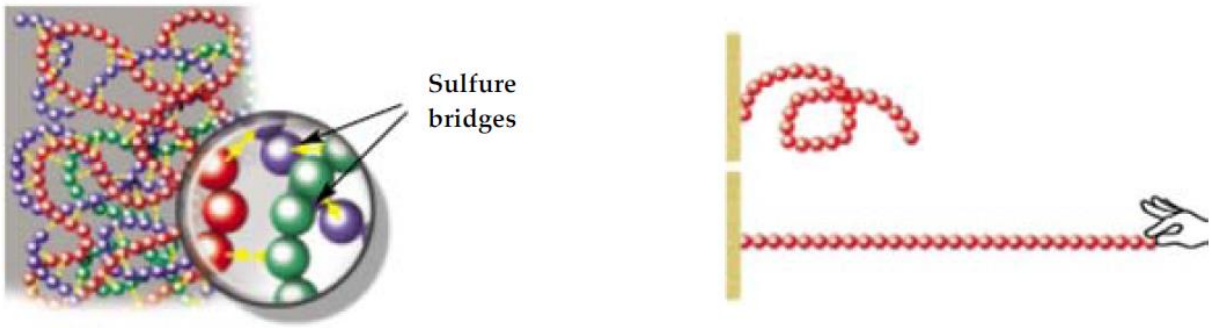

Figure 11-13: Creation of sulphured bridges between the chains giving the rubber elasticity behaviour

Nevertheless, this is not a perfect elastic behaviour because the molecular chains located between each sulphur links, rub with their external environment (i.e. others chains), leading to a friction phenomenon, which is at the origin of the viscous behaviour of the material, as shown in the Figure 11-14.

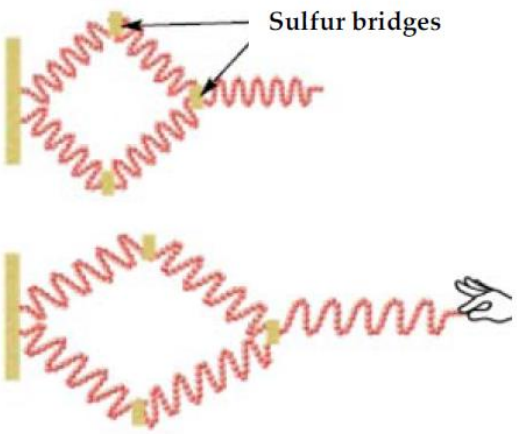

Figure 11-14: Sulphured bridges linked to rubber viscous behaviour

More generally, the rubbers mechanical properties are characterized by a wide variety of non linearities which are succinctly listed hereafter:

- **The Payne effect:** This visco elastic property leads to Young's modulus decrease when the dynamic amplification (or deformation rate) increases. This effect is more pronounced on rubber charged of carbon black.

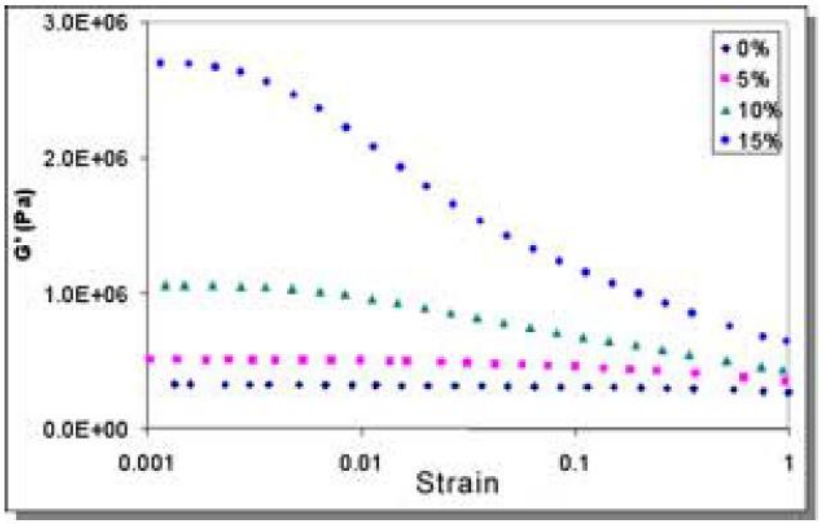

Figure 11-15: Payne effect

- **Temperature dependency:** The Young's modulus decreases when the temperature increases.
- **Frequency dependency:** The Young's modulus increases when the exciting frequency increases.
- **Static pre-loading:** This induces a non-symmetric repartition of the deformation rate in the material linking to Payne effect.
- **Mullins effect:** The stress-strain curve depends on the maximum loading previously encountered. The phenomenon can be idealized for many purposes as an instantaneous and irreversible softening of the stress-strain curve that occurs whenever the load increases beyond its prior all-time maximum value. At times when the load is less than a prior maximum, nonlinear elastic behaviour prevails.

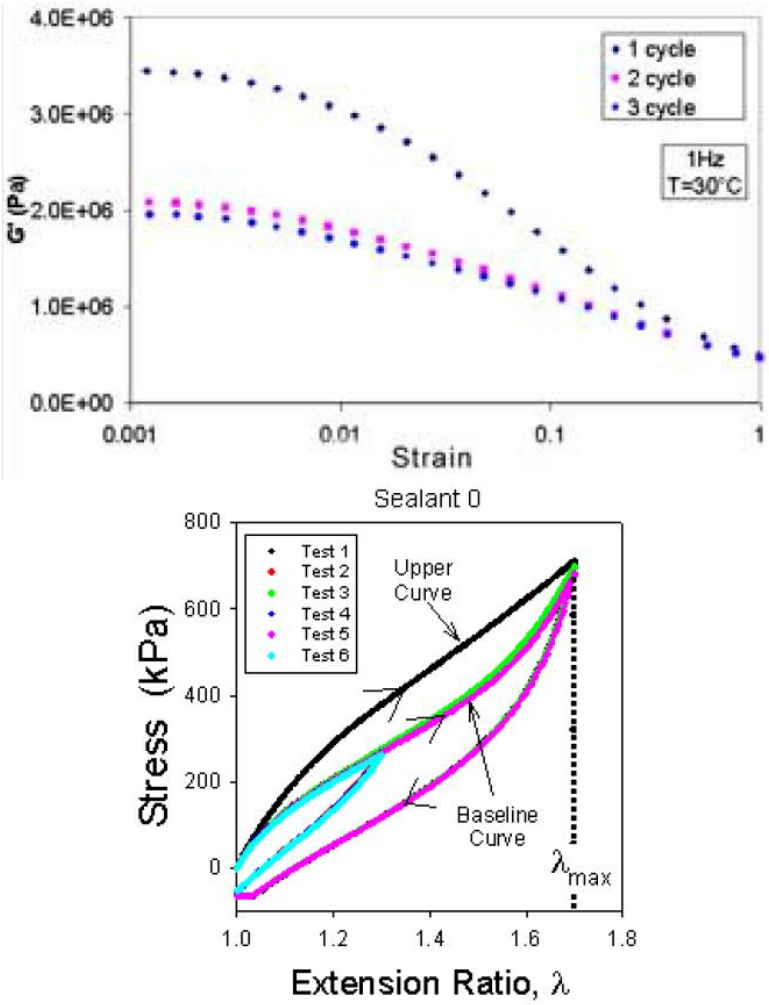

Figure 11-16: Mullins effect

The complex rubber behaviour can be idealized by the following simplified model analogy allowing apprehending the non-linear behaviours.

The molecular environment can be presented as a "pipe" around the chain:

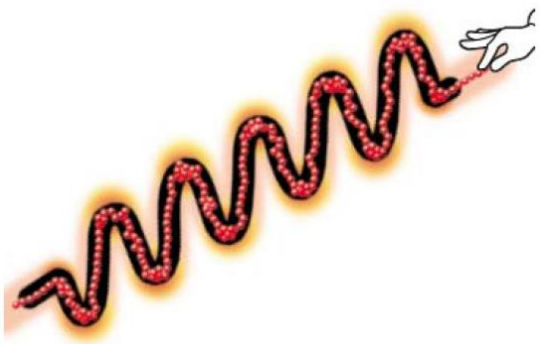

Figure 11-17: "Pipe" behaviour of the rubber

When a load is applied:

- The movement is slowed down

- Frictions appear between the chain and the pipe
- A dephasing appears between the load and the displacement

From this analogy, different rubber specific behaviour can be highlighted:

a. Frequency dependence:

Between two cycling loads, the molecular chain returns to a "balancing" statement. It is the creep phenomenon. The creep velocity depends on the molecular mobility, as shown on the Figure 11-18.

⇒ The mechanical behaviour depends on the frequency of the applied load/displacement:

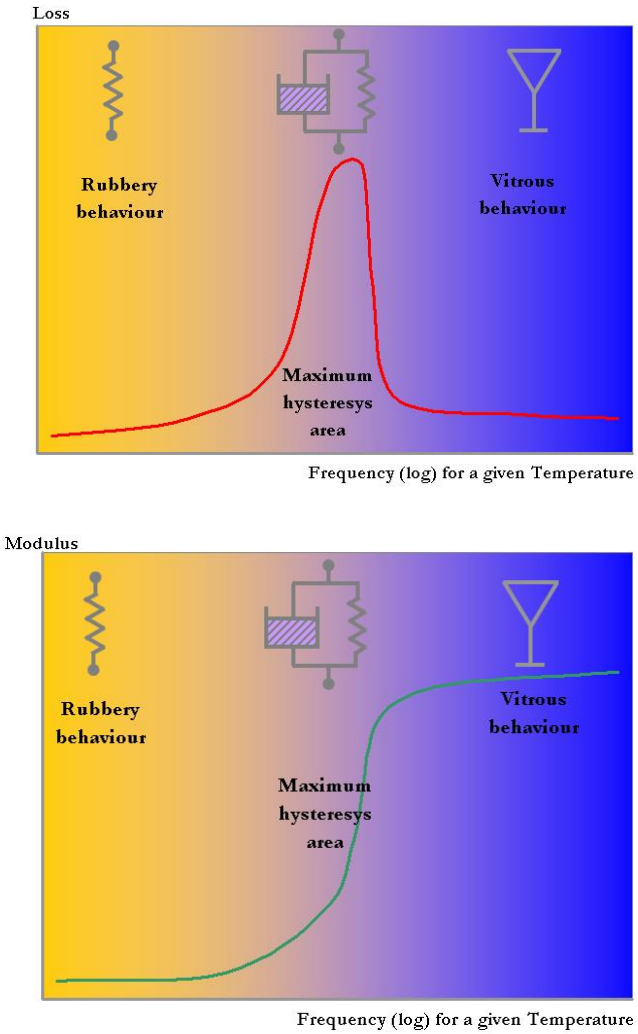

Figure 11-18: Frequency dependence effect

When the load is applied with a velocity:

— **lower than** the velocity of the mobility molecular in the "tube", the return to the "balancing statement" is in advance with the load: the stiffness of the rubber is low.

— **slightly upper than** the velocity of the mobility molecular in the "tube", the return to the "balancing statement" is in late with the load: this is the hysteresis phenomenon.

— **significantly greater than** the velocity of the mobility molecular in the "tube", there is no return to the "balancing statement". Permanent tensions appear inside the material: the stiffness of the rubber is high.

When the stiffness increases, the elastomer closes to a vitreous material which generates more friction in the molecular chains and thus higher damping. This effect is more important if the rubber is naturally damping.

b. Temperature dependence:

When the temperature increases or frequency decrease, the molecular mobility increases too. The temperature dependence is equivalent with the time or frequency dependence. High strain rate or frequency is equivalent to low temperature and low strain rate or frequency is equivalent to high temperature

The Williams–Landel–Ferry Equation (or WLF Equation) is an empirical equation associated to time–temperature equivalence. With this equation, it is possible to obtain large frequency range dependence with different dynamic tests in temperature.

As the mechanical behaviour depends on the molecular mobility, it depends on the temperature too, as shown on the Figure 11-19.

Thus when temperature increases, the "tube" diameter increases also and the molecular chains slide easier in the "tube" leading to decrease the Young's modulus.

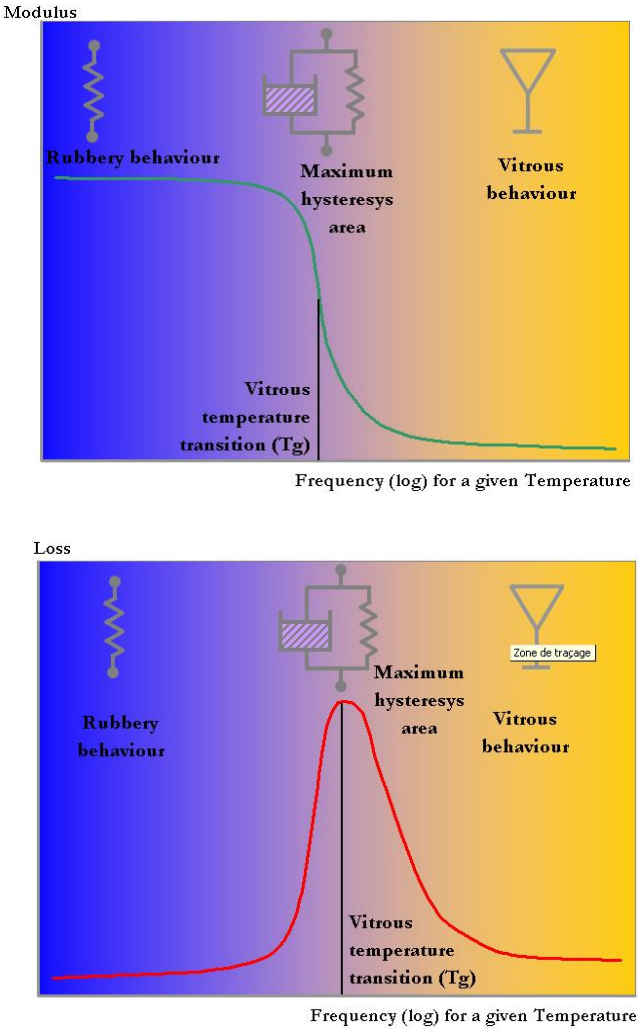

Figure 11-19: Temperature dependence effect

c. Damping dependence:

The damping properties are linked to molecular chains frictions. The easier the chains can move, the lower the damping is. By analogy with the "tube" it can be deduced that:

— The higher the frequency is, the higher the damping is.

— The higher the displacement is, the higher the damping is.

— The higher the temperature is, the lower the damping is.

T_g is a key parameter for rubber as it characterizes the vitreous/ rubbery transition temperature. Thus the higher this value is, the higher the transition closes the ambient temperature. This directly leads to conclude that the higher the T_g is, the higher the damping is

Other parameters influence the T_g and thus the damping:

— The chemical composition of the visco elastic material (e.g. carbon black, oil, and chemical components)

— State of internal stress

— Environmental temperature

— Type of stress

11.2.4 Elastomer type selection

11.2.4.1 Overview

For a development of an elastomer based device, it is important that the elastomer is selected among several types of elastomer families.

The choice between the different families for space application is determined by several parameters (e.g. behaviour in space vacuum, out gassing, ageing, working temperature, T_g). The task is a hard trade off often supported by characterisation tests.

However, in order to help this selection, we can highlight the following key parameters for space applications. Elastomer materials can be classified in 3 main families for which the main properties for selection are provided:

- Natural rubber
- Black synthetic rubbers (like SMACTANE SP)
- Silicon rubbers

11.2.4.2 Natural rubber

11.2.4.2.1 Origin

The natural rubber comes from the HEVEA tree: the sap of this tree (called latex) is collected and then coagulated, to become finally an elastomer material.

11.2.4.2.2 Chemical nature

The chemical name of the natural rubber is the "polysioprene cis 1-4 natural", with a molecular weight of 100 000 to 1 000 000 mainly composed of carbon and hydrogen atom.

11.2.4.2.3 Compounding

Natural rubber is generally vulcanized thanks to sulphur system. To increase its mechanical properties, it is reinforced by black carbon, and it can be protected from external aggression (e.g. oxygen, UV, ozone) thanks to various additives.

11.2.4.2.4 Thermodynamically aspects

Its glass Temperature (T_g) is low: between -75 °C and -65 °C (Nota: The T_g is strongly linked to the compounding, so these values are for indication only).

11.2.4.2.5 Mechanical strength aspects

Its mechanical properties are very good compared with the others rubber families: Natural rubber is dedicated for high loaded applications.

11.2.4.2.6 Dynamical aspects

Due to its low Tg, its damping is not very high for usual operational temperatures (-30 °C to +50 °C): the tan δ factor is between 0,1 and 0,2 (Nota: the tan δ is strongly linked to the compounding, so these values are for indication only).

However, compared with the usual synthetic rubbers, the natural rubber has a low temperature dependency (and so a low frequency dependency too).

11.2.4.2.7 Ageing aspects

It is sensitive to the "on ground" ageing that is why protective additives are included inside its compounding. Its maximum hot using temperature is ~80 °C. But if the radiation rate is not too strong, its ageing "in orbit" is good.

11.2.4.2.8 Manufacturing aspects

The usual moulding methods can be used to manufacture natural rubber parts. During the moulding phase, natural rubber can be easily bounded on various metallic substrates (e.g. Aluminium, steel, Titanium) and on organic substrates too if these organic substrates are in accordance with the moulding temperature (such as PEEK, polyimide).

11.2.4.3 Black Synthetic rubbers

11.2.4.3.1 Origin

Synthetic rubbers come from the oil industry. There are various families of synthetic rubber, with each one specific properties. For example, there are the polychloropren rubbers (CR), nitrile rubbers (NBR), the butyl rubbers (IIR) …

11.2.4.3.2 Chemical nature

Synthetic rubber are made with long molecular chains, composed of Carbon, Hydrogen, Oxygen or halogen atoms.

11.2.4.3.3 Compounding

As the natural rubber, synthetic rubbers are generally vulcanized thanks to sulphur system. To increase their mechanical properties, they are reinforced by black carbon and they can be protected from external aggression (oxygen, UV, ozone,…) thanks to various additives.

11.2.4.3.4 Thermodynamically aspects

As all rubber, the glass Temperature (T_g) of synthetic rubbers is lower than the room temperature (between -70°C and 20°C). This value is strongly linked to the compounding.

11.2.4.3.5 Mechanical strength aspects

Their mechanical properties are good (not as good as that of natural rubbers).

11.2.4.3.6 Dynamical aspects

With specific synthetic rubbers as SMACTANE®, a high damping factor (tan δ>1) can be obtained for usual operational temperatures (-30 °C to +50 °C). In this case, the temperature and frequency dependencies are strong and so, it is necessary to work with a short temperature range.

11.2.4.3.7 Ageing aspects

Compared with natural rubbers, they are less sensitive to the "on ground" ageing. Their maximum hot using temperature can be up to ~120 °C. And if the radiation rate is not too strong; their ageing "in orbit" can be good.

11.2.4.3.8 Manufacturing aspects

The usual moulding methods can be used to manufacture synthetic rubber parts. During the moulding phase, synthetic rubbers can be easily bounded on various metallic substrates (Aluminium, steel, Titanium …) and on organic substrates too if these organic substrates are in accordance with the moulding temperature (such as PEEK, polyimide).

11.2.4.4 Silicon rubbers

11.2.4.4.1 Origin

Silicon rubbers are a synthetic rubbers coming from pure Silicium reacting with methyl chlorure.

11.2.4.4.2 Chemical nature

The chemical name of silicon rubbers is the "polysiloxane". Their main molecular chain is composed of Silicium and Oxygen atoms.

11.2.4.4.3 Compounding

There are two main silicon rubber families:

- The silicon rubbers vulcanizing at room temperature [20 – 80]°C called RTV: Their molecular weight is low. These are bi components systems composed of the polymer and a reagent to be mixed together to begin the vulcanization phase. No compound possibility like the other black synthetic rubber.
- The silicon rubbers vulcanizing at hot temperature [140-200]°C called MQ, VMQ or PVMQ: Their molecular weight is high. They are vulcanized thanks to peroxide system. And as all synthetic black rubbers, various additives can be added to improve specific properties (hardness, mechanical strength).

11.2.4.4.4 Thermodynamically aspects

Its glass Temperature (T_g) is very low: between -130 °C and -100 °C (Nota: The T_g is strongly linked to the compounding, so these values are for indication only).

11.2.4.4.5 Mechanical strength aspects

Its mechanical properties are fair compared with the others synthetic black rubber families.

11.2.4.4.6 Dynamical aspects

Due to its low T_g, its damping is fair for usual operational temperatures (-30 °C to +50 °C): the tan δ factor is between 0,1 and 0,5 (Nota: the tan δ is strongly linked to the compounding, so these values are only indicative values).
Silicon rubbers have a low temperature dependency (and so a low frequency dependency too).

11.2.4.4.7 Ageing aspects

They are not very sensitive to the ageing. Its maximum hot using temperature can be up to ~240°C.Generally speaking, silicon rubbers are dedicated for very hot and very cold applications.

11.2.4.4.8 Manufacturing aspects

The usual moulding methods can be used to manufacture silicon parts. Regarding to bounding aspects with other metallic substrates, it is important to take the appropriate precautions: Silicon bounding is not as good as black rubbers bounding.

11.3 Attenuator device development

11.3.1 Overview

This paragraph provides the main recommendations for shock attenuator device development.

11.3.2 Attenuator requirement definition

11.3.2.1 Introduction

It is of prime importance to correctly specify the attenuator device to develop in order to obtain the right attenuation behaviour.

11.3.2.2 Performance specification

It is necessary to clearly specify the device attenuations performances with respect to the different types of mechanical environments (e.g. sine, random, shock). Due to the complex elastomer behaviour sensitive to temperature, it is essential to detail for each performance specification, the applicable temperature range.

As an example, the performances definition can be expressed as:

- The applicable working temperature range is (5 – 40) °C.
- The amplification on the device mode is lower than 3.
- The in plane and out of plane device modes is lower than 150 Hz.
- The filtering performance is at least of a factor 2 at 200 Hz and a factor 4 at 400 Hz.

As well as the definition of the device performance, it is worthwhile to define exactly the way to characterize it.

Such approach allows a clear understanding of both parts (customer and developer) with respect to the required performance, and avoids a free interpretation of the way to characterize the specified performances leading to a device not adapted to the true conditions of use.

It is important that such specification defines the complete test setup to verify the performance (e.g. the boundary conditions representative of spacecraft mounting conditions, the equipment definition, the nature of the run to apply as well as the input level, the allowed notching).

As an example the test setup can be expressed as:

- The test can be realized with a representative rigid dummy equipment with a CoG eccentricity of 50 mm
- The device can be directly mounted on the shaker slip table
- The performance can be verified with thanks to:
    - A 1 g input sine run,
    - increasing sine sweep rate of 2 octave per minute,
    - run on 5 Hz – 2 kHz,
    - Along the in plane and out of plane directions,
    - 15 g notching is allowed on the dummy mass CoG.

11.3.2.3 Environment definition

A good understanding of the complete attenuator environment is worthwhile to develop a well-adapted device in accordance with the real needs.

It is important that the complete environment definition is as close as possible from the real conditions of use, otherwise the attenuator device development could irremediably lead to a device that is over or under dimensioned or at least unrealizable.

It is also important that the environment definition takes into account all the condition cases of use. The most important requirements are listed hereafter, but this list is not exhaustive and can be completed by other specific:

- Temperature range for different working environment (for example, a working temperature range for sine, another one for shock events and a last one for in orbit conditions).
- The available volume for the device and the Interface Requirement Definition (IRD)
- All the mechanical environments to sustain (e.g. quasi static, sine, random, and shock)
- The preloading conditions with the applicability with respect to the different mechanical environments
- The performances evolution w.r.t the elastomer ageing
- The out gassing requirements
- The equipment to protect physical properties (mass, inertia and cog eccentricity from interface plane)
- The qualification status of the equipment to protect (definition of the frequencies to avoid)
- The irradiation requirements
- The device thermal conductivity requirements (is it necessary to use a thermal skirt)

11.3.2.4 Important factors affecting isolator selection / definition

Beyond the stiffness and damping properties which basically characterize an isolator, other factors play an important role for the selection. The important points for isolator selection and definition are:

- Type and direction of disturbance.

  A good understanding of the environment type of the equipment to protect is mostly important in order to select the right solution for isolator selection and definition.

  A good knowledge of the type of the dynamic environment to isolate is important for the definition of an isolator. The three main categories of environments can be (1) period vibration occurring at discrete frequencies, (2) random vibration gathering wide range of frequencies and amplitudes or (3) transient phenomena. Usually combination of these three categories occurs in most isolation systems. In the specific case of shock attenuator performance, the environment is mainly transient near the shock source, with increasing of sine period with the distance. The good characterisation can lead to the choice of the isolator solution which complies with the three key points:

  1. Deflection capability is enough to accommodate the maximum dynamic environment motion.
  2. Avoid load-carrying capability exceedance (based on evaluation of the environment maximum loads).
  3. Avoid isolator degradation due to overheating problems or fatigue deterioration due to long-term high-amplitude loading.

  The direction of the disturbance can have an effect on the determination of the isolator complexity. A higher number of disturbances (in several directions) can significantly increase the complexity of the isolator.

- Allowable response of a system to a disturbance

  This is the maximum allowable transmitted shock or vibration and maximum displacement due to a disturbance which can be expressed by different ways (maximum acceleration or displacement due to shock, specific natural frequency and maximum transmissibility or level at that frequency, maximum acceleration or velocity or displacement levels).

  The definition of this maximum allowable response helps to select the appropriate isolator. If such allowable is not available, it is important that this parameter is defined immediately by similarity with other equipment or situation.

- Space and location available for isolator

  Vibration and shock isolation should be considered as early as possible in the system design in order to estimate the isolator size. The size depends on the nature and magnitude of the expected dynamic disturbances and the load to be carried.

  The location of isolator is very important to the dynamics of the equipment mounted on them in order to minimize displacement and improve isolation efficiency. Most particularly, it is important that they are located such that they avoid the rocking modes.

  If the isolator cannot be located so as to provide a right centre of gravity location, the system analysis is more difficult and more space is allowed around the equipment for rocking motion. The isolator can be double checked to ensure that they are capable of withstanding the additional loads and motion from the non-translational movement of the equipment. This is particularly true when the centre of gravity is a significant distance above or below the plane in which the isolator are located.

  Rule of thumb: the distance between the isolator plane and the centre of gravity should be equal to or less than one-third of the minimum spacing between isolators. This helps minimize rocking of the equipment and the resultant high stress in the isolator.

- Space available for equipment motion

  The isolator choice can depend on the available limit place around the equipment. It is important to select the isolator spring constant o keep motion within this limit. The motion is the sum of (1) the static deflection due to the equipment weight supported by the isolator, (2) the deflection caused by the dynamic environment and (3) the deflection due to any steady state acceleration.

  Elastomeric device working in compression thanks to non-linear load deflection characteristics (called snubber) can be used to limit the motion of the equipment. It is implemented at the point of excessive motion. It is important to select their stiffness carefully to avoid transmission of high impact loads into the supported equipment.

- Ambient environment

  The ambient conditions can strongly affect the isolator characteristics by degrading the physical integrity leading to make it non-functional or change the operating characteristics (without permanent damage). Thus it is important to determine the operating environment of the isolator and select device providing the correct characteristics in this environment.

- Fail safe operations

  Many pieces of equipment are mounted on isolators on which the equipment remains supported in the event of mechanical failure of the isolator. This feature can be provided by a metal-to-metal interlock or by snubbers.

- Interaction with support structure

  As the supporting structure is not infinitely stiff, its response can affect the components that are flexibly attached to it. Thus if the stiffness of the isolator is high compared to the stiffness of the foundation, the foundation deflects more than the isolator and actually nullifies or limits the isolation provided by the isolator itself. A maximum efficiency from the selected isolator is achieved when the support structure stiffness is at least 10 times the isolator one.

  As supporting structure has inherent flexibility, its resonances could cause amplification levels coupled with the isolator, thus it is important that resonance frequencies are avoided in relation to isolated system natural frequencies.

11.3.2.5 Model specification

In order to realize a different system or sub-system analysis (equipment / system coupled analysis, launcher coupled load analysis), it is necessary to specify the numerical models (CAD or finite element model) to be delivered. If any, it is expected that the refining of such model is also specified, as well as the type of format delivery and the expected schedule.

11.3.3 Attenuator device development logic

11.3.3.1 Introduction

Once the entire attenuator requirements have been fully defined, the attenuator can be developed. The device development logic is detailed hereafter.

11.3.3.2 Attenuator pre-dimensioning

The pre-dimensioning step consists into deriving the attenuator performances and environment constraints into attenuator characteristics and estimate the global behaviour.

It is thus necessary to find the right compromise to match the performances taking into account the whole environments with the elastomer constraints.

The pre-dimensioning process would thus consist into a trade-off considering:

a. the whole mechanical environment versus the isolation frequency:
   - sine dimensioning if $F_{isolation} < 100$ Hz
   - random environment dimensioning if $F_{isolation} > 100$ Hz

b. the specified performances to determine where to tune the mode frequency

c. the thermal working range

Such trade off can be based:

- on experience on previous programs and on prototypes behaviour or
- on a cinematic analytical approach

The final objective of this trade-off is to determine the attenuator main characteristics compatible with the environment, performances and thermal constraints:

- 3 axis stiffness's of the device
- Global behaviour: number of mode along each direction and their frequency depending of the equipment physical properties.

In case performances are not completely matched some constraints can be slightly downgraded (like amplification on the mode or mode frequency) in order to be compatible for the whole environments.

Once mechanical characteristics are determined it is necessary to derive it into a device design. This necessarily means a choice of a material and a detailed design of the elastomeric parts.

11.3.3.3 Material characterization

Due to the wide and complex elastomer nature, the selection is a delicate task which consists into determining the elastomer family and its chemical composition of material giving the good performances in the temperature range of interest. It is a specialist purpose. However, to help determining easier the material choice, some tools are approaches are generally used:

- Material database like SPACEMAT, which gather the main characteristics of material used in the space industry (e.g. mechanical properties at a given temperature: Young's modulus and Poisson's ratio, damping, temperature ranges of use, master's curve, out gassing, and irradiation), as shown in the Figure 11-20.

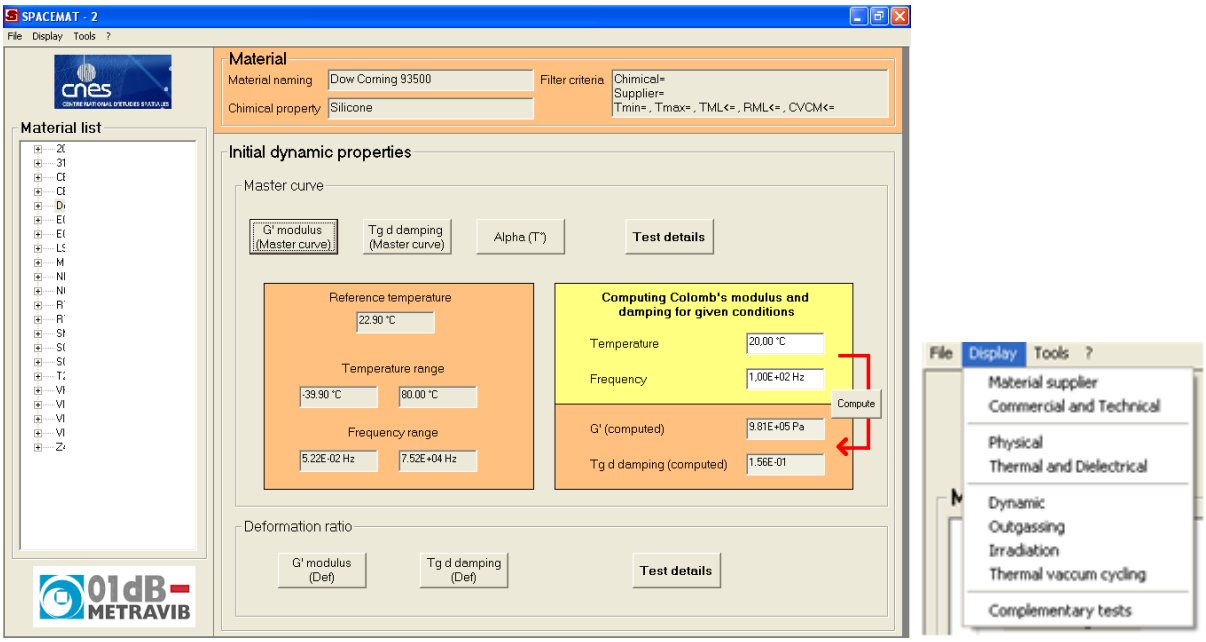

Figure 11-20: Overview of the SPACEMAT database

It also allow to compare one with the other ones the material characteristic to finely tune the right material to select, as shown in Figure 11-21.

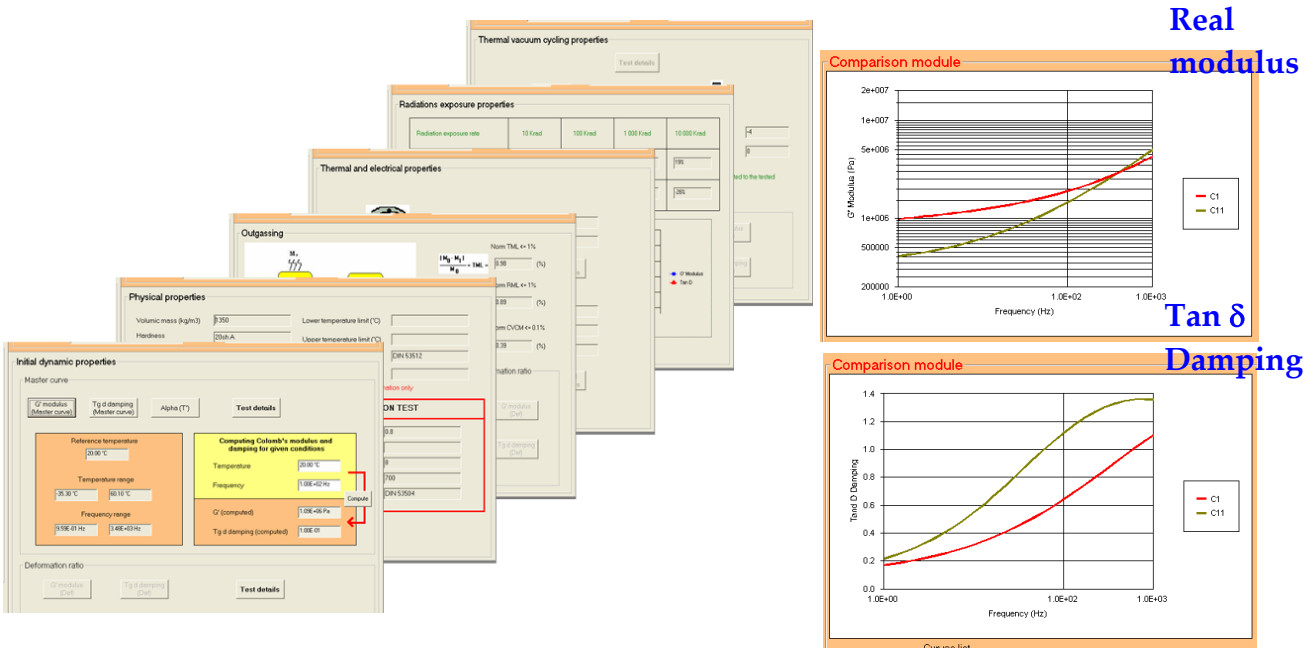

Figure 11-21: Comparison of several materials characteristics

- If a material doesn't exist, it can be characterized by Dynamic Mechanical Analysis (DMA) and the test results can complete the database.

  The DMA is realized with a visco analyzer device (see Figure 11-22).

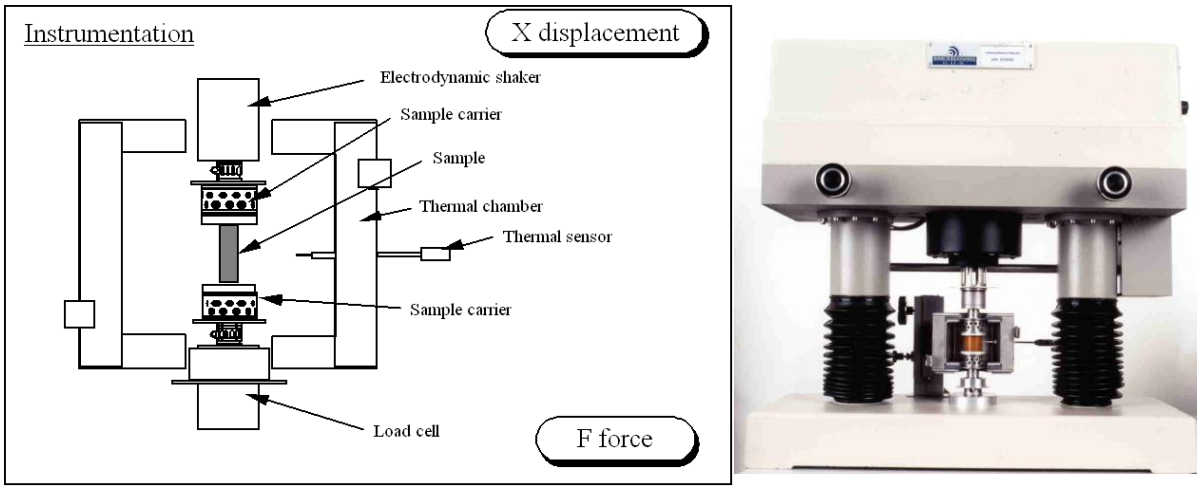

Figure 11-22: DMA Visco analyzer device

This device allows measuring the intrinsic mechanical properties of visco elastic material (e.g. as a function of the temperature, the frequency, and the deformation rate) among:

— The complex stiffness: $K^*=F/x$

— The damping: tan δ

— The glass temperature T_g

— The complex Young's modulus as a function of the geometrical factor α: $E^*=K^*/\alpha$

— Fatigue

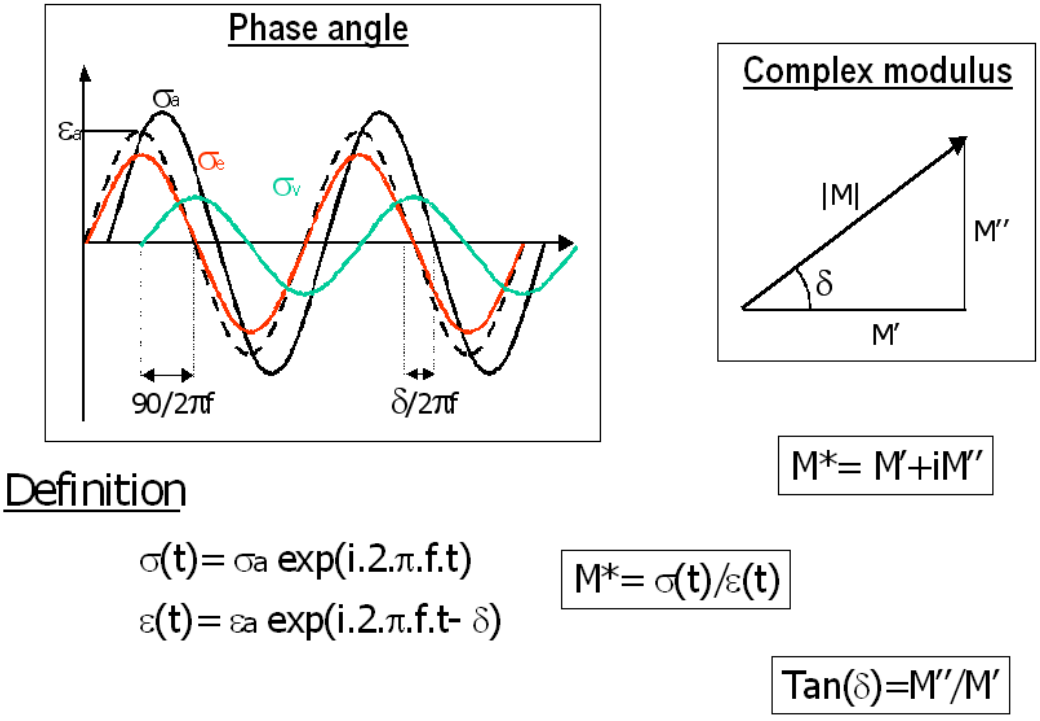

Figure 11-23: Visco analyzer output

11.3.3.4 Design preliminaries

Once the material is selected it is necessary to detail the elastomeric part design to recover at device level the target stiffness obtained in the trade off phase.

This is also the object to estimate the robustness design to sustain all the mechanical environments.

One critical point for the elastomer strength is to avoid too important deformation rate in the material which generally leads to adhesive or tear rupture. By experience, it is generally considered by the elastomer manufacturer **to avoid exceeding 30% deformation rate**.

Once detailed design is given, it could be estimated and verified the expected device final behaviour (e.g. modes frequencies, amplification on the mode, damping, and filtering capability) and verify it matches with the requirements.

11.3.3.5 Prototyping

To verify the attenuator device performances, there is no other way than realizing a prototype.

As the elastomer behaviour is complex and not easy to predict, it is difficult to ensure that the prototype has the exact expected behaviour. Thus the prototyping philosophy consists also to realize different prototypes with slight variation of the detailed design dimensions or materials composition in order to surround the target performances.

Simple test configuration allows verifying the main elementary performances like:

- stiffness directly by static test or indirectly by vibration mass test (measuring the modes in simple configurations)
- simple dynamic behaviour (not generally coupled which necessitate a more complex test configuration and hardware)
- simple shock filtering performance (by hammer impact instead of pyrotechnical approach)

Of course a more complete characterisation of the prototypes can be done to access to complete behaviour in real use configuration on a shaker also taking into account the temperature. In order to avoid main risks during qualification, it is recommended, as much as possible, to be representative of the tests environments. For performance assessment, it is important to respect:

- The shock nature (pyrotechnic or mechanical, near field or far field with modal content)
- The mechanical interfaces (potential impact on shock attenuation)
- The potential preload due thermo-elastic or gravity effects,

11.3.3.6 Attenuator design development

The prototypes experience allows finely tuning and freezing the detailed design of the attenuator.

The attenuator is generally composed of several metallic parts on which one the elastomer is moulded.

The attenuator design development thus includes the three main steps:

- Metallic parts design

  The detailed designed plans completely define the metallic parts which are manufactured classically without any special specificity.

- Elastomer design

  The elastomer parts design are detailed with the same definition than any other feature except that particular rules (see 11.4.4) limit the creation of all the design shapes.

- Moulds design

  The elastomer part are manufactured by moulding process (see 11.4) which thus also requires the manufacturing of moulds, i.e. the negative image of the elastomer parts.

  These particular features are necessary for the moulding process. They allow filling in the elastomer volume between the metallic parts in order to mould the quasi liquid elastomer chemical preparation before curing.

11.4 Attenuator device manufacturing

11.4.1 Overview

The attenuator manufacturing is a delicate step requiring a lot of know-how and experience in chemical elastomer preparation and moulding.

Elastomer technology is very complex as a lot of parameters (e.g. chemical composition, preparation protocol, moulding preparation, and curing) directly influence the final mechanical behaviour of the isolator device.

As this domain is very competitive elastomer manufacturing is mostly confidential. However, we could present the major aspects of the manufacturing process.

11.4.2 Manufacturing process

Elastomer is a very complex organic material. A lot of components enter in their definition (e.g. carbon black filler, sulphur, oil, and protecting agents) to improve physical properties, affect vulcanisation, prevent long-term deterioration, and improve processability. Major elements entering in elastomer composition are presented here before a short introduction to the manufacturing process.

The major compounding of elastomer are:

- **Reinforcement:** Reinforcement is necessary to obtain adequate tensile properties. This is generally achieved by carbon black particles which increase elastomer surface leading to increase tensile, modulus, hardness, abrasion resistance, tear strength, and electrical conductivity and decrease resilience and flex-fatigue life.
- **Addition of oil:** Oils are used to maintain a given hardness when increased levels of carbon black or other added fillers. They also function as processing aids and improve the mixing and flow properties.
- **Anti-degradents:** Elastomer are vulnerable to different type of agent actions leading to wide variety of degradation (e.g. chain scission, cross-link, and cracking). The degradation is more important in elastomer contain unsaturation in the blackbone structure. Anti-degradents is added to improve long-term stability.
- **Vulcanising agents:** *Vulcanization* is the process by which the elastomer molecules become chemically cross-linked to form a three-dimensional stable structure. Vulcanising agents (e.g. sulphur, peroxides, resins, and metal oxides) are used to improve the vulcanization rate, cross-link structure and final properties.
- **Mixing:** Adequate mixing is necessary to obtain a compound that process properly, cures sufficiently, and has the necessary physical properties for end use. Dedicated machine allow component mixing in an enclosed chamber within a two steps procedure to ensure that

premature vulcanization does not occur. Most ingredients are mixed at about 120 °C in the first step. The vulcanisation agents are added at lower temperature in the second step.

- **Moulding:** Compression, transfer, and injection-moulding techniques are used to shape the final product. Once in the mould, the rubber is vulcanized at temperature ranges from 100 °C to 200 °C. After removal from the mould, the rubber is sometime postcured in an autoclave to improve compression-set properties.

Moulding preparation requires important know-how. If any of the process steps is wrongly performed, the final product performance and/or reproducibility would be compromised.

The elastomer base preparation before moulding can be decomposed in the following important milestones:

- **Severe control of the elementary material lot delivery:** It is important that the material lot is of good quality, i.e. homogenous and pure and with the right chemical properties. Some materials pack can need to be subjected to acceptance tests.
- **Precise mixing of the components:** The elastomer material (before curing) is a viscous paste obtained by mixing in a dedicated order the chemical components. The knead process should lead to a homogenous paste. As it naturally increases the paste temperature by friction (about 50 °C at the beginning of the mixing), it is important that the paste temperature is closely controlled to avoid an undesired evolution of the chemical composition by cooling systems. This conditions the final material homogeneity and reproducibility. It is also necessary to control other parameters like pressure, kneading, and duration.

A good control of the complete process from the beginning to the end conditions the final product quality as well as the reproducibility warranty.

11.4.3 Moulding technology

The elastomer moulding is obtained by the simple "Compression – Transfer" technique allowing creation of complex shape with accurate tolerances and low influence of the operator in this process leading to good reproducibility compatible with space industry high levels quality requirements.

Such technique, detailed hereafter, requires moulds. The moulds are the negative image of the elastomeric parts enclosed between the metallic parts in order to realise a closed but non hermetic cavity to inject the elastomer paste.

The moulding process can be detailed as the following steps:

① The uncured rubber is transferred from a pot into the mould cavities when the mould is closed by press.

The control of the injected rubber quantity is achieved by weighting

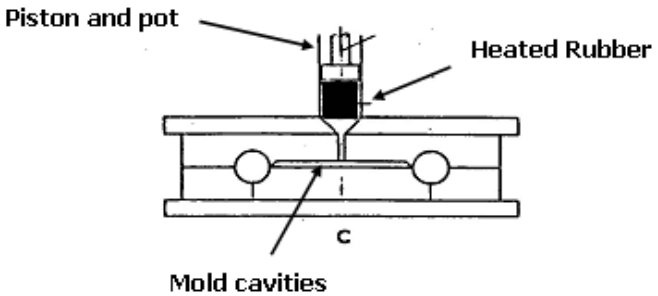

Figure 11-24: Moulding process

② The mould is closed by press and the Vulcanisation stage begins, as shown in Figure 11-25.

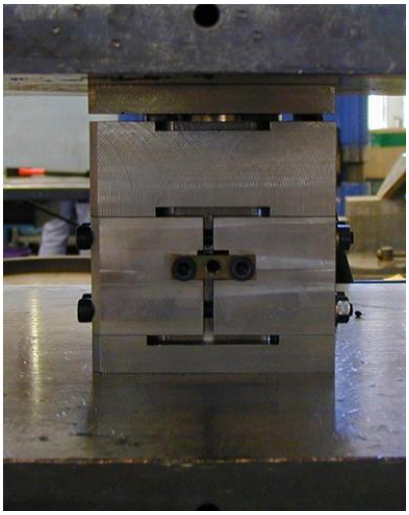

Figure 11-25: Mould under press for vulcanization

③ The damper is removed from the mould, as shown in Figure 11-26.

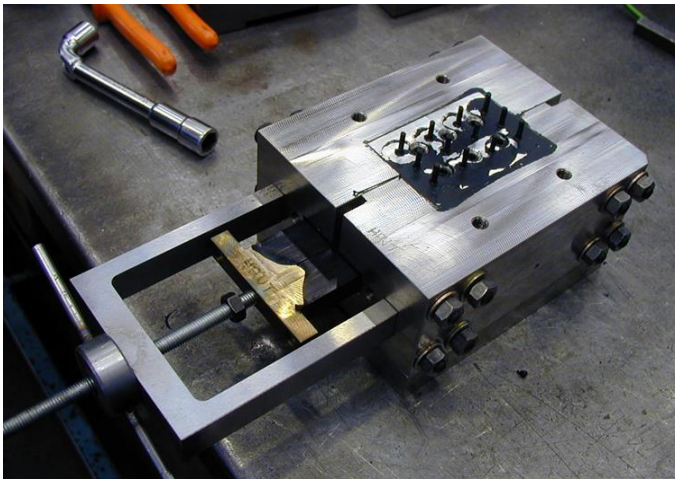

Figure 11-26: Damper removed from the mould

It should be noted that hot vulcanization is generally used in the space industry, instead of cold vulcanization, which presents less mechanical robustness.

After removal from the mould, elastomer pieces can be heated (at a lower temperature than the curing one) in order to improve the out gazing. However this operation is not systematically recommended as it slightly modifies the elastomer properties and accelerates the material ageing.

In case of a high reproducibility in the manufactured pieces, it should be necessary to sort the devices to get the more homogenous batch.

11.4.4 Manufacturing limitations

This compression-transfer technology presents some limitations or drawbacks which are presented hereafter:

- The rubber can self-heat during the transfer phase in the injection duct (leading to premature vulcanisation). Thus particular attention is paid in the duct mould design to avoid too tight piping.
- The technique makes it difficult to perfectly control the rubber temperature and homogeneity inside the mould which can have an impact to ensure a correct curing. Thus important experience is called upon for the moulder design.
- The mould design is defined to allow an easy removal without breaking the elastomer parts.
- The complexity of the moulded shape is limited by the different metal cores, to be removed from the mould at the end. Moreover, this can be a complex and long operation, longer than other simpler processes.
- The mould complexity explains the high mould manufacturing costs and thus limits also the number of samples and designs creatable.
- The technique does not allow moulding rubber thickness lower than 1 mm. This low thickness is difficult to master with this technique.
- The deburring phase can be difficult due to the risk of particular contamination.

11.5 Product assurance logic

The following is an example of a good product assurance policy logic for a development of an elastomer product:

a. Realise a mock-up device in order to:

   — verify and master the complete manufacturing process,

   — check the compliance w.r.t the performance requirement

   — Find the design robustness margins by extending the device solicitation beyond the specified ones.

   NOTE Such a prototype model cannot be used as flight hardware.

b. Manufacture prototypes with the process qualified by the mock-up.
   The flight prototypes are manufactured with generally additional spare samples to limit project failure risk.

   Due to the wide variety of components composing a rubber, some materials can outgass substances e.g. water and oils, which can be restrictive in use w.r.t. the application cleanliness requirement. Depending on the elastomer type (natural, silicone or SMACTANE families) the outgassing effect can be more or less important and thus it is necessary to limit the effect by a different adapted method.

11.6 Existing attenuator products

11.6.1 Overview

To illustrate the shock attenuators application in space industry, some examples of developed devices are presented in this chapter, highlighting the issue leading to identify an isolated solution and the performances achieved by the device.

11.6.2 Compact shock attenuators for electronic equipment

11.6.2.1 Purpose of shock isolation device

Electronic equipment are directly mounted on spacecraft structure, which is subjected to different transient events during the mission life (e.g. launcher, and appendages separation). If the qualification status of the equipment is too low with respect the imposed shock environment, it should be necessary to isolate them from the spacecraft, using ideally off the shelf isolation devices.

11.6.2.2 Shock isolation device principle

The compact shock attenuators for electronic equipment address for interface from M6 to M12 screws and for equipment weight range from 4 kg to 40 kg. They are thus intended to decrease the levels of shock waves to the equipment interface. These attenuators create a break of impedance.

They are sized to respect the following compromises:

- Be stiff enough not to introduce low frequency suspension modes.
- Be soft enough to filter shocks efficiently.

The device design is illustrated on the Figure 11-27.

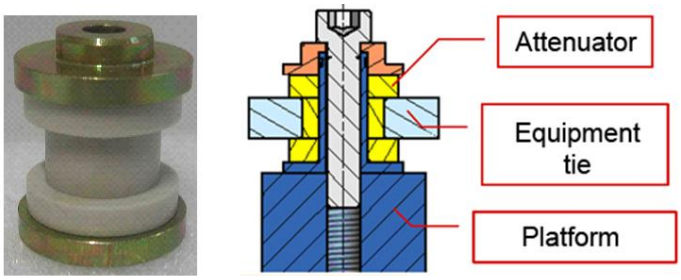

Compact shock attenuators for electronic equipments
Size range: from M6 to M12 screws
Equipment weight range: from 4 kg to 40 kg

Figure 11-27: Compact shock attenuators for electronic equipment assembly principle

The device development is realized by finite element model analysis, as shown in the Figure 11-28

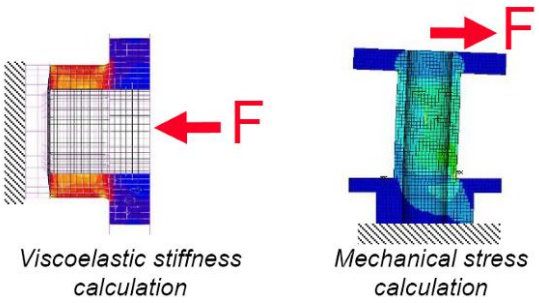

Figure 11-28: Finite element model analysis for shock device development

11.6.2.3 Performance achieved with the isolator device

The performance achieved with the isolator device is illustrated on the Figure 11-29, with attenuation performance greater than 20 dB.

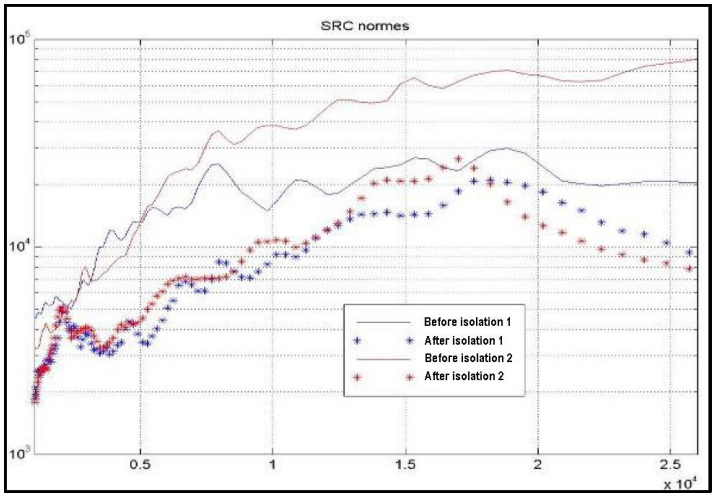

Figure 11-29: Attenuation performance for the isolator device

11.6.3 SASSA (shock attenuator system for spacecraft and adaptor)

11.6.3.1 Requirement specification analysis

A good understanding of the launch phases with their associated requirements and the spacecraft behaviour is a key step of the concurrent engineering phases.

The main functions of the Shock attenuation device are:

- To hold the spacecraft during all the launch phase
- To limit the shock spectrum generated by the launchers shock events (launcher separation) to a level lower than the clamped band release

In order to obtain the most efficient device, it requires a good understanding of both the launcher and the spacecraft requirements. In general, the non-linear behaviour specific to the use of elastomer leads to review the AR5 requirements in a different way. So, the flight events during the launch phase is analysed in a common work between EADS-ST and EADS-Astrium to assess what could be the new requirements for a spacecraft using a shock attenuation device at its interface.

The stiffness characteristics of SASSA are function of the loads applied which are mainly depending on the mass of the payload. Three classes of mass (low: 2000 kg, medium: 4100 kg, large: 6400 kg) have been considered within the range described.

At launcher system level, the SASSA brings some additional flexibility to the upper part of the launcher. It is necessary to limit this extra-flexibility in order to ensure the attitude control of the launcher, in particular during the atmospheric phase.

The stiffness of SASSA was defined such that the decrease of the first mode frequencies of the configuration [ACU 1194 H clamped + SASSA + CU rigid] is limited to the following values:

Lateral frequency (bending) ≥ 8 Hz (decreasing of 20 % from 10 Hz)

The MUA5 specifies the QSL (static and dynamic components) for the payload, at the CoG level.

Table 11-1: MUA5 Quasi-Static load

	Longitudinal (*)		Lateral (*)
	static	dynamic	Static + dynamic
Lift-off	– 1,7 g	± 1,5 g	± 2 g
Maximum dynamic pressure	– 2,7 g	± 0,5 g	± 2 g
Maximum acceleration (γ_L)	– 4,5 g	± 1,5 g	± 1 g
EPC tail-off	– 0,2 g	± 1,5 g	± 0,25 g
EAP jettison	+ 2,5 g		± 0,9 g

11.6.3.2 Baseline design presentation (QM for pre-qualification)

Main characteristics for SASSA unit are (see Figure 11-30 and Figure 11-31):

- Flanges for force fluxes distribution
- Interfaces unit/adaptor and unit/ clampband ring: 5 screws M8

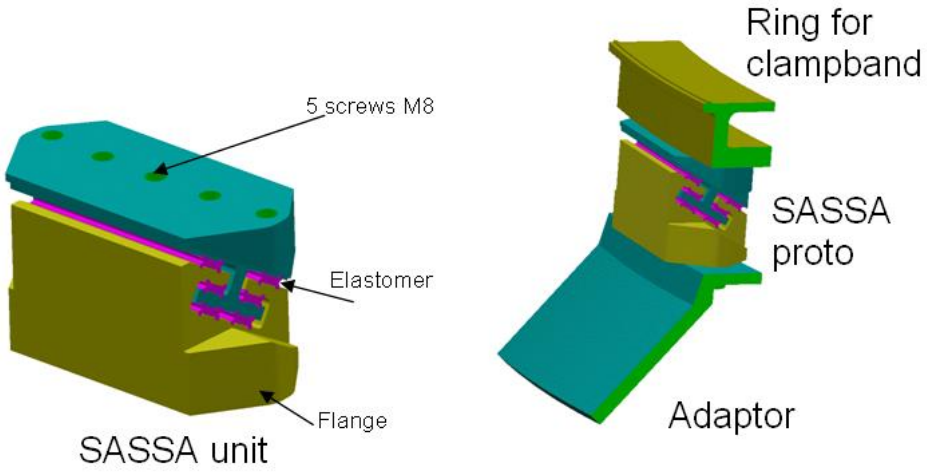

Figure 11-30: SASSA unit and assembly with adaptor and clampband ring

SASSA system configuration is presented in next figure. Main characteristics for SASSA system are:

- Twelve couple of unit each 30°. All allowable areas and screws are used to limit the forces flux at most.
- Inner space between two units makes easier the mounting, Outer space of two units are for pushers

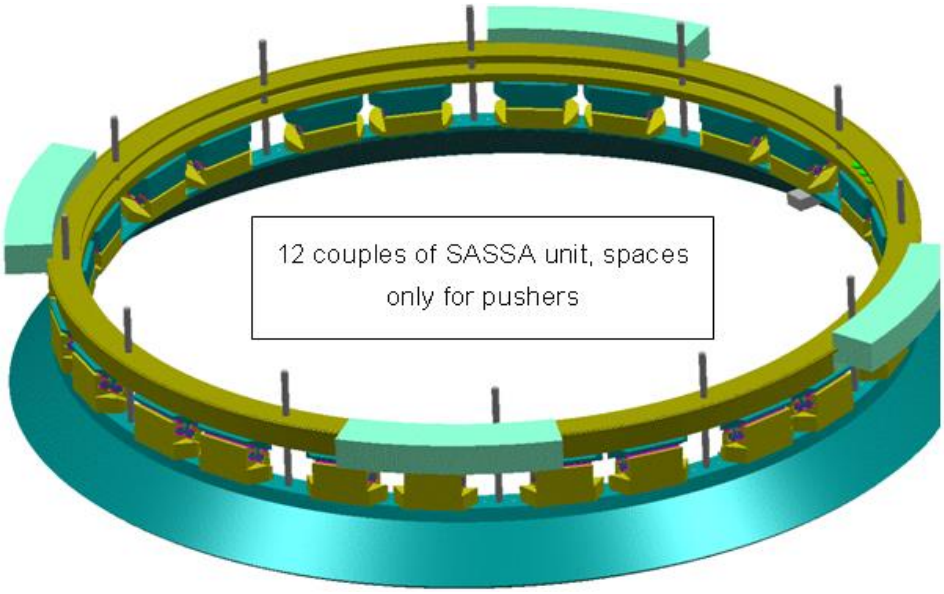

Figure 11-31: SASSA system overview

11.6.3.3 SASSA system qualification with Eurostar3000 STM

11.6.3.3.1 Strength and stiffness validation in lateral axis

The test set-up is made of four main structures: the STM3000, SASSA, a clamp ring CRSS and ACU 1194.

Figure 11-32: Test set-up in lateral, Momentum at S/C interface

The objective of SASSA strength qualification with a real test configuration is fulfilled. On the lateral mode at 6 Hz, the S/C base momentum: is 70 kN.m, which corresponds to 1 g QSL for 5 t with CoG at 1,46 m. This momentum corresponds to a SASSA module axial force at 12 KN. Moreover, the following observations were made:

- Q=8 for SASSA (Q= 13 for STM3000+SASSA+ACU)
- Linear behaviour without shock, no frequency or damping variation
- Good accuracy on frequency predictions
- No visible degradation on material, successful check of clampband after removal
- Good superposition of low levels (before and after qualification runs)

11.6.3.3.2 Pyrotechnic shock filtering - SHOGUN test with STM3000

SHOGUN configuration (free/free) leads to isolation modes around 1500 Hz with following performances:

- In low frequencies (first mode at 400 Hz): SASSA provides 5 dB up to 15 dB w.r.t. levels
- In High frequencies (modes above 1500 Hz): SASSA isolation provides 14 dB up to 24 dB w.r.t. levels

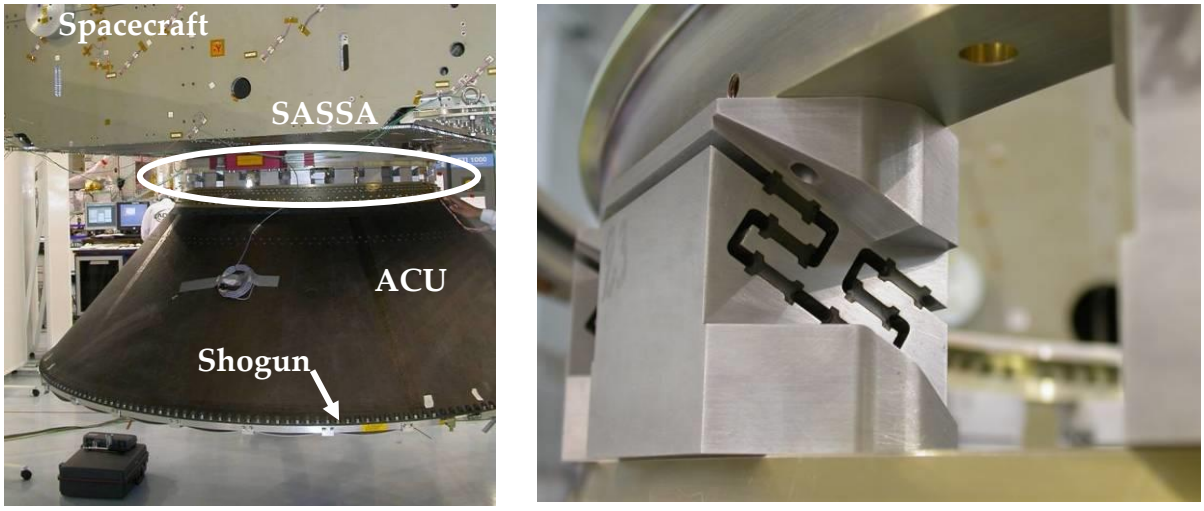

Figure 11-33: SASSA module configuration

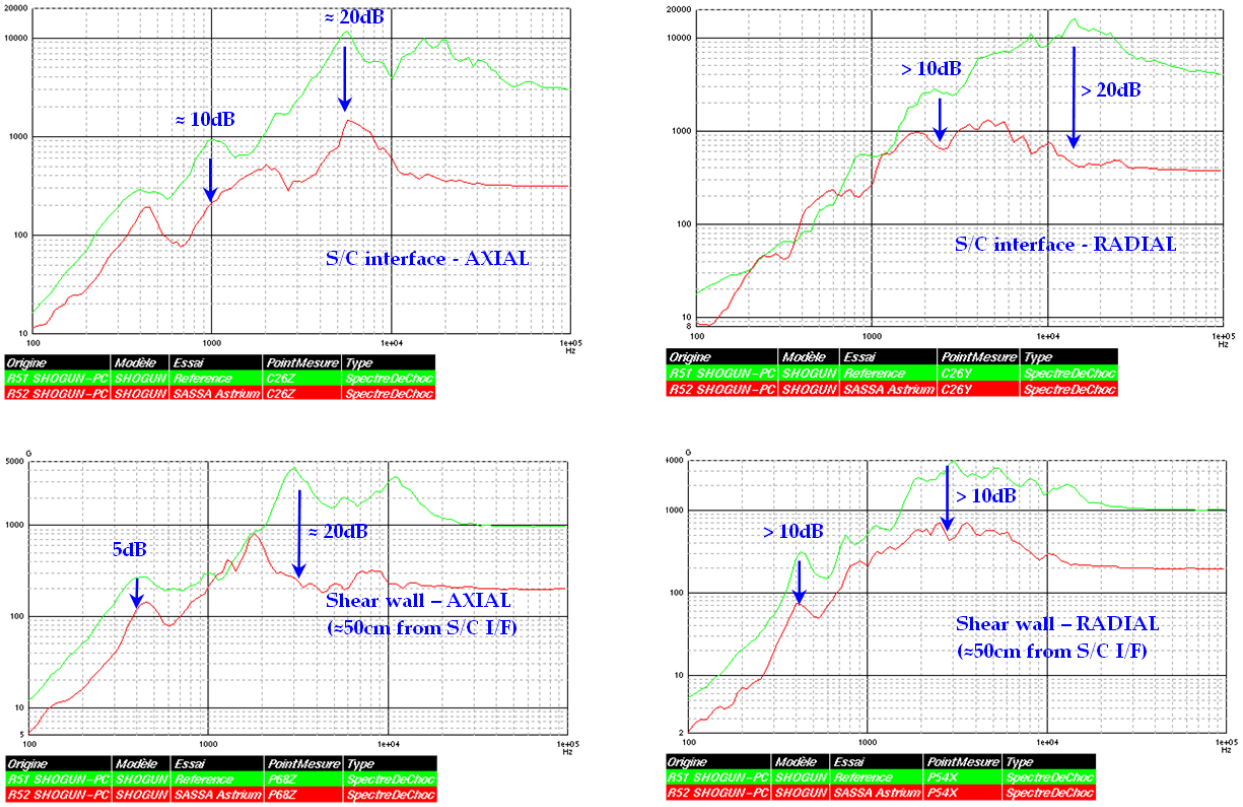

Figure 11-34: Example of SASSA performance in green without SASSA, in red with SASSA

11.6.3.4 SASSA lessons learnt

Development logic

The SHOGUN shock test performance was assessed with a preliminary design without a detailed design required for stress analysis. Therefore, the design was not enough mature for sine environment. In term of study logic, it is important to respect the following order:

1. Design activities
2. Environment tests validation
3. Performance tests validation

A dynamic test is mandatory for strength verification in case of any evolution in the design.

Industrial organisation and manufacturing

- In term of industrial organisation, it is recommended to centralise the elastomer moulding and metallic manufacturing activities. Tolerances and definitions of aluminium inserts are done with the definition of the mould and the retraction of the elastomer after de-moulding. Furthermore it is easier to do manufacturing drawing for aluminium inserts and for the mould.
- De-moulding in hot temperature and not in cold temperature (for example mould in water to win time) in order to avoid thermo-elastic stress, vacuum (high confinement of SASSA) and softening due to reversion of natural rubber
- Static acceptance test with realistic boundary conditions for unit and using of comparator to avoid tools flexibilities.

Specification

- Allowable volume was too constraining at the 1194 I/F. That led to too small section of aluminium inserts. Therefore, if possible, it is easier to use the 2624 I/F, if it is not possible, it is necessary to study in detail the volume in radial and the implementation of the pushers
- For stiffness or frequencies specification, it is important to analyse all the six DOF. Lateral mode should be as low as possible, but still ensuring sufficient margin with respect to the launcher control system. Also the longitudinal and torsional modes should be looked at, in order to improve the payload comfort (through coupled load analysis).

Prediction

- It is necessary to have MARC detailed model in the beginning, in order to find the errors of concept or manufacturing (example with layers too confined for mock-up 1)
- For stress or overfluxes analysis, it is necessary to have a detailed model. For stress or strain in unit (elastomer or aluminium) a non-linear MARC model is required and it is supposed to be correlated with test. This MARC model provides forces/displacements curves for all DOF, which provides simplified stiffness for system analysis and it completes tests which are not feasible for rotations. For system sine analysis with S/C or launcher a linear model is sufficient (SASSA is quasi-linear in the domain of system tests).

Tests validation

The main lesson for tests validation is that, if elementary tests with SASSA unit are well prepared and performed, tests at system level with complete SASSA are easier to manage/predict.

- For static tests, stiffness and strength can be assessed in translation with only one or two units. It is important for stiffness to take into account the tools flexibilities. For strength, it is required to combine longitudinal and lateral forces.
- For elastomer strength validation, it is necessary to perform a dynamic test. Representative conditions are possible with only 4 units of SASSA and a dummy mass.
- For shock attenuation performance, SHOGUN test was necessary for system characterisation, nevertheless it is well completed with mechanical shock with only 3 or 4 modules.

11.6.4 Shock isolators for EXPERT on-board equipment

11.6.4.1 Overview

Several shock isolators were designed and implemented inside the EXPERT vehicle, in order to protect different equipment from the shock environment met during the launch and during the re-entry phase too. Among these different isolators, one of them is used to decouple the Inertia Moment Unit (IMU) of the vehicle.

11.6.4.2 Main Technical specifications and assessments

- Mass of the IMU: 0,8Kg
- Mechanical environment:

  The mechanical environment met during the launch and the re-entry phase is mainly characterized by:

  — A high sine level between 60 Hz and 130 Hz (7,1g)

  — A high random level inside the 100 Hz-1000 Hz bandwidth (0,4 g^2/Hz, 3 min)

  — A high SRS shock: 100 g at 100 Hz, 2000 g from 1 kHz to 4 kHz

  — A 100 Hz to 160 Hz forbidden band
- Thermal environment: from 0 °C to 30 °C

The main design task for this shock isolator is to withstand the launch sine levels which are strong from 60 Hz. So, the cut off frequency of the decoupled system is selected lower than these 60 Hz. Finally the target is to have the 1st mode around 38 Hz with an amplification lower than 2, taking into account the temperature range and the dependence on the level.

11.6.4.3 Presentation of the design

The design of the isolator is based elastomer mounts moulded with the SMACTANE SP® rubber material, in order to achieve an amplification lower than 2. The rubber shape is directly bounded on aluminium interface during the moulding phase (see Figure 11-35).

Figure 11-35: View of the elastomer mount

As showed in the Figure 11-36, 4 mounts were tightened between two aluminium brackets. The aim is to avoid rocking modes for lateral vibrations. To get there, these aluminium brackets were designed to increase the footprint and to align the IMU Cog with the mount.

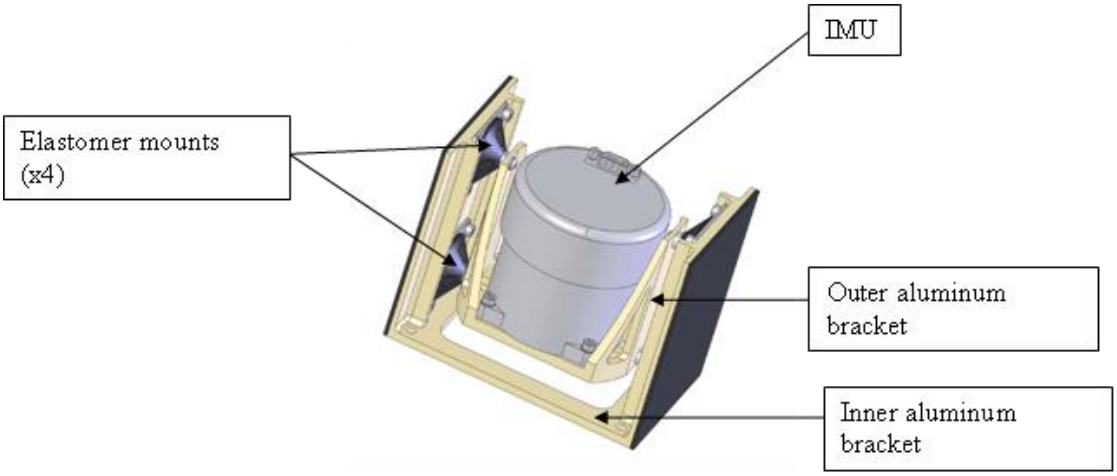

Figure 11-36: View of the complete isolator

In addition of that, rubber layers constrained by a carbon/epoxy plate were bounded on the external area of the outer bracket, to add structural damping on this metallic part to damp the flexure mode (~400Hz), and so to avoid a strong response under the lateral shock environment.

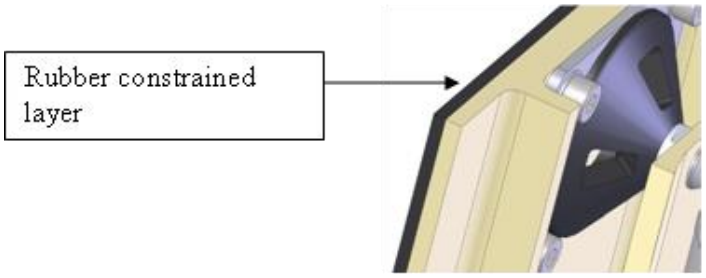

Figure 11-37: View of the rubber constrained layer

11.6.4.4 Performances

11.6.4.4.1 Introduction

Here are the main performances measured during the qualification tests campaign, as shown in Figure 11-38.

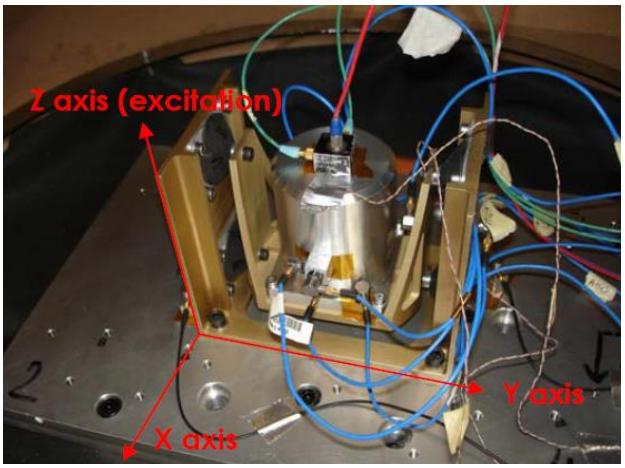

Figure 11-38: View of the isolator during vibration tests

11.6.4.4.2 Performances w.r.t. random loads

- Following Z axis: See Figure 11-39 and Table 11-2.

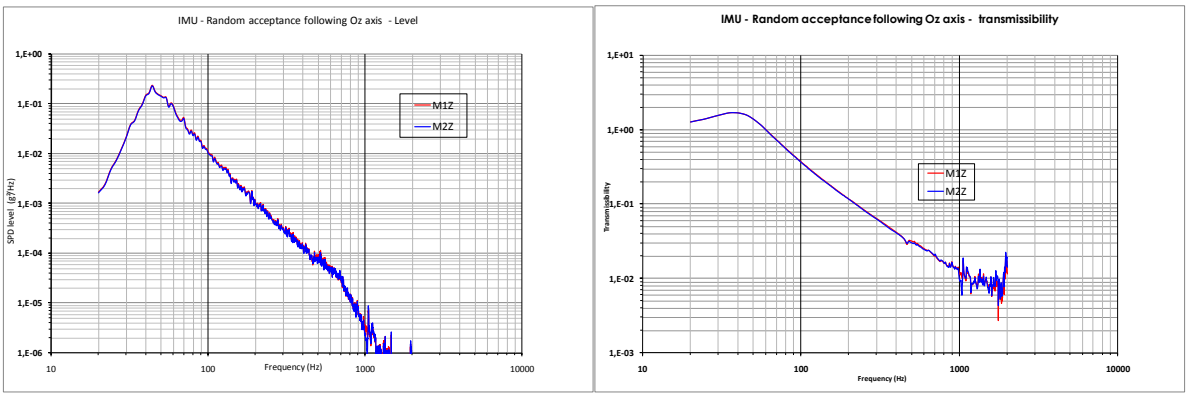

Figure 11-39: Random test level and identified transmissibilities – Z axis

Table 11-2: Amplification domain definition

Sensor	1st Eigen mode Fr (Hz)	Amplification at Fr	Cut off frequency Fc (Hz)
M1	38	1,65	63
M2	38	1,73	59

- Following Y axis: See Figure 11-40 and Table 11-3.

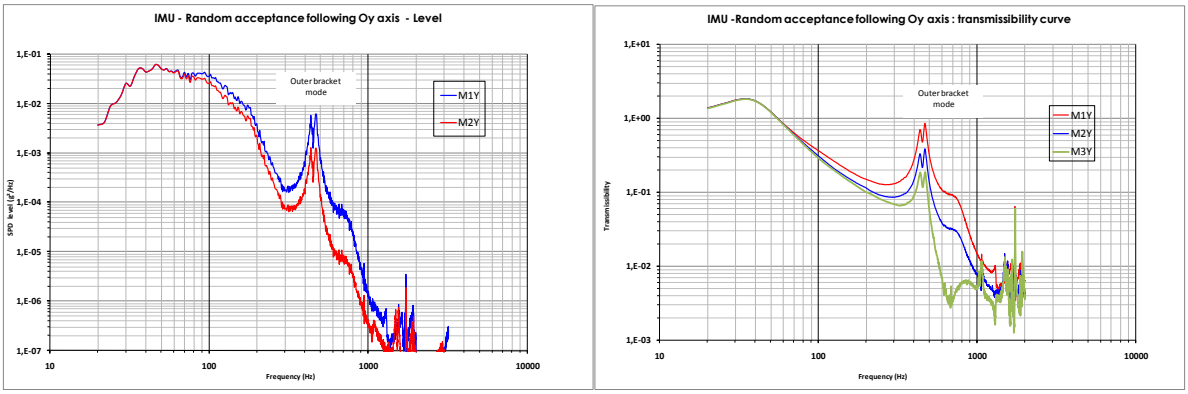

Figure 11-40: Random test level and identified transmissibilities – Y axis

Table 11-3: Amplification domain definition

Sensor	1st eigenmode Fr (Hz)	Amplification at Fr	Cut off frequency Fc (Hz)
M1	35	1,82	55
M2	35	1,82	55

As expected, the 1st mode is around 38Hz with amplification lower than 2 and no rocking mode can be identified.

11.6.4.4.3 Performances w.r.t. shock loads

Figure 11-41 shows the achieved attenuation performance, as identified during a system level shock test, and compared against the prediction.

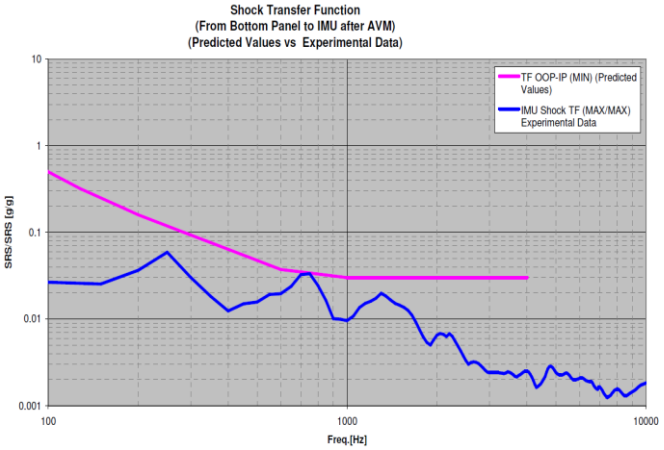

Figure 11-41: performances under shock levels

The rubber constrained layer further improves the attenuation performance in low frequency, with in particular no amplification on the main mode. The achieved attenuation exceeds 12 dB in lower frequency range, and exceeds 24 dB above 1000 Hz, hence confirming the suitability of the shock isolator design.

Part 3
Shock verification approach

12
General approach to shock verification

12.1 Rationale for shock verification

The scheme presented in Figure 12-1 aims at presenting in a synthetic way the general approach of shock verification.

This scheme is based on several questions to be answered, represented by the *yellow diamonds* ◆:

- Is the equipment a new one ? – It addresses the presence of a heritage for the considered equipment.
- Is the equipment similar ? – In case a heritage has been identified, it is important to evaluate the degree of similarity between the considered equipment and the equipment of the same family.
- Is the equipment sensitive ? – In case the equipment is a new development or the degree of similarity is insufficient, it is important to determine the equipment sensitivity.
- Capability to withstand the qualifying shock demonstrated ? – The fourth question is the same whichever the qualification approach has been chosen. It deals with the capability to withstand the qualifying shock with respect to the available data.

When the shock verification involves shock testing, those test campaigns are depicted by *blue squares* ■:

- The unit qualification shock test aims at qualifying the considered equipment at its own qualification level. See 13 and particularly 13.3 for more details.
- The system level test (generally Clampband on Structural or Flight Model or Shogun on Structural Model) aims at consolidating the different equipment shock specifications. It can also be used as an acceptance test for equipment not sufficiently verified at their own level, with the condition that the associated risk is clearly identified/assessed. See paragraph 13 and particularly 13.3 for more details.
- The delta qualification test at unit level can be necessary in case the capability to withstand the qualifying shock has not been demonstrated by the first qualification test. It can consist in changing test facility, test conditions or input level to meet the required levels.

In case the capability to withstand the qualifying shock has not been demonstrated, several possibilities exist:

- As previously mentioned a delta qualification test at unit level can be performed in order to reach the specified levels.
- Another way is to modify the design. This can be done either internally to the equipment or at its interface. Dedicated internal redesign can be looked at if the failure cause has been well identified. Interface redesign typically consists in adding a shock attenuation system to reduce shock levels at equipment base (see section 13). In both cases a redesign is a difficult task especially as this design modification is decided late in the programme.

- A third way is a Shock Damage Risk Analysis (see **Part 4**) which aims at evaluating the risk incurred by the equipment with respect to the known shock levels. Such a task is only chosen as a last resort since it bypasses the standard qualification process and represents a risk for the equipment. In this regard, the SDRA drives automatically the unit away from the qualification domain; but it either provides valuable data to ensure a successful qualification (in view of a sub-system or system level qualification test), or it provides a risk assessment on the capability of a spacecraft/equipment to withstand (or not) the required shock environment without damage.
- The three precedent ways focus on the equipment. A fourth way exist. It consists in reviewing the specified levels. This is usually done by a waiver requested to launcher authorities: the aim is to reduce the specified levels at the base of the spacecraft using better knowledge of the real excitation. This is always hazardous as such waivers are seldom accepted.

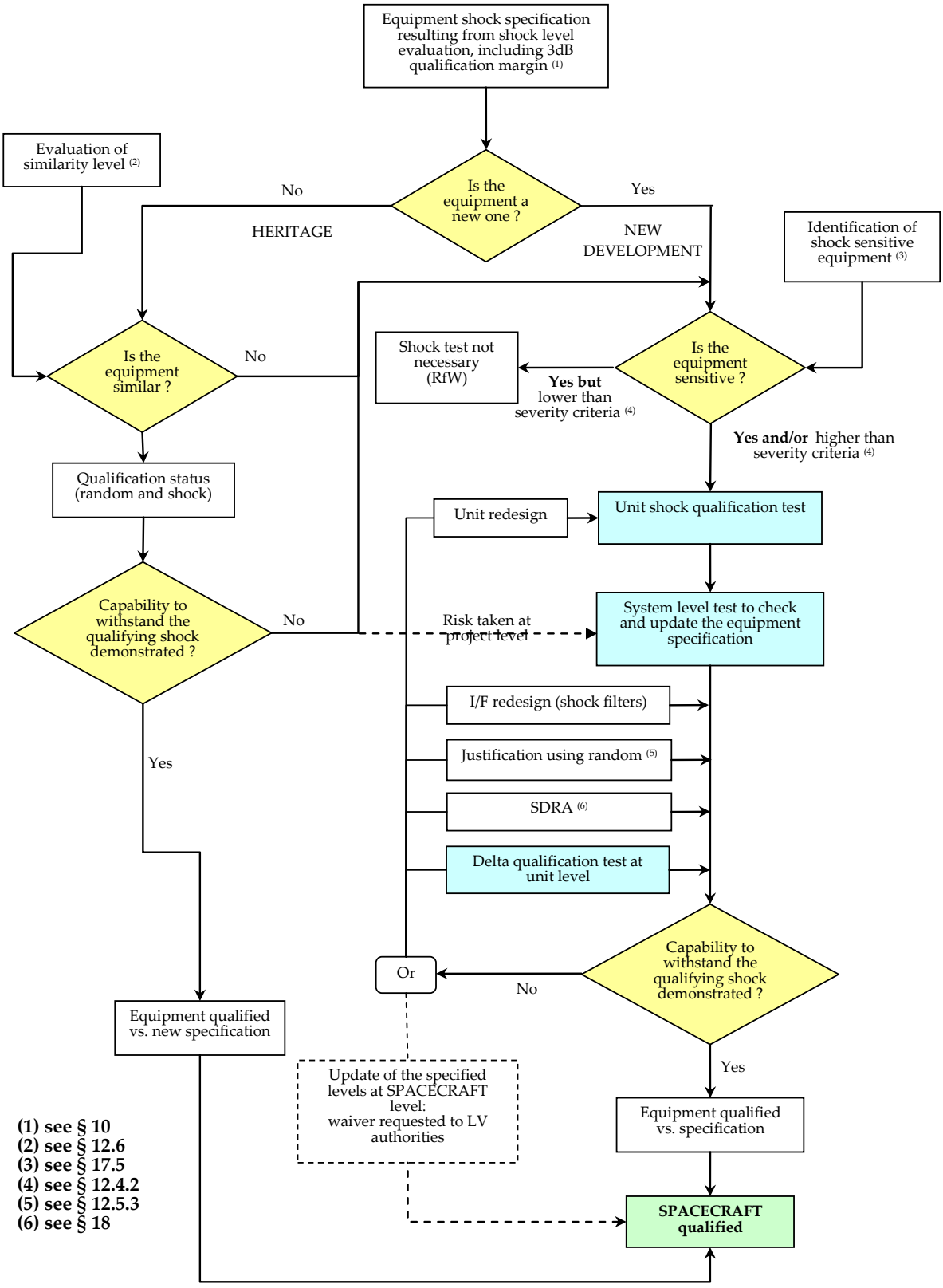

Figure 12-1: Principle of shock verification

12.2 Test rationale and model philosophy

12.2.1 Qualification test

12.2.1.1 Qualification shock test on QM unit

The objective of qualification testing is the **formal demonstration** that the design implementation and manufacturing methods have resulted in hardware conforming to the specification requirements. The purpose of qualification testing is **to demonstrate that the items perform satisfactorily in the intended environments with sufficient margins**. Such a test is commonly a contractual requirement with an associated test specification. This specification requires the qualification test levels to exceed the maximum predicted levels by a factor of safety which assures that, even with the worst combination of test tolerances, the flight levels do not exceed the qualification test levels. For shock environment, a margin of **minimum 3 dB** over the entire frequency band is usually added to the maximum expected flight environment (see 10.2). This margin accounts for hardware strength variability and shock environment variability.

A qualification test is usually performed on a hardware item (called Qualification Model QM) that is not meant to fly, but is manufactured using the same drawing, materials, tooling, processes, inspection methods, and personnel competency as used for the flight hardware. The purpose of a qualification test is to verify the design integrity of the flight hardware with a specific margin.

The qualification testing is usually performed at subsystem level. As a consequence, the representativeness of the test, in terms of support impedance (infinitely rigid support are often used to clamp the equipment) and category of source (mechanical instead of pyrotechnical for instance) is generally reduced. **It is important to pay dedicated attention to the selection of the test method / facility**, to avoid situations where the equipment would be submitted to a more stringent environment as compared to the expected environment at system level.

A qualification test is always followed by functional tests to ensure the correct working and performance of the item. Furthermore, the standard qualification test sequence (ECSS-E-ST-10-03C) specifies thermal vacuum after the mechanical environments (sine, random and shock) based on both the order in which the environments are encountered during flight and the purpose to perceive defects as early in the test sequence as possible. Experience has indeed shown that until the thermal-vacuum tests are performed, many failures induced during dynamics tests are not detected because of their short duration. In addition, the thermal-vacuum test on flight hardware at both the assembly level and the system level provides a good screen for intermittent as well as incipient hardware failures.

12.2.1.2 Case of re-test on QM unit

A re-test on QM unit can occur if a failure or malfunction has occurred during the shock test on the qualification unit. The best practice is to follow the standard NRB (Non-conformance Review Board) process. The main technical activity is to understand the reason of the failure. For this, suitable guidelines can be found in Part 4 – SDRA.

Then the qualification approach is re-assessed, going either in the direction of a design modification or of acceptance of a reduced specification by the System.

Then the QM full qualification sequence (including all mechanical environments) can be either resumed or restarted.

If it is chosen to restart the test from the beginning, fatigue issues should be addressed (other sensitive components may need to be changed even if not failed, in order to avoid fatigue). In any case, as the QM

has already been submitted to environmental tests, it is necessary to review the test tolerances in order to reduce the over-testing risk (define tighter test tolerances).

12.2.1.3 Case of qualification shock test on PFM unit

It is important to consider the shock environment as any other mechanical environment, and to take it into account when defining the model philosophy for the equipment development programme (typically at the EQSR, Equipment Qualification Status Review). Heritage/Similarity (section. 12.6) and Severity criteria (section. 12.4) are primary drivers for the definition of a suitable model philosophy.

Furthermore, it should be noted that there are proven suppliers which prohibit shock test on proto (flight) units through their company standards. Hence, such restriction needs to be taken into account when the model philosophy is defined.

Applying these guidelines should avoid situations where no QM model and no heritage are available to verify a potentially damaging shock environment.

But even if these guidelines are consistently followed, project constraints can be such that a shock qualification on flight hardware is unavoidable. The shock environment can be subject to changes in the course of the spacecraft development, due for instance to a change of the launcher (imposing a more stringent environment than the previous baseline launcher), or due to higher shock loads identified during a system level shock test.

Therefore shocks on PFM are not forbidden in this handbook, as well as in the ECSS "Testing" [RD-049]. However, the protoflight approach can present a higher risk than the prototype approach in which design margins are demonstrated by testing of a dedicated qualification product. In the case where shock testing is performed on a (proto) flight unit, the following strategy is recommended to be applied to minimize the risk:

- Perform only one shock application per axis
- enhancing development testing,
- assessing equipment sensitivity to shocks (through detailed SDRA – see chapter 16),
- implementing an adequate spare policy,
- reviewing the shock requirement (better estimation of environment, use of a database (see paragraph 8.2.6), or available data from a System STM test).
- selecting an adequate shock facility (section 13.2 and 13.3),
- paying a close attention to the calibration test (section 13.3.4.2),
- imposing more stringent requirements to the test execution (upper test tolerance, and number of applications, see section 13.1.2 and 13.1.7).

Finally, acceptance by the customer is a precondition for the protoflight approach for shock qualification.

12.2.2 Acceptance test

The purpose of acceptance testing is **to demonstrate conformance to specification and to act as quality control screens to detect manufacturing defects, workmanship errors, the start of failures and other performance anomalies**, which are not readily detectable by standard inspection techniques. The acceptance tests are formal tests conducted to demonstrate the adequacy and readiness of an item for delivery and subsequent usage. Acceptance testing should not create conditions that exceed safety margins or cause unrealistic modes of failure. Acceptance tests should be conducted on flight models under environmental conditions no more severe than those expected during the mission.

For shock environment, and for spacecraft programme, a flight acceptance test is not required at equipment, where the equipment design integrity has already been verified by a qualification test.

The acceptance testing is usually performed at system level, in conjunction with a system level functional test (i.e. separation shock test of spacecraft / appendages, and verification of compatibility with respect to the induced environment). All the items are then mounted on their real interface support and the shock sources are exactly those that are used during flight.

An acceptance test is always followed by functional tests to ensure the correct functionality and performance of the item.

12.2.3 System / subsystem distinction

Ideally, the time-history data used to develop the qualification test specification should be measured during a full scale system test in which the actual pyrotechnic device or devices are initiated. The full-scale test should be performed with hardware that is structurally similar to the real hardware if the real hardware is not available. Unfortunately in actual development program, the real hardware is rarely available early in the development stage, so that mock hardware is often used. As a minimum requirement, it is important that the mock hardware has the same weight and have the same attachment points as the real hardware. However, in many cases the hardware weight distribution becomes critical because it governs both the amplitude and the frequency content of the measured acceleration response at the base of the mock hardware, so that a different amplitude and frequency is observed with the real hardware. A control point measurement should be specified close to each test item or subassembly of interest, preferably at the attachment point, to measure the input pyroshock.

Since full-scale testing is expensive, data from a similar application can be used to develop qualification test specifications for subsystem test. This practice can result in over-test or over-design if a large margin is added to the test specification to account for the uncertainty in the data. If this practice is used, the test specification should be revised when better system data become available.

12.2.4 Model philosophy

The test baseline definition should be based on the project model philosophy. Several types of model philosophies can be employed according to verification requirements. Specificity of shock environment induces however particular rationale.

Classical philosophy includes **characterization testing** on STM (that can possibly be refurbished in PFM) for launcher-induced shocks, for spacecraft release shock, or for deployment of appendages. Once the different environments are characterized, subsequent specifications are derived for the corresponding subsystems. **The qualification demonstration is then achieved at subsystem level on QMs**.

Acceptance testing is performed at system level on PFM or FM.

NOTE for deployment tests the actuation device needs to be replaced.

NOTE for actuation devices that cannot be replaced (e.g. pyrovalve), the induced environment is usually characterized neither on STM (propulsive subsystem not included) nor on PFM. It cannot be considered as an acceptance test on PFM or FM due to evident constraint of such one-shot devices. As a consequence, it is important to pay attention on subsystem qualification (see 12.7.2).

Table 12-1 summarizes the model philosophy for system level shock testing.

Table 12-1: Model philosophy

System level	Shock testing
STM/QM	Launcher simulation test when applicable (e.g. SHOGUN/VESTA) S/C release or separation test Deployment test Pyrovalve shock test (when possible)
PFM/FM	Launcher simulation test on case by case basis(*) S/C release or separation test Deployment tests
(*) It is important to identify the risk of overshoot with respect to the intended flight environment, and where relevant, to implement the resulting corrective actions (i.e. replacement of shock sensitive units by representative dummies).	

12.3 Environmental test categories

12.3.1 Combination or separation of sources

Occasionally, a pyrotechnic device, such as an explosive bolt cutter, is combined with another mechanism, such as a deployment arm, to position items for a particular event sequence. In this case, a distinct velocity change is combined with the pyroshock event, and the low frequency slope of the shock response spectrum reflects this velocity change and can require an additional shock test to meet the velocity requirement. In some cases, two or more pyroshock events, such as stage separation and an explosive actuator, can be combined into a single test specification.

If the events shows significant differences in time/frequency characteristics, the resulting test specification can be difficult or impossible to meet. In some cases (different frequency content, very different sources, …), it could be relevant to consider distinct shock specification for each pyroshock event.

12.3.2 Pyroshock environmental categories

Pyroshock environments have been broadly divided into **three categories** [RD-053]: **near-field, mid-field, and far-field**. For most aerospace installations, the distinction between these three categories is the magnitude and spectral content of the environment, which depends on the type and strength of the pyroshock device, the source/hardware distance, and the configuration details of the intervening structure (especially discontinuities like joints, corners, lumped masses, and resilient elements, which can significantly attenuate the high frequency content of the pyroshock environment). The pyroshock environmental category usually has a strong influence on the hardware design and/or selection.

In broad terms, these categories can be described as follows:

- The near-field environment is dominated by **direct wave propagation from the source**, causing peak accelerations in excess of 5000 g temporal with a frequency content still important above 100 kHz (in particular for the linear sources) and SRS with a continuous growing tendency. For very intense sources, such as most line sources, the near-field usually includes structural locations within approximately 15 cm (6 in.) of the source (unless there are intervening structural discontinuities). For less intense sources, such as most point sources, the near-field usually includes locations within approximately 3 cm (1 in.) of the source. In a good aerospace system design, there should be no pyroshock-sensitive hardware exposed to a near-field environment.
- The mid-field environment is characterized by a **combination of wave propagation and structural resonances**, causing peak accelerations between 1000 and 5000 g and substantial spectral content above 10 kHz. For very intense sources, the mid-field usually includes structural locations between approximately 15 cm and 60 cm (2 ft) of the source (unless there are intervening structural discontinuities). For less intense sources, the mid-field can extend between 3 cm and 15 cm of the source.
- The far-field environment is **dominated by structural resonances**, with peak accelerations below 2000 g and most of the spectral content below 10 kHz. The far-field distances occur outside the mid-field. The typical far field SRS discloses a knee frequency corresponding to the dominant frequency response - See Figure 12-2. As dealt with in Part 2, these structural resonances in mid frequency range are less easily attenuated, as compared to higher frequency excitations.

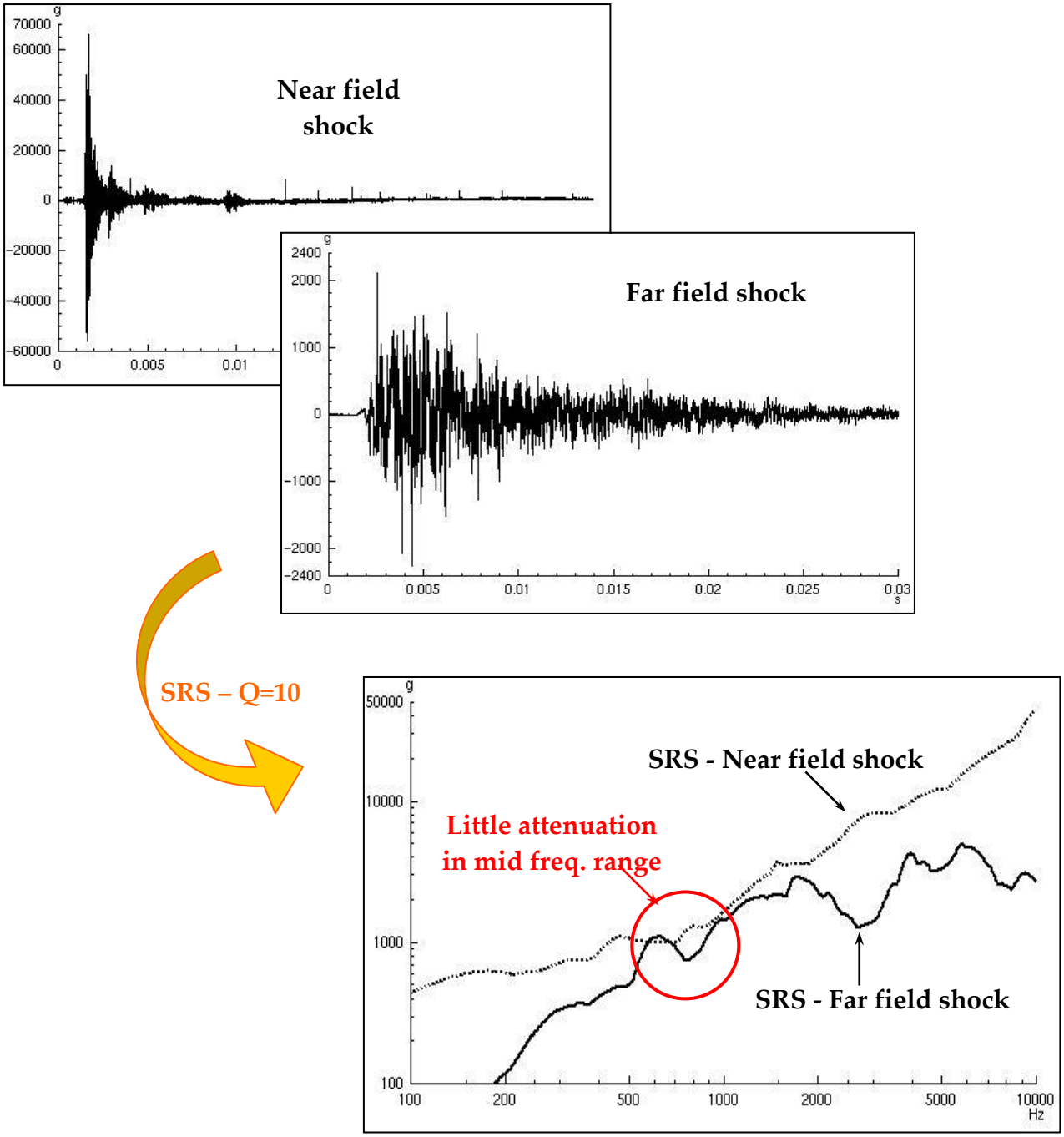

Figure 12-2: Typical near and far field SRS and time history

12.4 Shock sensitive equipment and severity criteria

12.4.1 Identification of shock sensitive equipment

When looking at the shock qualification status of an equipment, it is necessary to assess the equipment sensitivity to shock, since this is determinant to the equipment shock verification approach.

Shock sensitive equipment can be identified using the list of elements that are particularly sensible to shocks provided in paragraph 17.5. Such an evaluation should be done by both prime contractor and equipment supplier.

12.4.2 Severity criteria

12.4.2.1 Overview

Even if all units should be proven to be compatible to their shock environment, such a process does not always require a shock test for demonstration. In case of low shock levels, some non-sensitive units may not be endangered. The purpose of this section is thus to define severity criteria below which the unit is considered safe with respect to shock and for which no shock test is required.

A subdivision between unit types has been found necessary to define such severity criteria: electronic units, structural or non-sensitive equipment and other types of equipment.

Note that these criteria are expressed using standard SRS, which means using the usual Q=10 amplification factor.

12.4.2.2 Electronic units

12.4.2.2.1 Introduction

For electronic units, a no shock test approach is **best justified applying a verification by similarity**, for which a detailed guideline is provided in para. 12.6, including complementary activities to support such verification approach (para. 12.6.3.4).

On the other hand, the Handbook identifies some sensitivity threshold levels for various electronic components (para.17.5), and identifies some robust design principles with respect to shock (para. 18.3.1.6). Both aspects are relevant in view of the identification of a severity criteria, below which the unit is considered safe with respect to shock, and for which a no shock test approach could be supported:

- From the identification of sensitivity threshold levels (para.17.5), the lower bound relates to failure modes of relays, with level as low as a few hundred g's in relation to bouncing and transfer (whereas mechanical damage may be experienced for significantly higher levels).

  NOTE Relay sensitivity threshold levels have been characterised during a test campaign on several types of relays (EL215 – EL415 – E215 – GP3A – GP250 – GP2A – T12 – TL12 – PHL50A), see para. 17.5.2.1.3.

- From considerations for robust equipment design with respect to shock (para. 18.3.1.6), the equipment mechanical design and the influence of components / PCB mounting conditions, are identified to be primary drivers for the sensitivity of the equipment to shock.

The severity criteria proposed in this section can be called upon, under the strict condition that the following conditions are met, and should be justified in the frame of a Request For Waiver (i.e. necessitating the approval of the customer):

a. The electronic unit should be screened for presence of sensitive components, according to Table 17-1. The severity criteria assumes that all electronic components are mounted on PCB, hence accounting for filtering/decoupling effect from equipment housing response. Also in case the electronic unit contains some relays, it should be verified that those relays are of the same type of the ones used to establish the sensitivity threshold level.

b. Once the list of shock sensitive components is established, evidence should then be provided showing that all related processes in place are qualified and approved by the customer. This includes in particular the compliance with soldering methods and with mounting technology of components (heavy components, metal-case/glass-encased components, provision for stress relief), as specified in ECSS-Q-ST-70-08C and ECSS-Q-ST-70-38C ([RD-0121] and [RD-0122] respectively).

NOTE Process qualification for shock sensitive components (Table 17-1) should include shock test to environment greater than the severity criteria.

c. Highest PCB deflection is experienced during the response of the PCB main modes, and is decreasing when frequency increases. PCB deflection is detrimental for large and/or heavy components. For this reason, the severity criteria considers that the PCB fundamental mode (main flexural mode) should be covered by random equivalence (RRS).

d. The electronic unit should be exposed to a representative “flight” shock environment during a system level shock test, followed by functional tests.

NOTE The induced shock environment during the system level shock test should be verified to be lower than the severity criteria.

In the following severity criteria, a distinction is made between equipment **powered on** during shock and equipment **powered off** during shock.

12.4.2.2.2 Equipment powered on during shock

The severity criterion is defined by heritage as follows, and is illustrated in Figure 12-3:

- SRS at unit interface with increasing slope at 6 dB/octave below 2 kHz and a constant level of **200 g at 2000 Hz** and above, and
- The Random Response Spectrum (RRS – see 12.5.3.2) on the main PCB modes and the equipment housing mode, covers the unit shock level.

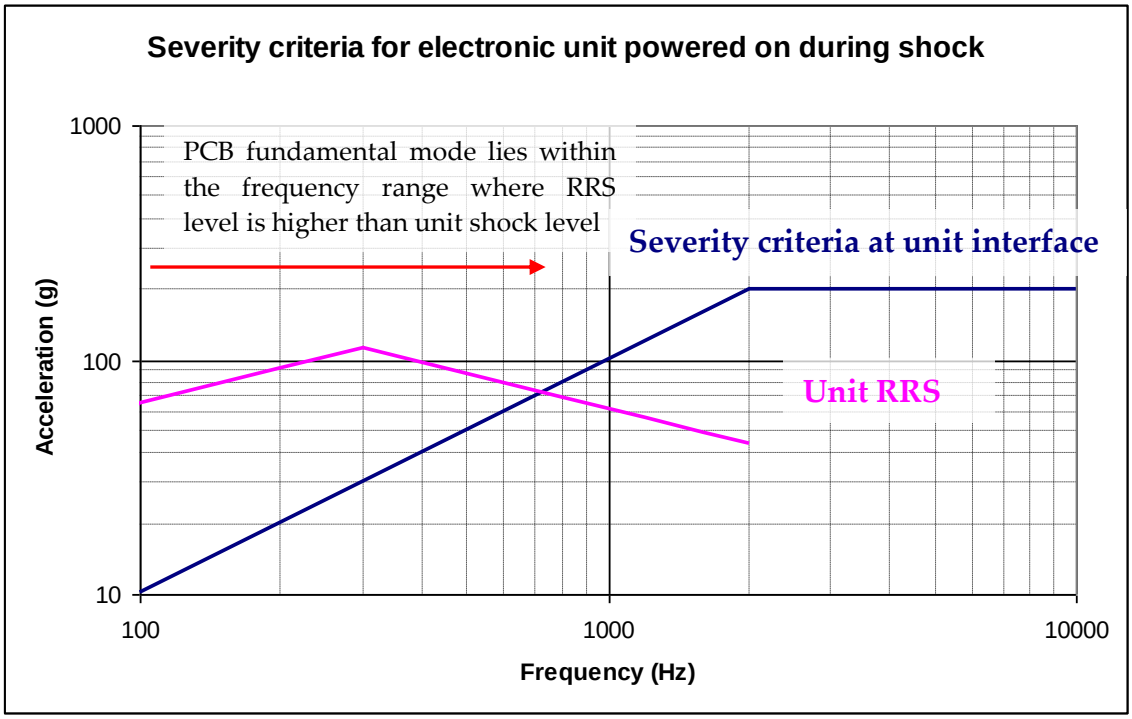

Figure 12-3: Severity criteria for electronic unit powered on during shock

NOTE The justification of the high frequency threshold comes from relays bouncing which can occur by experience with levels above 200 g (time history) measured at relay interface. The SRS of such shocks had a level between 200 g and 600 g above 1 kHz, as illustrated by Figure 17-10 and Figure 17-11 in the Handbook Part 4. The 200 g SRS threshold thus appears as a conservative value to be considered as a severity criteria.

12.4.2.2.3 Equipment powered off during shock

The severity criterion is defined by heritage as follows, and is illustrated in Figure 12-4:

- SRS at unit interface with increasing slope at 6 dB/octave below 2 kHz and a constant level of **500g at 2000 Hz** and above, and
- The Random Response Spectrum (RRS – see 12.5.3.2) on the main PCB modes and the equipment housing mode, covers the unit shock level.

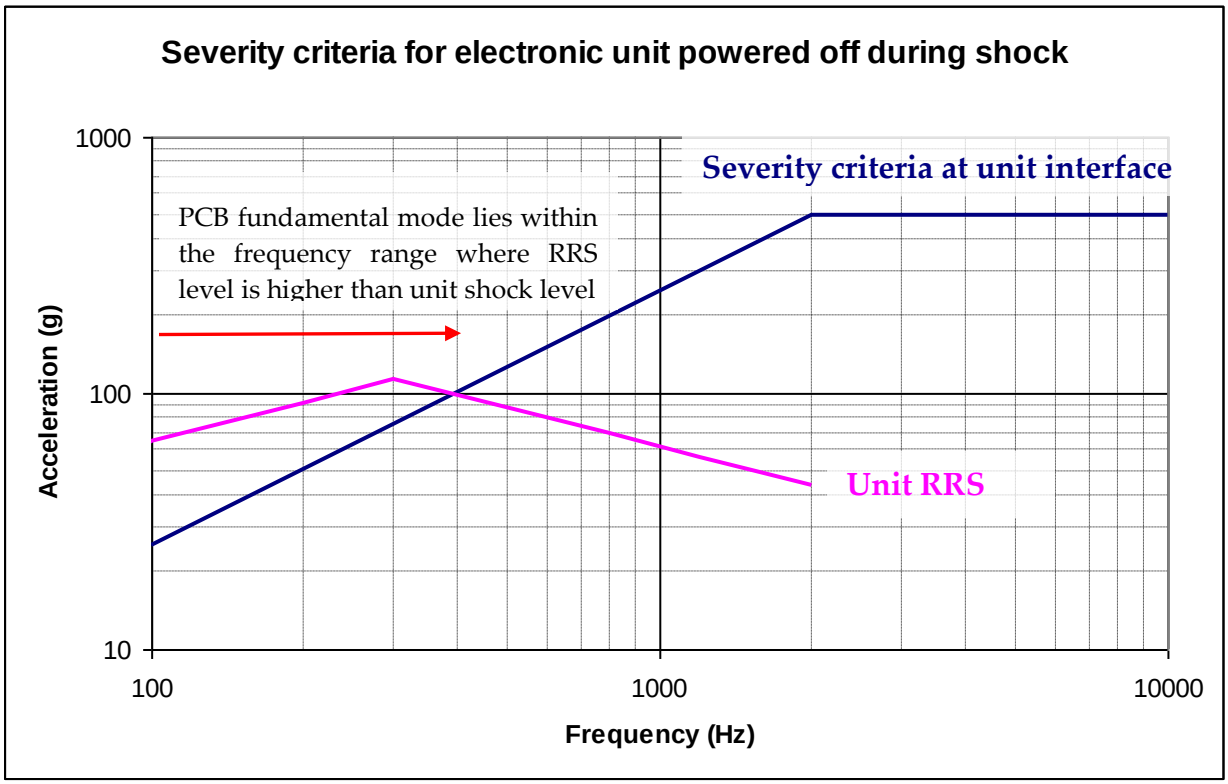

Figure 12-4: Severity criteria for electronic unit powered off during shock

NOTE The justification of the high frequency threshold comes from relays and quartz susceptibility to shock. This aspect is discussed in the Part 4 of the Handbook. This threshold is also consistent with usual practice on programme which usually require shock test for specification higher than 500 g on the plateau.

12.4.2.3 Structural and non-sensitive equipment

This section is related to equipment which do not contain any component sensitive to shocks (see 17.5.2 of Part 4). The main equipment that are in this category are usually structural equipment without any electronics. This rule does not apply to units with functional alignments.

In this case the so-called "0,8 f rule" can be used. The "0,8 f rule" defines a severity criteria in term of SRS at unit interface equals to 0,8 multiplied by the considered frequency.

This severity criterion is recalled in Figure 12-5:

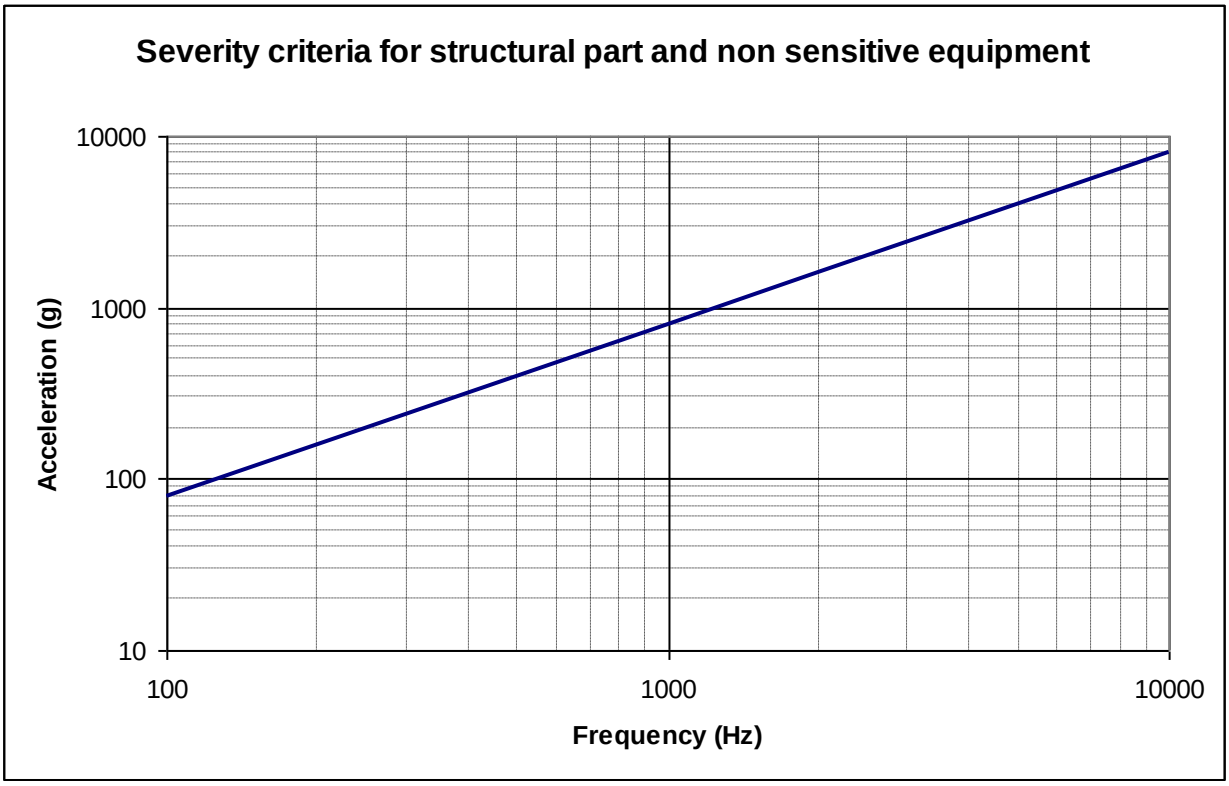

Figure 12-5: Severity criteria for structural part and non-sensitive equipment

This rule is based on return of experience (See Part 4) and does not precisely focus on space equipment related needs. As a consequence the usage of the "0,8 f rule" is limited to structural and non-sensitive equipment (primary structure - bracket - reflector - antenna - tanks) for which the original background of this widely used empirical "rule of the thumb" can be considered as applicable.

12.4.2.3.1 Shock severity using PVSS and applicability of 0,8f rule

a) Pseudo Velocity Shock Spectrum (PVSS)

Despite some limitations, the shock spectrum is widely used to describe the shock severity of a shock signal (refer to the introduction of this handbook). The most common representation is by using (pseudo) acceleration Shock Response Spectrum, commonly referred as SRS.

A complementary way to describe the shock severity is the pseudo velocity shock spectrum representation, or PVSS, which is computed from the velocity time history data (integration of acceleration time history data). Indeed many authors ([RD-082], [RD-083],[RD-085], [RD-086], [RD-087] and [RD-088]) have justified either experimentally or theoretically that the stress is proportional to the velocity. The pseudo velocity is the parameter that is proportional to stress, and as such indicates the severity of the shock signal in a structure.

The maximum stress is given by:

$$\sigma_{max} = K\rho c v_{max}$$

Where:

- σ_{max} is the maximal stress in the structure (in plane longitudinal or transversal)
- c = $\sqrt{E/\rho}$ is the wave velocity (E = Young's modulus, and ϱ = density)
- v_{max} is the maximum pseudo velocity
- K is a shape factor useful for bending waves or bending modal responses ([RD-088]). This shape factor has been evaluated for beams, thin rectangular plates, tapered rods and wedges. Many authors have shown that this factor could be as high as 10. K=1 for compression waves or modal responses in compression. An example of K factor is given in [RD-085] for beam submitted to bending waves. $K = \frac{h}{\eta}$, where η is the maximum cross-sectional distance from neutral axis and $\eta = \frac{I}{A}$ is the radius of gyration.

It can be demonstrated that the relation $\sigma_{max} = \rho c v_{max}$ is deduced from the Hooke relation , and is therefore always valid whatever is the mechanical regime : propagation of compression wave, modal response established in a stationary vibration or modal transient response in the phase following the propagation compression wave , intermediate regime between propagation wave and modal transient response.

The difficulty arose with the bending waves, which are dispersive (meaning that each frequency component of the wave is travelling at its own velocity).

Hence to estimate stresses resulting from bending waves, the previous relationship needs to be corrected, as follows : $\sigma_{max} = K\rho c v_{max}$,introducing a K factor depending of the geometrical characteristics of the structure (see Table 12-2 for typical K factors).

Table 12-2: Beam shape factor dynamic bending stress

Beam cross section	Shape factor K
Solid rectangle	$\sqrt{3}$
Solid round beam	2
Thin hollow tube	$\sqrt{2}$
Thin hollow square	$\sqrt{6}/2$

The analytical expression of shape factor K is further detailed in [RD-086], from which the following 2 examples are extracted:

Example 1 – Clamped-free beam, simple bending

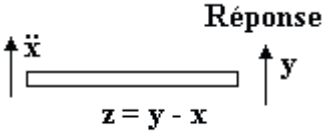

The maximum bending stress can be expressed as $\sigma_{\max} = \frac{4\sqrt{3}}{\lambda_n^2}\rho c v_{\max}$

The K factor is then identified as $K = \frac{4\sqrt{3}}{1{,}875^2} = 1.97 \approx 2$

Example 2 – Clamped-free beam with lumped mass, simple bending

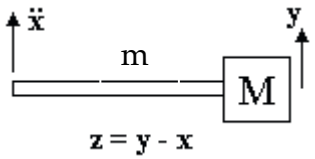

The maximum bending stress can be approximated as $\sigma_{\max} \approx 3\sqrt{\frac{M}{m} + 0{,}23}.\rho c v_{\max}$

The K factor is then identified as $K \approx 3\sqrt{\frac{M}{m} + 0{,}23}$, depending of lump mass M and solid beam mass m. As an example, for M=2.m, it results K=4,48.

b) Shock spectrum equations and main characteristics of Pseudo Velocity Shock Spectrum – PVSS

Newton's law can be applied to a free-body diagram of an individual system, as shown in Figure 12-6

A summation of forces yields the following governing differential equation of motion:

$$m\ddot{z} + c\dot{z} + kz = -m\ddot{y} \qquad (\text{with relative displacement } z = x - y)$$

Additional substitutions can be made as follows,

$$\omega_n = \sqrt{\frac{k}{m}} \quad \text{and} \quad 2\xi\omega_n = \frac{c}{m}$$

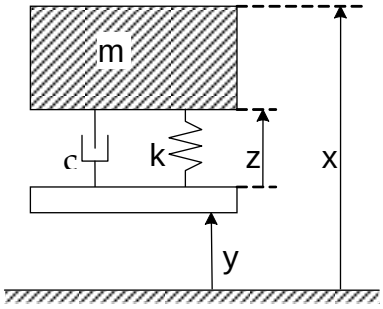

Figure 12-6: SDOF system

Note that ξ is the damping ratio, and that ω_n is the natural frequency in radians per second. Furthermore ξ is often represented by the amplification factor Q, where $Q = 1/(2\xi)$.

Substitution of these terms into the previous equation yields an equation of motion for the relative response:

$$\ddot{z} + 2\xi\omega_n\dot{z} + \omega_n{}^2 z = -\ddot{y}(t)$$

- $z(t)$ is the relative displacement, this quantity is useful for evaluating the distortions and strains within the responding structure,
- $\dot{z}(t)$ is the relative velocity, useful for determining the stresses generated within the responding structure due to viscous damping and the maximum energy dissipated by the responding structure,
- $\dot{y}(t)$ is the absolute velocity, useful for determining the kinetic energy of the structure,
- $\ddot{z}(t)$ is the relative acceleration, useful for determining the stresses generated within the responding structure due to the combined elastic and damping reactions of the structure.

The quantity $\omega_n{}^2 z$ is called **pseudo acceleration**. The Shock Spectrum derived from this quantity is called pseudo acceleration Shock Spectrum (commonly referred as SRS).

The quantity $\omega_n z$ is called **pseudo velocity**. The Shock Spectrum derived from this quantity is called Pseudo Velocity Shock Spectrum (PVSS) .

If we called U the energy stored in the spring, $U = \frac{kz^2}{2}$ or $\frac{U}{m} = \frac{k}{m}\frac{z^2}{2} = \frac{(\omega z)^2}{2}$

It comes $\omega z = \sqrt{2\frac{U}{m}}$. This is the **pseudo velocity**. Pseudo velocity is the square root of twice the peak energy per unit mass that is stored in the oscillator during the shock.

Effectively the pseudo velocity is computed from the pseudo acceleration by dividing by the pulsation ω:

$$pseudo\ \ velocity = \frac{pseudo\ \ acceleration}{\omega}$$

c) Estimating shock severity

Some sources claim that the shock severity is best characterised by PVSS plotted on 4 coordinate paper (4CP). This type of representation shows three regions: rattle space (peak deflection) – velocity change – maximum acceleration. However it is not adequately popular, and not used within European industries.

NOTE The 4CP representation provides: z (relative displacement), ωz (pseudo velocity) and $\omega^2 z$ (pseudo acceleration).

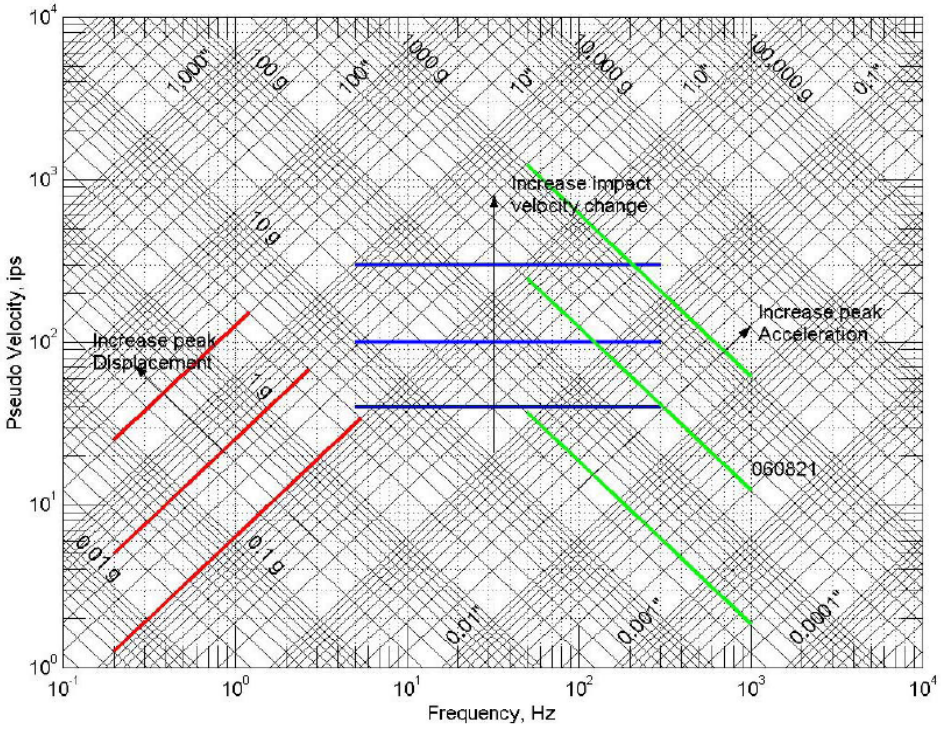

Figure 12-7: Principle of 4 coordinates plot

This representation is only a graphical issue: if the case under interest is concerned by a risk of exceeding the acceptable structural stress, then a graphical representation highlighting the pseudo-velocity can be used. Only the pseudo-velocity is proportional to the stress. As such a combination of acceleration SRS and PVSS plotted on a log-log graph provides already the most essential information (velocity change and maximum acceleration) to determine the shock severity of a signal.

The following example provides an illustration for the estimation of shock severity.

On an aluminium plate, excited by a detonation produced by an expandable tube (generating traction/compression and bending waves), several accelerometers were measuring out of plane acceleration and several strain-gages were measuring compression and bending strains . Figure 12-8 below shows the pseudo acceleration shock spectrum and the pseudo velocity shock spectrum (deduced one from the other by a rotation of 45°). It can be seen that the evolution of PVSS at near 3m/s is approximately the same for all the points of measurement spread on the plate. All these curves can be enveloped by a horizontal line, that we call the "velocity change" of around 3m/s in this case.

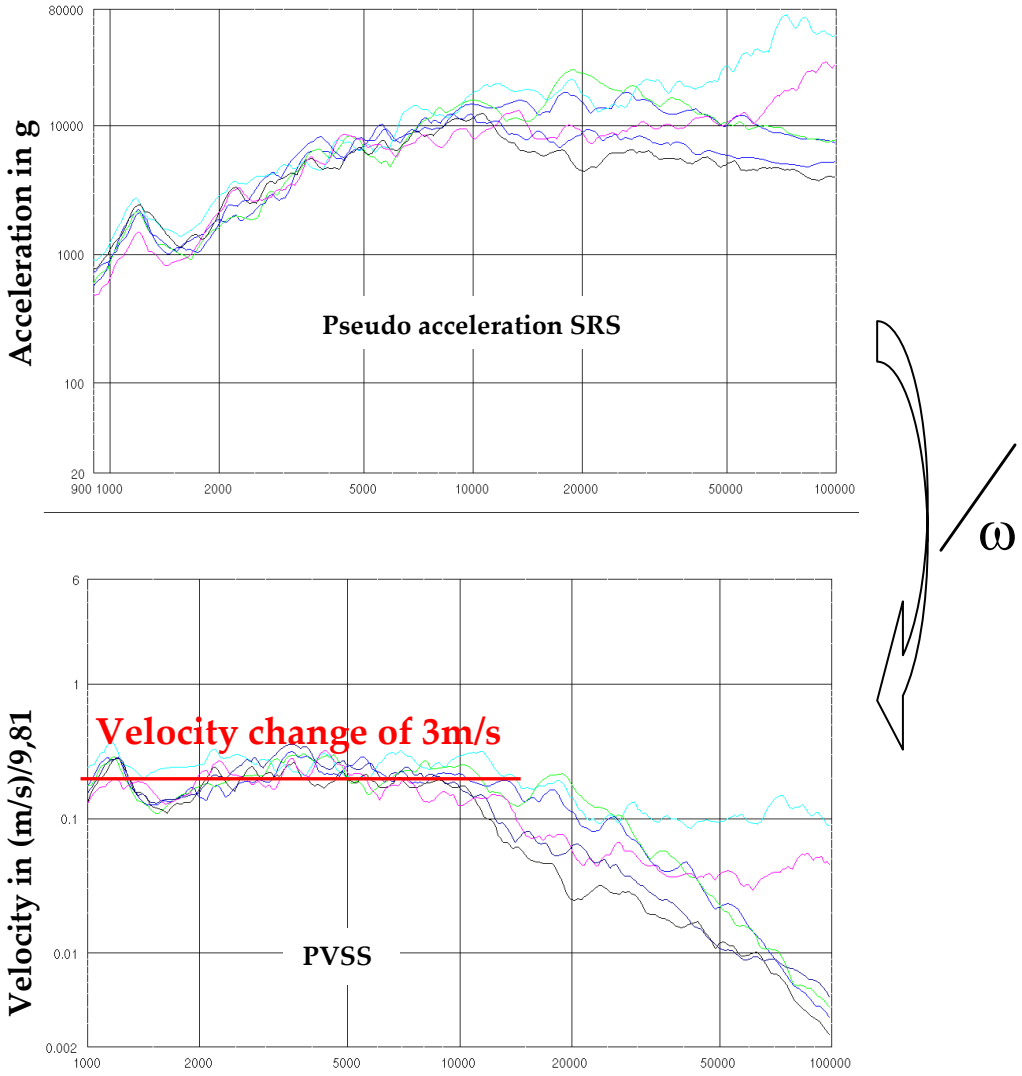

Figure 12-8: Comparison between pseudo acceleration and pseudo velocity shock spectrum

A superposition of the bending and the compression strains measured at a given point J8 are represented in the Figure 12-9 (compression in dark blue – bending in light blue).

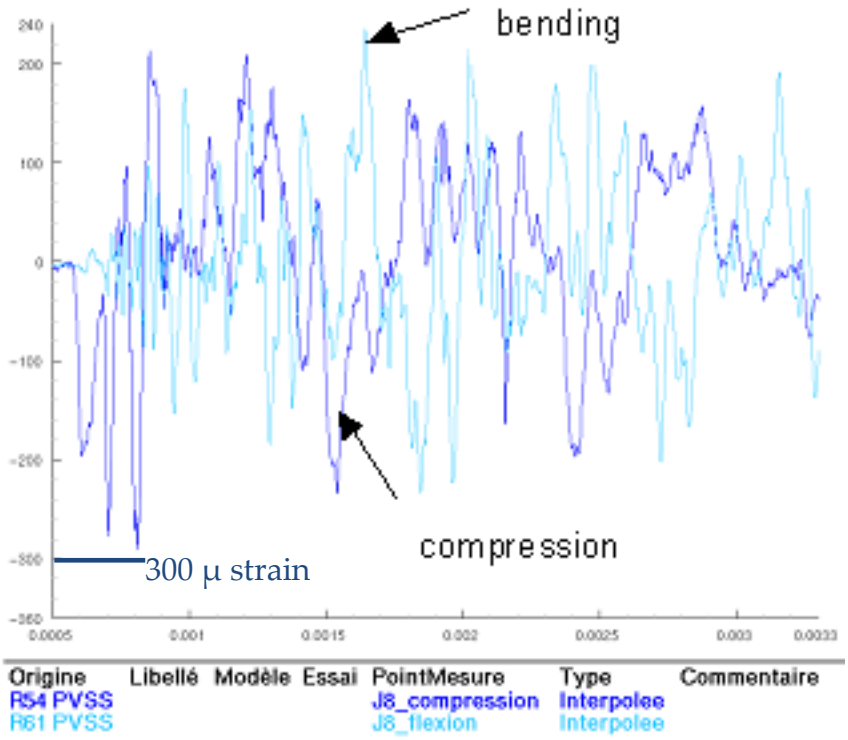

Figure 12-9: Strain gauges measurements

It can be seen that for this case the amplitudes of the compression and bending strains are comparable, but such observation highly depends from the source characteristics (symmetrical versus asymmetrical separation system).

The relation $\sigma_{max} = \rho c v_{max}$ permits to calculate the maximum of the compression stress resulting from the maximum of the previously identified velocity change (3m/s):

$$\sigma_{max} = 2700.5300.3 = 42.9 M.N/m^2 = 42.9 MPa$$

This comes in rather good agreement with the stress identified through the Hooke relation (considering 300 μ strain, as measured by the strain gauge J8):

We may compare that result to the compression stress deduced from the measured strain: .

$$\sigma = E \,.\, \varepsilon = 0{,}8 \,.\, 10^{11} \,.\, 300 \,.\, 10^{-6} = 240.\, 10^5 \text{ N/m}^2 = 24 \text{ MPa}$$

Both maximum stresses would better agree if an average value of the velocity change would be considered (2m/s instead of 3m/s, corresponding to a stress of 28.6MPa).

This points out the difficulty in estimating the velocity change in presence of modal local responses which evidently are not considered in the model.

The calculation of the stress resulting from the bending is depending from the knowledge of the coefficient K. The technical literature gives some values for particular cases. Moreover, the transformation of the bending strain in stress would not be so direct than it is for compression.

The design of the pyro source is essentially determining the severity of the induced shock.

The two following figures (a) and (b) give the superposition of bending (in red) and compression (blue or black), measured on an aluminium plate, the source being for figure (a) an expandable tube and for figure (b) a SHOGUN generating high bending waves.

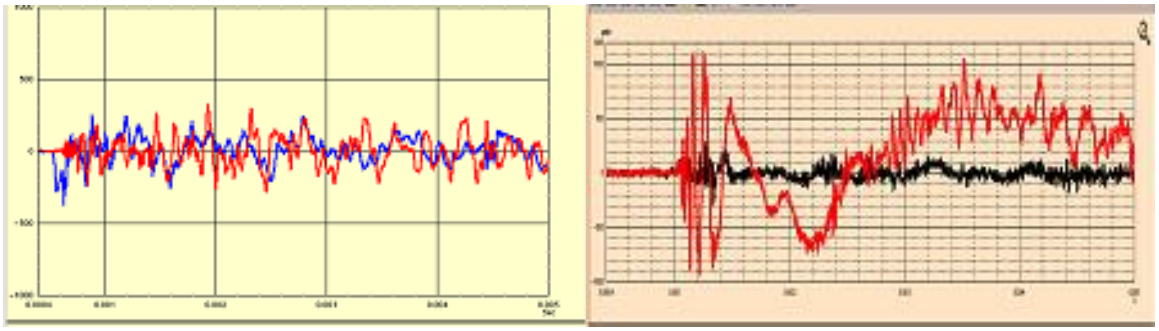

(a) (b)

Figure 12-10: superposition of bending (in red) and compression (blue or black), measured on an aluminium plate

The propagation regime is evident for the red curve (bending) on Figure 12-10 (b) and is followed by modulations which correspond to modal response regime. In this case, the amplitude of stress in propagation phase is higher than the one in modal phase and the bending strain is much higher than the compression one. It is not the case for the other source on Figure 12-10 (a). This source is much more balanced (expandable tube with double separation, on each side of the tube), leading to much lower bending effect.

It has been demonstrated that the plateau region of the PVSS is proportional to the maximal stress according to the relation $\sigma_{max} = K\rho c v_{max}$ for plates, rods, beams, working either in longitudinal or transversal direction. The knowledge of the coefficient K is of prime importance when the calculation of the stress is made for bending waves . Some are given in the literature. Its estimation can be obtained from calculation or measurement extracted from a test result. When the structure is more complex, presenting bifurcation or dissymmetrical shapes, as it is often the case for Space Structures or satellites, then this relationship cannot be applied.

d) Background and applicability of the 0,8 f rule

This rule is presented in some standards, such as [RD-099]:

Extract from [RD-099]: "Past experience has shown that the high frequency shock environment does not pose a hazard to typical aerospace equipment at shock spectrum amplitudes (with Q=10) below 0,8 times the frequency in Hz. Accordingly, VOL I of [RD-099] does not require shock qualification testing of units for which the maximum expected shock spectrum does not exceed a value of 0,8 times the frequency in Hz; as long as the qualification random vibration test spectrum, when converted to an equivalent 3σ response in the frequency range specified, exceeds the qualification shock spectrum.

The above content presents in the same document two likely origins of this rule-of-thumb:

- The first one, based on return of experience: but no corresponding technical paper was found and no study is reported. The fact is that this rule has been used in many cases as a practical way to screen the equipment to be assessed for pyroshock risk. For those who applied this rule, it was in general evident that either specific electronic components (such as relays, tantalum capacitors, quartz) or mechanisms (valves, roll bearings, worm screw,…) were not covered by this rule and had to be considered specifically.

- The second possible origin, is derived from the relation $\sigma_{max} = K\rho c v_{max}$. If we consider K=1 (assuming that compression wave is predominant) and the yield limit for steel at 100 inch/s (2,54 m/s), it comes with a conservatism factor of 2: acceleration (g) = (2.π.f .v)/9,81= 0,81 x f (Hz). It seems that this result has been "adopted" improperly and generalized to all type of wave or modal regime (in plane or out of plane), without any other consideration (type of material, type of structure and associated geometry, type of wave and directions).

Conclusion on the applicability of the "g=0,8 f" rule

It can be concluded that **the rule "g=0,8 f" has no proper justification for electronic equipment verification**. The application of this rule should be strictly limited to structural parts.

Even if used for structural parts, this rule should be followed with great caution, because:

- It assumes that the mode of deformation of the structure is compression ; the bending deformation requires the use of a correction coefficient K whose range of possible values is from 1 to 10 according to the references,
- If the expected failure mode is a peeling effect resulting from inertia loads, thus directly proportional to the acceleration, it is more appropriate to implement the pseudo acceleration SRS (which is the default SRS usually implemented).

12.4.2.4 Other sensitive units

For other sensitive units such as mechanisms, brittle material, optical systems or optical connectors, no generic severity criteria can be established. This means that for such equipment shock test are always recommended unless the compatibility is demonstrated through coverage with lower frequency environment (see paragraph 12.5).

12.4.3 Synthesis

The applicable severity criteria are summarised in Table 12-3.

Table 12-3: Severity criteria

Equipment category		Severity criteria
Electronic equipment	Powered-on during launch	SRS at unit interface with increasing slope at 6 dB/octave below 2 kHz and a constant level of 200 g at 2000 Hz and above, and Coverage with Random Response Spectrum (RRS) is verified in correspondence to the PCB fundamental mode.
	Powered-off during launch	SRS at unit interface with increasing slope at 6 dB/octave below 2 kHz and a constant level of 500 g at 2000 Hz and above, and Coverage with Random Response Spectrum (RRS) is verified in correspondence to the PCB fundamental mode.
Structural and non-sensitive equipment		0,8 f rule: SRS at unit interface equals to 0,8 multiplied by the considered frequency (see § 12.4.2.3.1)
Other sensitive unit		No generic severity criteria. Compatibility usually achieved through coverage by lower frequency environment (see § 12.5)

12.5 Equivalence between shock and other mechanical environment

12.5.1 Quasi static equivalence – effective mass method

12.5.1.1 Definition

The SRS equivalence to the quasi-static qualification aims at providing a conservative equivalence from SRS levels to verify the instrument qualification compliance based on its quasi-static qualification levels. The method is based on the modal analysis results (eigenfrequencies and associated effective masses), the equivalent acceleration is computed at the unit basis when submitted to the specified shock spectrum using the following formula:

- **In case of decoupled main modes**: Decoupled modes are successive modes for which frequency ratio between two consecutive modes is at least $\sqrt{2}$.

  The SRS equivalence to quasi-static loads is given by the formulae:

$$\gamma_{QS\ equivalent} = \frac{\Sigma_i M_i^{effective} \times \gamma_{SRS}(f_i) + M_{residual} \times \gamma_{SRS}(High\ \ frequency)}{M_{Total}}$$

  This approach is a worst case estimation (conservative) as it considers that all the effective masses at different frequencies occur at the same time in phase. It is applicable for low number of mode and only at high frequency (> 100 Hz) for which the damping factor is not too large.

- **In case of coupled main modes**: the SRS equivalence to quasi-static loads is given by the formulae:

$$\gamma_{QS\ equivalent} = \frac{\sqrt{\Sigma_i\left[M_i^{effective} \times \gamma_{SRS}(f_i)\right]^2 + \left[M_{residual} \times \gamma_{SRS}(High\ \ frequency)\right]^2}}{M_{Total}}$$

  This approach is more realistic when number of mode increase as it considers the quadratic summation thus all the event doesn't occur at the same time.

Where in both cases:

- f_i is the unit eigenfrequencies,
- $M^{effective}{}_i$ is the effective masses associated to the eigenfrequencies « i »,
- M_{Total} is the unit total mass,
- $M_{residual} = M_{Total} - \Sigma_i M^{effective}{}_i$,
- γ_{SRS} (f) is the acceleration of the specified shock spectrum at the frequency « f ».

12.5.1.2 Example of application

The methodology has been applied on an equipment (mass 11.7kg) supported by an instrument main panel, interface with the spacecraft thru iso-static mount.

First, the specification at instrument interface has been derived at equipment interface for in plane and out of plane excitation considering the first lateral (in plane X and Y) and axial (out of plane Z) modes frequencies of the instrument on its iso-static support.

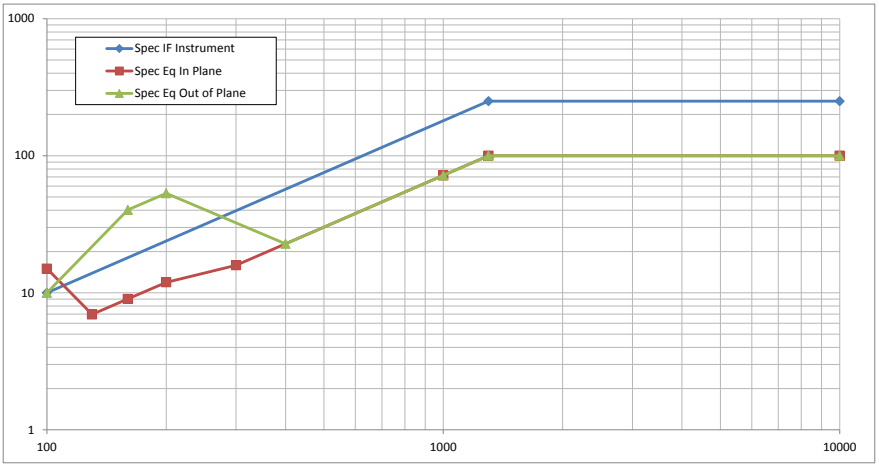

Figure 12-11: Specification derivation at equipment interface

Then a modal analysis is performed on the equipment detailed model up to the frequency of the specification main plateau (1.3kHz in this example)

Table 12-4: Equipment modal analysis on [0-1300Hz]

N	Frq(Hz)	Mxx	Myy	Mzz	Ixx	Iyy	Izz
1	111.97	0.1	5.8	0.2	50.2	0.9	0.2
2	112.6	3.7	0.2	1.8	0.3	33	1.9
3	298.5	5.8	0	1.6	0.6	39.4	2.4
4	324.79	0	2.1	0.1	17.1	0.1	0
5	357.84	0.4	0.1	3.6	0.3	2	0.1
6	518.39	0	2.3	0.1	18.2	0.2	0
7	603.87	0.7	0.1	2.7	0	6.6	0.4
8	903.14	0	0	0	0	0	0
9	953.36	0.4	0	0.2	0.1	3	0.2
10	971	0	0.1	0	0.8	0.1	0
Cumulated Meff		11.1	10.8	10.3	87.6	85.3	5.2
Residual Mass		0.6	0.9	1.4	5.8	3.7	0.3
Rigid Mass		11.7	11.7	11.7	93.4	89	5.5

The two different summations have been performed for the equipment on the three axis, considering only the 3 main modes per axis for the linear summation (identified in bolt on the following figure, considering decoupled approach) and quadratic summation when considering all the modes (coupled approach). A special care should be taken on the shock spectrum interpolation up to the plateau on the equipment modes frequencies: no linear but logarithmic interpolation should be applied.

Table 12-5: Quasi-static shock equivalence

		X			Y			Z		
N	Frq(Hz)	Effective mass (Kg)	Shock spectrum value (g)	Interface force (N)	Effective mass (Kg)	Shock spectrum value (g)	Interface force (N)	Effective mass (Kg)	Shock spectrum value (g)	Interface force (N)
1	111.97	0.1	10.77	10.56	**5.8**	10.77	612.64	0.2	13.98	27.42
2	112.6	**3.7**	10.59	384.44	0.2	10.59	20.78	**1.8**	14.21	250.94
3	298.5	**5.8**	15.82	900.30	0	15.82	0.00	1.6	32.60	511.68
4	324.79	0	17.54	0.00	**2.1**	17.54	361.40	0.1	29.40	28.84
5	357.84	0.4	19.81	77.74	0.1	19.81	19.43	**3.6**	26.11	922.13
6	518.39	0	31.54	0.00	**2.3**	31.54	711.73	0.1	31.54	30.94
7	603.87	**0.7**	38.20	262.34	0.1	38.20	37.48	**2.7**	38.20	1011.90
8	903.14	0	63.31	0.00	0	63.31	0.00	0	63.31	0.00
9	953.36	0.4	67.76	265.89	0	67.76	0.00	0.2	67.76	132.95
10	971	0	69.34	0.00	0.1	69.34	68.02	0	69.34	0.00
	Residual	0.6	100	588.60	0.9	100	882.90	1.4	100	1373.40
Decoupled sum		1547.08	QS (g)	**13.48**	1685.76	QS (g)	**14.69**	2184.96	QS (g)	**19.04**
Coupled sum		1204.35	QS (g)	**10.49**	1341.21	QS (g)	**11.69**	2026.20	QS (g)	**17.65**

It demonstrates that quasi-static shock equivalence remains below 19g whatever the coupled or decoupled approach is considered which is lower than equipment quasi-static specification and qualification level. This validates the acceptability of shock level for this equipment based on its quasi-static qualification level.

12.5.1.3 Applicability and limitations:

This methodology is applicable when a detailed finite elements model of the sub-system is available allowing calculating a modal analysis up to the shock specification main plateau, especially to perform the coupled method. This is mandatory to have a good estimation of effective mass distribution up to the shock specification plateau (typically 1kHz to 2kHz) not to apply a too large residual mass to the plateau level (the highest one) which could be very conservative

This method is usually very conservative for large units (main modes below 100Hz) for which the underlying assumption on full in phase excitation is not valid.

12.5.2 Use of sine vibration test data

Sine vibration test data can only be used when the frequency range of the sine event is matching the one for the shock event. In most cases it happens when a sine environment is specified up to 140 Hz.

As the SRS is the response of a 1dof system for each frequency, the computation of the SRS level equivalent to the sine level is directly the sine level multiplied by the Q factor (conventionally 10).

In the general case, the equipment does not exhibit any mode in low frequency, and in such a case the comparison become artificial, as the SRS corresponds to the peak response of an array of SDOF systems.

In situation where the equipment/instrument presents some low frequency modes, the Q factor identified during the sine test should also be used for the SRS computation.

The following figure shows an example of the use of sine levels (most preferably using test data) to cover low frequency shock specification.

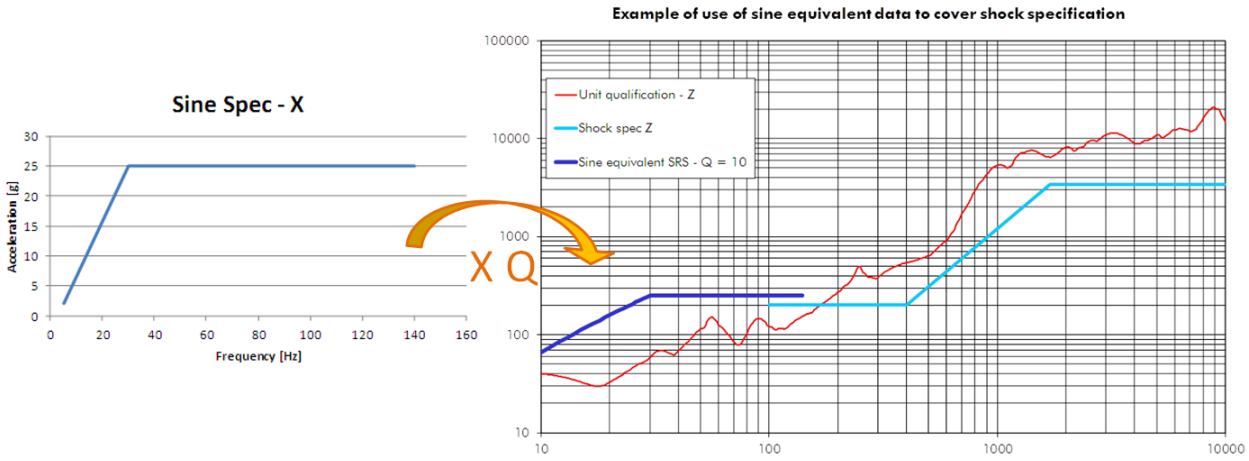

Figure 12-12: Sine shock equivalence

12.5.3 Use of random vibration test data

12.5.3.1 Introduction

Random environment can be used to cover shock environment, owing that appropriate equivalence methods are applied. The reason why random environment can be used to cover shock environment is that random vibration can produce maximum response (i.e. maximum strain) capable of damaging an equipment in a similar way than a shock.

The comparison of severity between a random or a shock signal, is based on the mechanical effect (RMS or peak responses respectively) induced in an array of SDOF systems.

To use random environment to cover shock environment it is necessary to compare a random environment characterized by its PSD with a shock environment usually represented by its SRS (see annex A of [RD-081], and [RD-089]). The way it is done is to convert PSD into an "equivalent SRS". Several digital signal processing tools are available such as RRS, RRS_{Miles}, ERS and URS. They are detailed in the following section.

12.5.3.2 Signal processing tools to convert random PSD into Response Spectrum

12.5.3.2.1 Overview

When comparing the severity of a mechanical shock versus a random vibration, a difficulty arises coming from the **statistical aspect of the random vibration** (the shock being deterministic). It is important that the equivalent environment is directly comparable to a SRS, namely that it **represents the variations of the RMS responses of an array of SDOF systems submitted to a random input signal of PSD *W(f)***, as a function of the SDOF natural frequency f_k, for a given damping factor $Q = \frac{1}{2\xi}$. The random acceleration input is assumed to be weakly stationary and Gaussian. Mean values of responses are assumed to be zero.

12.5.3.2.2 Definition of RRS and RRS_{Miles}

The approach generally adopted by the Space Community consists in calculating a **Random Response Spectrum (RRS),** corresponding to the RMS responses of an array of SDOF systems excited at its base with the PSD *W(f)***.** Different conventions exist on the probability limits of the peak value, in the following formula the RRS is defined for a **3σ peak value**:

$$RRS(f_k) = 3.z_{RMS}(f_k)$$

Where:

z_{RMS} is the RMS value of the absolute response of the SDOF system (1σ), and corresponds to an acceleration

$$z_{RMS}(f_k) = \sqrt{m_0} = \sqrt{\int_0^\infty |T_k(f)|^2 . W(f) df} \quad \text{with} \quad T_k(f) = \frac{1 + 2i\xi\frac{f}{f_k}}{1 - \left(\frac{f}{f_k}\right)^2 + 2i\xi\frac{f}{f_k}}$$

A simplified approximation of the integral in RRS formulation is often used. It is known as the **Miles Formula** and denoted **RRS_{Miles}**. It is an **exact estimation when the PSD is constant** over the considered frequency band. RRS_{Miles} provides however a reasonable approximation of RRS when the

PSD presents a smooth variation. On the contrary, the approximation by the Miles Formula becomes crude in the region where notches have been applied.

$$RRS_{Miles}(f_k) = 3\sqrt{\frac{\pi}{2}.f_k.Q.W(f_k)} \text{ with } Q = \frac{1}{2\xi}$$

This formula yields the acceleration responses in g's of a SDOF linear system (for 3σ peak value, with 99,7% probability not to be exceeded).

The signal processing tools (RRS and RRS_{Miles}) which generate a response spectrum from a PSD have the advantage to allow the comparison of severity between a random and a shock signal.

However such tools have also the disadvantages to:

- Limit the probability distribution to 3σ peaks, whereas such distribution generally exceeds 3σ (see Figure 12-13).
- Discard the effect of the test duration: for a random vibration, the longer the time duration of the random signal, the higher the probability can be to exceed a given level (i.e. to exceed 3σ peak value).

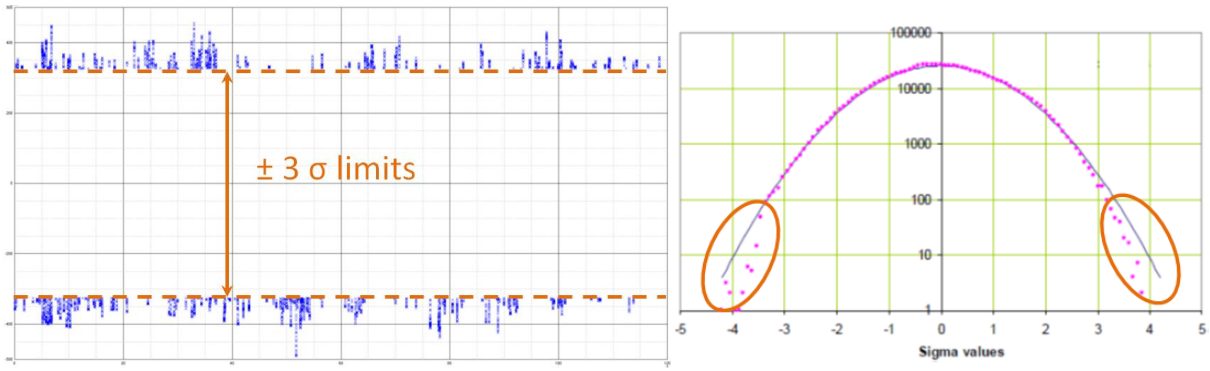

Figure 12-13: Peak values exceeding 3σ limits (temporal signal and statistical distribution)

In order to overcome these disadvantages, more precise approaches have led to the definition of **Extreme Response Spectrum (ERS)** and **Response Spectrum with up crossing risk (URS)**, as detailed in annex A of [RD-081].

12.5.3.2.3 Definition of ERS

The **ERS** represents an approximation of the maximum response of a SDOF submitted to a PSD *W(f)* during a duration *T* with an associated risk of 63.2% to overpass the given spectrum. The mathematical formulas are given hereafter.

$$ERS(f_k) = z_{RMS}(f_k).\sqrt{2.\ln(n_0^+ T)}$$

Where:

n_0^+ is the mean number per second of 0 crossing with positive slope, n_0^+ can be approached by $n_0^+ \approx f_k$

The complete expression of n_0^+ is: $n_0^+ = \frac{1}{2\pi}\sqrt{\frac{m_2}{m_0}}$ with $\begin{cases} m_0 = \int_0^\infty |T_k(f)|^2.W(f)df \\ m_2 = (2\pi)^2 \int_0^\infty f^2.|T_k(f)|^2.W(f)df \end{cases}$

T is the total duration of the random test

In the ERS formulation the peak value is defined with an associated risk of 63.2% to overpass the given spectrum, as such the **associated probability is defined too low** to guarantee that the peak value is actually seen higher in reality. In other words, the ERS overestimates the random equivalence (peak value may be seen lower in reality). This limitation is overcome with the URS formulation, which allows to define specifically the risk α of up crossing the peak value.

12.5.3.2.4 Definition of URS

The **URS** corresponds to the largest peak observed over a time T with a given accepted risk α of up crossing this peak. The mathematical formulas are given hereafter.

$$URS(f_k) = ERS(f_k).\sqrt{\frac{-\ln\left(1-(1-\alpha)^{1/n_0^+ T}\right)}{\ln(n_0^+ T)}} = z_{RMS}(f_k).\sqrt{2\cdot\ln\left(\frac{1}{1-(1-\alpha)^{1/n_0^+ T}}\right)}$$

For $\alpha << 1$, the following approximation can be used:

$$URS(f_k) \approx ERS(f_k)\cdot\sqrt{1-\frac{\ln(\alpha)}{\ln(n_0^+ T)}} \approx z_{RMS}(f_k)\cdot\sqrt{2\cdot\ln\left(\frac{n_0^+ T}{\alpha}\right)}$$

The choice of α, comprised between 0 and 1, depends on the application:

- If this equivalence is used to specify an equipment to a shock environment, it is important to ensure that a conservative approach is used, by enveloping the largest peak observable. Therefore, α should be very low and the hypothesis $\alpha << 1$ is applicable.
- On the contrary, if URS is used to compare to a shock specification or measured data, the conservative approach consists in minimizing the URS amplitude, and consequently to take $\alpha \approx 1^-$.

In practical terms, when using the URS formulation for deriving random equivalence and comparing to a shock specification (general case for the use of random to cover shock), the risk α of up crossing the peak value should be defined equal to at least **0,99**. Hence the case with a low α should not be used for covering a shock specification by a random equivalence, as the severity of the associated URS will be overestimated.

12.5.3.2.5 Example 1 – Comparison of RRS-ERS-URS equivalence

In the following Figure 12-14, are illustrated the various random equivalences computed from a typical PSD:

- Extreme Response Spectrum,
- URS with a risk of 99% ($\alpha = 0.99$),
- URS with a risk of 1% ($\alpha = 0.01$), for illustration only
- The complete RRS representation,
- The application of the Miles formula

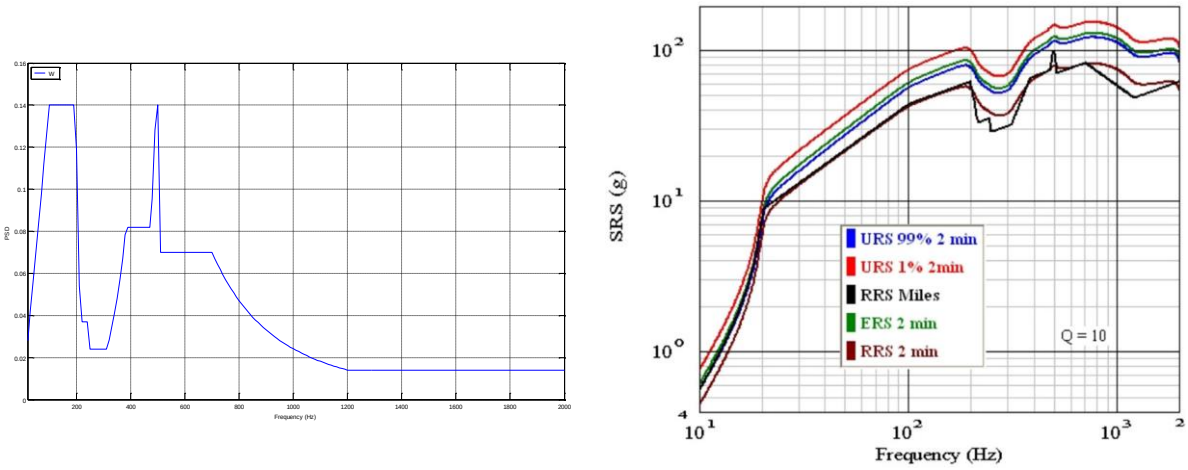

Figure 12-14: Example of PSD, and Comparison between ERS, URS, RRS and RRS_{Miles}

Some general observations can be made:

- The RRS_{Miles} formulation provides an exact estimation of the RRS in frequency ranges where the PSD is constant, and a reasonable approximation when the PSD presents a smooth variation, but it becomes crude in the region where notches have been applied.
- The gain offered by the ERS and URS (with an accepted risk of up crossing of α=99%) representations is obvious. As a rule, the higher the risk of overpass, the lower the URS is.
- The observed difference between URS (α = 99%) and RRS in the above example is about 3dB in the mid frequency range (URS > RRS).

12.5.3.2.6 Example 2 – Comparison of environment severity between SRS and random equivalence

A comparison of environment severity between SRS and random equivalence (RRS and URS) for a given random signal (represented by its time history or its PSD) is presented in Figure 12-15.

Two representative test configurations have been considered to support this comparison, with recording of temporal signals. SRS and random equivalence (RRS and URS) are computed from the time history and acceleration power spectral density respectively. For the comparison of environment severity, the SRS is considered as the reference, against which the RRS and URS are evaluated.

NOTE To illustrate the limitation of RRS, they are computed for 3σ peak value and considering also the peak values identified from the time histories (5σ for test configuration A, and 3.6σ for test configuration B).

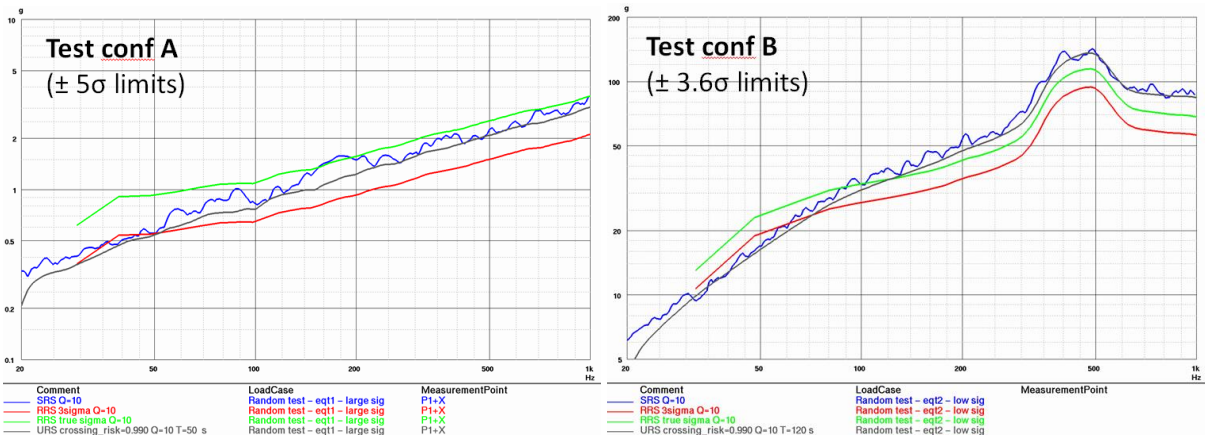

Figure 12-15: Comparison of environment severity SRS – RRS – URS

From these two representative test configurations, it is verified that the RRS computed at 3σ, globally underestimates the environment severity (SRS being the reference for this comparison). The estimation becomes more precise in lower frequency range, in correspondence to fundamental modes of an instrument for instance. The reason being that the probability of exceeding 3σ peak value, decreases when the frequency decreases.

It is also shown that the RRS should never be computed for the peak values identified from the time history, as the environment severity is globally overestimated (at least for test configuration A, characterised with 5σ limits).

On the other hand, **the environment severity is adequate estimated by the URS (99%), which matched the lower bound of the associated SRS, over the entire frequency range.**

12.5.3.3 Applicability of random equivalence w.r.t. shock

If the PSD profile presents some strong variations due to implementation of notches during the random test in reference, the equivalence into shock environment can be made through the RRS formulation, which corresponds to 3σ peak value. But by limiting the probability distribution to 3σ peak, the resulting severity is under-estimated.

To overcome this limitation, ERS and URS formulations allow the estimation of the peak value (as function of the random test duration) which **generally exceed 3σ.** As such the interest of such formulations lies in the consideration of a greater peak value, leading to an higher random equivalence, which in turn may allow the coverage of the specified shock environment.

However the choice for the accepted risk of up crossing α should be defined to ensure that the peak value is estimated in a pessimistic manner. To this end, the ERS should not be used, as the associated probability is defined too low to guarantee that the peak value is actually seen higher in reality. Instead the **URS formulation should be used, with an accepted risk of up crossing of α = 99 %.**

NOTE When used for shock equivalence, the URS should be calculated with risk of very large up-crossing probability (α =99%). If this URS is larger than the specified SRS, it is shown thus that the random vibration is more severe than the shock, with a high probability.

12.6 Similarity between equipment – Verification by similarity

12.6.1 Introduction

Reuse of electronic unit from one programme to another is often applied or desired, since it offers the opportunity for reduced cost, schedule and technical risk. However, the new electronic unit may present some changes with respect to the previously qualified unit, due to obsolescence of components and/or unique performance/functional requirements imposed to the new unit.

Verification by similarity is the process which demonstrates that the new unit is suitable for its new application, without a dedicated qualification programme on an EQM unit. However, such process can impose complementary verification activities.

Unfortunately, if the overall process is well defined ([RD-050], [RD-05], [RD-090]), the associated similarity criteria are often defined on a case by case basis. Furthermore the similarity criteria for shock may differ from the similarity criteria for vibration, as both environments (random and shock) have their own specificities. For example, the fatigue damage potential is a specific similarity criteria for vibration, and high frequency responses at component level is a specific similarity criteria for shock.

If the changes between the previously qualified unit and the new unit are considered as minor, as defined hereafter, a verification by similarity may apply. Based on accepted practices for verification by similarity with respect to shock, a guideline is herein proposed, and is recommended as a basis for similarity criteria for shock. Such guideline may not fully cover all type of electronic units, all missions, all verification strategies, therefore some adaptations may be necessary.

In any case, the adopted set of similarity criteria is reviewed and approved by the customer.

12.6.2 Similarity criteria for shock

In the following, the adopted convention is to consider unit ② as the new unit, and unit ① as the previously qualified unit.

Two units can be declared having similar shock withstanding, if the following criteria are met:

- Unit ① was a representative flight equipment, and was qualified through a rigorous qualification process, in line with applicable standard.
- Unit ① was not verified by similarity or analysis.
- Supporting documentation for unit ① is available and includes specifications, drawings, qualification test procedures, qualification and acceptance test reports.
- Units ① and ② were produced by the same manufacturer using identical tools, qualified manufacturing processes, and quality control procedures.
- The shock environment, in terms of SRS and shock duration encountered by unit ① during its qualification or flight history has been equal to or more severe than the qualification environments intended for unit ②.
- Units ① and ② should perform similar functions, with ① having variations only in terms of performance such as accuracy, sensitivity, formatting, and input-output characteristics.
- Consider Unit ① and ② mechanically similar, when all of the following apply:

— Architecture similarity:
  - The overall architecture is unchanged (e.g. stacked design),
  - The mounting configuration is unchanged,
  - The mounting configuration of PCB is unchanged (e.g. edge guide, stiffener, frame),
  - The PCB characteristics are unchanged (dimensions and thickness).

— Dynamic similarity:
  - The main natural frequencies of the chassis are within 10% of the original frequencies, and with similar mode shapes,
  - The first natural frequency of each PCB is within 10% of the original frequency,
  - Local modes of the PCB have similar mode shapes / frequencies.

— Similarity in component family:
  - Component families are unchanged (i.e. both units perform similar functions),
  - Shock sensitive components are accommodated in same areas of the PCB (i.e. close to edge, middle of PCB, …),
  - Mounting conditions of shock sensitive components are unchanged,
  - When the sensitivity of a components depends on its orientation with respect to the PCB, the orientation is unchanged (e.g. relay),

NOTE Minor design changes involving substitution of piece parts and materials with equivalent reliability items can generally be tolerated. Design dissimilarities resulting from addition or subtraction of piece parts and particularly moving parts, ceramic or glass parts, crystals, magnetic devices, and power conversion or distribution equipment usually compromise verification based on similarity, as such parts are particularly sensible to shocks.

NOTE Non-critical components can be re-distributed on the boards between two programmes.

As such, the similarity assessment aims at defining differences that can dictate complementary activities.

Effectively, the verification by similar is closely linked to a Shock Damage Risk Assessment (SDRA) process, with identification of shock sensitive components (para. 17.5 from Part 4), with consideration for robust design with respect to shock (para. 18.3.1.6), and it often comes in support to the equipment design and verification with respect to shock (para.18.3.1.5).

12.6.3 Example of process for verification by similarity

12.6.3.1 At complete unit level

Two units can be considered as similar if their global withstanding, in regards of shock environment, is the same. Therefore, their architecture is based on the same mechanical concept (typically the case for modular units).

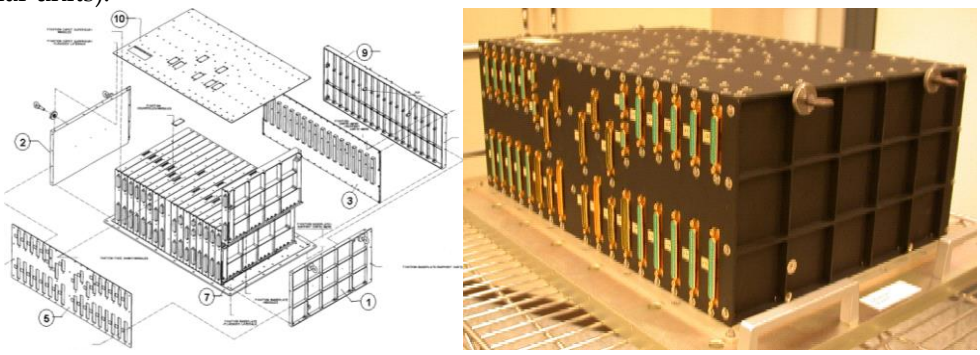

Figure 12-16: Example of modular concept

Table 12-6: Example of global characteristics comparison

		Unit ① - Heritage	Unit ② - New
Dimensions	Length [mm]	508.5	559.5
	Width [mm]	345	345
	Height [mm]	195	195
Mass	[kg]	23.17	27.4
CoG	X [m]	0.247	0.271
	Y [m]	0.162	0.164
	Z [m]	0.081	0.085
Inertia	IXX [kg.m²]	0.333	0.368
	IYY [kg.m²]	0.570	0.749
	IZZ [kg.m²]	0.705	0.907
Material	Baseplate	aluminium alloy AW 5083	aluminium alloy AW 5083
	Housing	aluminium alloy 6061 T6	aluminium alloy 6061 T6
	Structure	aluminium alloy 6061 T6	aluminium alloy 6061 T6
	PCB	Polyimide	Polyimide
Number of modules		18	20
Number of fixation points Unit/platform		32	34
Number of fixation points Module/Baseplate		11	11
Number of fixation points Module/ top plate		6	6
Baseplate thickness	[mm]	4 externally 5 internally	4 externally 5 internally
Module width	[mm]	24	24

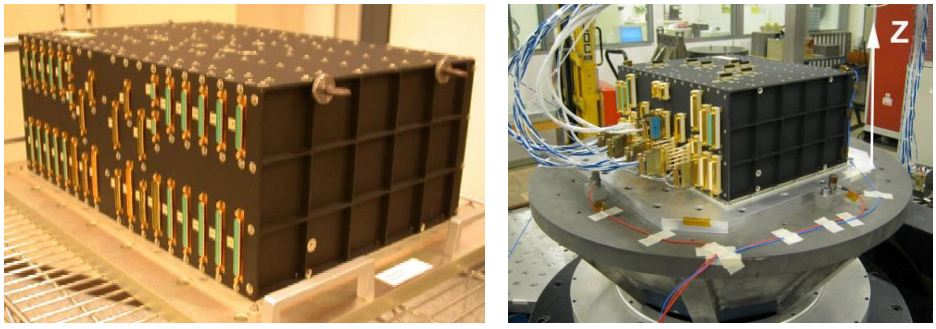

Figure 12-17: Example of similar units

In addition, the similarity for the mechanical behaviour needs to be established, particularly for what concerns the main natural frequencies of the chassis (within 10% of the original frequencies).

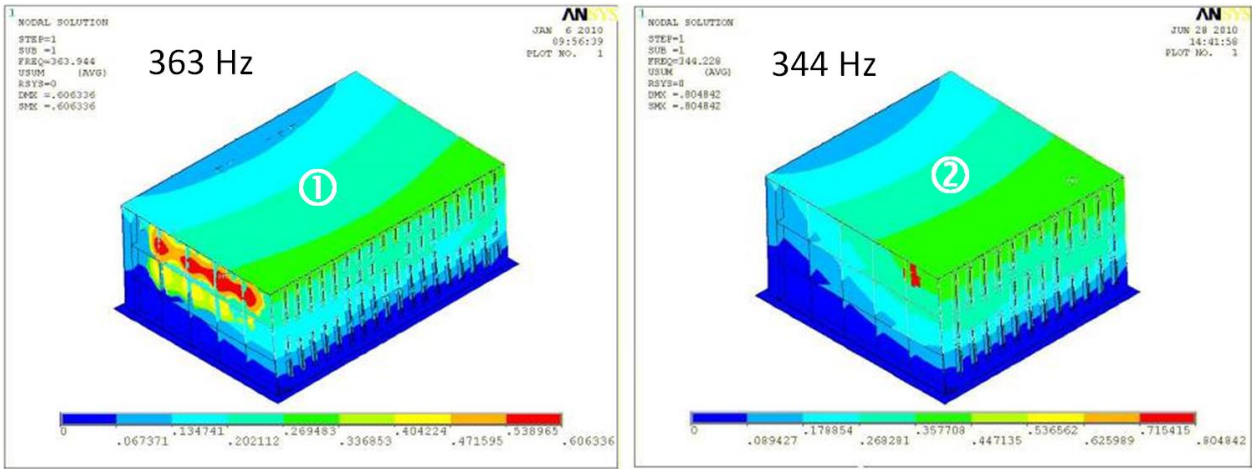

Figure 12-18: Comparison of the first natural frequency of similar units

In summary, to establish similarity at global unit level, the following information should be detailed:

- Description of the architecture concept,
- Table with global characteristics comparison,
- Comparison of the first natural frequencies of the units.

12.6.3.2 At Sub-equipment level (module, PCB,…)

The architecture of the main parts inside the units should be similar. For that, the following characteristics should be shown as similar:

- Description of the architecture of the sub-assembly,
- Philosophy of the fixation points: sub-equipment in regards of complete unit, PCB on structure,…
- PCB: dimensions, thickness,
- Local modes of the boards (the first natural frequency of each PCB is within 10% of the original frequency).

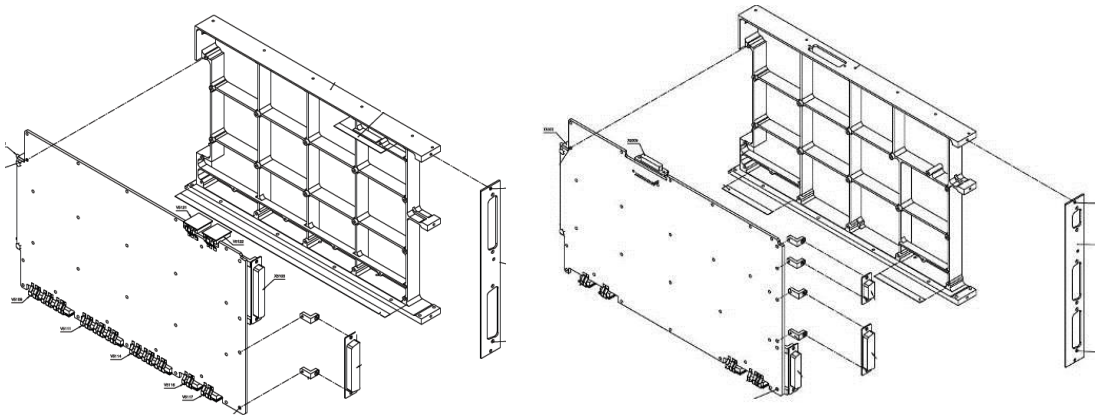

Figure 12-19: Global view of similar modules

12.6.3.3 At component level (module, PCB,…)

A listing of sensitive components in the units should be established to show that all the families, present in unit for which a shock heritage exists, are also mounted (with the same conditions) in the unit for which the similarity is verified.

The following table shows an example of critical components listing.

Table 12-7: Critical components listing

Component Family	Type	Location	Unit ① - Heritage	Unit ② - New	Mounting Conditions
Relay	TL26	PCB	✓	✓	
	GP250	PCB	✓	✓	
Inductors and Transformers	Self S3R	Housing	Diameter: 29mm Height: 13mm Weight: 26.5g	Diameter: 27mm Height: 12.5mm Weight: 28g	
	SELF 28,6uH 13,4ADC	Housing	Diameter: 38mm Height: 16.5mm Weight: 70g	✓	
	SELF 61.2uH 4.3ADC	PCB	Diameter: 24mm Height: 11mm Weight: 16.6g	✓	
	SELF 12.6uH 5.2ADC	PCB	Diameter: 16mm Height: 7.5mm Weight: 6.8g		
	SELF 2.9mH	PCB	Diameter: 18.1mm Height: 8mm Weight: 8g	✓	
	SELF COIL CORE	PCB	Diameter: 15.5mm Height: 7.8mm Weight: 6.9g	✓	
	Inductor VFMR Driver On	PCB	Diameter: 11mm Height: 5.8mm Weight: 2g	✓	
	SESI15SR	PCB	✓	✓	Glued with EG7655
	TFO RM5i	PCB	✓	✓	Glued with EG7657
	SMQ1553	PCB	✓	✓	Glued with EG7656
Heavy Components	PM948S-4	PCB	✓	✓	Dimensions: 17 x 18.5 x 15mm³ Weight: 6.8g
	CTC21-D	PCB	✓	✓	
	SMD1 without leads	PCB	✓	✓	
	DIL14	PCB	✓	✓	Without thermal mounting
	SMD05 with leads	PCB	✓	✓	
	Shunt SMV	PCB	✓	✓	
	DIL14	PCB	✓	✓	With thermal mounting: glued with stycast on ceramic plate
	FP20 - Qtech	PCB	✓	✓	
	DIL-28	PCB	✓	✓	
	FP24	PCB	✓	✓	
Hybrids	CQFP256	PCB	✓	✓	
	CQFP220 (µST)	PCB	✓	✓	
SOCS	SMD05	Housing	✓	✓	
	SMD1		✓	✓	
	SMD2		✓	✓	

A particular attention should be taken in regards of the **mounting conditions of the components** (on PCB or structure) in the different units. Heritage can apply only if the same type of mounting conditions have been used in the heritage unit.

Additionally, the critical parts in the unit should be located in the same areas from one similar unit to the other.

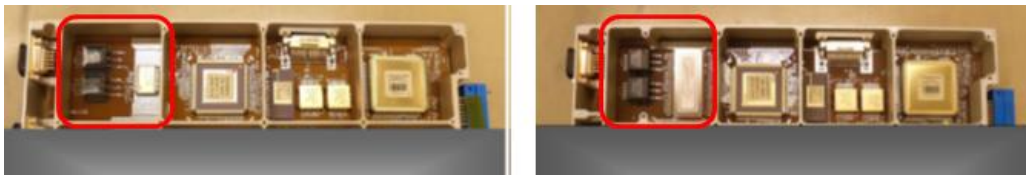

Figure 12-20: Critical parts location – Program ① (left) vs. Program ② (right)

When applicable (typically for relays), the orientation of the components should be the same. Whereas the non-critical components can be re-distributed on the boards from one program to the other.

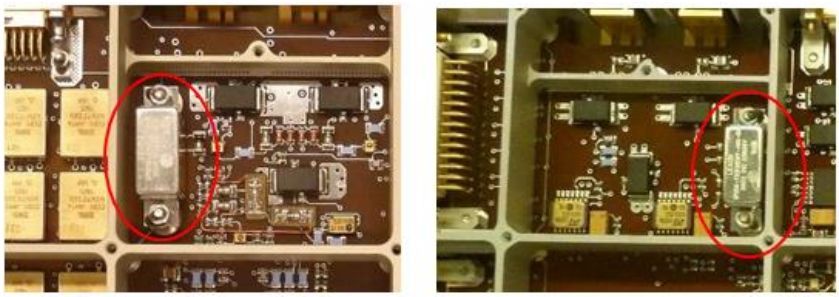

Figure 12-21: Relay orientation

12.6.3.4 Complementary activities to support a verification by similarity

By complying to the previously defined similarity criteria (para. 12.6.2), the suitability of the unit for its new application may be established based on previous heritage.

But more often than not, the similarity assessment may result in the identification of differences that can dictate some complementary activities. As such, the extend of the differences needs to be carefully assessed, and possible complementary activities identified. Should be considered valid, only those which further demonstrate the similarity assessment at component level.

In case of incomplete evidence of qualification heritage of some components (including the associated mounting conditions), the complementary activities should then comprise either a qualification shock test on the new unit (EQM or PFM, see paragraph 12.2.1.3 for precautions related to shock test on PFM units), or a shock test at qualification level on a dedicated test vehicle, consisting in a representative chassis equipped with PCB populated with the shock sensitive components in question, and with a representative distribution of components/ballast masses.

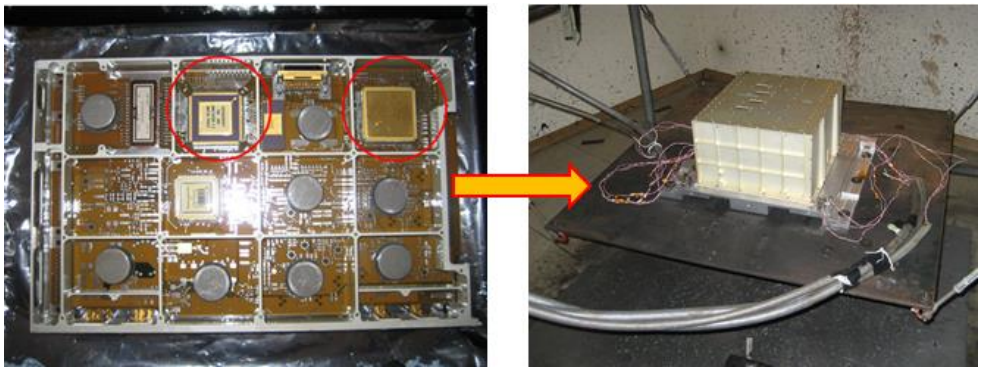

Figure 12-22: Shock test on a test vehicle, including representative PCB/components distribution

12.7 Specific guidelines for shock verification

12.7.1 Optical instrument

12.7.1.1 Overview

The optical instrument is a particular equipment of a spacecraft as it constitutes the payload and thus the core mission. The mission performance and success is thus strongly dependant of its performance. However, the optical instruments are a particular category of system gathering a wide variety of components whose sensitivity with respect to shock is more or less pronounced.

The complexity of optical instruments together with programmatic aspects impose some specificities to the shock verification, which are further detailed in this section.

12.7.1.2 Optical instrument definition and sensitive components

The optical instruments are generally composed of the following main sub-systems:

- **Optical units**: they are generally an assembly of different parts (mirror and fragile elements) potentially sensitive to shock. It can be distinguished two different categories:
  - Optical components (e.g. mirrors, lenses, and filters) are composed of fragile material (e.g. SiC, C-SiC, Zerodur, glass, and Germanium) very sensitive to mechanical rupture under shock environment. The detectors are generally close to the optical units.
  - Structural elements in fragile material (e.g. SiC, C-SiC, and Zerodur) which is also very sensitive to mechanical rupture under shock environment.
- **Electronics** are not addressed in this part of the shock handbook but in Part 4.
- **Mechanism**: this category can be split into two subtypes:
  - Orientation of the optical elements (like motors …) is not addressed in this part but in Part 4.
  - Release device which is not directly sensitive to shock but is an internal shock source in the instrument close to some sensitive parts.
- **Mechanical assembly and interfaces** which is determinant for the instrument performance. This includes a wide variety of categories:
  - Parts sensitive to misalignment (optical bench, lenses assembling)
  - Structural mechanical connections:
    - iso static mounting,
    - bonding with glue
    - molecular adhesion bonding

These four categories are illustrated on Figure 12-23 to Figure 12-25.

However, the shock damage type at instrument level can be split in two main categories:

- Fragile rupture of a component: this case can occur but would be due to a wrong appreciation of the damage risk and an insufficient design dimensioning. Materials are generally strength enough.
- Tilts of the optical assembling which impacts directly instrument performances. The case is more realistically problematic than the first one.

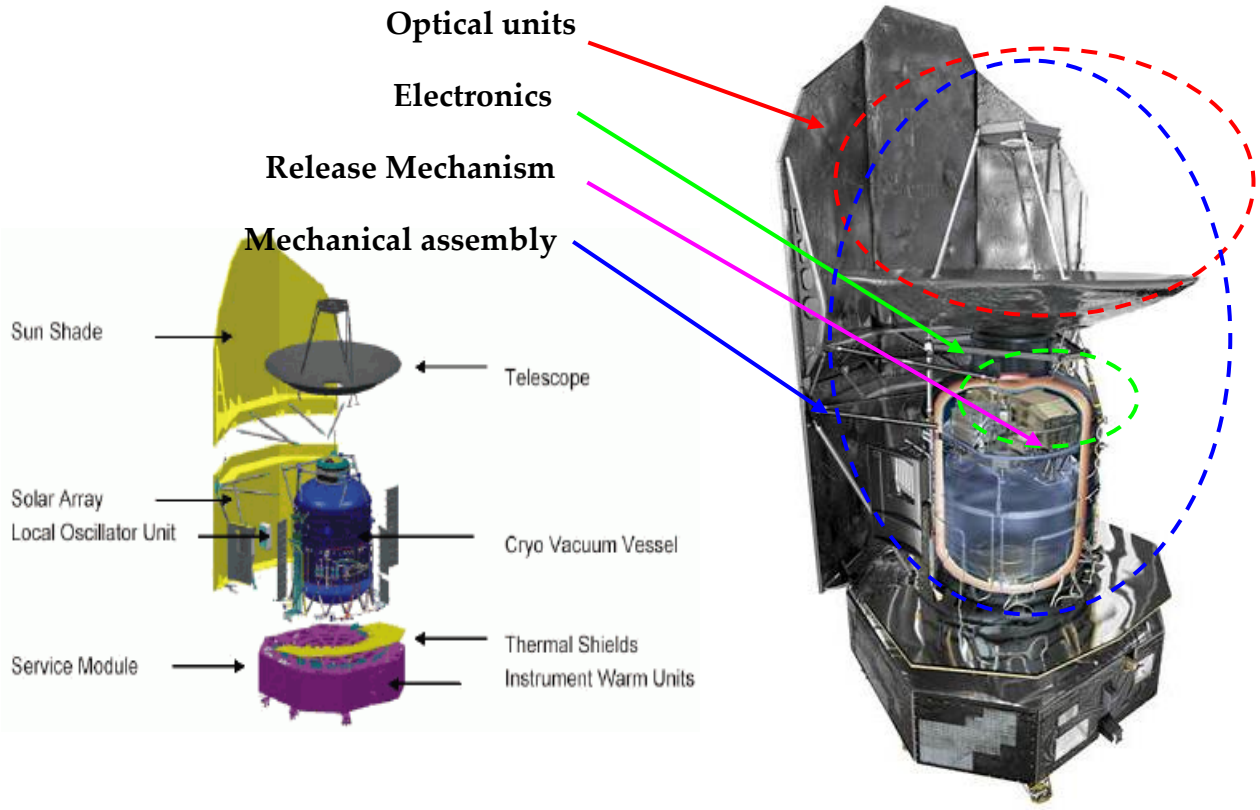

Figure 12-23: Overview of the HERSCHEL space telescope architecture and instrument categories

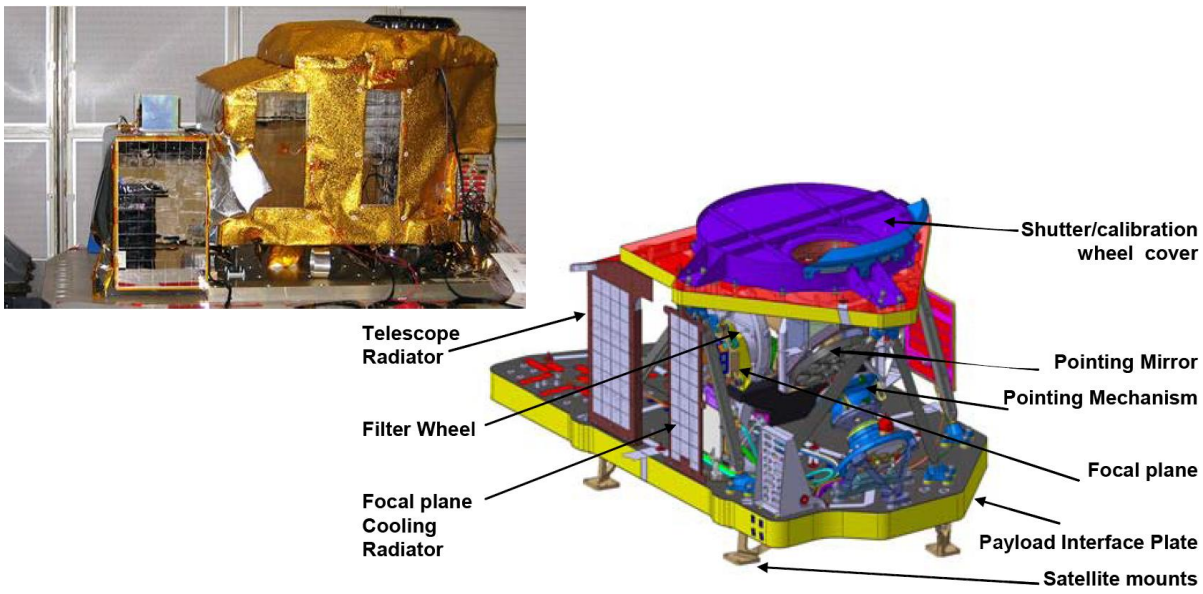

Figure 12-24: Overview of the GOCI instrument architecture

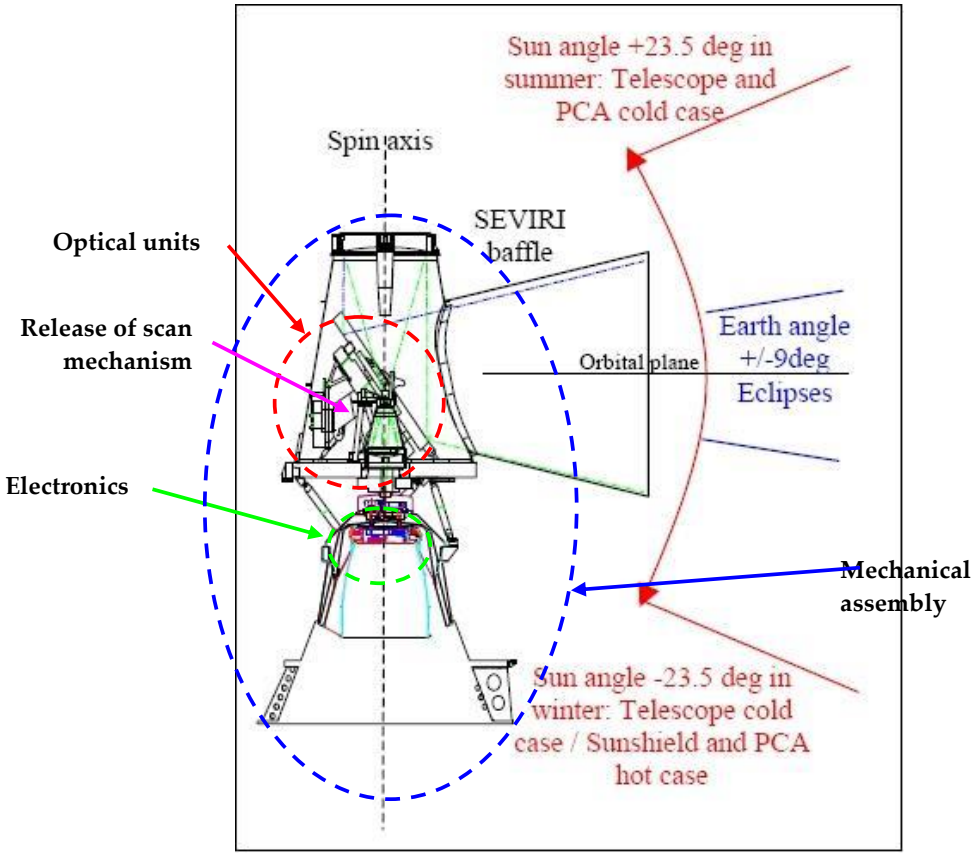

Figure 12-25: Overview of the SEVIRI instrument architecture

12.7.1.3 Typical instrument architecture and accommodation on the spacecraft

Depending on the spacecraft size, the accommodation of the optical instrument on the main spacecraft structure can be far or close to the shock source. This directly induces a different level of verification to apply in order to sustain the shock environment.

In case of a big spacecraft, instruments are generally accommodated on the top of the structure, far from the different shock sources leading to relatively low shock levels (e.g. order of magnitude is around 200 g @ 1kHz), as shown on the Figure 12-26:

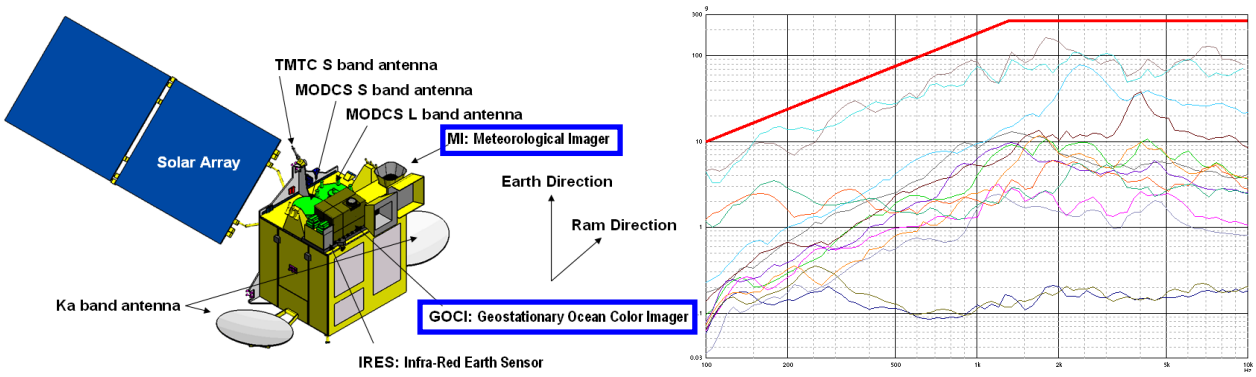

Figure 12-26: Overview of typical shock levels on top of big spacecraft far from shock source

In case of a small spacecraft, instrument are also generally accommodated on the top of the structure but on a confined structure, closer from the different shock sources leading to relatively high shock levels (e.g. order of magnitude is around 1 kg @ 3 kHz), as shown on the Figure 12-27.

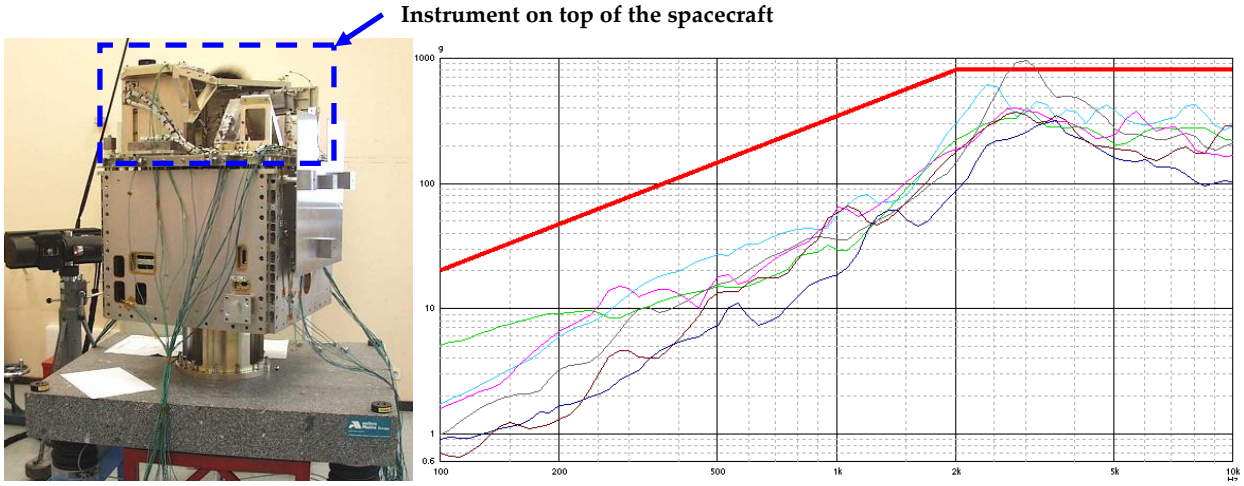

Figure 12-27: Overview of typical shock levels on top of small spacecraft far from shock source

12.7.1.4 General design rules w.r.t. shock

12.7.1.4.1 Overview

The optical instruments are generally designed in order to achieve a given mission performance and not relatively to the potential shock environmental conditions. The main design driver for optical instruments is thus to get a stable structure, calling for fragile materials which are generally decoupled from the main spacecraft structure by iso-static mountings in order to reduce as much as possible external disturbance from the spacecraft. Moreover, it is important that the location of the instrument on the spacecraft is at the best location to fulfil the mission requirements.

The iso-static mounting aims to provide a mechanical decoupling which is benefit for the shock isolation.

Shock is a part of the mechanical environment of the optical instrument. As the knowledge about the shock sensitivity of the different component is limited, their qualification is often covered by other environment (like random or quasi-static equivalent) or by the shock test that can be performed on a shock bench that imposes non-representative but conservative interface loads due to the fact that the system test base plate is more rigid than the spacecraft flight panel.

The kind of shock depends of the source location which could be close to the instrument (internal shock device for clamped element release) or far field (launcher or spacecraft interface events). In case of far field the shock signal is naturally filtered of its high frequency content and generally remain only the low frequency modal content.

12.7.1.4.2 Consideration of accommodation in the spacecraft

The accommodation of the optical instrument on the spacecraft is generally driven by the mission requirement. The instrument is located at the best place in order to fulfil the spacecraft mission. Thus different interface conditions with the spacecraft can generally be met in instrument accommodation, for example:

- at the top of the spacecraft far from the interface, as illustrated on the Figure 12-28 for the HERSCHEL space telescope

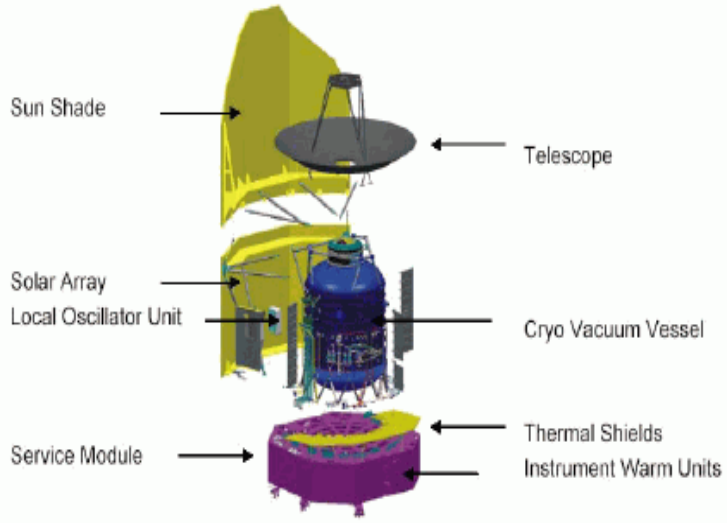

Figure 12-28: Overview of the instrument location on the HERSCHEL spacecraft

- close to the spacecraft interface, as illustrated for SEVIRI instrument on Meteosat Second Generation (MSG) on the Figure 12-29.

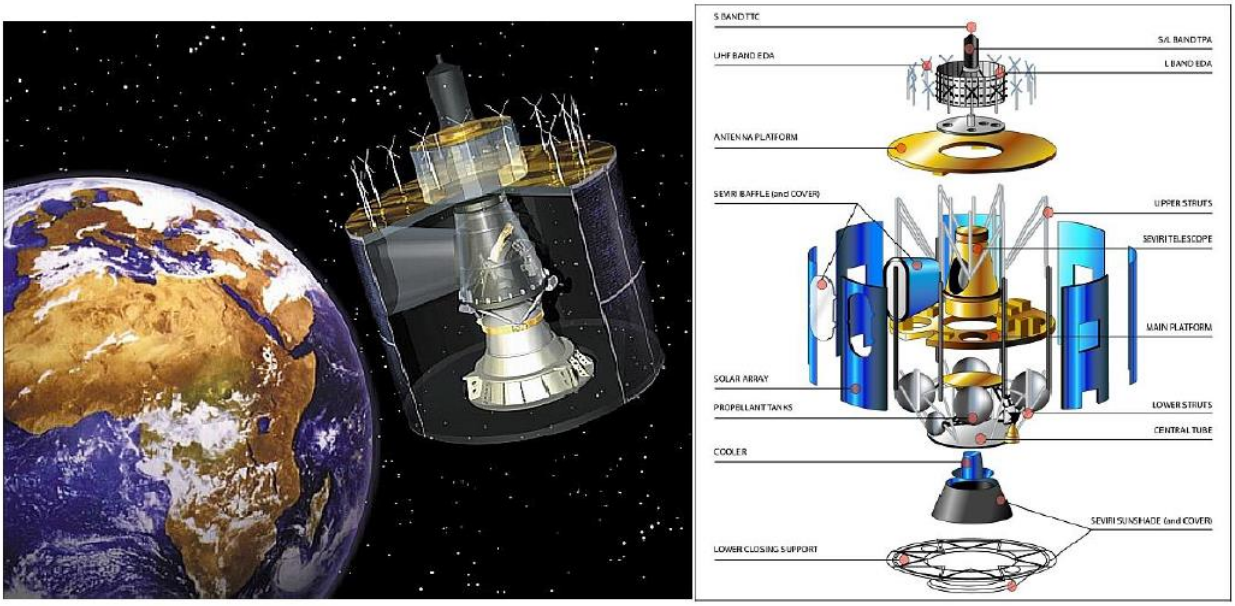

Figure 12-29: Overview of SEVIRI instrument location on the MSG spacecraft

12.7.1.4.3 Identification of dimensioning shock

Optical instrument are complex systems including sensitive component, for which it is important to limit as much as possible the shock levels and their impact. Due to the potential criticality of some instrument component with respect to the shock, it is of high importance to get a good estimate of the overall instrument life shocks and their characteristics.

Among the wide range of shock event, we could distinguish two main categories:

- External shock sources due to:
  - the launcher:
    - Launcher pyrotechnical events (fairing separation, inter-stage separation)
    - Spacecraft to Launcher separation (by means of Clampband or pyronuts).
  - the spacecraft: spacecraft appendage release (e.g. solar array, antenna, clamped mechanism).

  The first assessment should consist in the identification of transmissibility of the shock from the shock source to the most sensitive components (see Part 2). If this transmissibility is too important, it is fundamental to undertake recovery actions to isolate the instrument or the sensitive part at its interface from the external shock.
- Instrument internal shock source due to mechanism release (some instrument internal mechanisms are protected from the launch loads and released once in operation for service).

  The optical instruments sensitive components are generally far from the external shock sources, the dimensioning shock levels are induced by internal shock source. Consequently optical instrument release mechanisms mostly rely on low shock devices, such as:
  - Low shock actuators (NEA, Lacroix …) which exist for wide range of bolt section
  - Shape memory alloys actuator
  - Paraffin wax actuator

  They are generally based on a smoothed released of the mechanical constraint due to a relatively low dynamic of the mechanism limiting the shock levels.

12.7.1.4.4 General design rules

Owing to the heritage on a wide range of previous programs, the accommodation in the spacecraft can generally help to reduce shock levels at instrument interface, by considering the main structure complexity leading to break the path for shock waves to propagate, as well as the number of interface. However, even if several factors help to reduce the shock transmission (number of interfaces, length, direction change, mass impedance damping effect …) the effect can't cumulate infinitively and the cumulate of no more than two effects is generally observed.

It can also be mentioned that the damping of the shock levels are generally more efficient close to the shock source than far away from it (at the instrument interface for example).

Moreover, as optical instruments are generally accommodated far from the shock source, the assessment of the equipment compatibility with respect to the shock can be provided by the **random qualification level or equivalent quasi-static**. This is justified by the fact that as the external shock sources are generally far from the instrument interface and thus the shock frequency content at the instrument interface has mostly the "low frequency" modal behaviour of the structure underneath. The "high frequency" signal content has generally been filtered in the propagation of the spacecraft structure.

This is illustrated in the Figure 12-30, showing a comparison between the input level at the spacecraft interface with the shock level measured at the instrument interface (far away from the spacecraft interface).

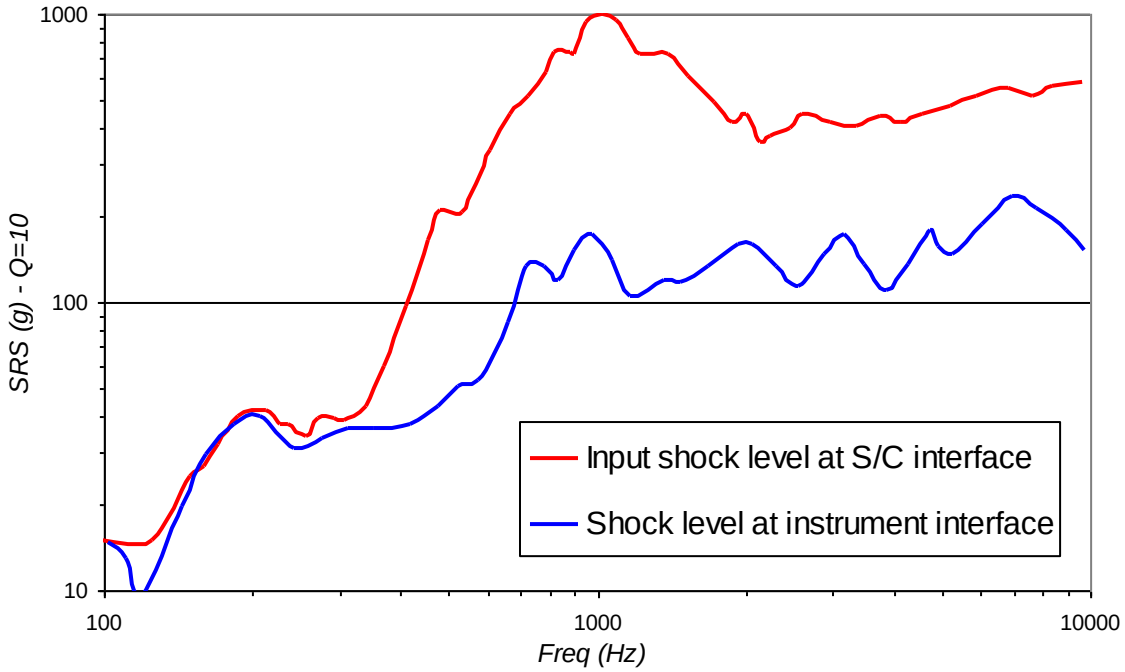

Figure 12-30: Overview of shock level close to the shock source at spacecraft interface at the left and far from the SC/ bottom at the instrument interface at the right

As the shock signal becomes dominated by low frequency modal content, the compatibility to shock environment can be covered by the other low frequency environments (sine, random and quasi-static). These methods are detailed in paragraphs 12.5.

12.7.1.5 Verification logic w.r.t. shock

In order to apply shock verification logic for optical instruments, it is necessary to have a good knowledge of:

- the shock environment, i.e. identify all the shock sources applicable to the optical instrument (e.g. internal or external sources, far field or close to the instrument).
- the expected shock severity, i.e. an estimate of the frequency content and the magnitude of the shock signals at the optical instrument interface or directly at a component interface.
- the instrument heritage sensitivity, i.e. identify the potential optical instrument components sensitivity to shock (e.g. due to their design, optical alignments, gluing, or specific fragile materials) based on a heritage and knowledge about their sensitivity to shock.

This knowledge of the shock environment (with identification of dimensioning shock), the shock severity and the instrument heritage sensitivity determines the verification logic to apply at system and sub-system level.

In case the knowledge / confidence level in one of the three previous points is considered too low, some risk reduction measures need to be implemented. The risk reduction logic verification depends of the type of environment to qualify and the size and complexity of element to qualify.

The complexity, long engineering optimisation, high sensitivity and cost of optical instrument lead generally to avoid directly testing the system. Consequently the risk reduction logic generally calls for a STM approach which allows:

- qualifying the representative structural elements
- identifying the environments to apply to the subsystems and verify the dimensioning hypothesis thanks to shock covering methods by random environment.

The STM approach can be consolidated by mechanical analysis in order to estimate the confidence margin which is not accessible in tests. These consist on transient analysis of a representative finite element model coupled instrument and main spacecraft structure to get representative impedance at the instrument interface.

More generally, the risk reduction actions can be considered as mandatory:

- for important or complex subsystems for which it is impossible to do testing (due to the important dimensions of the units).
- when the subsystem level shock testing is not representative of the true environment on the spacecraft (due to interface load too important with respect to the true environment).

The optical instrument qualification is achieved when the following points are fulfilled:

- A system level shock test on a representative spacecraft STM (STM service module + instrument STM) which concludes about the structural element and instrument qualification levels. The necessary level of representativity depends on the identification and qualification needs.
- Internal instrument components qualification given by a shock test or a random equivalence at optical instrument subsystem level.
- Specific test on the optical instrument allowing covering the internal instrument shock cases.

12.7.2 Propulsion sub system

12.7.2.1 Overview

Propulsion sub-system is made of an assembly of several units that have the particularity to be both mechanisms and pressurized items. Therefore their sensitivity to shocks is specific. And depending on the design philosophy, the units of propulsion sub-system can be Single Point Failure for the satellite.

Moreover, one of these units is a also shock source itself : the pyrovalve. Its function is to definitely open or close a fluid circuit, and its actuation requires a squib that generates high levels in the near to far field. And this shock source is the only one in the spacecraft that cannot be tested at system level on a proto-flight model.

This results in several specificities in the design and verification of the whole propulsion sub-system versus shock.

12.7.2.2 Propulsion sub-system description

12.7.2.2.1 General accommodation

Propulsion sub-system can have various architectures depending on the mission and the size of the satellite. However, two basic configurations can be identified:

- Mono-propellant propulsion system
- Bi-propellant propulsion system

In Figure **12-31** and Figure **12-32** a simplified flow diagram for both configurations is given together with the implementation on actual satellite.

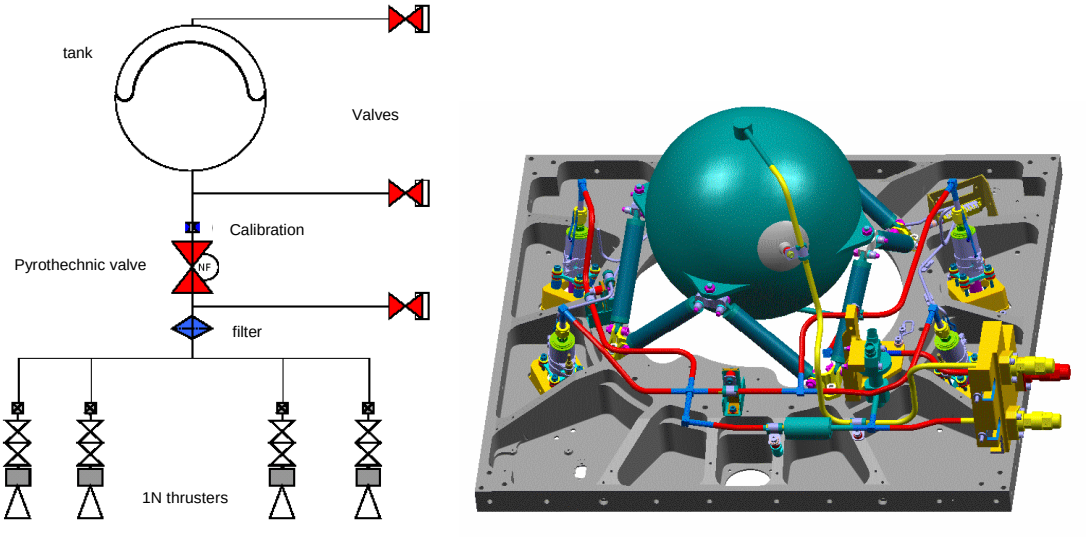

Figure 12-31: Mono-propellant propulsion system for Myriade satellite (CNES): flow diagram and physical layout

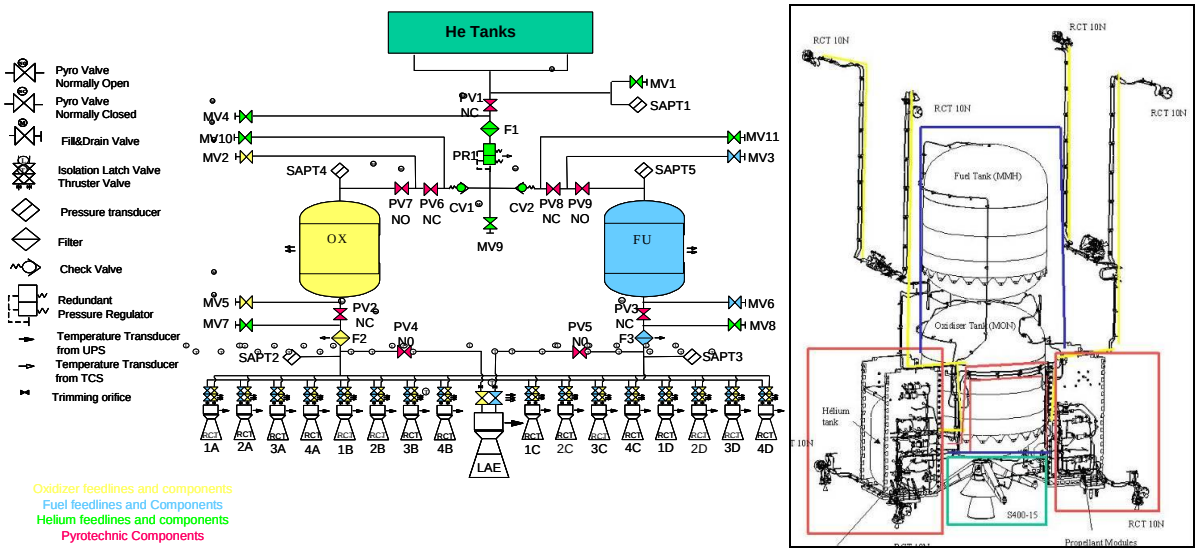

Figure 12-32: Bi-propellant propulsion system for AlphaBus platform: flow diagram and physical layout

12.7.2.2.2 Propulsion sub-systems with associated sensitivity

a. **Propellant tanks:** the propellant tanks, even if placed close to shock source, are not sensitive (because considered as structural parts). Only the PMD (Pressure Management Device), if present inside the tank, could be sensitive to shock.

b. **Pressurization tanks**: typically filled with helium, the pressurization tanks are insensitive to shock (i.e. considered as structural parts)

c. **Thrusters:** these equipment are sensitive to shock. The most sensitive parts are the nozzle due to its filigree design and the valves due to the presence of the actuation mechanism (movable parts).

d. **Pyro-valves:** this equipment is interesting from both point of views, it is a strong pyro shock source and it is sensitive to external shocks. Its sensitivity to external shocks belongs to two aspects of its functionality: the presence of the mobile part (the punch) that can change position and the risk of starting the squib.

   The pyro-valve is described in detail in 12.7.2.3.

e. **Fill and Drain Valves:** FDV are used during ground phases but not during launch. Therefore they are not subjected to shocks which are experienced only in flight (see 12.7.2.3). Moreover the mechanism of the FDV is a manual screwed system with an important torque and security system which is therefore low sensitive to a highly transient phenomena as the shock is.

f. **Filters:** Filters for propellant and pressurization fluids are normally present on sub-system to limit pollution of the circuit that could be generated by Pyrovalves firing. The filter in itself is a passive structural item with reduced sensitivity to shock. Anyway due to its function is often placed close to the internal shock source thus it could experience high shock levels.

g. **Pressure Regulator:** The presence of mobile parts, bellows and springs make the Pressure Regulator sensitive to shocks. Anyway, sensitivity is limited due to the typically robust housing of commercially available items.

h. **Pressure Transducer:** It is used to monitor pressure and provide input for propellant gauging, its sensitivity to shock is quite important. Indeed a PCB with electronic components and a sensor (strain gauges) are present in this equipment.

i. **Valve:** Latch valve is an electrically actuated valve. The valves can be actuated in both directions during all lifecycle of the satellite. Several parts of the valve are sensitive to shock (movable parts, seal). Main functional sensitivity is the possibility that the valve changes its status due to shock which would lead to uncontrolled leak or malfunctioning of the sub-system.

j. **Check (Non-Return) Valves:** This valve is a passive element, functionality is assured by pressure drop and not actuation. Therefore this valve is not too sensitive to shock, indeed a jamming of the component or a crack on the diaphragm is hard to achieve.

k. **Tubing:** Tubing is not a concern for shock qualification of the propulsion sub-system, owing that some design and verification rules are respected, see 12.7.2.4.

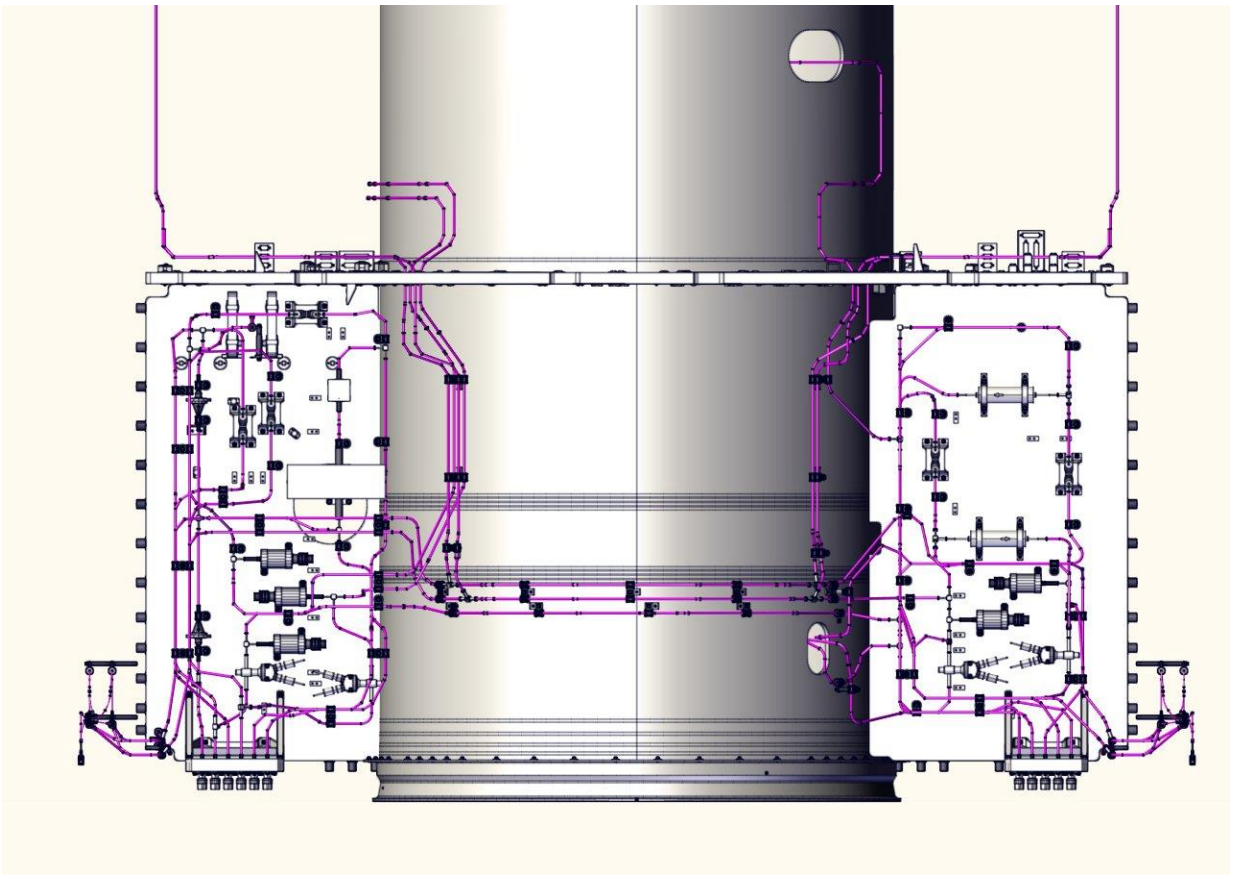

Figure 12-33: Example of propulsion lines (in purple)

12.7.2.3 Propulsion shock source

12.7.2.3.1 Overview

As stated above, one of the units in the propulsion sub-system is a shock source itself : the pyrovalve. It is a pyrotechnic device, and as most of the other units are accommodated very close to it they are submitted to very high levels in the near- and mid-field ranges.

The main issue is then to derive the shock environment due to the pyrovalve actuation.

12.7.2.3.2 Description of the pyrovalve shock

In Figure **12-34** is indicated a schematic exploded view of a PV. The initiators are located in the upper body thus close to the interface. Therefore the shock rejected by the pyrovalve at its interface is significant.

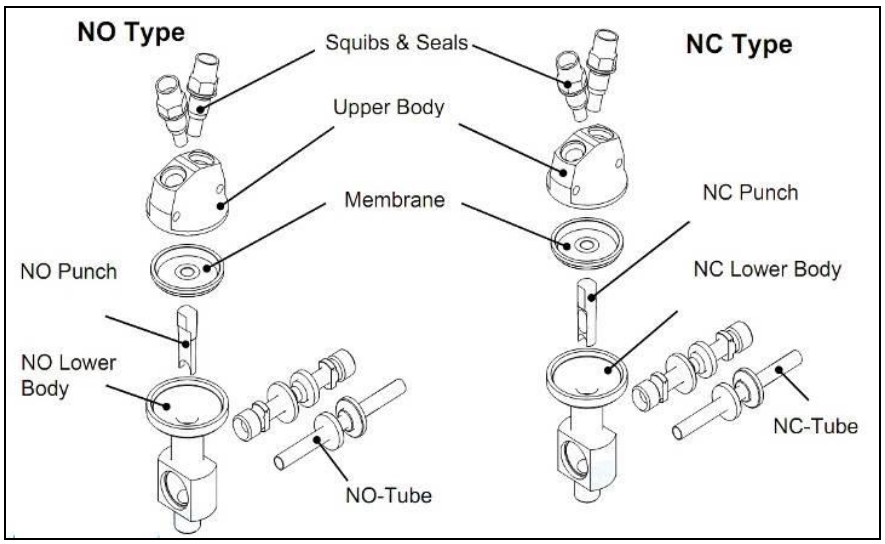

Figure 12-34: Exploded view of NC and NO pyrovalves

The function of the pyrovalves is to definitely shut down or open a fluid circuit. The energy needed for actuation is supplied by a pyrotechnic system and transmitted by the deformation of a titanium flexible membrane. This membrane ensures a perfectly proof tightness between the pyrotechnics chambers and the fluid circuits before, during and after the actuation.

Each valve consists of two standard initiators, connected in parallel, providing firing redundancy. Both initiators are fired at the same time in order to perform the correct actuation of the valve (opening or closing).

The firing of the squib results in the ram inside the valve being propelled downwards towards the tubing. In the case of a Normally Closed PV, the ram travels down into a receptacle at the base, and is latched in a position that renders the valve open. The Normally Open (NO) PV, operates in a similar way, but the tube is sheared by the ram on its travel. A near perfect seal is created by the rams wedge shape.

Combustion products are prevented from contaminating the system by titanium flexible membranes located between the chamber and the ram.

A pyrovalve can be mounted directly on panels. However for simpler coupling to the propulsion tubing, it is usually mounted on brackets. In the following Figure 12-35 are shown some typical mounting.

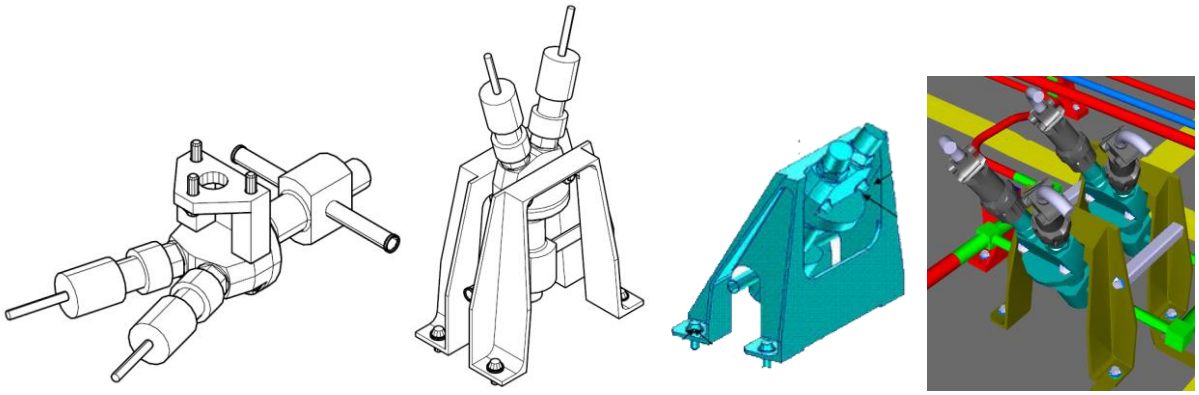

Figure 12-35: Lay down support | single bracket (vertical) | single bracket (angled) | double bracket

12.7.2.3.3 Shock environment derivation

a. Approaches

Due to the lack of heritage measurements on PFM spacecraft, specification for PV induced environment could be obtained basically by two approaches.

The first one consists in performing a test on a Qualification Model (QM) of the complete propulsion sub-system (equipment and tubing). Moreover, this QM should be fully representative of the satellite in the vicinity of the propulsion sub-system to allow the identification of shock propagation paths and therefore the definition of shock levels at the various interfaces.

The second one consists in performing a characterization test on a structure similar than the flight one but with the objective of deriving the most of information on levels at equipment interface and not of qualifying the complete sub-system. This approach is most used on commercial telecommunication satellites: with this approach the results are more generic and qualification of sub-system can evolve with evolution of single equipment without the need of a new QM test on the complete sub-system. On the other side the shock qualification of the complete sub-system is never proven by a test in actual flight configuration.

b. Guidelines for characterisation tests

In this section are addressed the main points to be considered when a characterization test campaign is foreseen to investigate the shock environment generated by pyrovalve firing.

The main objective of the campaign is to identify the levels at propulsion equipment interface in order to define the relevant specifications.

A valuable characterization should allow constituting a database that gives the possibility to extend results to various configuration of propulsion system to anticipate possible evolutions (in technology and design).

A secondary objective is to evaluate the levels injected on the platform (if it is not possible to exclude by design that significant levels are transmitted).

Test campaign results should be detailed enough to identify possible design choice on shock reduction (e.g. isolators and equipment layout).

To fulfil these objectives, it is important to pay special attention to the test setup:

- It should be fully representative of the supporting structure and its boundary conditions (global and local stiffness and mass).
- It should be representative of the surrounding structures if the transmissibility to the platform is of any interest.
- The PV and its mounting should be the same than the flight ones (e.g. brackets, connections, and isolators)
- The equipment should be the flight ones or could be replaced by dummies representative in term of mass and stiffness (particularly of importance for equipment mass higher than 200 gr).
- The PV are always connected to the other equipment by tubing (see Figure 12-32). The tubing should be considered in the setup if it affects the shock transmissibility or the stiffness of the assembly. Anyway, if some common tubing design rules are respected (see 12.7.2.2), the experience shows that tubing effect is negligible.

It is important to pay special care on instrumentation, mainly for two aspects:

- The PV shock is mainly a near field shock: so it is important to select the correct accelerometers (see part 3, 13.4)
- One objective being to build a database of results, it is important to ensure that the number of accelerometers is sufficient, and their positions are selected in such a way that they allow the evaluation of transmissibility to equipment versus different design parameters (e.g. distance, mass, connections, and surrounding structure).

In the following Figure 12-36 the setup for characterization test performed for an actual Telecom satellite family is given. This test campaign follows the second approach : various test setups have been tested.

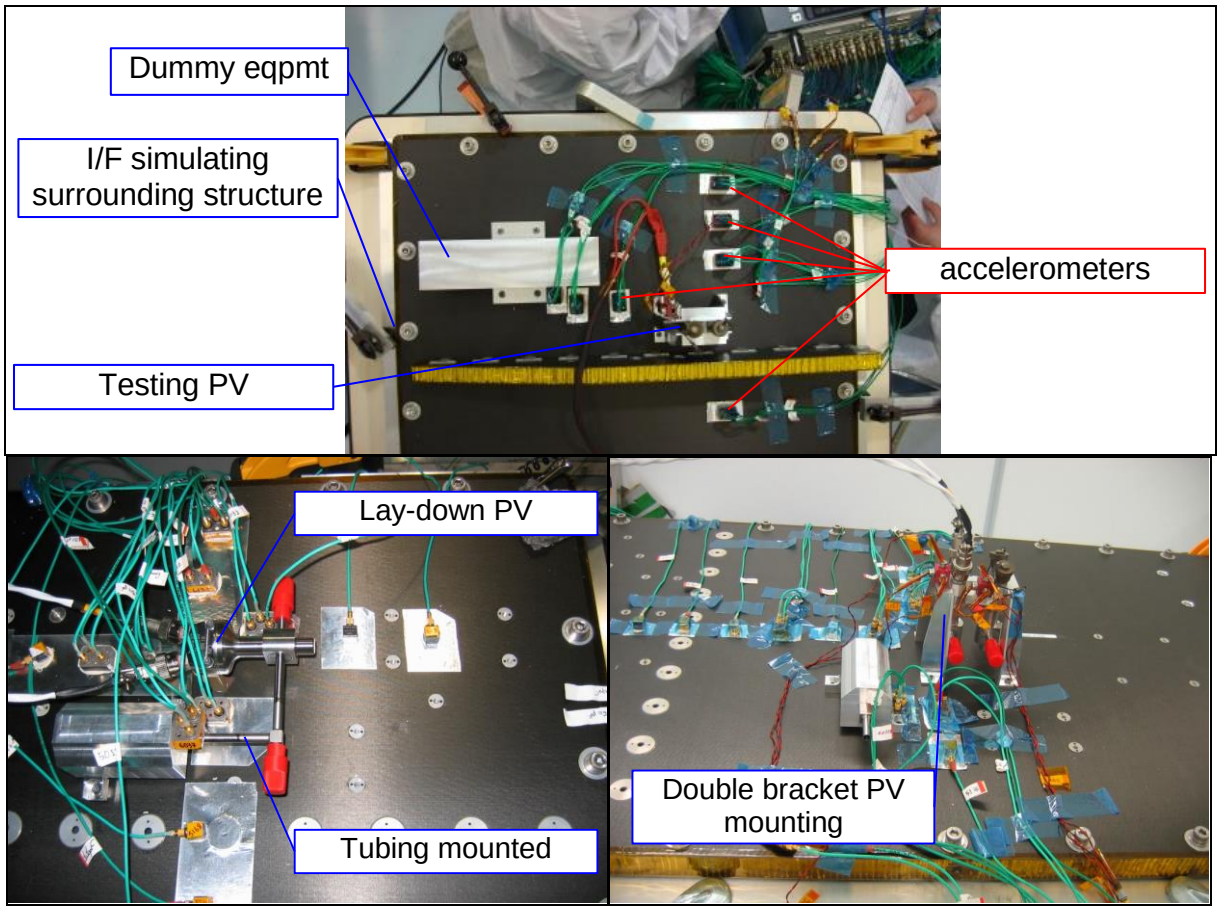

Figure 12-36: Test configurations for complete characterization test.

It can be noticed that different types of PV mounting, various positions for equipment (and dummies) and a dense instrumentation is considered, even the effect of a local stiffness (sandwich stiffener) has been evaluated.

The test shown above was planned to get extensive database and to be applicable on an evolving propulsion system's layout. This test is fulfilling all the objectives (primary and secondary).

In the following Figure 12-37 is shown another test setup following the first approach (test performed on ALPHABUS platform) which fulfils the primary objective of getting levels at propulsion unit interface (accelerometers at each equipment interface), which allows estimating transmissibility to surrounding structure but which is not robust enough to get an extensive database of results (only one configuration is characterized)

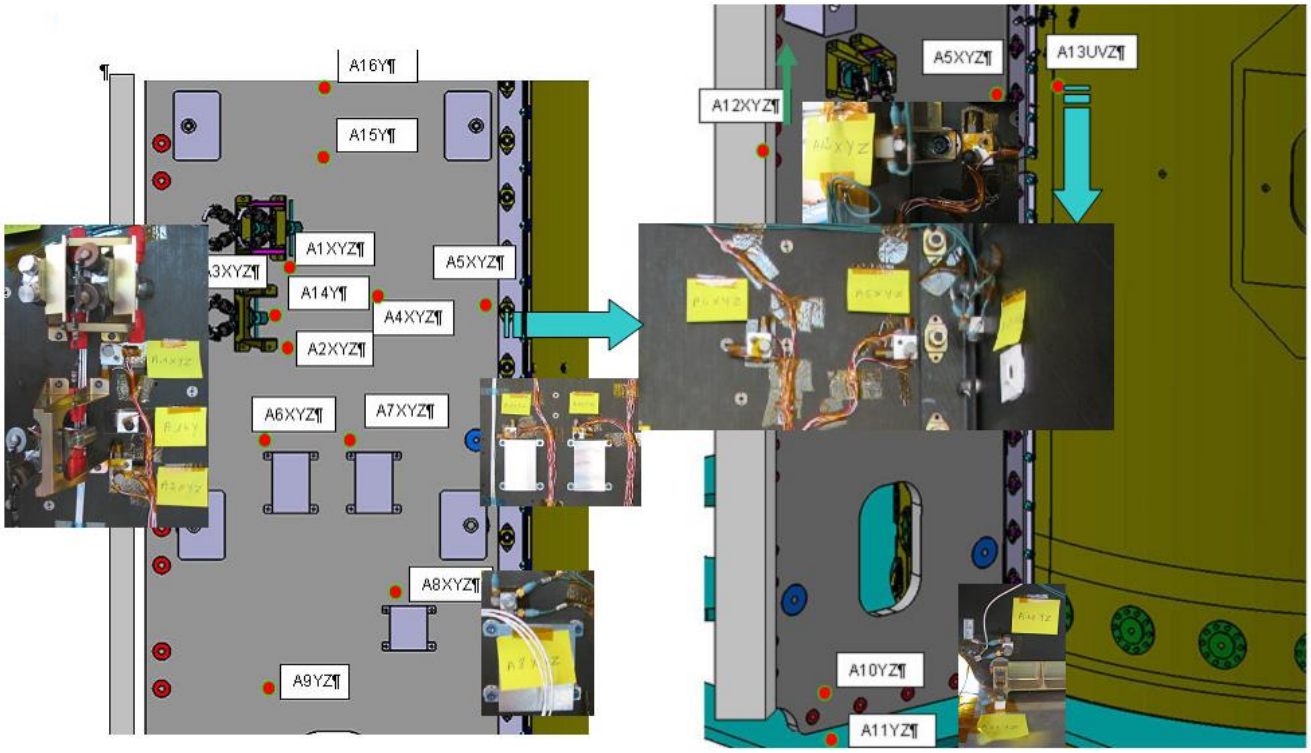

Figure 12-37: Test configurations for dedicated characterization test (AlphaBus).

c. Typical attenuation rules

As indicated in the previous chapter the evaluation of attenuation rules should be a result of the characterization test. In this chapter, some attenuation rules based on Alphabus pyro-shock test campaign are evaluated.

Attenuations due to distance and transmissibility to surrounding structure have been analyzed.

The main results can be resumed as follows for in-plane and out-of-plane directions:

— Out of plane:
  - d < 150 mm: no attenuation
  - 200 mm ≤ d < 300 mm: attenuation 3 dB (for f>2 kHz)
  - 300 mm ≤ d < 500 mm: attenuation 3 dB (for f<1 kHz) and 6 dB (for f>1 kHz)
  - d ≥ 500 mm without obstacle: attenuation 7 dB
  - d ≥ 500 mm with obstacle: attenuation 9 dB
  - interface: attenuation of 6 dB

— In plane:
  - d < 150mm: no attenuation
  - 200 mm ≤ d < 300 mm: attenuation 3 dB
  - 300 mm ≤ d < 500 mm: attenuation 3 dB
  - d ≥ 500 mm without obstacle: attenuation 3dB
  - d ≥ 500 mm with obstacle: attenuation 9 dB
  - interface: attenuation of 6 dB

Globally 6dB of attenuation (up to 10000 Hz) can be considered while going to the surrounding structure.

These attenuation factors only relate to this tested configuration, nevertheless a good agreement is found with respect to the generic attenuation rules for point source excitation, as presented and discussed in the paragraph 8.3.1. In-house experience by the satellite manufacturer or generic attenuation factors can be taken into account for preliminary specification and design, but it is important that they are confirmed by a dedicated characterization or qualification test representative of the actual flight configuration.

d. Qualification margins

To define the specification, the measured test values should be increased by the classical qualification margin of +3 dB (see section 10.2 of Part 2).

The margin of 3 dB is applicable under the hypotheses that a dedicated characterization test representative of the configuration has been performed and that a sufficient database of results is available. Indeed the experience shows that the dispersion is limited at iso-configuration.

Anyway if heritage results are used to define specification or if important design evolutions are applied, the qualification margin for preliminary design should be increased. The value is then evaluated on a case by case basis.

In these cases a dedicated characterization test should be considered in the development plan.

12.7.2.4 General design rules

12.7.2.4.1 Specific rules for tubing lay-out

The concern for tubing is the relative displacements on a tubing section between two suspension point (equipment or brackets). Even the relatively low displacements caused by shock could generate high stresses on a rigid tubing line.

Therefore tubing should guarantee an important flexibility by design. A layout containing long non-straight lines and the use of suspension at tubing to bracket I/F should solve the rigidity concerns (see Figure 12-33).

Besides the design rules, detailed inspection at sub-system and system levels should be implemented in the development and qualification plan. Typically the minimum inspection/test required are X-ray on welding, pressure proof test on the line at sub-system level, after system integration after system environmental tests.

The use of heritage design and processes plays an important role in increasing the reliability of the tubing assembly.

12.7.2.4.2 Shock reduction solutions

In some cases, in order to reduce shock levels coming from PV, isolation system can be implemented. One solution can be to apply isolators at PV or bracket to platform interface. This solution has the strong advantage that it can be implemented very late in the design (or integration) phases.

Another solution can be to separate mechanically the PV from the others propulsion's equipment as per Figure **12-38**. With such a solution, the attenuation of shock is obtained by the longer path from PV to equipment and the presence of several links (see c for an estimation of reduction due to path length and links).

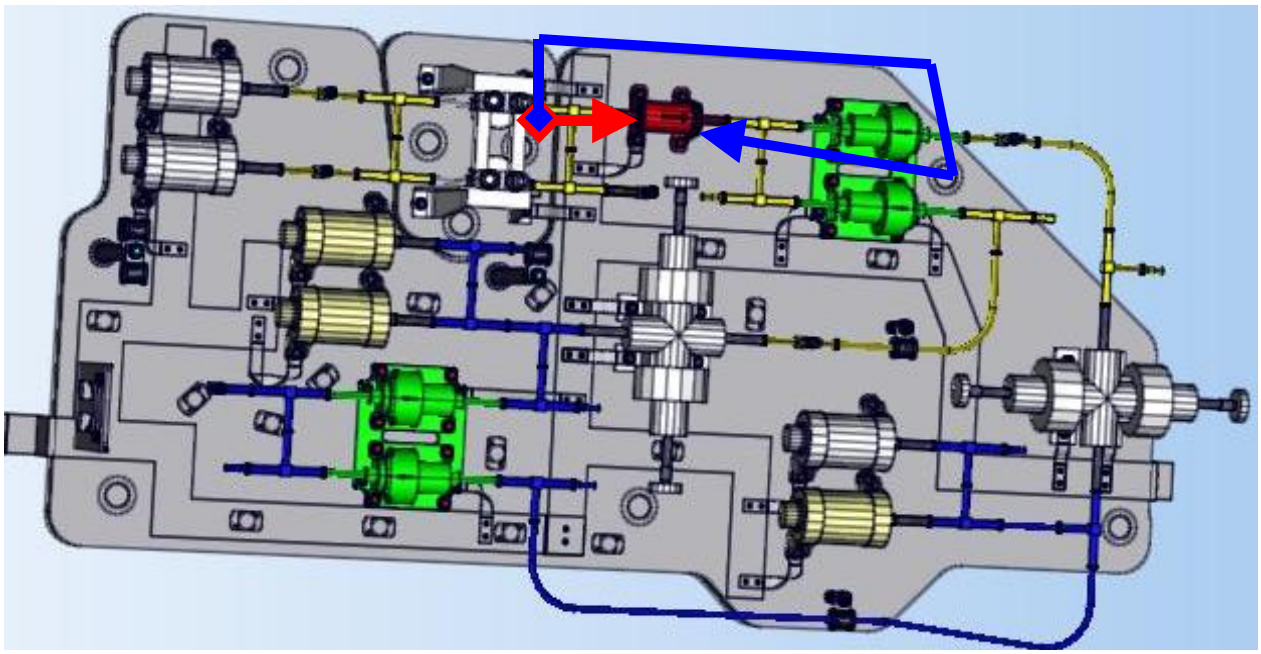

Figure 12-38: Example of PV mechanically isolated from the other equipment

12.7.2.5 Verification of the propulsion sub-system w.r.t. shock environment

12.7.2.5.1 Shock environment for the propulsion sub-system

The propulsion sub-system can be subjected to several shock environments:

- Launcher induced shocks or separation shocks
- Solar arrays and Reflector release
- Propulsion pyro-valve actuation

Depending on the spacecraft layout, the three shocks can be of interest for the propulsion sub-system, as shown in following Figure 12-39 (configuration with propulsion equipment accommodated on a shear wall, close to both launcher interface and appendages release mechanism).

In the same figure, the relevant shock levels measured in the given configuration are given for qualitative comparison purposes. For functional reasons PV are often the closest shock source, imposing a stringent shock input in the mid to near field domains. Whilst for far field event the other environments typically drive.

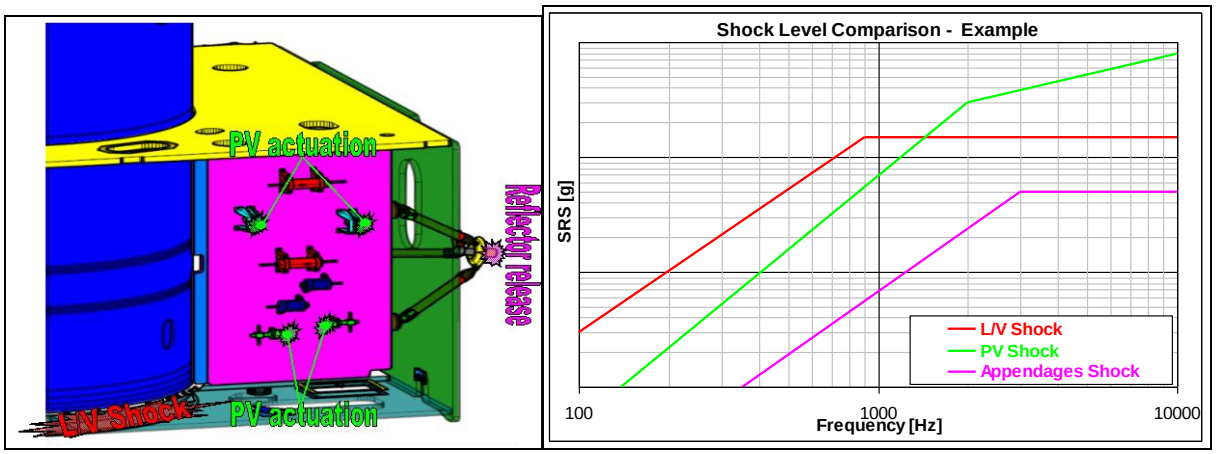

Figure 12-39: Example of shock event and measured levels

12.7.2.5.2 Verification at unit level

As for any sub-system, all the propulsion units should be tested at elementary level with respect to the defined environment. Classical procedures defined in 13.3 apply in that case.

However, some modifications can be applied as follows.

Theoretically all shock environments should be combined together and covered by one single specification. But PV injecting high shock levels at higher frequency than other shock sources as launcher separation, it could be foreseen (on a case by case basis) to separate the two environments in order not to over-stress the equipment.

For the same reasons (high levels and high frequency content) pyrotechnic shocks test is advised to better simulate this environment.

12.7.2.5.3 Verification at System level

For classical shock sources, verification at system level consists in actuating on the PFM the device causing the shock environment and checking that the levels measured (plus the 3 dB qualification margin) at units interfaces are covered by their qualification status. This is explained in paragraph 13.3.2 and is not covered in this chapter.

However, propulsion sub-system self-induced shocks cannot be tested on PFM satellite. This is due mainly to the stringent requirement on pollution prevention which applies to this sub-system. Indeed once actuated a pyro-valve needs to be replaced. But this can cause the loss of the hermetical sealing of the circuit thus leading to possible pollution issues on the circuit. To avoid this risk the PV firing test on PFM spacecraft is not recommended.

Three issues are caused by this limitation:

- The unavailability of heritage system test results to evaluate the shock environment;
- The lack of demonstration of the system design robustness against these self-induced shocks.
- The lack of demonstration of the actuation's functionality after the other mechanical aggressions.

Therefore a specific validation against this self-induced shock is mandatory. This validation is obtained by a specific approach to be defined at subsystem level. Usually two approaches are applied: either testing the full sub-system (for unique spacecraft as for science missions) or characterizing the pyrovalves shock sources in order to allow design modifications. The following table summarizes the two possible approaches.

Table 12-8: Qualification processes comparison

	QM approach (MYRIADE)	Characterization test approach (TELECOM)
Levels estimation / specifications definition	By dedicated QM test	By characterization test
Measures dispersion	3 dB margin on measured levels	Several test for characterization 3 dB margin on measured levels
Manufacturing dispersion (on PV)	Process control 3 dB margin on measured levels Acceptance test on PV (DLAT)	Process control 3 dB margin on measured levels Acceptance test on PV (DLAT)
S/S Qualification	By dedicated QM test	Not tested in actual flight configuration, Qualified by specific qualification logic
Sensitivity to design evolution	High: new QM test needed for design evolution	Low: characterization test covers several configuration and can cover important differences in the design of the sub-system.
Equipment qualification	Equipment test	Equipment test
S/S acceptance (PFM or FM)	Not done for PV shock, covered by: – qualification on QM – process control – equipment acceptance	Not done for shock, covered by: process control equipment acceptance
System Acceptance (PFM)	Not done for PV shock, covered by: – heritage – inspection – process control – functional test	Not done for PV shock, covered by: – heritage – inspection – process control – functional test

Finally the verification at system level is completed by rigorous functional test of the propulsion subsystem mounted on spacecraft. These verifications cover all aspects of propulsion functioning with the exclusion of the firing of the pyrovalves. Pyrovalve correct behaviour is however checked (i.e. Electrical check out of squibs: squib wire resistance and squib insulation resistance).

The tests requested on the propulsion assembly are divided in three main categories: integration, safety, performance. These tests allow verifying the propulsion assembly at both sub-system and system level.

13
Shock testing

13.1 Shock test specifications

13.1.1 Test levels and forcing function

The test levels correspond usually to the expected flight levels increased by the qualification margin (minimum of 3dB – see Part 2 10.2). These flights levels are obtained using:

- Similarity-heritage methods
- Numerical methods

Those methods are thoroughly described in Part 2.

The required shock spectrum can be achieved using a representative transient, usually exponential decay, with effective duration (see 15.3.1) specified around 20 ms - 30 ms for far-field. Half-sine transients are thus not recommended as they are generally not representative of real pyro shock events. **The shock transient should contain all necessary shock frequency components simultaneously as opposed to a serial application.**

13.1.2 Number of applications

The number of applications has always been subject to discussions among European industries and agencies, mainly due to a lack of clarity into this requirement. This section intends to provide the reader with the necessary justifications for an adequate number of applications in pyroshock testing (both at equipment and system levels).

The requirement on a number of applications finds its origin into the verification of the life cycle of the tested unit. The life cycle is defined as the total number of shocks to be withstood by the flight unit for each specific shock event (launcher induced shocks, spacecraft release shock, internal shocks) during its complete life (including ground tests and in-service shocks). Hence the verification of the full compatibility of the unit with the intended shock environment, implies that the qualification margin is verified, and that **the number of applications covers the complete life cycle of the tested unit.**

At this point 3 distinctions need to be made, between equipment QM testing, equipment PFM testing and system level testing:

- **Equipment QM testing** – The number of applications typically varies from 1 to 3 along each direction. A single shock application is considered sufficient only in case the equipment sees its dimensioning shock only once in its life cycle (i.e. in orbit). Multiple shock applications need to be foreseen in case the equipment is exposed to its dimensioning shock more than once during its life cycle (on ground and in orbit). In this case the provision for an additional retest should be considered i.e. the number of shock applications equals the number of dimensioning shocks seen by the equipment under test during its life cycle plus one.

NOTE As a return of experience from electronic unit shock testing, it has also been shown that several consecutive shock tests at high levels can influence the behaviour/integrity of relays and quartz. Example of relays with plastic deformation of the brackets supporting the mobile part or frequency shifts of Local Oscillator quartz are presented in Part 4. In that specific case, **3 shocks per axis** can reveal some unexpected behaviour of the unit, and **are therefore recommended**.

- **Equipment PFM testing** – In itself a PFM programme presents already a higher risk than the prototype approach in which design margins are demonstrated by testing on a dedicated qualification product, hence, in case a shock testing is required on a PFM unit, it is important that the number of applications does not exceed 1 per axis.

  As discussed in section 12.2.1, a PFM programme should be accompanied by a strategy for risk mitigation, which should consist in enhancing development testing, in increasing the design factors of safety and in implementing an adequate spare policy.

- **System level testing** – System level tests for self-induced shock environments are usually performed by utilizing flight pyrotechnic devices on a flight structure. As a consequence, duplication of the flight shock environment can be reasonably achieved, but a qualification margin is generally unachievable. For qualification and proto-flight testing for self-induced shocks, multiple firings allow accounting for firing-to-firing variability, and in this case, a minimum of 2 firings is recommended.

  But conducting multiple firings on a FM satellite is usually considered impractical, and only one firing is applied. The system level test is then used to demonstrate the adequacy of the equipment level shock requirement, and in this case the qualification margin is demonstrated at equipment level.

13.1.3 Mounting conditions

The following mounting conditions of the unit need to be established:

- Representative mounting points, including fasteners dimensions
- Representativeness of the supporting structure,
- Shock isolator if used on real configuration,
- Bracket if used on real configuration,
- Thermal filler if used on real configuration.

13.1.4 Test article operation

It is important that the tested equipment is **powered-on and properly monitored** where relevant (e.g. equipment powered-on during launch).

For propulsive elements, it is required in ECSS-E-ST-35C that the test configuration is flight representative especially with respect to operative pressure. For instance, if the functional behaviour (e.g. closed or open valve) of the unit is modified with or without any pressure, this standard requires that the most representative conditions are used for the test. Moreover, this implies that if additional equipment is necessary to pressurize the unit during test, it is mounted in a representative configuration or at least without interference with the tested unit configuration (e.g. not too close to the unit interface).

13.1.5 Safety and cleanliness

The applicable safety and contamination and cleanliness requirements on the unit under test H/W part of the PA requirements for the unit. Beside the requirements borne by the unit under test, there can be additional safety requirements and safety procedures from facility point of view to be taken into account. To ensure safety and cleanliness during shock test as a minimum the following points are checked with regard to the applicable specifications prior to a test campaign:

- Compliance to environmental conditions i.e. temperature, humidity etc.
- Compliance to contamination levels
- Recording of environmental and contamination conditions e.g. temperature gauges, particle counters, witness plates

13.1.6 Instrumentation

The sensor type, number, location and mounting condition affect greatly the test result and it is therefore important that they are prepared with particular attention.

The following are recommendations for carrying out a correct instrumentation of the equipment shock test:

- A minimum of two sensors at opposite corners of the tested unit. For some test setups and test specimen configuration it is advisable to use more sensors to characterise the shock input, in particular in cases for which large scattering is expected e.g. large specimen, elastic support structures etc..
- Locate measurement points designated to record the shock levels at equipment interface at the closest location with respect to the physical interface.
- Ensure that such instrumentation is able to demonstrate good shock levels homogeneity at the equipment interface.
- Ensure that such instrumentation is able to measure the shock levels in all three axes and not only in the main excitation direction. Use of a mounting cube is acceptable provided that its natural response is not excited. For pyro shock tests mounting cubes should be avoided due to excitation in range of cube resonance frequency.
- Ensure that the selected instrumentation and acquisition system is able to acquire the shock levels with the resolution and in the frequency band required (see also Section 13.4 for sensor selection).
- Provide a complete set of photos covering the entire instrumentation.

13.1.7 Test tolerances

In addition to a specification should always be provided a test tolerance as it is impossible to precisely get the required shock environment, whatever the test facility is.

The definition of the test tolerance is a compromise between the risk of under-testing, versus the risk of over-testing, considering also the potential conservativeness of the specified environment.

The ECSS-E-ST-10-03C specifies a test tolerance of -3 dB/+6 dB across the full spectrum, which is achievable on most shock bench, owing that an adequate calibration test campaign is conducted:

- The lower test tolerance of -3 dB is a minimum requirement to ensure coherence with the qualification margin.

  The lower test tolerance is sometimes tailored to 0 dB up to the corner frequency (typically around 1 kHz – 2 kHz), to guarantee a minimum qualification margin of 3 dB within the critical

frequency range of the unit. Such tailoring is typically adopted once the specified shock environment has been consolidated with a system level shock test.

- Whereas the upper test tolerance of +6 dB acts as the upper bound to reduce the risk of failure.

  Yet again, it is important to pay dedicated attention to critical frequency ranges of the tested unit, in order to limit the potential over-testing within those ranges.

As discussed in the paragraph 13.1.6, a minimum of two sensors should be placed at opposite corners of the tested unit. The verification of the requirement on test tolerance is done considering the average of those two sensors, with an additional constraint on homogeneity (no more than 6 dB between the two sensors, in order to ensure a proper excitation of the unit).

NOTE In cases for which large scattering is expected e.g. large specimen, elastic support structures etc. the homogeneity of 6 dB may be difficult to achieve. Any deviations are discussed on case by case basis with the customer to ensure avoidance of over or under testing.

NOTE A reported practice consists in a qualification by slices, the unit being rotated after a few applications for example. The number of shock applications per direction for the axis are agreed with the customer to avoid over testing.

13.1.8 Test success criteria

The test is considered as successful if:

- The tolerances presented above are not exceeded.
- The maximum of the measured transverse excitation values does not exceed the transverse specification applying upper tolerance.
- The equipment functional behaviour is within the specifications after the test, and its structural integrity is preserved.
- All test data is recorded, stored and suitable for further exploitation.

13.2 Criteria for test facility selection

To choose a test facility, it is necessary to be aware of the following concerns:

- Representativeness w.r.t. real shock environment: this means the capability of the test facility of allowing a correct representativeness of the produced shocks. The following points are of relevance:
    - *Type of shock environment*: it is important that the **test facility is adapted to the desired type of shock environment** (near-field, mid-field or far-field – see 12.3). For instance near-field pyrotechnical shock characteristics can only be reached by test facilities using pyrotechnical shock sources whereas far-field pyrotechnical shocks characteristics can be obtained by more various test facilities.
    - *Shock duration*: It is also important that the test facility, e.g. a shaker is able to generate shocks as a **unique impulsion lasting for the specified effective duration**. The "effective transient duration," Te, is the minimum length of time that contains all significant amplitude time history magnitudes beginning at the noise floor of the instrumentation system just prior to the initial most significant measurement, and proceeding to the point where the time history amplitude is a combination of measurement noise and substantially decayed structural response (see 15.3.1). Special care needs to be taken for tests on electrodydnamic shaker systems in order to ensure representative transient duration.
- Physical adequacy with test specimen: this means that the test facility respects the needs in terms of mass capacity and dimensions.
- Adequacy with test specification: this means the capability of the test facility to generate shock that respect the specification. A pre-test with a mass dummy is recommended. This covers the following points:
    - *Shock levels over frequency* taking into account the test tolerance (see 13.1.7). This concerns the capability of the test facility to tune the generated shock levels to comply with the specified levels (usually in the form of a SRS). This point is not as obvious as it appears: some test facilities can be unable to sufficiently tune the frequency content of the generated shock to be compliant with the required shock levels, including test margins.
    - *Boundary conditions*: this concerns the capability of the test facility to represent the specified boundary conditions, which generally means an equipment clamped on its interface. In this case it implies the representativeness of stiffness of the supporting structure w.r.t. to the real mounting conditions of the specimen.
    - *Multi-axis shock ability*: this concerns the capability of the test facility to produce shocks in several directions with respect to the specification.
    - *Space correlation of interface accelerations*: this concerns the capability of the test facility to generate representative and homogeneous inputs around the test specimen (see 13.1.7).
- Repeatability: this means the capability of the test facility to generate completely repeatable shocks. This means that with identical initial conditions, two successive shocks produce the same response, or at least with a discrepancy much lower than the test tolerances. Typical achievable repeatability values are summarised in the subsequent table.

Method / Type of facility	Typical Achievable Repeatability i.e. difference in SRS between
Facility under procedure II	• For usual shock levels: between 1 and 2dB • For high shock levels (not reachable with others test benches): between 2 and 3dB
Facility under procedure III	0,2 to 2 dB
Facility under procedure IV	Lower than 1 dB

- Advanced criteria in term of representativeness of shocks: the following are relevant criteria to ensure representativeness:
  - The frequency content and the frequency density of the generated is as close as possible the real shock environment, if such a piece of information is known.
  - The relative phasing of the different frequency components is as close as possible to the real shock environment, if such a piece of information is known.
- Capability of the data handlings system: this concerns to the capability of the test facility to condition, record and store a sufficient number of sensor signal with a sufficiently high sampling rate and to deliver the test data in a format which is suitable for further exploitation.
- Experience of test house or test engineer: this can also be a selection criteria in particular for complex setups and configurations.

13.3 Test methods and facilities

13.3.1 Basis

The following procedures are derived from [RD-049], [RD-052].

13.3.2 Procedure I – System level shock test

13.3.2.1 Test configuration

A crucial point, as for any mechanical test, is the representativeness of the test configuration and especially the system boundary conditions. Boundary conditions of most current system level shock tests are discussed here below:

- Clampband release: LV adaptor and spacecraft hoisted on a crane (representative of free-free condition), and clampband tension set as close as possible to its maximum value during flight. The assembly is hoisted using a dedicated lifting frame; a foam mat (thickness around 10 cm) is placed under the test article in order to damp the free fall (drop height around 5 cm) of the LV adaptor once the clampband is released. See Figure 13-1 (left picture).
- SHOck Generator UNit (SHOGUN): Identical boundary conditions as clampband release. The Shogun device is bolted to the LV adaptor lower interface, and then actuated. The shock impulse is created by the expansion pyrotechnic linear cord and the rupture of the weakened section.

- VESTA (Vega Shock Test Apparatus): spacecraft and adapter are integrated on the VEGA 4th stage structure with a flight representative boundary condition. The complete assembly is then supported by air springs placed beneath the 4th stage structure.
- Appendage release (solar array or antenna reflector): it is not necessary to have a free-free configuration as the boundary conditions for the appendage and its supporting structure are made by the neighbouring parts of the structure and not by the spacecraft global boundary conditions. However installation of zero-g compensation equipment is usually necessary.
- Real launch vehicle stage separation: When fully representative LV stage separations are performed at system level, the test configuration and the associated boundary conditions are more complex as several pieces of structure are involved. An example is given in Figure 13-1.

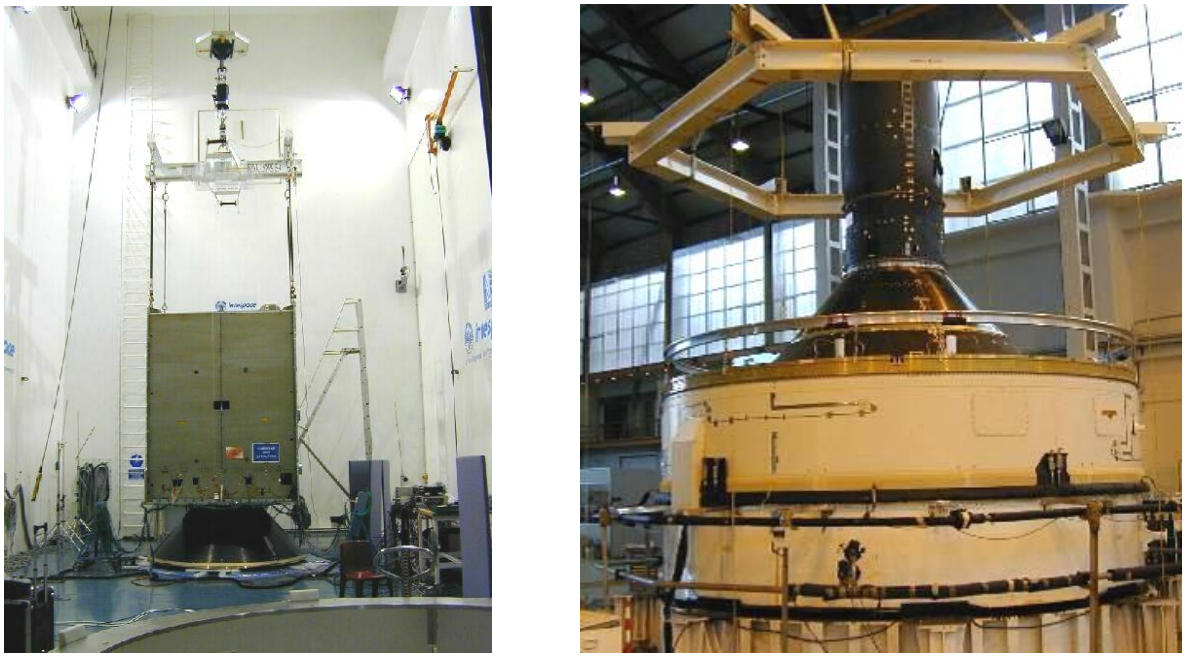

Figure 13-1: Examples of system test configuration and boundary conditions (clampband release on the left and Ariane 5 VEB separation on the right)

13.3.2.2 Shock test required by Launcher Authority

13.3.2.2.1 Spacecraft separation test

a. Clamp-band release

Spacecraft separation test is usually part of the fit-check operation. This functional test is also useful for shock verification purpose (in particular for non-recurring spacecraft specimen). As for any shock test, the boundary conditions are essential. Therefore, a drop test is mandatory for the spacecraft separation test in order to reproduce the physical separation of the Spacecraft from its adapter. A single release test without liberation of the Spacecraft is not representative enough and should not be conducted for shock verification.
In a nominal situation, the demonstration of the spacecraft's ability to withstand the separation shock generated by its separation from the launch vehicle should be based on the following method :
A clamp-band release test is conducted with the tension of the band set as close as possible to its maximum value during flight. During this test, interface levels and equipment base levels are measured. This test can be performed on the STM, on the PFM or on the first flight model provided that the spacecraft structure close to the interface as well as the equipment locations and associated supports are equivalent to those of the flight model.

The induced shocks generated on spacecraft equipment units measured during the abovementioned test are then increased by:

- +3 dB uncertainty margin aiming at deriving flight limit environment from the single test performed in flight-like configuration; [NB: In case two clamp band release tests are performed, the maximum of the two test is retained and this +3dB uncertainty margin can be removed.]
- +3 dB qualification factor aiming at defining the required minimum qualification levels, to be compared to the qualification status of each spacecraft subsystem and/or equipment.

These obtained shock levels are then compared to the qualification status of each spacecraft subsystem and/or equipment.

NOTE If the drop test is not performed at the maximum tension foreseen during flight, additional margin may be required by the launcher authority.

A typical scattering on spacecraft interface shock levels, observed by two consecutive clamp-band release tests, is shown in the following figure. A good agreement was observed in the low frequency range up to the main breathing frequency, whereas a larger scattering (typically +/-3dB) was observed in the higher frequency range.

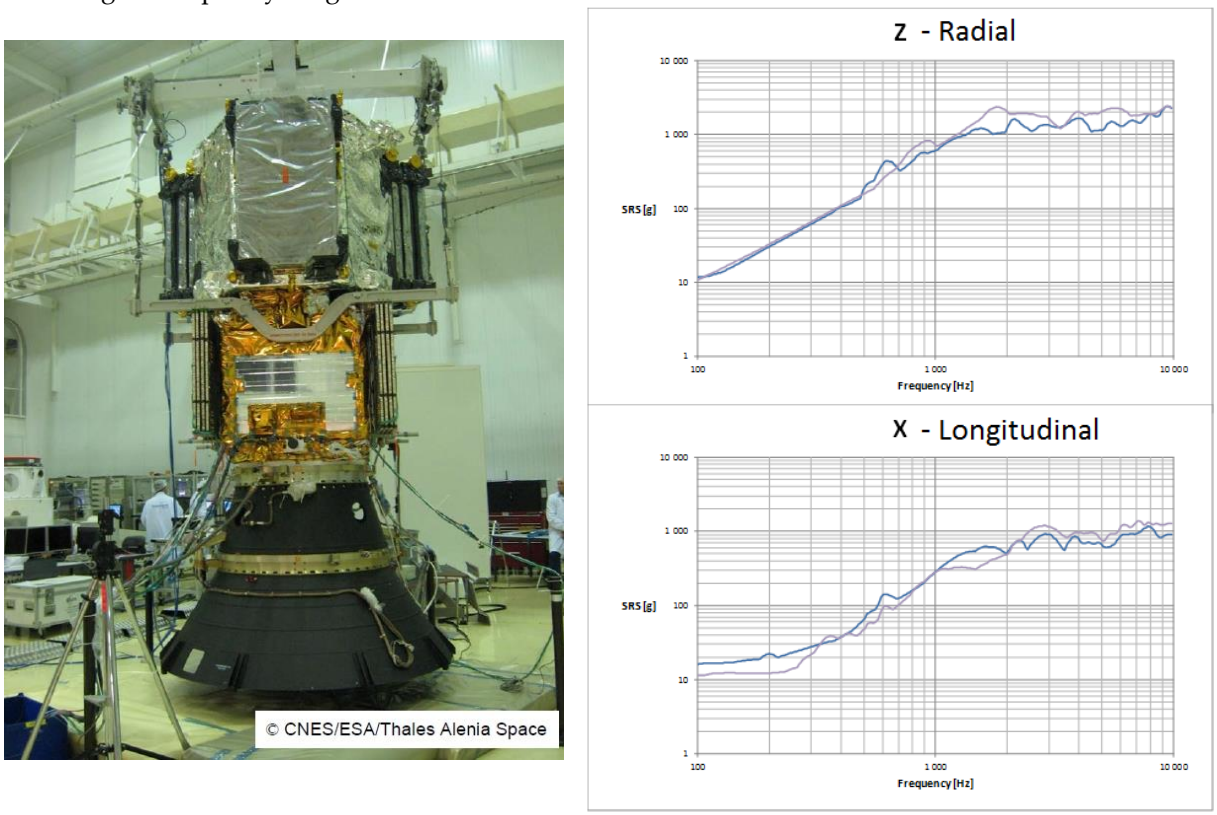

Figure 13-2: Two consecutive clampband release tests on Proteus platform – Comparison of shock levels at spacecraft interface

b. Pyronuts release system

Similarly to the clampband separation test, a particular attention should be paid to the boundary conditions. They should be as representative as possible, compared to the flight conditions.

Thus the spacecraft should be hung as shown in Figure 13-3 and after firing, the pyronut is dropped.

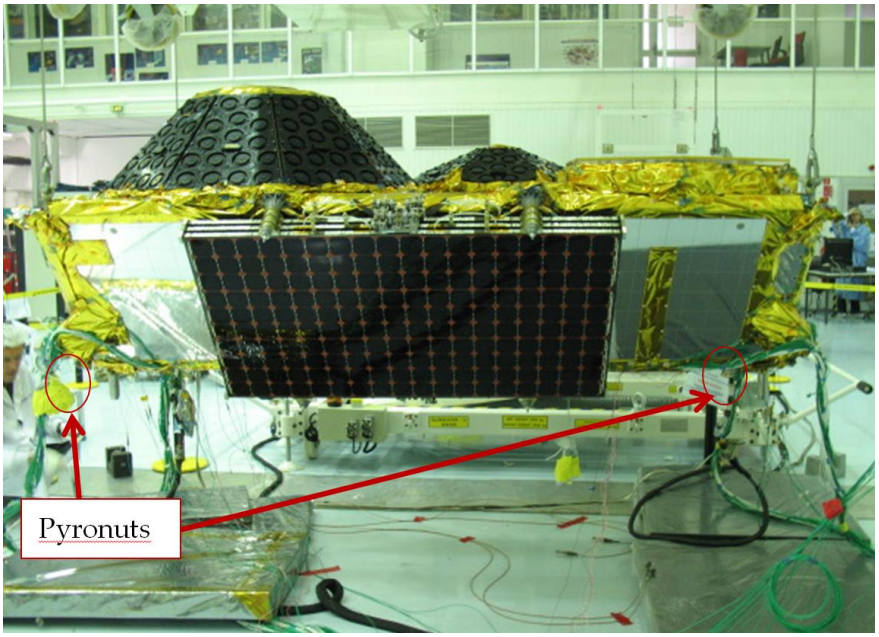

Figure 13-3: Configuration for shock test with pyronuts

13.3.2.2.2 Launch Vehicle induced shock test

Specific shock methods required to cover specificities of Launcher shocks in case the Launcher shocks are not covered by the spacecraft release event. This is typically the case for Ariane 5 and VEGA, but this can also concern launchers in case the severity of the LV induced shock is seen higher than the severity of the spacecraft release event.

Ariane 5/SHOGUN method.

This paragraph presents the current derivation method for Ariane 5 based on a Shogun test, and is representative of a HSS1 like separation system for the fairing. Owing to continuous development on the launcher, the induced environment by the launcher towards the spacecraft has seen its severity reducing over the past years, and the introduction of a new design of the fairing separation system will further improve the situation from mid 2015.

As compared to other launch vehicles, the Ariane 5 qualification methodology is different since shocks induced by separation of stages are not covered by shocks induced by clampband release, neither in level nor in type of shock. Hence a specific test device, the **SHOGUN** (SHOck Generation UNit), is proposed by the Ariane 5 launcher authorities in complement to the clampband release test, to cover the specificity of these high energy stage separation shocks.

This device is not able to generate all qualifying Ariane 5 shock levels. Hence an alternative spacecraft qualification approach is required. This approach combines the average shock level at the spacecraft interface with a “shock transfer function” between the spacecraft interface and the equipment interface as shown in the following flow chart.

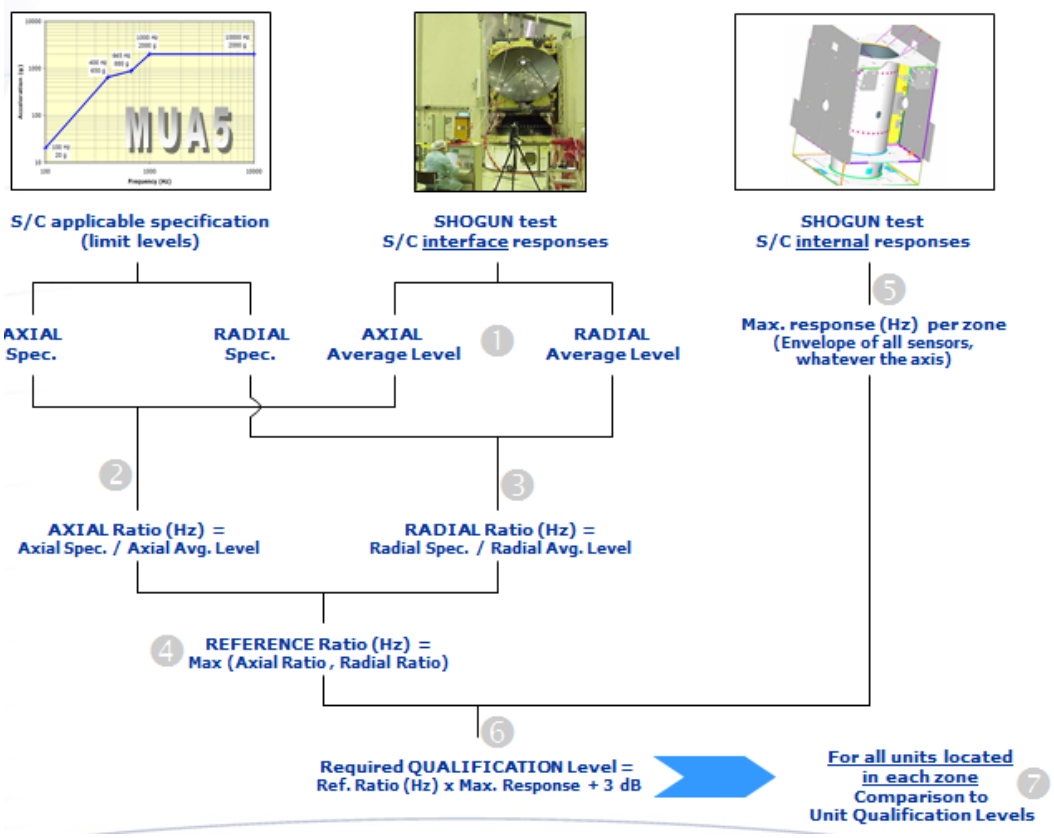

Figure 13-4: Scaling "max ratio" methodology

1. From shock measurements at SC interface during Shogun test, calculation of the average level of each direction separately : axial & radial,
2. Determination of the ratio between the LV axial limit level (applicable specification) and the Shogun axial average level for all frequencies,
3. Determination of the ratio between the LV radial limit level (applicable specification) and the Shogun radial average level for all frequencies,
4. **Calculation of the "reference ratio", which corresponds to the maximum of axial and radial ratios** ***(Nota : reference ratio is frequency dependent),***
5. From Shogun test data, determination for each spacecraft internal zone (bottom deck, shear walls, lateral walls, upper deck, etc. …) of the maximum recorded shock environment (envelope of all the measurements located in the zone, whatever the axis),
6. For each spacecraft zone, application of the "reference ratio" to the maximum shock response, to determine the predicted flight limit environment in the zone due to the applicable interface shock specification

   ➔ definition of unit level shock requirement throughout the spacecraft, including addition of +3dB margin to derive qualification environment level,
7. Comparison of resulting spectrum with equipment qualification level, derived from unit specifications of maximum tested levels (shock, random, sine, CB release, design factor)

This "max ratio" methodology is highlighted through the following example :

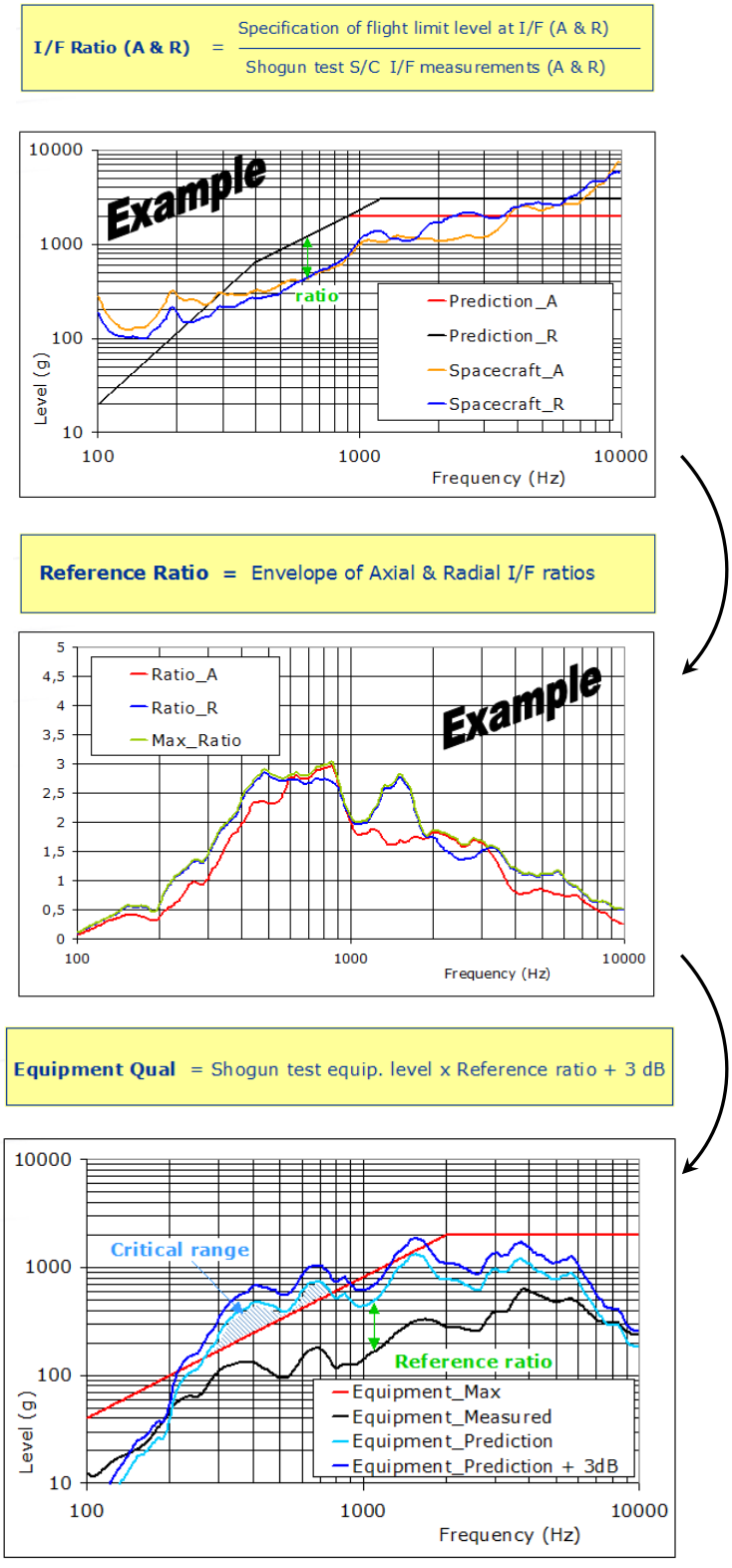

Figure 13-5: Example for "max ratio" application

This process is the standard approach recommended by Arianespace. However, the use of the maximum ratio as a reference ratio requires a **well-balanced input levels** at S/C interface in terms of axial and radial magnitudes (typically axial and radial averages agree at all frequencies to within 3 dB). Otherwise, the methodology becomes too much conservative and constraining.

Indeed, using the max ratio means that equipment response (i.e. its maximum) is rather driven by the minimum response at the S/C interface than by the maximum one. This is not usually the case in a shock condition (not harmonic) but the margin provided with this max ratio methodology brings good robustness for the global shock qualification process. In case of unbalanced inputs, the max ratio could become unrealistic and it could generate high virtual amplification factor and virtual concerns at unit level.

If it can be demonstrated at unit level that response is driven by a dedicated direction, the associated ratio can be used instead of the max ratio. For instance, close to the interface ring, it can be demonstrated that unit radial response is due to radial input and axial response due to axial input.

As it is a deviation to the standard recommended methodology, the application of a "directional" ratio should be justified to Arianespace and approved.

VEGA/ VESTA method

Similarly to Ariane 5, The VEGA induced shocks by fairing or stage separation events are not covered by shocks induced by the spacecraft release. As such, a specific tool has been developed, so-called **VESTA** (VEga Shock Test Apparatus), in order to support the qualification of spacecraft.

VESTA aims at generating a shock at the spacecraft bottom interface representative of the Vega separation events (fairing jettisoning and interstage 3-4 separation). Since the driving event is the fairing separation for most of the frequency spectrum, VESTA simulates the release of the fairing belt at the base of the payload adapter. The belt release is, indeed, much easier to manage, in terms of necessary hardware and operations.

The tool (see Figure 13-6) is built from several stage/component full scale mock-ups used during the VEGA development and consists in a flight representative model of the VEGA upper composite. It is composed by the following parts:

- VEGA 4th stage flight representative structure
- A VEGA 937 payload adapter
- The fairing boat-tail sector
- The fairing HSS (Horizontal Separation System)
- A payload clamp-band
- Shock acquisition system.
- Firing box unit

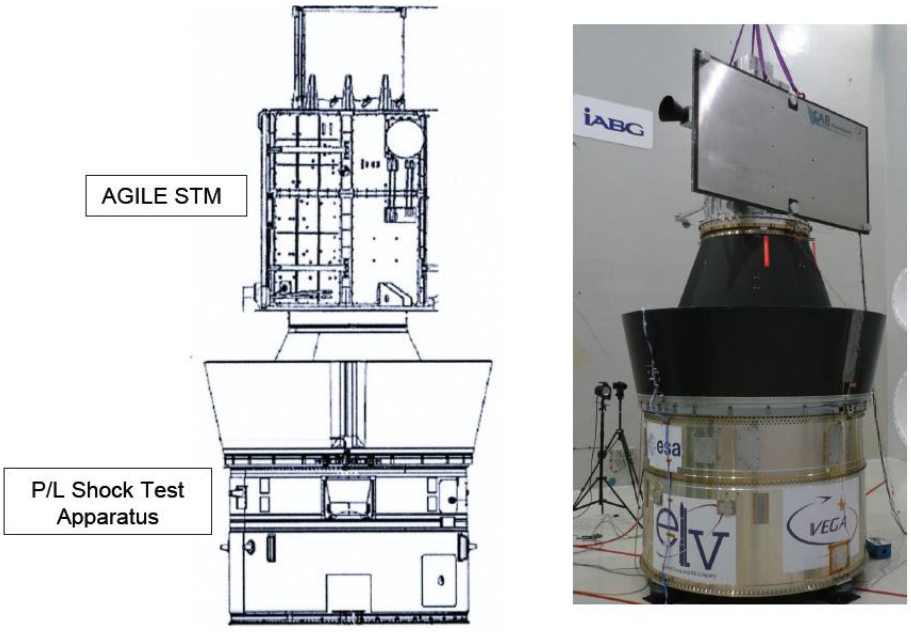

Figure 13-6: VESTA with AGILE STM

The shock level at the spacecraft base is driven by the tension applied in the HSS belt. Repeatability of the shock input is assured by the application of the tension in the HSS belt with an accurate procedure (same procedure as per flight) and measurement/monitoring of the load in the tensioning bolts. The SRS is dominated by the response of the adapter ring mode at about 800 Hz, which is experienced as a global mode by the Spacecraft.

The main peculiarity of the VESTA tool is that the shock levels can be tuned by adjusting the tension of the HSS belt at a certain value. This allows to meet possible constraints identified by the customers on the maximum levels in order not to over-test the test article. It is worth to note that the test can be conducted up to the HSS tension foreseen at the time of the Fairing separation (i.e. including thermal effects during flight).

The tool has already been validated by test and has demonstrated to be a suitable tool for the qualification of payloads to be flown on VEGA. In particular, the validation test campaign has been conducted using the AGILE STM (see Figure 13-6), while the first test campaign has been conducted on a Lisa Path Finder PFM spacecraft.

The above test campaign allowed to verify the validity of the linear extrapolation recommended for the evaluation of the shock levels at the in-flight value of the HSS belt tension when test results at low tension value are known (see Figure 13-7).

Then the following "linear extrapolation law" can be used (where T2 and T1 are two different values of HSS belt tension):

$$SRS(f, T_2) = SRS(f, T_1)\frac{T_2}{T_1}$$

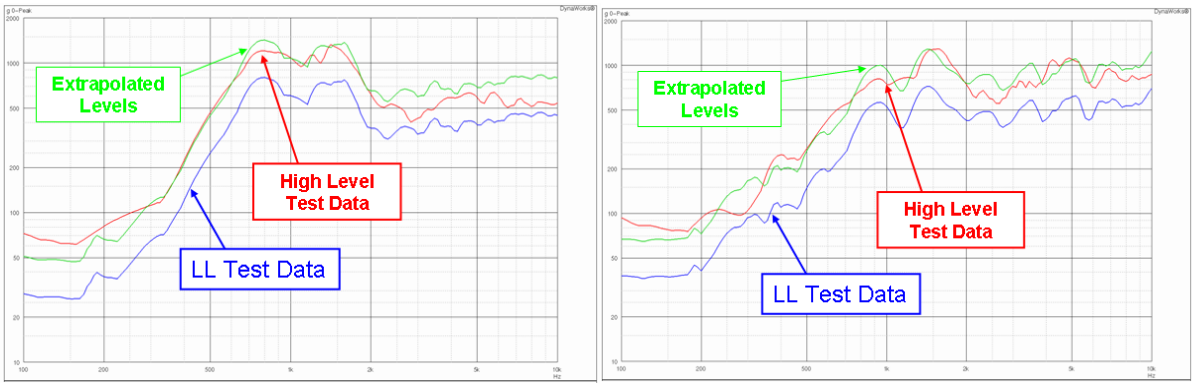

Figure 13-7: Effect of HSS belt tension on shock levels and validation of linear extrapolation (axial levels on the left, radial levels on the right)

As far as the test sequence is concerned, the following methodology should be followed:

- A base line of two tests is recommended
- Low Level test: first test at a low HSS tension (TL) of 20-25kN (i.e. ~1/4 flight tension)
- High Level test: second test at higher tension (TH), as high as possible considering spacecraft constraints.

After the above tests are performed and the linear extrapolation law is verified, the following methodology is recommended for the evaluation of results at sub-system level (see flow chart in Figure 13-8):

8. If TH is lower than the in-flight HSS tension, apply the "linear extrapolation law" to the results of the High Level test with T2=80 kN and T1=TH for each measurement location (on each measurement direction).

9. Shock limit levels determination:

   (a) For f ≤ 3kHz, the SRS derived from the linear extrapolation law (see point 1 above) are considered as flight limit levels (FLL). In fact, the fairing separation event induces levels at the top of S/C adapter is higher than stage event levels in this frequency range.

   (b) For f > 3kHz, the SRS derived from the linear extrapolation law (see point 1 above) is multiplied by the ratio between the level found at point 1 at the top of the S/C adapter interface and the VEGA UM applicable levels.

   NOTE The above approach is based on experiences gathered from the VEGA maiden flight and may be re-assessed as new flight data become available.

10. Definition of unit level shock requirement throughout the spacecraft, including addition of +3dB margin to derive qualification environment level

11. Comparison of resulting spectrum with equipment qualification level, derived from unit specifications of maximum tested levels (shock, random, sine, CB release, design factor, …)

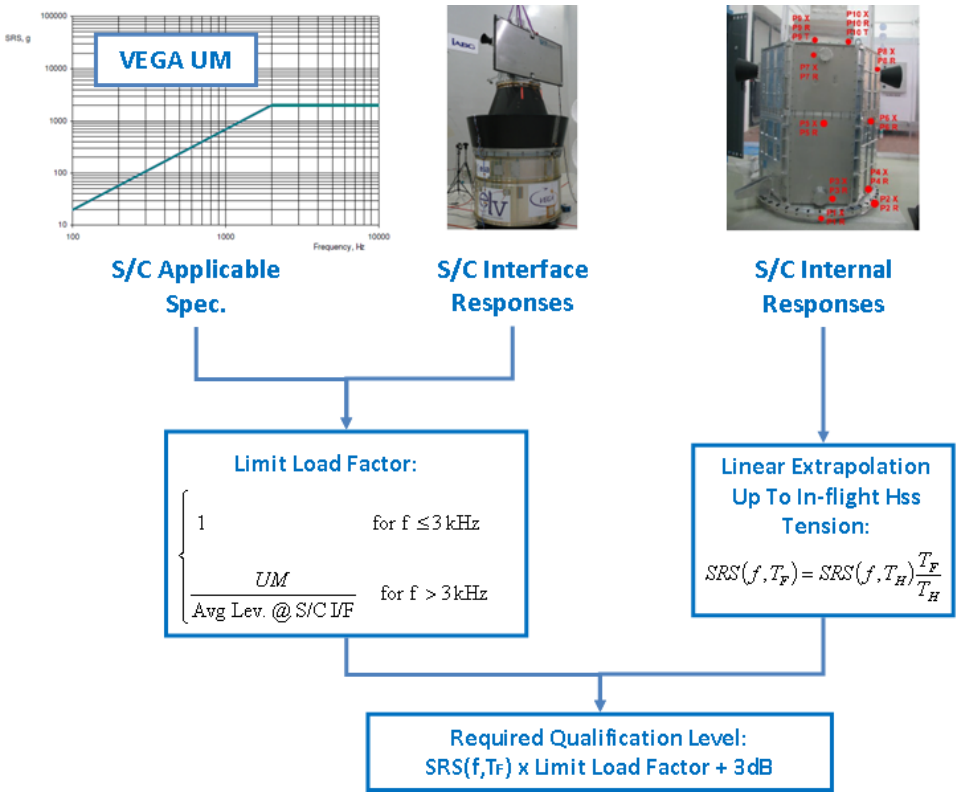

Figure 13-8: Methodology for VESTA test results evaluation at S/S level

13.3.2.3 Shock test required by Spacecraft

13.3.2.3.1 Actuation of hold-down and release mechanisms (HDRM)

Several appendages are typically stowed for launch configuration in order to fit the fairing volume, and then released and deployed once in orbit. This is the case on almost all spacecraft, with the solar arrays stowed as a stack of panels and deployed in several phases in space. For telecommunications satellites large reflectors are also stowed and released once in orbit. On scientific spacecraft sometimes it is necessary to open protection covers in space.

Courtesy of THALES ALENIA SPACE

Figure 13-9: Example of a telecommunication spacecraft with deployed and stowed appendages (solar arrays and reflectors)

The proper functionality of the associated mechanisms and sometimes the deployment kinematics are validated on ground through specific tests. This is usually verified during a release test where the acceleration levels are also measured in order to validate the qualification of the spacecraft with respect to the associated shock environment.

Courtesy of THALES ALENIA SPACE

Figure 13-10: Example of release of solar arrays (left: intermediate position; right: final position)

Courtesy of THALES ALENIA SPACE

Figure 13-11: Example of release of reflectors

An adequate instrumentation is therefore defined following the path of the shock wave, and the SRS are computed at the interface of the concerned equipment units. A qualification margin of 3 dB is added to these measurements. Qualification of the spacecraft with respect to this shock environment is then declared when all the units' qualification status is above the measurement at their interface including a qualification margin.

13.3.2.3.2 Latching "shock"

When an appendage is released, the final operation consists in latching it so that it remains in its final position. Latching mechanical environments are abusively called "shocks" as they are a sudden event. But they are in fact a very low frequency event (of the order of 1Hz) and demonstration of the acceptability of the induced environment is usually established based on the max temporal response.

13.3.2.3.3 Pyrovalves actuation

Pyrovalves are part of the propulsion subsystem as they allow to definitely open or close a fluid circuit. As described in details in Section 12.7.2, they cannot be actuated at system level on a flight satellite, as it would be necessary to replace the pyro-valves which are welded to the tubing. Therefore no test is performed at system level on a flight satellite, and the qualification with respect to the associated shock environment is demonstrated through a specific methodology.

The principle of this methodology is to perform test on a representative test bench and derive a Maximum Expected Environment (MEE) taking into account the scatter in the measured levels (see Section 12.7.2.3.3 for detailed explanations). Qualification of the concerned units is then declared when their respective qualification levels are above the MEE+3dB.

13.3.2.4 Test sequence

The standard test sequence (called "Test Block" in ECSS-E-ST-10-03) for a system level shock test contains as a minimum:

- Test Readiness Review (TRR, as per clause 4.3.2.2 of ECSS-E-ST-10-03).
- Test rehearsal: A test rehearsal (also called dry run), is performed prior the live firing of the pyro devices. During the test rehearsal, the procedure to be executed during the test campaign is checked. Checking in this stage, means that the procedure is followed with the shock actuators disarmed and in safe condition. As part of the dry run, the measured data are checked, verifying the absence of influence of the firing signal (short and high power) on the other measured channels (i.e. over the ground). It is worth to be mentioned that some tap test(s) are performed before the dry run, to check that all instrumentation is working correctly.
- Test Performance: Test execution according to specified procedure.
- Post Test Review (PTR, as per clause 4.3.2.3 of ECSS-E-ST-10-03)

  As part of the PTR, and before further use of the recording of pyroshock data, it is important to ascertain the quality of these data based on so-called shock validity criteria (see chapter 15). For general use, the simplified criteria (see paragraph 15.3) is sufficient for determining the validity of pyroshock data. However for some more advanced applications, such as FE simulations which require using some "perfect" time history measurements, the refined criteria based on velocity validation procedure should be applied (see paragraph 15.4).
- Test Review Board (TRB, as per clause 4.3.2.4 of ECSS-E-ST-10-03).

13.3.2.5 System test specificities

At system level, instrumentation is a tough job. It is usually a balance between the necessity to characterise the environment at an equipment interface and to have a good global knowledge of the system behaviour with respect to shock. Therefore the **instrumentation choice should be made carefully**.

Here are some advices to build a correct instrumentation for a shock test at system level:

- The best characterisation of the shock environment for a given equipment necessitates to evaluate the main shock propagation paths. As a matter of fact it is necessary to set the measurement points near an equipment foot at the closest location from the shock source along the shortest shock propagation path. This allows to have the most dimensioning environment.
- Measurement point should be placed very close from the equipment foot: even a few centimetres distance is sufficient to get a measurement different from what is intended because of local phenomena.
- In case an equipment is mounted on a bracket, the shock environment should be placed on the bracket at equipment foot and not directly at the bracket interface: this is necessary to have the right shock environment for the equipment.

A major rule is to always have a complete set of photos covering the entire instrumentation (see Figure 13-12). All instrumentation point should be seen in both close-up (to see its very precise location) and in a more general view (to locate it with respect to the system). This traceability rule is absolutely necessary to build a satisfying test report enabling a good test exploitation.

(general view on the left, close-up on the right)

Figure 13-12: Example of shock instrumentation

The test success criteria consists in validation of input levels and inside measurements (typically 90 % of correct measurements).

13.3.3 Procedure II – Equipment shock test by pyrotechnic device (explosive detonation)

13.3.3.1 Test facility presentation

13.3.3.1.1 Presentation

Pyrotechnic devices generally consist in a fixture excited by an explosive charge. This facility is suited for hardware exposed to near-field pyroshock. However it could also be used for stringent far-field shock environment, pending on the ability of the shock bench to filter the direct shock waves propagation and to bring a modal content in the low frequency band.

Simplest test benches using explosive detonations are composed of single or double plate(s), made either of steel or aluminium.

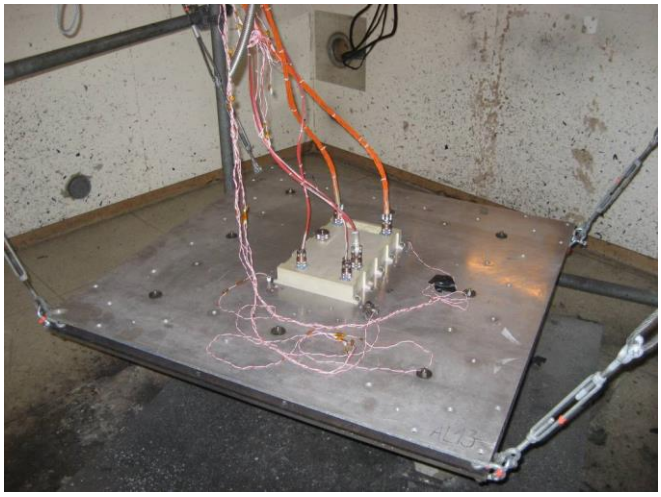

Figure 13-13: Resonant bi-plate

The kind of test set-up is usually suited to qualify units along out of plane axis. However, it leads to difficulties to reach acceptable levels along in plane axes (for unit directly mounted on the second plate) if the specification has to be covered along the three axes at the same time. It can be reached but with an over-testing along out of plane axis, as illustrated here under.

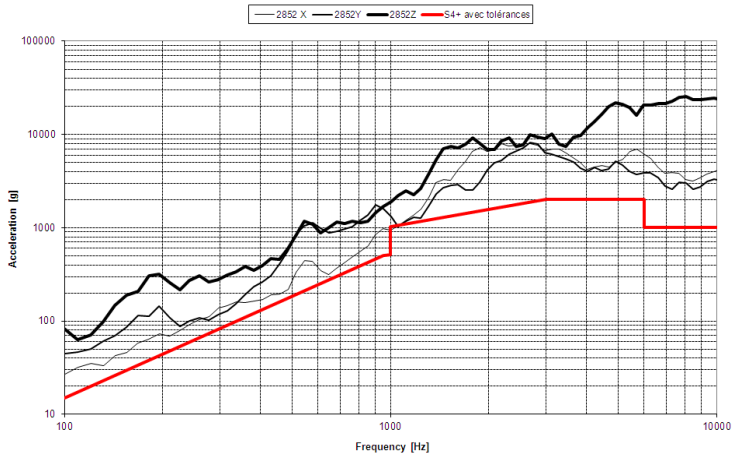

Figure 13-14: Resonant bi-plates set-up – Multi axial shock

More complex structures can also be used, especially to qualify the units axis by axis:

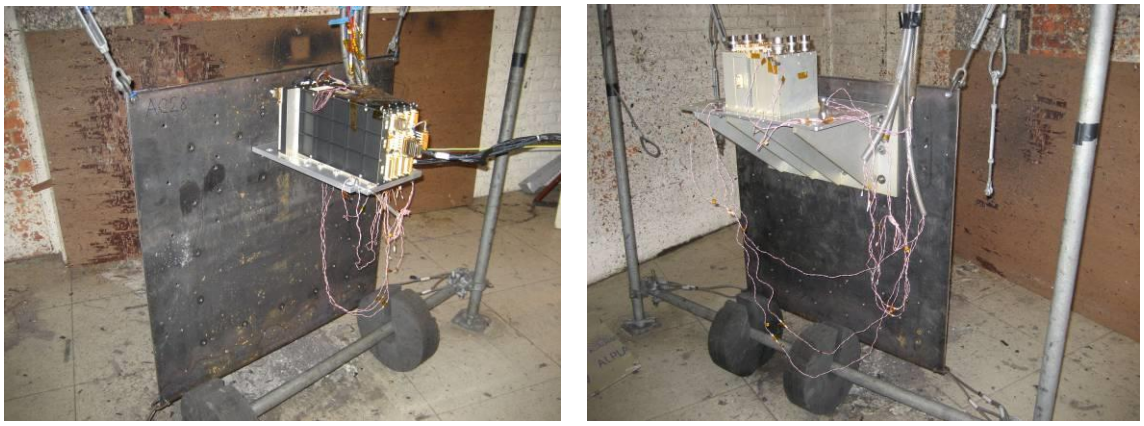

Figure 13-15: Other configurations using explosive excitation

13.3.3.1.2 Illustrations of the different technologies:

The method consists in exciting a resonant plate by explosive charge (e.g. plastic explosive, mild detonating cord) either in direct contact or via a pressure shock wave.

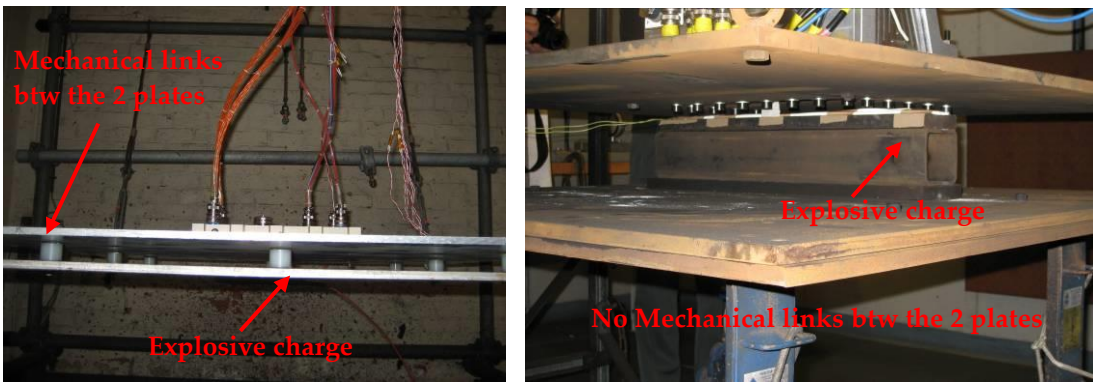

Figure 13-16: Excitation through direct contact (left) and pressure shock wave (right)

A typical time history, achieved with a resonant bi-plate, is shown hereunder.

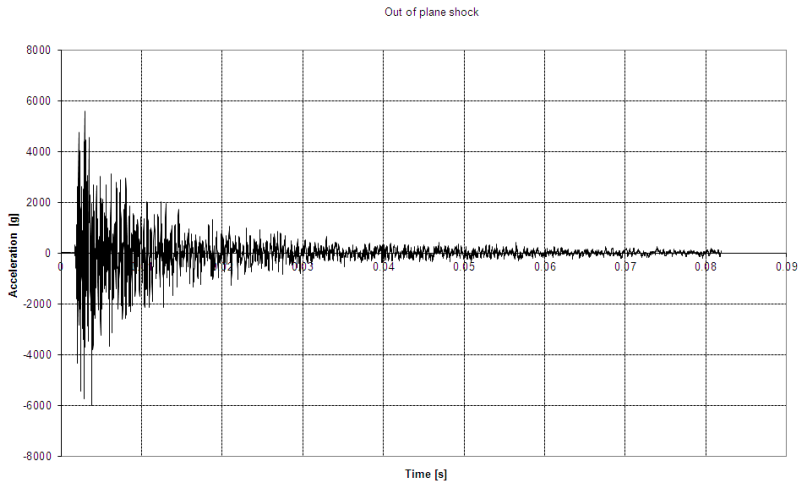

Figure 13-17: Typical time history achieved with resonant bi-plate set-up

Usually, pyrotechnic test benches are used when high shock specifications are required. It is important to pay particular attention to the test tolerance in order to avoid any stringent overtest. Figure 13-18 illustrates a good tuning where high frequency levels are globally within 6 dB over the test requirement.

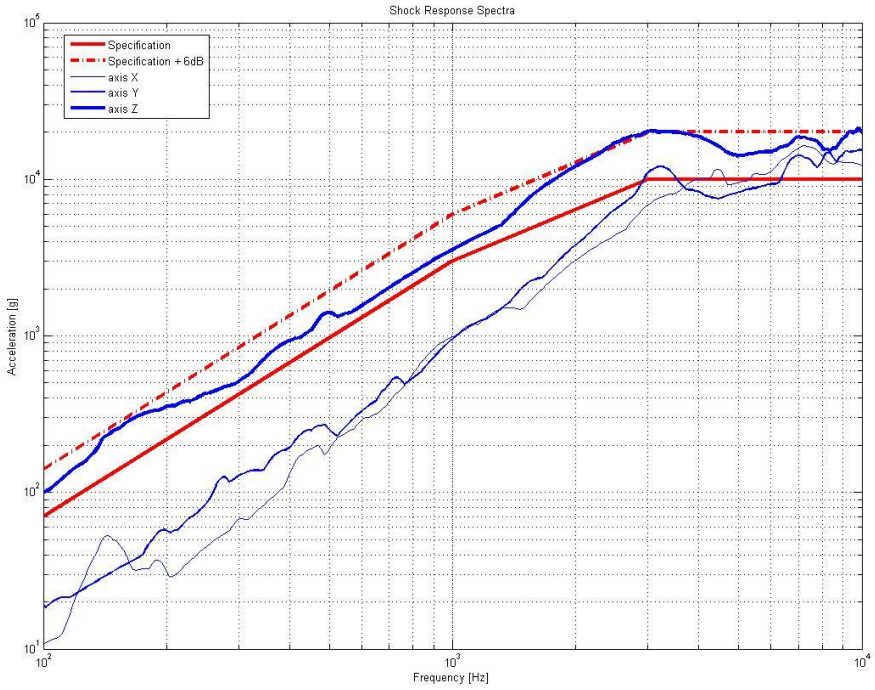

Figure 13-18: Example of pyroshock test for high specification

A fine tuning phase is sometimes difficult to achieve with such a facility.

An adequate tuning requires usually several tests which need to be taken into account in the overall schedule. Following figures show a good calibration stage (in regards of an usual specification) performed on a pyroshock bench leading to results inside the specified test tolerances.

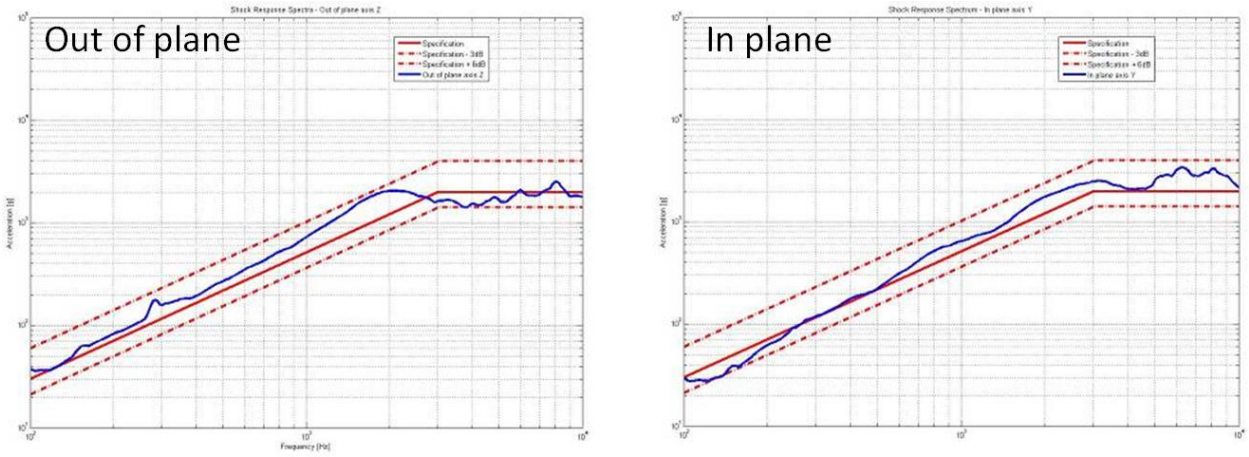

Figure 13-19: Results obtained on a pyroshock facility after adequate tuning

13.3.3.1.3 Repeatability

For "standard" shock levels, a good repeatability can be expected with a test facility using explosive detonation for excitation.

The following graphs show the example of three consecutive identical shocks with measurements along the three axes. It can be seen that the maximum difference between the three shocks is between 1 and 2dB.

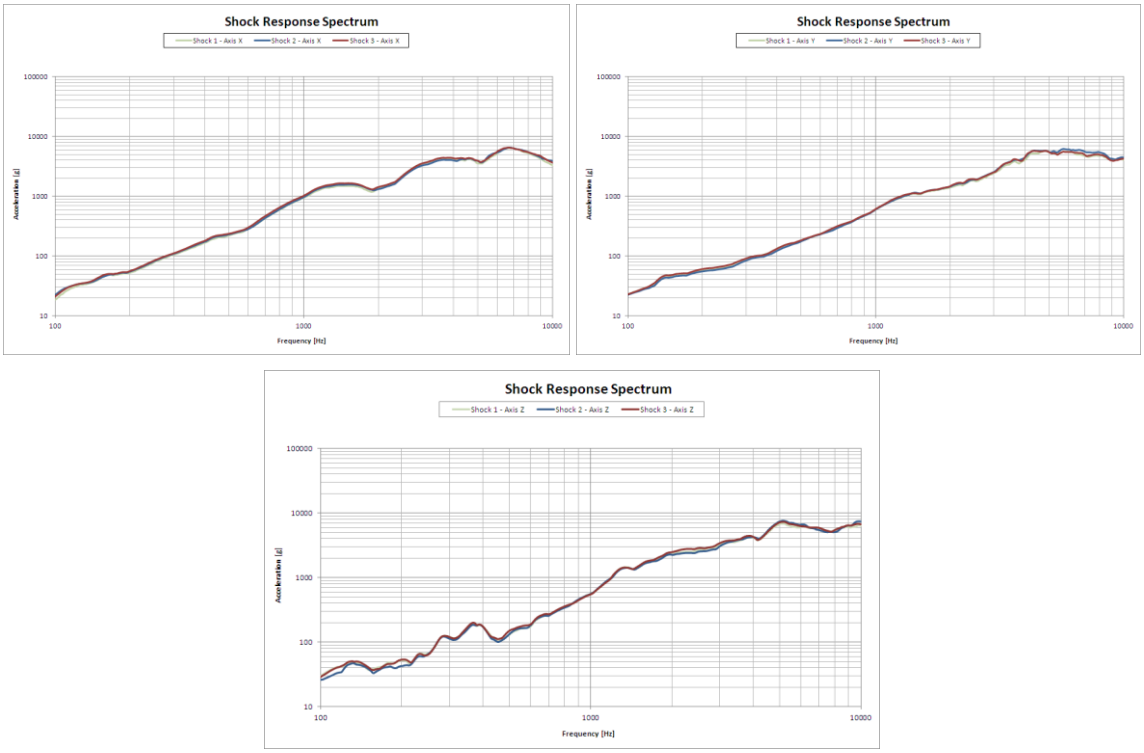

Figure 13-20: Achieved repeatability on a pyrotechnic shock bench (explosive detonation) – Mid intensity shock

For higher shock levels, which imposes using a pyroshock test facility (not reachable by mechanical impact), can lead to a higher dispersion between similar shocks due to the deformation of materials of the test set-up (steel or aluminium plates). In this particular cases of very high levels, the dispersion can reach up to 3dB.

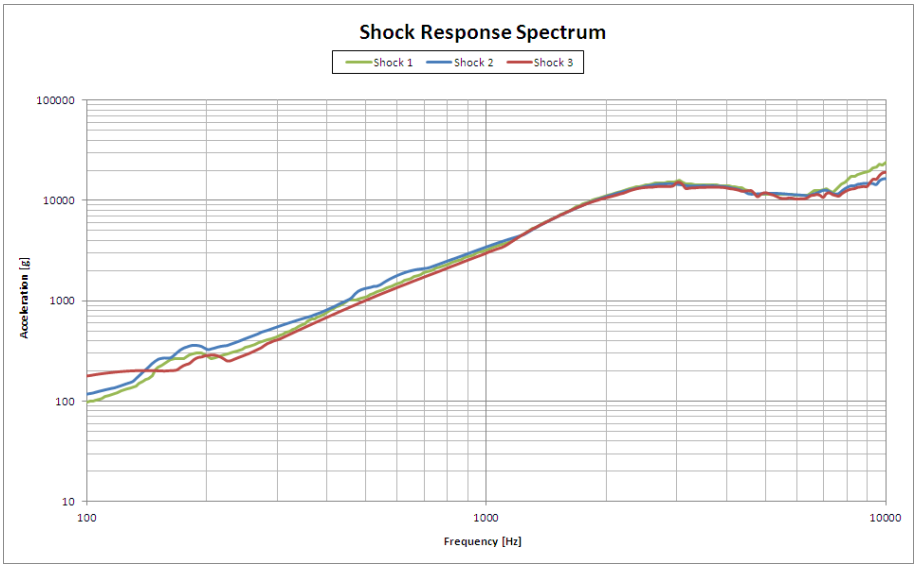

Figure 13-21: Achieved repeatability on a pyrotechnic shock bench (explosive detonation) – High intensity shock

13.3.3.1.4 Representativeness of the interface conditions

Representative conditions are not often known by the equipment providers: mounting on Chotherm, gluing on heat pipes, etc… Additionally, generic shock qualifications (for "products" approach) cannot be dependent of the way of mounting on platform. Thus, the shock tests are always applied on a rigid interface.

When the unit is built with external dampers, the shock qualification has, of course, to be performed using these elements.

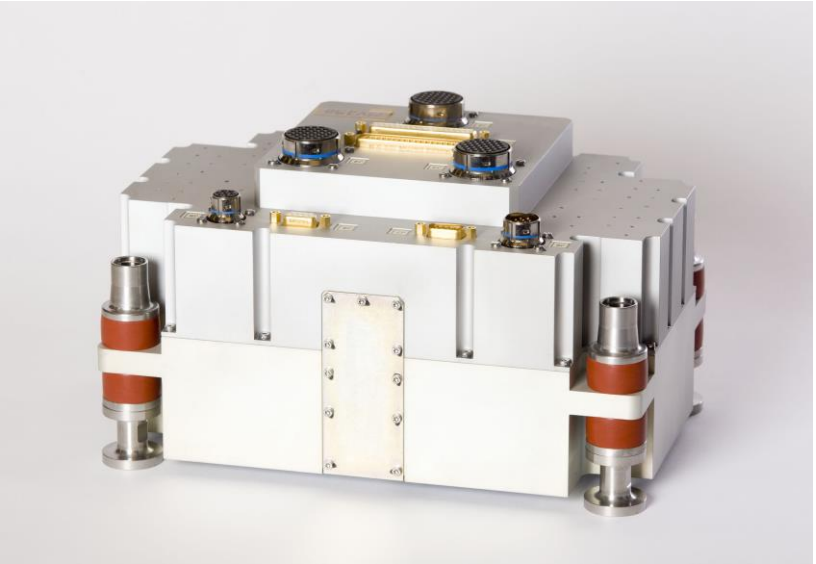

Figure 13-22: Example of a unit with external dampers

13.3.3.2 Test sequence

The standard test sequence for a given axis is as follows:

- Calibration tests on dummy of the unit to test

  Before the test item is attached to the test bench, it is necessary to attach a dummy and obtain measured data under test conditions to be compared with the desired test response. It is important to pay attention so that the pre-test shocks do not degrade the resonating plate configuration.

- Perform calibration shocks until two consecutive shock applications to the representative dummy produce SRS within specified tolerances for at least one axis.
- Carry out the test readiness review
- Nominal shock sequence on test item in its operational mode (e.g. usually three consecutive shocks)
- Carry out the post-test review: a post-test evaluation is carried out to identify any failure in the structural configuration of the test item that even not having a direct impact on the failure of the functioning of the material, it can lead to failure in its in-service environment conditions.
- Data validation:

  Before the recording of pyroshock data are utilized, it is important to ascertain the quality of these data based on so-called shock validity criteria (see chapter 15). For general use, the simplified criteria (see paragraph15.3) is sufficient for determining the validity of pyroshock data. However for some more advanced applications, such as FE simulations which require using some “perfect” time history measurements, the refined criteria based on velocity validation procedure should be applied (see paragraph 15.4).

- Repeat this sequence for each orthogonal axis to be tested if the previous test shock did not meet the test specification in the other axes.

13.3.4 Procedure III – Equipment shock test by mechanical impact (metal-metal impact)

13.3.4.1 Test facility presentation

13.3.4.1.1 Mechanical bench – current technologies

a. Overview

Mechanical impact devices consist in a resonant structure (resonant plate or beam) excited by a mechanical impact of e.g. dropping mass, pendulum or projectile (cannon, airgun, pneumatic piston or powder actuated tool). This **facility is well suited for hardware exposed to far-field shock** environment, inducing similar effects as pyrotechnical shock loads on spacecraft components.

An important rule is that the mechanical impact point on the resonant structure is not located under the unit, to avoid direct transmission of the shock through the baseplate of the unit (i.e. to avoid creating a situation where the maximum of the environment occurs in a location that is not monitored).

b. Mono-plate technology – drop mass

The plate technology is the most used for shock testing [RD-055]. In this family, two sub-families can be distinguished: bi or mono plate.

Major advantages of such concepts are **its low operational cost, predictable behaviour and easy operation**. It generates a spatially uncorrelated excitation of the test unit, thus inducing similar effects than pyrotechnical shock loads on spacecraft components.

If the drop height is controlled and the impact angle of the drop mass constrained then this method inherits a very good repeatability.

The **shock response is driven by the flexion modes of the plate**. **The definition of the plate defines the frequency knee of the SRS**. The definition of a plate bench is preliminary driven by the definition of the plate material, its dimension (size, thickness) and the boundary conditions **constraining** the plate. Also the impact position, the mass of the drop mass and the drop mass/anvil material combination play a role in the tuning of the SRS. It is important to study the position of the equipment on the plate in order to avoid an installation in the nodal line of the natural modes. A Mono plate test bench is the simplest technology but usually it presents a limitation in terms of specimen mass (up to typically 15kg).

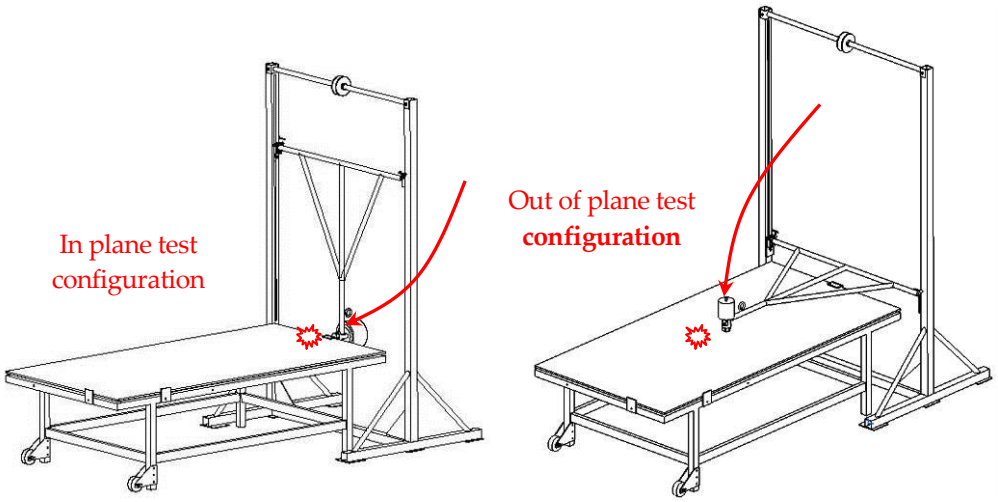

Figure 13-23: Example of a resonant plate bench (ESA/ESTEC)

In plane test

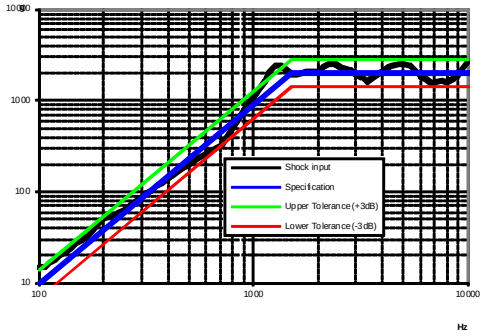

Out of plane test

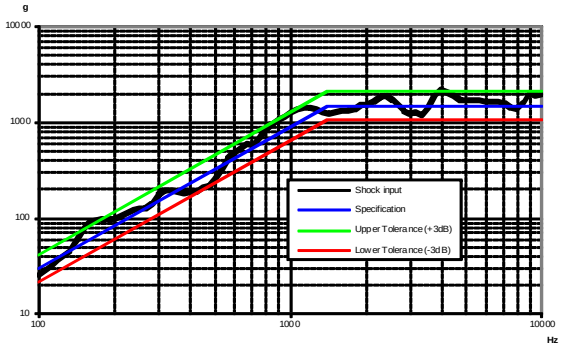

Figure 13-24: Examples of achieved levels on a plate bench (ESA/ESTEC)

The main characteristics of a shock generated by a plate system can be seen in Figure 13-24

— In Plane direction: The 1st elongation traction/compression mode of the plate (around 1200 Hz in that case) is driving the SRS response. In practice, the equipment is placed close to the centre of the plate, in order to limit the amplification seen at this frequency. Another characteristic of the shock input is the poor frequency content of the excitation below the corner frequency.

NOTE In order to overcome the usual limitation of in plane testing (poor frequency content below the corner frequency), the in plane testing is often realized with the addition of a bracket which transfers an out of plane shock input (out of plane test configuration) into an in plane shock towards the unit. Precaution should then be given to the limitation of the cross-axis responses, this is often achieved by centering the bracket in the middle of the ringing plate, in regards of the impact location.

— Out of plane direction: The spectrum is obviously more "full", and a large family of modes are excited across the whole spectrum. The shape of the spectrum is influenced by the location of the unit on the plate (for a generic shock specification,

a good location is usually close to the impact point, i.e. close to the centre of the plate). The low frequency excitation (below 300 Hz) usually exceeds the specification, additional devices such as dynamic absorbers or clamps need to be implemented to decrease the excitation.

c. Mono-plate technology – powder actuated gun

The testing principle is based on the plate technology as describe above. The vibration modes of the used plate / shock table are excited by an impact caused by a powder actuated gun. The following picture shows a test setup during calibration for out-of-plane excitation.

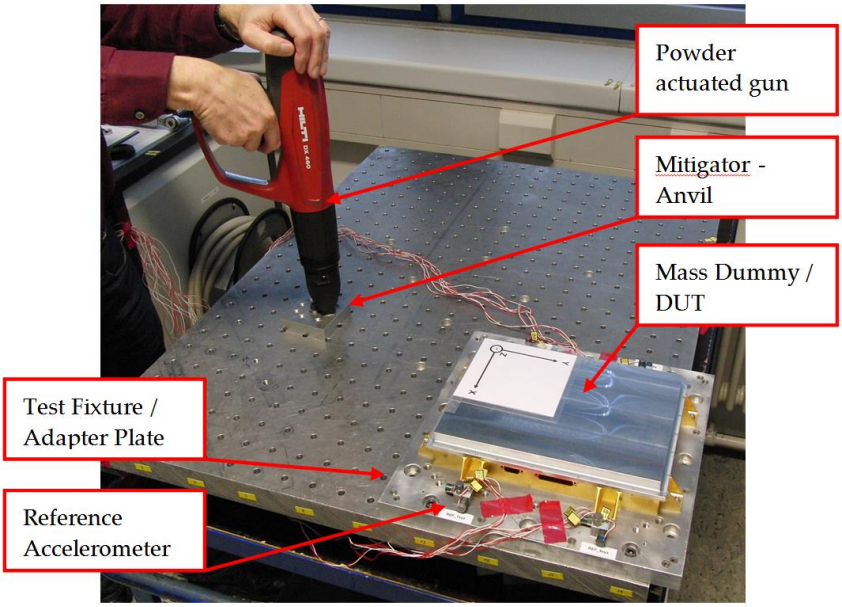

Figure 13-25: Out-Of-Plane excitation with powder actuated gun

The specimen is attached via its test fixture onto the shock table. Its position as well as the impact point and the parameters of the excitation are determined during a series of pre-tests using a mass dummy.

The following listing shows the main parameters to tune the requested SRS:

— gun (type of gun, cartridge size),

— ringing plate (size, thickness, material, boundary conditions),

— material of the anvil plate,

— position of item under test on the ringing plate,

— position of impact on the ringing plate,

The following picture shows a typical measured time history with corresponding SRS, as well as the specified reference with tolerance bands (+/- 6dB in this specific case).

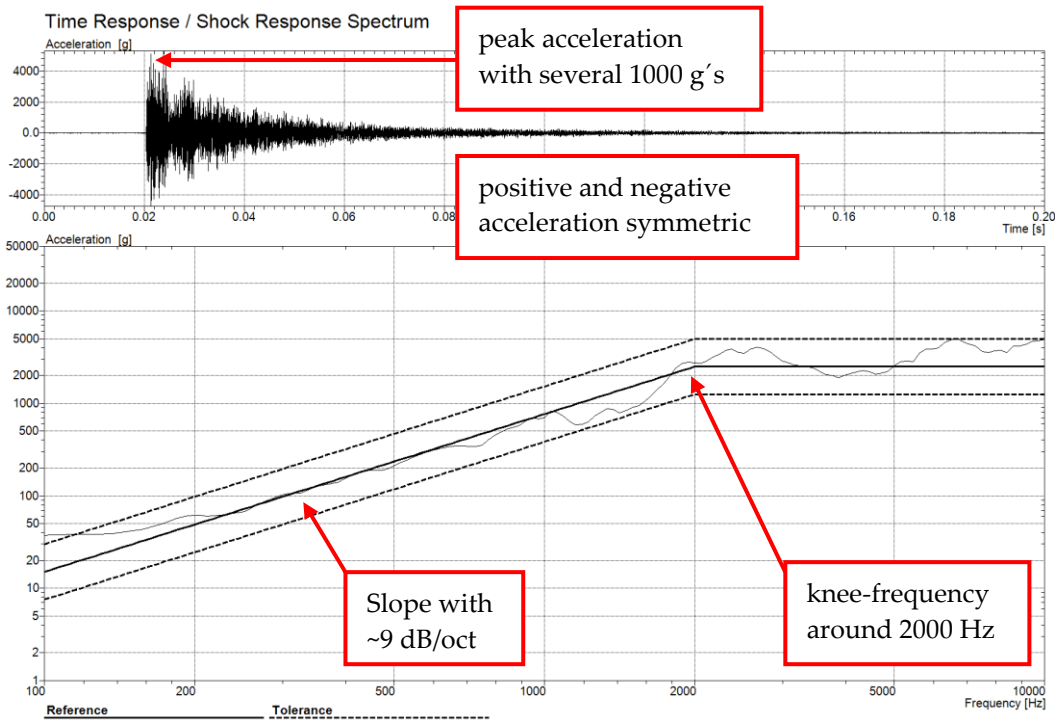

Figure 13-26: Typical time history and SRS of a powder actuated gun test

With this test method, the three environmental categories can be achieved (fair field up to near field), hence answering a large variety of shock specifications for small and mid-size units.

The high frequency excitation (typically above 5kHz, due to pyrotechnic actuation) can exceed the upper test tolerance, therefore this should be addressed during the calibration phase; this is particularly important in the situation where high shock levels are specified.

This test method can also be used for testing of larger assemblies (i.e. instrument), however attention should be paid to the representativeness of the test configuration with respect to the flight configuration, especially for what concern the boundary conditions. Indeed experience has shown that shock testing on larger assembly can lead to large over-testing / high transmissibility, if the test condition induces a more severe shock imposition to the test specimen. This situation can typically be experienced when a pure in phase shock loading is imposed to the test specimen simultaneously to all interface points, leading to a greater excitation of the main modes of the test specimen, whereas in reality such shock imposition will not be encountered at instrument level.

This potential problem can however be overcome owing that a detailed calibration phase is followed, which allows the identification of impact location avoiding a pure in phase imposition of shock loads at the instrument interface points (see Figure 13-27).

To achieve sufficient representativeness of the test configuration, especially for what concern the boundary conditions, calibration is a key element in order to generate a representative environment towards the sensitive sub-systems. As discussed above, this can be achieved for instruments, but past experience has shown that such test method should not be used on a spacecraft as a substitute to a fully representative separation shock test, due to the incorrect representation of the boundary condition / mechanical impedance with respect to the flight configuration, resulting in the transmission of low frequency modes of the ringing plate into the spacecraft.

Another limitation of such test on larger assemblies, lies in the fact that this test method is often used to identify the transmissibility functions from the instrument interface towards internal locations. And as the shock impulse is applied in out of plane of the ringing plate, low cross axis excitations are generated, therefore the transfer functions should only be computed considering the instrument input level along the main axis of excitation as the reference.

Hereafter are shown some examples of calibration test configuration (Figure 13-27), of test configuration for instrument shock testing (Figure 13-28), and an example of achieved levels during such an instrument shock testing (Figure 13-29).

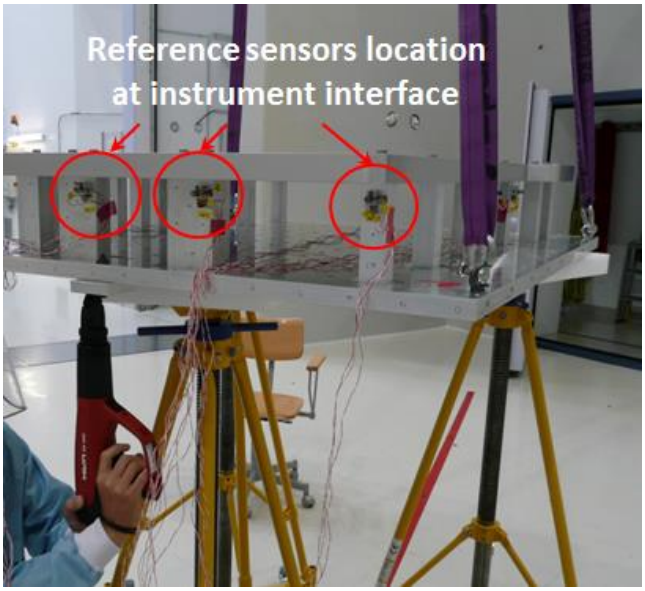

Figure 13-27: Instrument shock test with powder actuated gun - Calibration test for identification of adequate test parameters

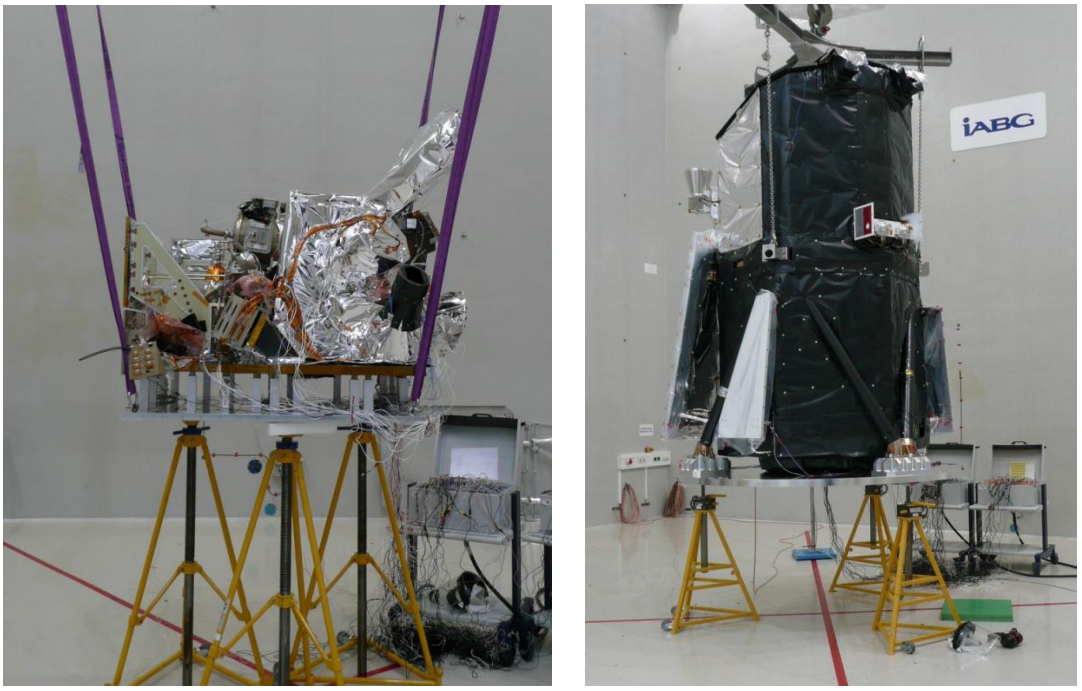

Figure 13-28: Examples of test configurations for instrument testing

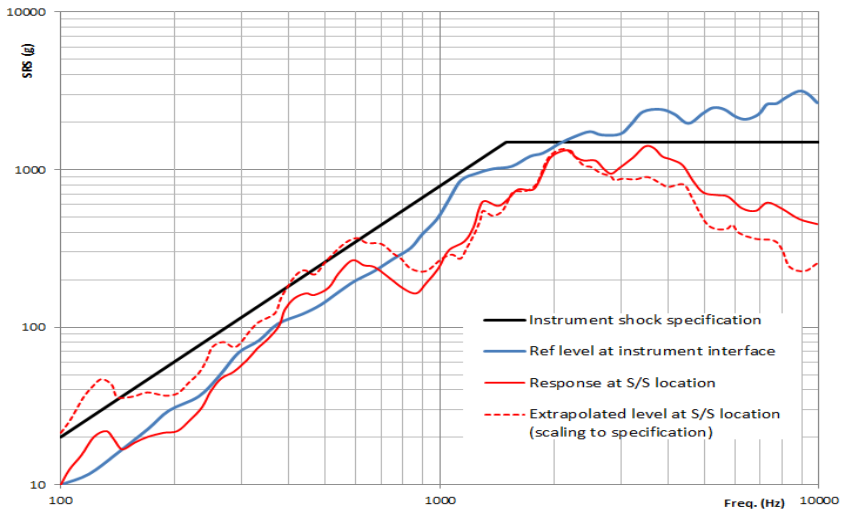

Figure 13-29: Example of achieved levels during instrument shock testing

d. Bi-plate technology

Resonant bi-plates technology is the terminology used for shock test bench composed of a baseplate supporting the excitation device (explosive charge or mechanical impact) and another one, on which is mounted the unit under test. The dimensions of the plates can vary from one set-up to the other. These two mechanical tools are linked together by means of spacers, dampers or threaded rods.

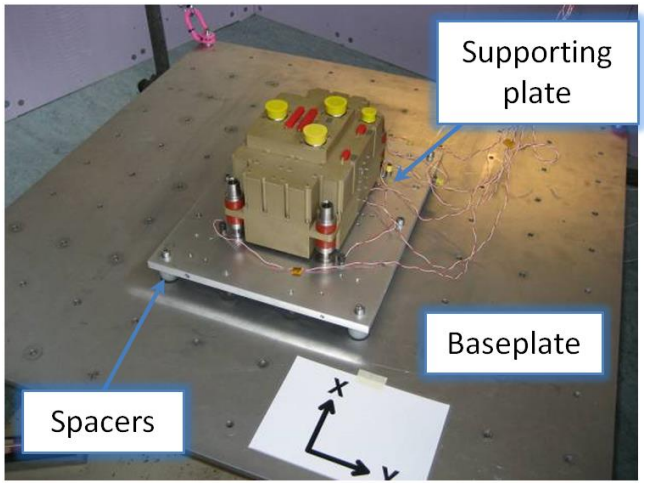

Figure 13-30: Example of bi-plate set-up for shock along out of plane axis

Number and type of spacers (steel, aluminum, nylon, etc…) are important parameters which allow tuning of the SRS at the feet of the unit under test.

The main advantages of this technology are:

— The mechanical filtering of the shock response, at high frequencies, thanks to the decoupling between the baseplate and supporting plate. The shock wave is filtered through the interfaces between the two plates;

— Larger and heavier equipment can be tested, while sill achieving an adequate homogeneity of shock levels around the unit.

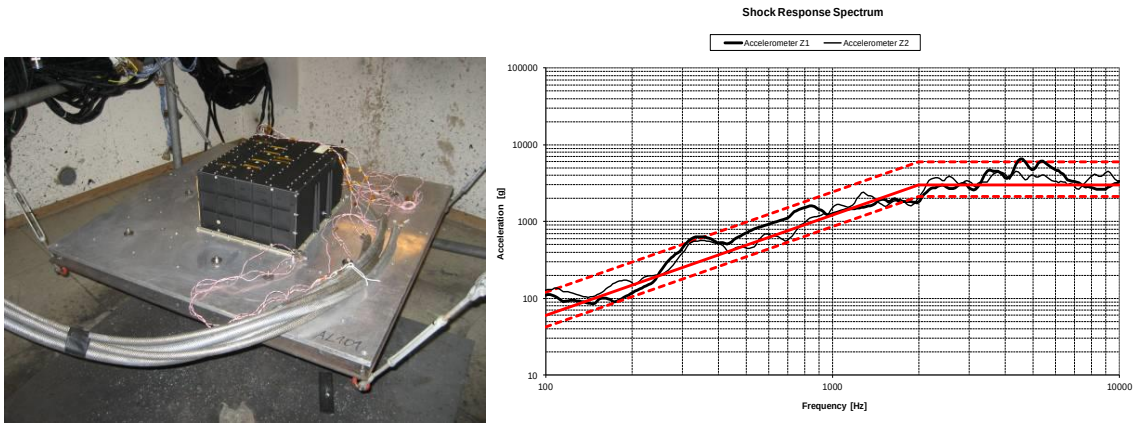

Figure 13-31: Example of set-up and results for shock along out of plane axis on large unit

On the other hand, the main disadvantage of bi-plates technology lies in the difficulty in generating sufficient excitation in in-plane directions (out-of-plane levels being significantly higher than in-plane levels).

e. Beam technology – Hopkinson bar

The resonant beams have a response "damped sinus" like. This response is the response of the main mode to the excitation applied to the bench. This means that the frequency content of the shock is quasi mono frequency.

Depending on the categories of beam based bench, it is possible to tune the main modes or to damp some undesirable mode.

This kind of beam is known as Hopkinson beam. The equipment is mounted on an expander (one for in plane axes, one for out of plane axis) located at an extremity of the beam and allowing positioning of the tested equipment either for in plane or out of plane orientation. The impact is done on the other extremity. The SRS's elbow is driven by the traction/compression mode of the beam. The tuning of the main frequency can be done either by a modification of the length of the beam or by adding an extra mass that leads to modify the free-free boundary condition to clamped condition.

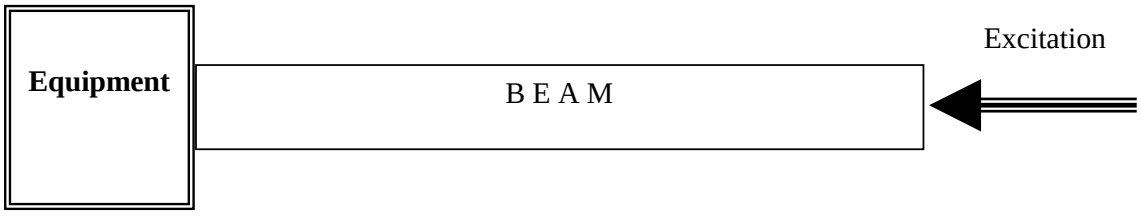

Figure 13-32: General principle of a Hopkinson bar

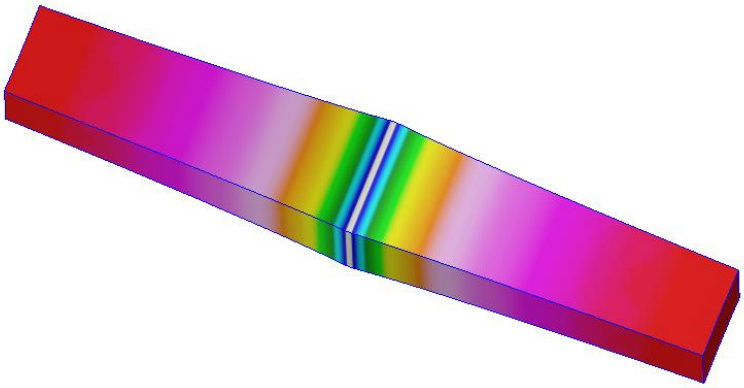

Figure 13-33: mode of traction / compression of a beam

One of the main restrictions for this technology is the size of the equipment to test given that dimensions of used expanders are limited by their associated mass. The correlated advantage is a good homogeneity of induced levels.

Another limitation of those benches is the response, in damped sinus like. This response is basically mono frequency and could basically be far from a real shock response, which is a multi-frequency response.

That's why it is possible to improve the frequency content by adding additional resonators located either close to the impact extremity or directly on the expander.

Figure 13-34: Example of a test bench (in plane configuration) based on Hopkinson bar

13.3.4.1.2 Cross correlation between resonant plate and pyrotechnic shock

The subsequent figures illustrate that the low-pass filtered acceleration time histories at the interface of a unit are quite well correlated in the case of qualification shock using a resonant plate (a). However, this is not so true when the equipment is mounted on a honeycomb panel submitted to a pyrotechnic shock e.g. bolt cutter (b). As a result, the equipment response estimated on the base of a single I/F acceleration overestimates the true acceleration measured in pyrotechnic test conditions in particular in the out of plane direction.

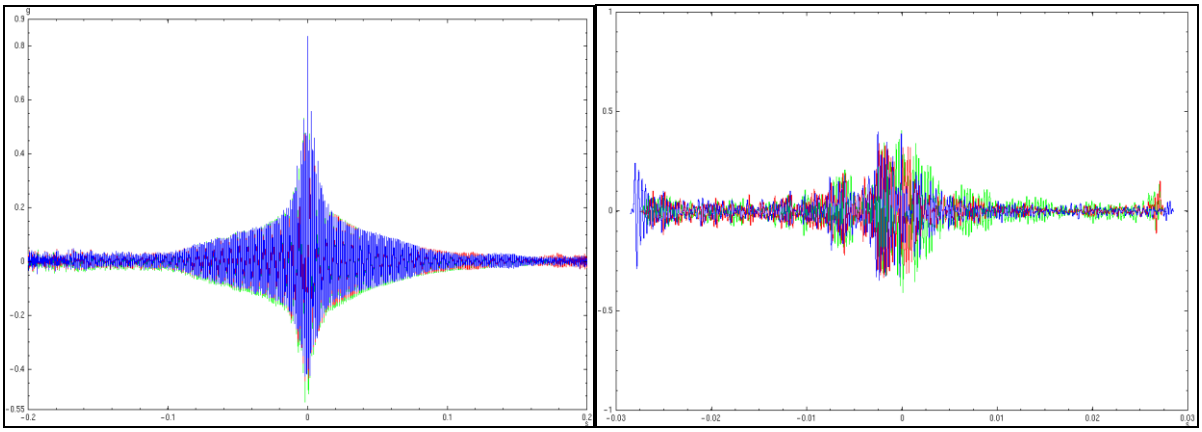

(a) Qualification with a resonant plate (b) Pyrotechnic shock

Figure 13-35: Cross correlation between I/F accelerations low pass filtered at the equipment transition frequency –[RD-0109]

13.3.4.1.3 Other shock machines

a. Overview

Other shock machines are used for standardized tests on components and mounting technology qualification (half sine tests). These however should not be used for equipment testing, as the input does not satisfy the requirement on shape of time history.

b. Free fall shock machine

The Free fall shock machine is designed to produce classical shock wave shapes by dropping a table supported on its side by Thompson rods and bearings. The table drop height can be set at pre-determined heights for shock pulse repeatability. Acceleration levels are generated by drop height while time duration is a function of the programmer provided; elastomer pads for half-sine, lead pellets for sawtooth and pneumatic cylinders for square wave pulses.

Figure 13-36: Free fall shock machine

c. Pneumatic Shock Machine

These machines produce a shock pulse in the vertical direction using compressed air to force the carriage to impact on the shock machine base. Elastomer pads re used between the carriage and the base in the impact area to produce half-sine pulses, lead pellets for sawtooth pulses and pneumatic cylinders for square pulses. The design of the programmers affect the time duration of the pulse while the air pressure and drop height are used to accelerate the carriage to determine the magnitude of the shock pulse.

Figure 13-37: Pneumatic shock test machine

13.3.4.2 Test sequence

The standard test sequence is as follows:

NOTE The test sequence may need to be adapted considering controllability and linearity of the test bench.

- Calibration tests on dummy of the unit to test

  Before the test item is attached to the shock apparatus, attach a representative dummy. For small units (i.e. switches, electric boxes) a simple mass dummy is sufficient, for complex units (i.e. antennas, subsystems) a structural model is recommended to achieve repeatable results between calibration shocks and the actual test.

  The specimen needs to be mounted onto the test table in representative conditions i.e. using the same attachment points, use of fillers etc. If the specimen is normally mounted on shock isolators to attenuate the shock then ensure the isolators are functional during the test.

- Perform calibration shocks to identify test parameters which allow achieving input SRS within the specified test tolerances, and also to demonstrate adequate repeatability.
- Once an adequate calibration is achieved, perform in the same configuration a low level shock, typically at half energy (e.g. by reducing the dropping mass height).
- Install the equipment on the test bench and repeat low level shock to check if sensors are still responding normally and analyse the level discrepancy between the two low level runs (1st with dummy mass, 2nd with specimen).

  If necessary remove the test article and modify the test set-up accordingly. In that case re-perform calibration shocks..

  NOTE Depending on the test method an additional full level test without test article could be necessary because moving from one level to another can degrade calibration (transverse excitation in particular).

- Conduct the test readiness review
- Nominal shock sequence on test item in its operational mode (e.g. usually three consecutive shocks).

  NOTE 1 If the homogeneity criterion (less than 6 dB between sensors) is not fulfilled, rotate test specimen implying a number of shocks doubled.

  NOTE 2 Recommended to perform a data validation as minimum for the first shock event.

- Conduct the post-test review

  NOTE the mechanical shock in general, provides a more severe low frequency environment (comparatively large velocity and displacement) than the actual pyroshock event and hence, any structural failures, e.g., deformed fasteners or mounts can be more akin to those found in the real flight configuration.

- Repeat this sequence for each orthogonal axis to be tested if the previous test shock did not meet the test specification in the other axes.

- Data validation:

  Before the recording of pyroshock data are utilized, it is important to ascertain the quality of these data based on so-called shock validity criteria (see chapter 15). For general use, the simplified criteria (see paragraph15.3) is sufficient for determining the validity of pyroshock data. However for some more advanced applications, such as FE simulations which require using some "perfect" time history measurements, the refined criteria based on velocity validation procedure should be applied (see paragraph 15.4).

- Carry out the Test review board

13.3.5 Procedure IV – Equipment shock test with an electrodynamic shaker

13.3.5.1 Introduction

Performing a shock test on a shaker can be convenient for the following reasons:

- Shakers enable both classic and complex oscillatory shock pulses to be applied.
- The tests can be performed by a single facility – usually the same facility performing the sine and random vibration tests. Therefore costs can be considerably lower.
- The unit is normally already instrumented for sine and random, so the shock test is simply a follow on test – in an undisturbed configuration for low level sine assessments.
- If the time base input from a real transient event is available, a realistic input can be applied to the particular unit – reducing the need for severe over-designs, whilst maintaining adequate margins.
- There is a high degree of reproducibility of the shock inputs.
- Once the input is stored in the system, there is minimum set up time for repeat tests. Even for complicated waveforms subsequent repeat tests are achieved in a fraction of the original timescale. The wavelet test being a test in one direction – whereas an impulse normally requires two tests per axis (+ve and –ve directions).

On the other hand, electrodynamic and electrohydraulic shakers have limited magnitude, spectra, and directional capability. In both cases, the specific spectral capacity is highly dependent on the particular design of the device. A vibration shaker can be able to achieve a shock magnitude that reaches into the lower portion of the far-field region, but would probably be unable to achieve the desired far-field spectral content, since most electrodynamic shakers are unable to provide sufficient excitation above 3 kHz.

Shaker based shock testing raises a number of interesting problems where secondary shocks are concerned:

- Ensure that the mean acceleration of the table is zero (just as it is for vibration).
- Due to the need that the shaker table returns to the same position after each bump, Ensure that the resulting velocity waveform has a mean value of zero. This is best defined as follows: ensure that a transient which is suitable for simulation on a shaker has an acceleration and velocity time history – both of which have total integral values of zero. In practical terms this means to ensure that not only the area above and below the zero line for the acceleration / time history are equal, but that the area above and below the velocity / time history are also equal.

For shock testing on shakers this requirement means that the primary pulse are preceded and followed by acceleration pedestals – which are of opposite sign to the shock pulse. Because of the limited displacement available on shaker systems this can cause problems if long duration high level shocks are required, particularly if excessively large pedestals cannot be used. Since in the simple case the secondary and primary shocks occur with the displacement in one direction, it is often necessary to bias the shaker table to its upper or lower stroke limit to provide the maximum performance.

Recommendation: for classical pulses on a shaker – such as the half sine input pulse, pre and post modifications should be included in accordance with Figure 13-38 or similar specification. It is also recommended that the tails be minimized as much as possible to preserve a reasonable match to the SRS of an unmodified pulse.

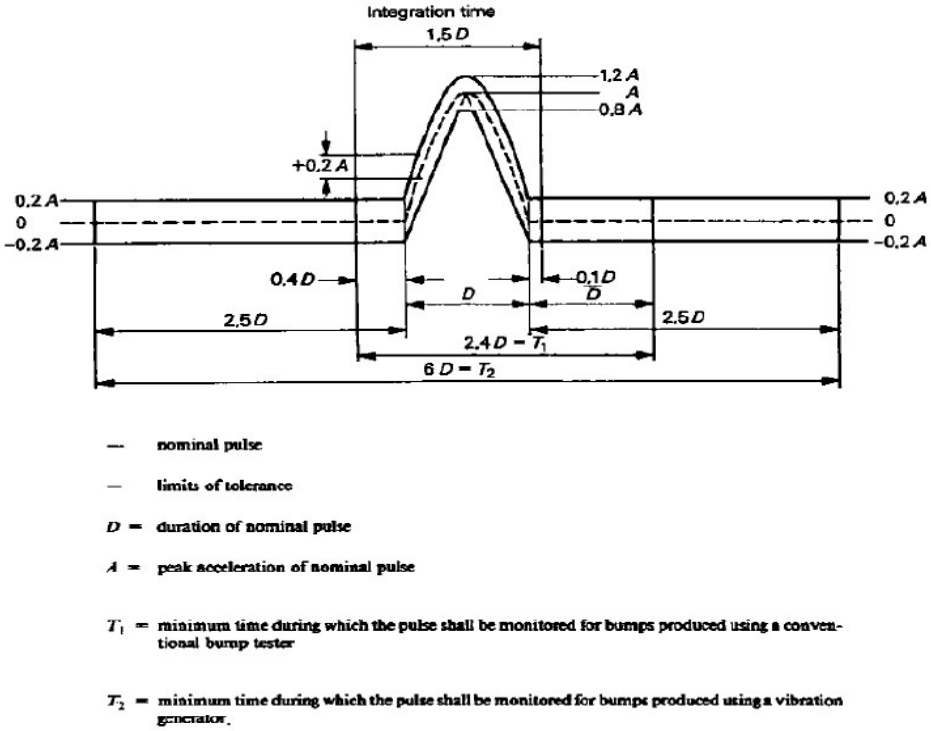

Figure 13-38: Basic Pulse Shape definition

Shaker manufactures do not usually specify the acceleration limit for shock performance. This is because there is such a large variety and variation of shock waveform that can be specified when compared with vibration waveforms.

The input acceleration transient also produces a velocity and displacement transient. Throughout this transient, it is important that all instantaneous values of displacement lie within the stroke limitation of the shaker. Limitations imposed by asymmetrical displacement pulse shapes can frequently be reduced by off-setting the neutral position of the armature within the total stroke range.

An electrodynamic shaker does not have an inherent peak velocity limit. The frequently stated velocity limit is actually a system limit imposed by maximum power amplifier voltage.

It is obvious that the force limit for a given shaker system depends on the size of the system installed. The maximum wideband continuous force rating of most electrodynamic shakers is governed by the ability to cool the armature producing the force. Most armatures are designed to withstand the resulting accelerations for long periods. The basic limitation on performance during shock testing is generally not the acceleration – but the stress distribution through the armature structure during the transient. This stress distribution is strongly dependent on the amplitude vs. frequency content of the shock input, as well as the test item and fixture. Very high shock inputs – thousands of g units, exceed the capabilities of most shakers, so other techniques such as resonant fixtures are sometimes introduced.

13.3.5.2 Test facility presentation

13.3.5.2.1 Electrodynamic shaker system

Some electrodynamic exciters can be programmed to generate short duration transient motion. Particular designs of shaker allow achieving a shock magnitude higher than 1000 g, but generally speaking shakers have limited magnitude, spectra, and directional capability.

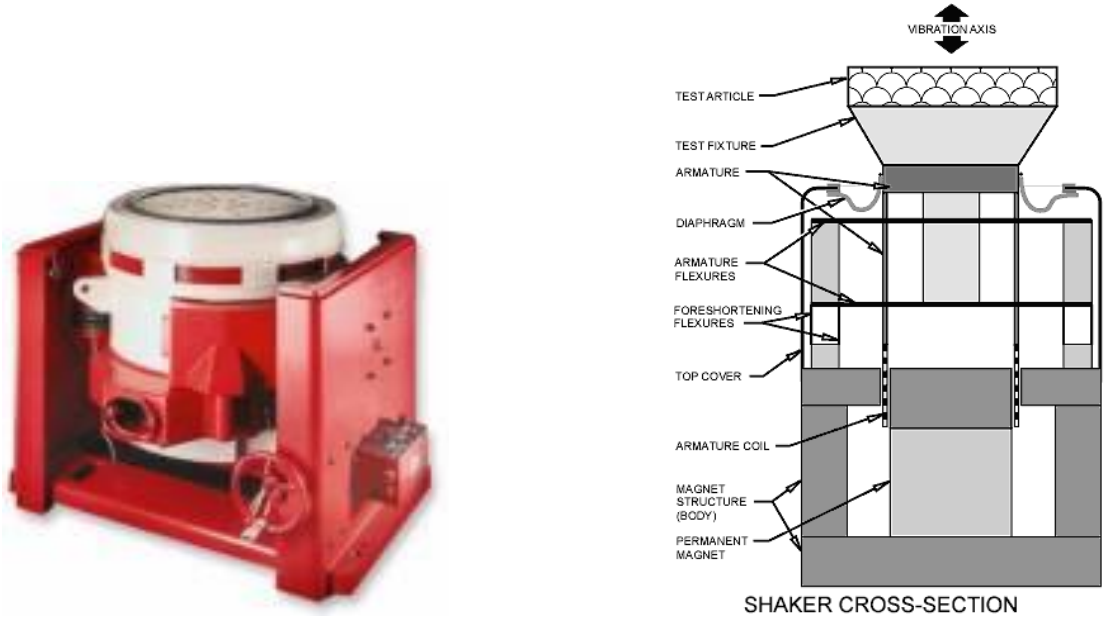

Figure 13-39: Electrodynamic exciter

13.3.5.2.2 Examples of shock testing using electrodynamic shaker

a. Example 1

The PFM LRPT Deployable Antenna (METOP spacecraft) was subjected to the following qualification level shock test: base input SRS equivalent to a half sine impulse of 112 g (peak) 0,5ms duration (Q = 10) (test tolerance 0dB to +3 dB) with a test analysis up to 4000 Hz. The damped SRS is shown in Figure 13-40 along with the test set up (Figure 13-41). For information the antenna flight mass was approximately 12 kg. It is interesting to note the use in Y-axis of a balance mass on the "free" corner of the large square head expander. During test, the SRS inputs were monitored/evaluated at each of its three discrete interfaces shown in Figure 13-41.

The tests were conducted using a Ling Electronic Industries C340 160kN thrust shaker.

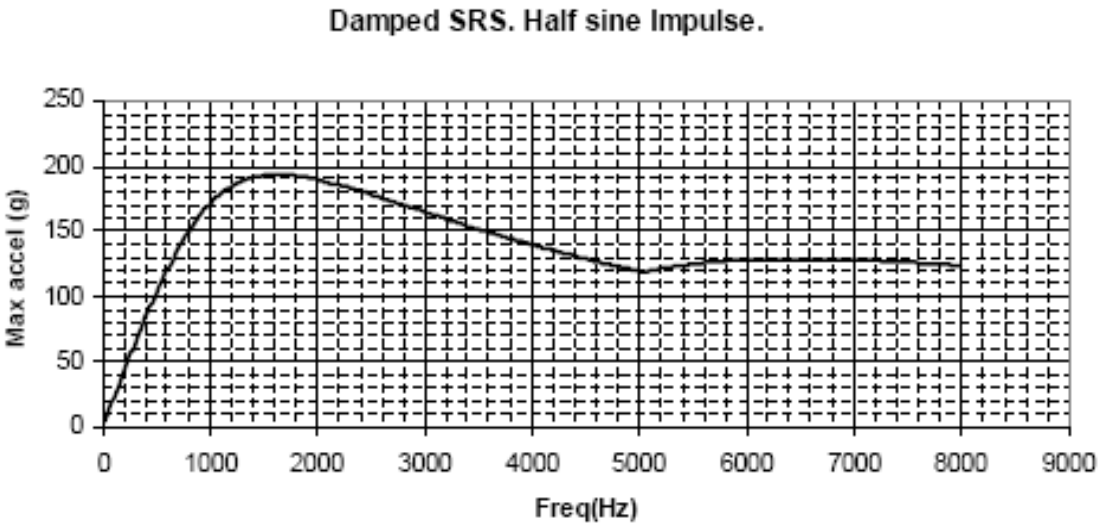

Figure 13-40: Damped Base Input SRS for the METOP LRPT Qualification Tests

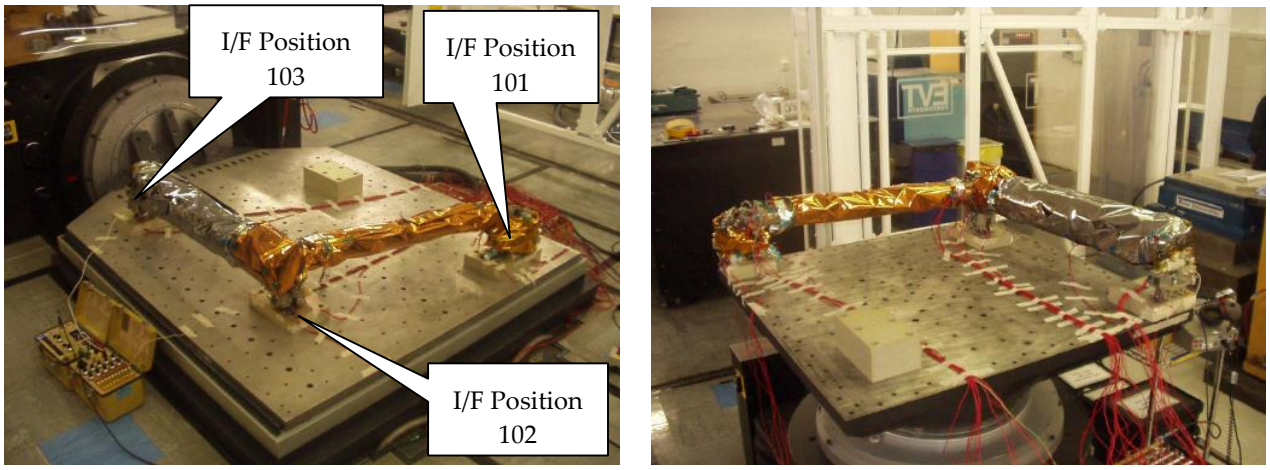

Figure 13-41: METOP LRPT Lateral X Input Testing (left) and Vertical Y Input Testing (right)

The control plots (Figure 13-42) show that the shaker was able to input reasonable approximations to the input requirements at some of the interfaces – particularly 101Y. However, owing to the very large footprint of the LRPT antenna, it was not possible to control the shaker sufficiently to input the same values at each interface location. The shaker limitations are also evidenced by the high frequency responses. The results obtained however were judged to be acceptable.

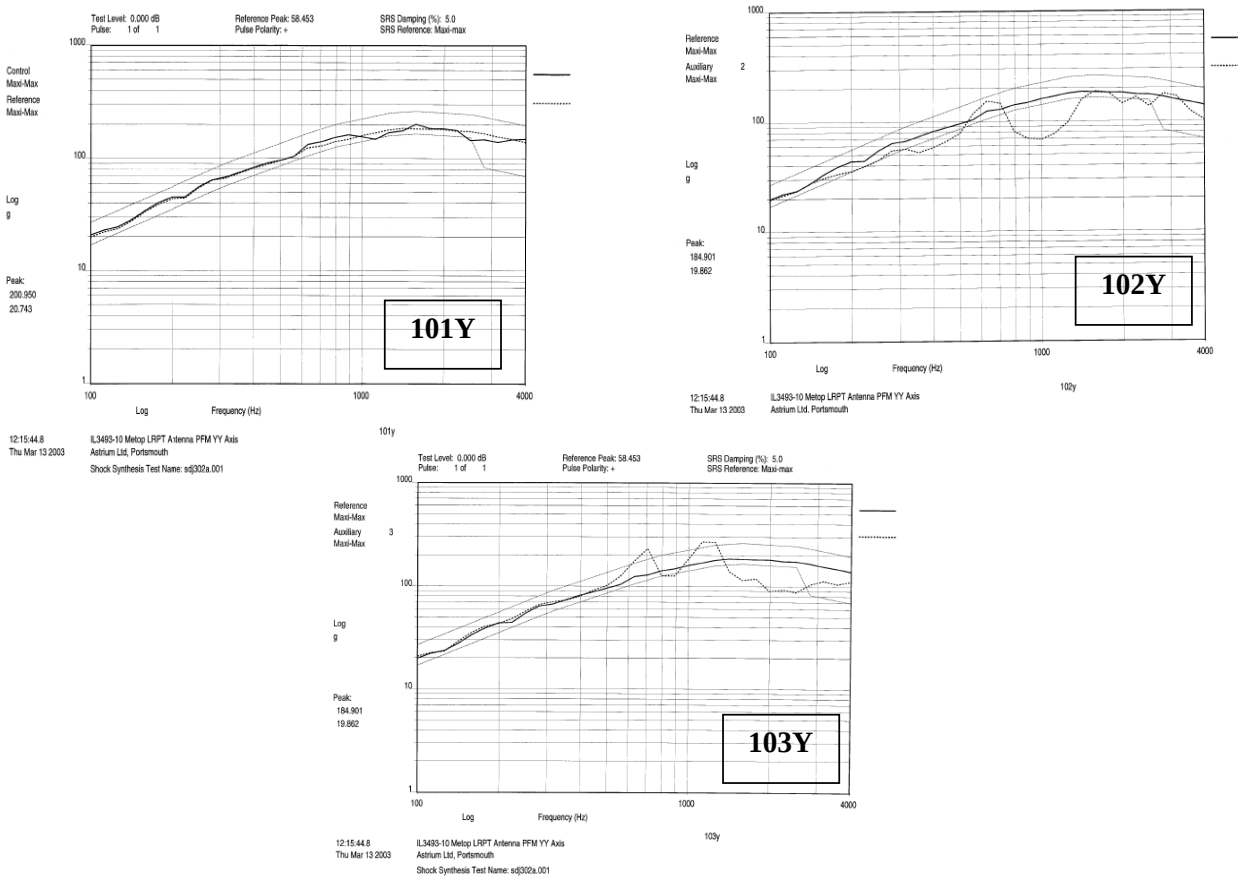

Figure 13-42: METOP LRPT Y Axis Shock Test

b. Example 2

The METOP DTA antenna shaker based shock test set-ups are shown in Figure 13-43. Two shakers were used during the test programme: the Ling Electronic Industries C 340 160kN thrust shaker and the Ling Dynamic Systems V 954 40kN thrust shaker. The antenna shown is of fixed (non-deployable) quadrafilar design of total flight mass of approximately 3 kg. During test, one control accelerometer adjacent to the cone/shaker interface was used on test. The PFM DTA Deployable Antenna was subjected to the following qualification level shock test: base input SRS defined by a curve obtained by linear connection of the following points on a logarithmic chart.

100 Hz	37g
900 Hz	350g (Q>10)
	310g (Q=10)
2000 Hz	350g (Q>10)
	310g (Q=10)
4000 Hz	300g

(Tolerance –0,+3dB on SRS g)

From the bare fixture tests the V 954 shaker was found to be more suitable for lateral shock testing, as its slip table is smaller and has higher natural frequencies. The DTA test programme used the C340 shaker up to the start of the lateral shock testing, and then continued on the smaller V 954 shaker.

Figure 13-43: Metop DTA Lateral Test on the Ling C340 (left) and on the Ling V954 (right)

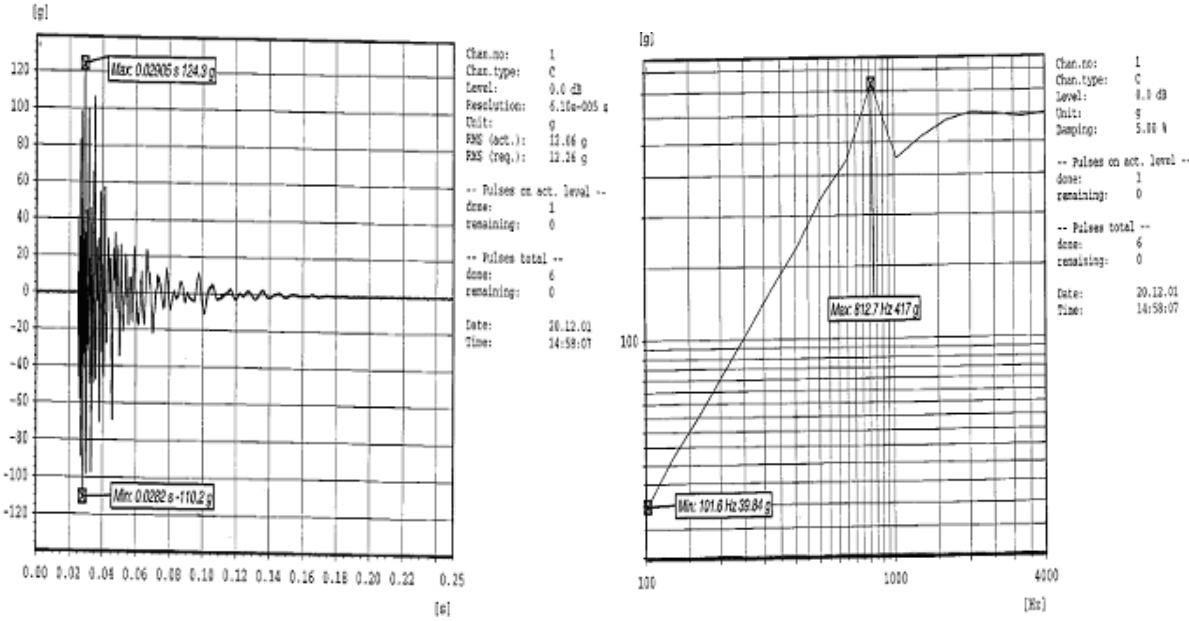

Figure 13-44: METOP DTA X Axis Shock Test Control Plot on Ling V954 Shaker

Some conclusions were drawn from these tests:

- For units with large foot prints (even lightweight units) significant variation of transmissibility can result across such interfaces due to head expander / slip table flexibility.
- Control above typically 2,5 kHz can be problematical hence extreme high frequency inputs on a shaker can be a limitation. Slip table or head expander attenuation characteristics at high frequency can render shaker driving impossible. The use of a smaller shaker can be advantageous for higher frequency input achievement.

13.3.5.2.3 Induct-A-Ring technology

This technology has substantially improved shaker armature capacity to withstand high level shocks (maximal temporal up to 600 g) by combining mechanical durability and electrical simplicity. Most conventional armatures utilize a complicated armature construction of electrical windings, epoxy bonded joints, high amperage flexures (to deliver input power to the coil), and high pressure hoses (to bring cooling water in and out of the coil). Each of these components is subjected to the same vibration and/or shock levels applied to the test specimen. Repeated high level operation often leads to fatigue failures, water leaks, cracked epoxy joints, burned out windings, or voltage breakdown in the coil.

By comparison, the induct-A-Ring armature is a simple two-piece metal structure. No electrical current leads or water cooling connections are needed. There are no electrical windings. All points on the armature are at ground potential at all times. There is no possibility of voltage breakdown. No electrical insulation is utilized anywhere in the armature assembly because there is zero voltage potential between any two points on the ring, and between the ring and ground.

Table 13-1: Induct-A-Ring vs. conventional armature design (source Unholtz-Dickie T2000 series)

	UD Induct-A-Ring	**Conventional Shaker Design**
Armature Construction	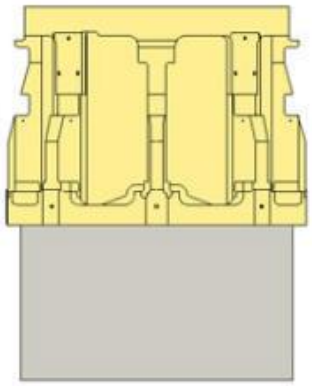 Solid metal, forged aluminium ring bolted to upper casting.	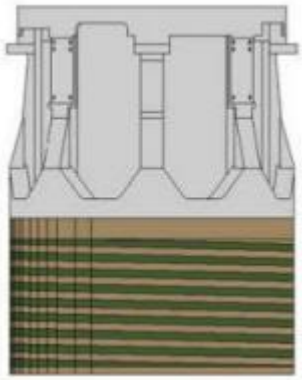 Insulated copper wire is held together with epoxy joints. Armature is epoxy bonded to upper casting.
Electrical Connection	Inductively Coupled - No electrical current leads required. All points on moving armature remain at ground potential.	Fragile 1000 Amp current connection bridging shaker suspension required. Armature is at high voltage potential. Voltage break down and shorting (arcing) are possible.
Armature Cooling	Air Cooled - simple and effective	Design requires fragile water connection to bridge the armature suspension to cool the coil. These hoses and fittings are subjected to high vibration stress.
Rated Acceleration	200 g sine / 600 g shock	100 - 150 g max sine

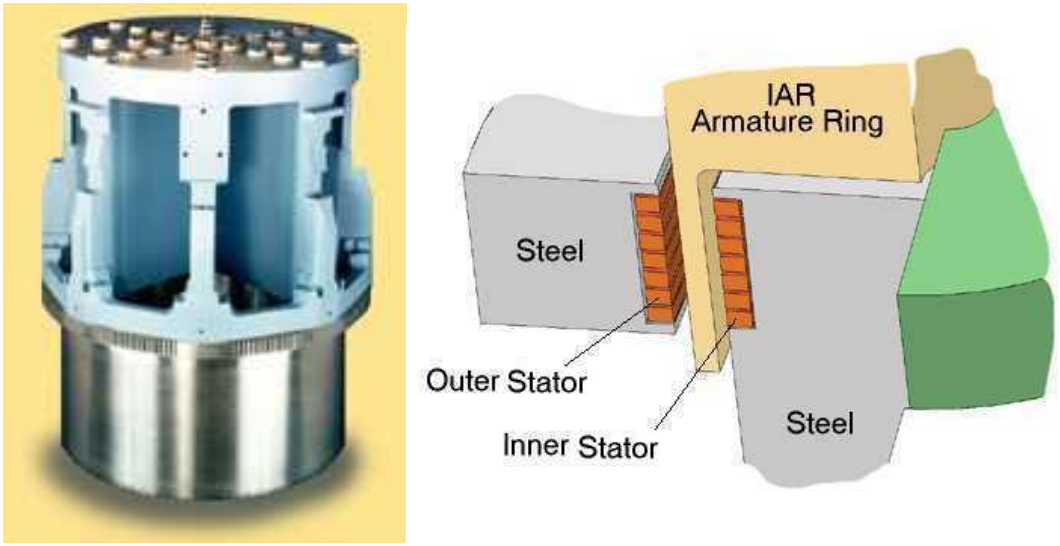

Figure 13-45: Induct a ring shaker Armature ring in its magnetic gap (source Unholtz-Dickie T2000 series)

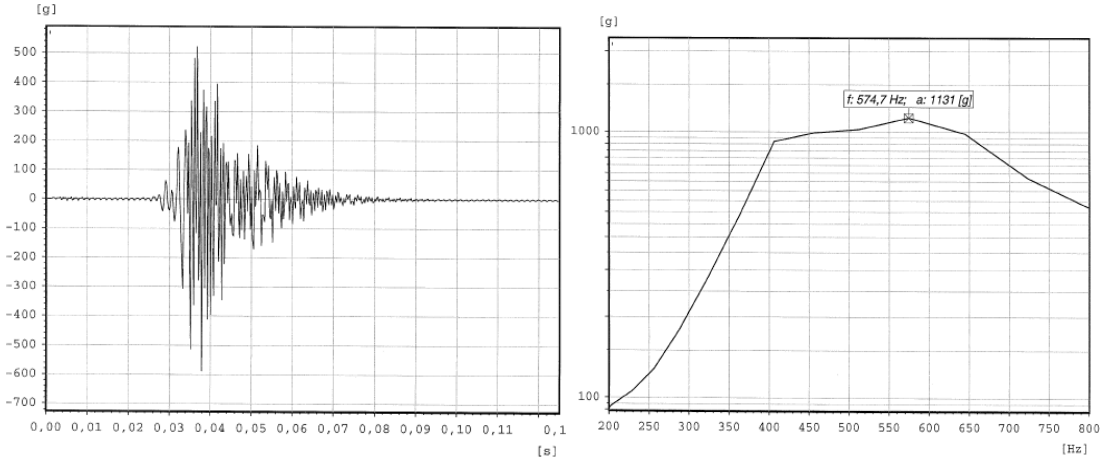

(a) (b)

Figure 13-46: (a) Time history and (b) corresponding SRS on shaker

Figure 13-46 shows on the left an example of time history measured on the table on an induct-A-ring shaker. On the right, the corresponding SRS. The example corresponds to a low frequency content shock. This shaker is capable of frequency content up to 5 kHz, corresponding to the compression resonance frequency of the moving coil.

Mechanical amplifier installed on an induct-A-ring shaker

In order to increase the levels delivered by the induct a ring shaker, a mechanical amplificatory could be implemented. Its drawing is represented below (see Figure 13-47). It has permitted to reach 3700 g SRS at 1600 Hz.

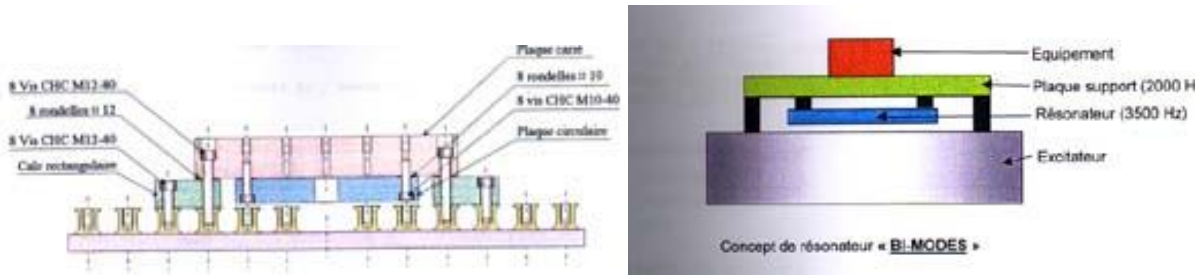

(a) (b)

Figure 13-47: (a) Drawing of the mechanical amplifier – (b) Principle of the mechanical resonator

Figure 13-48: Mechanical amplifier

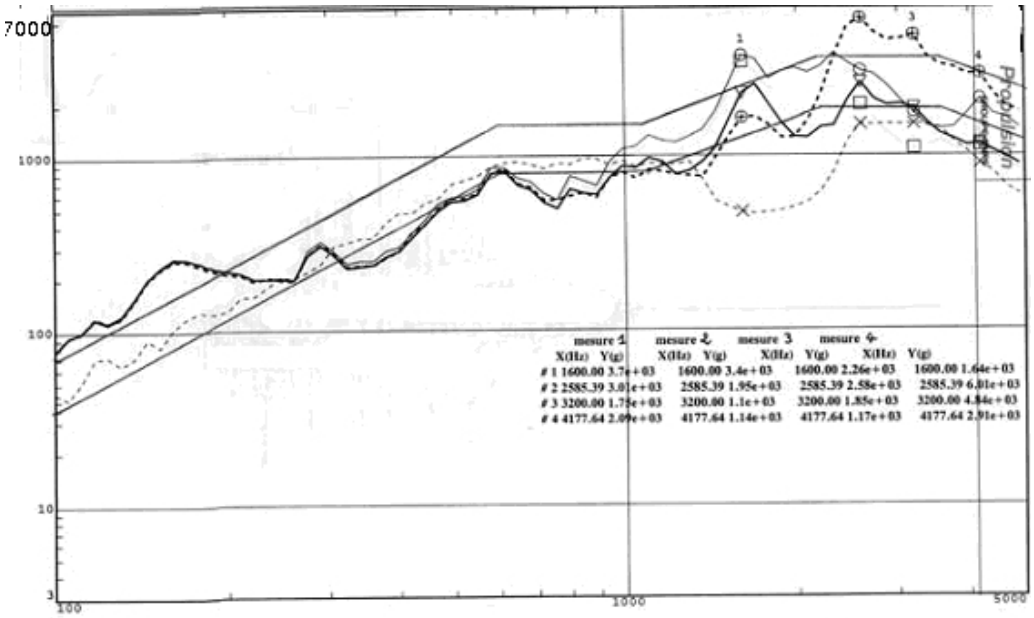

Figure 13-49: SRS of the excitations obtained with the additive effect of the mechanical amplifier

13.3.5.3 Shaker test specificities

13.3.5.3.1 SRS specification and time domain input for electrodynamic shakers

Any transient waveform can be presented as an SRS, but the relationship is not unique; **many different transient waveforms can produce the same SRS**. As such, the generated transient could be very different from real pyroshock environment while still complying with the specified SRS. Thus, **a pre-requisite before the qualification run is that a specific agreement concerning the time history from the customer is met**.

Tests on a simple cantilever beam have been performed to investigate peak responses on a test specimen for different base input motions whose SRS characteristics are consistent at a designated Q = 10. Tests were base-lined for two families of excitation:

- an impulsive transient – i.e. classical half-sine with pre and post pulse modification for net zero displacement.
- a series of longer duration / reduced peak complex waves generated by wavelets whose form resembles that of a modulated sine wave.

Waves are oscillating functions of time or space or both. Wavelets are small waves. A wavelet has oscillating wave-like characteristics and its energy is concentrated in time over relatively small intervals. Wavelets are especially useful for simultaneous time and frequency analysis of transient, non-stationary (e.g., structurally time-varying) signals. Wavelets are mathematical functions that cut up data into different frequency components, and then study each component with a resolution matched to its scale (See Figure 13-50).

The following sections give basic introduction to the theory behind wavelets, along with supporting example (see [RD-080]).

A shock response spectrum can be met using a series of wavelets. The wavelets are synthesised into a time history on a control computer. The control computer applies the time history to an electromagnetic shaker. The shaker then applies the shock pulse to the test item. The control computer then verifies the resulting shock pulse.

The equation for an individual wavelet is:

$$W_m(t) = \begin{cases} 0, \; for \; t < t_{dm} \\ A_m \sin\left[\frac{2\pi f_m}{N_m}\left(t - t_{dm}\right)\right] \sin\left[2\pi f_m \left(t - t_{dm}\right)\right], \; for \; t_{dm} \le t \le \left[t_{dm} + \frac{N_m}{2 f_m}\right] \\ 0, \; for \; t > \left[t_{dm} + \frac{N_m}{2 f_m}\right] \end{cases}$$

Where:

— $W_m(t)$ is the acceleration of wavelet m at time t

— A_m is the wavelet acceleration amplitude

— F_m is the wavelet frequency

— N_m is the number of half-sines in the wavelet (an odd integer, bigger or equal to 3)

— T_{dm} is the wavelet time delay

The total acceleration at any time t for a set of n wavelets is:

$$\ddot{x}(t) = \sum_{m=1}^{n} W_m(t)$$

Selection of the proper wavelet parameters to fulfil a given shock response spectrum is a trial-and-error process. Prior experience is a valuable guideline. Note that the wavelet is designed to have zero net velocity and zero net displacement. A time history of sample wavelet is shown in Figure 13-50.

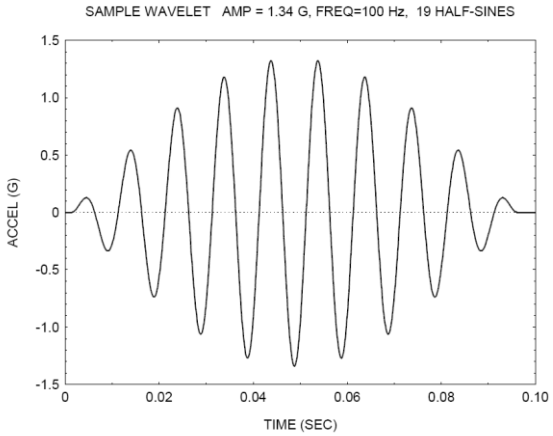

Figure 13-50: Time history of sample wavelet

An example is given in Table 13-2. Let us consider the following specification:

1. Require that both the positive and negative spectral curves meet the specification.
2. Assume tolerance bands of ± 3 dB.
3. Use 1/6 octave spacing.
4. Allow 0,400 second duration.

Table 13-2: Example of SRS specification

MIL-STD-810E Crash Hazard, SRS Q=10	
Natural frequency(Hz)	Peak acceleration (g)
10	9,4
80	75
2000	75

The objective is to synthesize an acceleration time history which satisfies the specification via wavelets and to optimize the time history to minimize the peak acceleration, velocity, and displacement values. A synthesis can be performed using the approach in Table 13-3.

Table 13-3: Method for synthesizing an acceleration time history via wavelets

Step	Description
1	Generate a random amplitude, delay, and half-sine number for each wavelet. Constrain the half-sine number to be odd. These parameters form a wavelet table.
2	Synthesize an acceleration time history from the wavelet table.
3	Calculate the shock response spectrum of the synthesis.
4	Compare the shock response spectrum of the synthesis to the specification. Form a scale factor for each frequency.
5	Scale the wavelet amplitudes.
6	Generate a revised acceleration time history.
7	Repeat steps 3 through 6 until the SRS error is minimized or until an iteration limit is reached.
8	Calculate the final shock response spectrum error. Also calculate the peak acceleration values. Integrate the signal to obtain velocity, and then again to obtain displacement. Calculate the peak velocity and displacement values.
9	Repeat steps 1 through 9 many times.
10	Choose the waveform which gives the lowest combination of SRS error, acceleration, velocity, and displacement.

The method in the above table is a rough outline.

For the example, the time delays are arranged in a "reverse sine sweep" manner. In other words, the highest frequency component has zero delay. Each successive wavelet moving downward in frequency has a progressively longer delay. The delay step is proportional to the wavelet frequency. The two wavelet components having the lowest frequencies, however, are allowed to begin at time zero.

This synthesis method produced the wavelet series producing the peak time history values shown in Table 13-4. The acceleration, velocity, and displacement time histories are shown in Figure 13-51 and Figure 13-52. The shock response spectrum is shown in Figure 13-51. The spectral curves satisfy the tolerance bands.

Table 13-4: Peak Values of Synthesised Time History

Parameter	Maximum	Minimum
Acceleration (G)	13,2	-12,9
Velocity (in/sec)	25,2	-23,3
Displacement (inch)	0,344	-0,122

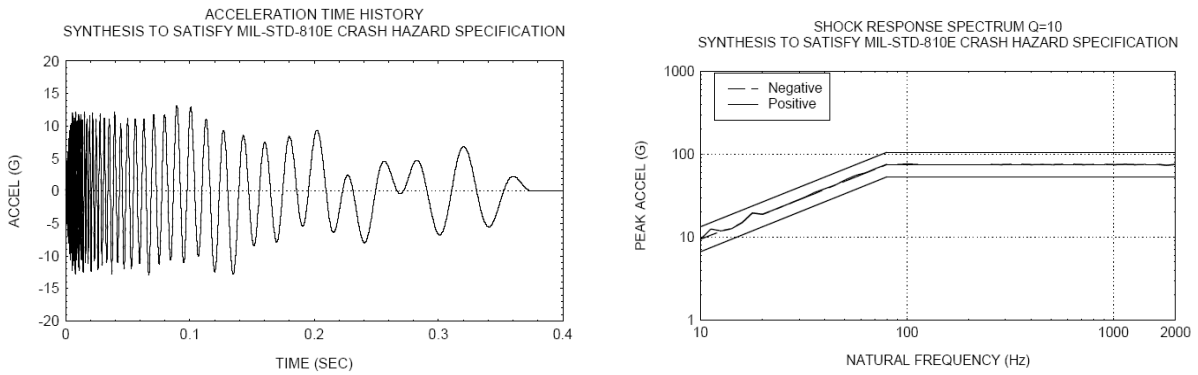

Figure 13-51: Wavelet acceleration time history and SRS

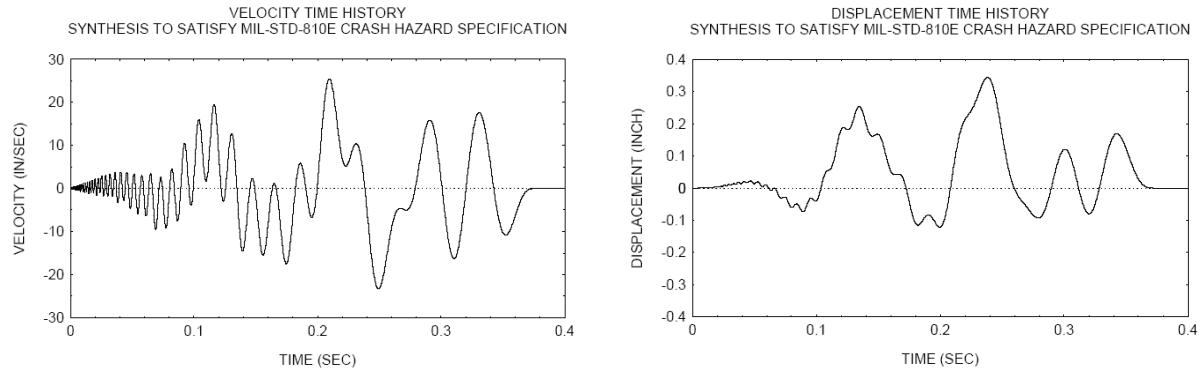

Figure 13-52: Wavelet velocity and displacement time history

Note that the reverse sine sweep method tends to produce lower acceleration, velocity, and displacement values than a random delay method. Minimization of these parameters is highly desirable due to shaker table limitations

Most control systems in use by the Environmental Test Facilities (EVT) contain built in routines to aide in the creation of wavelets for shock testing.

The goal of tests on cantilever beam was for both families of excitation to generate a consistent SRS across both regimes of excitation at the industrial normal assumptions of Q = 10. Since we know that the response of a multi-DOF system is generally insensitive to damping for impulsive excitation, then the lesser peak from the wavelet relies on 'steady state' build-up of response to achieve the appropriate amplification.

One key element of the test specimen was to select a specimen whose inherent damping/loss characteristics were low. For mathematical simplicity choice of a simply supported specimen would have been ideal since the eigen-functions in a modal analysis are simple. However, realisation of the boundary conditions was more difficult and in addition, achievement of minimised damping in the specimen with such boundary conditions would also have been difficult without introducing significant energy dissipation. Hence, with focus on minimised loss characteristics a Fixed-Free specimen was chosen.

For general aerospace materials such as typical wrought aluminium materials and steels the differences in material loss factors are not that great and providing we avoided materials which were intrinsically selected for relatively high loss factor then the choice of material for the specimen was not seen as significant. Owing to time and financial restraints, the material selected was aluminium – since material was readily available with minimum required machining. The test set-up employed is shown diagrammatically and with a photo in Figure 13-53.

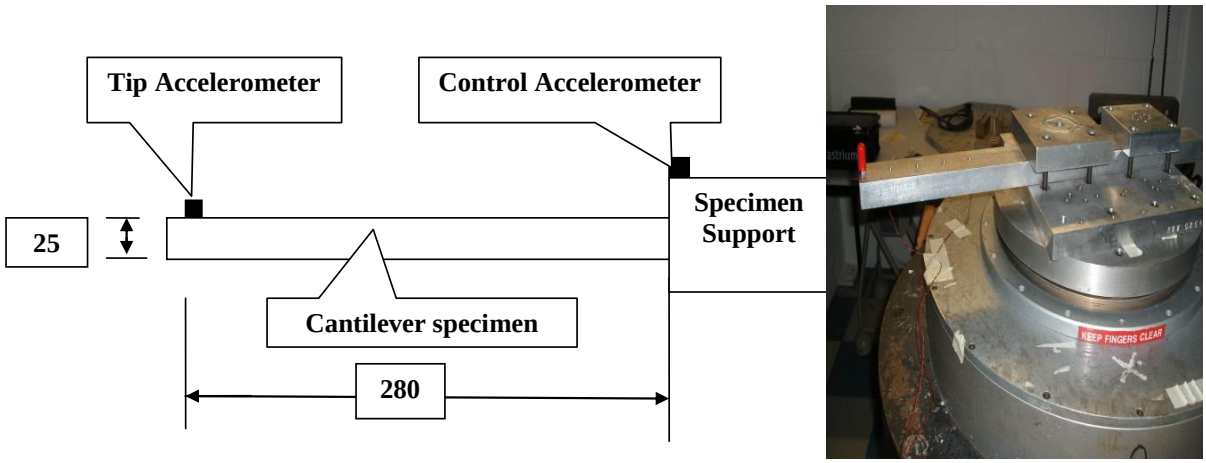

Figure 13-53: Test set-up

Examples of base input accelerations (impulsive input and wavelet input) applied on the test specimen are shown in Figure 13-54. Note that the SRS for each of the four (4) test inputs are approximately consistent for Q = 10 as shown in Figure 13-55. Note also that the peak acceleration input in the time domain for the wavelets (around 40 g) are less than the peak impulse acceleration (80g) of the half sine impulse, which is the primary reason for such wavelet approach as shaker thrust demand is less.

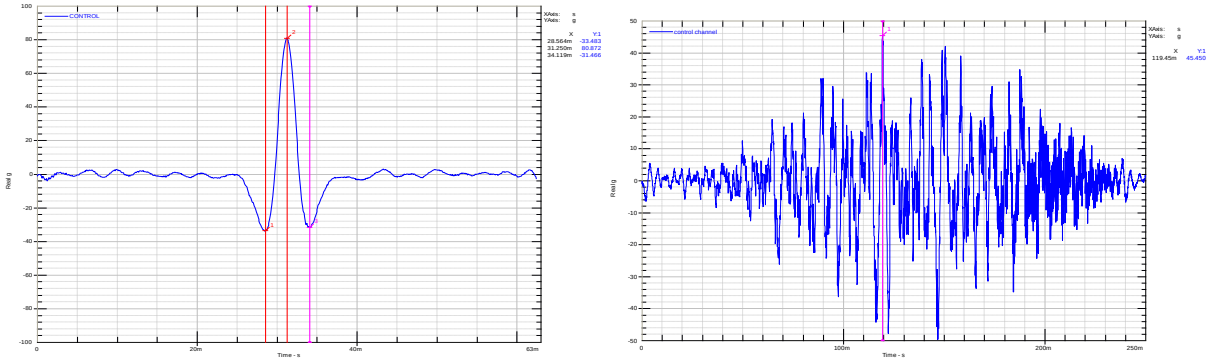

Figure 13-54: Base input accelerations applied to test specimen

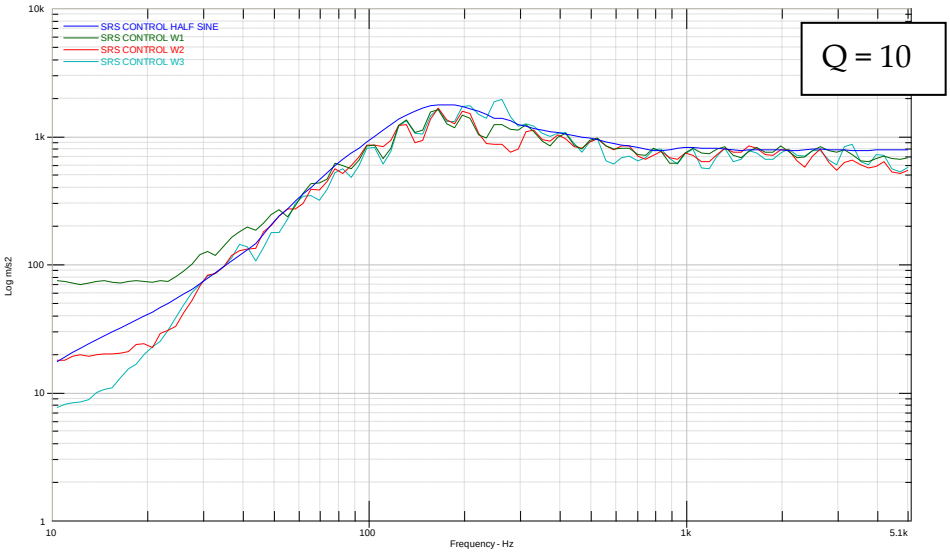

Figure 13-55: Comparisons of SRS for half sine and alternative wavelet base inputs

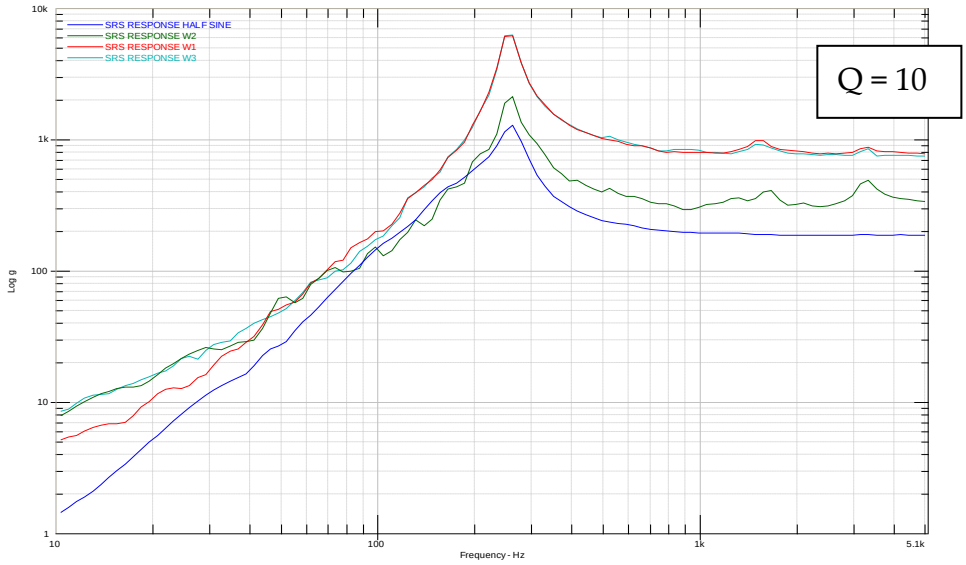

Figure 13-56: Comparisons between tip responses for the half sine and alternative wavelet base inputs

Peak response from the wavelet excitation tests typically show peak time domain responses in excess of 700g compared with approximately 150 g from the half sine impulsive input. Figure 13-56 shows 'overlay' plots for the four tip response SRS (Q = 10) considered during testing. The SRS ripple in Figure 13-55 for the wavelet SRS are generally marginally below the SRS profile for the impulse SRS, hence one would possibly expect in the absence of this 'ripple' if pure spectra were achieved with exact overlay (over the impulse SRS) then wavelet induced peak responses would have been marginally greater than shown by these tests.

In summary, these tests validate the initial pre-test hypothesis of influence of the time domain forcing function of the wavelet/harmonic form versus impulsive. Assumption of damping influence insensitivity on impulsive response cannot be applied when considering the wavelet / harmonic form. It can be seen that with near consistent SRS' for the industrial norm of Q = 10 can yield response from wavelet excitation much greater than those resulting from impulsive excitation when the test item damping is much lower than expected.

13.3.5.3.2 Overall recommendations and points of note relating to shaker based shock testing

The following general notes and recommendations can be addressed relating to Shaker Based Shock Testing:

- Modal damping of the test can be a key consideration. It has been shown that significant over test could result if an impulsive test is translated to a wavelet test based upon SRS consideration alone and modal damping is low. In this respect a logical conclusion is to access input SRS (damping).
- Specification achievement above 1.5 kHz - 2,5 kHz can be problematical due to shaker control and shaker transmissibility affects since the resonance frequency of the shaker armature is usually in this frequency regime.
- Consideration should be given to shaker selection for reasons given in previous point two). It has been shown that a small / stiffer shaker arrangement can be beneficial for high frequency achievement.
- Test item foot print size can result in significant input variation across the test item which can mean over/under test relative to each interface.

- For shaker axial tests (non-slip table) balancing of the test item set-up can need to be considered.
- The wavelet approach can be advantageous in terms of environmental representativeness. Inputs into units from Spacecraft shock tests typically are transient followed by post transient free vibration response resulting from dominant local Spacecraft modes of say either a panel or breathing modes of say a central cylinder. It could be questioned that a short duration impulsive test (e.g. half sine) does not represent such response of Spacecraft systems and in this context a wavelet based periodic modulated or damped sinusoid is more representative. Conversely, the primary advantage of a wavelet relative to an impulse is the ability to address shaker thrust limitation i.e. to achieve a required SRS but with lower peak input acceleration – it should be noted that this achieved at the expense of pulse duration representativeness. However it is important to pay attention to limit the time signal duration has much as possible, and to forbid serial application of the shock frequency components (see section 13.1.1).

13.4 Test monitoring

13.4.1 Accelerometers

Accelerometers are the **most widely used type of transducer for measuring shock events**. Small size, light weight and wide bandwidth are the common attributes that make them so useful for vibration and shock measurements. However not all accelerometers are suitable for all shock measurements.

The old adage "garbage in, garbage out" is very appropriate for shock measurements. Non-linear distortion, clipping, over-ranging, cable noise, intermittent connections, mass loading, environmental influences can all affect the measurement.

There are several different sensor technologies that are available and the following discussion details the more popular designs and their appropriateness for shock measurements [RD-056], [RD-057], [RD-058], [RD-059], [RD-060], [RD-061], [RD-062], [RD-063], [RD-064])

13.4.1.1 Piezoelectric accelerometers (PE)

Piezoelectric accelerometers work on the principle of **stressing a piezoelectric element and measuring electrical output** caused by the dynamic force that had been applied. This could be from a vibration or a shock input. Many accelerometers use man-made piezoelectric materials (e.g. lead zirconate titanate) which conveniently can be manufactured to suit particular design requirements. Other designs use "natural" materials such as quartz or tourmaline.

With stiffness values on the order of 104^{E9} N/m^2, which is similar to that of many metals, piezoelectric materials produce a high output with very little strain. In other words, piezoelectric sensing elements have essentially no deflection and are often referred to as solid-state devices. It is for this reason that piezoelectric sensors are so rugged and feature excellent linearity over a wide amplitude range. In fact, when coupled with properly designed signal conditioners, piezoelectric sensors typically have a dynamic amplitude range (i.e.: maximum measurement range to noise ratio) on the order of 120 dB.

Sensors without integrated electronics are typically referred to as **charge mode sensors**.

A wide variety of piezoelectric accelerometer configurations are available. Piezoelectric accelerometers mainly use the piezoelectric crystal in a **compression mode or a shear mode**. Each method has its own particular advantages and disadvantages for different applications.

The typical element configurations are shown in Figure 13-57. The red represents the piezoelectric crystals, while the arrows indicate how the material is stressed. **Accelerometers typically have a seismic mass**, which is represented by the grey colour.

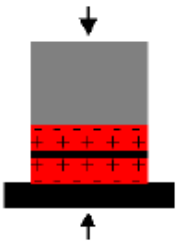 **Compression design**	 **Shear design**
Disadvantages: High sensitivity for a given resonance frequency compared to other designs, resulting in an extremely Rugged accelerometer Higher sensitivity to base strain Higher sensitivity to thermal transient effects Require low-noise coaxial cable	**Advantages:** Well balanced blend of wide frequency range Low off axis sensitivity Low sensitivity to base strain Low sensitivity to thermal inputs. **Disadvantages:** Require low-noise coaxial cable

Figure 13-57: Comparison of piezoelectric accelerometers in compression mode and shear mode

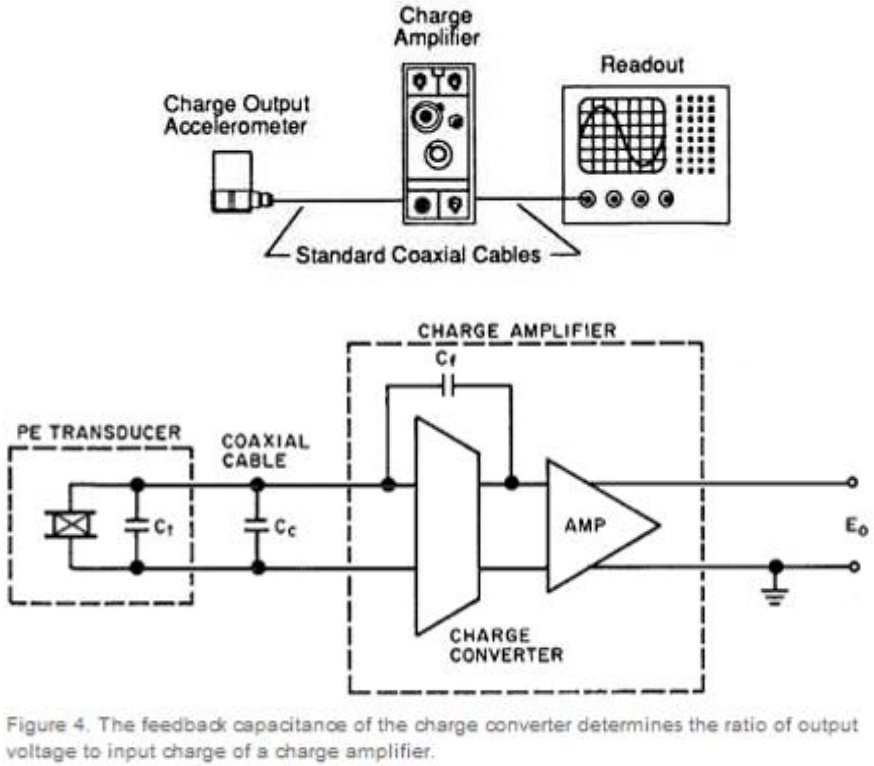

Figure 13-58: Piezoelectric accelerometers principle

13.4.1.2 Piezoelectric accelerometers with integrated electronics (IEPE)

These accelerometers have many different names depending on the particular manufacturer.

With the advent of hybrid microelectronics, it was possible to add a voltage amplifier of a charge amplifier inside the accelerometer casing. This meant that the output from the accelerometer could be at high level and also low impedance. The low impedance output allows the accelerometer to be used with simple cabling, not requiring the special low-noise cable that is essential with normal piezoelectric accelerometer.

Sensors containing built-in signal conditioners are classified as Integrated Electronics Piezoelectric (IEPE) or **voltage mode sensors. Other acronyms are used but are registered trademarks (e.g. ICP® for PCB Group, Inc.).**

The same type of constructions also applies to IEPE sensors (compression/shear designs), the only difference lies in the integrated microelectronic signal conditioning circuitry. In addition to providing crucial impedance conversion, IEPE sensor circuitry can also include other signal conditioning features, such as gain, filtering, and self-test features.

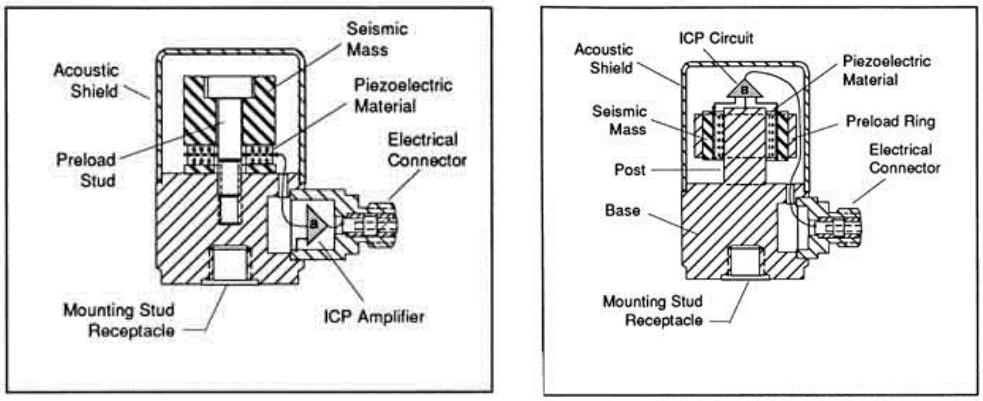

(a) (b)

Figure 13-59: Piezoelectric accelerometers with integrated electronics

(a) Compression design – (b) shear design

Piezoelectric accelerometers with integrated electronics have a limited operating temperature range, because of the integral amplifier, which also defines the dynamic range of the device. The overall performance depends on the quality of the piezoelectric sensor design, adding electronics does not overcome the limitations of a poorly designed sensor.

IEPE conditioning enhances the measurement system's signal-to-noise ratio.

A special feature of IEPE transducers is that power supply and measuring signal are transmitted via the same cable. So, an IEPE transducer requires, like a transducer with charge output, only one single-ended shielded cable. Figure 13-60 shows the principle circuit diagram.

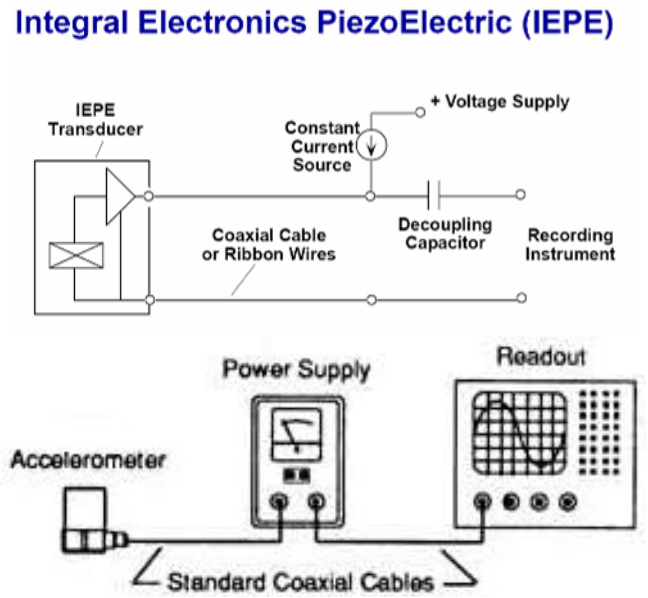

Figure 13-60: IEPE principle

The integrated sensor electronics is powered with constant current in the range between 2 and 20 mA. A typical value is 4 mA. Some battery powered instruments even work at 1 mA. The constant current I_{const} is fed into the signal cable of the sensor. The supply current and the length of the cable can influence the upper frequency limit.

The de-coupling capacitor C_c keeps DC components away from the signal conditioning circuit. The combination of C_c and R_{inp} acts as a high pass filter. Its time constant should be sufficiently high to let all relevant low frequency components of the sensor signal pass.

Important:

- Under no circumstances a voltage source without constant current regulation should be applied to an IEPE transducer.
- False polarization of the sensor cable can immediately destroy the built-in electronics.

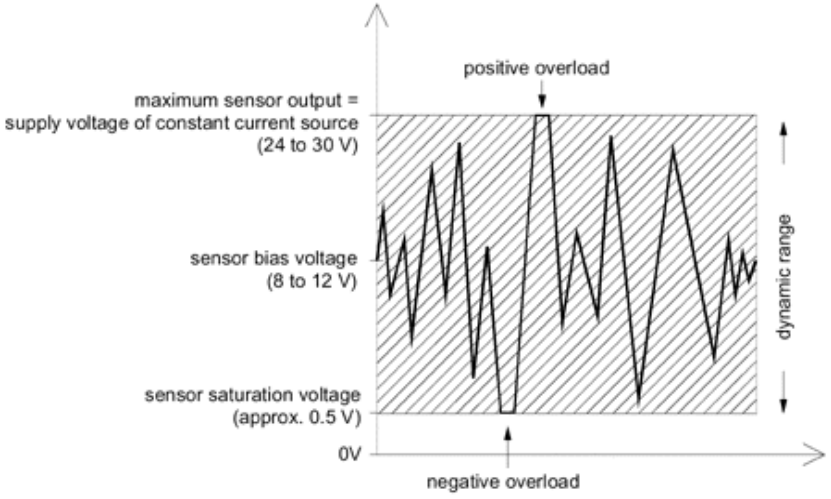

Figure 13-61: Dynamic range of IEPE accelerometers

In Figure 13-61 there can be seen that IEPE transducers provide an intrinsic self-test feature. By means of the bias voltage at the input of the instrument the following operating conditions can be detected:

- UBIAS < 0,5 to 1 V: short-circuit or negative overload

- 1 V < UBIAS < 18 V: output within the proper range
- UBIAS > 18 V: positive overload or input open (cable broken or not connected)

13.4.1.3 Piezoresistive accelerometers (PR)

The term 'piezoresistive' implies that an accelerometer's sensing flexure is manufactured from silicon as a microelectro mechanical system (MEMS). Piezoresistive accelerometers use silicon strain gauge sensing elements, in a Wheatstone bridge arrangement. The electrical resistance of the gauges changes in proportion to applied mechanical stress. Since silicon is a single crystal material, it is not only strong but is virtually free of mechanical hysteresis with inherently good linearity.

The piezoresistive accelerometer offers the advantages of lighter weight, smaller size, higher output and higher frequency response. A limitation in PR accelerometers is their tremendous amplification at resonance (as high as 1000:1), which can lead to sensor failure due to high-frequency inputs.

Unlike the piezoelectric accelerometer, the piezoresistive accelerometer is useful for measuring steady state acceleration (zero frequency).

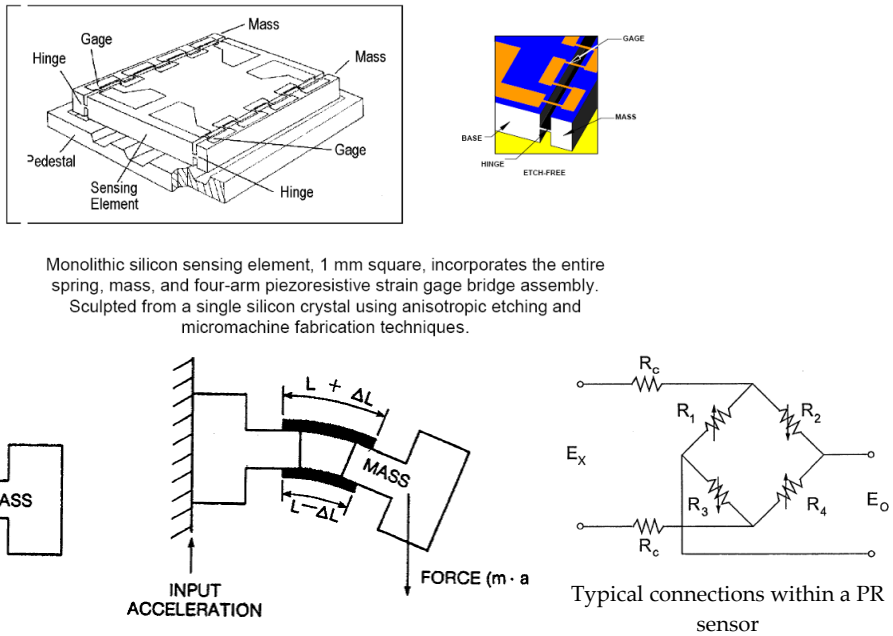

Figure 13-62: Piezoresistive accelerometer

The above sketches represent a simple application to piezoresistive gauges to produce an output proportional to acceleration. Strain gauges bonded on each side of the beam measure the strain on the surface of the beam. With acceleration applied to the structure, the beam bends. As the beam bends in one direction, the resistance of one gauge increases and the other decreases.

Early design of piezoresistive accelerometers featured extremely high resonance frequencies, very low damping and correspondingly extreme values of resonant amplification. These characteristics often caused zero-shift problems due to high frequency electronic limitations. To mitigate the aforementioned problem, more recent design (like 7270 AM 6 from Endevco) contains a mechanical isolation to mitigate high-frequency stimuli, or contains design features to reduce the amplification at resonance (like sensor 3501 by PCB).

13.4.1.4 Shock sensor selection criteria

When selecting accelerometers, it is important to pay attention to the critical sensor parameters, such as:

- Amplitude range and linearity,
- Resonance frequency and mounting effect,
- Electrical (for IEPE) and mechanical filters,
- Transverse sensitivity,
- Base strain sensitivity,
- Eventually the temperature sensitivity.

A good knowledge of the nature and severity of the shock environment to be measured is a key element for the selection of adequate accelerometers:

- For general purpose instrumentation (far-field measurement), Piezoelectric sensors can be used; whereas for a more intense shock exposure IEPE sensors should be selected. For sensors at direct vicinity to a pyrotechnic shock source, Piezoresistive sensor is often the only choice.
- IEPE and PR accelerometers are low impedance output devices and do not suffer from triboelectric cable noise problems. Where violent cable motions are expected, IEPE or PR accelerometers should be selected.
- The accelerometer's resonant frequency should be as high as possible, or at least decoupled from the expected shock environment, in order to avoid saturation (excitation of accelerometer resonance). As a general recommendation, the accelerometer's resonant frequency should be at least 5 times greater than the highest frequency content of the expected shock environment.
- As a consequence of the above recommendation on decoupling, PE accelerometers should not be used on a direct loadpath from a pyrotechnic shock source. PE accelerometers, having a resonant frequency typically around 50kHz, should be strictly limited to far-field measurement.
- Accelerometers with built-in electrical filter offer a better protection against ringing of the crystal element, and hence are well suited for far-field high-g shock measurement. Adding a mechanical filter offers an additional protection against high frequency content excitation, and hence such accelerometers are better suited for mid-field high-g shock measurement.
- Sensitivity to base strains is of importance, since these can be introduced into the accelerometer by distortion of the structure being measured. If the accelerometer cannot be mounted to a rigid block, an accelerometer with low base strain sensitivity should be used.
- Measurement of near-field to mid-field pyroshock requires the selection of Piezoresistive accelerometers. Such accelerometers are capable of responding to and surviving extremely fast rise times, typical of a high-G shock event. Special attention is required when selecting PR accelerometers, to ensure that the recording of shock responses is not affected by dynamic offset. To achieve this a dedicated attention should be paid to the mounting condition (always on a mounting block, with flat and smooth matting surfaces, and using a torque wrench). PR accelerometers with mechanical filter or with low amplification at resonance should be used.

The Table 13-5 provides the performance specifications for the most commonly used shock sensors. This table is not exhaustive and restrictive. Other sensors or newer versions can be used, if their characteristics are equivalent or superior to the ones provided in Table 13-5.

Table 13-5: Usual shock sensors and associated characteristics (not limited list)

Type	Photo	Max. sinusoidal accel pk (g)	Overload limit (shock) (g)	Mech. Filter (Res. Freq.)	Mounted resonant Frequency (Hz)	Electrical Filter (Res. Freq.)	Mass (gr)	transverse Sensitivity %	Frequency Range & Linearity	Sensitivity	Strain base Sensitivity g pk /με
B&K 4393 **PE**		±5000	25000	No	55 kHz	No	2,4	< 4	12 kHz (±5%)	3,1 pC/g	0,0005
B&K 8309 **PE**		±15000	100000	No	180 kHz	No	3	< 5	39 kHz (±5%)	0,04 pC/g	0,2
B&K 4374 **PE ****		±5000	25000	No	85 kHz	No	0,65	<5	18,5 kHz (±5%)	1,1 pC/g	0,0005
Endevco 2225 **PE**		±20000	20000	No	100 kHz	No	2	< 5	10 kHz (±2%)	0,75 pC/g	0,03
Endevco 2220 D **PE**		±1000	5000	No	50 kHz	No	3,1	< 5	10 kHz (±5%)	3 pC/g	0,05
Endevco 2222 C **PE ****		±1000	10000	No	32 kHz	No	0,5	< 5	10 kHz (±5%)	1,4 pC/g	0,04
Endevco 2255 B1 **IEPE**		±5000	100000	No	270 kHz	Yes	2	< 5	20 kHz (±1dB)	1 mV/g	0,2
Endevco 2255 B01 **IEPE**		±50000	100000	No	300 kHz	Yes	2	< 5	20 kHz (±1dB)	0,1 mV/g	1

Type	Photo	Max. sinusoidal accel pk (g)	Overload limit (shock) (g)	Mech. Filter (Res. Freq.)	Mounted resonant Frequency (Hz)	Electrical Filter (Res. Freq.)	Mass (gr)	transverse Sensitivity %	Frequency Range & Linearity	Sensitivity	Strain base Sensitivity g pk /με
Endevco pyrotron 7255 A 01 **IEPE**		±50000	300000	15 kHz		Yes	5	< 5	10 kHz (±1dB)	0,1 mV/g	
Endevco pyrotron 7255 A 1 **IEPE**		±5000	25000	15 kHz		Yes	5	< 5	10 kHz (±1dB)	1 mV/g	
PCB 3501A12 60KG **PR**		±60000	180000	No but low Q	> 120 kHz	No	3	< 3	10 kHz (±1dB)	0,003 mV/g	0,1
Endevco 7270 A 20k **PR**		±20000	60000	No	350 kHz	No	1,5	< 5	50 kHz (±5%)	0,01 mV/g	2mV/με (200 g/με)
Endevco 7270 A 60 k **PR**		±60000	180000	No	700 kHz	No	1,5	< 5	100 kHz (±5%)	0,003 mV/g	2mV/με (600 g/με)
Endevco 7270 A 200 kg **PR**		±200000	200000	No	1200 kHz	No	1,5	< 5	150 kHz (±5%)	0,001 mV/g	2mV/με (2000 g/με)
Endevco 7270 20kM6 **PR**	 Actual size	±20000	60000	≈ 10 kHz		No	5	< 5	10 kHz (±5%)	0,01 mV/g	

Type	Photo	Max. sinusoidal accel pk (g)	Overload limit (shock) (g)	Mech. Filter (Res. Freq.)	Mounted resonant Frequency (Hz)	Electrical Filter (Res. Freq.)	Mass (gr)	transverse Sensitivity %	Frequency Range & Linearity	Sensitivity	Strain base Sensitivity g pk /με
Endevco 7270 60kM6 **PR**	 Actual size	±60000	180000	≈ 10 kHz		No	5	< 5	10 kHz (±5%)	0,003 mV/g	
PCB 357 A09 **PE ****		±2000	10000	No	> 50 kHz	No	0,6	< 3	10 kHz (±5%)	1,7 pC/g	< 0,1
PCB 357 A08 **PE ****		±1000	10000	No	> 70 kHz	No	0,16	< 5	12 kHz (±5%)	0,35 pC/g	
DJB A23E **PE**		±5000	10000	No	50 kHz	No	4,5	5	10 kHz (±2%)	8 pC/g	0,01
DJB A28E **PE ****		±5000	10000	No	45 kHz	No	0,25	5	10 kHz (±2%)	0,4 pC/g	
PCB 350 B03 **ICP ***		±10000	50000	23 kHz	> 100 kHz	13 kHz	4,5	7	10 kHz (±1dB)	0,5 mV/g	0,002
PCB 350 B04 **ICP**		±5000	50000	23 kHz	> 100 kHz	13 kHz	4,5	7	10 kHz (±1dB)	1 mV/g	0,002
PCB 350 B21 **ICP *****		±100000	200000	No	> 200 kHz	No	4,4	7	10 kHz (±1dB)	0,05 mV/g	0,2

Type	Photo	Max. sinusoidal accel pk (g)	Overload limit (shock) (g)	Mech. Filter (Res. Freq.)	Mounted resonant Frequency (Hz)	Electrical Filter (Res. Freq.)	Mass (gr)	transverse Sensitivity %	Frequency Range & Linearity	Sensitivity	Strain base Sensitivity g pk /με
PCB 350 B23 **ICP**		±10000	50000	23 kHz	> 100 kHz	13 kHz	4,5	7	10 kHz (±1dB)	0,5 mV/g	0,002
PCB 350 B24 **ICP**		±5000	50000	23 kHz	> 100 kHz	13 kHz	4,5	7	10 kHz (±1dB)	1 mV/g	0,002
PCB 350 C02 **ICP**		±50000	150000	23 kHz	≥100 kHz	13 kHz	4,2	≤7	10 kHz (±1dB)	0,1 mV/g	
PCB 352 B01 **ICP ****		±5000	10000	No	> 65 kHz	No	0,7	< 5	10 kHz (±5%)	1 mV/g	
PCB 352 A25 **ICP ****		±2000	10000	No	> 80 kHz	No	0,6	<5	10 kHz (±5%)	2,5 mV/g	
PCB 352 C23 **ICP ****		±1000	10000	No	> 70 kHz	No	0,2	<5	10 kHz (±5%)	5 mV/g	
PCB 352 A73 **ICP ****		±1000	10000	No	> 70 kHz	No	0,3	<5	10 kHz (±5%)	5 mV/g	
PCB 356 A01 **ICP** Tri-axis		±1000	10000	No	> 50 kHz	No	1	< 5	8 kHz (±5%)	5 mV/g	
Kistler 8715A5 **IEPE**	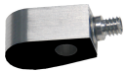	±5000	8000	No	> 70 kHz		2.1	< 3	10 kHz (±5%)	1 mV/g	0.005

Type	Photo	Max. sinusoidal accel pk (g)	Overload limit (shock) (g)	Mech. Filter (Res. Freq.)	Mounted resonant Frequency (Hz)	Electrical Filter (Res. Freq.)	Mass (gr)	transverse Sensitivity %	Frequency Range & Linearity	Sensitivity	Strain base Sensitivity g pk /με
Kistler 8743A10 **IEPE**		±10000	12000	No	≥100 kHz	No	4.5	1.5	10 kHz (±7%)	0.5 mV/g	0.005
Kistler 8743A20 **IEPE**		±20000	24000	No	≥100 kHz	No	4.5	1.5	10 kHz (±7%)	0.25 mV/g	0.005
Kistler 8743A50 **IEPE**		±50000	60000	No	≥100 kHz	No	4.5	1.5	10 kHz (±7%)	0.1 mV/g	0.005
Kistler 8743A100 **IEPE**		±10000	11000	No	≥100 kHz	No	4.5	1.5	10 kHz (±7%)	0.05 mV/g	0.005

* ICP is a trademark of PCB Group, Inc., which identifies uniquely PCB sensors that incorporate built-in electronics (IEPE)

** These ultra-small vibration transducers provide virtual transparency applied to lightweight structures, as such they can be installed on a Printed Circuit Board to measure the response to the pyroshock

*** Although sensor PCB 350 B21 features a high shock limit, the absence of mechanical/electrical filter prevents using it for near-field high-g shock measurements

13.4.1.5 Charge amplifiers

13.4.1.5.1 Overview

Accelerometers with charge output generate an output signal in the range of some picocoulombs (pC) with a very high impedance. To process this signal by standard AC measuring equipment, it needs to be transformed into a low impedance voltage signal. Preferably, charge amplifiers are used for this purpose. The input stage of a charge amplifier features a capacitive feedback circuit which balances the effect of the applied charge input signal. The feedback signal is then a measure of input charge. Figure 13-63 shows a typical charge input stage.

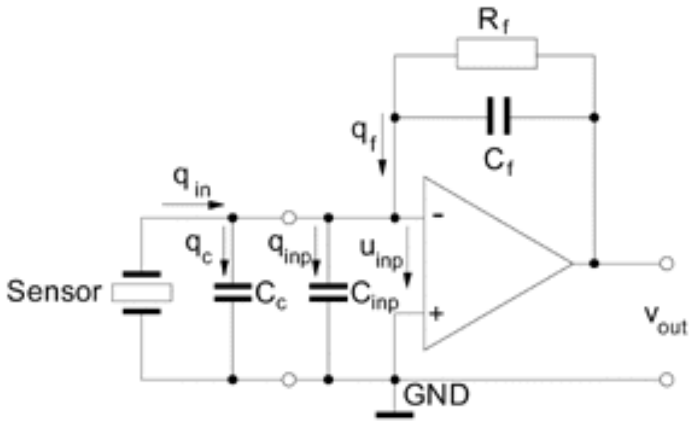

Figure 13-63: Charge amplifier

The input charge q_{in} is applied to the summing point (inverting input) of the amplifier. It is distributed to the cable capacitance C_c, the amplifier input capacitance C_{inp} and the feedback capacitor C_f. The node equation of the input is therefore:

$$q_{in} = q_c + q_{inp} + q_f$$

Using the electrostatic equation:

$$q = u.C$$

and substituting q_c, q_{inp} and q_f:

$$q_{in} = u_{inp}.(C_c + C_{inp}) + u_f.C_f$$

Since the voltage difference between the inverting and the non-inverting input of a differential amplifier becomes zero under normal operating conditions, we can assume that the input voltage of the charge amplifier u_{inp} is equal to GND potential. With $u_{inp} = 0$ we can simplify the equation:

$$q_{in} = u_f.C_f$$

and solving for the output voltage u_{out}:

$$u_{out} = u_f = q_{in} / C_f$$

The result shows clearly that the output voltage of a charge amplifier depends only on the charge input and the feedback capacitance. Input and cable capacitances have no influence on the output signal. This is a significant fact when measuring with different cable lengths and types.

Referring to Figure 13-63, the feedback resistor R_f has the function to provide DC stability to the circuit and to define the lower frequency limit of the amplifier. The circuit in Figure 13-63 represents only the input stage of a charge amplifier. Other stages like voltage amplifiers, buffers filters and integrators are not shown.

13.4.1.5.2 High-impedance voltage amplifiers

Instead of charge amplifiers, high impedance voltage amplifiers can be used with charge mode transducers. In this case, however, it is important to consider the capacitances of sensor, cable, and amplifier input (Figure 13-64).

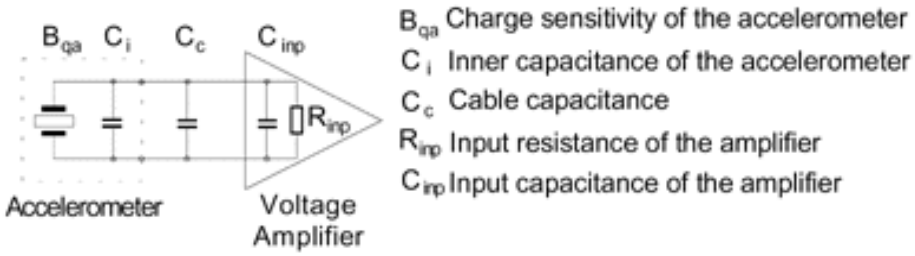

Figure 13-64: Charge mode sensor at voltage amplifier

The voltage sensitivity of an accelerometer with known charge sensitivity B_{qa} and inner capacitance C_i is calculated to:

$$B_{ua} = B_{qa} / C$$

B_{qa} and C_i can be found in the sensor's data sheet.

Taking into account the capacitance of the sensor cable C_c and the input capacitance C_{inp} of the voltage amplifier, the resulting voltage sensitivity B'_{ua} becomes lower than B_{ua}:

$$B'_{ua} = C_i / (C_i + C_c + C_{inp})$$

A typical 1,5 m low noise cable model has a capacitance of approximately 135 pF.

The lower frequency limit f_l can also be influenced by C_c, C_{inp} and R_{inp}:

$$f_l = \frac{1}{2 \pi R_{inp}(C_i + C_c + C_{inp})}$$

The lower frequency limit increases with decreasing input resistance.

Example: A charge mode accelerometer with inner capacitance Ci = 1,4 nF is connected to a typical scope input with R_{inp} = 10 MΩ and C_{inp} = 20 pF. The sensor cable has a capacitance of 135 pF. The lower frequency limit is then at about 10 Hz.

13.4.1.6 Accelerometer mounting

13.4.1.6.1 Overview

Mounting of the transducer is as important as the selection of the transducer in many applications. If the motion of the test structure is not accurately transmitted to the transducer, it cannot be accurately measured.

13.4.1.6.2 Surface Preparation

Transducer mounting technique and surface preparation can affect the amplitude-frequency response of the measurement, particularly at high frequencies. It is important to prepare a smooth and flat machined surface where the accelerometer is attached. Inspect the area to ensure that no metal burrs or other foreign particles interfere with the contacting surfaces.

Prior to mounting accelerometers, clean the mating surfaces with a hydrocarbon solvent.

In case of stud mounting, the application of a thin layer of silicone grease between the accelerometer base and the mounting surface also assists in achieving a high degree of intimate surface contact required for best high-frequency transmissibility.

13.4.1.6.3 Stud Mounting

The best way to mount a transducer is “stud mounted” (see NOTE). Stud mounting provides higher transmissibility than any other method. The direct coupling, stud mounted to a very smooth surface, generally yields the highest mechanical resonant frequency and, therefore, the broadest usable frequency range.

NOTE Some transducers feature an integral threaded fixing stud.

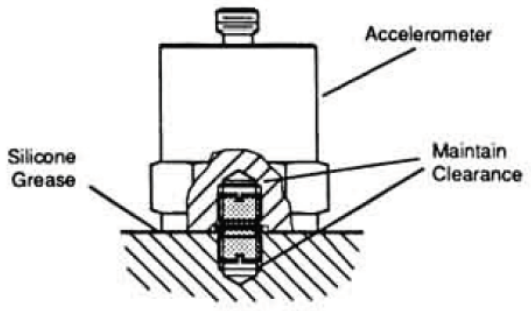

Figure 13-65: Accelerometer stud mounting

First, grind or machine on the test object a smooth, flat area at least the size of the sensor base, according to the manufacturer's specifications. Then, prepare a tapped hole in accordance with the supplied installation drawing, ensuring that the hole is perpendicular to the mounting surface. Install accelerometers with the mounting stud and make certain that the stud does not bottom in either the mounting surface or accelerometer base. Acceleration is transmitted from the structure's surface into the accelerometer's base. Any stud bottoming or interfering between the accelerometer base and the structure inhibits acceleration transmission and affects measurement accuracy (e.g. strain induced errors).

A torque wrench should be used to mount all accelerometers to ensure repeatability in the installation of the transducers and to prevent thread damage. The mounting torque recommended by the manufacturer should be followed. A thread-locking compound can be applied to the threads of the mounting stud to guard against loosening.

The sensors exposed to a stringent shock exposure (for instance at the spacecraft interface or close to a shock source) should be stud mounted.

13.4.1.6.4 Adhesive Mounting

Stud mounting is often impractical, since it alters the mounting surface. For far-field measurement (i.e. general purpose instrumentation in a spacecraft), an adhesive mounting is preferred. Furthermore most miniature accelerometers can only be mounted using an adhesive.

When adhesively mounting accelerometers, the amount (thickness) of adhesive can play a critical role in achieving good frequency response. A thin film or minimal amount of adhesive promotes higher transmissibility and hence a broader frequency response. The adhesive also influences the accelerometer's mounted resonance frequency.

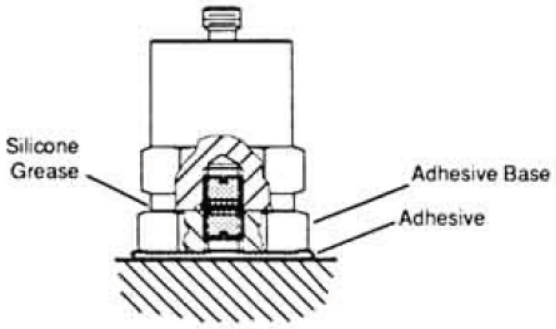

Figure 13-66: Accelerometer adhesive mounting

Prior to mounting accelerometer, clean the mating surfaces with appropriate solvent.

It is important that great care is taken when dismounting an adhesively mounted transducer. It should not be removed with impacts. All traces of adhesives should be removed using recommended solvents only. Most damages to miniature accelerometers are caused by improper removal techniques.

The type of adhesive recommended depends on the particular application: **For general purpose** (such as far-field measurement in a spacecraft) a **cyanoacrylate instant adhesive** (Loctite™ type 454) has the best coupling characteristics over a wide frequency range; whereas **for a more intense shock exposure, a two components adhesive** (dental cement, type X 60) is a preferred solution.

13.4.1.6.5 Triaxial mounting blocks and isolation adapters

Many installations require the transducer to be mounted on an adapter block for triaxial (three orthogonal axes) measurement. The block itself becomes part of the structure being measured, and acts as an additional spring mass system. Therefore a good mounting block should be as small, lightweight, and stiff as possible.

When mounting blocks are used in direct vicinity to a shock source, the sensors should be stud mounted onto the block, and the block itself should be cemented (two components adhesive) and screwed onto the mounting surface.

Figure 13-67: Accelerometer triaxial mounting blocks

13.4.1.7 Accelerometer cabling

The selection of connectors and cables has a direct impact on the ruggedness and reliability of the sensor installation. This is why it is so important to use the cable specified by the transducer manufacturer. Such cables usually include a special noise-reduction treatment.

It is good practice to clamp down loose cables, as shown in Figure 13-68. This also helps to reduce dynamically induced noise generated by the cables.

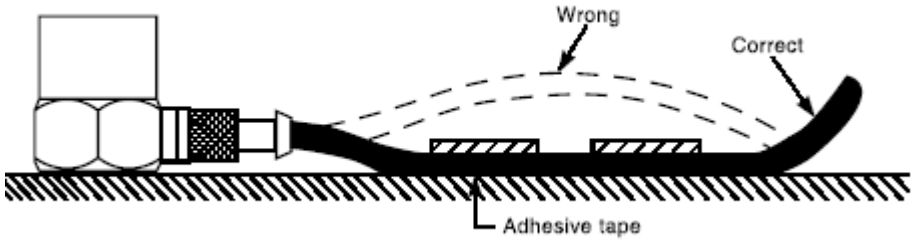

Figure 13-68: Securing cables

Additional shielding is often necessary in order to insure clean vibration signal transmission, for instrumentation in direct vicinity to a shock source. This is realised by isolating the cable from the structure with a double face adhesive, and by covering the cable with an aluminium tape.

13.4.2 Strain gauges

13.4.2.1 Overview

Although the usage of strain gauges is not usual during pyro test campaigns, essentially because all the specifications are based on SRS extracted from acceleration measurements, it is however recommended to use them when the physical phenomenon such as strain compression and bending waves needs to be characterised/understood. Enough experience has been gained today for enabling the use of strain gauges in pyroshock campaigns, with a reasonable associated cost. The range of amplitudes covers 10 μm/m (close to the electrical ground noise, which mitigation is necessary to get clean measurements in this lower part of the range) to 3000 μm/m, distance from the source greater than 20 cm. For measurements in near field conditions (less than 20 cm from the source) the risk of excitation of the cable resonance increases when approaching the source. So far, validation of cable mounting conditions in near field conditions (less than 20 cm from a linear source) has not been achieved.

Strain gauge measurements do not replace corresponding acceleration measurements but are complementary.

13.4.2.2 Type of resistance elements

- Foil strain gauges: foil strain gauges come with a resistance element - a several micro-meters thick foil resistor of Cu-Ni or Ni-Cr alloy. These gauges feature accurate size and uniform characteristic through photo-etching technology, as well as comparatively low production costs. A versatile lineup is the extra. All this makes foil strain gauges the most popular tool used for strain measuring in general.
- Wire strain gauges: these gauges use a resistor wire or Cu-Ni or Ni-Cr alloy, 13 μm - 25 μm in thickness, for the resistance element. They serve in paper gauges, extra long size concrete

measurement gauges, high elongation gauges, and special purpose gauges such as high temperature gauges, as well.

- Semiconductor strain gauges: their resistance element is formed by monocrystal such as silicon, whose gauge factor is as large as 90 - 200. This makes them suitable for detection of microstrains as well as manufacturing of high sensitivity sensors. They even eliminate the need for an amplifier in measurement of impact wave forms. These gauges are however largely affected by temperature, and are also poor in non-linearity. Their applications can be limited, accordingly.

For the purpose of strain measurement induced by pyroshocks, the foil strain gauge is so far the most adapted.

Backing matrix materials: the material of a backing matrix affects a gauge's characteristics same as the material or a resistance element. Generally, a backing matrix uses polyimide or some other organic material. High temperature gauges use ceramics; and weldable gauges use metals such as Inconel 600.

13.4.2.3 Gauge size

13.4.2.3.1 General considerations

The strain gauge size limits the frequency range of the gauge.

- Gauge length is an important consideration in strain gauge selection, and is usually the first parameter to be defined.
- Dimensions listed for gauge length (as measured inside the grid end loops) and grid width refer to active grid dimensions. Overall length and width refer to the actual foil pattern, not including alignment marks or backing.
- The matrix size represents the approximate dimensions of the backing matrix of the gauge as shipped. Matrix dimensions are nominal, with a usual tolerance of ±0,015 in [±0,4 mm]. If the gauges are encapsulated, the matrix can be smaller by as much as 0,01 in [0,25 mm]. Most patterns also include trim marks, and, for use in a restricted area, the backing matrix can be field-trimmed on all sides to within 0,01 in [0,25 mm] of the foil pattern without affecting gauge performance.

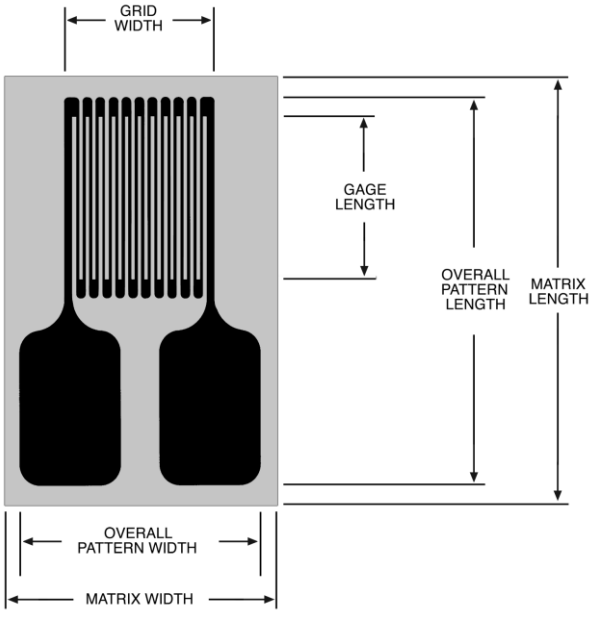

Figure 13-69: Gauge dimensions

The active grid length, in the case of foil gauges, is the net grid length without the tabs and comprises the return loops of the wire gauges. The backing dimensions are designed for the optimum function of the strain gauge.

13.4.2.3.2 Relation between the gauge length and the highest measured frequency

One general rule is that the gauge length is lower than $1/10^{th}$ of the measured wavelength.

Example: if the test objective is to measure a phenomena around 250 kHz, with a compression wave speed of 5200 m/s, it comes $\lambda=5200/250.10^3 = 2cm$, thus a maximal gauge length of 2 mm is necessary. As the frequency of 250 kHz can be seen as a top-level request, the length could be extended up with consideration of other criteria such as particular irregularities in the material under stress that could limit the gauge length: e.g. size of holes, and irregularities in loading distribution.

Table 13-6: Relation between the gauge length and the maximal frequency

Length (mm)	**Max Frequency** (kHz)
1	500
2	250
3	166
6	83

13.4.2.4 Conditions of bonding (gluing or adhesion) of the strain gauge to the structure

Because a strain gauge can perform no better than the adhesive with which it is bonded to the test member, the adhesive is a vitally important component in every strain gauge installation. Although there is no single adhesive ideally suited to all applications, the suppliers offer a wide selection of adhesives to cover the spectrum of stress analysis testing, and for use in transducer manufacturing. The adhesives should be specially formulated and selected for highest performance under the recommended environmental conditions, and are packaged to provide for ease of mixing and application.

Each adhesive is accompanied by specific instructions for its proper handling — storage mixing, application, curing, and, if appropriate, post-curing. The adhesive containers are also dated to assure freshness of the contents.

NOTE It is usually a misguided economy to attempt installing strain gauges with out-dated adhesive, or adhesive that has not been stored as recommended. It should also be noted that conventional industrial and consumer adhesives are not generally suitable for bonding strain gauges. Since different adhesives are intended for different types of applications and different environmental conditions, it is obviously important to select the most appropriate adhesive for each strain measurement.

The gauges can be bonded either in room temperature or in elevated temperature. The elevated temperature requires the gauges to be installed on their support material in a thermal enclosure, thus limiting the cases where it could be employed.

Nevertheless, for the purpose of measuring pyroshock deformation responses, it has not appeared a significant difference between the room and elevated temperature bonding until at least 100 kHz. This can be compared with the calculation of the resonance frequencies of the mounted gauges (It is in fact the calculation of the resonance frequency of the joint unit of adhesive with the gauge behaving like an inert mass).

Example of gauges characteristics that led to a frequency of resonance of 3 MHz for the elevated temperature adhesive and 1 MHz for the room temperature adhesive, which is well in agreement with the fact that no difference was observed up to 100 kHz:

- Weight of a gauge: some mg
- Thickness of the adhesive:
  - Elevated temperature Adhesive M610 < 10μm
  - Room temperature Adhesive E10: 100 μm
- Stiffness: 3000 MPa for araldite
- Density: 1200 kg/m3 for araldite

13.4.2.5 Sensitivity

13.4.2.5.1 Overview

The output voltage of the gauge signal conditioning amplifier is given by the relation:

$$Vout = Vbr.A.(K/4).\varepsilon.10^{-6}$$

Where:

- Vbr is the supply voltage of the gauges bridge
- K is the gauge sensitivity
- A is the conditioning module amplification
- ε is the deformation

As it is stated in 13.4.2.7, high resistances allow higher voltages for a given power level.

The strain sensitivity k or gauge factor of a strain gauge is the proportionality factor between the relative changes of the resistance. The gauge factor of each production lot is determined by sample measurements and is given on each package as the nominal value with its tolerance. The reference temperature is the ambient temperature for which the technical data of the strain gauges are valid, unless temperature ranges are given. The technical data quoted for strain gauges are based on a reference temperature of 23 °C.

13.4.2.5.2 Strain Gauge Wire Material Selections

Although the sensitivity factor S is usually provided by the strain gauge vendors, engineers still need to choose the right gauge wire materials for their applications. Pros and Cons of common strain gauge wire materials are given hereafter:

- *Constantan* (Advance, Copel alloy) is the oldest and most widely used strain gauge materials. It has a high enough electric resistivity (r = 0,49 mW·m) to achieve a proper resistance for a small gauge length. It has a relatively low temperature induced strain in the temperature range of -30 °C to 193 °C (-20 °F to 380 °F). This material is thus considered to have self-temperature-

compensation. It has almost constant sensitivity across a wide range of strain. *Annealed Constantan* can even be used in the plastic region with strain > 5 %. But, The resistance of Constantan drifts continuously when the temperature raises above 65 °C (150 °F), which can become troublesome for strain measurements over a long period of time or in high temperature.

- Isoelastic alloy is suitable for *dynamic* strain measurement in vibration and impact. It has higher sensitivity (3,6 vs. 2,1 for Constantan), which improves the signal to noise ratio. It has higher resistance such that most isoelastic strain gauges have resistance of 350 W compared to 120 W in common Constantan strain gauges, which also increases the strain sensitivity. It has better fatigue properties among strain gauge materials. But, isoelastic alloy does not have self-temperature-compensation property unlike Constantan or Karma. It is too sensitive to changes in temperature, so that it is not suitable for measurements which last a long period of time with temperature fluctuations. Sensitivity reduces from 3,1 to 2,5 when strain exceed 7500 μm/m.
- *Karma* alloy has similar overall properties to Constantan.

13.4.2.6 Factors affecting optimum excitation

Following are factors of primary importance in determining the optimum excitation level for any strain gauge application:

1. *Strain gauge grid area* (active gauge length x active grid width).
2. *Gauge resistance*. High resistances permit higher voltages for a given power level.
3. *Heat-sink properties of the mounting surface*. Heavy sections of high-thermal-conductivity metals, such as copper or aluminium, are excellent heat sinks. Thin sections of low-thermal-conductivity metals, such as stainless steel or titanium, are poor heat sinks. Also, the shape of the gauged part can create thermal stresses in portions of the structure due to gauge self-heating. Long warm-up times and apparent gauge instability can result. The situation often arises in low force transducers, where thin sections and intricate machining are fairly common.

13.4.2.7 Thermal Considerations

Changes in temperature during the test duration are almost unavoidable. The mismatch of thermal expansion coefficients between gauge wire, backing, and specimen induces so called apparent strain which contributes to errors in the static or low frequency strain measurements. As we are here interested by the high frequency content, we can easily filter the low frequency content to eliminate the low frequency evolution, if necessary (that is not the case in general).

13.4.2.8 Potential Error Sources

13.4.2.8.1 Overview

In a stress analysis application, the entire gauge installation cannot be calibrated as can some pressure transducers. Therefore, it is important to examine potential error sources prior to analysing data.

Some gauges can be damaged during installation. It is important therefore to check the resistance of the strain gauge prior to stress.

Electrical noise and interference can alter your readings. Shielded leads and adequately insulating coatings can prevent these problems. A value of less than 500 MΩ (using an ohmmeter) usually indicates surface contamination.

Thermally induced voltages are caused by thermocouple effects at the junction of dissimilar metals within the measurement circuit. Magnetically induced voltages can occur when the wiring is located

in a time varying magnetic field. Magnetic induction can be controlled by using twisted lead wires and forming minimum but equal loop areas in each side of the bridge.

Temperature effects on gauge resistance and gauge factor is not an issue as stated above.

13.4.2.8.2 Recommended preliminary verifications

- Measure the base resistance of the unstrained strain gauge after it is mounted, but before wiring is connected.
- Check for surface contamination by measuring the isolation resistance between the gauge grid and the stressed force detector specimen using an ohmmeter, if the specimen is conductive. This should be done before connecting the lead wires to the instrumentation. If the isolation resistance is under 500 MΩ, contamination is likely.
- Check for extraneous induced voltages in the circuit by reading the voltage when the power supply to the bridge is disconnected. Bridge output voltage readings for each strain-gauge channel should be nearly zero.
- Connect the excitation power supply to the bridge and ensure both the correct voltage level and its stability.
- Check the strain gauge bond by applying pressure to the gauge. The reading should be unaffected.

In all cases, it is recommended, before a firing, to check the good behaviour of the whole acquisition chain, from sensor (strain gauge in our case) to data acquisition and even data basis management system by making a test with a hammer excitation. The data at the final stage of the acquisition chain should be carefully examined, in order to verify the coherence of the data (superposition of the first and reverse sides gauges signal in the initial phase of compression, temporal coherence with spatial location of the gauges …).

13.4.3 Load cells

Load cells can be used at the base of an equipment to measure interface force during a shock event. An example of load cell use at equipment interface is given below.

It is important that the usage of load cells is made with care as the boundary conditions are modified by the presence of the load cells. This effect is all the more important that the supporting structure is not stiff.

In the following example a specific baseplate has been installed in order to implement load cells at the interface of the unit on a sandwich panel. The excitation is a pyroshock generator. With respect to the configuration without the cells and the additional baseplate, the average accelerations at the interface of the unit are quite similar up to 10 kHz (Figure 13-71). However, the accelerations at the top of the unit are filtered above 3kHz, as illustrated on Figure 13-72. As the measured forces are dominated by frequency components below 1kHz, these measurements can be considered representative of the unit configuration without the force cells.

With this application case, the quality of the load time histories is excellent along the three directions, as illustrated on Figure 13-73. Peak values are measured along the normal axis, with a maximum amplitude reaching 700 N.

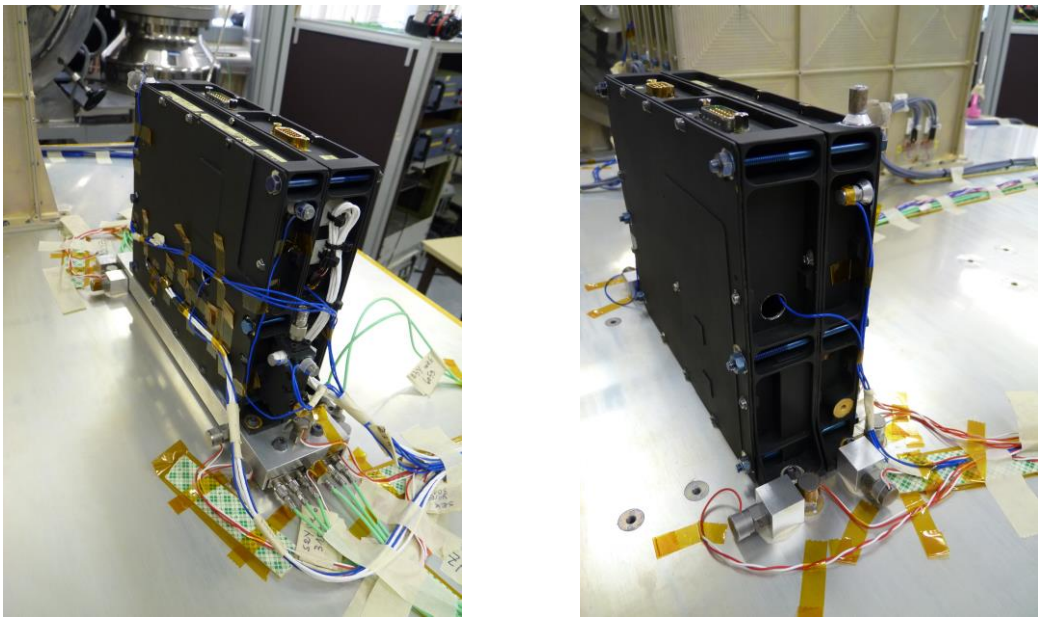

Figure 13-70: RF unit with tri-axial load cells at the base

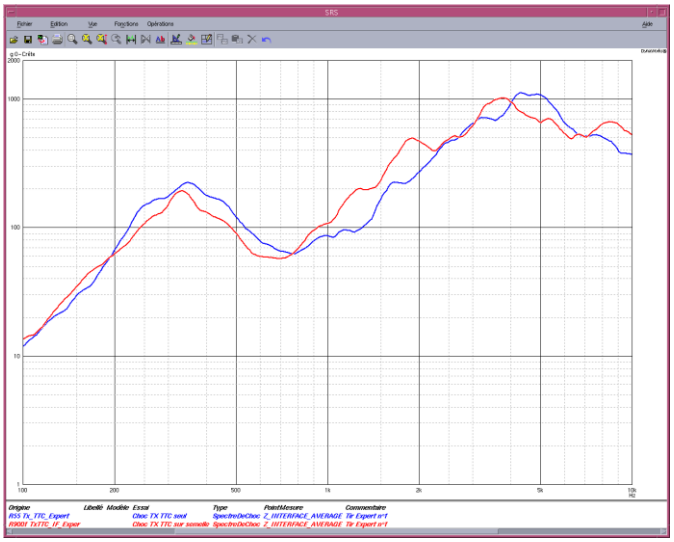

Figure 13-71: Average acceleration (Z) with and without the load cells

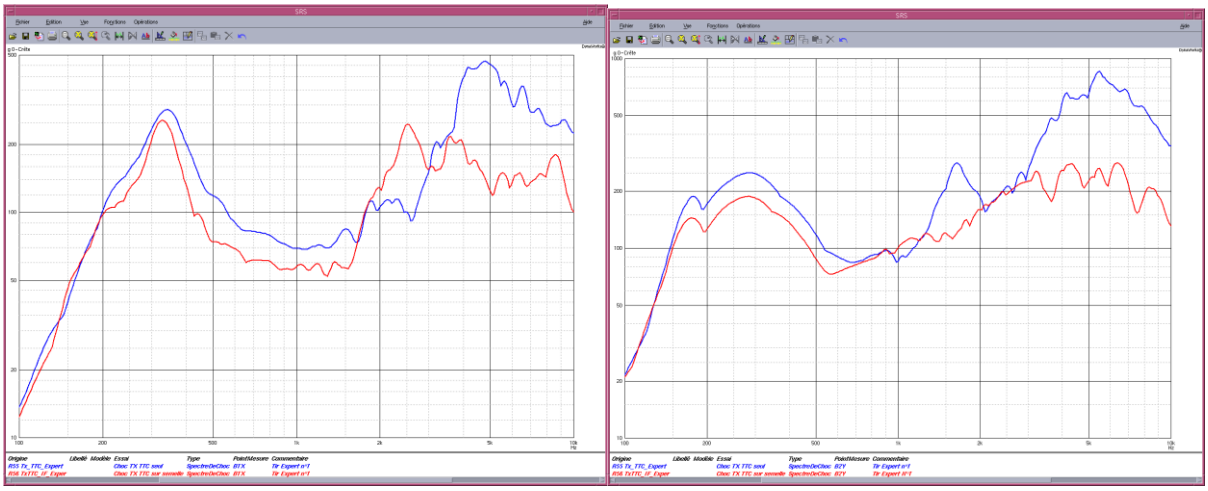

Figure 13-72: Top unit responses (X, Y, Z) with and without the load cells at the interface

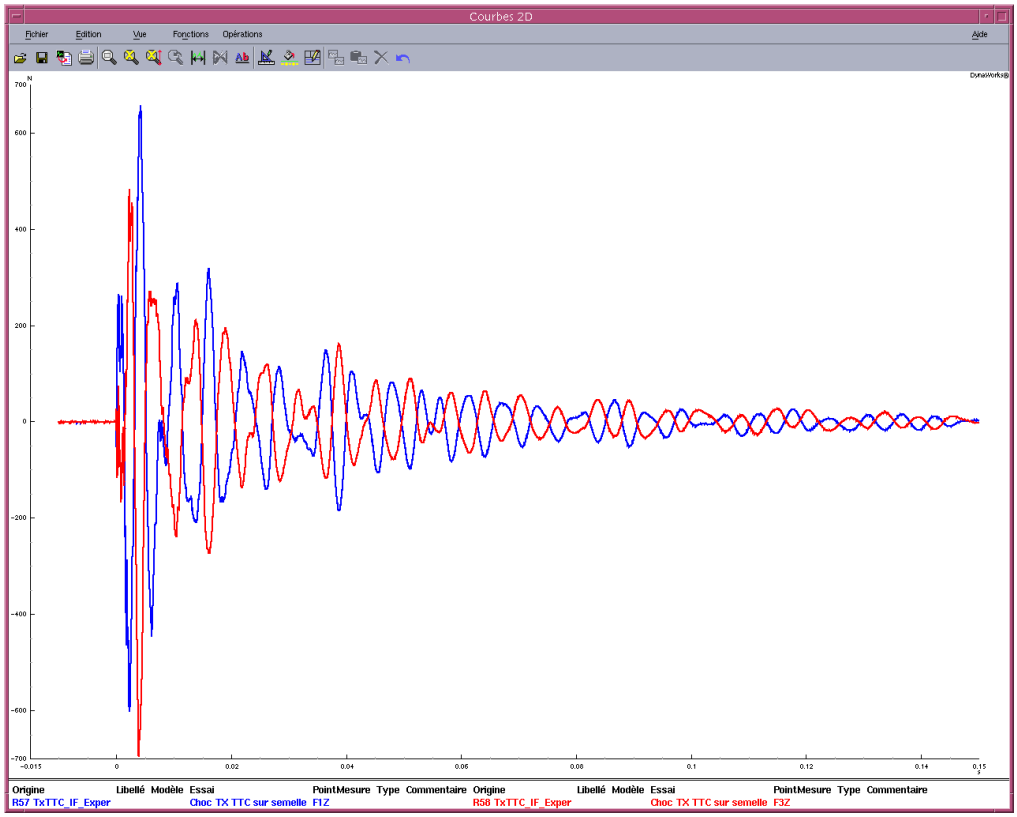

Figure 13-73: Measured I/F loads (Z)

13.4.4 Laser vibrometer

A Laser Doppler Vibrometer (LDV) is a scientific instrument that is used to make non-contact vibration measurements of a surface. The laser beam from the LDV is directed at the surface of interest, and the vibration amplitude and frequency are extracted from the Doppler shift of the laser beam frequency due to the motion of the surface. The output of an LDV is generally a continuous analog voltage that is directly proportional to the target velocity component along the direction of the laser beam.

Some advantages of an LDV over similar measurement devices such as an accelerometer are that the LDV can be directed at targets that are difficult to access, or that may be too small or too hot to attach a physical transducer. Also, the LDV makes the vibration measurement without mass-loading the target, which is especially important in many applications.

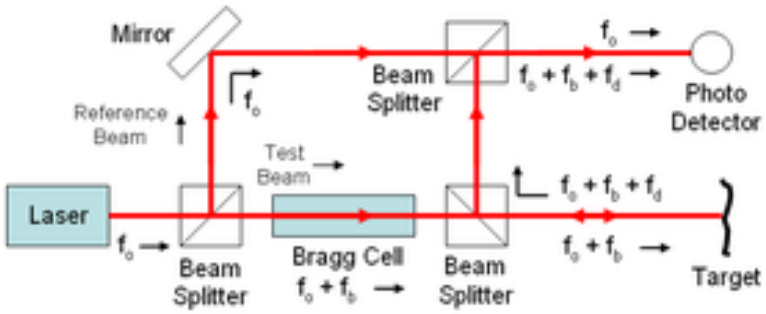

Figure 13-74: Basic components of a Laser Doppler Vibrometer

Principles of operation

An LDV is generally a two beam laser interferometer that measures the frequency (or phase) difference between an internal reference beam and a test beam. The most common type of laser in an LDV is the helium-neon laser, although laser diodes, fiber lasers, and Nd:YAG lasers are also used. The test beam is directed to the target, and scattered light from the target is collected and interfered with the reference beam on a photodetector, typically a photodiode. Most commercial vibrometers work in a heterodyne regime by adding a known frequency shift (typically 30–40 MHz) to one of the beams. This frequency shift is usually generated by a Bragg cell, or acousto-optic modulator.

A schematic of a typical laser vibrometer is shown above. The beam from the laser, which has a frequency f_0, is divided into a reference beam and a test beam with a beamsplitter. The test beam then passes through the Bragg cell, which adds a frequency shift f_b. This frequency shifted beam then is directed to the target. The motion of the target adds a Doppler shift to the beam given by $f_d = 2*v(t)*\cos(\alpha)/\lambda$, where v(t) is the velocity of the target as a function of time, α is the angle between the laser beam and the velocity vector, and λ is the wavelength of the light.

Light scatters from the target in all directions, but some portion of the light is collected by the LDV and reflected by the beamsplitter to the photodetector. This light has a frequency equal to $f_0 + f_b + f_d$. This scattered light is combined with the reference beam at the photo-detector. The initial frequency of the laser is very high (> 1014 Hz), which is higher than the response of the detector. The detector does respond, however, to the beat frequency between the two beams, which is at $f_b + f_d$ (typically in the tens of MHz range).

The output of the photodetector is a standard frequency modulated (FM) signal, with the Bragg cell frequency as the carrier frequency, and the Doppler shift as the modulation frequency. This signal can be demodulated to derive the velocity vs. time of the vibrating target.

Types of Laser Doppler vibrometers

- Single-point vibrometers – This is the most common type of LDV.
- Scanning vibrometers – A scanning LDV adds a set of X-Y scanning mirrors, allowing the single laser beam to be moved across the surface of interest.
- 3-D vibrometers – A standard LDV measures the velocity of the target along the direction of the laser beam. To measure all three components of the target's velocity, a 3-D vibrometer measures a location with three independent beams, which strike the target from three different directions. This allows a determination of the complete in-plane and out-of-plane velocity of the target.
- Rotational vibrometers – A rotational LDV is used to measure rotational or angular velocity.
- Differential vibrometers – A differential LDV measures the out-of-plane velocity difference between two locations on the target.
- Multi-beam vibrometers – A multi-beam LDV measures the target velocity at several locations simultaneously.
- Self-mixing vibrometers – Simple LDV configuration with ultra-compact optical head. These are generally based on a laser diode with a built-in photodetector.
- Continuous Scan Laser Doppler Vibrometry (CSLDV) – A modified LDV that sweeps the laser continuously across the surface of the test specimen to capture the motion of a surface at many points simultaneously

Example 1 – Vibrometer used at vicinity of expandable tube

The pyro source is an expandable tube. Two LDV were used in this test campaign :

- LDV 1 with a range of 10m/s and a frequency bandwidth of 1.5 MHz
- LDV 2 with a range of 30m/s and a frequency bandwidth of 80 kHz

Close near the two laser beam impacts were installed two classical accelerometers (type 1 and type2, as shown in the Figure 13-75 and Figure 13-76.

The analog output of the LDV is a velocity, as shown on the Figure 13-77. It should be derived to get the acceleration. Each imperfection in the velocity (in particular due to optical drop outs resulting from optical misalignments) is amplified after application of the derivation, and should to be corrected (by elimination of all the signal interval presenting a non-normal peak) : see Figure 13-78, where some minor peaks at the end of the signal haven't been totally eliminated. The Figure 13-79 represents a superposition of the two OOP accelerations obtained from the two LDV after derivation and peak elimination.

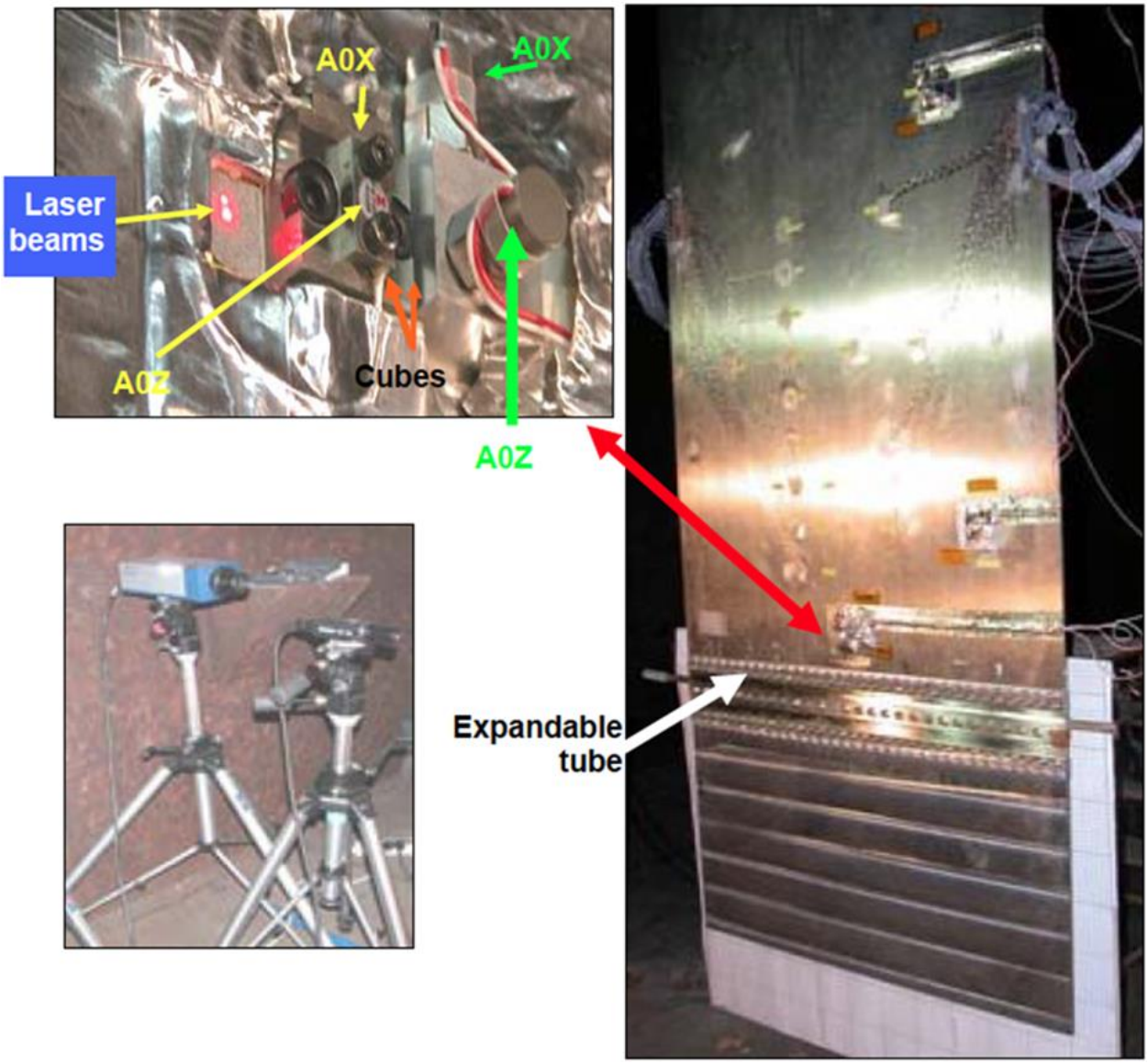

Figure 13-75: The instrumented plate (top left), the laser vibrometers (bottom left), and the location of the laser target for the vibrometers (right). Two types of accelerometers have been used (type 1 and type 2)

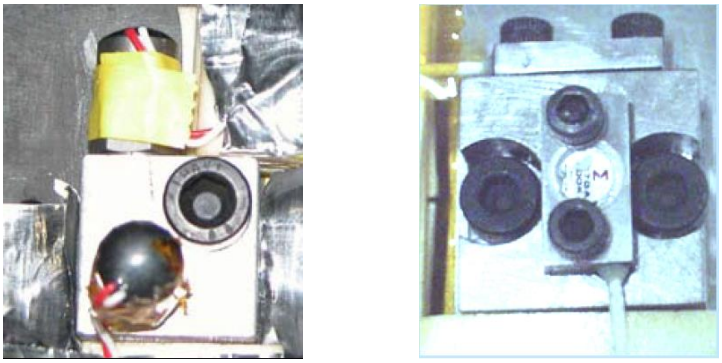

Figure 13-76: Type 1 accelerometer and Type 2 accelerometer

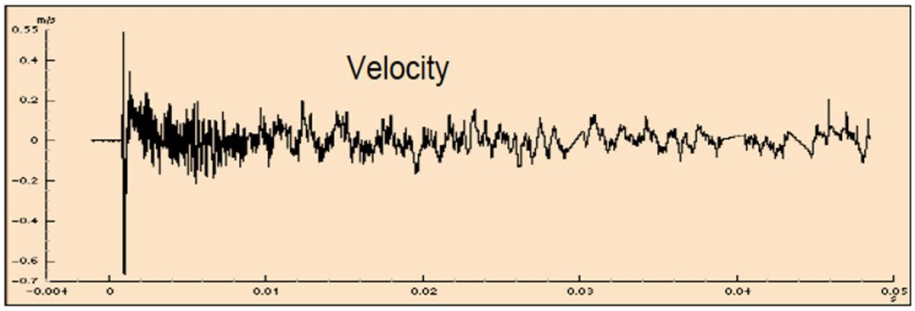

Figure 13-77: Out of plane velocity signal from the vibrometers

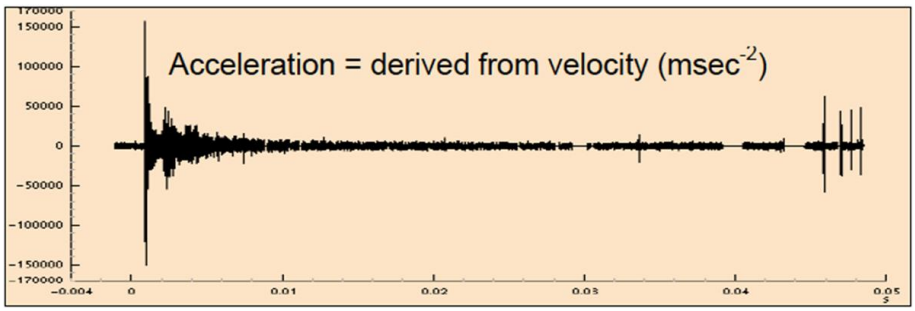

Figure 13-78: Acceleration signal derived from velocity

Figure 13-79 shows the superposition of the two accelerations (in m/s^2) extracted from the two vibrometers (10m/s and 30m/s), evidencing that the high performance vibrometer should be used for shock application.

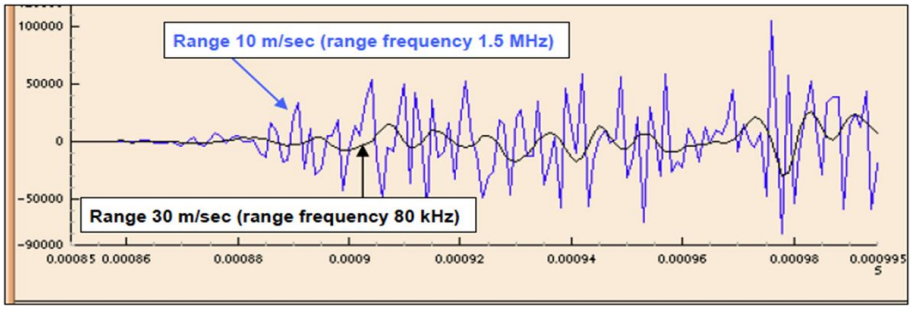

Figure 13-79: Superposition of acceleration signals from both vibrometers (10 and 30m/s)

A general concern with a classical accelerometer, is the sensitivity of the accelerometer reading to the deformation of the structure to which it is mounted: Such deformation induces a low frequency so-called "dynamic offset" in the signal, as shown on the Figure 13-80. The similarity in trend between the low pass filtered signal and the compression wave measured very close from the accelerometer is indeed obvious.

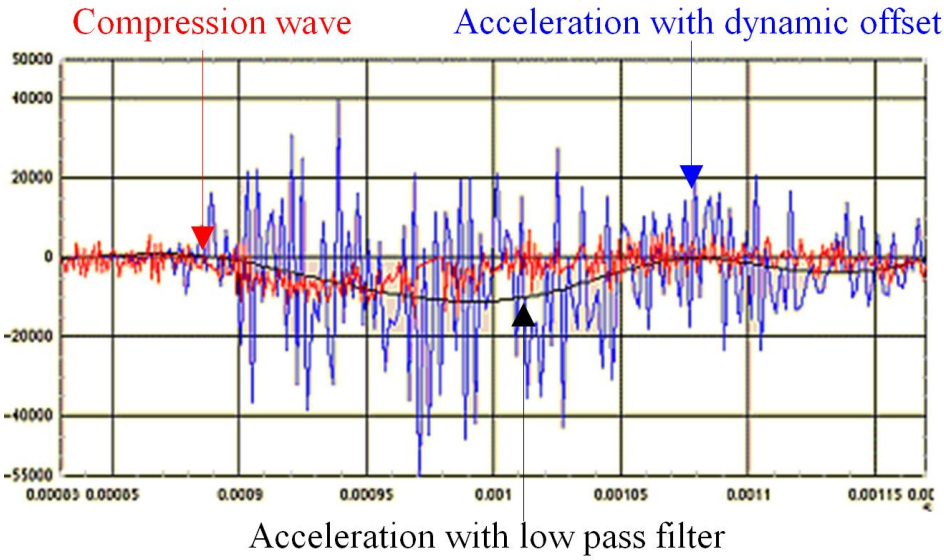

Figure 13-80: So called "dynamic offset" on the acceleration compared to the compression wave deformation wave measured close to the accelerometer

It is necessary to remove such low frequency contents from the original signal, in order to recover a meaningful SRS. It is shown in Figure 13-81, that the SRS computed from the original signal has a suspicious trend over the entire frequency range. Eliminating the dynamic offset (through Prony correction method in this case) allows recovering a meaningful SRS, which agrees very well up to 20kHz with the SRS computed from the vibrometer reading.

This example shows the relevance of advanced measurement technique (laser vibrometer), for measuring true environment, in areas where a classical measurement technique is reaching/overpassing its limitation (typically close to a shock source).

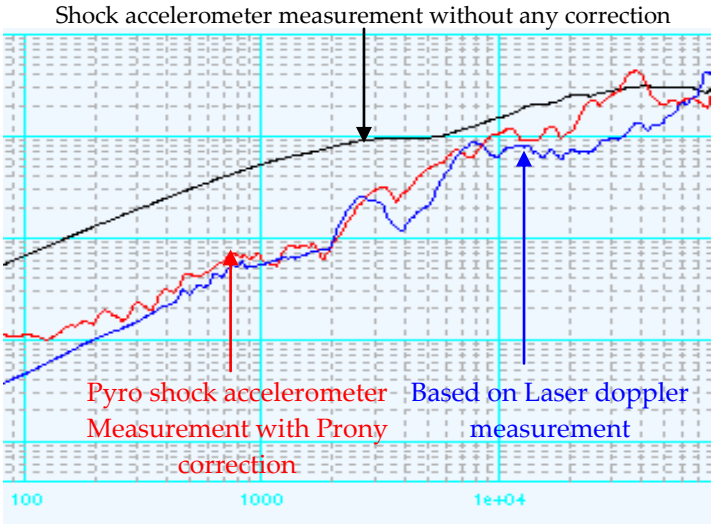

Figure 13-81: Comparison of the SRS's as measured by vibrometer and classical accelerometer (with and without PRONY correction)

Example 2 – Vibrometer used to characterised the transmissibility from equipment supporting structure to the equipment base plate

A laser vibrometer has been used to measure the in plane base acceleration on a unit mounted on a sandwich panel and submitted to a pyrotechnic shock generator. The test set-up is illustrated on Figure 13-82. It has been verified that a derivation of the velocity measured by the laser vibrometer and a small collocated accelerometer were giving the same acceleration. Indeed, Figure 13-83 shows that the two SRS are very similar as they present less than 2 dB differences in small frequency ranges between 100 Hz to 20 kHz, which is the cut-off frequency of the vibrometer.

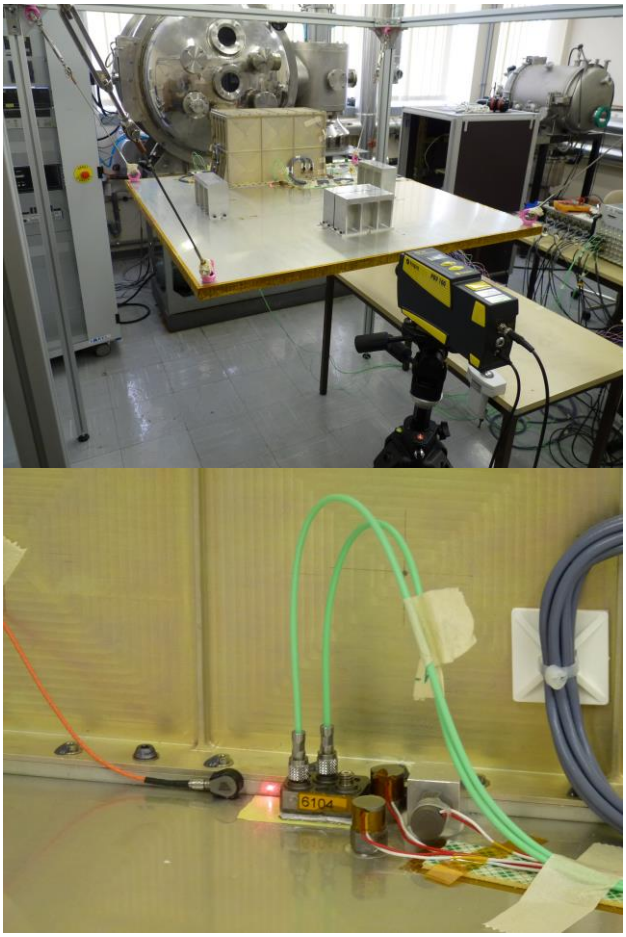

Figure 13-82: Laser vibrometer measurement of the in-plane acceleration

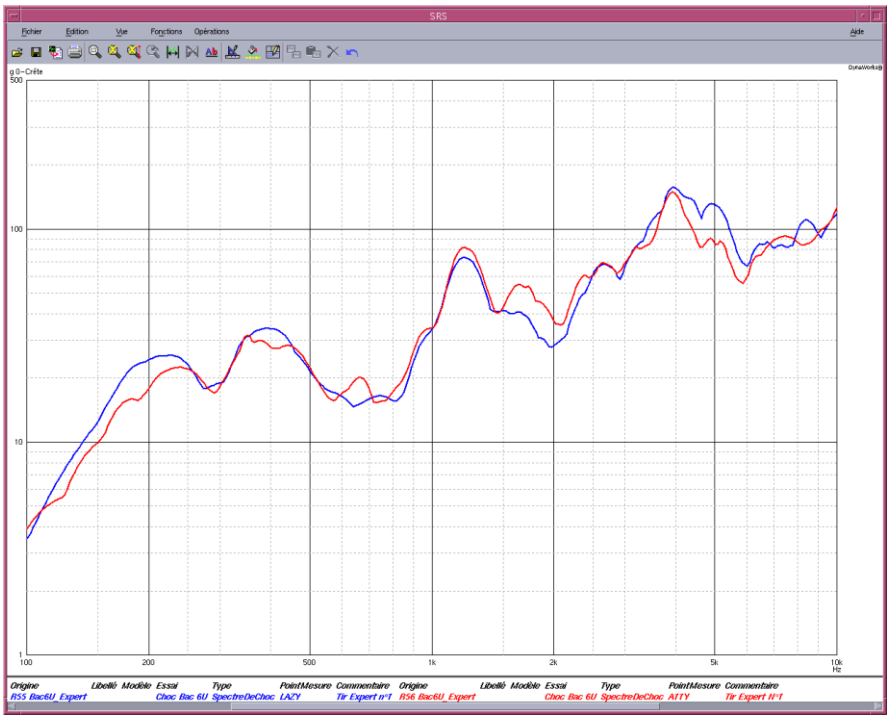

Figure 13-83: Different in-plane acceleration measurements at the same location

13.4.5 Acquisition systems

13.4.5.1 Overview

The selection of a suitable data acquisition system is primarily based on the characteristics of the recorded transient.. The acquisition chain (from sensors selection to readout equipment) is processed in accordance with the two main types of transient capture requirements:

1. Acquire far and mid field transients e.g. simulated by standard shock benches (procedure III) or generally speaking far from a pyrotechnical shock source
2. Measure near field transients originated from the firing of a pyrotechnical actuator, in direct vicinity to the source

Frequency and acceleration characteristics, associated with near field, mid field and far field are presented in paragraph 12.3.2.

In both cases, there is a need for high bandwidth data acquisition combined with a very good anti-aliasing filter (see paragraph 13.4.5.7.2) to ensure a correct acquisition of the time domain data over the entire pass-band. The anti-aliasing filter needs to guarantee excellent phase linearity to record the true transient amplitude levels. Also the channel to channel phase match (<0.5º) can be an criteria in particular for the assessment of transient waveform propagation in a structure. The data acquisition system needs to provide a high throughput rate (around 15MSamples/s) and sufficient disk space for high sampled recording and storing the time signals for the required channel count. Post processing and quick view capabilities to determine the quality the acquired transient signals (see also shock validity criteria, in paragraph 15), to analyse waveform propagation and to calculate shock response spectra with adjustable amplification factors and frequency resolution are also common for both cases.

However, there are also differing set of requirements towards the data acquisition system pending on the type of shock to be captured.

13.4.5.2 Far field and mid field measurements

Typically as induced by system test far from source, and by procedure III. The resulting shock environment is dominated by structural resonances with a frequency content below 10kHz. The absence of high frequency excitation reduces the risk of sensor ringing, saturation and overload of the data acquisition system. The available choice of instrumentation is large and in most cases standard of the shelf acquisition equipment can be used.

The sampling rate should be defined to cover an acquisition bandwidth of 10kHz. Thus, for far field excitation, a sampling rate of at least 50kHz per channel should be considered. In case excitation is expected up to 10kHz, for instance mid field simulations, then a greater sampling rate should be adopted (e.g. 100kHz).

For the setup, no specific precautions needs to be taken with respect to grounding/ ESD perturbations.

The use of a digital trigger with pre-trigger recording is a good practice.

13.4.5.3 Near field measurements

Typically as induced by system test at direct vicinity to source and by procedure II. The resulting shock environment contains high frequency excitation well above 10kHz. The high frequency excitation combined with very high peak acceleration levels (in excess of 5000g), can cause ringing of sensor and/or overload of the readout equipment. Utmost care should be taken in the selection and the setting of the various constituents of the acquisition chain in order to avoid saturation of signals (sensors selection should then be made according to recommendations provided in 13.4.1.4).

The sampling rate to be defined in accordance with the expected frequency content. The useful bandwidth is typically 100kHz which implies a sampling rate of 500kHz per channel (and more) should be selected.

For the setup, stringent precautions should be taken, in particular with respect to grounding of all equipment and specimen as well as to prevent ESD perturbations. Common measures are to segregate the firing box chain and acquisition system, shielding of sensors/cables which are mounted close to the source, proper grounding of specimen and support equipment to a dedicated Earth point.

Manual trigger is often applied to avoid interference potentially induced by firing box.

For system test in general (procedure I) and near field shock simulation (procedure II), dry runs are performed prior to the actual test to verify the setup and procedures.

Good practice also, is to consider redundancy for critical items such as distributed frontends and when possible to use different types of shock sensors to guarantee that useful data will be generated, this can include the use of Laser Doppler Velocimeter (see paragraph 13.4.4).

13.4.5.4 Concerns with acceleration measurement with transducers: zero shift during shock, or dynamic offset

One concern often met when measuring a mechanical shock is the presence of a non-constant zero shift, or an evolutionary offset. Its consequence is to overestimate the SRS in the lower frequencies, often up to 2 kHz; this error could not be easily corrected and could lead to SRS errors up to 20 dB.

Figure 13-84 represents the same signal, but with different time scales. The plot on the right discloses the presence of low frequency phenomenon, that is not physical as the corresponding displacement obtained by a double integration of the signal is not equal to zero at the end of the shock transient.

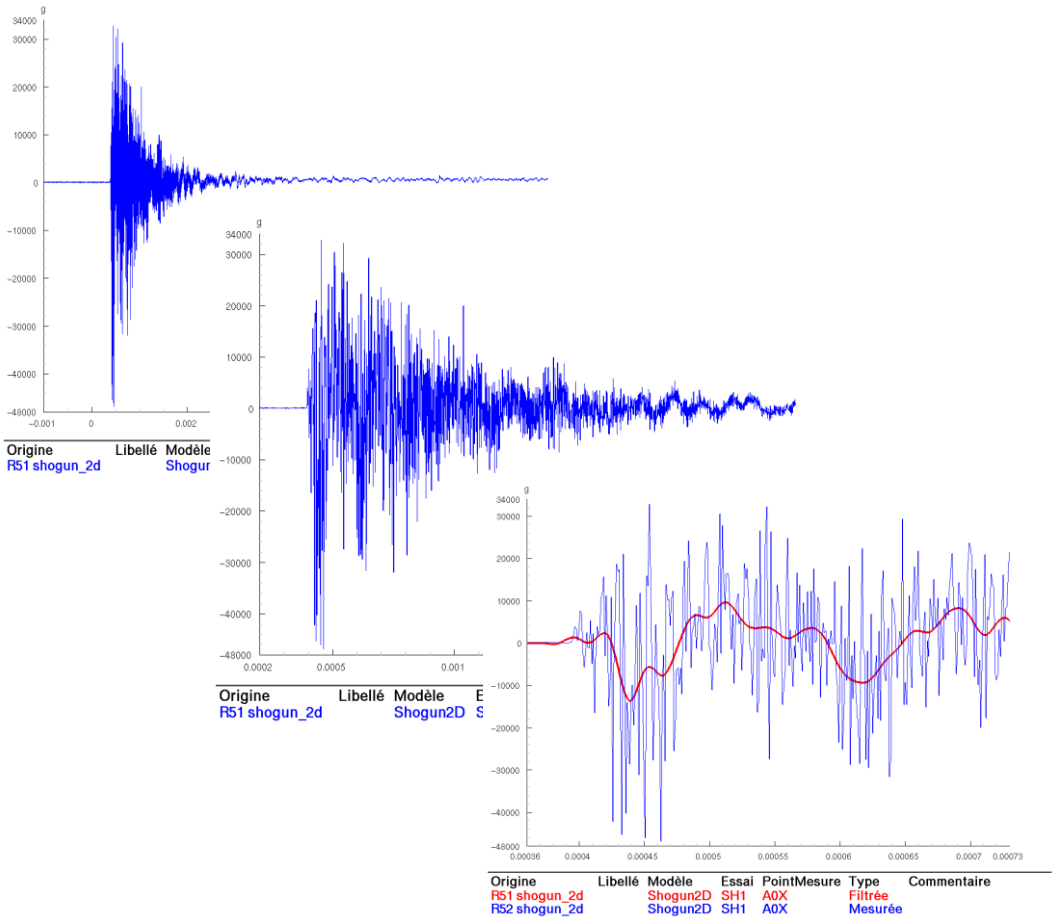

Figure 13-84: Same time history at 3 different scales – evolutionary offset

Two main causes are advanced to explain this phenomenon:

a. **Cause 1**: The importance of the amplifier or conditioner bandwidth

A study [RD-075] has been carried out with the objective to compare several commonly use shock amplifiers to examine their output characteristics under momentary overload. The author obtained three charge amplifiers through McDonnell Douglas, Huntington Beach for this test, and five other devices were obtained in-house. Instead of analysing their topologies and studying the circuit designs (which in most cases is impossible), the author approached this evaluation as an end user, and examined the data from that point of view. Also for business ethics reason, all unit identifications remain anonymous. The study concluded on two observations. First, a high "maximum charge input" rating does not alone qualify a unit as a good shock amplifier. Secondly, wide bandwidth seems to correlate well with good overload characteristics. From this amplifier evaluation the author concluded that, in the presence of high amplitude, **fast rise-time transient** inputs as found in near-field shock measurement, three out of the six test amplifiers exhibited DC offset after the transient response. While an obvious DC offset can be detected easily by the test engineers, the minor zero shifts can be left unchecked and cause serious low frequency errors in Shock Response Spectrum.

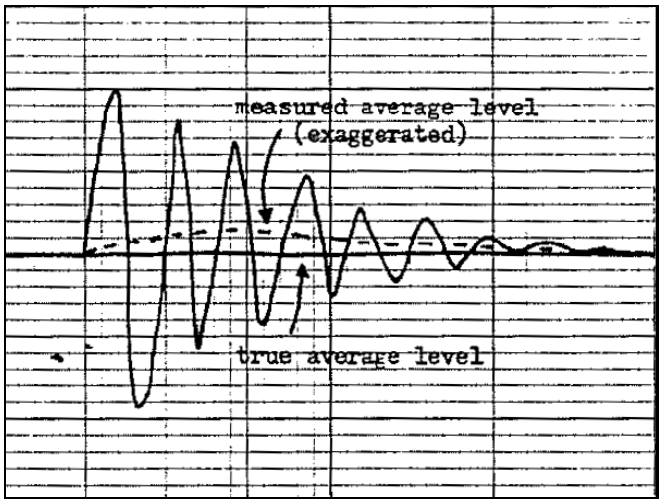

Figure 13-85: Illustration of the effect of polarity dependent slew rate on the average value of a high frequency transient

A series of unpublished tests on charge amplifiers [RD-076] show that there can be measurable differences in the slew rates of positive going and negative going voltages at high frequencies. The slew rate is defined as the maximum rate of change of voltage that the instrument is capable of providing. In other words the slew rate can be faster in one direction than the other. The effect of these higher frequency polarity dependent slew rate is to cause the average, or DC value of the amplifier to be biased during the time that the high frequency is present. It appears as a low frequency shift in the average value as illustrated on Figure 13-85.

A good quality charge amplifier would probably not exhibit this phenomenon for frequencies within its normal bandwidth but for higher frequencies, e.g., a high level, high frequency signal from an accelerometer shocked near its resonance, can produce the low frequency shift without appearing at the output. In addition to polarity dependent slew rates, the high frequency saturation of the charge amplifier can cause a similar average shift. The typical piezoelectric transducer is an undamped single-degree-of-freedom system with a Q of 20 to 50. Typically, the **flat frequency response is approximately 20 % of those at resonance frequency and rises rapidly close to the resonant frequency.** The output of the charge amplifier is filtered to eliminate the energy from the resonant peak. **It is also important that the gain of the charge converter, at the input of the charge amplifier, is capable of accepting the energy of the resonant peak without saturation**.

If there is sufficient energy to saturate the charge converter, then it saturates while the energy within the pass band of the amplifier's filters remain within the specification values. The signal at the output of the amplifier appears normal and within specifications, while the charge converter gets saturated. The effect of the saturation can come out as a longer return to the average or zero value. In other words the average can be higher or lower than the true value (depending on saturation polarity because of the slower recovery rate of the charge converter).

These anomalies can cause a low frequency component to appear at the output of an amplifier generating an error in the SRS computation. Polarity dependent slew rates can occur in the entire chain of instrumentation.

b. **Cause 2**: The sensitivity of the accelerometer transducer to the strain wave

Previous studies have permitted to measure the compression and bending deformations inside plate under pyroshock excitation. The known **sensitivity of the transducer to base strain** is given by the 7270 sheet i.e. 0,5 mV for 250 μstrain, thus equivalent to 500g.This amount could seem negligible when compared to maximum temporal value of 50000g (1 %), but in fact it should be compared to the frequency domain by the corresponding SRS, and then the ratio is

much higher. [RD-077] presents a method of mitigation of the dynamic offset based on Prony decomposition (see also **Figure 15-8**). This correction is recommended for all shock measurements which do not satisfy to the quality criteria, in particular the Piersol criteria based on the SRS symmetry (see Figure 13-87).

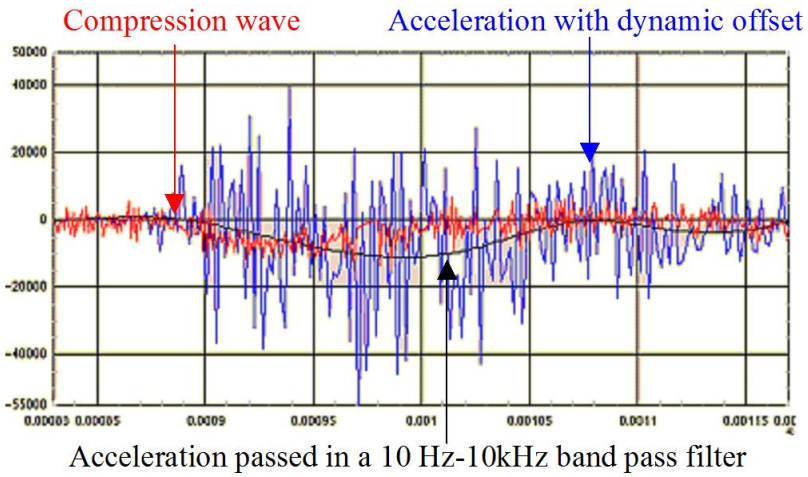

Figure 13-86: Example of evolutionary offset

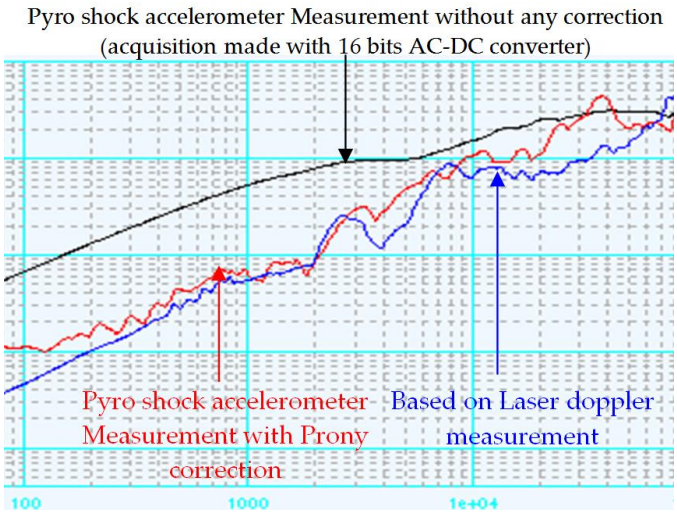

Figure 13-87: Example of mitigation of offset through Prony decomposition

13.4.5.5 Concerns with strain measurement via cables glued to the structure

In this example (see Figure 13-88), the gauges are located at positions 1, 2, 17, 3, 4 and 5. The cables are in red. The source is constituted by four sectors, each of them being an expandable tube shaped along a quarter of circle. The mechanical excitation of the cable preceding the transducer excitation leads to false signal preceding the signal delivered by the transducer itself. But even from this instant, the effect of the cable is still active. It could be seen very clearly on Figure 13-89 disclosing a dissymmetry of strain in the recto and verso side measured by the gauge 1.

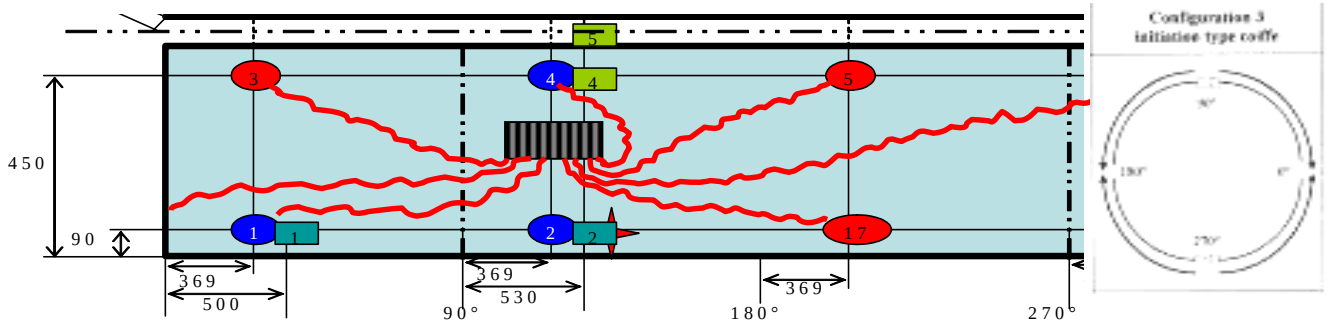

Figure 13-88: test configuration with strain gauges

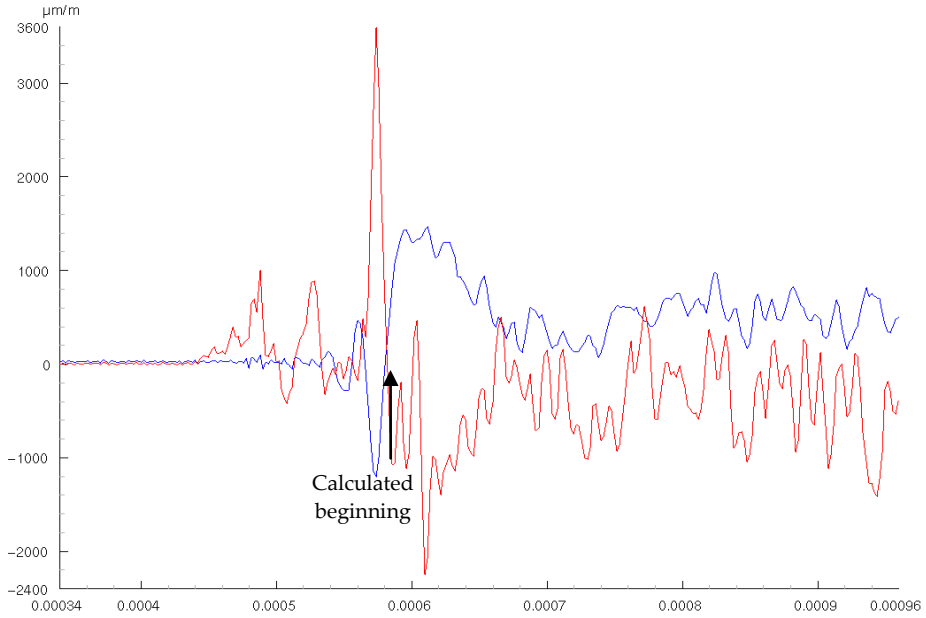

Figure 13-89: Perturbation of strain gauge signal due to glued cables

The solution for avoiding this problem is to reduce as much as possible the length of the cable bonded to the structure, or to decouple the cable from the structure by the most appropriate solution.

13.4.5.6 Analog versus digital

13.4.5.6.1 Overview

The bandwidth of the tape recorders, in LBG1 record mode, is function of the tape speed according to Table 13-7.

Table 13-7: LBG1 tape recorder bandwidth

TABLE 6-7. WIDE BAND AND DOUBLE DENSITY FM RECORD PARAMETERS

	Tape Speed	Carrier Center Frequency	Carrier Deviation Limits(1)		Modulation Frequency	Response Band Limits
	Wide Band FM		Plus Deviation	Minus Deviation		
	(mm/s) (in/s)	(kHz)	(kHz)	(kHz)	(kHz)	(dB(2))
	Group I					
	47.6 (1-7/8)	6.750	9.450	4.050	dc to 1.250	±1
	95.2 (3-3/4)	13.500	18.900	8.100	dc to 2.500	±1
	190.5 (7-1/2)	27.000	37.800	16.200	dc to 5.000	±1
	381.0 (15)	54.000	75.600	32.400	dc to 10.000	±1
	762.0 (30)	108.000	151.200	64.800	dc to 20.000	±1
	1524.0 (60)	216.000	302.400	129.600	dc to 40.000	±1
	3048.0 (120)	432.000	604.800	259.200	dc to 80.000	±1
Double Density	Group II					
	47.6 (1-7/8)	14.062	18.281	9.844	dc to 7.810	±1, −3
	95.2 (3-3/4)	28.125	36.562	19.688	dc to 15.620	±1, −3
95.2 (3-3/4)	190.5 (7-1/2)	56.250	73.125	39.375	dc to 31.250	±1, −3
190.5 (7-1/2)	381.0 (15)	112.500	146.250	78.750	dc to 62.500	±1, −3
381.0 (15)	62.0 (30)	225.000	292.500	157.500	dc to 125.000	±1, −3
762.0 (30)	1524.0 (60)	450.000	585.000	315.000	dc to 250.000	±1, −3
1524.0 (60)	3048.0 (120)	900.000	1170.000	630.000	dc to 500.000	±1, −3
3048.0 (120)	6096.0 (240)	1800.000	2340.000	1260.000	dc to 1000.000	±1, −3

Notes:
(1) Input voltage levels per subparagraph 6.4.1.
(2) Frequency response referred to 1-kHz output for FM channels 13.5 kHz and above, and 100 Hz for channels below 13.5 kHz.

It is sometimes advisable to lower the LBG1 bandwidth for pyroshock measurement; high frequencies phenomena can indeed appear. As the usage of digital filters is not recommended, it is therefore recommended to filter at the acquisition stage with the analog recorder acting as an analogical filter.

From the return of experience, the following synthesis can be drawn:

The ideal situation consists in recording the data numerically meantime saving (securing) them into analogical. Possible discrepancies between numerical and analogical have causes that are highlighted hereafter:

- A spectrum aliasing, when numerical acquisition is carried out without anti-aliasing filter. The behaviour of the conditioning module associated to the transducer is not known in high frequencies, above 100 kHz. It has never been characterized so far. The data sheet of the product only displays basic characteristics, e.g. for the DC amplifier Endevco Model 136:
- Broadband frequency response: DC to 200 kHz -3 dB referenced to 1 kHz
- Filter characteristics: 4 pole butterworth

- Corner frequency (-3 dB): 10 kHz ±12 % (other corners available by changing internal module 31875: from 10 Hz to 80 kHz)

This can be understood as follows: the response without specific filter is a broadband frequency response: DC to 200kHz and a 4 pole Butterworth specific low pass filter is set up with a 80 kHz of corner frequency.

- unexplained discrepancies between analogical and digital (see Figure 13-90) – This phenomenon is frequent when measurements come from sensors strongly excited in high frequencies, especially above the conditioning module cut-off frequency; The report of these variations at least makes it possible to engage an investigation into the causes, which is likely to reduce the errors of measurement. One of the possible causes could come from content in high frequencies beyond the cut-off frequency making the equipment working in non-characterized propagative conditions.

Figure 13-90: Analog versus digital signals – example

In Figure 13-90 the classical over estimation of the analog data SRS in the low frequencies is visible and is due to the noise of the analog data. Spurious spikes are also visible in medium frequency.

The comparison between the analog and digital measurements is powerful because it allows to rise attention on the abnormal behaviour, which can be investigated in order to mitigate the source of measurement errors.

That's why analog measurements are used as back up.

13.4.5.6.2 Conclusions

a. The ideal solution is to acquire digitally and to save analogically. The comparison between both type of results should disclose usual differences in low frequencies (below 100 Hz) due to the lower signal to noise ratio of the analog recorder. Eventual differences in the range 1 kHz to 80 kHz (if 120 IPS and LBG1 mode for the analog recorder) should be closely analysed and the causes should be disclosed in order to identify and to fix if possible the eventual anomalies.

   Choose an effective range for the tape recording larger than that of numerical acquisition (to reduce the risk of saturation, which is irremediable).

   Choose a speed for the magnetic recorder just adapted to the need for the useful frequency range (with the aim to avoid later numerical filtering which is prohibited), whereas one can allow a frequency band higher than the correct requirement in numerical acquisition with an aim of exploration.

b. In case where one cannot implement simultaneously the two modes (nominal numerical acquisition and tape recording in backup), it is necessary to prefer the numerical acquisition which in general gives better results. it is necessary however:

   1. to encourage the presence of anti-aliasing filters, especially for measurements in near field

   2. not to forget that the choice of an input dynamic range results in fixing the threshold in lower part of which one is not able to characterize the SRS with precision: for example, for an input range of 200000g and a dynamics of 11bits+sign, the step of quantification corresponds to 200000/2048 i.e. approximately 100g. As one needs at least 3 steps to characterize the signal and that the amplitude of the SRS reaches 3 times the amplitude of the temporal one, the threshold is at 1000g, which is very high. Consequently, the SRS is not usable below this threshold in low frequency.

c. In case only analog recording is available, that all the more gives interest to a preliminary firing to refine the choices of input range and speed of recording.

13.4.5.7 Preventive techniques for clean measurement

13.4.5.7.1 Application

Recommendations in sections 13.4.5.7.2 to 13.4.5.7.8 are valid for near, mid and far field measurements.

13.4.5.7.2 Anti-aliasing filters

[RD-079] highlights the sensitivity of the SRS to the type of anti-aliasing filter; if the sampling frequency is 1 MHz, the risk of aliasing is often considered very low, due to the intrinsic effect of the low pass filter inherent to the conditioning module.

The use of anti-aliasing filters is recommended; if not used, pay attention to the eventual differences between results extracted respectively from analog and digital acquisitions in the range 1kHz to 100 kHz. If no differences, aliasing did not occur.

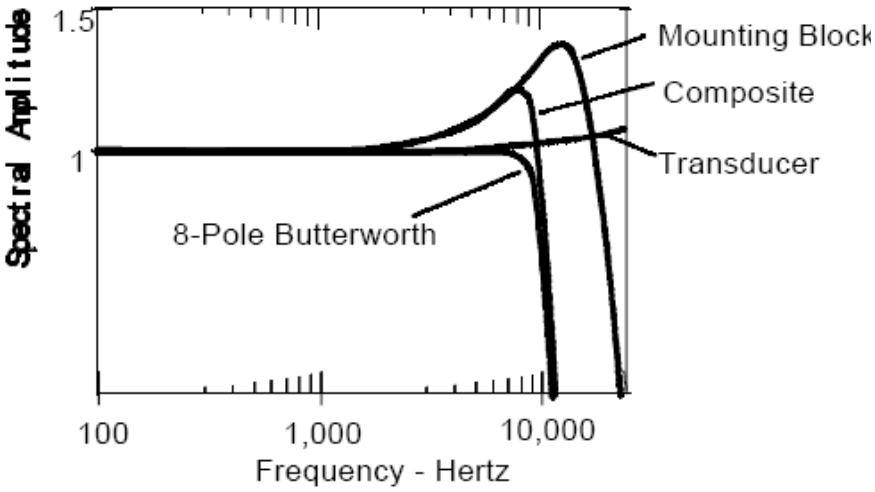

Figure 13-91: Effect of anti-aliasing filter

13.4.5.7.3 Characteristic of the anti-aliasing filters

High frequency data (above 10 kHz for the PCB 350 B03 or 100 kHz for the Endevco 7270) are inaccurate because of a variety of factors including transducer resonance, frequency dependant sensitivity of signal conditioning systems and noise. Therefore the data is often low passed by a combination of mechanical and electrical filters.

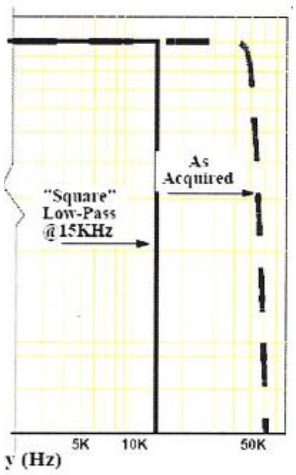

Figure 13-92: Low pass filter at 1,5 x MSRSF

The data should be analytically low-pass filtered with a square, zero-phase filter at 1,5 x the Maximum Analysis Frequency before SRS being computed.

NOTE All filters in the data acquisition and analysis systems affect phase distortion, therefore, the SRS. These errors can be a function of the relative amplitudes of the spectral components, the frequencies of the spectral components and the phase of the spectral components. Because of the random distribution of the amplitudes, frequencies, and phase in different transients, each time history exhibits different errors which results in different errors for each. These errors cannot be calibrated. If a given time history is repeatedly analysed (and no other errors exist; then the data consistently has the same errors and the same SRS is computed each time. This instills a false sense of security in the use.

13.4.5.7.4 AC coupling or DC coupling

The output of the piezoresistive conditioning module is always slow in evolution. It does not bring any concern, as it can be easily eliminated after acquisition. The DC coupling can be used as the AC coupling.

In this latter case, chose a cut off frequency near 2 Hz or 0,1xLFA (Lowest Frequency Analysis), whichever is higher. Type of filter: eight poles, Butterworth.

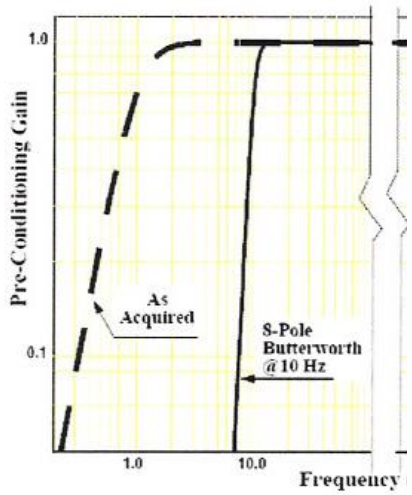

Figure 13-93: High pass filter at 0,1 x LFA

13.4.5.7.5 Highest Shock Response Spectrum Frequency

In the following, HSRSF refers to Highest Shock Response Spectrum Frequency, and MAF refers to Maximal Analysed Frequency. In general these two values are identical if one supposes that only the SRS is used for analysis.

Table 13-8: Recommended Highest Shock Response Spectrum Frequency

	Near field	Mid field	Far field
Recommended HSRSF	100 kHz	10 kHz	5 kHz

However the real limit of the HSRSF is given by the Nyquist frequency (half of the sample frequency) diminished by a factor depending on the low pass anti-aliasing filter which was used; for example, for SF = 1 MHz and a LP anti-aliasing filter constituted by an 8 poles Butterworth 48 dB/oct and a dynamic range of 60 dB, a ratio of 2,5 corresponds. Thus the HSRSF should be 400kHz, instead of 100kHz as recommended above in Table 13-8. It is however necessary to reconstruct the signal up to 400 kHz as described in [RD-078].

13.4.5.7.6 Sampling Frequency and Shannon interpolation

When an analog signal is digitized, the computer samples the signal magnitude at a series of equally spaced points along the time history. The resultant digitized data is a series of discrete points representing the original signal. If the data is digitized at too slow rate, discrete sampling points can cause the amplitude of the peaks to be represented at a lower value. This is illustrated on Figure 13-94(a) where it can be seen that the amplitude can be in error by as much as 29 % if the sample rate is 4 times the frequency of the signal. Figure 13-94(b) shows a sine wave sampled at a rate slightly different from four times the signal frequency.

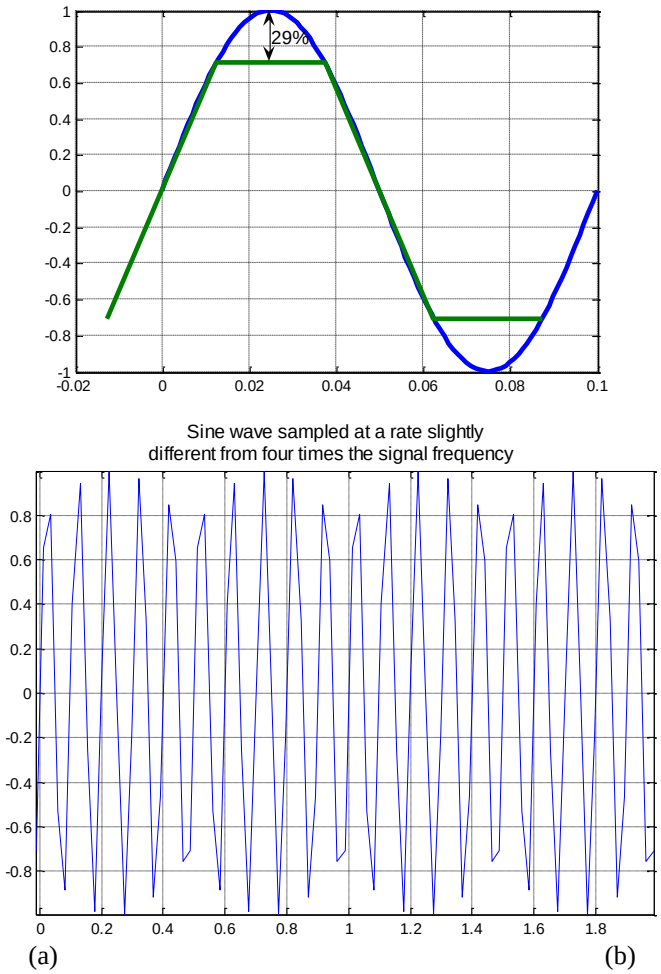

Figure 13-94: (a) under-sampled sine wave – (b) sine wave sampled at a rate slightly different from four times the signal frequency

1/ Classical recommendations between sampling frequency and maximum frequency of the signal

Generally speaking the acquisition chain used during pyrotechnical shock test is tuned according to the following rule:

$$f_{samplingfreq} = a \cdot f_{max} \quad \text{, with } a = 10$$

to ensure a good quality of the shock spectrum at f_{max} .

The value of f_{max} corresponds either to the cutting frequency of the anti-aliasing filter or to the upper bound of the frequency content of the signal due to its own nature or to the filtering done by the sensor itself.

2/ Discussion about sampling frequency

Factor a = 10 recommended above seems exaggeratedly high with respect to the one given by the Shannon theorem.

Remember that the Shannon theorem gives a condition on the sampling frequency f_e that is necessary to rebuild a continuous signal x(t) from its samples x[nT] (with $T = 1/f_e$): $f_e \geq 2f_{max}$.

Under that condition one can re-build x(t) from its samples using the following interpolation formula:

$$x(t) = \sum_{n=-\infty}^{+\infty} x(nT) \frac{\sin(\pi(t-nT)/T)}{\pi(t-nT)/T}$$

Usually this reconstruction is omitted and the shock response spectrum (SRS) is directly computed on the samples x[nT]. In that case the factor a = 10 is recommended. If the reconstruction of the signal is effectively done, then a factor a = 2.5 is enough.

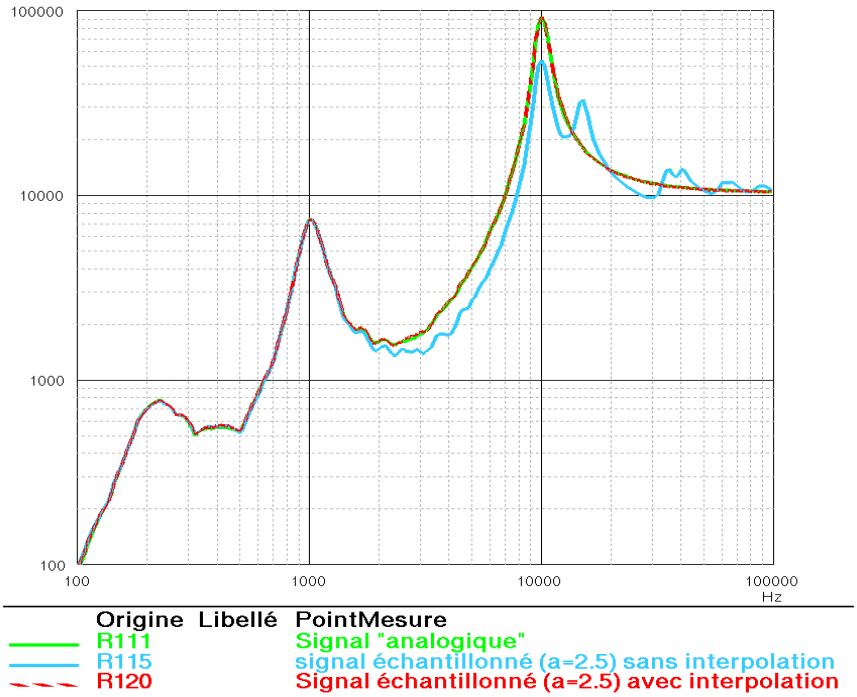

Figure 13-95: (a) Effect of the application of the Shannon interpolation formula for fe=2.5*fmax

The figure above clearly shows:

- the error introduced when computing directly the shock response spectrum on the samples for a = 2.5 (at the limit of the Shannon theorem) – blue curve: the SRS is under-estimated of 5 dB at 10 kHz (corresponding to f = f_e/2.5);
- the perfect correction realized by the use of the interpolation formula – red curve

3/ Conclusion

- using a factor a = 10 allows to get rid from the original time signal reconstruction by interpolation
- It is recommended therefore to either use a = 10 or to perform reconstruction.

NOTE: this discussion doesn't deal with the issue due to the slope of the anti-aliasing filter that can justify using a > 2.5.

As shown in the following table, in practice a factor a = 7 is often considered as sufficient for the applications considered in this handbook.

Table 13-9: Recommended Sampling Frequency

	Near, Mid and Far fields
Recommended	10 times HSRSF
Minimal	7 times HSRSF

As a guideline, the recommended best practice for sampling rate is > 50kHz for far field, and >500kHz for near field)

13.4.5.7.7 Impact of the dynamic acquisition range on the SRS at low frequencies

This problem comes from confrontation between the very high range requested for near field measurement with Endevco 7270 transducer, i.e. usually 200000 g and the fact that one seeks to exploit SRS of low level at low frequencies. It is then important to take care of the validity of the SRS levels at low levels.

Example: let us suppose a range of 200 000 g and an analogical/numerical converter of 11 bits + sign, thus a quantification step of 200000/2048= 97 g.

One needs approximately 3 steps to correctly represent the first half period of an exponential sine decay, corresponding thus to a minimal amplitude of 300 g and like the ratio between the temporal peak value and the corresponding SRS temporal is on average 3 for pyro shocks, it results that precision of SRS should be acceptable for SRS values above 1000 g. A 15 bits + sign converter would give a step of quantification of 200000/32768= 6,1 g what leads to an acceptable precision of SRS to the top of 54 g.

Table 13-10: Recommended analog to digital converter

	Near field	Mid field	Far field
Recommended analog to digital converter	15bits + sign	15bits + sign	11 bits + sign

13.4.5.7.8 Detection of unknown noise source

For Procedure I and Procedure II to detect emission from extraneous sources, e.g. EMI, configure an accelerometer without sensing element and process its response in the same manner as for the other accelerometer measurements. If this accelerometer exhibits any character other than very low level noise, consider the acceleration measurements to be contaminated by an unknown noise source.

13.5 In-flight shock monitoring

13.5.1 Overview

The monitoring of shock, as well as many other kinds of environment (e.g. low frequency dynamics, acoustic, thermal, etc…), is also performed during flight by means of the telemetry sub-systems available on launchers and/or on satellites. As far as the shock environment is concerned, its monitoring is especially performed on launchers in order to verify the shock levels actually induced at payload interface during the launch phase.

The following scheme shows the basic elements belonging to a telemetry subsystem. Several other elements (e.g. batteries, amplifiers, conditioners, etc…) can be part of this sub-system, nevertheless they are not reported in the following scheme.

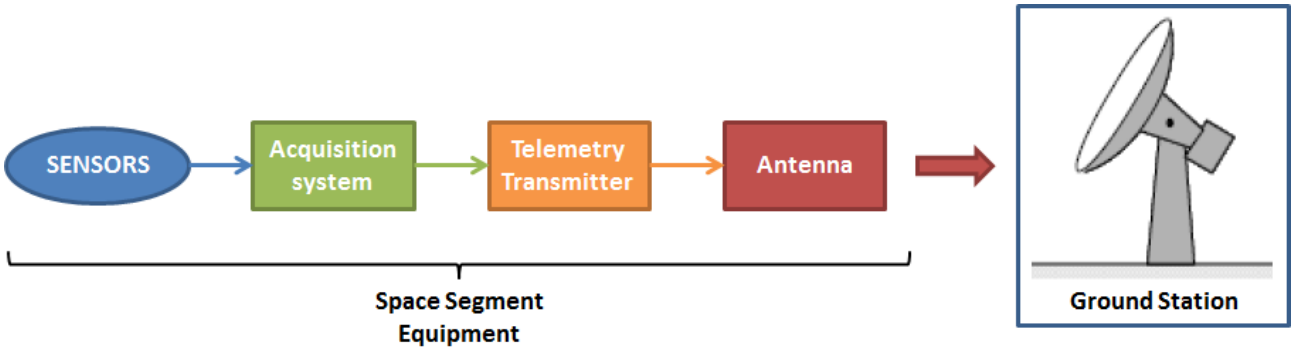

Figure 13-96: Telemetry sub-system basic architecture

As seen in the above figure, beyond the elements already described in the previous paragraphs (i.e. sensors and acquisition systems), on board telemetry systems include all the items necessary for the transmission of data to the ground stations that allow the downloading of measured data to be provided to concerned users (e.g. Launch vehicle/Satellite design authorities) for post-processing activities.

It is important to pay attention to the following section ,detailing the acquisition systems that are currently used on European launchers. A description of such systems and some recommendations to be followed for the settings of the main parameters for a correct acquisition are provided.

13.5.2 VEGA in-flight acquisition systems

The VEGA telemetry sub-system is derived from the Ariane 5 one, in fact most of the hardware used for this system are COTS developed and qualified in the frame of the Ariane programme.

The VEGA Telemetry Sub-System architecture has a modular structure and foresees:

1. The acquisition units:
   (a) One central acquisition unit (UCTM – Unité Central de Télé-Mesure)
   (b) Several peripheral units (UCAT – Unité de Conditionnement et d'Acquisition de Télémesure)
2. The telemetry transmitter
3. An antenna sub-system (two antennas)

The acquisition system is composed by several units (see Figure 13-97). In particular there are several peripheral units that allow the acquisition of sensor measurements in the different stages of the launcher. All these units are then connected to a central unit (located on the upper stage) that allows both the acquisition of additional sensors and the final processing of the telemetry data acquired by all other units, that are sent to the telemetry transmitter and then transferred to the ground station.

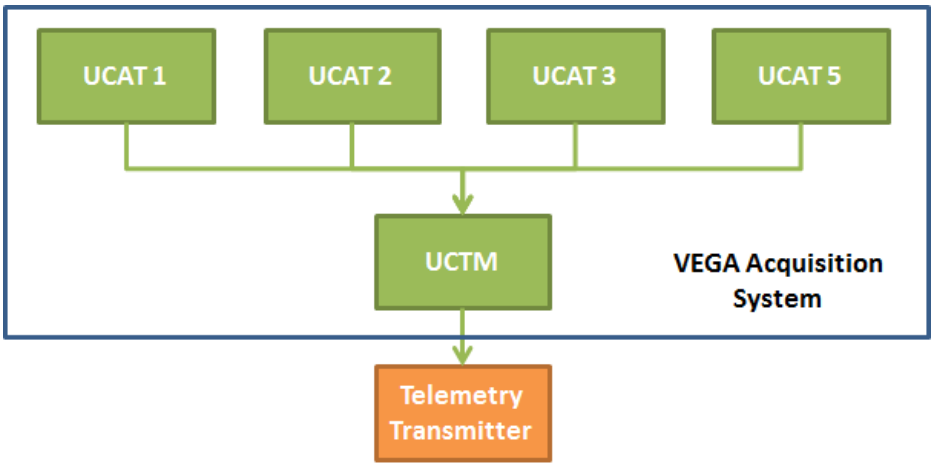

Figure 13-97: VEGA telemetry acquisition system architecture

UCTM and UCATs are modular equipment and their configuration depends on the particular mission needs (for example, qualification versus a generic production flight) in terms of type and number of channels to acquire.

UCTM is capable of being programmed in terms of sampling frequencies and measurement ranges that are used during different flight phases to cope with specific requirements. Due to the big amount of data processed by UCTM and to the constraints in terms of data that can be downloaded by the ground stations, there are some limitations in the possible settings of UCTM that can be summarized as follows:

- Not all the values of sampling frequency are allowed: a limited number of sampling frequencies is allowed. Usually, each value of allowed sampling frequency is attributed to a certain family of sensors (e.g. sampling frequencies in the order of few Hz are used for thermal sensors, about 500 Hz are used for low frequency dynamic accelerometers and so on).
- The data are downloaded in digital format with an amplitude resolution of 8 bits.

The above limitations are crucial especially for the shock measurements. In fact due to the limitation in terms of sampling frequency, shock data are usually acquired at a sampling frequency of about 8000 Hz which prevents a post-processing of flight data in the complete frequency spectrum used for shock specifications (100-10000 Hz). Moreover, the limitation in the amplitude resolution needs to be carefully taken into account when the sensors full scale values are defined.

Concerning the sampling frequency, it is recommended that the highest possible value from the available family is used. Moreover it is recommended that the Shannon interpolation (refer to paragraph 13.4.5.7.6) is used in order to increase as much as possible the frequency range that can be analysed with the available sampling frequency. For VEGA, the sampling frequency for shock sensors is set at about 8000 Hz since, despite the constraints of the telemetry system, it allows to analyse the frequency range for which the “plateau” of the shock specification is defined and this is the frequency range in which the major criticalities were identified during the VEGA development.

As far as the amplitude resolution is concerned, particular attention should be put on the definition of the sensor full scale value. Considering in particular the shock sensors, the full scale value should be high enough in order to avoid the saturation of the measure during the shock transient and low

enough in order to have a measure with a good amplitude resolution (i.e. with a good accuracy). The best compromise between these parameters is chosen. In these regards, Figure 13-98 shows two measures for which a too high full scale value was defined, which led to discard those measurements due to insufficient resolution. On the other hand, Figure 13-99 shows two measures for which the full scale value was correctly defined and relevant measures used for post-processing.

Considering the above, it is highly recommended to use test data as a basis for the definition of the shock accelerometer full scale value, with limited margin with respect to test data.

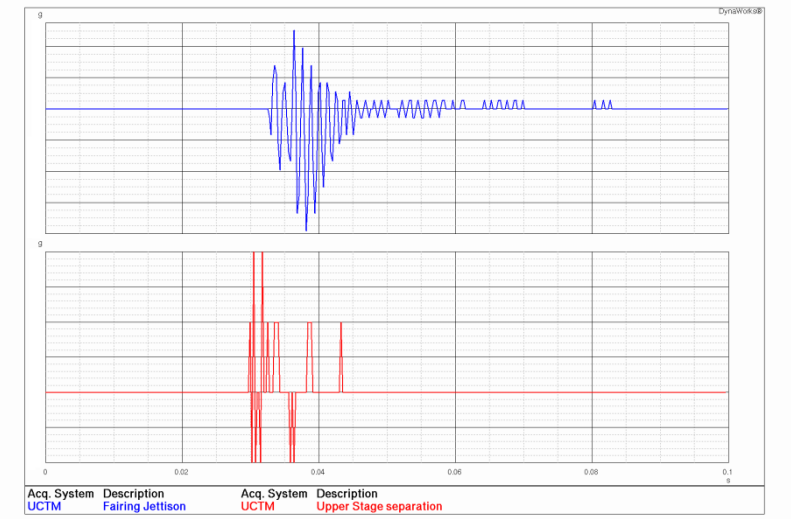

Figure 13-98: Example of UCTM shock measures with incorrect full scale value

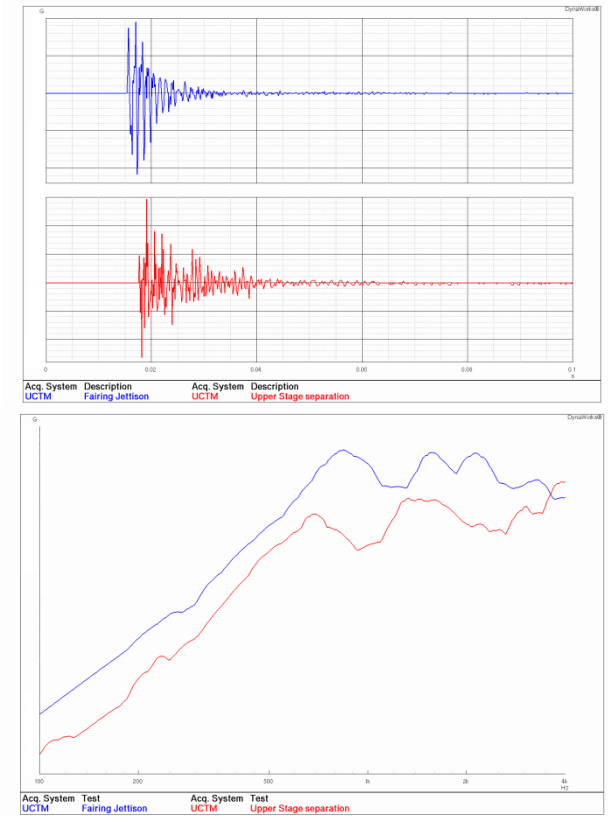

Figure 13-99: Example of UCTM shock measures with correct full scale value and relevant SRS

14
Data analysis tools for shock

14.1 Introduction

Time history constitutes the primary (and the most natural) accessible data since almost all physical signals are obtained by receivers recording variations with time. It contains obviously all the pertinent information and it is essential to save any time history in order not to lose any information.

But a shock measurement in the form of a time-history is not directly useful for engineering purposes, e.g. comparing shocks severities, or understanding its effect on components. A reduction to a different form is often necessary to obtain a more readable form or to extract information that is not directly accessible in the time history, like frequency content.

Several digital signal processing have been used to characterize time signals and extract useful information for phenomena comprehension. That is not the question here to make a complete inventory of digital signal processing tools, neither a lecture on signal processing. The aim of this section is to present some practical tools developed to study shocks transients.

14.2 Shock Response Spectra (SRS)

14.2.1 Basis

This section is based on [RD-065] and [RD-066].

14.2.2 Definition

The shock response spectrum (SRS) is a calculated function based on an input transient. It allows to characterize the shock effect on a **dynamical standardized system** in order to estimate its **severity or its damaging potential**. Thus it allows to compare shocks with each other or to establish equivalence criterion between a measured transient environment and a laboratory simulation of that transient environment.

The method consists in applying a time history as a base excitation to **an array of single degree-of-freedom (SDOF) systems** and then calculating for each of them the **temporal maximum of their response**. The SRS can be defined for any input or response parameters of interest (relative displacement, pseudo velocity/acceleration, absolute velocity, or absolute acceleration). For aerospace structures, it is common to define the input transient in terms of a pseudo-**acceleration.** Without any other information, the SRS per default is be the pseudo-**acceleration SRS (s**ee Figure 14-1 and Figure 14-2).

The peak accelerations for the SDOF systems are gathered in a SRS which is a log-log plot of these values over a range of natural frequencies, see Figure 14-2.Every SDOF system in the array represents an independent natural frequency in the SRS plot.

The natural frequency of each SDOF is an independent variable. Thus, the calculation is performed for a number of independent SDOF systems, each with a unique quality factor Q=10, assuming conventionally the same damping (5 %) for each SDOF.

The choice of damping should be carried out according the structure subjected to the shock under consideration. When this is not known, or studies are being carried out with a view to comparison with already calculated spectra, a Q factor Q=10 is conventionally chosen.

Any arbitrary set of unique natural frequencies can be used for the shock response spectrum calculation. A typical scheme, however, is based on a proportional bandwidth, such as 1/24 octave. This means that each successive natural frequency is $2^{1/24}$ times the previous natural frequency. The SRS resolution is determined by this bandwidth and is independent of the transient duration.

There are several SRS values that can be of interest for different applications, namely, the maximum absolute response of the SDOF versus frequency that occurs:

- during the application of the transient, called the primary SRS,
- after the transient is over, called the residual SRS,
- in the positive direction, called the positive SRS or SRS+,
- in the negative direction, called the negative SRS or SRS-,
- at any time in either direction, called the maximax SRS (most usually used).

A typical maximax SRS is shown in Figure 14-1. The SRS acceleration is also called the maximum or peak absolute response.

NOTE 1 Primary and maximax SRS can differ when time signal has a non-negligible zero shift (also called DC-offset). See 15.5.2.

NOTE 2 SRS are often presented on a log-log graph. It is important to take care with this representation because of the real gap between two curves are visually minimised at high frequencies. A lin-lin representation allows sometimes to clearly visualise gaps.

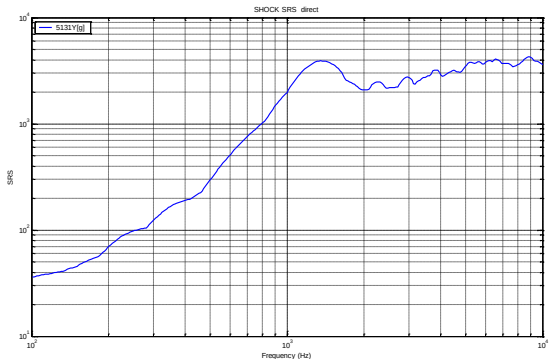

Figure 14-1: SRS example

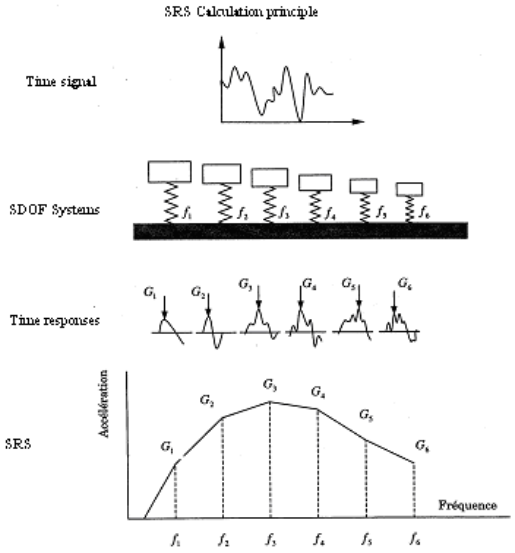

Figure 14-2: Shock Response Spectra principle

14.2.3 SRS properties

SRS main properties are given hereafter:

- If the velocity change is zero between the beginning and the end of the transient, the shock response spectra should have an initial slope of 6 dB/octave and raising to 12 dB/octave at around the corner frequency. The modal response brings some local responses that superpose to the slopes.
- SRS should be globally increasing (i.e. without taking into account local maxima) in low frequency range up to a maximum value. If the curve is decreasing or flat at the beginning, it could indicate a problem of zero offset or a truncation error. One of the dangers of these errors is they can propagate when specification are derived from incorrect measured SRS [RD-066]. See **Figure 4-4**.

  NOTE The slope N of a line on a log-log graph is defined as $N = \frac{\log_{10} \frac{A_2}{A_1}}{\log_{10} \frac{f_2}{f_1}}$,

  where
  N=1 corresponds to a 6 dB/octave line.
  N=2 corresponds to a 12 dB/octave line
- The value of the SRS at higher frequency converges towards the absolute maximum value of the transient acceleration as the natural frequency of the SDOF exceeds the lesser of the highest frequency in the Fourier spectrum of the transient, or the upper frequency limit of the data acquisition system. The time history at the base of the considered SDOF acts indeed as a quasi-static excitation. The SDOF's response follows consequently the time history oscillations. (see **Figure 4-4**)
- The amplification factor of a component in a signal depends on the signal form. Considering a Q-factor of 10 for SRS calculation, it is comprised between 1,6, corresponding to a half-sine time signal, up to 10, corresponding to a perfect sine signal with a sufficient number of periods. SRS of real signals have generally an amplification comprised between 3 and 4. In other words, a shock spectrum response (Q=10) performed on a shock signal has an amplitude about 3 to 4 times higher than the maximum of the time history due to the transient (non-harmonic) nature of the signal. This order of magnitude is useful to determine accelerometers calibration during a test campaign.

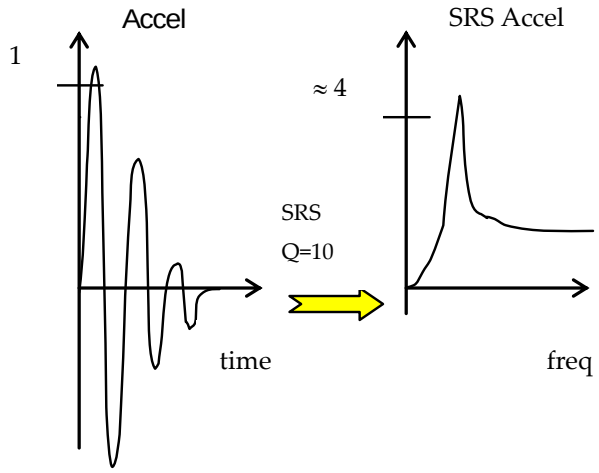

Figure 14-3: SRS peak amplitude derived from typical transient shock signal

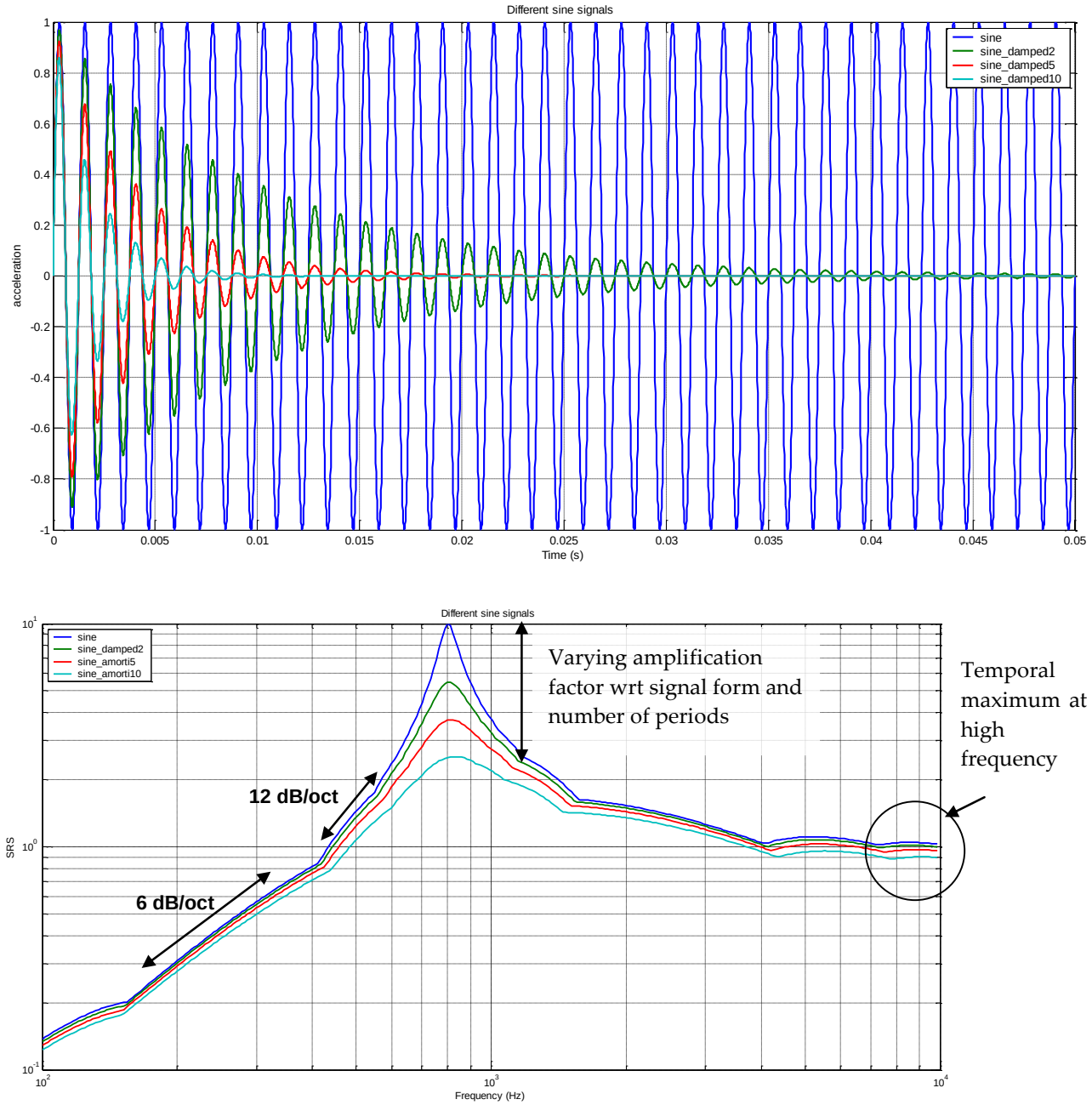

Figure 14-4: Example of SRS calculations, as function of transient signal characteristics

- The SRS is not linear with regard to the addition of time signals. That is to say that the SRS of time signals sum is not equal to the sum of the individual time signals SRS.
- The SRS is, in return, linear with regard to a scalar multiplication. That is to say that the SRS of a time signal multiplied by a scalar α is equal to α times the SRS of the time signal.
- The SRS calculation is not a bijective calculation. Some information is definitively lost (like the phase or the effective duration information). It is thus essential to save any time history in order not to lose any information. Both the transient time history and resulting spectrum are critical to the environmental definition and test verification.

14.2.4 SRS algorithm

The following algorithm can be used to calculate the Shock Response Spectra of a source time signal [RD-067].

The equation to be solved by the algorithm (SDOF system excited at the base by an acceleration) is:

$$\ddot{x} + 2\beta\omega\dot{x} + \omega^2 x = -a(t)$$

With $\ddot{x}$ the relative acceleration,β the damping coefficient, ω the pulsation and a(t) the excitation.

The algorithm approximates the excitation a(t) by a linear piecewise function as shown in Figure 14-5.

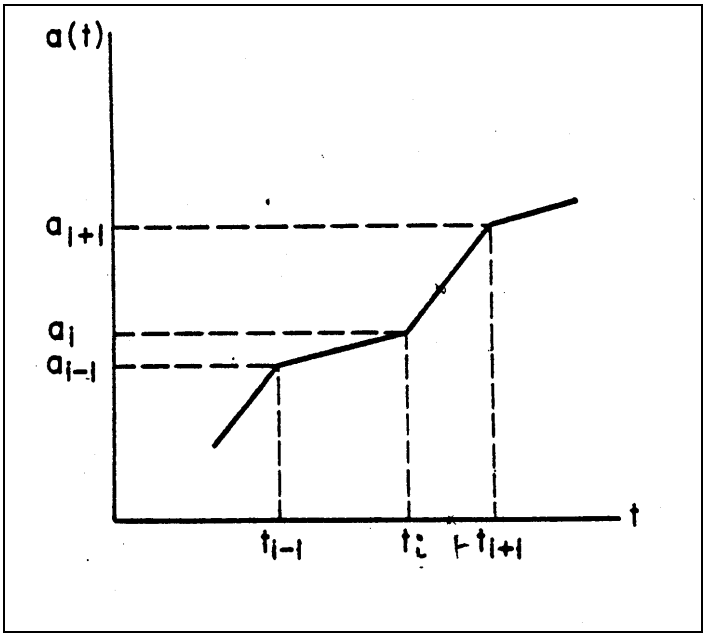

Figure 14-5: Digitalization of input transient

The SDOF equation is now:

$$\ddot{x} + 2\beta\omega\dot{x} + \omega^2 x = -a_i - \frac{\Delta a_i}{\Delta t_i}(t - t_i) \qquad t_i \le t \le t_{i+1}$$

With $\Delta t_i = t_{i+1} - t_i$ and $\Delta a_i = a_{i+1} - a_i$

Δt_i is supposed constant.

The solution of this equation for $t_i \le t \le t_{i+1}$ is given by:

$$x = e^{-\beta\omega(t-t_i)}\left[C_1 \sin\omega\sqrt{1-\beta^2}(t-t_i) + C_2 \cos\omega\sqrt{1-\beta^2}(t-t_i)\right] - \frac{a_i}{\omega^2} + \frac{2\beta}{\omega^3}\frac{\Delta a_i}{\Delta t_i} - \frac{1}{\omega^2}\frac{\Delta a_i}{\Delta t_i}(t-t_i)$$

where C_1 et C_2 are constants:

$$C_1 = \frac{1}{\omega\sqrt{1-\beta^2}}\left(\beta\omega\, x_i + \dot{x}_i - \frac{2\beta^2 - 1}{\omega^2}\frac{\Delta a_i}{\Delta t_i} + \frac{\beta}{\omega}a_i\right)$$

$$C_2 = x_i - \frac{2\beta}{\omega^3}\frac{\Delta a_i}{\Delta t_i} + \frac{a_i}{\omega^2}$$

Consequently, the final solution is:

$$\vec{x}_{i+1} = A(\beta, \omega, \Delta t_i)\vec{x}_i + B(\beta, \omega, \Delta t_i)\vec{a}_i$$

in which:

$$\vec{x}_i = \begin{Bmatrix} x_i \\ \dot{x}_i \end{Bmatrix} \qquad \vec{a}_i = \begin{Bmatrix} a_i \\ a_{i+1} \end{Bmatrix}$$

$$A = \begin{bmatrix} a_{11} & a_{12} \\ a_{21} & a_{22} \end{bmatrix} \qquad B = \begin{bmatrix} b_{11} & b_{12} \\ b_{21} & b_{22} \end{bmatrix}$$

The elements of matrix A and B depend only fromβ, ω and Δt_i .

The final step consists in determining from x_i and $\dot{x}_i$ the absolute acceleration $\ddot{x}_i$.

The shock response algorithm is usually based on the implementation of the ISO 18431−4 standard which is based on a digital recursive filtering relationship. Some Shock-Response-Spectrum recursive algorithms were also developed for SRS computation by Smallwood- Light ([RD-091]) and Kelly-Richman ([RD-092]).

Depending on application it is possible to compute:

- Absolute Acceleration
- Relative Velocity
- Relative Displacement
- Pseudo Velocity

14.2.5 Recommendations on SRS computation

The following are general considerations to be followed:

- The sampling rate for the input time history should be 8 times greater than the highest shock response spectrum calculation frequency and at least superior to 5 times (See 13.4.5.7.6)
- The recommended frequency range for a SRS of a near-field time source is 100 Hz-100 kHz.
- The recommended frequency range for a SRS of a medium or far-field time source is 100 Hz-10 kHz.
- The minimum sampling rate of the SRS should be 12 points per octave, with an optimum number of 24 points per octave. Note that the higher the used Q-factor is the higher the frequency sampling should be.
- For measurements on structures that experience no net velocity change due to the transient event, the signal should be forced to yield a net velocity change of zero from the beginning to the end of the transient event before the SRS computation. This condition is achieved by calculating the mean value of the acceleration signal, and subtracting this mean value from all data values.

14.2.6 Q-factor

It is sometimes useful to let the quality factor Q varying in order to evidence some frequency components. The SRS result depends strongly on the way the different frequency components combine themselves. Some frequencies can indeed be hidden by other peaks. An example in Figure 14-6 is that shows this particularity. The source signal is the combination of 2 frequency components:

- A highly damped 500 Hz component and
- A slightly damped 300 Hz component.

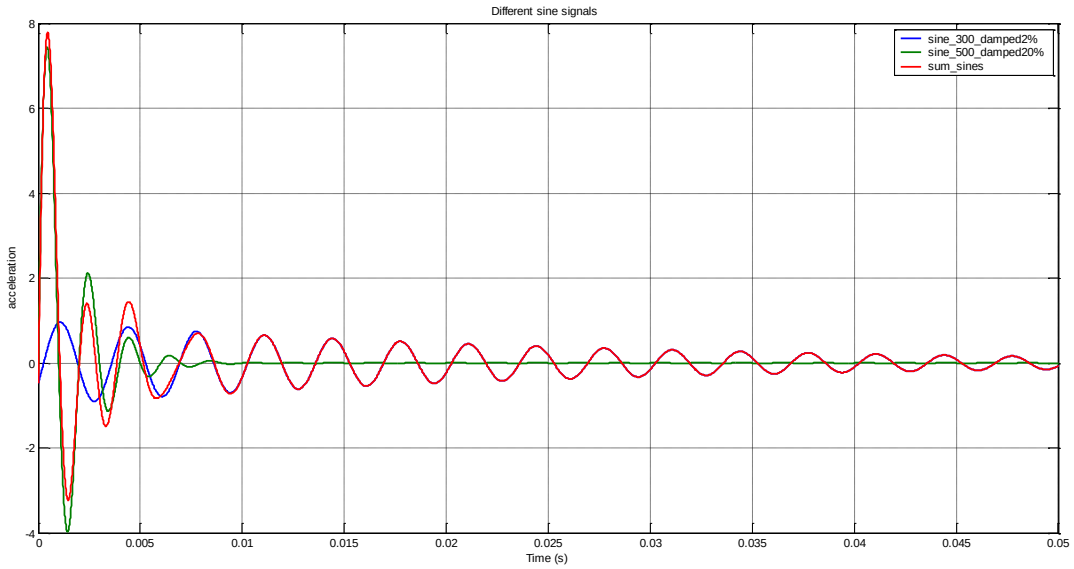

Figure 14-6: Example of transient signals

The SRS of these signals with a classical Q-factor of 10 gives the following results (Figure 14-7):

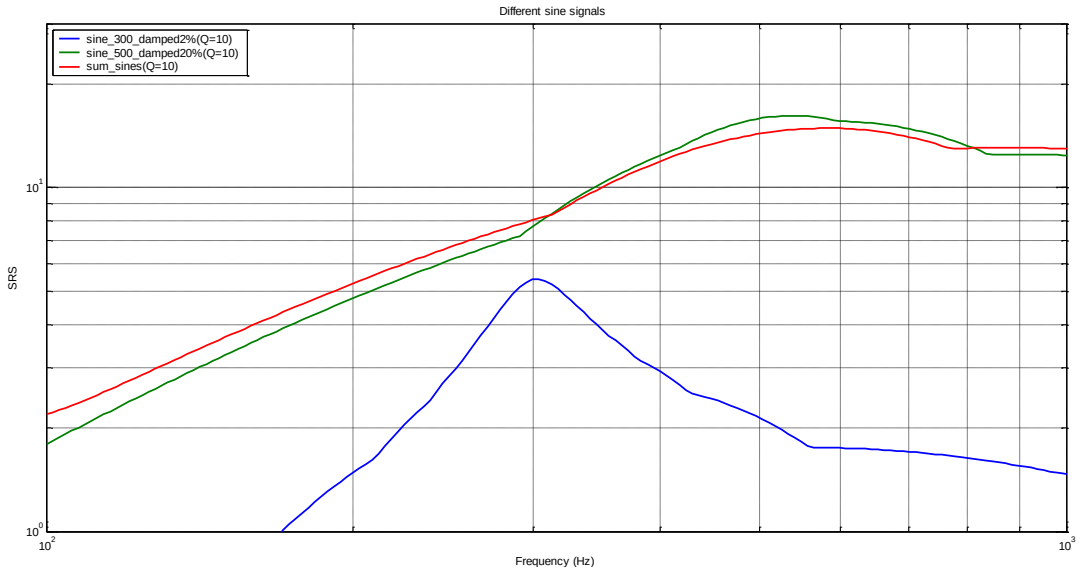

Figure 14-7: SRS of transient signals with Q=10

It can clearly be seen that the SRS of the sum is below the 500Hz component SRS between 300 Hz and 800 Hz. Moreover, the 300 Hz component is not visible on the SRS of the sum. It is hidden by the other component.

Thus, it appears that the 300 Hz component makes the SRS of the sum less severe on the SDOF systems with a Q-factor of 10. But this hidden component can be very severe on a real system with an eigenmode around 300 Hz as the following SRS results, calculated with a Q-factor of 50, shows it:

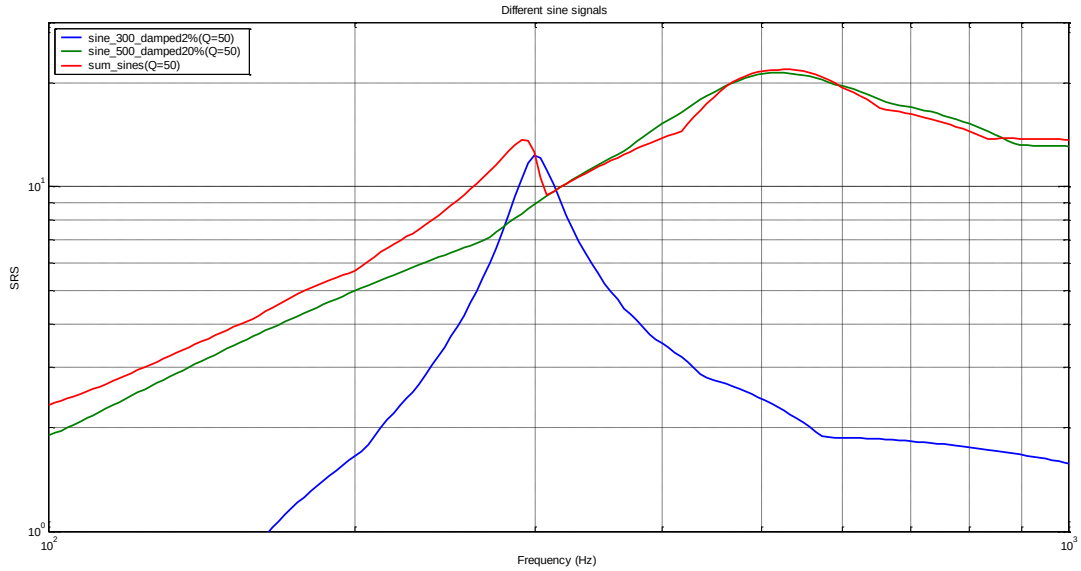

Figure 14-8: SRS of transient signals with Q=50

Increasing the Q-factor amplifies the SDOF responses on the natural frequencies of the source signal and consequently allows to detect hidden peaks.

Another example corresponding to a real test measurement at system level is given in Figure 14-9. It shows a SRS computed with different Q-factors ranging from 10 to 300: many hidden peaks appear with the increasing Q-factor. It should be noticed that the higher the Q-factor, the higher the frequency sampling of the SRS should be to get a sufficient frequency resolution.

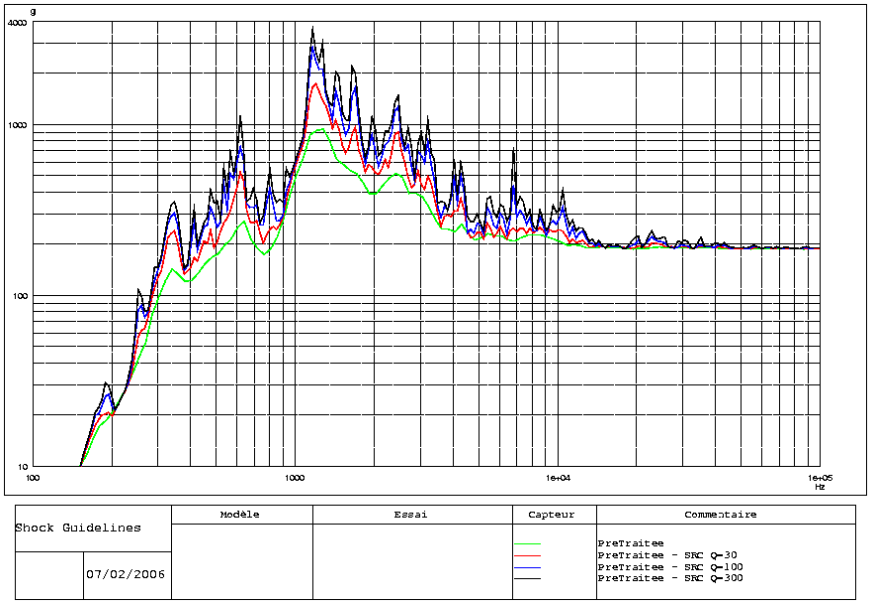

Figure 14-9: Impact of a varying Q-factor on SRS data

Varying Q-factor allows to discriminate between damped and undamped component of a given signal. As it has been seen previously the damping of a component is directly linked to the SRS peak value, just as the Q-factor used to compute SRS has a direct impact on the SRS peak value. These variations are not independent. As a matter of fact, the more damped the component is, the lower the impact is of a Q-factor variation on its SRS peak value. Thus when multiplying the Q-factor by 3 (from 10 to 30 for instance):

- If the impact on the SRS value is higher than 2 the component is considered as undamped (harmonic),
- If the impact on the SRS value is below than 1,5 the component is considered as damped.

14.2.7 SRS limitations

The notion of severity is relative to the considered dynamical system. Thus, real systems do never correspond to the standardized system: they do not have the same natural frequencies, and the real damping can be very different from 5 % (Q=10).

Damage can be caused by amplification on an eigenmode. A source time signal with a frequency component near this eigenfrequency can be very severe, whereas another time signal with a high but different frequency component can be less severe for the considered unit. The difficulty comes generally from a very approximate knowledge of the mid and high frequency eigenmodes of real systems.

The SRS tool allows to compare shocks transients with each other, to consider envelopes and then specify shocks levels. This is today the universal tool for describing shocks, specify them or pronouncing qualification. However, it is not a perfect tool:

The SRS **does not have a unique relationship with the transient signal** from which it is computed; i.e., it is possible for different transients to have the same SRS. These shocks have consequently the same effect on any of the SDOF with a Q-factor of 10 but can have a different effect on the considered system. In particular, it is often possible to at least coarsely approximate the maximax SRS for a complex, multi-cycle transient environment by an appropriately shaped single pulse transient in the laboratory. Of course, the required single pulse used for the simulation has a much higher maximum level and a different effective duration than the actual environment, raising serious questions about the real severity of the simulation.

The SRS does not allow to describe completely the frequency content of a signal. Some frequencies can be hidden by others peaks. Changing the Q-factor is the method to reveal these hidden peaks.

The SRS is based on the response of a 1-DOF system which is not representative of real multi-DOF systems. This limitation is all the more important that the studied system has eigenmodes at close frequencies.

14.3 Fast Fourier Transform (FFT)

14.3.1 FFT definition

The FFT is a **reversible operation** that allows to transform a source signal in **the time domain into the frequency domain** [RD-068]. The FFT allows thus to identify the natural frequencies of a time signal.

$$X(f) = \int_{-\infty}^{\infty} x(t) e^{-j2\pi ft} dt$$

Measured signals are always digitized. The algorithm used is thus the DFT (Discrete Fourier Transform).

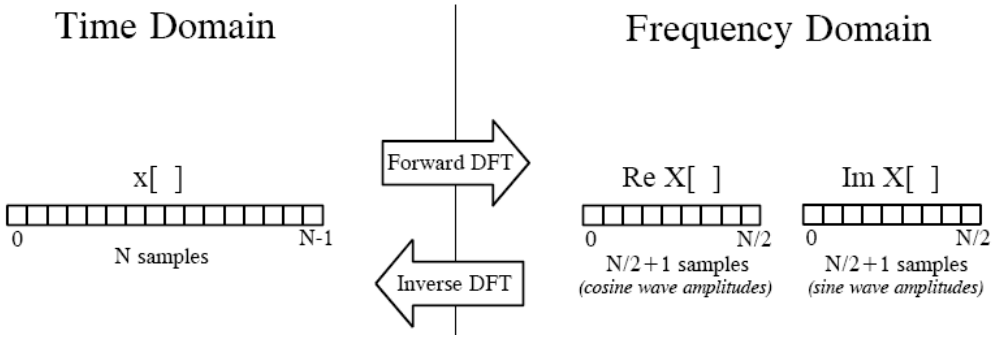

Figure 14-10: DFT Terminology

14.3.2 Precautions

The spectral analysis is recommended for periodic steady-state signals or stationary random signals in order to proceed to averages or statistical analysis. This kind of analysis is not correctly adapted to short transient or non-stationary signal like shocks.

The frequency resolution is inversely proportional to the time signal duration. For instance, if the time duration of a measured signal is about 40 ms, the frequency resolution of its FFT is about 25 Hz.

The FFT is not a priori normalized. As for shocks transients, the time amplitude of a component is decreasing exponentially, the FFT amplitude is not significant of the time signal amplitude.

In return, time signals that have been recorded in the same conditions and on the same duration can be compared in terms of FFT amplitudes.

14.4 Time-Frequency Analysis (TFA)

14.4.1 General

If the FFT and its inverse give two kind of global representations of a signal in the time and frequency domain, they do not include any information on the time structure of the signal itself. A time representation of a signal gives little information on its frequency behaviour and its FFT does not provide any element on the instant of emission and duration of a specific component.

The TFA attempts to provide a specific representation with two variables, time and frequency (see Figure 14-11) [RD-069][RD-070][RD-071]. This is not a gain in information but a redistribution of information in order to understand the different transient phenomena in the signal. These representations can indeed evidence some non-stationary components of signals, characterizing precisely the shocks transients. Several methods engender time-frequency representations with varying properties and performances.

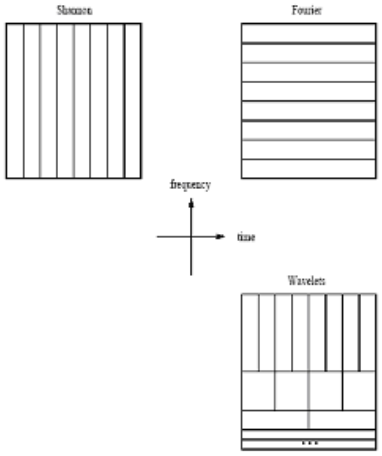

Figure 14-11: Divisions of the time-frequency plane

14.4.2 Linear Time-Frequency Transform (TFT)

14.4.2.1 Overview

The linear time-frequency representations decompose the signal on elementary components (the atoms).

The most common linear TFT are:

- The Short-Time Fourier Transform (STFT)
- The Wavelet Transform (WT)

14.4.2.2 Short-time Fourier transform

A simple and intuitive solution consists in pre-windowing the signal x(t) around a particular time t, calculating its Fourier transform for each time instant t. The resulting transform, called the short-time Fourier transform (STFT, or short-time spectrum), is defined by:

$$F(t, f, h) = \int_{-\infty}^{\infty} x(u)h^{*}(u-t)e^{-j2\pi fu}du$$

Where *h(t)* is a short time analysis window localized around t=0 and f=0. The obtained spectrum is thus "local" around t. The time resolution of the STFT is proportional to the effective duration of the analysis window *h*. The frequency resolution of the STFT is proportional to the effective bandwidth of the analysis window *h*. Consequently, there is a **trade-off between time and frequency resolutions**: on one hand, a good time resolution requires a short window *h(t)*; on the other hand, a good frequency resolution requires a narrow-band filter, i.e. a long window *h(t)*. Hereunder is an example of trade-off between time and frequency resolution.

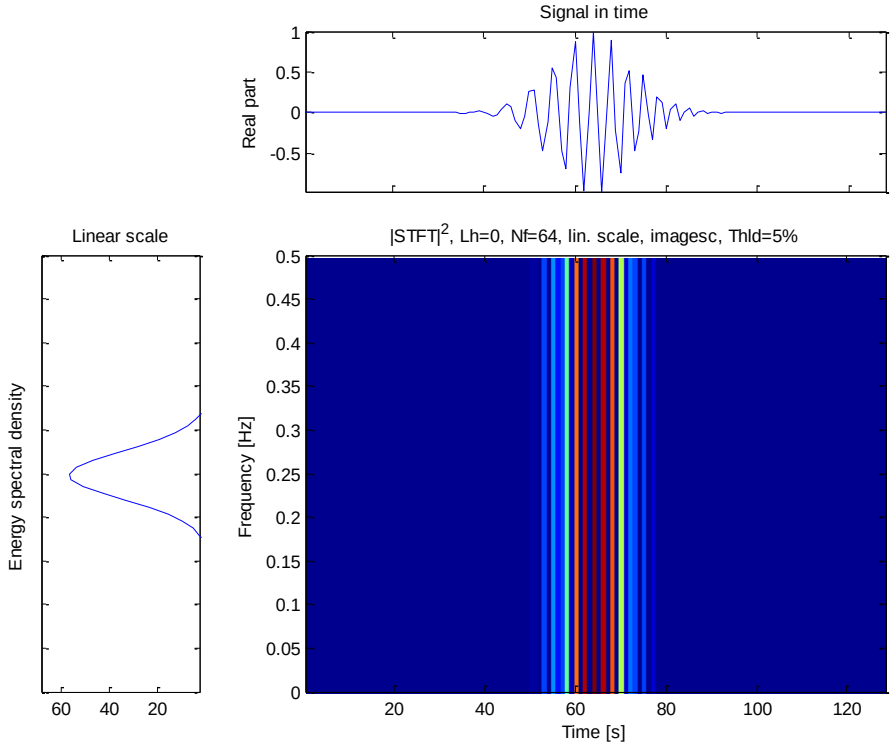

Figure 14-12: Best time resolution with the STFT, but with no frequency resolution: the window h is chosen as a Dirac impulse

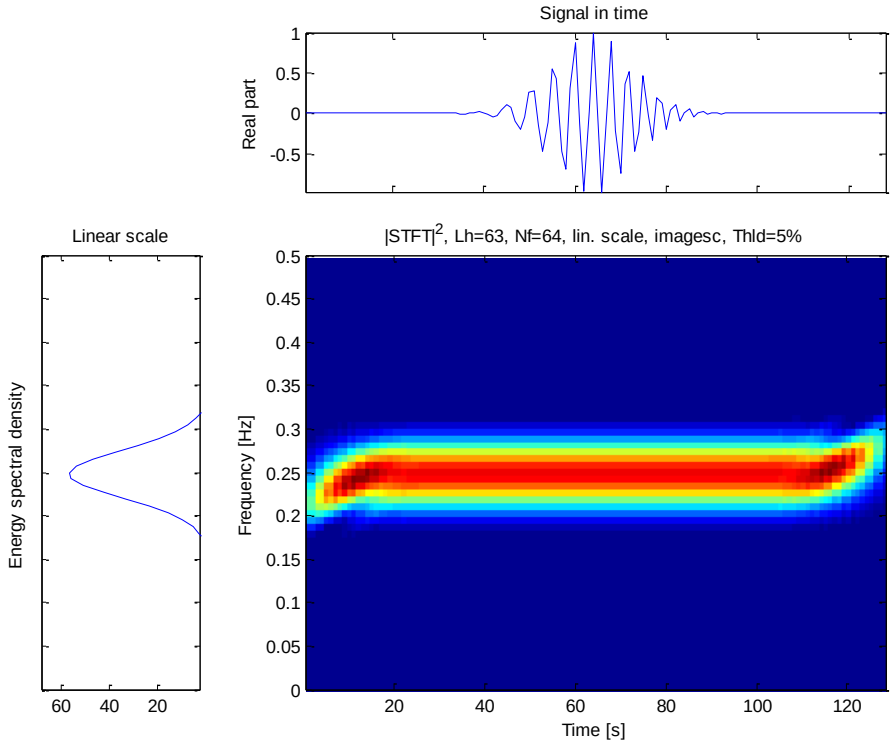

Figure 14-13: Best frequency resolution with the STFT: the window h is chosen as a constant

The STFT is similar to an array of band-pass filters with constant bandwidth.

14.4.2.3 Wavelet Transform (WT)

The idea of the wavelet transform (WT) is to project a signal x on a family of zero-mean functions (the wavelets) deduced from an elementary function (the mother wavelet) by translations and dilations:

$$T_x(t,a,\Psi) = \int_{-\infty}^{\infty} x(u)\Psi_{t,a}^{*}(u)du$$

where $\Psi_{t,a}(u) = |a|^{-1/2}\Psi(\frac{u-t}{a})$. The variable a corresponds now to a scale factor, in the sense that taking $|a| > 1$ dilates the wavelet Ψ and taking $|a| < 1$ compresses Ψ.

The basic difference between the wavelet transform and the short-time Fourier transform is as follows: when the scale factor a is changed, the duration and the bandwidth of the wavelet are both changed but its shape remains the same. And in contrast to the STFT, which uses a single analysis window, the WT uses short windows at high frequencies and long windows at low frequencies. This partially overcomes the resolution limitation of the STFT: the bandwidth Δf is proportional to f, or

$$\frac{\Delta f}{f} = \text{constant}$$

The WT can also be seen as a filter bank analysis composed of band-pass filters with **constant relative bandwidth**. Time and frequency resolutions depend on the frequency: the frequency resolution (resp. time resolution) becomes poorer (resp. better) as the analysis frequency increases.

The type of mother wavelet to use is a delicate question. The main criteria for the choice of the wavelet is the similarity between the mother wavelet and what is intended to be identified in the time history. For instance Morlet wavelet, based on a sine convoluted with a Gaussian signal, is quite good adapted to far-field shock measurement.

An example of a wavelet transform using so-called Morlet wavelets is given (this example uses the same data presented in the following sections):

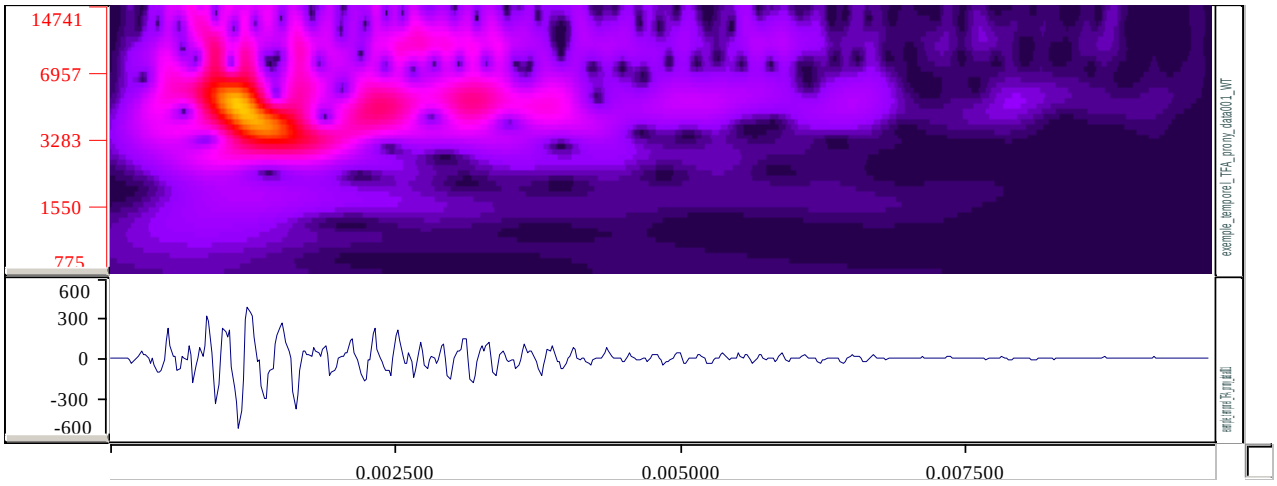

Figure 14-14: Example of a wavelet transform using Morlet wavelets

14.4.3 Quadratic Time-Frequency Transform

14.4.3.1 Overview

Another approach consists in **distributing the energy of the signal along the two variables time and frequency**. This leads to energy time-frequency distributions, which are quadratic transforms of the signal.

The most common quadratic TFT are:

- The Spectrogram
- The Wigner-Ville distribution
- The Pseudo-Wigner-Ville distribution
- The Smoothed pseudo-Wigner-Ville distribution

14.4.3.2 Spectrogram

If we consider the squared modulus of the STFT, we obtain a spectral energy density of the locally windowed signal $x(u)\ h^*(u-t)$. Thus, we can interpret the spectrogram as a measure of the signal energy contained in the time-frequency domain centred on the point (t; f) and whose shape is independent of this localization.

The spectrogram being the square magnitude of the STFT, it is clear that the time-frequency resolution is limited as it is for the STFT.

Moreover, as it is quadratic representation, the spectrogram of the sum of two signals is not the sum of the two spectrograms. Thus, as every quadratic distribution, the spectrogram presents interference terms. However, one can show that these interference terms are limited if the signal components are well separated. This is the main advantage of this representation.

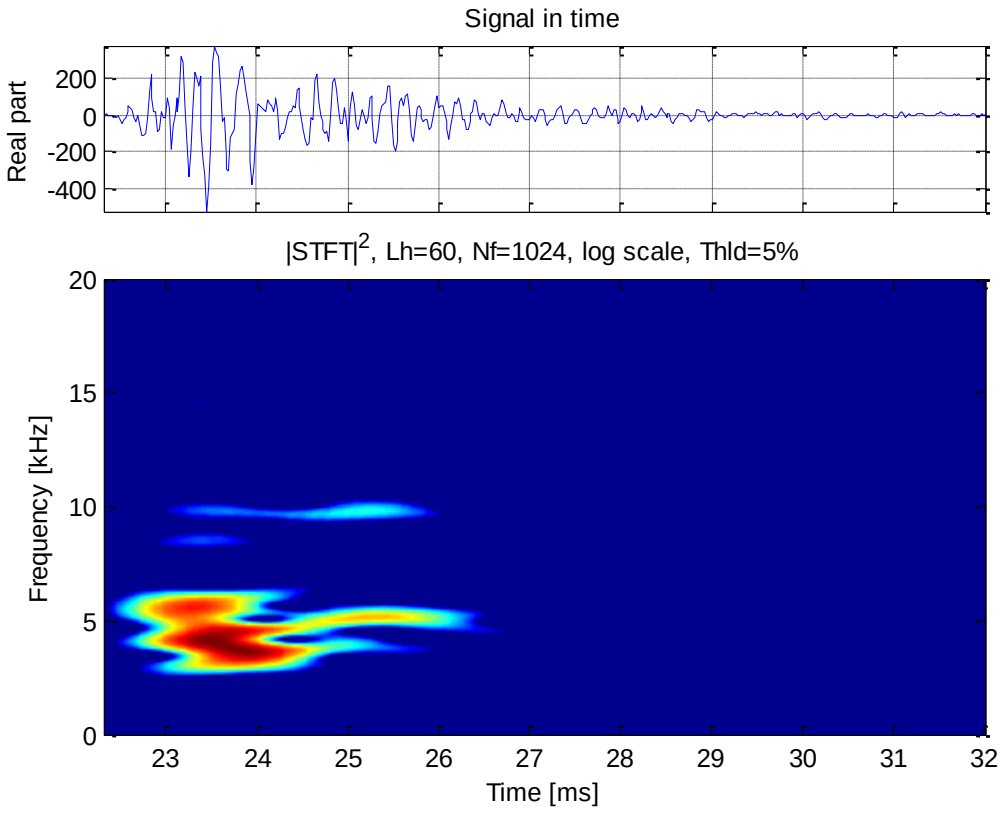

Figure 14-15: Example of Spectrogram

14.4.3.3 Wigner-Ville Distribution (WVD)

A time-frequency energy distribution which is particularly interesting is the Wigner-Ville distribution (WVD) defined as:

$$W_x(t, f) = \int_{-\infty}^{\infty} x(t+\tau/2)x^*(t-\tau/2)e^{-j2\pi f\tau}d\tau$$

This distribution satisfies a large number of mathematical properties. In particular, it is real-valued, it preserves time and frequency shifts, it localizes perfectly linear chirp and satisfies the marginal properties (i.e. if we integrate the time-frequency distribution along one variable (t or f), we obtain the energy density corresponding to the other variable).

Unlike the spectrogram interference terms, the WVD interference terms can be non-zero regardless of the time-frequency distance between two signal terms. **These interferences are the major drawback** of this distribution since they can overlap the signal terms and thus make it difficult to visually interpret the WVD image. However, it appears that if these terms are not present, the good properties of the WVD cannot be satisfied.

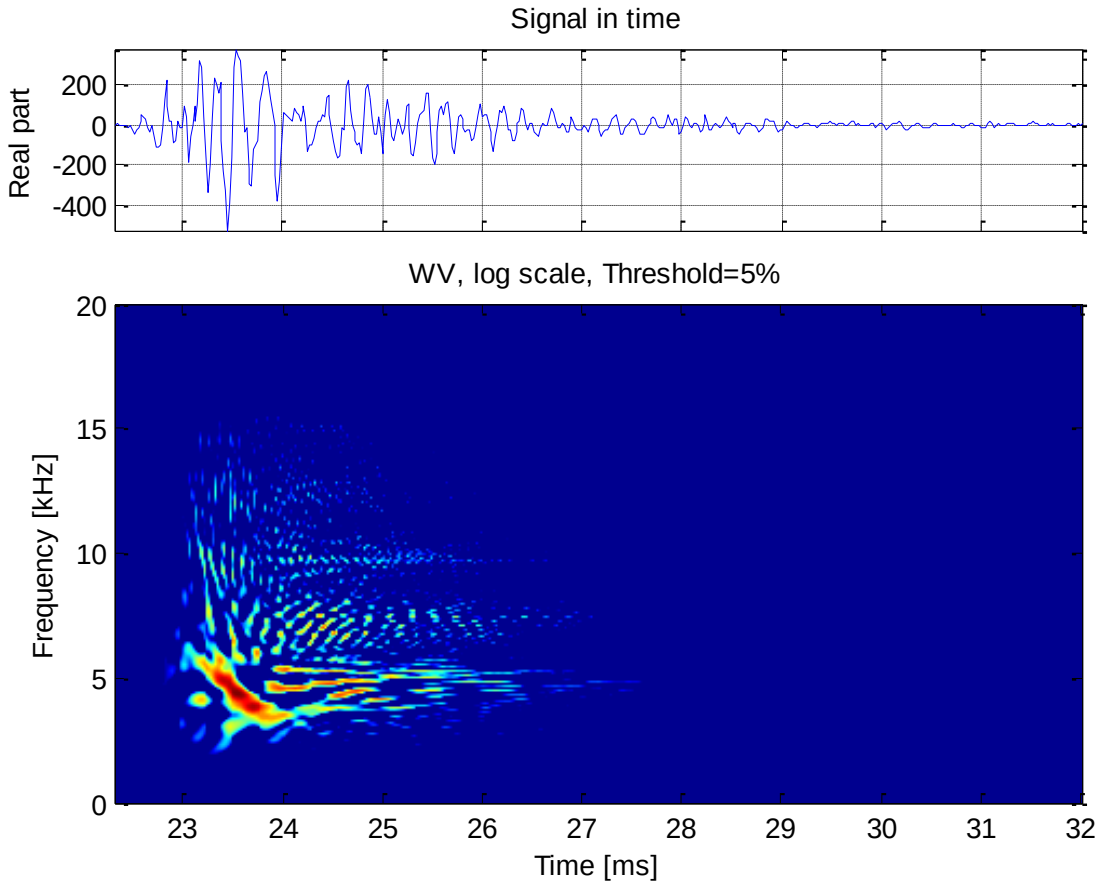

Figure 14-16: Example of Wigner-Ville distribution

14.4.3.4 Pseudo Wigner-Ville Distribution (PWVD)

In order to overcome the interference of the WVD, the Pseudo Wigner-Ville distribution is defined as:

$$PW_x(t,f) = \int_{-\infty}^{\infty} h(\tau)x(t+\tau/2)x^*(t-\tau/2)e^{-j2\pi f\tau}d\tau$$

Where *h(t)* is a regular window. This windowing operation is equivalent to a **frequency smoothing** of the WVD. However, the consequence of the improved readability is that many properties of the WVD are lost.

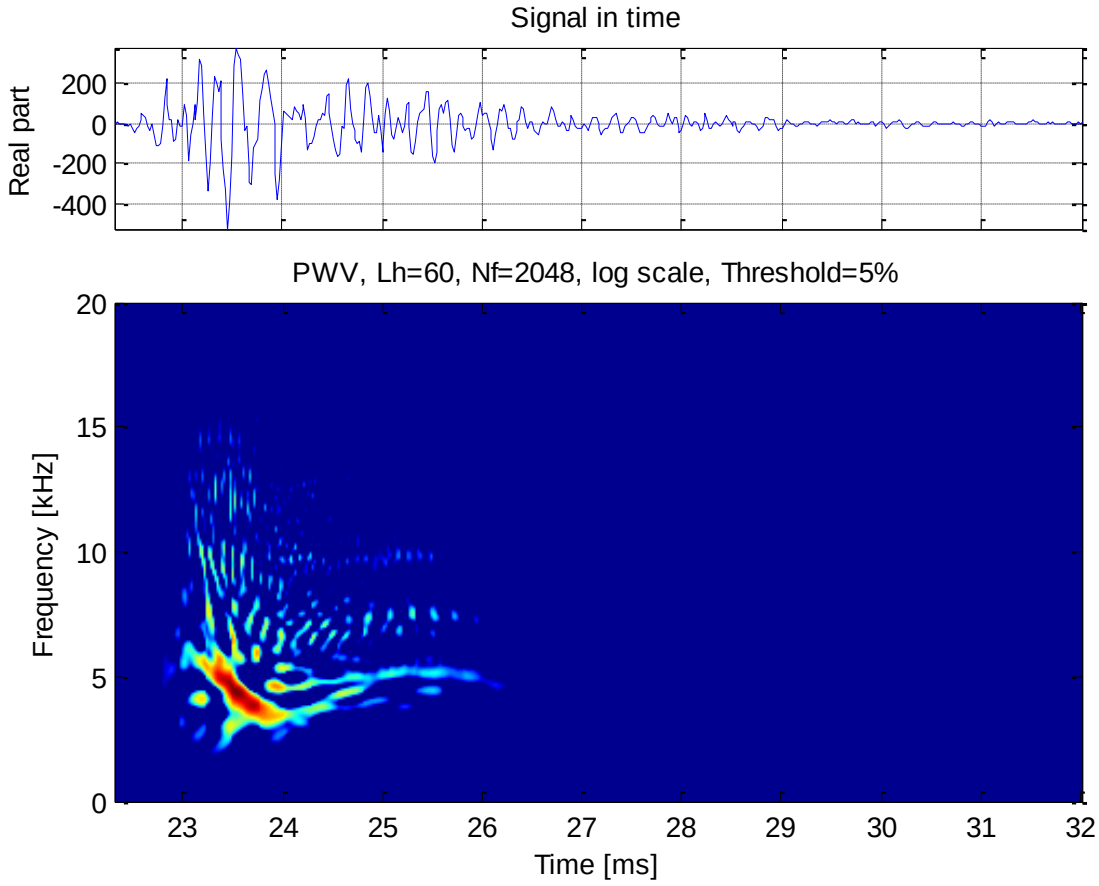

Figure 14-17: Example of Pseudo Wigner-Ville distribution

14.4.3.5 Smoothed-Pseudo Wigner-Ville Distribution

The problem with the previous smoothing function is that it is controlled only by the short-time window *h(t)*. If we add a degree of freedom by considering **a separable smoothing function**

$$\Pi(t, f) = g(t)H(-f)$$

where *H(f)* is the Fourier transform of a smoothing window *h(t)*, we allow a progressive and independent control, in both time and frequency, of the smoothing applied to the WVD. The obtained distribution

$$SPW_x(t, f) = \int_{-\infty}^{\infty} h(\tau)\int_{-\infty}^{\infty} g(s-t)x(s+\tau/2)x^*(s-\tau/2)ds.e^{-j2\pi f\tau}d\tau$$

is called the smoothed-Pseudo Wigner-Ville distribution.

The previous compromise of the spectrogram between time and frequency resolutions is now replaced by a compromise between the joint time-frequency resolution and the level of the interference terms: the more you smooth in time and/or frequency, the poorer the resolution in time and/or frequency.

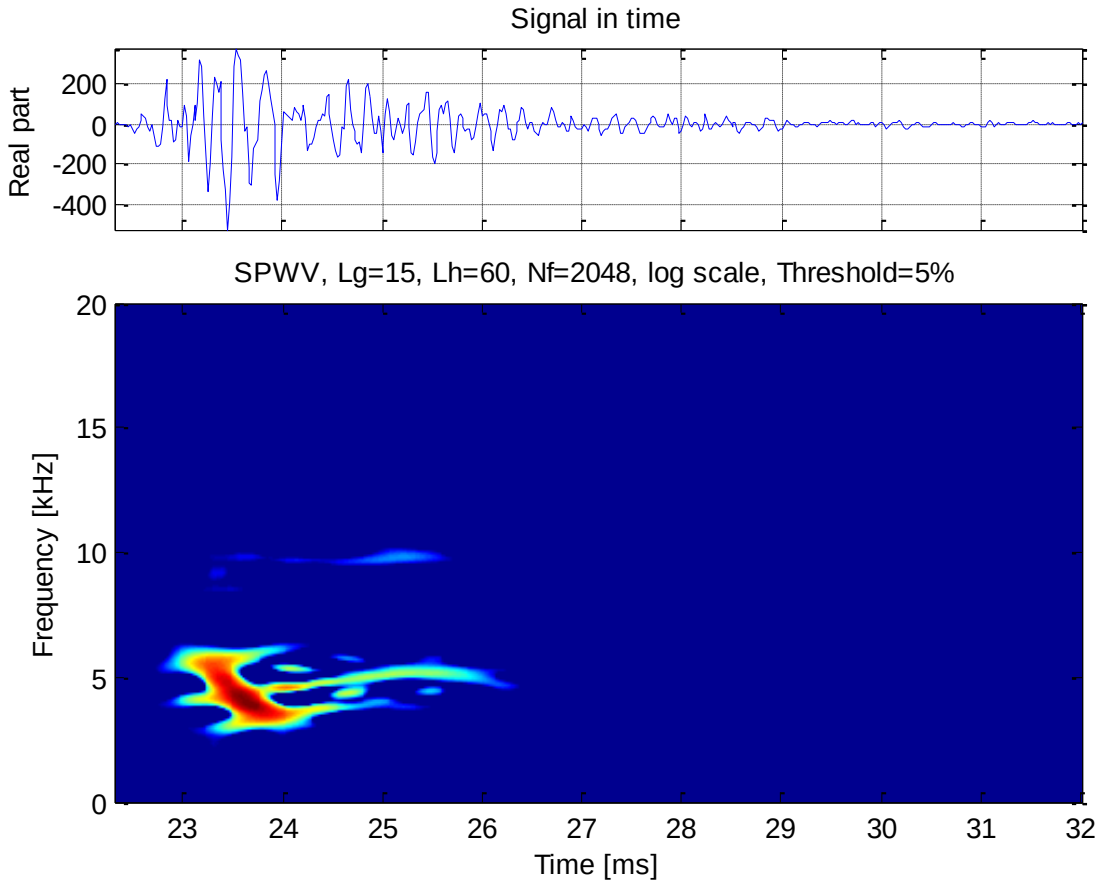

Figure 14-18: Example of Smoothed Pseudo Wigner-Ville distribution

An interesting property of the smoothed-pseudo WVD is that it allows a continuous passage from the spectrogram to the WVD by choosing correct smoothing windows *g* and *h*.

14.4.4 Interpretation and precautions

These digital signal processing tools are **designed for expertise** and can be delicate to use. A correct use needs some experience in the domain of time-frequency analysis. The different representations of the same time signal show that the choice of a transformation is not obvious. The Wigner-Ville is generally difficult to interpret because of the interference terms. It is thus more a theoretical tool.

Nevertheless, the previous representations illustrate the recombination of high frequencies appearing at the beginning of the transient into lower frequencies. It allows to detect accurately the different transition between frequencies and where is localized the energy in the time-frequency plane.

14.5 Prony decomposition

14.5.1 Definition

A Prony mode is a standardised signal whose shape is an exponentially damped sine wave. As such signal looks like measured shock time histories, this decomposition technique been used as a data processing tool: the main idea is that shock measurements can be **decomposed as a sum of Prony modes** [RD-072].

Two decomposition schemes exist (basic and advanced schemes) which are described in the following chapters (14.5.2 and 14.5.3).

14.5.2 Basic scheme

The basic signal is a simple exponentially damped sine wave (see Figure 14-19). All waves are simultaneous but can have different phasing. Such a model is therefore characterised by four parameters per mode: magnitude, frequency, damping and phasing. Due to the simultaneous arrival and the sharp initial rise of a Prony mode, such a scheme is better adapted to near-field measurement with high-frequency content. An example corresponding to a Shogun pyroshock measurement is given in Figure 14-20 and Figure 14-21.

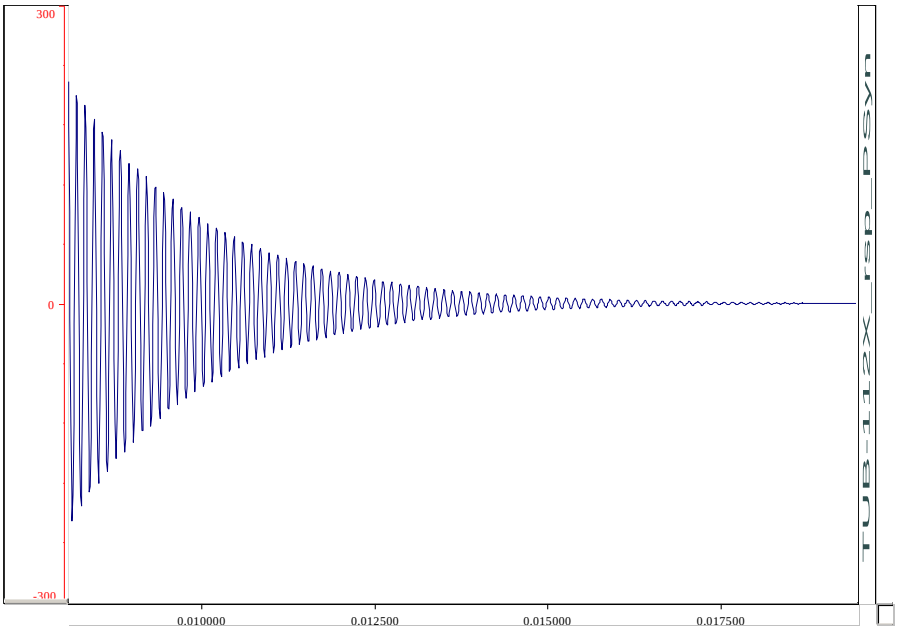

Figure 14-19: Example of a single standard Prony mode

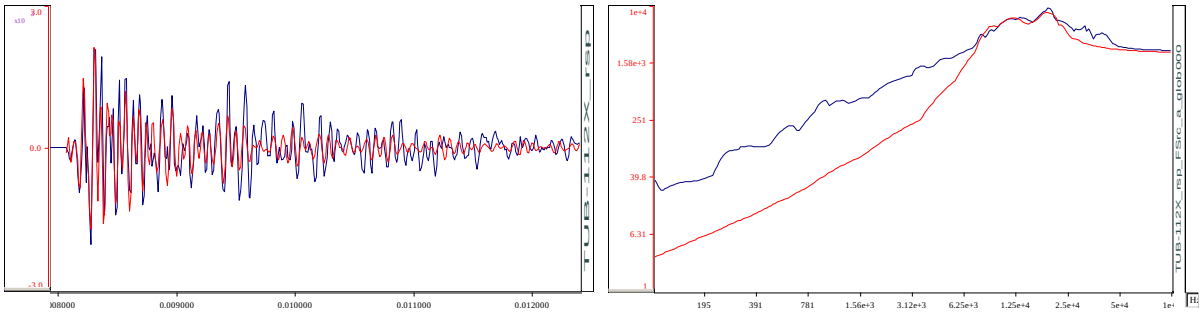

Figure 14-20: Example of a measurement (blue curve) reconstructed using 12 Prony modes (red curve) and the associated SRS

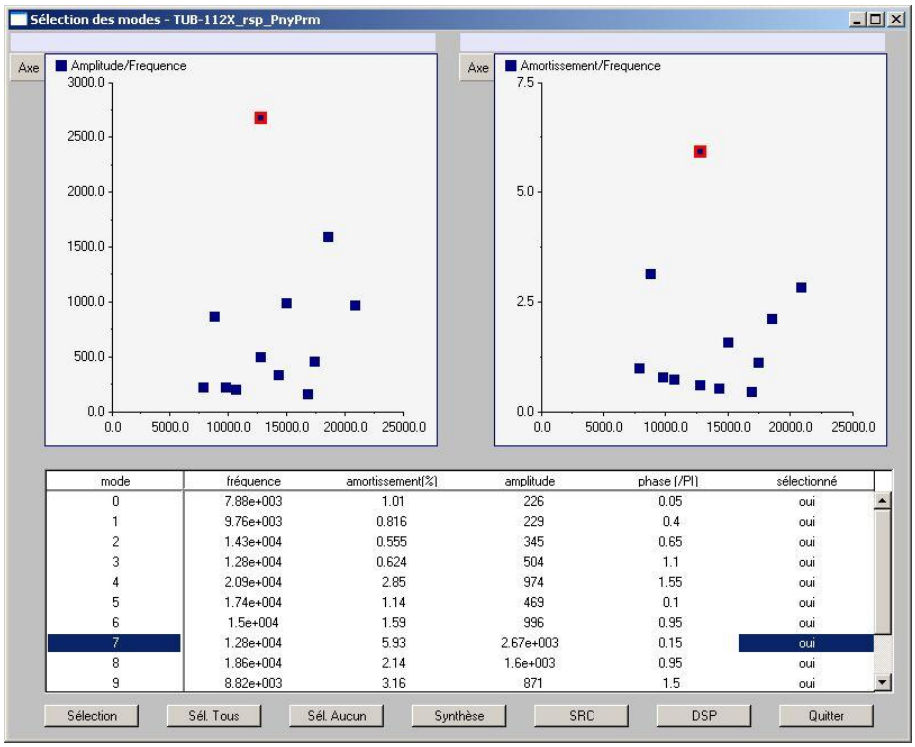

Figure 14-21: Listing of the identified modes with their corresponding parameters

14.5.3 Advanced scheme

The advanced scheme is a limited bandwidth exponentially damped sine wave, which means that the standard Prony mode is convoluted with a basic Gaussian pulse to limit its frequency bandwidth (see Figure 14-22). The waves have different arrival dates, so that it is possible to represent the chronology of arrival of the various components. Such a model is therefore characterised by four parameters per mode (magnitude, frequency, damping and arrival date) plus one global parameter that drives the Prony limited bandwidth. Due to the differentiate arrival and the smooth initial rise of a limited bandwidth Prony mode, such a scheme is better adapted to far-field measurement. A measurement example (the one that has been intensively used in the previous sections) is given in Figure 14-23 and Figure 14-24.

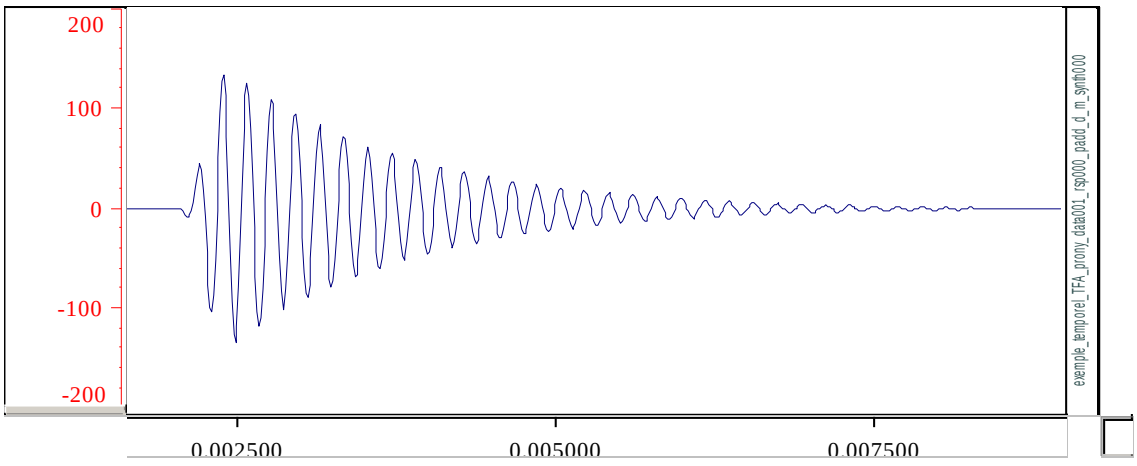

Figure 14-22: Example of a single limited bandwidth Prony mode

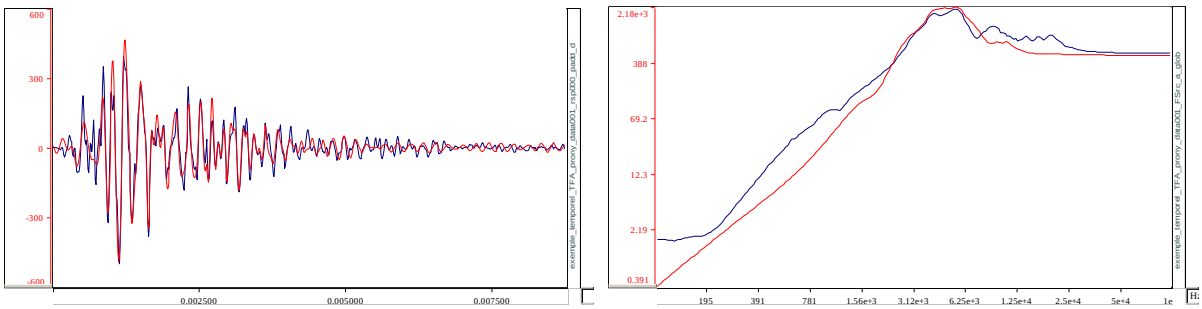

Figure 14-23: Example of a measurement (blue curve) reconstructed using 14 limited bandwidth Prony modes (red curve) and the associated SRS

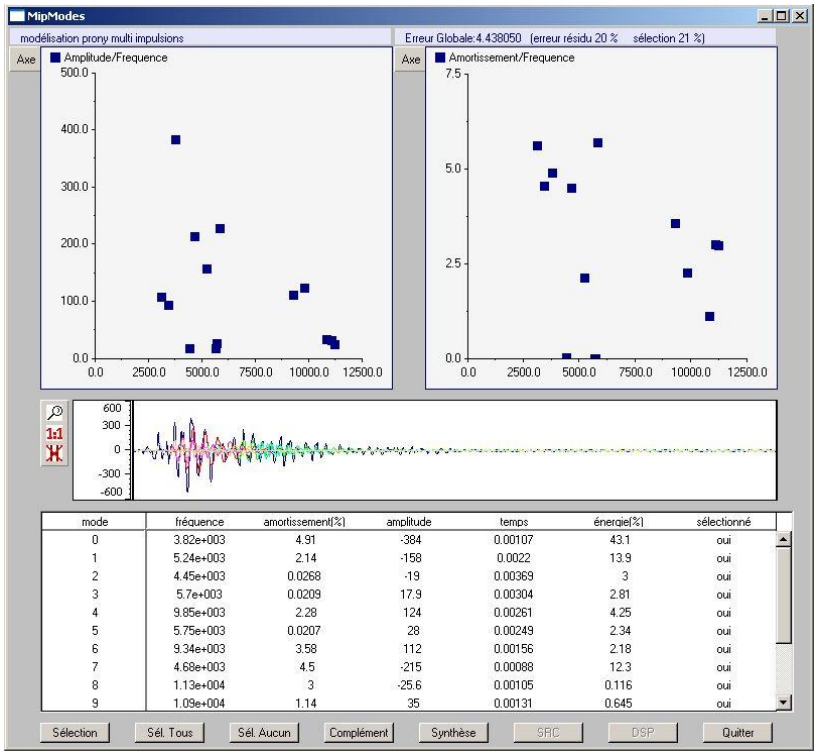

Figure 14-24: Listing of the identified modes with their corresponding parameters

14.5.4 Use and limitation

To have a correct representation of a shock time history, typically **5 to 15 modes are required**, depending on the precise aim of the Prony decomposition.

One of the main interest of such a Prony decomposition is that it provides a **characterisation of a shock environment with a limited number of parameters**: typically 4 or 5 parameters per mode, which means that a shock environment can be defined by several dozen of parameters. This can be very useful for the following purposes:

- Get a **detailed quantitative characterisation** of a shock environment, especially a quantitative representation of the time-frequency structure of the shock measurement.
- **Simplify a shock environment** while keeping its main physical characteristics in both frequency and time domains. Especially this allows to get a simple definition of a shock environment which respects its duration and the relative phasing of its main components.

- **Compare different shock environments** on specific parameters not easily available through other post-processing tools such as damping or arrival date or with a higher precision for magnitude or frequency.
- **Track some specific components** of shock measurements throughout a structure to have a more precise image of the wave propagation.

The main limitations of such a tool are presented hereafter:

- Prony mode extraction usually offers a lot of parameters potentially leading to somewhat different results. As a consequence experience is needed to use it properly.
- Shock measurements that have a **very wide frequency content** can lead to difficulties in Prony modes extraction. As a matter of fact the algorithms usually concentrate on the components with the highest magnitude (usually at high frequency) which can hide lowest magnitude components (usually at low frequency) which are thought of interest as low frequency environment is usually the most dimensioning. Such a problem can be circumvented by doing either a simplification of the shock environment (by filtering for instance) or by splitting the measurement in different sub-signals to be summed up.
- Shock measurements that have a **very dense frequency content** can lead to difficulties in Prony modes extraction. In such a case, it would need a very high number of modes to correctly represent the measurement. It can be difficult to get the Prony modes of interest due to automatic focus on a certain frequency range exhibiting a large number of components of similar magnitude. The resulting precision is consequently lower and the model can even become unusable because of a too high number of parameters.

14.6 Digital filters

14.6.1 Basis

This section is based on [RD-068].

14.6.2 Definition and parameters

Filtering a shock signal is sometimes necessary in order to isolate a specific frequency component in the signal. The theory behind filtering is quite complex and the aim of this section is not to detail the design of such filters. But it is important to observe some precautions and good practices in order to avoid bad results or misunderstanding.

A filter aims to preserve frequency components of a signal in a defined passband with a certain tolerance and to eliminate the other frequency components with a certain attenuation (in dB/octave for instance) in the stopband.

The frequency domain parameters of digital filters are (Figure 14-25):

- **Frequency response type** (low-pass, high-pass, band-pass or band-reject)
- No or minimum **passband ripple** (the **passband** refers to frequencies that are passed)
- The **stopband** contains frequencies that are blocked: a good **stopband attenuation** is needed
- The **transition band** is between: a **fast roll-off** means that the transition band is very narrow
- The division between the passband and transition band is called the **cut-off frequency,** generally expressed as reduced frequency or fraction of Nyquist frequency

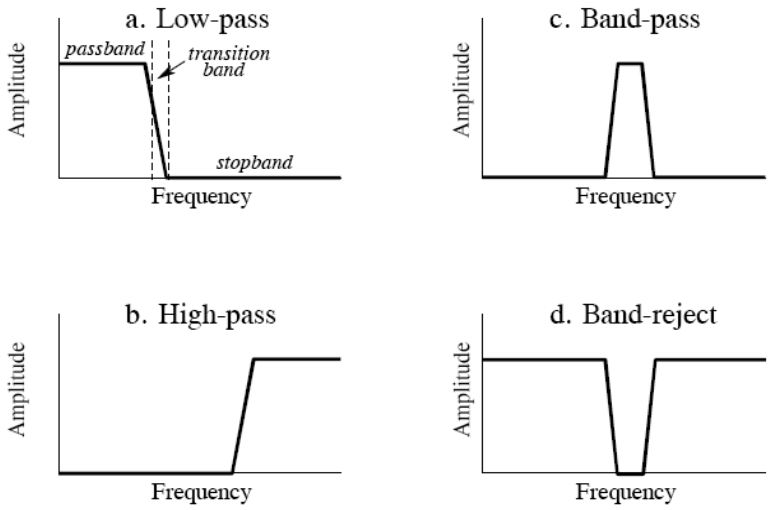

Figure 14-25: Different frequency response types for digital filters

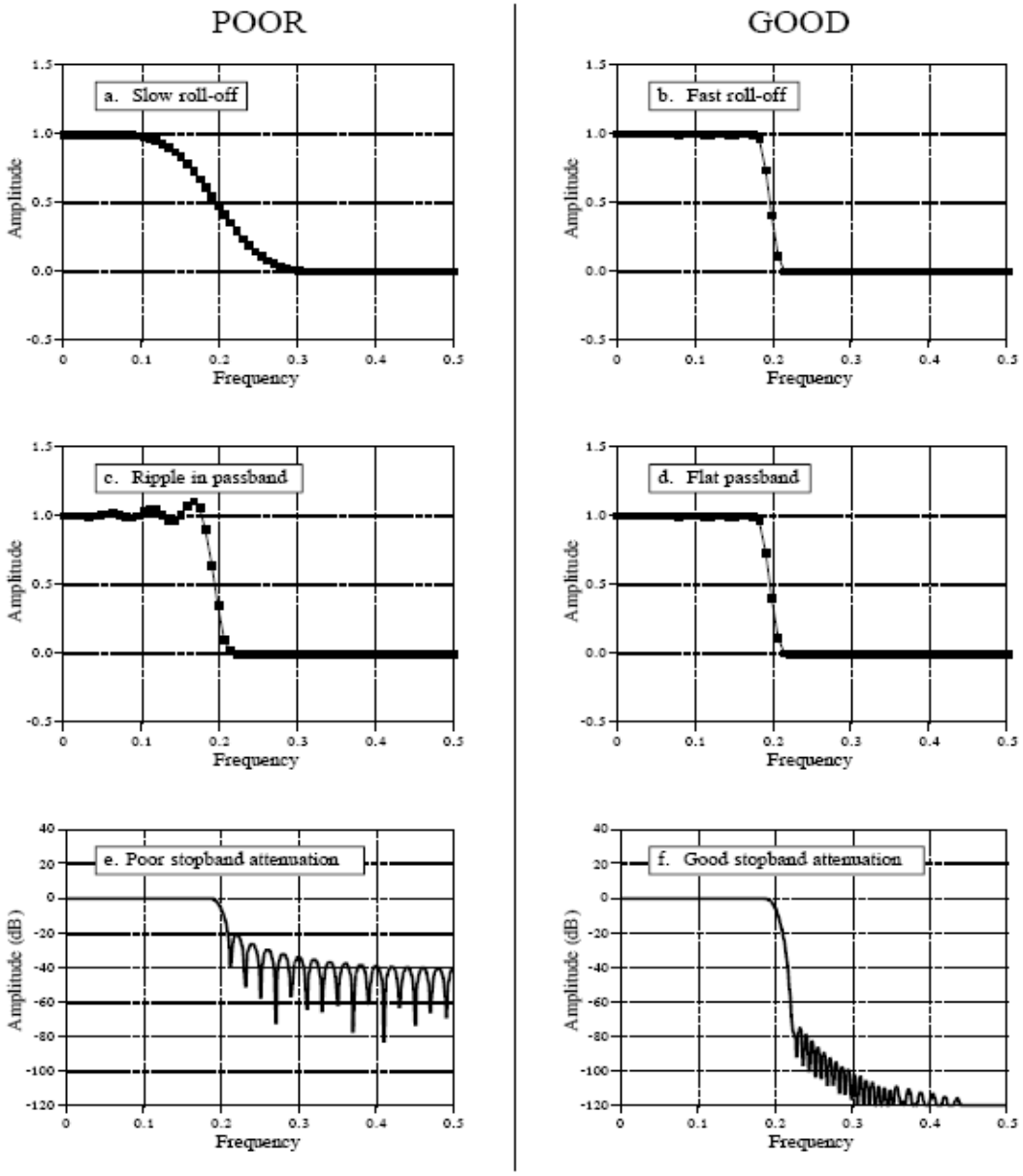

Figure 14-26: Influent parameters of digital filters frequency response

NOTE The reduced frequency 0,5 in the above graphs corresponds to the Nyquist frequency, namely half the sampling frequency of the time history signal.

Digital filters can be implemented in two ways, by ***convolution*** (also called *finite impulse response* or ***FIR***) and by ***recursion*** (also called *infinite impulse response* or ***IIR***). Filters carried out by convolution can have far better performance than filters using recursion, but execute much more slowly.

14.6.3 FIR filters

The convolution of the ideal frequency response with the frequency response of a chosen window causes **ripple**. This ripple finds its greatest deviations near the discontinuity at the cut-off frequency. For many applications the ripples in the frequency response are unacceptable. It is possible to decrease the amount of rippling by using different types of **windows**. The performance of a window is governed by its frequency response. Since the frequency response of the window is convolved with

the desired frequency response the objective is to find a window which has a frequency response which is as impulsive as possible. That is, the frequency response should have a narrow main lobe with most of the energy in this lobe and side lobes which are as small as possible.

Some current windows used in practice are:

- **Rectangular**
- **Triangular** (this window shows less ripple but broader transition bands than the rectangular one).
- **Hamming** (All but 0,04 % of the Hamming windows energy is in the main lobe)
- **Kaiser** (The Kaiser window yields an optimal window in the sense that the side lobe ripple is minimized in the least squares sense for a certain main lobe width.)
- **Chebyshev** (The Chebyshev window uniformly minimizes the amount of ripple in the side lobes for a given main lobe width and filter length).

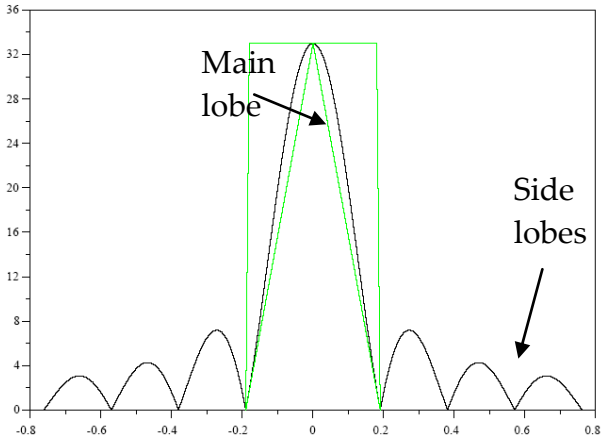

Figure 14-27: Frequency response of the rectangular window

14.6.4 IIR filters

The primary attribute of IIR filters is their speed, typically more than an order of magnitude faster than the FIR filters. This is because they are carried out by *recursion* rather than *convolution.* The design of these filters is based on a mathematical technique called the *z-transform*.

Current examples of IIR filters are:

- Butterworth,
- Chebyshev (type I and II),
- Elliptic

The Chebyshev response is an optimal trade-off between ripple and roll-off. As the ripple increases, the roll-off becomes sharper. When the ripple is set to 0 %, the filter is called a **Butterworth filter**. A ripple of 0,5 % is often a good choice for digital filters. One distinguish two types of **Chebyshev filters:**

- **Type 1** filters, meaning that the ripple is only allowed in the *passband*.
- **Type 2** filters**,** meaning that the ripple is only in the *stopband*. Type 2 filters are seldom used.

The **elliptic filter** has ripple in *both* the passband and the stopband. Elliptic filters provide the fastest roll-off for a given number of poles, but are much harder to design. It is frequently the first choice of filter designers.

14.6.5 Precautions

The following are important precautions to be taken:

- Many filters introduce a **nonlinear phase shift** near the filter cut-off frequency that can distort the signal time history. This can be corrected with **bidirectional filtering**. In that case, the passband ripple applies twice.
- After designing a frequency filter, it is recommended to check if it corresponds to the desired parameters. Verify its frequency response and to use it on a theoretical time signal (e.g. a sine sweep) and/or on the useful time signal and compare the FFT of the original and transformed signal.
- The **round-off error** from the limited number of bits can degrade the response of an IIR filter or even make it unstable. Ensure that double precision is used when using digital IIR filters.
- When using IIR filters, the beginning and the end of time signal are not correctly filtered because the algorithm based on level of recursion cannot find previous values.
- Mention each filtering operation.

15
Shock data validation

15.1 Overview

Before the recording of shock response data are utilized, it is important to ascertain the quality of these data based on shock validity criteria. The **Piersol procedure** [RD-073] and [RD-074] is recommended for determining the validity of shock data, where:

- the time histories are visually inspected,
- the noise perturbation is evaluated,
- the comparison of positive and negative SRS's are computed.

15.2 Visual inspection

All shock signals are **visually inspected for evidence of** the following **anomalies**:

- Obvious wild points, dropouts, magnitude limitations (malfunction),
- Signal terminations (accelerometer failure or separation from the structure),
- Sharp, randomly occurring spikes (noise due to a loose connector or other intermittent noise sources),
- Asymmetrical signal (electrical isolation, grounding problem, accelerometer/amplifier saturation, DC and dynamic offsets).

In most cases, if a pyroshock signal reveals any of the above anomalies, the data are considered invalid. However corrections for certain anomalies are possible, specific cases are also discussed herein.

Some illustrations of anomalies detected by visual inspection are presented in Figure 15-1, Figure 15-2 et Figure 15-3.

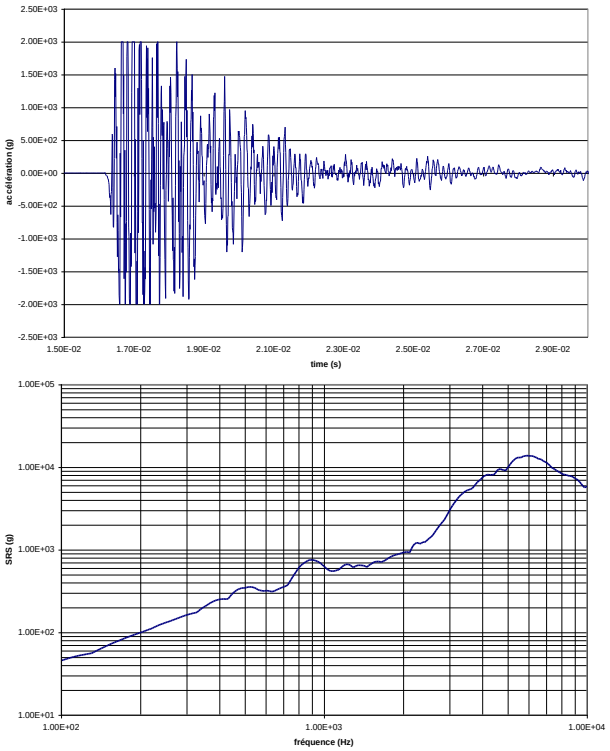

Figure 15-1: Magnitude limitations and associated SRS

It is important to notice that nothing on the above SRS allows to detect the time signal anomaly. In some cases, the SRS magnitude in the useful frequency range (typically between 100 and 10000 Hz) was profoundly modified by this type of anomaly without being able to directly detect it on the SRS.

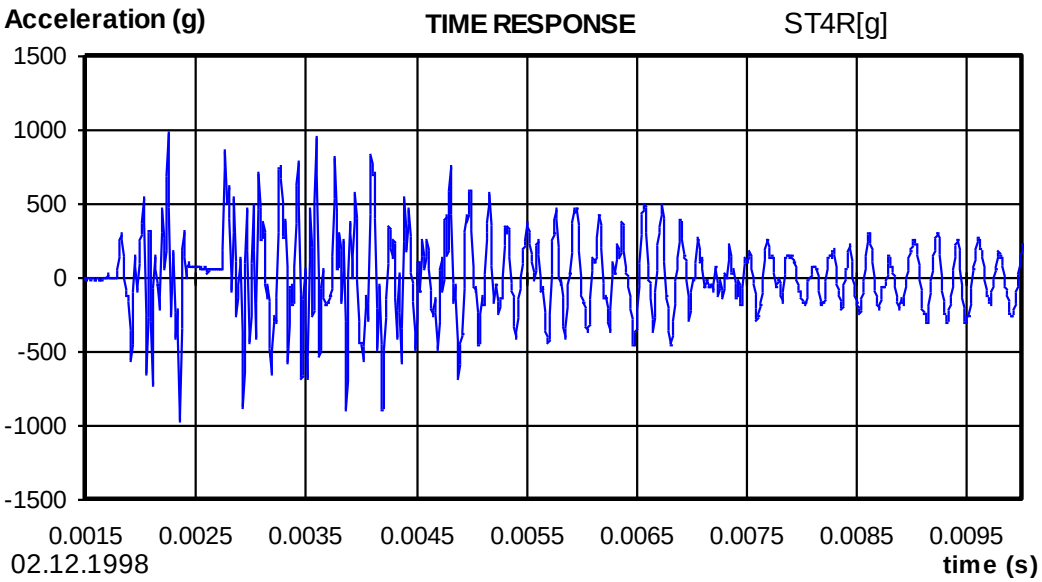

Figure 15-2: Erroneous time signal due to wild points

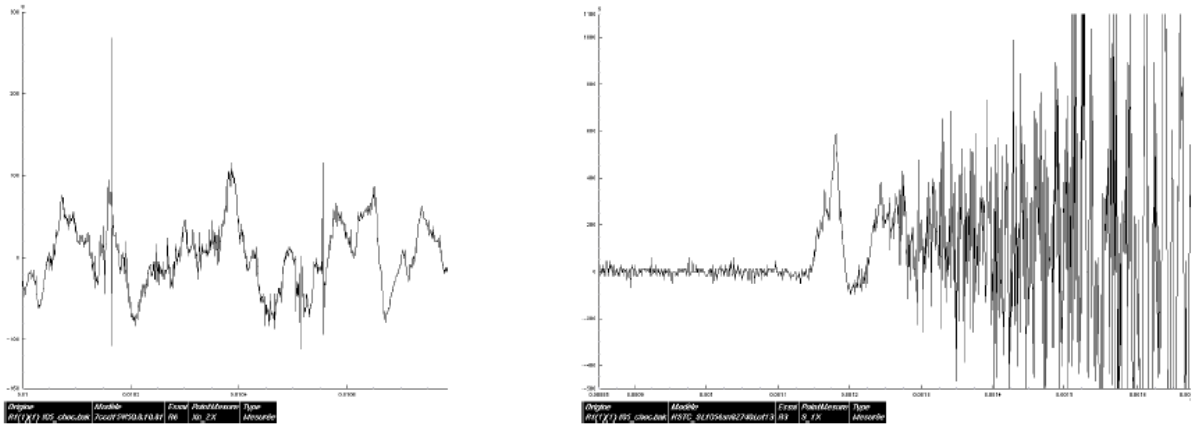

Figure 15-3: Spike example and asymmetrical signal before shock

15.3 Data analysis – simplified criteria

15.3.1 Duration analysis

The data processing should be conducted on the effective duration of the measured time history data. The effective shock duration is defined as the minimum length of time that contains at least 90 % of the energy associated with the shock event (sliding RMS value over a short horizon). For the determination of the effective shock duration, the information inherent in the complex transient should be preserved, and the information related to instrumentation noise should be minimised.

In most cases, the judgment of an experienced analyst is satisfactory in determining the effective duration, in place of a rigorously applied analytical definition.

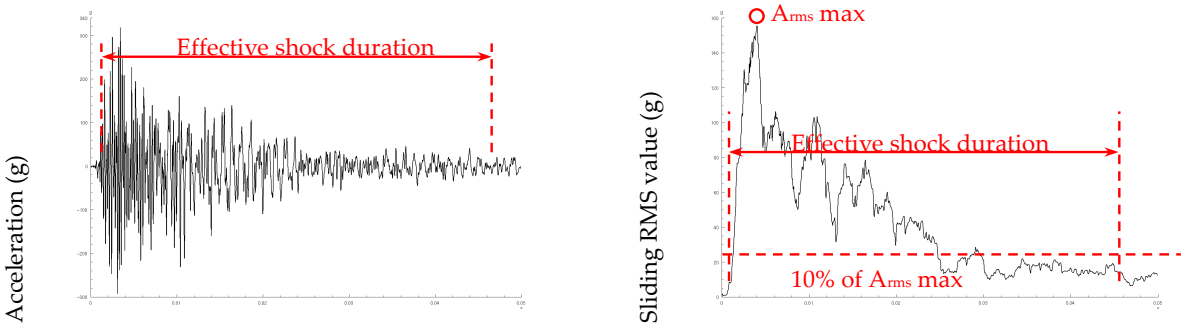

Figure 15-4: Shock effective duration

15.3.2 Validity frequency range

15.3.2.1 Overview

Purpose of this section is the definition of the validity frequency range. Generally speaking, its definition does not follow a single rule, but it depends on different aspects such as signal duration, limitation due to the sampling, perturbation due to the noise or inaccuracy due to acquisition system.

The combination of all these aspects results in the definition of the validity frequency range. This is the frequency range to be used to verify the validity criteria.

15.3.2.2 Signal duration

The cut off frequency (f_c) is defined by $fc = \left(\frac{\text{signal duration}}{3}\right)^{-1}$ and corresponds to the lower frequency, which can be observed if we take into account 3 periods.

15.3.2.3 Background noise

The noise SRS should be computed from a segment of the signal measured after the transient has diminished into the noise (or before, if a sufficient segment of the signal is available). The duration of this segment should be the same as the duration of the transient segment.

The pyroshock should be considered valid at those frequencies where the noise SRS is more than 6 dB below the pyroshock SRS.

15.3.2.4 Data sampling

The data sampling limits the validity frequency range in the upper band. For instance if a sampling of 50 kHz (Δt = 2e-5s) is considered, the frequency range can be extended up to 7000 Hz - 8000 Hz (at least, 6 to 7 points are required to approximate one period of the signal).

On the next graphs, the effect of an improper sampling on the SRS calculation can be visualized. A theoretical signal has been used composed of three frequency components at respectively 5000, 9000 and 16000 Hz. This reference signal has been sampled at 1 MHz. It has been then resampled at 40 kHz with an algorithm that preserves the frequency content below the resampled frequency (see the FFT). On the SRS, it can be noticed a difference between both signals superior to 2 dB after 11 kHz (grey area).

The optimal sampling frequency should be as per Section 13.4.5.7.6.

(a)

(b)

(c)

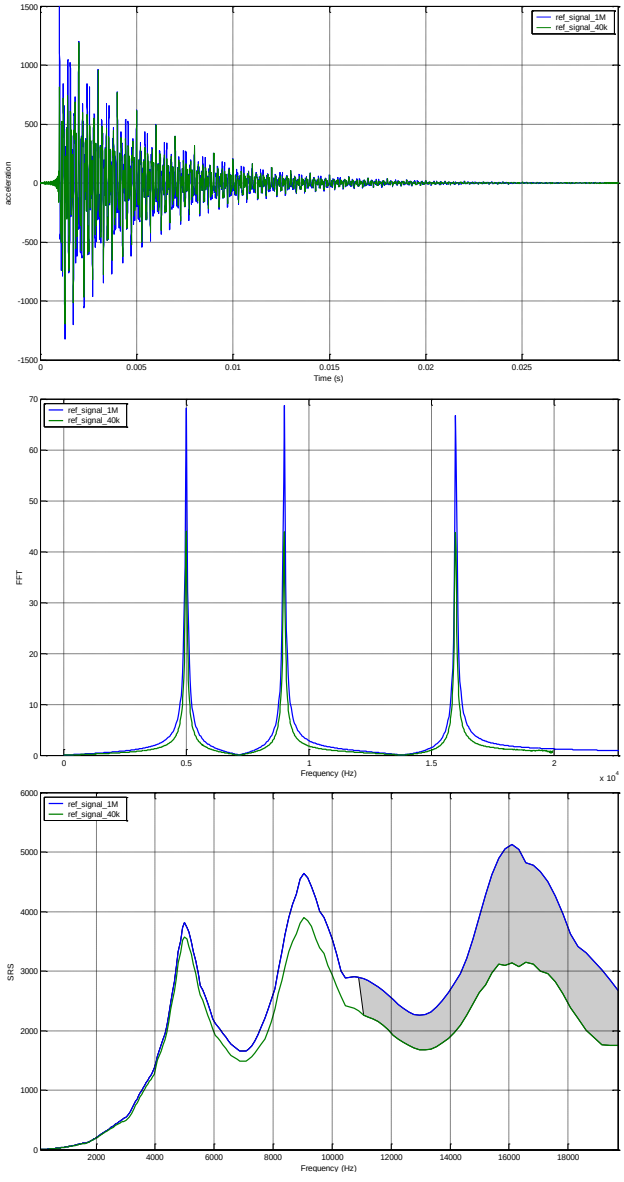

Figure 15-5: (a) reference and resampled time signals; (b) reference and resampled FFT; (c) reference and resampled SRS

15.3.3 Final validity criteria - Positive versus negative SRS

The ratio between SRS+ and SRS- (cf. **4.1.4.2** for definition) should be computed for all signals. These two SRS should agree at all frequencies, above the beginning of the validity frequency range (as defined previously) within ± 6 dB.

If they differ by more than ± 6 dB (i.e. 0,5 and 2) at any frequency, the pyroshock data should be considered invalid at all frequencies.

15.4 Data analysis – refined criteria – Velocity validation

For general use, such as derivation of shock specification or shock severity assessment, the simplified criteria are enough for determining the validity of pyroshock data. However some more advanced applications, such as FE simulations, require using some "perfect" time history measurements.

In addition to the simplified criteria, as presented above, a velocity validation procedure should be applied. The velocity signal is obtained by integration and should look like a lowpass filtered version of the acceleration signal with a zero velocity value at the end of the measurement (for shock tests with no net velocity change). This integrated signal can be used to detect anomalies in the measurement system e.g., cable breakage, slew rate of amplifier exceeded, data clipped, unexplained accelerometer offset.

It is important to take care to distinguish between a rapid trend indicative of a spurious acceleration signal and a slower trend due to an integrated noise problem (which can generally be corrected with a highpass filter).

The signal should be considered invalid if a rapid shift of the velocity mean value is revealed, more precisely if the mean value of the velocity signal exceeds the peak-to-peak range of the fluctuating portion of the velocity signal. This example is given in Figure 15-6.

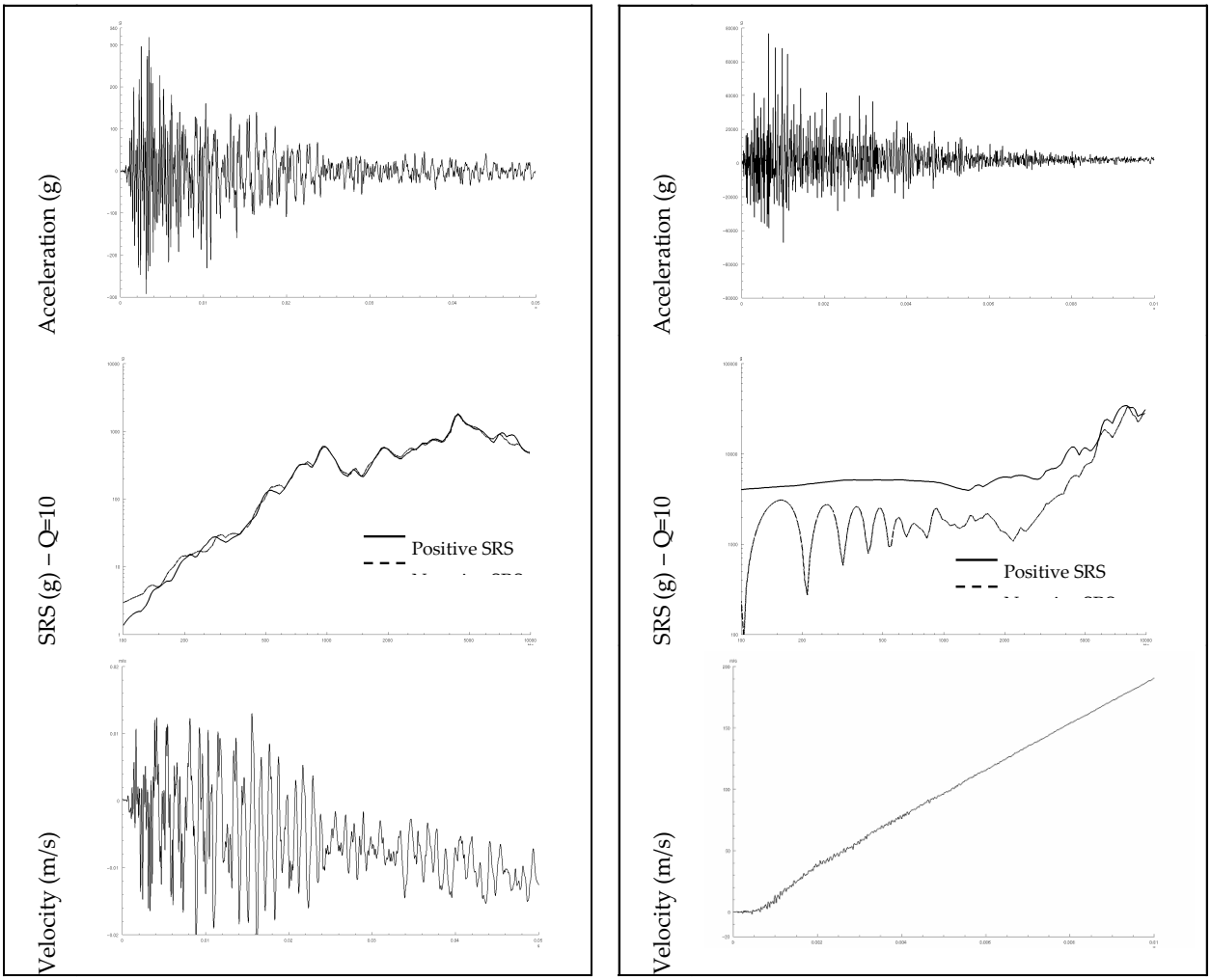

Acceleration and velocity time histories, Positive versus negative SRS for valid pyroshock data

Acceleration and velocity time histories, Positive versus negative SRS for valid pyroshock data

Figure 15-6: Illustration of velocity validation

15.5 Corrections for anomalies

15.5.1 Overview

Corrections for certain anomalies are possible. If wild points or noise spikes are easy to be corrected, other corrections for other anomalies such as dynamic offset or power line pickup require a more dedicated attention from an experienced analyst.

Recommendations for zeroshift correction and power line pick up correction are provided hereafter.

15.5.2 Correction for zeroshift

Zeroshift [RD-056] is commonly defined as failure of the electrical output of the piezoelectric accelerometer to return to its original zero baseline after an acceleration transient. This shift can be of either polarity and of unpredictable amplitude and duration.

Zeroshift effects can be created in the accelerometer, the cable, and/or the electronics. In addition to the effects within the ferroelectric material, other sources such as slippage of internal parts, cable noise, straining of sensing element, inadequate system low frequency response, and overloading of electronic circuits can also lead to zeroshift.

No cause dominates as a major source of zeroshift. Therefore to minimise the actual zeroshift in a given test, all of the causes are also minimised or eliminated (through proper component selection and instrumentation system setup). The best approach to the zeroshift problem is prevention.

It is important to dedicate a careful attention to the shock data validation. Especially **all data affected by a zeroshift problem should be clearly identified**. These "erroneous" signals can be easily identified, either directly after visual inspection (for the most severe cases), or looking at the Shock Response Spectrum (incorrect slope in the low frequency band of the spectrum – slope much lower than 6 dB/oct).

Illustrations of zeroshift in shock signals are shown in Figure 15-7.

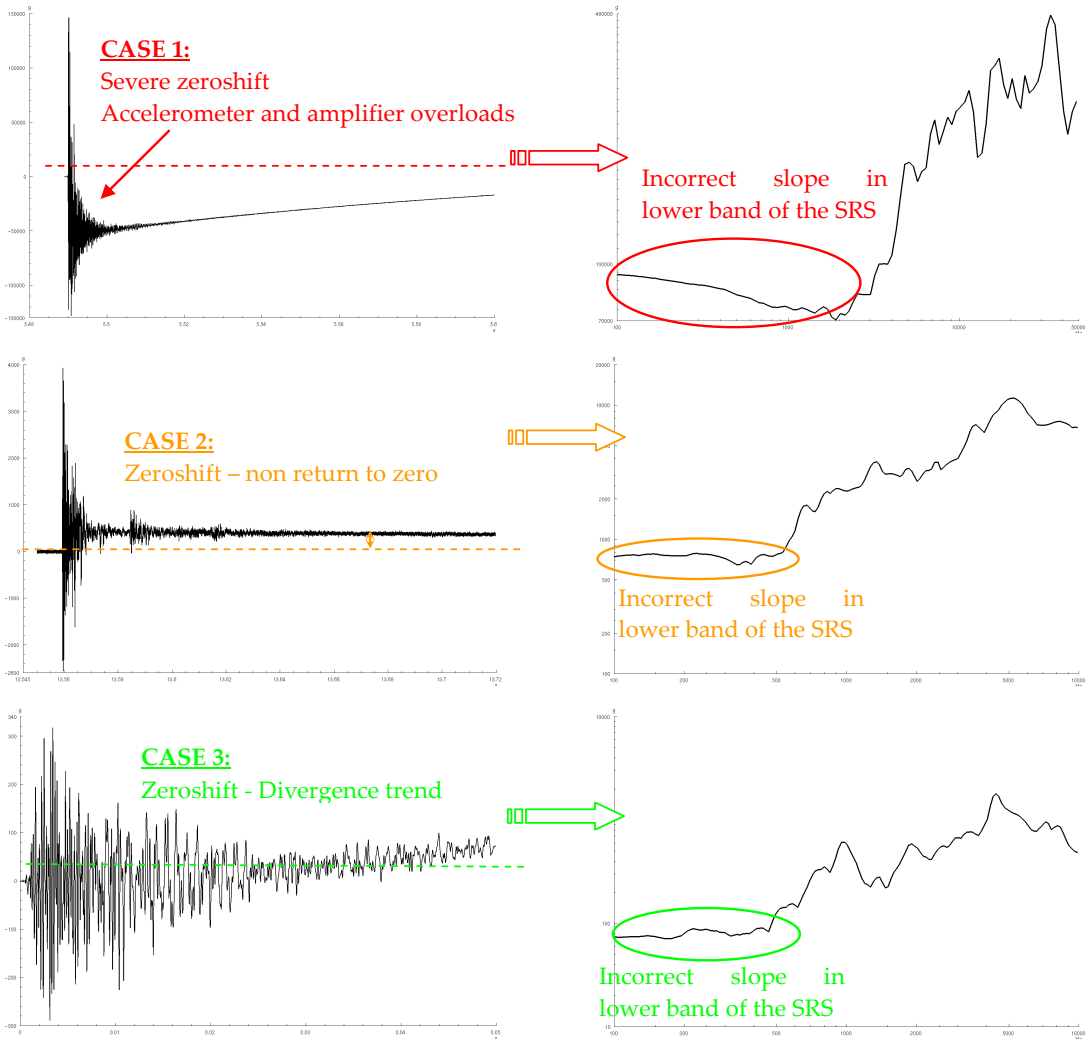

Figure 15-7: Illustrations of zeroshift effect

Compensating for zeroshift requires making assumptions and interpretations, which can be then the source of unacceptable errors (resulting in unintentional overtest of the specimen).

Corrective actions to treat zero-shift problems exist but it is important to **apply them on a case by case basis** and with **great precaution**.

When encountering a zeroshift problem, the following procedure is recommended:

- Discard all time histories affected by severe zeroshift, which are usually caused by overloading of sensor or amplifier. If a zeroshift due to saturation of a piezoelectric transducer or amplifier is identified, consider the data as spurious, no corrective editing or trend removal should be attempted.

  The following criterion is proposed for the classification of zeroshift (from severe to limited):

  — Severe zeroshift: A zeroshift should be considered as severe, when it is clearly attributed to saturation of an amplifier or piezoelectric transducer element. Case 1 presented in Figure 15-7 is a good illustration for a severe zeroshift problem, which cannot be corrected in any case (nonlinear system response, causing a loss of information at all frequencies).

  Another rejection criteria could be as follows: if a pyroshock signal reveals zeroshift with mean amplitude higher than $1/8^{th}$ of the maximum temporal, the measurement should be rejected.

  — limited zeroshift: In most cases where a zeroshift is not due to saturation of an amplifier or piezoelectric transducer element, the presence of the zeroshift in the data signal only distorts the low frequency content in a computed SRS.

  Example of slight zeroshifts are presented in Figure 15-7 (*case2* and *case3*):

  Case 2: A step signal superimposed to the shock signal is usually indicative of an accelerometer malfunction called "crystal domain-switching", but such a result could also be indicative of saturation in the accelerometer amplifier. Experience has shown that the loss of information affects essentially the low frequencies (where the slope is incorrect in lower band of the SRS). The measure can usually be corrected (see below), under the condition that the mean amplitude of the zeroshift is lower than $1/8^{th}$ of the maximum temporal.

  Case 3: A divergence and monotonic trend are not indicative of a sensor or acquisition system malfunction. The measure can usually be corrected (see below).

- Try to use another data in direct vicinity, not affected by this problem.
- For limited zeroshift, any correction procedure requires a detailed knowledge of the sensor and acquisition characteristics, as well as a proper engineering judgment. The following correction procedures could be used:

  — High pass filter (cut-off frequency f_c). The subsequent data analysis computations would be limited in the lower frequency range by 1,5 f_c (no mechanical signal below this frequency),

  — Prony decomposition to remove non-physical Prony modes.

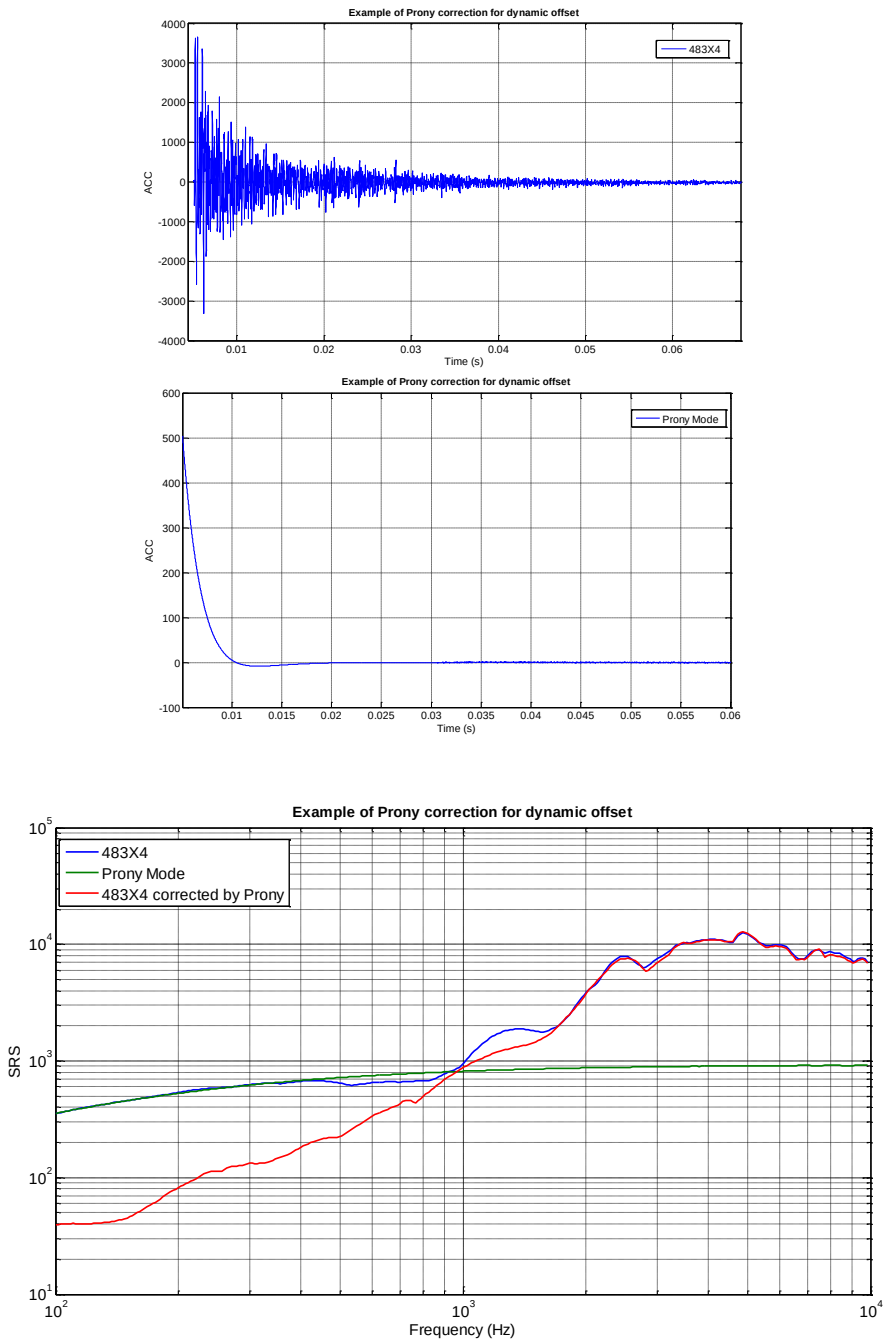

Figure 15-8: Example of dynamic offset correction using Prony decomposition

— Extract decaying function by classical curve fitting technique: characterise polynomial function (4^{th} order is usually used) from the integrated displacement signal, and remove it (becomes 2^{nd} order) from the acceleration signal,

— Calculate the mean over a sliding horizon and remove it from the original signal.

- The selected correction procedure should be consolidated, by comparing different corrected signals together (find similar behaviour, and check slope of SRS in the lower frequency band).

15.5.3 Correction for power line pickup

15.5.3.1 Overview

The contamination of a measured signal by power line pickup (at 50Hz within Europe, often with multiple harmonics) commonly occurs if the data acquisition system is not properly shielded and grounded. Power line pickup produces a periodic oscillation superimposed on the signal time history of interest. If the pickup is strong, the detection is easily made by visual inspection on the time history of interest, as illustrated in Figure 15-9.

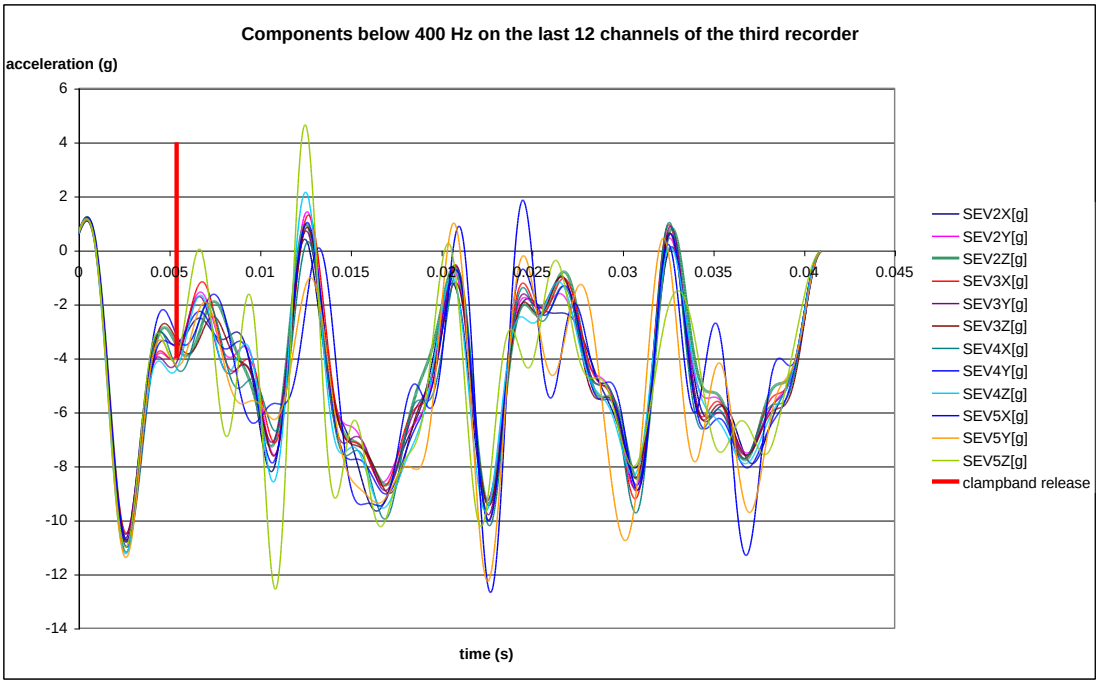

Figure 15-9: Illustration of power line pickup

Unless it is very severe, power line contamination is not a reason to reject measurements for spectral analysis purposes, although it can somewhat limit the time domain interpretations of such data.

15.5.3.2 Power line pick-up cleaning principle

Power line pick-up cleaning process is as follows:

- Isolate the power line component by filtering
- Compare them taking into account the different channel gains
- If identical, remove this component because of its electrical nature
- Remove the mean perturbation to all channels taking into account the different channel gains

15.5.3.3 Power line pick-up cleaning steps

Some components have been identified in the measured signals which do not correspond to any mechanical vibration. Those levels are not relevant for shock study and can be removed. There is no perfect way to clean the signals from the low frequency interference. However, if the undesired components can be identified and isolated, they can be removed by subtraction or filtering.

Since the electrical disturbances are the same on all channels, it is possible to identify the electrical noise by checking the components which are exactly the same. This is done by:

- Filtering the signals with a high pass filter to remove the offsets in the measures (when necessary) and then with a low pass filter to remove the high frequency components.
- Looking at both the temporal filtered signals and the Fourier transforms.
- Multiplying the levels by the ratio between calibration gains for channels with different calibration gains (so that the electrical components are amplified with the same ratio for all channels).
- Removing the channels which show some other levels than the electrical components
- Calculating the average of the remaining channels, which gives the best approximation for the electrical components.
- Comparing this average to the filtered signals and checking that the average almost equals the signals, and ensuring that there is low scatter between the signals used to calculate the average. Check with Fourier transform that the average contains the same components at the same levels than the signals.
- Subtracting the average to all channels (with a correction factor for different calibration gain). The resulting signal is free from the electrical components.

Remark: in Europe, electrical components are often multiple of 50 Hz.

15.5.3.4 Precautions

The filters used are filters with non-dephasing behaviour. All filters responses are checked to verify their quality.

The filters do not work at the really beginning and at the end of the signals. This is not a real issue, since the shock event does not usually begin exactly at the beginning of the recorded signal and ends before the end of the recording. This implies the necessity of calculating SRS from the beginning of the shock to its end, removing the time laps where the filtering is poor.

Part 4
Shock damage risk assessment

16
Introduction to shock damage risk assessment and objective

16.1 Overview

Following system and equipment level testing, the qualification status of the shock sensitive equipment are assessed by comparing the qualification shock levels (including 3 dB margin) to the shock qualification requirement at equipment interface (or shock allowable derived by sine/random testing – see Part 3 – Shock Verification Approach).

In the ideal case, the capability of the spacecraft to withstand or, if appropriate, to operate in the induced shock environments is demonstrated after this operation. And the shock qualification is achieved.

But in some cases, the shock qualification cannot be directly achieved (shock environment not completely validated by system level and unit level testing). In general, this problem is discovered too late to perform a delta qualification at unit level.

Several recent ESA programmes as ENVISAT, ARTEMIS, SMART-1and MSG were in this position and had to face the demonstration of their spacecraft integrity with respect to a stringent shock environment. In this frame, some special techniques have been established in order to get a sufficient confidence in the absence of degradation risk against shock.

The so-called Shock Damage Risk Assessment (SDRA) is built on a good knowledge of failure modes of shock sensitive equipment on good engineering practices for the derivation of shock level at components interface, and for the identification of the qualification status of the shock sensitive equipment.

It is of importance to underline that a Shock Damage Risk Analysis is by itself not a qualification, however it can provide an assessment if the spacecraft can withstand the required shock environment without damage/degradation or not.

16.2 Assessment context

Such demonstration activities are performed in the frame of different contexts due to the project development differences. In particular, the time schedule can be compatible or not with the performance of additional testing at system level or equipment level. Nevertheless the methodologies and approaches used are the same. They are based on the evaluation of the damage risks against shock for the sensitive equipment.

— **Sub Case 1:** Case of a satellite following proto-flight verification test at system level. The assessment objective is then to evaluate the risk on equipment induced by such a test.

— **Sub Case 2:** Case of equipment not fulfilling the shock qualification requirement and no sufficient heritage exists. In case shock verification is to be achieved on PFM unit, the risk is assessed. For a new development (QM available), SDRA is used to support designs choices in order to minimize the risk of failure during qualification.

— **Sub Case 3:** Case of an alert on component that impacts all programmes on which some equipment has this component.

16.3 Outputs of SDRA and associated limitations

Due to the high frequency nature of pyroshocks, the induced phenomena are not easily numerically or analytically simulated, and therefore the notion of safety margin becomes ambiguous, in the same way a probability risk level cannot be precisely estimated. Instead, the level of confidence in a SDRA is directly and obviously related to the conservatism considered for the various analysis parameters. When conducting a SDRA, it is essential to justify the conservatism in the assumptions made.

In this regard, the SDRA drives automatically the unit away from the qualification domain; but it either provides valuable data to ensure a successful qualification (in view of a sub-system or system level qualification test), or it provides a risk assessment on the capability of a spacecraft/equipment to withstand (or not) the required shock environment without damage.

17
Unit susceptibility with respect to shock

17.1 Overview

The susceptibility of equipment to pyroshocks cannot be straightforwardly assessed. This assessment is made possible, if a consistent approach is strictly followed.

The first step of this evaluation consists in an immediate screening of equipment criticality with respect to shock, and in the identification of the associated critical frequency ranges. Some special techniques have been established and are presented in this chapter.

The evaluation of damage risk with respect to shock is built on:

- Good engineering practices for the derivation of qualification shock levels at unit interface,
- The identification of the critical frequency ranges,
- A good knowledge of failure modes of shock sensitive equipment,
- Good engineering practices for the identification of the compatibility status of the shock sensitive equipment, based upon a set of general evaluation criteria and taking the type of equipment into account,
- Consideration of mission related aspects.

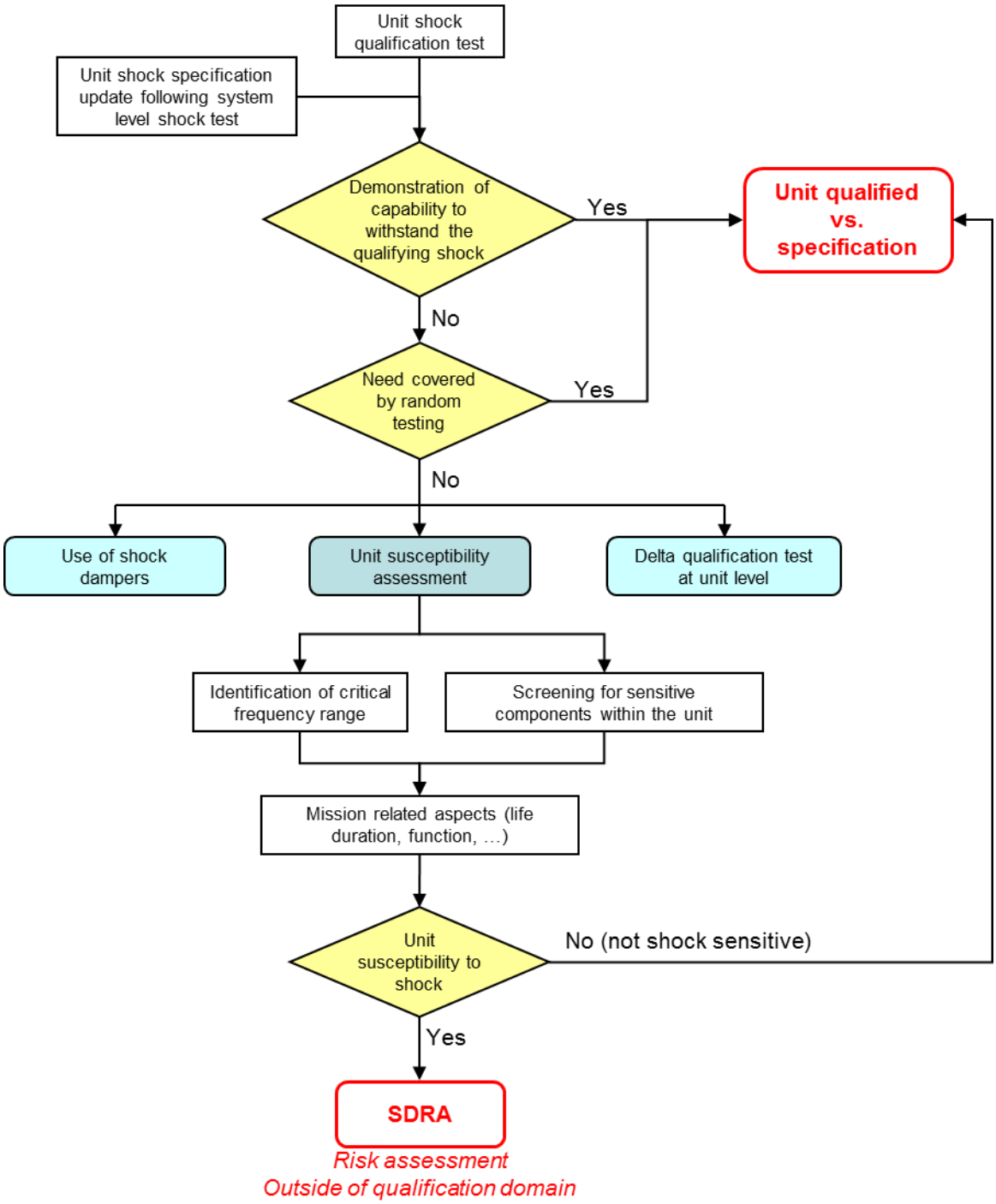

Figure 17-1: SDRA rationale

17.2 Derivation of qualification shock levels at unit interface

Prior any Shock Damage Risk Assessment, it is recommended to review the methodology previously used to derive the qualification shock levels at unit interface.

Indeed, an excessive conservatism in the derivation methodology could result in declaring wrongly most of the equipment non-qualified.

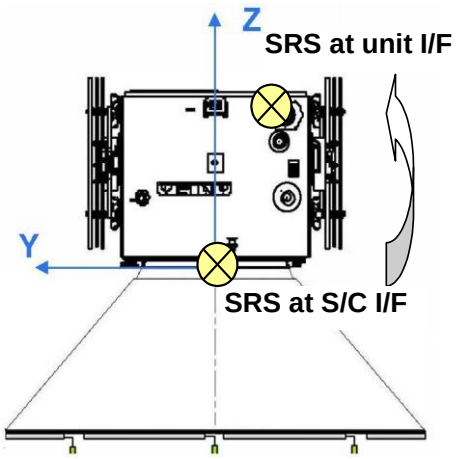

Figure 17-2: Principle of computation of SRS ratio

This conservatism could come from:

- A too stringent launcher shock specification. This should be reviewed with the launcher authority, and justified on the basis of relevant flight data measurements,
- Pollution of recording of shock response data. Most typical problem are zero-shift or dynamic offset affecting the time histories, this results in an incorrect slope for the SRS in the lower frequency range,
- An improper usage of system level test data (SRS ratio method for instance, or by extrapolation from another type of shock excitation),
- The construction of the unit specification from measurements, by an excessive simplification (constant slope line and plateau on a log-log graph).

These topics are addressed in details in the Part 2 of the present Handbook (Refer to Part 2 – Shock Derivation to Sub-Systems).

17.3 Identification of critical frequency ranges

This operation simply consists in comparing the qualification shock levels (including 3 dB margin) to the shock levels achieved during equipment level testing (or shock allowable derived by random testing – see Part 3 – Shock Verification Approach).

Further compatibility assessment should then be limited to the identified non-coverage (so-called critical frequency ranges) with respect to the qualification shock levels.

In the comparison of shock levels (unit / system), care should be taken for the selection of the SRS Q factor. Experience has shown that the selection of the Q factor depends on the environmental category of the pyroshock data:

- For far-field shock environment (structural modal responses predominant and high in the low frequency range below 2 kHz): A standard Q factor of 10 can be retained in the comparison of shock levels.
- Whereas for Medium-field shock environment (typically induced by a local pyrotechnical device, used for spacecraft separation or appendages deployment), experience has shown that high frequency modes of the spacecraft (for instance, breathing mode of sandwich panel with high Q factor, excited by a cable cutter or a pyro-nut) could be easily transmitted inside an equipment. In that case, it is recommended to compute the SRS with two different Q factors (typically 10 and 100) to reveal pseudo-harmonic frequency content.

NOTE Near-field shock environment is generally not encountered at spacecraft level.

Figure 17-3 shows that increasing Q factors, some frequency contents of the system shock (pyrotechnic cutter) can be particularly critical. The same behaviour can be observed on qualification shock accelerations (Figure 17-4) but the emphasized frequencies can be different than the ones at system level. As a result, the test of some sensitive components that appear qualified considering a Q factor of 10 can be non-conservative if higher internal Q factors are considered, as illustrated by Figure 17-5. On this figure, it should also be noted the very different nature of the two shock excitations. The shock at system level has narrow band frequency content (almost a damped sine wave) whereas the qualification shock has a broader band frequency content.

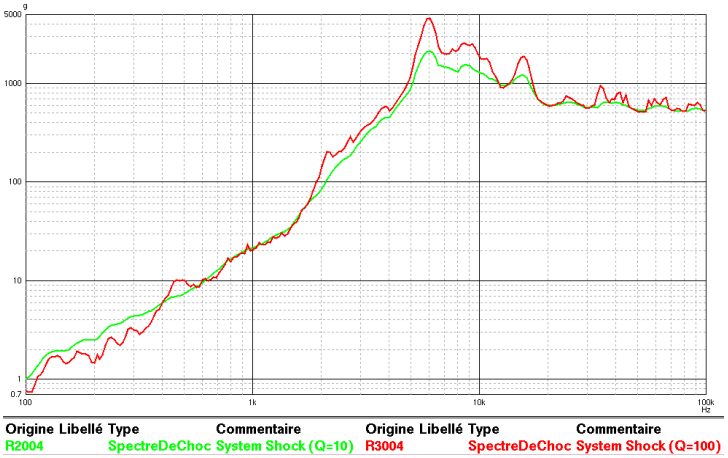

Figure 17-3: Shock measurement (pyrotechnic cutter) at system level - SRS with varying Q

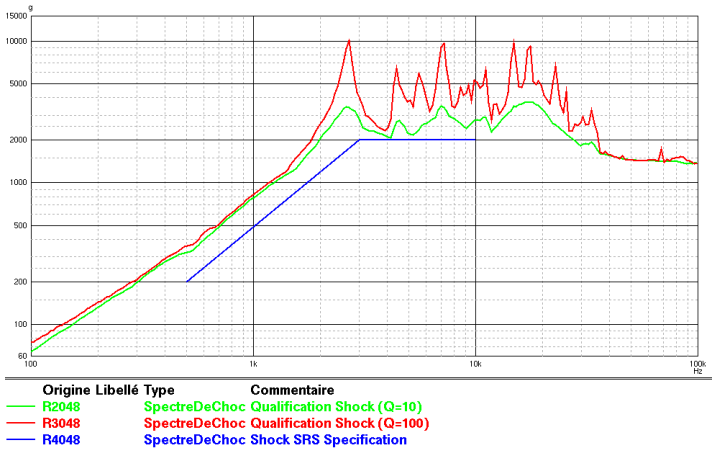

Figure 17-4: Example of qualification mechanical shock test - SRS with varying Q

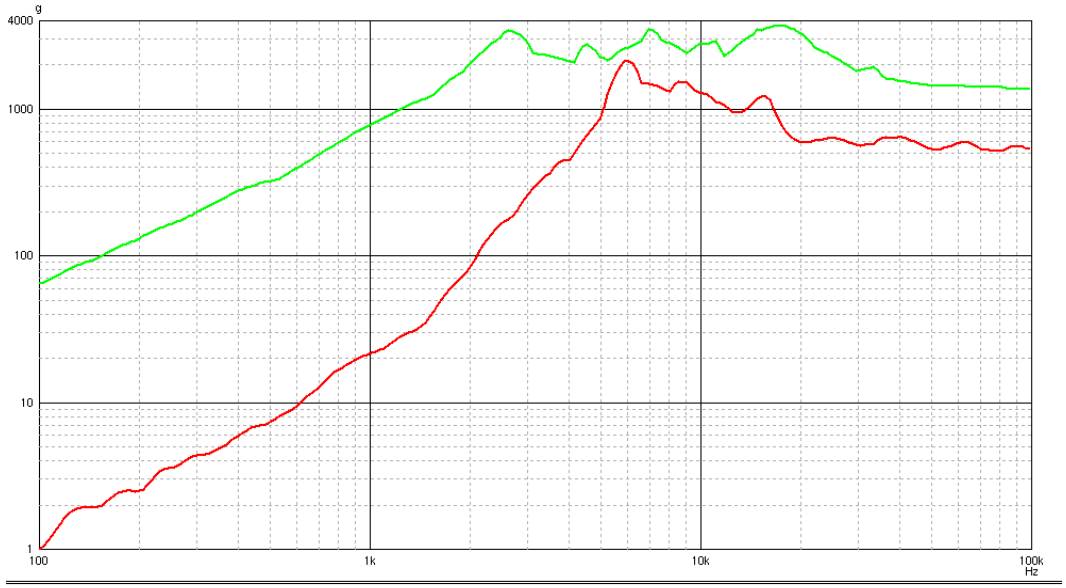

Origine	Libellé	Type	Commentaire
R2005		SpectreDeChoc	Qualification Shock (Q=10)
R2004		SpectreDeChoc	System Shock (Q=10)

(a)

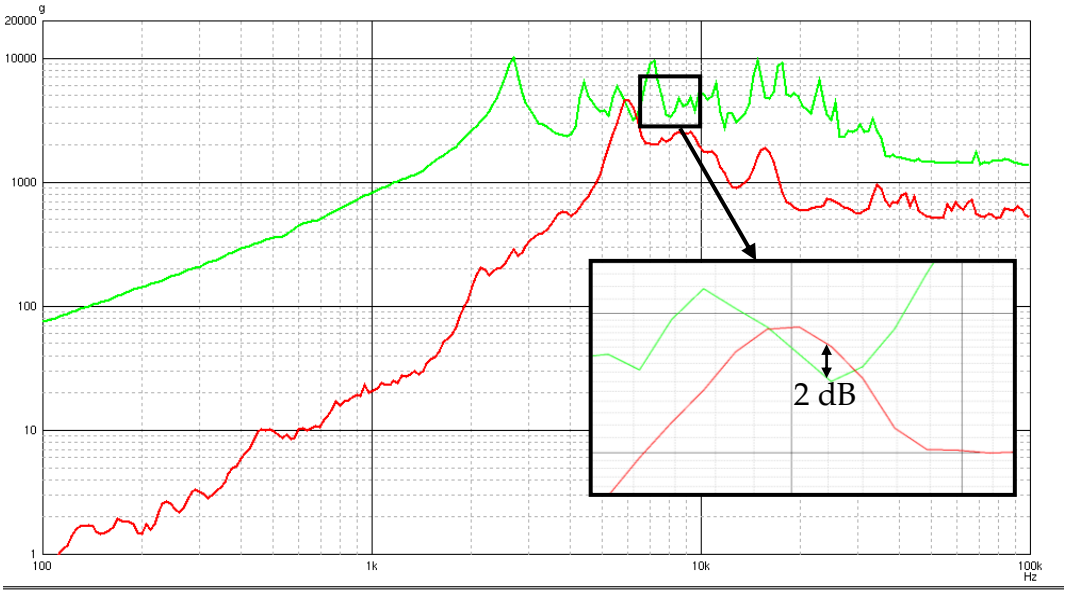

Origine	Libellé	Type	Commentaire
R3005		SpectreDeChoc	Qualification Shock (Q=100)
R3004		SpectreDeChoc	System Shock (Q=100)

(b)

Figure 17-5: Comparison between qualification and system tests – SRS with Q=10 (a) and 100 (b)

17.4 Considerations related to life duration and mission

The damage tolerances and their associated criteria are depending on the mission of the equipment and its sub-system. In case that an equipment is not straightforwardly qualified, then a "dedicated qualification" can be necessary in relation to its compatibility with the mission, spacecraft general design and operations.

For instance, let's consider a relay to illustrate the impact of the mission on the damage tolerance:

The damage modes of a relay are bouncing, transfer and degradation. Assuming that the unit (housing this relay) is switched-off during the shock event, the bouncing can be allowed, whereas the transfers can be allowed only if the unit is re-initialised before it is switched-on. For some types of relays, the transfer can damage definitively the mechanism, thus decreasing dramatically the bouncing threshold.

Thermal cycling is another aspect to be considered in the analysis of the shock damage. In some cases, minor cracks initiated during the shock event can reveal to be disastrous some time later as thermal cycling propagates the phenomenon. **This is the reason why it is always recommended to perform some thermal cycling after a shock test.**

17.5 List of shock sensitive components/units

17.5.1 Overview

The identification of the sensitive components in the unit under investigation in regards of the critical frequency ranges allows the determination of the unit susceptibility to shock.

Based upon return of experience from unit development / qualification testing, failure case histories and engineering judgment, rules for failure modes of shock sensitive components have been established. In this respect, this section intends to list the failure modes of the most commonly used components.

Three categories of shock sensitive components can be distinguished:

- Electronic components
- Functional mechanical assemblies
- Mechanisms

17.5.2 Electronic components and associated degradation modes

The shock sensitive electronic components are listed in the table below.

Table 17-1: Shock sensitive electronic components vs. failure modes

Electronic components	Failure modes			
	Mode 1	Mode 2	Mode 3	Remarks
Relay	Bouncing	Temporary or permanent transfer	Non reversible mechanical damage	
Quartz	Relief of residual stress in the quartz ⇒ frequency shift that can be temporary during the shock application or definitive	Solder overstress or adhesive crack at clip interfaces	Broken crystal	Quartz are usually mounted on a damping material
Magnetic components (RM) Transformer and self	Crack initiation in ferrite	Electrical lead wire rupture		The internal part is fragile, in particular if the component is composed of ferrite or ceramic
Hybrid	Adhesive rupture at substrate level or other small part level (getter, absorber)	Crack in glass feed-thru	Packaging or lid structural failure	Packaging is often made of brittle material Particles in hybrids are detected by a PIND test
Tantalum capacitor	Bending of the PCB leading reversible electrical peak of current due to local destruction of the dielectric	Bending of the PCB leading to internal over-stresses with non-reversible total destruction by short circuit – Avalanche phenomenon	Tantalum capacitor can also be of large dimensions, hence with same failure modes as for heavy/large components	
Heavy or large component	For heavy components (> 5 gr), overstress at the attachment due to loads, e.g. capacitor, transformer, shielded components …	For large components, overstress at the attachment due to PCB bending		
Optical components	Fibre optic pigtail cleavage	Damaged fibre surface in connectors		
Low insertion force DIP socket	Disjunction of the component			
Semiconductors (IC) components, Hybrid components, relays, capacitors with cavities	Dislodging of mobile particle			Particles are detected by a PIND test

17.5.2.1 Relay

17.5.2.1.1 Failure modes

Various types of issues can be encountered with relays:

- The first and most common one is a contact chatter, or electrical bouncing. It can be unacceptable for some applications depending on the electrical design (i.e. functional equipment during shocks).
- The second one is a change of the movable part position in a bi-stable relay, or so called transfer. This phenomenon can be either temporary during the shock or permanent.
- The third one is an irreversible damage (damaged contact, locked mechanism,…)

17.5.2.1.2 Examples of relay failure

The qualification test campaign of a small payload unit has given the following results:

- Transfer of a TL relay after the shock along X-axis, but the relay could still be activated
- Transfer of the relay after the shock along Z-axis, but the relay could still be activated
- Transfer plus temporary locking of the relay (before it could be activated again) during an additional shock along X-axis.

Figure 17-6 indicates the excitation axes with respect to relay orientation. Figure 17-7 shows an X-ray picture of the relay after the complete test sequence. The relay is irreversibly damaged (plastic deformation of the brackets supporting the mobile part). The mounting conditions of the component on the Printed Circuit Board were such that it created a local resonance of the component around 1700 Hz (Q = 80), at the origin of the failure. See also the section 18.3.1.6.1 for additional examples on the importance of the relay mounting conditions on the relay functional issues.

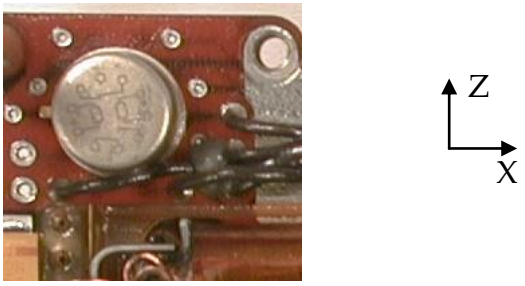

Figure 17-6: Relay orientation w.r.t. unit axes

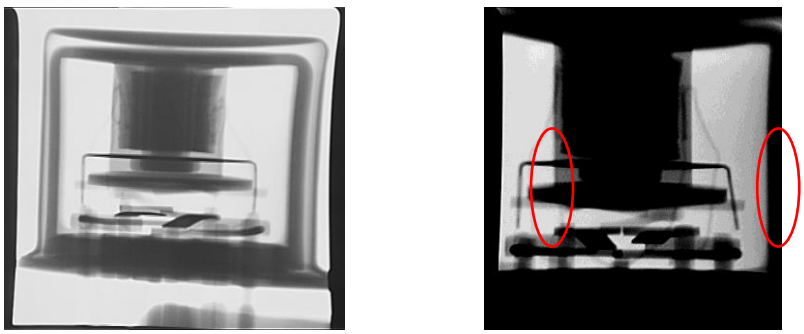

(a) (b)

Figure 17-7: (a) TL relay before shock – (b) Damaged TL relay after a qualification shock test on a payload unit

Figure 17-8 shows the X-ray of another type of TL relay mounted on a PCB that was submitted to an acceleration exceeding 4000 g (temporal) during a process qualification. Once again, the relay is irreversibly damaged.

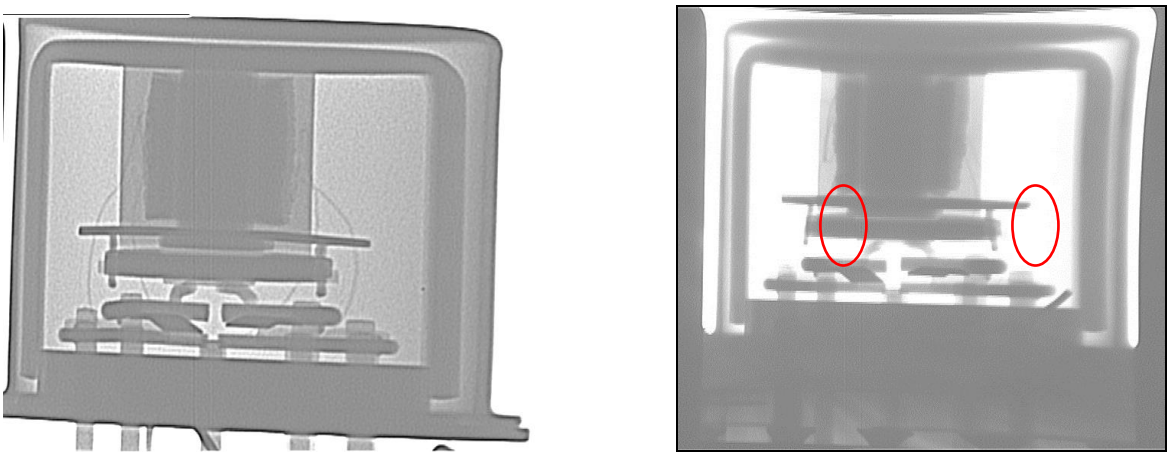

(a) (b)

Figure 17-8: (a) TL relay before shock – (b) Damaged TL relay after a process qualification shock test

17.5.2.1.3 Relay shock sensitivity threshold

Procurement specifications are generic in nature and are not always reflecting the qualification need for equipment submitted to a stringent shock environment. The situation has improved with the introduction of a high level mechanical shock (up to 750g@0.5ms half sine, compared to previously defined level of 100g/6ms) for several of relay types, as specified in ESCC generic specifications [RD-095] and [RD-096].

NOTE 100g@6ms half sine specification on relay is inherited from MIL-STD-202G, Method 213B, Test Condition C. Such low level is neither representative of the qualification level for equipment nor representative of the frequency content associated to the shock specification typically defined for electronic units.

The adequacy of the specified levels from the procurement specification should be verified as part of the Equipment Qualification Status Review (EQSR). In the situation where those specified levels are not covering the qualification need for an equipment submitted to a stringent shock environment (i.e. depending on the electronic unit design, on the relay type and on the severity of the shock environment), some delta-qualification activities need to be conducted.

In order to better understand the behaviour of relays with respect to shock environment and to gain confidence in the domain, a test campaign ([RD-097] and [RD-098]) has been carried out on several types of relays at ESTEC test facility. This test campaign has been conducted in the frame of ENVISAT qualification process; the purpose was to determine the shock levels inducing bouncing or transfer.

A total of 9 different types of relays have been shock tested. Three specimens of each type of relay have been shock tested, to assess the repeatability from relay to relay.

The mounting conditions were:

- a bracket for EL215,EL425,E215,GP2,GP250,GP3A and PHL50A
- a piece of printed circuit board for the T12 and TL12

As shown below, the test bench consisted in a cube of aluminium being hit by a pendulum hammer. The shock was of metal/metal impact type, with a shape enveloped by an exponential decay. The test bench has been instrumented to monitor the transient shock acceleration close to the specimen mounting. A relay status detection circuit has also been used for setting the relay mode (latch or reset) and for monitoring the relay contacts during the shock impact.

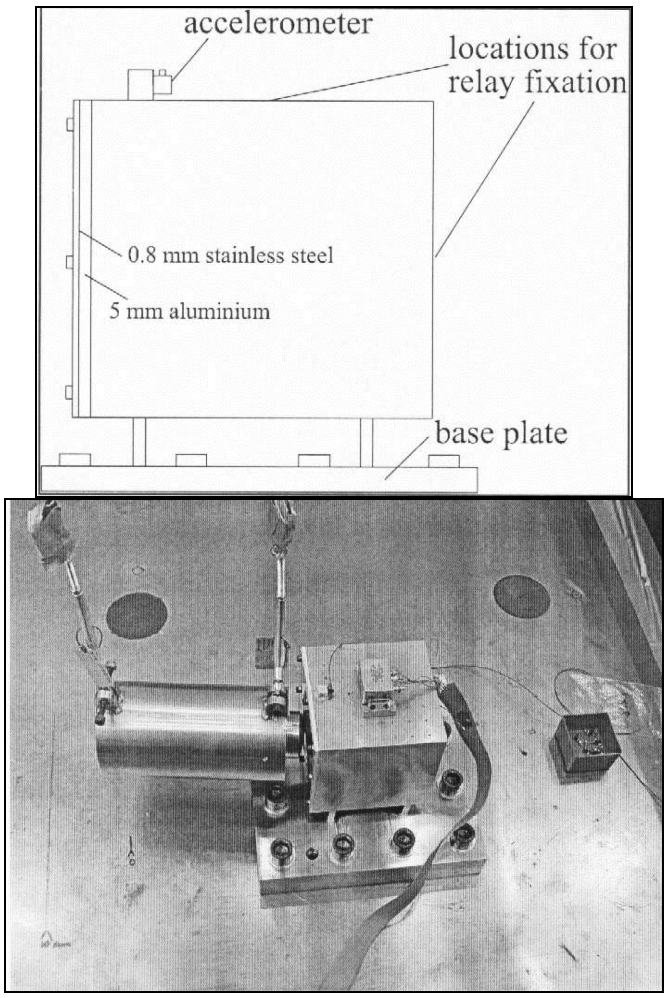

Figure 17-9: Relay test set-up

In order to establish SRS thresholds for these relays, a typical SRS of the applied shocks is illustrated hereunder. It appears that the peak of the SRS is about three times higher than the maximum of the time history. To be more precise, a conservative ratio of 2 should be applied between 1000 Hz and 3000 Hz and the SRS threshold should be the peak acceleration of the time history above 3000 Hz. Finally, the SRS of such a shock can be fully defined by its peak acceleration G, as illustrated on Figure 17-11.

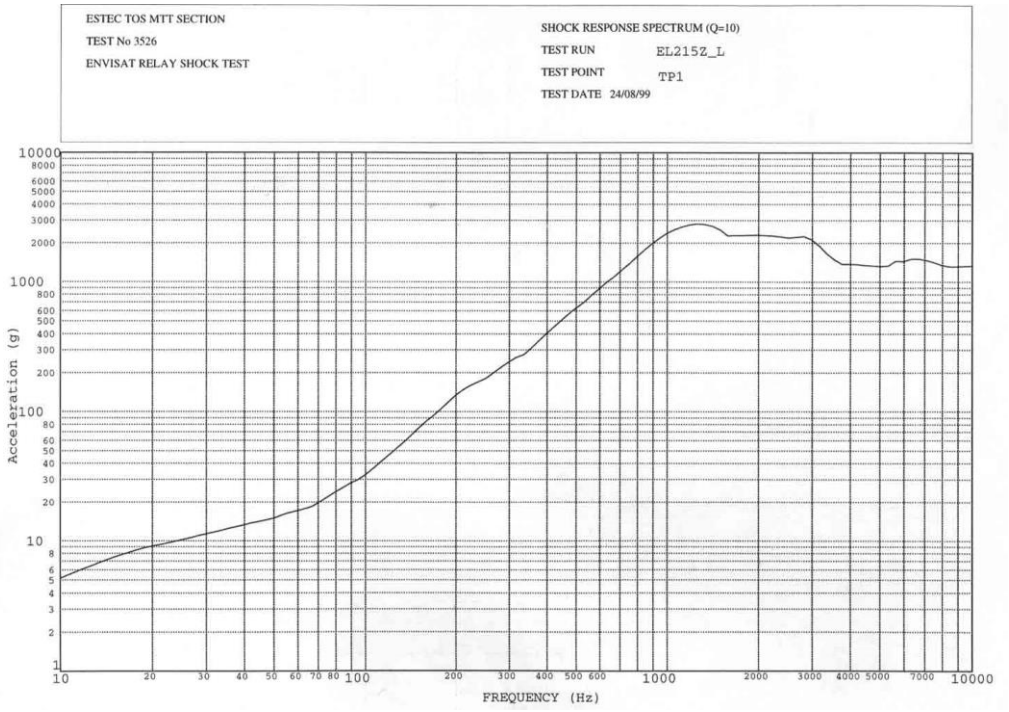

Figure 17-10: SRS of a typical qualification shock applied on relays

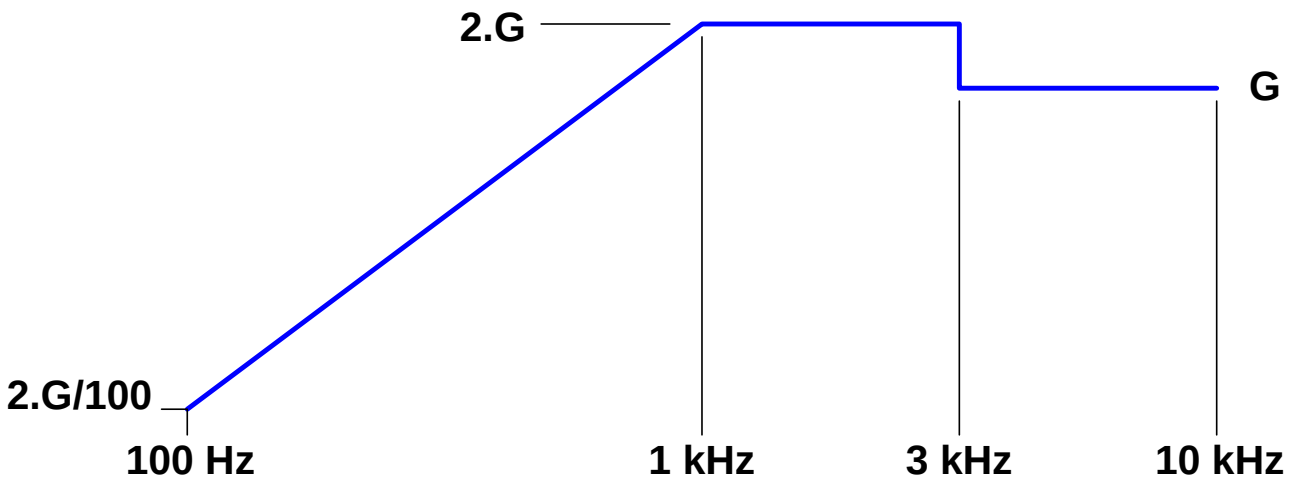

Figure 17-11: Schematic SRS of a typical qualification shock (peak acceleration G) applied on relays

Except for monostable relays, no bouncing has been reported for acceleration levels lower than 200g peak acceleration. Transfer phenomena have been reported on most bi-stable relays at varying levels above 500g. Some relays have been damaged (PHL50A, and GP2).

The highest levels applied in relation to the damage modes (bouncing, transfer, irreversible damage) are summarized in Table 17-2.

Table 17-2: Highest applied G levels without failure vs. type of relay

Relay	No bouncing experienced below:	No transfer experienced below:	Highest level without damage
EL215	600g	2600g	2600g
EL415	280g	2220g	2220g
E215	500g	1790g	1790g
GP3A	520g	520g	1730g
GP250	540g	1390g	1840g
GP2A	570g	1270g	2040g
T12	630g	1580g	1900g
TL12	510g	1800g	2000g
PHL50A	280g	1250g	1250g

Note that the levels which are indicated in the table are maximal values of the **time history** of the acceleration.

The considered failure modes (either bouncing, transfer and/or non-reversible degradation) can be frequency dependent. But as the sensitive range of frequency is not known, the level is given in the time domain.

17.5.2.2 Quartz

17.5.2.2.1 Failure modes

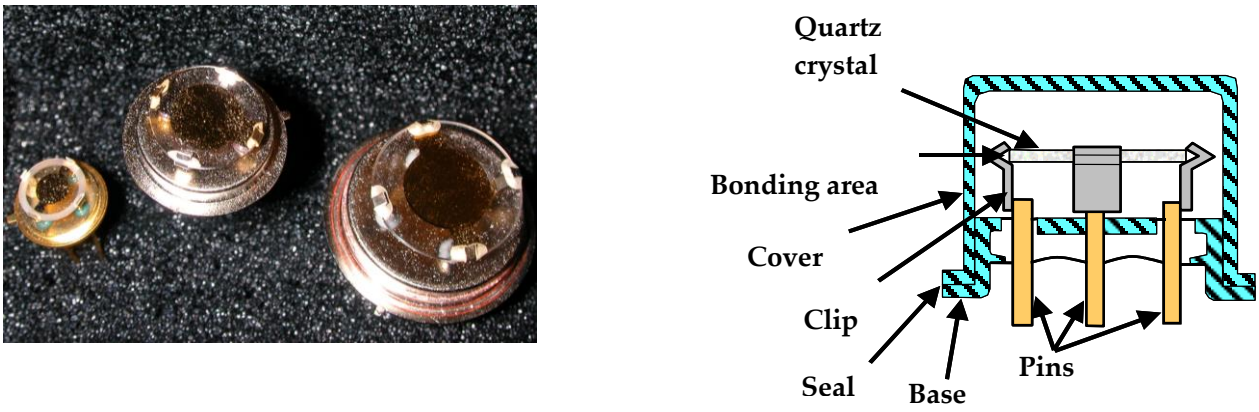

Figure 17-12: Quartz detail

When a quartz component is submitted to a shock excitation, two phenomena can occur:

- Dynamic shift of its central frequency during the shock
- Permanent shift of its central frequency after shock exposure. This is often considered as the most critical issue.

These two effects are illustrated in Figure 17-13.

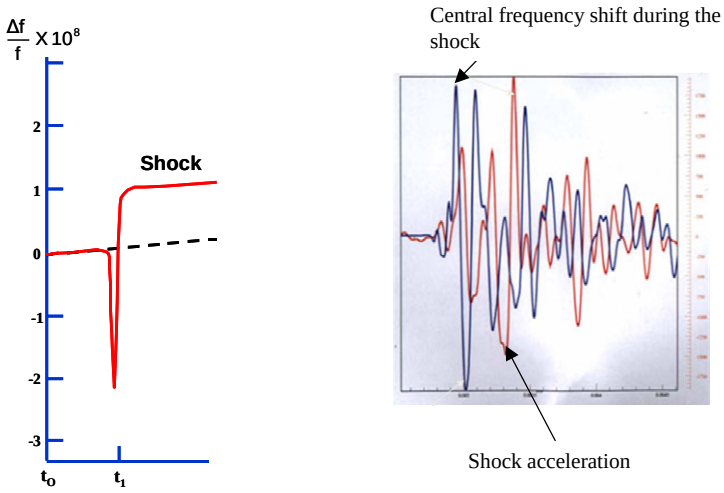

Figure 17-13:Quartz frequency shift during shock exposure

Quartz are components characterized by a very few internal resonances that present a very high Q factor. These resonances can be identified experimentally by using the quartz as a sensor and applying a calibrated force to compute a transfer function, as indicated on Figure 17-14. A typical response of a 100 MHz crystal with 2 clips is illustrated on Figure 17-15. In this case, there are only 3 resonances below 10 kHz. Figure 17-16 shows the associated mode shapes computed by finite elements.

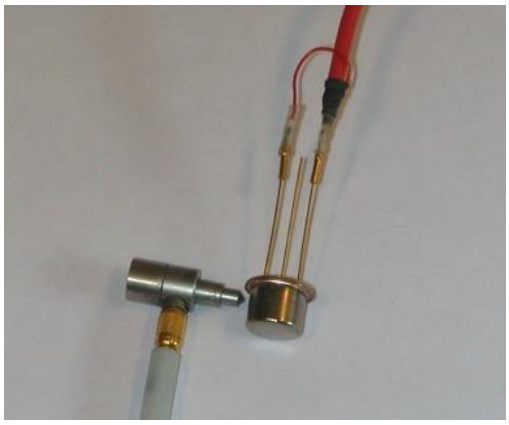

Figure 17-14: Modal characterization of a quartz

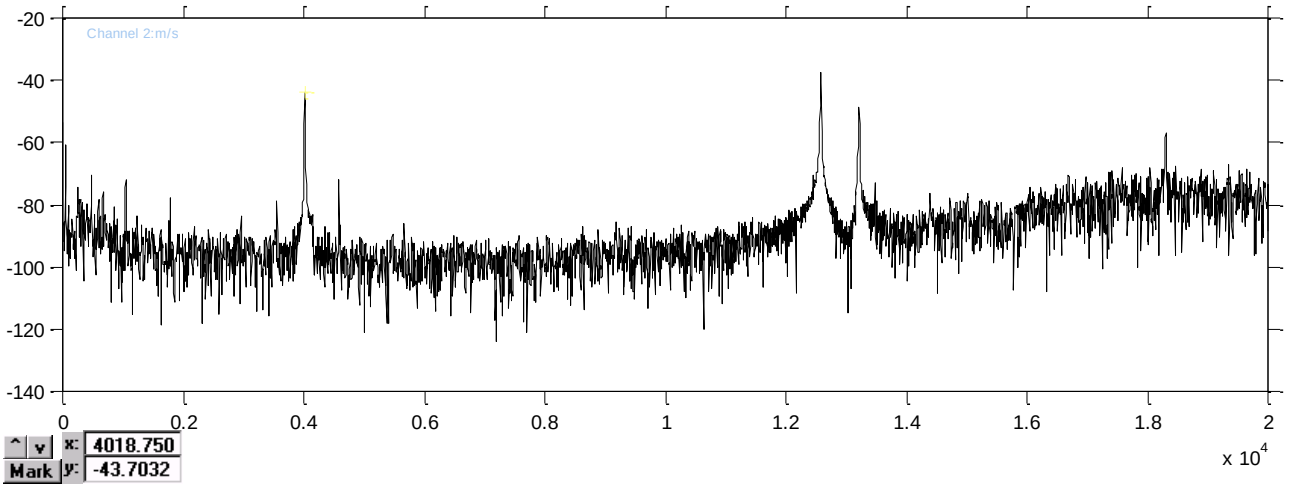

Figure 17-15: Typical response of a quartz to a calibrated force (transfer function)

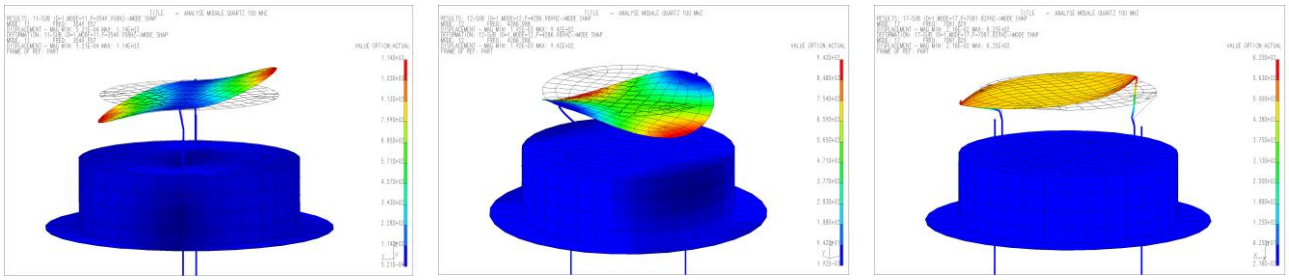

Figure 17-16: First mode shapes of 100 MHz quartz with 2 clips

Various shock tests performed on quartz components show that an excessive excitation of these resonant frequencies can result in a permanent frequency shift of the resonator eventually associated to an apparent irreversible damage (broken quartz, clip attachment or bonding).

Therefore, when analysing a quartz issue, it is important that the SRS is calculated to reflect a realistic Q factor of the critical resonances.

Last but not least, an excessive shock exposure can accelerate the aging of the quartz, i.e. the frequency shift over the years.

17.5.2.2.2 Examples of quartz failure

Example 1 – Permanent frequency shift

As illustrated by Figure 17-17, an electronic unit was successfully submitted to a first qualification level (so-called Level 1), but presented an excessive shift of the quartz central frequency for a higher shock level (+6 dB or so).

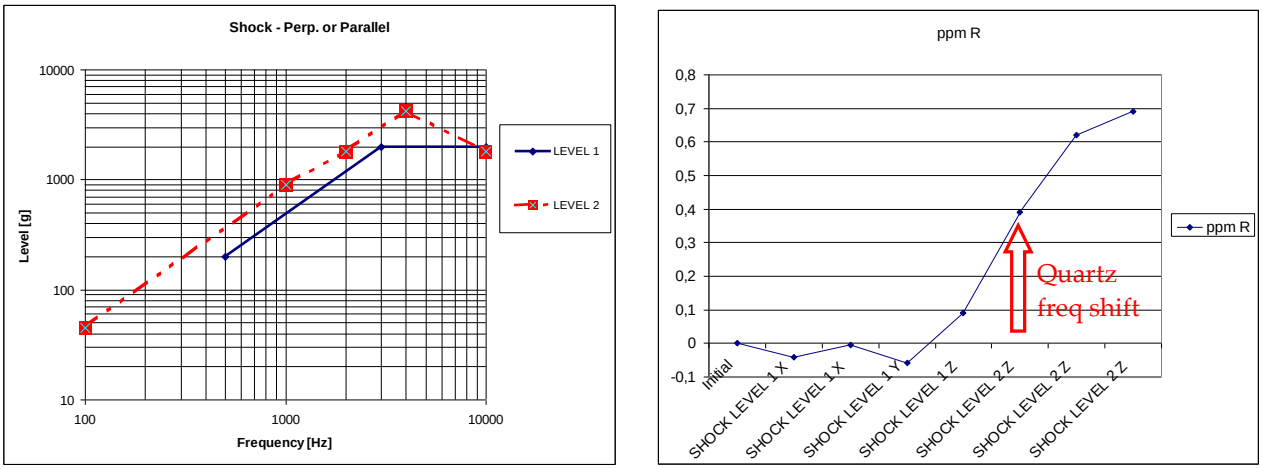

Figure 17-17: (a) Payload unit shock specifications – (b) associated Local Oscillator frequency shifts in ppm

A permanent frequency shift is associated to a stress relief on the quartz crystal. This can occur without any apparent damage of the component but it can also be linked to mechanical defects such as crack initiations at either interface of the elastic clips maintaining the quartz crystal, as illustrated by Figure 17-18.

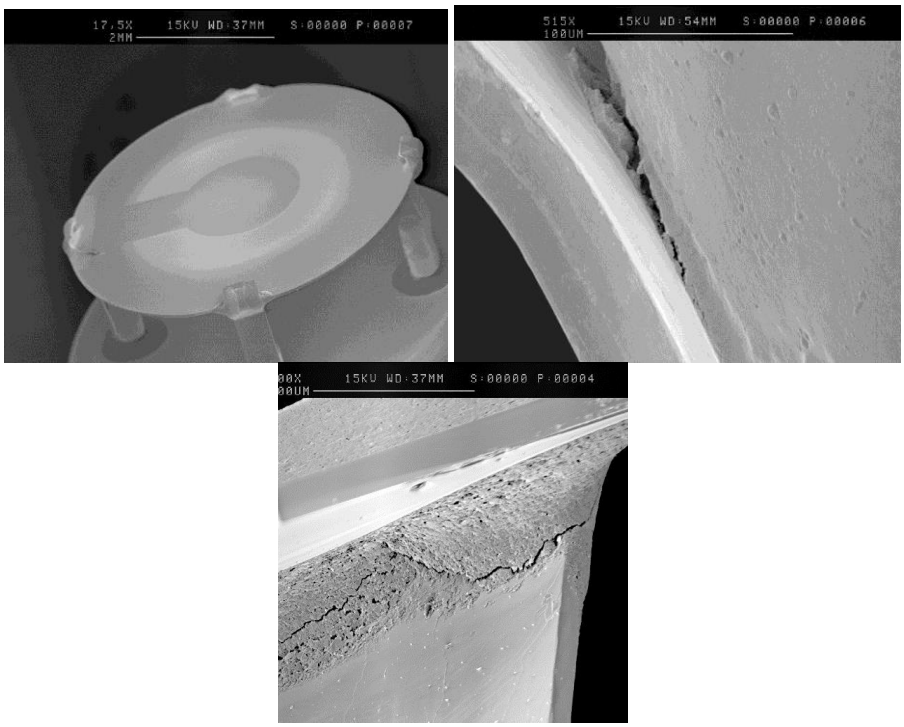

Figure 17-18: Examples of crack initiation due to shocks at the interfaces of an elastic clip carrying the quartz crystal

Example 2 – Broken crystal

Another qualification test on an electronic unit has resulted in a broken quartz crystal, as illustrated by the X-ray on Figure 17-19. The specification was the Level 1 indicated on Figure 17-17.

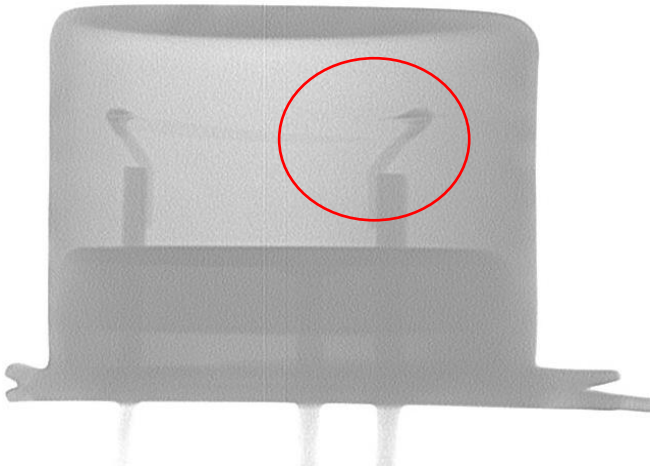

Figure 17-19: Broken quartz crystal due to shocks

Example 3 – Dependence with respect to shock characteristics (half sine versus metal on metal)

A quartz whose fundamental resonance was measured at 6075 Hz along X axis has been submitted (bonded on a PCB) to two different shock tests:

- A 600g half-sine, 0,5 ms (Figure 17-21)
- A metal on metal shock (Figure 17-22)

Figure 17-20 shows the cumulative frequency shift of the local oscillator after each axis of the various tests. It is relatively low (< 0,2 ppm) after the three half sine shocks. The frequency shift is still acceptable after the first two shock at level 1 (along Z and Y), but it raises dramatically to 0,8 ppm after the shock along X axis. The SRS level is 3000 g at 6075 Hz considering a Q factor of 10 but it reaches 10000 g considering a Q factor of 600.

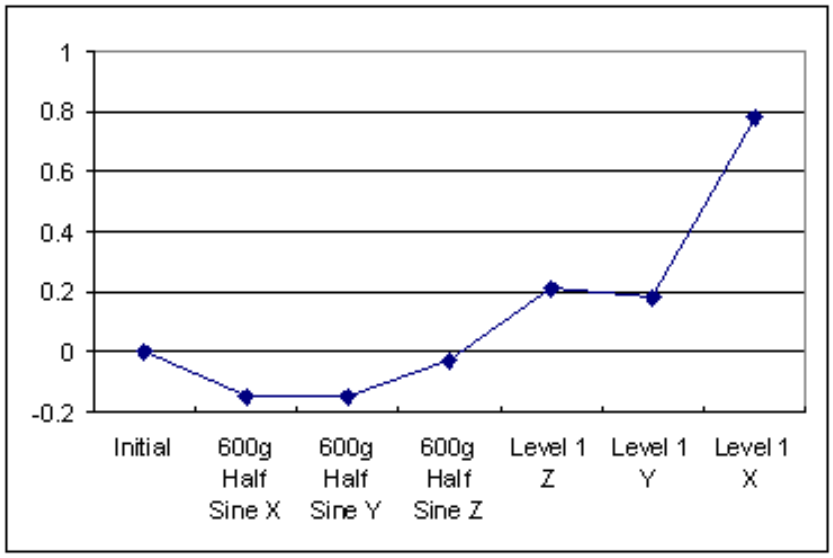

Figure 17-20: Cumulated Quartz frequency shift (ppm) after various shock tests

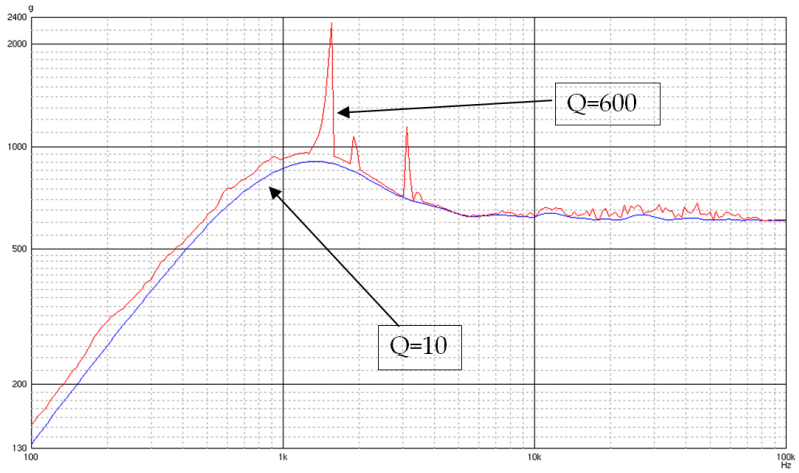

Figure 17-21: SRS of a 600g/0,5ms half-sine (Q=10 and Q=600)

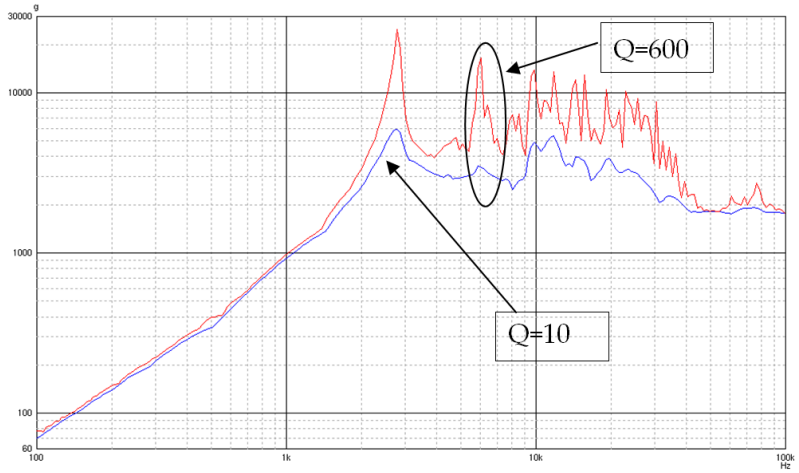

Figure 17-22: SRS of metal on metal shock at level 1 (Q=10 and Q=600)

Example 4 - Shock effect on ageing

Four quartz (FM) have been submitted to a shock test at level 1, illustrated by Figure 17-22. The aging test before the shocks estimates the frequency shift is well below 1 ppm after 20 years, as indicated in

Table 17-3. After the shocks, the frequency shift varies from 0,126 ppm to 1,005 ppm. However, the aging test performed after the shock estimates the shift is around 4,28 ppm over 20 years for one of the quartz. Thus, this level of shock is not acceptable for the quartz without a mechanical filter.

Table 17-3: Aging results on quartz before and after shocks at level 1

S/N	Frequency before Shocks (Hz)	Estimated aging over 20 years before shocks (ppm)	Frequency after shocks (Hz)	Shift after shock tests	Estimated aging over 20 years after shocks (ppm)
64801	95539871	-0,292	95539914	0,450	-0,264
64812	95540019	-0,445	95540031	0,126	-4,28
64814	95540103	-0,332	95540128	0,262	-0,492
64815	95539869	-0,035	95539965	1,005	0,355

17.5.2.3 Magnetic component (RM), transformer and self

17.5.2.3.1 Failure modes

Magnetic components often have a magnetic circuit made of ferrite material. This material has good electrical properties but is also characterized by a fragile rupture.

The other failure mode for these components is the electrical lead wire rupture.

17.5.2.3.2 Failure examples

Example 1 – RM rupture

Pyrotechnic tests with increasing amplitude have been performed on various sizes of magnetic components bonded on a rigid substrate. The test vehicle and the test setup are described on Figure 17-23. The results are illustrated in Figure 17-24 up to Figure 17-27. It appears that the larger is the component the lower is the level to rupture. All allowable SRS levels exceed 2000 g for frequencies above 3000 Hz.

Similar test have been performed with components (RM size 4, 5 and 7) reported on a PCB (Figure 17-28). The results on Figure 17-29 show that no damage was observed for SRS levels up to 3000g at frequencies above 1000 Hz.

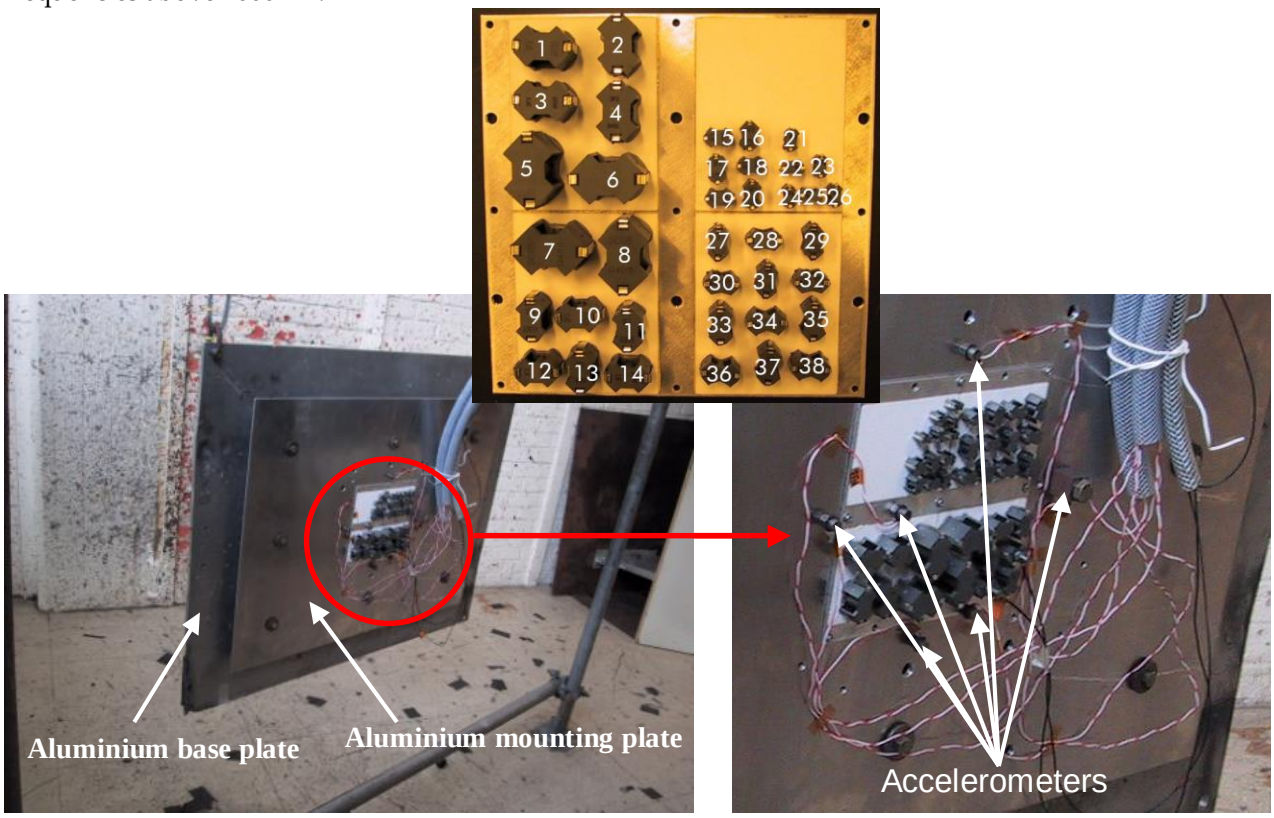

Figure 17-23: Pyroshock Test Set-up – RM glued on alumina substrate with ME 7155

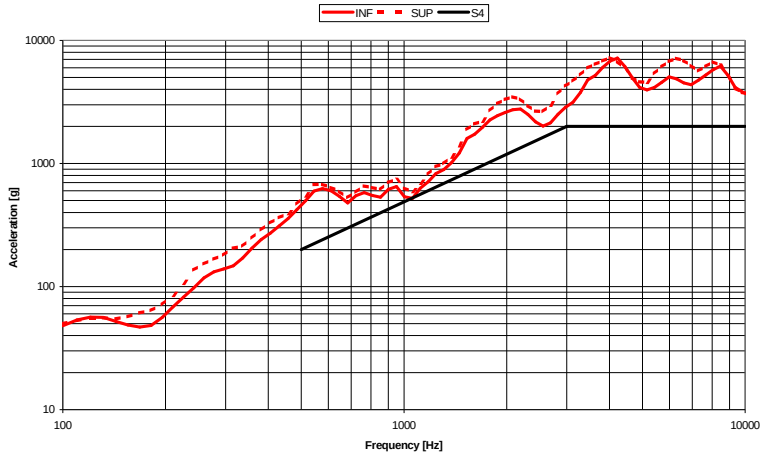

Figure 17-24: RM12 - SRS Level to Rupture (red line)

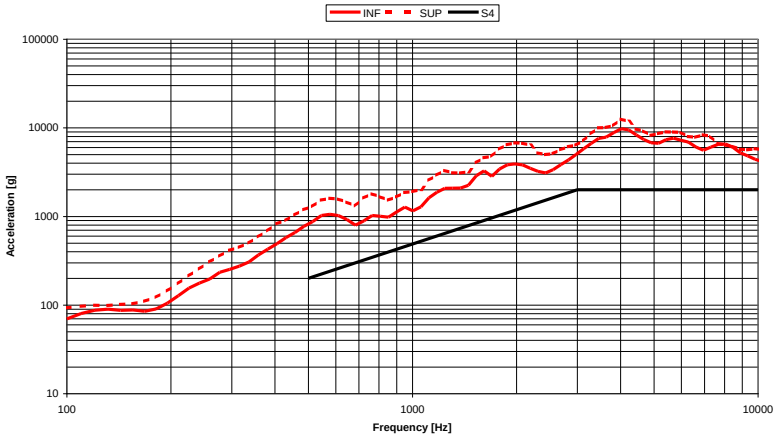

Figure 17-25: RM10 - SRS Level to Rupture (red line)

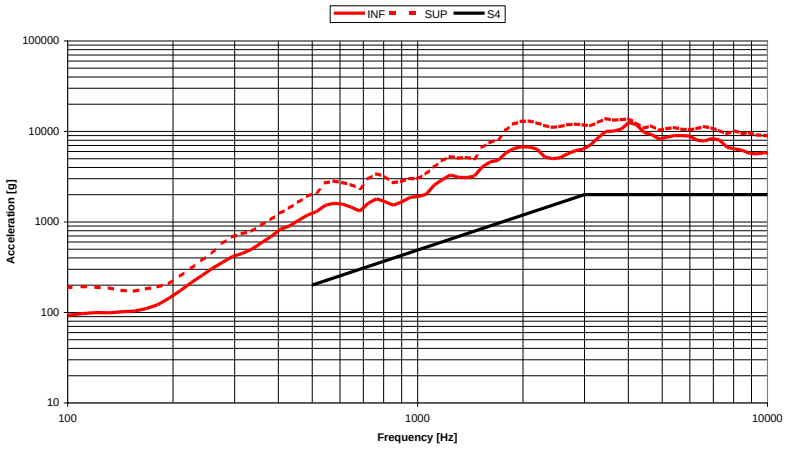

Figure 17-26: RM 6,7,8 - SRS Level to Rupture (red line)

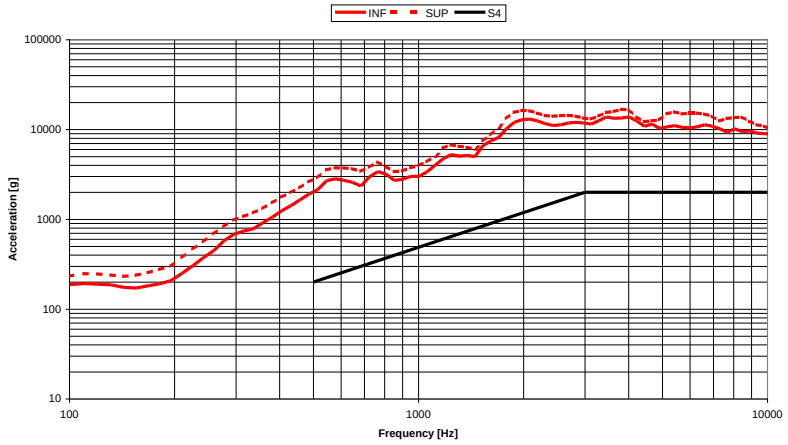

Figure 17-27: RM 4,5 - SRS Level to Rupture (red line)

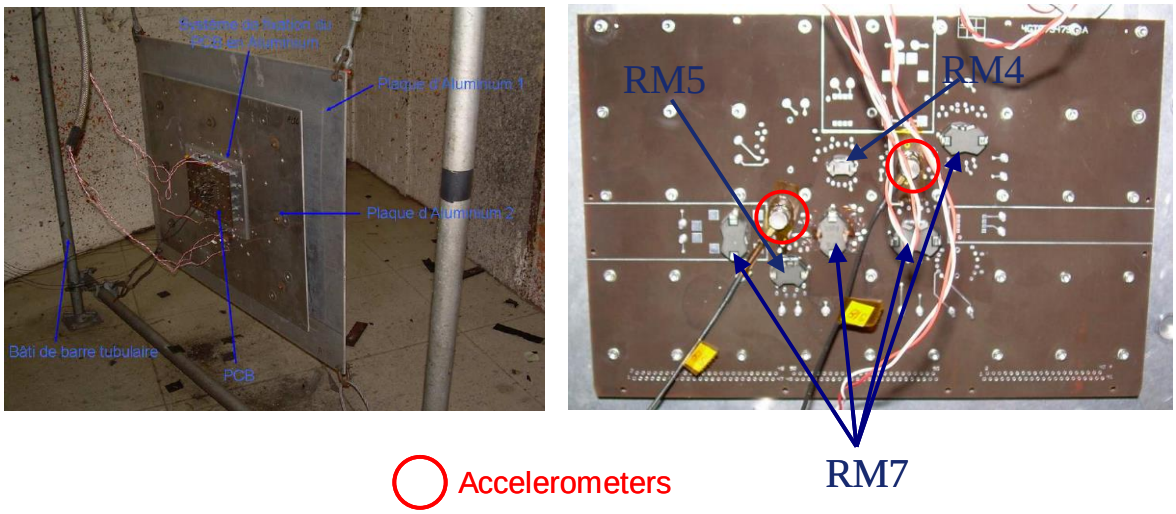

Figure 17-28: Pyroshock Test Set-up – RM reported on a PCB

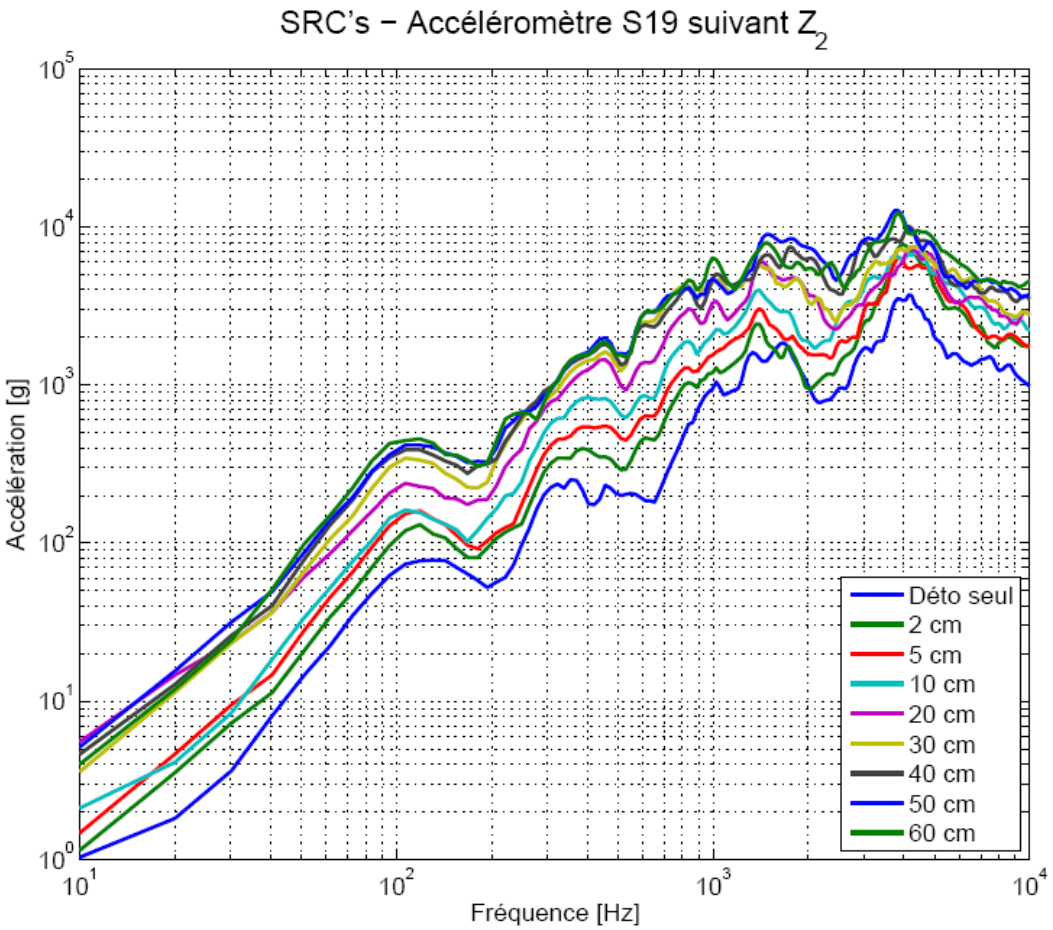

Test n°	Charge	Etat RM	Remarques
1	Détonateur seul	OK	—
2	2 cm de cordeau explosif	OK	—
3	5 cm	OK	—
4	10 cm	OK	—
5	20 cm	OK	—
6	30 cm	OK	—
7	40 cm	OK	—
8	50 cm	Casse RM5.2 + RM4.1 fissuré	Acc_S18 décollé
9	60 cm	Casse RM5.2 + Casse RM4.1	—

Figure 17-29: SRS Levels to Rupture for RM reported on PCB

17.5.2.4 Hybrid

17.5.2.4.1 Failure modes

Hybrids present several risks of failure:

- Adhesive rupture at substrate level or other small part level (getter, absorber)
- Crack in glass feed-thru
- Packaging or lid structural failure
  Note that part of the packaging is often made of a brittle material
- Mobile particles in the cavity

17.5.2.4.2 Failure examples

Example 1 – Housing deformation

Figure 17-30 shows a plastic deformation of an hybrid interface plate after half sine shock qualification test whose level was 2000g and duration 0.5ms. Such defect can lead to functional issues as it modifies the thermal contact between the hybrid and its supporting structure.

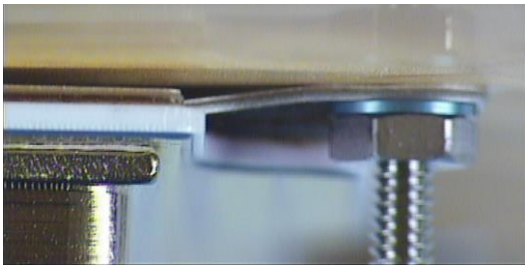

Figure 17-30: Deformed hybrid interface plate

Example 2 – Multiple damages on an hybrid (packaging structural failure, pin bond failure and glass seal damage)

Figure 17-31 shows multiple damages on an hybrid consecutive of high shock loads application, in excess of 3.f severity (i.e. 3000g @ 1000Hz).

The damage has propagated from the mounting points causing excessive stress to the braze joint, glass seals and wire bonds resulting in the failure of the module.

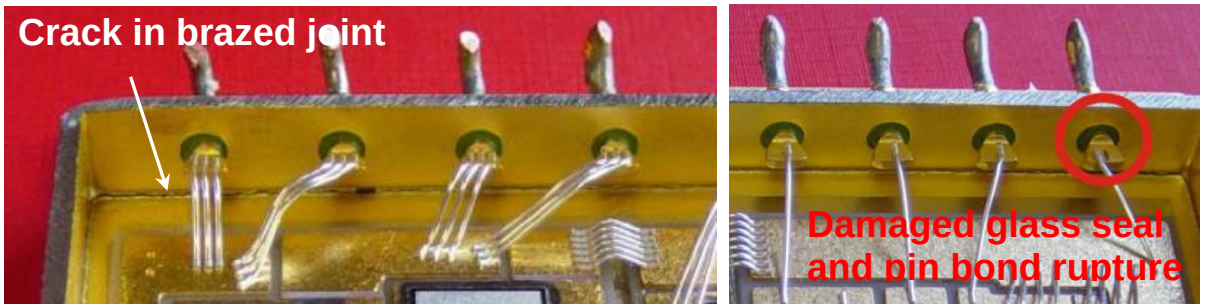

Figure 17-31: Multiple damages on hybrid

17.5.2.5 Tantalum capacitor

Figure 17-32 represents an example of test measurement setup of sensitivity threshold of tantalum capacitor. The PCB is clamped along two edges. The dimensions have been chosen to obtain a given bending resonance frequency for the PCB. An accelerometer is measuring the OOP acceleration. In this specific example, a risk was identified for PCB deflection exceeding 1mm (for a PCB of dimension 100 mm). However the sensitivity threshold depends on the capacitor dimensions and on the induced PCB deflection.

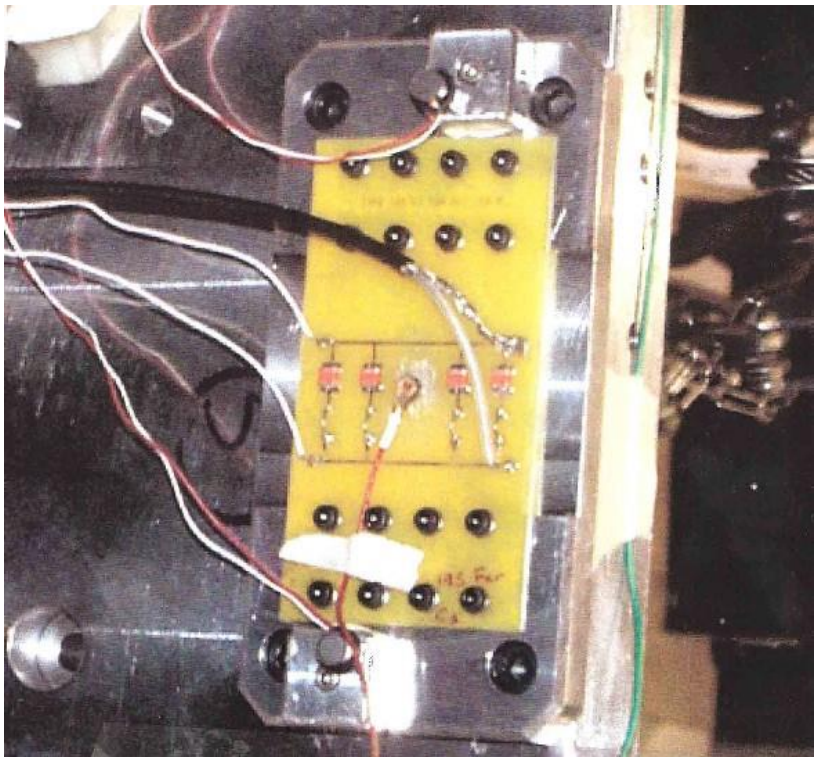

Figure 17-32:Tantalum capacitor

The tantalum capacitor can also be heavy and of large dimensions, and hence falls in the category of large and heavy components, for which adequate mounting condition (i.e. staking with adhesive compound) and method for stress relief should be implemented, as per ECSS-Q-ST-70-08C [RD-0121].

Figure 17-33: Heavy/large tantalum capacitor (secured with adhesive compound and with provision for stress relief)

17.5.2.6 Heavy or large component

Example 1 – Large deflection of PCB resulting from an insufficient support/reinforcement of the PCB combined with high shock loads (above 2000g SRS, depending on the induced PCB deflection), can lead to adhesive failure and rupture of solder joint, as illustrated in Figure 17-34 ; or can lead to pin / lead-wire rupture, as illustrated in Figure 17-35.

An adequate mounting condition should be implemented as per ECSS-Q-ST-70-08C and ECSS-Q-ST-70-38C (in particular with staking applied for components weighing more than 5gr). It should be noted that conformal coating cannot be considered as a suitable staking method.

NOTE Refer to [RD-0121] for requirements for the manufacture and verification of manually-soldered, high reliability electrical connections; and [RD-0122] for requirements for electrical connections of leadless and leaded surface mounted devices (SMD).

Figure 17-34: Adhesive failure and rupture of solder joint after a stringent shock test

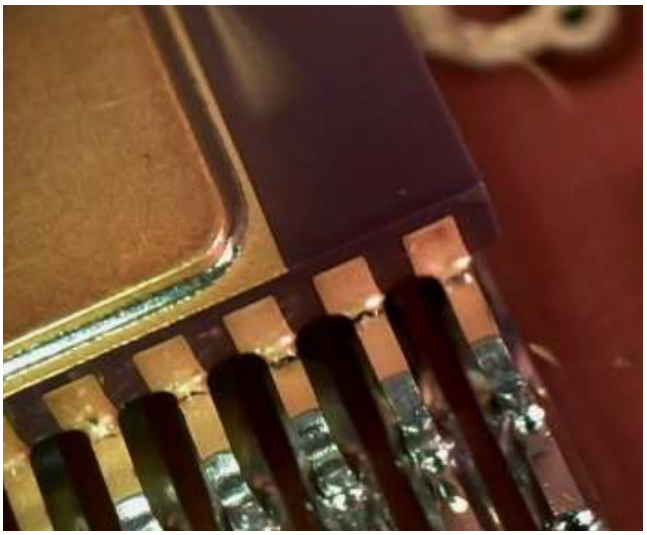

Figure 17-35: Pin / lead-wire rupture (component heavier than 5gr, without staking)

Example 2 – Lead wire rupture between solder joint and winding of coil

In the following example, the winding wires had sheared between the solder joint and the winding of a coil. This coil was insufficiently secured (only with two lacing cords, and without adhesive), which allowed movement in the plane of the PCB. As such a certain amount of stress has been induced in the coil leads between the coil exit point and the fixed connection of the lead in the solder joint to the board, which resulted in rupture of the lead wire (vibration/shock).

This illustrates that for heavy components, such as coils (typically heavier than 5 gr), adequate mounting technology should be implemented, as per ECSS standard ECSS-Q-ST-70-08C. Such components should be secured by either mechanical means or application of adhesive and should not impair stress relief.

Accordingly typical mounting technology for coils consist in a staking solution with additional mechanical means (for example lacing and/or staking), while stress relief design should be implemented for the lead wire.

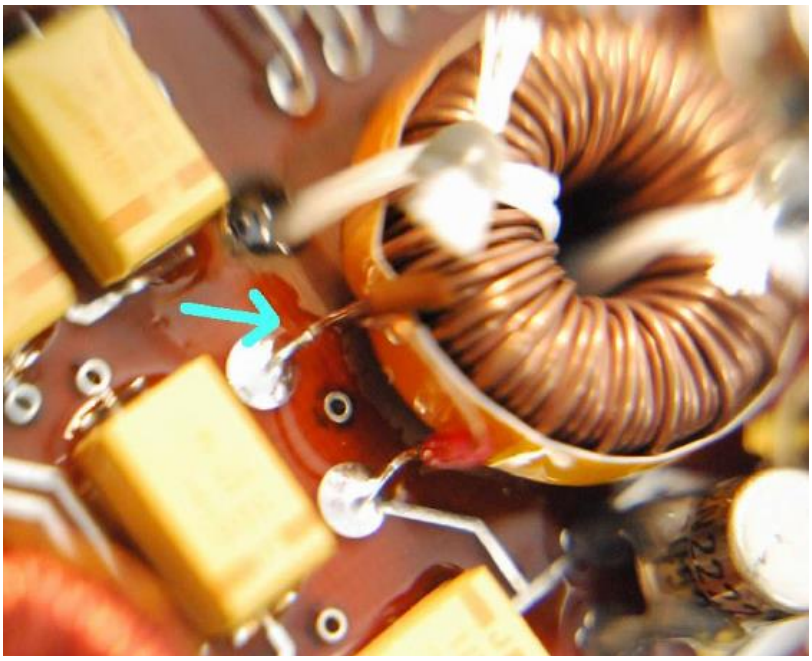

Figure 17-36: Sheared lead between solder joint and winding of coil

This example can be extended to any heavy components weighing more than 5gr, for which adequate mounting condition (i.e. staking with adhesive compound) and method for stress relief should be implemented, as per ECSS standard ECSS-Q-ST-70-08C [RD-0121].

17.5.2.7 Optical components and connectors

Optical modules and two different types of optical fibre connectors were submitted to increasing levels of half sine shock, as illustrated on Figure 17-37. No damage has been observed up 2000 g SRS. Transmission losses of the connectors have been measured after the shocks and do not exceed 0,3 dB.

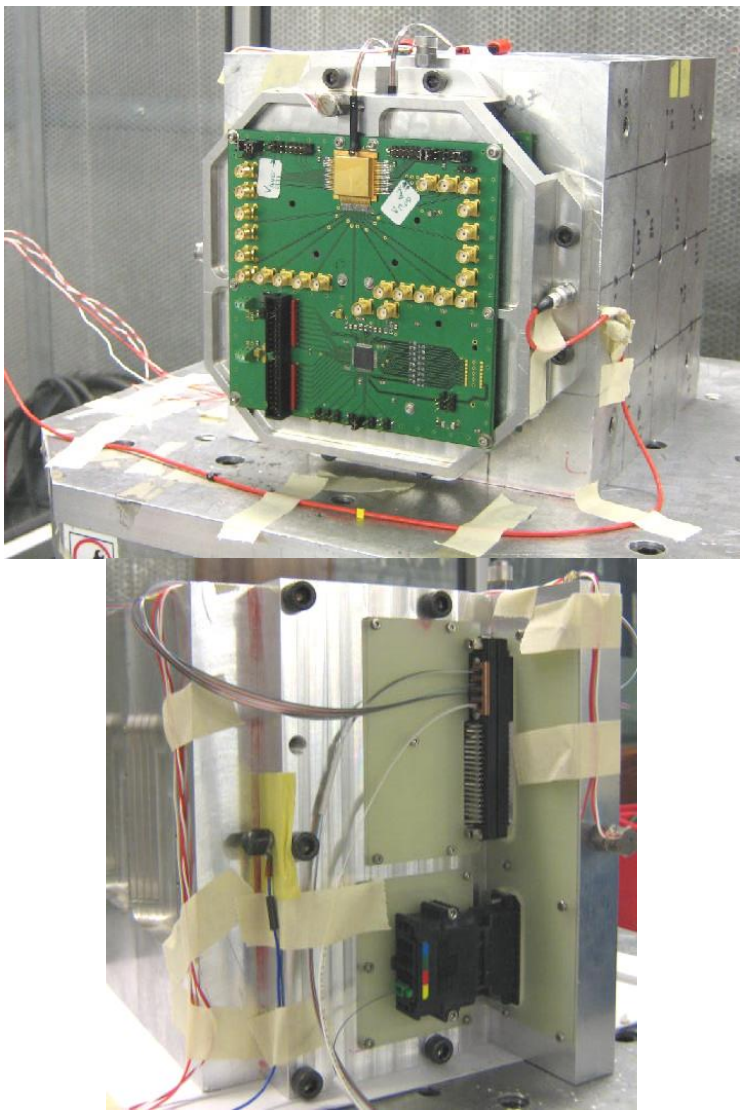

Figure 17-37: Shock test set-ups with optical components and connectors

17.5.2.8 Components mounted on low insertion force DIP socket

The low insertion force DIP socket usually consists of components with 2 rows of parallel legs of 8 to 40 pins, going through the PCB.

The problem has arisen because of the shim in tantalum which has been made for reducing the component sensitivity to Electromagnetic Radiations; this shim was cut in a sheet of tantalum 1 mm thick. The shim is stuck on the track and tin lead and glue adheres badly so it creates a weakness. The rule is not to use a track or shim of the same material as the track below the shim. A manufacturing sheet has been written to reinforce bonding of the shim. It is important that the thickness of adhesive is the smallest possible to avoid increasing the thermal resistance.

At least each equipment has a card with this type of support. To ensure that the component does not pull off, the shim was bonded on the PCB and between the shim and the component was applied charged varnish to permit component disassembling; if we did not have a good holding of the component via a shim, when this component is mounted on the low insertion force DIP socket, it raises the component on the PCB. If the shim is badly glued, or if there is no shim, one can get a component pulling off during the mechanical shock.

The components mounted on low insertion force DIP socket can dissipate. It can then be necessary to put a stiffener bar, on which are mounted the components. That makes the length of leg through the hole even shorter since the leg length is much less when the component is mounted on an outgrowth of stiffener which allows heat dissipation.

The threshold risk of component pulling off is identified around 1000 g to 1300 g SRS along OOP direction.

17.5.2.9 Mobile Particles in the cavities of electronic components

17.5.2.9.1 Overview

This defect is characteristic

- in 99 % of the cases of the solid-state components
- for the remaining, of the relays, the condensers with cavity

The mobile particles come primarily from

- alloy of welding of the chip on the substrate
- closing of the housing by electric welding
- silicium composing the chip
- peeling of internal protections of the housing

17.5.2.9.2 Particles generated at the time of the welding of the chip on the substrate

The particles are generated during the brazing of the chip, mainly by an eutectic gold/silicium, which is the alloy generating the most particles but which is also used the most because it has other advantages (good thermal characteristics and low costs in particular).

That relates to all the transistors and integrated circuits with ceramic or metal cases.

17.5.2.9.3 Particles of electric welding of the case

The particles are generated during the closing of the cap by a brazing silicon. That relates to all the metal cases closed by an electric welding (welding known as integral).

This welding having to ensure elsewhere the tightness of the cavity by component, the manufacturer has tendency to accentuate welding current accentuating the risk of cinder. If diameter is higher than 50 µm, they can generate, specifically for the T099, T039, T05,… a short-circuit between a wire and the edge of chip or between two tracks if there is no protection.

17.5.2.9.4 Silicium particles

Silicon constituting the chips can itself present cracks likely to generate particles. The sawing known as integral allows to generate in theory less particles.

That relates to all the semiconductors with cavity (e.g. all those seen previously as well as the diodes with case glass: D035, D0-7,…).

17.5.2.9.5 Particles of protections peeling

The particles come from the peeling of metal protections out of nickel or gold of the internal wall of the cases.

That thus relates to all the semiconductors with metal case (including the hybrids).

17.5.2.9.6 Statistics

In 1985, 15 % of the failures noted during the admission tests on the ground of the ARIANE equipment originated in the mobile particles in the electronics components. A simple test in heat was enough to highlight this defect.

In Defence sector, a prime contractor reports that the particles represent the second cause of defects on the integrated circuits all technologies, the integrated hybrid circuits and the discrete components.

The application of a PIND test has corrected that problem: a **PIND** test is a Particle Impact Noise Detection Test. The purpose of a PIND test is to detect loose particles inside a device cavity. The test provides a non-destructive means of identifying those devices containing particles of sufficient mass that, upon impact with the case, excite the acoustic transducer. See [RD-0101], [RD-0118].

Figure 17-38 presents the superposition of SRS of the PIND shock test, applied on chosen types of components, and the levels measured on PCB's of a stacked equipment. It appears that the lower frequencies are not covered. That concerns mainly the risk with heavy mobile particles, which could have resonance frequencies lower than those of the smaller mobile particles.

The following diagram proposes a rationale to help in the decision of specific action in order to mitigate the risk of mobile particle.

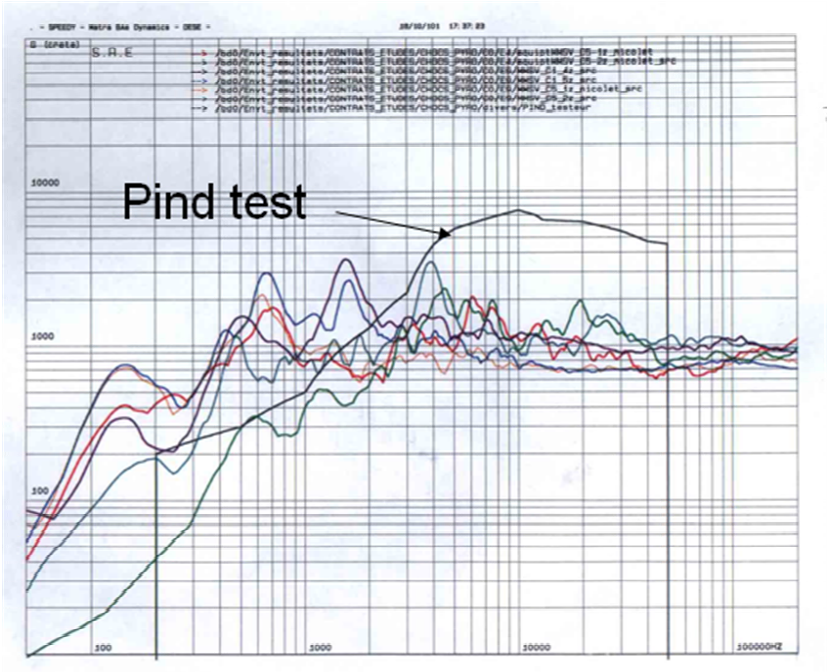

Figure 17-38: Pind test SRS

17.5.2.10 Synthesis on threshold levels

The following table presents a synthesis of the threshold shock levels for each failure mode of the sensitive components. Note that **G** values in Table 17-4 refer to the following SRS:

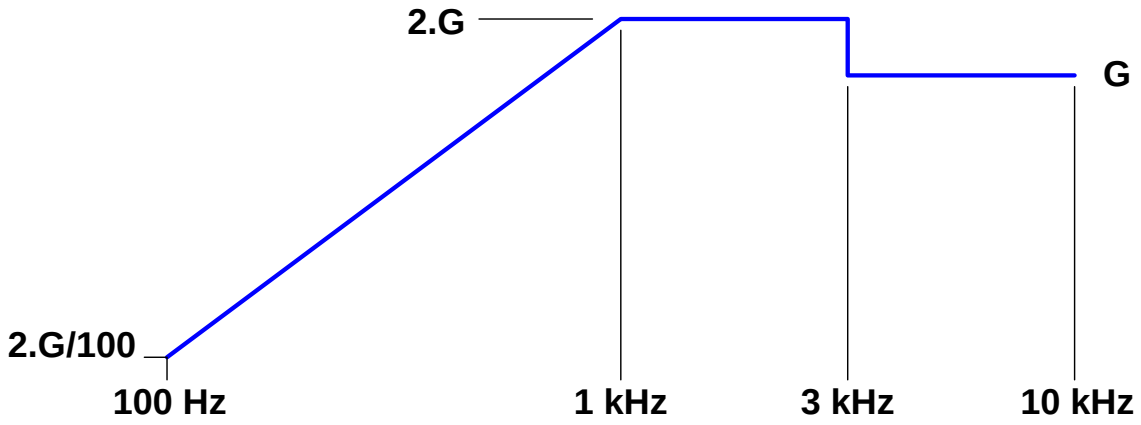

Figure 17-39: Schematic SRS defined by a G value

Table 17-4: Components – Sensitivity threshold for the various failure modes

ELECTRONIC COMPONENTS	Sensitivity threshold for the various failure modes			
	Mode 1	**Mode 2**	**Mode 3**	**Remark**
Relays	*Bouncing* **G**=200g SRS in all directions	*Transfer* **G**=600g SRS in all directions	*Mechanical damage* **G**=1200g SRS in all directions	
Quartz	*Relief residual stress* **G**=600 g SRS in all directions	*Solder overstress / adhesive crack* **G**=600 g SRS in all directions	*Broken crystal* 2000 g SRS at quartz resonances	Criteria to be verified with representative Q factors (>100). These values are typical for quartz with frequencies between 50 and 100MHz.
RM, Transformer and Self	*Crack in ferrite* 2000 g SRS (above 3000 Hz)	*Lead-wire failure* Apply stress relief and staking solutions		
Hybrid	*Adhesive rupture* Design and size dependent	*Crack glass feed-thru* Design and size dependent	*Structural failure* Design and size dependent	
Tantalum capacitor	*Local destruction dielectric* Capacitor size and PCB deflection dependent – ensure acceptable deflection	*Short circuit* Capacitor size and PCB deflection dependent – ensure acceptable deflection	*Lead-wire failure* Apply stress relief and staking solutions	
Heavy or large component	*Heavy component / Lead-wire failure* Apply stress relief and staking solutions – ensure acceptable deflection	*Large component / Lead-wire failure* Design and size dependent – ensure acceptable deflection – apply staking solution		
Optical components (optical fibre connector…)	*Fibre pigtail cleavage* 2000g SRS (above 2000 Hz)	*Damaged fibre* 2000 g SRS (above 2000 Hz)		
Low insertion force DIP socket	*Disjunction of the component* SRS of 1000 to 1300g in OOP			
Semiconductors (IC) components, Hybrid components, relays, capacitors with cavities	*Dislodging of mobile particle* Compare expected levels to the PIND TEST levels if applied, and validate the not covered range of frequencies by the PIND test			

17.5.3 Functional mechanical assemblies

17.5.3.1 Overview

Some mechanical assemblies are particularly critical as minor deformations/displacements largely affect their performance. These functional issues after shock testing can be linked to slightly sliding threaded fasteners, local plastic deformations or pre-stress release.

17.5.3.2 RF channel filters (IMUX, OMUX,…)

These units are made of resonant cavities. The dimensions of the cavities are directly linked to the nature of the RF filter. Screws around the cavity perform additional tuning. Minor changes in the cavity configuration (volume, screw position) or in the assembly of the cavities modify the original filter shaping. In case a dielectric resonator technology is used, the electrical contact of the resonator with the cavity is critical for the RF performance. Any modification of the contact could indeed result in electrical glitch while thermal cycling.

17.5.3.3 Iso-static mount and bonding

17.5.3.3.1 General

An Iso-static mount is designed to provide sufficient strength and stiffness for the dimensioning mechanical environment, to provide low sensitivity to thermal gradients and to decouple the sensitive item (mirror, telescope, optical bench, …) thermo-mechanically from the primary structure.

In the following figure is shown a typical iso-static mount arrangement of a mirror.

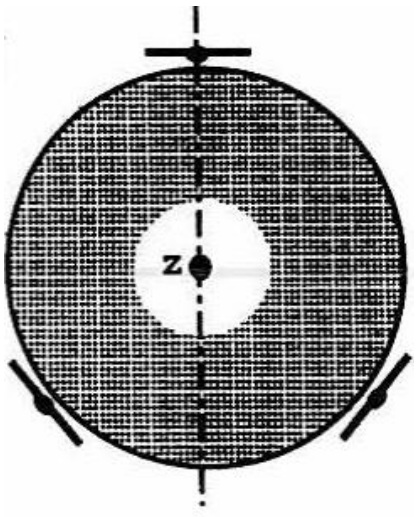

Figure 17-40: Typical iso-static mount of a mirror

Induced stresses in the ISM should not exceed the yield precision limit for stability reason. In this respect, the material characteristics should be precisely characterised (strength, yield precision limit), stress concentration factor should be accounted for where relevant, and the local dynamics should be considered (e.g. Q factor, torque, force, bending moment).

The computation of the induced stresses results either from structural analysis or from analytical derivation based on the geometrical/material characteristics of the ISM.

The associated degradation modes are permanent deformation, residual tilt or misalignment that degrades the optical performance of the system.

Usually, for a stress level below the yield precision limit, it is considered that no degradation can occur. This is valid for the classical precision required in optical instruments. If exceptional stability performance is specified, this principle is verified through adequate analysis.

The yield precision limit in metals usually used for ISM (INVAR, Titanium), is a few times less than the classical yield limit. This should be characterized by specific tests on the material.

17.5.3.3.2 Bonding

- Classical bonding

  To limit stress concentration as much as possible, mirrors can be interfaced onto a "mirror cell/flange", consisting in a cylindrical piece joining the mirror in x points (glued junctions) to the main structure via the 3 iso-static mounts.

  The bonding strength should be evaluated, paying addition to a possible degradation of the glue mechanical performance due to thermal-vacuum test (adhesive properties from manufacturer datasheet can be optimistic).

Figure 17-41: MSG M3 mirror iso-static mount

- Molecular adhesion mirror

  Molecular adhesion is used as an alternative for classical bonding on high precision optical mirrors, used for example in spatial communication between satellites on orbit. The optical contacting of two substrates is a phenomenon during which the surfaces of the substrates are placed in close contact and bonding occurs by propagation of a bonding front between the substrates. This type of bonding is effective till a certain force is applied to the bonded part. Then the separation occurs immediately and the corrective process is very long. It is therefore important to verify that the threshold level of acceleration is not met during the vibration and the shock tests.

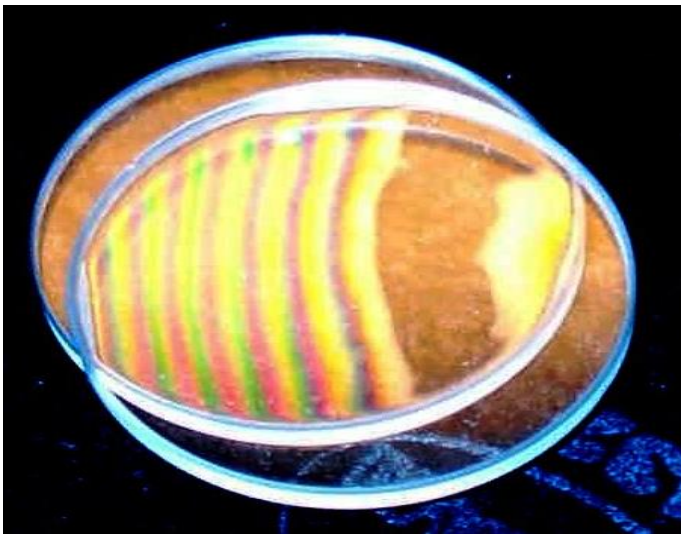

Figure 17-42: Molecular adhesion bonding front

Example – Bonded joint failure (between mirror flange and mirror)

Insufficient protection/isolation with respect to the input shock environment combined with excitation of mirror main modes can result in overstressing the bonded joint between the mirror flange and the mirror, as illustrated in Figure 17-43.

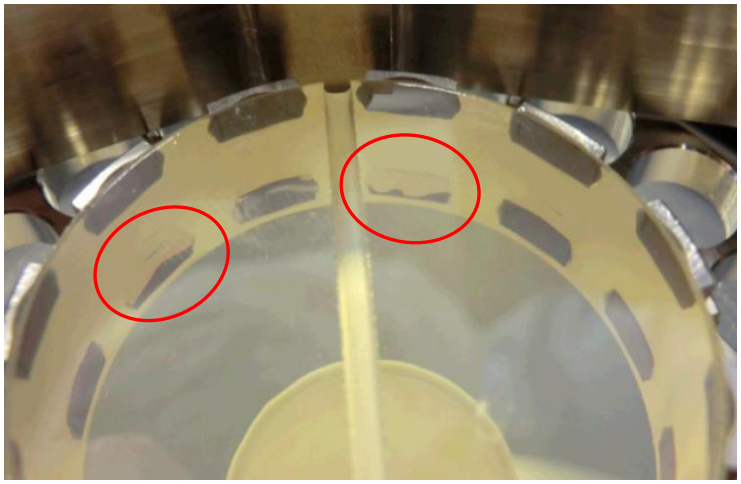

Figure 17-43: Mirror bonded joint failure

17.5.4 Mechanisms and associated degradation modes

A mechanism is by nature a complex assembly of components which are linked together to enable a relative motion. The components used in the mechanisms, which are reputed sensitive are:

- Bearings, gears, worm wheels, endless screws, gimbal bearings – their degradation mode is an excessive marking. This is further discussed in section 18.3.2.
- Alignment critical parts – Their degradation mode is a slippage in interfaces resulting in failure or performance change.
- Clearance seals – Their degradation modes is change in the gap, which could result in contact/friction/wear/stiction or debris generation.
- Valves – Their degradation modes are a limited leakage in quantity and time, a significant or permanent leakage and a structural degradation, which involve a malfunction of the valve mechanism. They are further discussed in section 18.3.3.
- Life sensitive components – Their degradation modes is an accelerated fatigue for multiple shocks.
- Others components such as flexible pivots, preload locking systems or RF switches (position switch can occur when the shock level exceeds 2000g SRS) are also known to be sensitive. Furthermore a mechanism can include an optical component (i.e. encoder, mirror, …), for which misalignment, permanent deformation or failure of brittle material can occur.

The life duration impacts on the selection and the severity of the damage criteria. For example, the residual marking in bearings is practically forbidden for long life duration mechanisms. In the opposite, for the mechanisms, which are activated only a few times during their life, the residual marking size allowed is limited by their functionalities.

18
Shock damage risk analysis

18.1 Required inputs for detailed SDRA

The first step of the damage risk with respect to shock, described in chapter 17, consists in localizing (in frequency) and characterizing (by screening all the shock sensitive units and components and associated degradation modes) the damage risk with respect to shock. Once this first step has been achieved, a detailed analysis should be performed in order to quantify more precisely the damage risk with respect to shock on all the units that have been identified as potentially sensitive.

A complete evaluation of the sensitivity against shock requires the knowledge of parameters such as:

- Units design via engineering drawings, unit architecture (especially for electronic boxes with detailed description of PCB, components, mounting technologies)
- Geometrical data, material, mass and stiffness properties
- Dynamic behaviour in terms of resonant frequencies and Q factors, preferably obtained from sine survey test or random test on FM units (or only QM if FM data not available) or from FEM analysis. If both are available, a test-analysis comparison is recommended in order to assess if the FEM is correlated and trustful to derive non usually measured parameters (e.g. effective masses, effective transmissibilities, and mode shapes)
- Function description, mission criticality
- Qualification data for the equipment in terms of an equivalent SRS derived from the random qualification levels
- Heritage shock data from similar units by subcontractor's data
- Qualification data for the components and the mounting technologies (shock tests or random vibrations)
- Identification of the aforementioned unit category and subsequent comparison with the foreseen qualification shock levels derived by scaling the measured levels to the flight levels and adding 3 dB margin

The SDRA context is also another criterion to be taken into account when beginning such an analysis. The identified critical frequency ranges where the considered unit is not formally qualified often depend on the particular shock source that generates the shock environment. Launcher induced shocks have indeed the particularity to introduce some important low frequency contents that can directly excite some natural frequencies of the spacecraft structure whereas the high frequency part of the spectrum is relatively damped when propagating inside the spacecraft. These low frequency modes, generally below 1000 Hz, can then excite natural frequencies of units and consequently generating some non-negligible stress and/or displacement (e.g. mechanisms, PCB deflexion). The first mode of the unit is then a key parameter to assess the shock damage risk.

Internal pyroshocks, such as solar array or antenna release, generate mainly high frequency content (i.e. above 4000 Hz). The involved physical phenomena are then quite different than for the launcher induced shocks. This frequency span mainly concerns small components (e.g. electronic components like relays, quartz) inside the equipment. Functional aspects of the unit can also be impacted like relay bouncing or transfer, valve transient leakage. The detailed design of the unit (e.g. PCB location and layout, type of component, type of mounting technology) is then the key parameter to assess the shock damage risk.

18.2 Evaluation of transmissibility between equipment and sensitive components interfaces

18.2.1 Overview

In the overall SDRA process, once the shock level in terms of SRS has been derived at the equipment interface (see 17.2), the next step is to assess how this level is transmitted inside the unit at the sensitive components interface. This assessment is a difficult task and cannot be considered as completely mature. It relies mainly on rules-of-thumb and/or FE analyses, as measurements are almost never available inside the unit.

As described in the previous section vibration test results and detailed FE analysis are the two key elements to derive accurately the transmissibility inside the units. The use of these two different and complementary information allows to gain confidence in the derivation of the level. Test, if appropriate instrumentation plan, can be used directly to extract the transmissibility (see 18.2.2) or can be used to correlate a FEM that allows to derive the transmissibility at sensitive component interface (see para. 18.2.4).

18.2.2 Derivation by extrapolation from test data

The transmissibility between equipment I/F and sensitive equipment is used for the evaluation of shock levels at sensitive component interface.

Ideally it could be derived from a representative shock test using a dedicated instrumentation, but it is generally based on the available measurements performed during sine surveys (up to 2000 Hz).

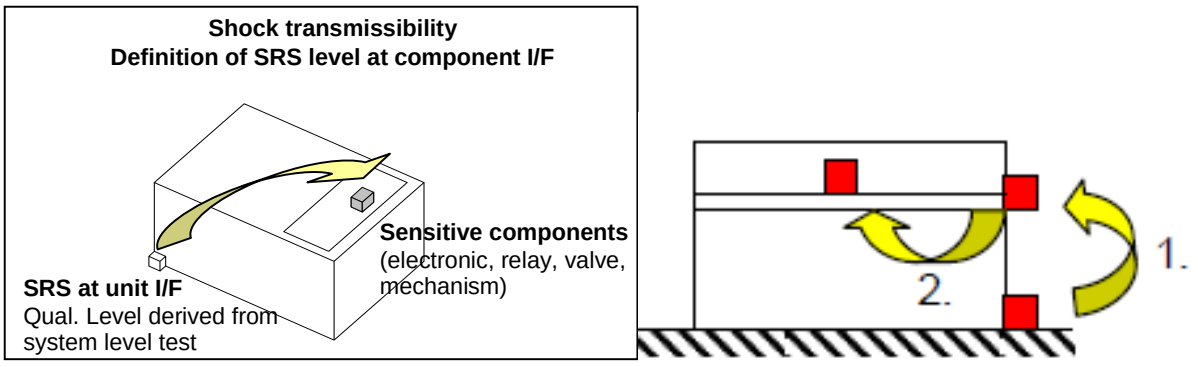

Figure 18-1: Equipment shock transmissibility

The derivation of the shock transmissibility can be evaluated with the following steps:

a. In the sine survey test, identify the sensor closest to the shock sensitive component.

   Extract from the sine survey the transmissibility $FRF^{sine1}(f)$ between the equipment interface and this sensor (see Figure 18-1. The sine survey transmissibility corresponds to a steady state modal response and is different of the transmissibility extracted from the shock regime measurements.

b. In most cases, the sensor location differs from the sensitive component location. Therefore, the transmissibility $FRF^{sine2}(f)$ between these two locations should be evaluated.

c. $$\text{SRS at component I/F} = \text{SRS at unit I/F x } TF_1^{shock}(f) \text{ x } TF_2^{shock}(f)$$

Where :

$TF_1^{shock}(f)$ = shock transmissibility between unit I/F and sensor location

$TF_2^{shock}(f)$ = shock transmissibility between sensor and component location

$$\sqrt{FRF_i^{sine}(f)} \le TF_i^{shock}(f) \le \sqrt{2xFRF_i^{sine}(f)} \qquad (i = 1,2)$$

For the reasons indicated below, in most cases, a good approximation for TF^{shock} is

$$TF_i^{shock}(f) = \sqrt{FRF_i^{sine}(f)}$$

A rationale and a limitation for such formulation are the following:

- Sine transmissibility amplifications are severe and cannot be used directly as shock transmissibility functions. The amplification found on low damped modes is high because the excitation is stationary. A shock is a transient excitation and full amplification of low damped modes cannot be reached. Experimental observations allows to derive this rule-of-thumb: shock transmissibility at low frequencies (below 2000 Hz) is comprised between the square root of the sine transmissibility and the square root of twice the sine transmissibility as illustrated on Figure 18-2 on a small RF unit (see also Part 3, **14.2.3**). Note that the considered shock is a qualification shock performed on a thick resonant plate with a hammer impact as a shock generator. As a result, the cross correlation between all interface points is stronger than it would be during a pyrotechnic shock and the shock transmissibility at low frequency can thus be overestimated.

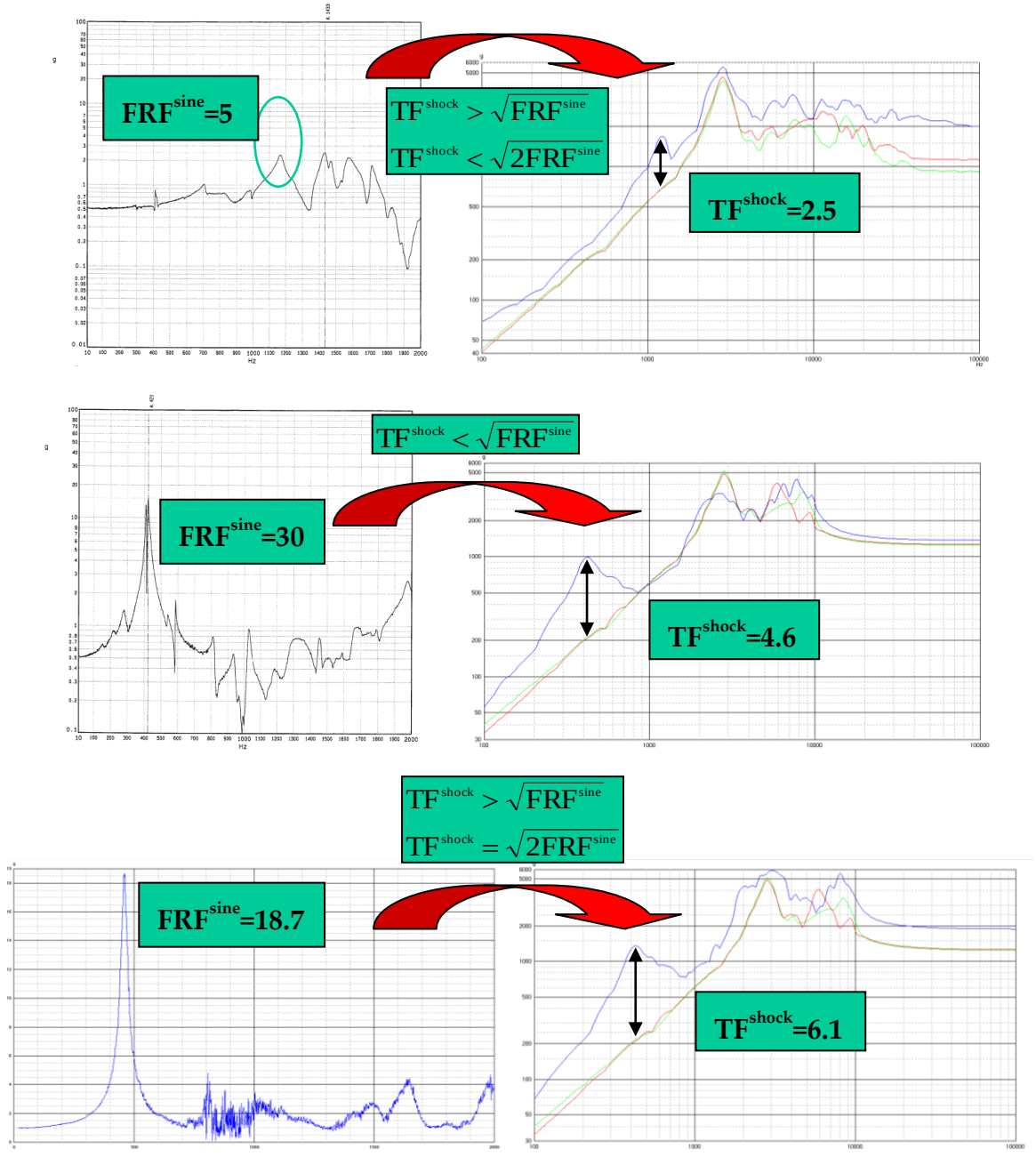

Figure 18-2: Comparison of the amplification factors between sine and shock tests on a small RF unit

- In case only random test results are available, i.e. expressed in terms of PSD_{in} and PSD_{out}, it is recalled that the transmissibility function can be obtained applying the formula:

$$FRF^{random} = \sqrt{\frac{PSD_{out}}{PSD_{in}}}$$

Assuming linearity of the unit mechanical behaviour, FRF^{random} is equal to FRF^{sine}.

- Sine transmissibility functions are obtained from a test where the specimen is clamped on a stiff interface and excited by the base uniformly in one direction. The boundary conditions in the real shock environment, e.g. on a satellite panel, can differ from a clamped condition, furthermore the shock is a multi-axis excitation source. As a result, this may affect not only the amplitude of the shock transmissibility function but also the modal behaviour.

  And extreme case is presented in Figure 18-3, with a comparison between the transmissibility identified through sine survey, and the SRS level as recorded during the pyrotechnic shock test (measurement point is located on a PCB of the equipment). The mode shape that is largely excited during the pyro shock is a torsion mode at 750 Hz around an OOP axis, with some shear of the different metallic PCB frames stacked together. This phenomenon cannot occur during a single axis excitation such as the sine survey vibration. It is worth mentioning that the pyrotechnic source consisted in a pyrozip separation system, located close to the equipment interface, hence not fully representative of far-field shock environment usually experienced in a satellite.

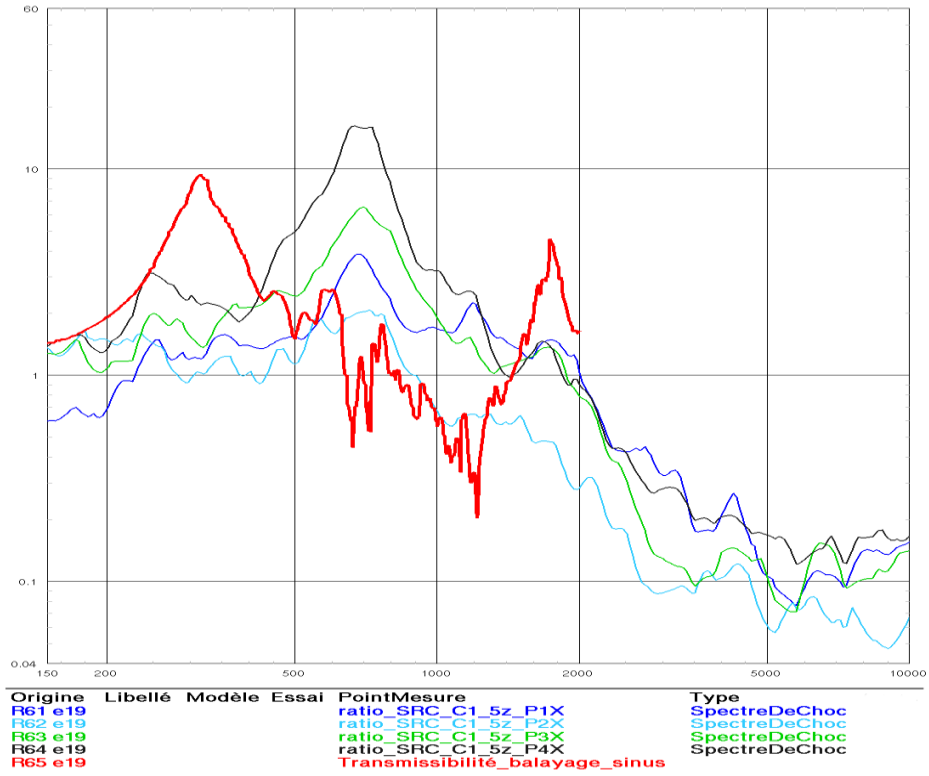

Figure 18-3: Sine survey and SRS ratio for a given measurement

18.2.3 Shock response prediction based on transmissibility

An attempt has been made to summarize the previous sections and propose a shock transmissibility general approach in terms of SRS covering the usual frequency band of far-field shock, i.e. from 100 Hz to 10 kHz. As an illustration, the Figure 18-4 starts from a shock specification at the interface of a subsystem and a FRF representing the subsystem response under a sine excitation on a rigid interface (obtained from a shaker test or by FEA). The proposal consists in using the sine transmissibility up to 2000 Hz as specified in section 18.2.2. Then, in the mid frequency band defined between 2000 Hz and the transition frequency (as explained in 18.2.4.4.2), a 6 dB corridor seems a reasonable assumption as shown in section 18.2.4.4.2 and Figure 18-15. Beyond the transition frequency, a decreasing corridor is proposed that ends with a maximum value equal to the specification at 10k Hz, as no more acceleration is transmitted to the observed point due to global modal behaviour inside the subsystem.

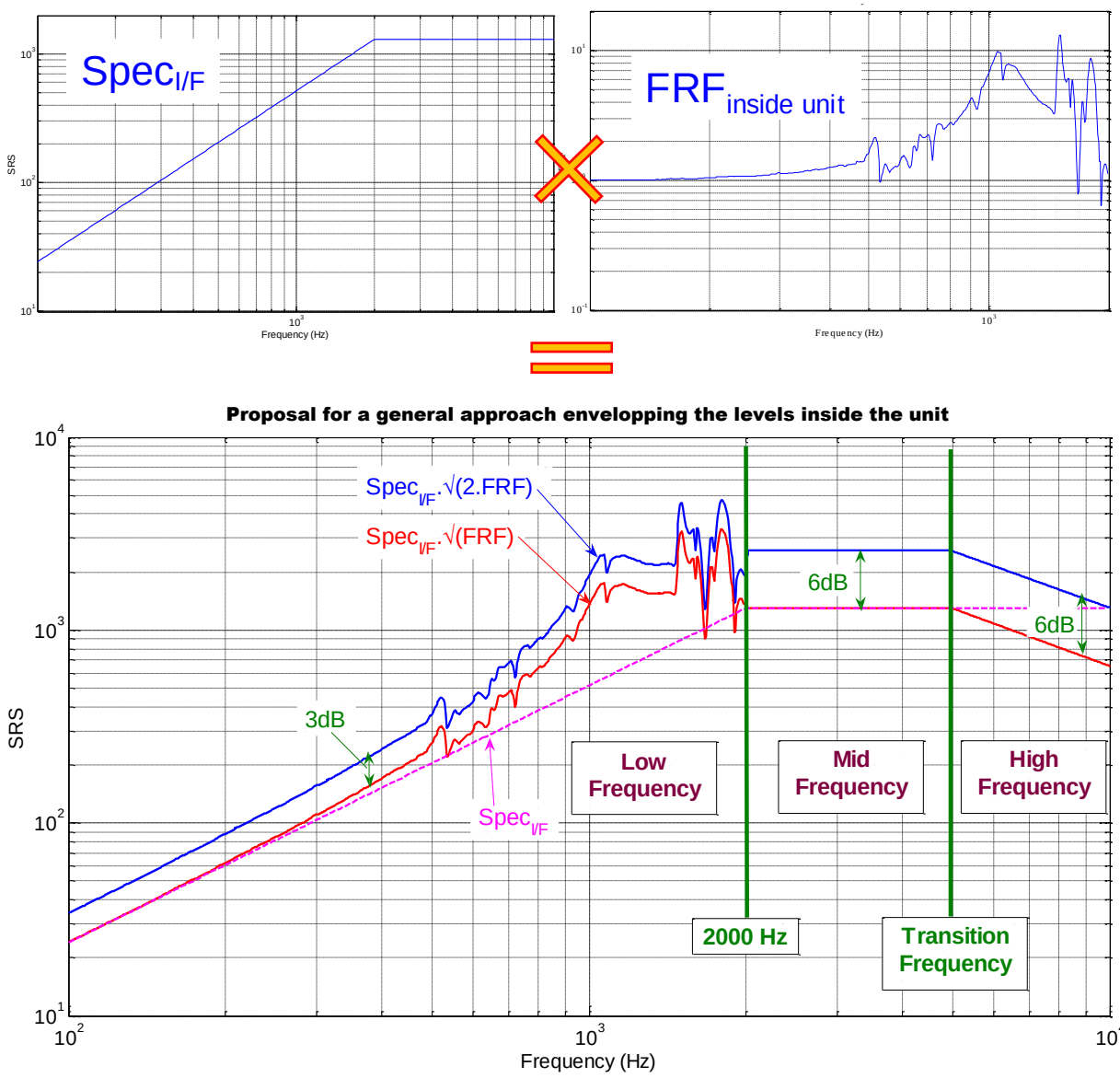

Figure 18-4: Proposal for a general approach of shock transmissibility

This proposal is based on a lower and upper SRS bound that depends on the degree of conservatism for the derivation of this transmissibility. The conservative approach consists in deriving the transmissibility considering the upper envelope whereas a less conservative approach considers the lower envelope.

The 3 dB corridor below 2000 Hz is relatively tight as the FRF comes from a real test. Further margin should be added to reach 6 dB if the FRF is the result of a FEA.

The proposed approach is defined for electronic units exhibiting internal modes beyond 2kHz. For more complex mechanical assembly (a large instrument for example), some adaptations of this method are necessary to account for a lower transition frequency. Application of this method to instruments is further detailed in paragraph 8.3.6.1.

18.2.4 Guideline for equipment shock analysis

18.2.4.1 Overview

If a detailed FEM of the equipment is available, it can be used to evaluate a shock environment in the unit at locations where no measures are available. Formally, this situation is comparable to the shock derivation at subsystem interface in a spacecraft as described precisely in **Part 2** – Shock Derivation to Subsystems. Similar limitations apply to these numerical analyses with regard to the meshing size, damping introduction, source modelling, components modelling, junctions modelling As a matter of fact such a numerical method is unable to get precise evaluation of shock environment at component interface but it can be useful to estimate conservatively a level when used with an appropriate margin policy.

Depending on the context and the available information, more appropriate approaches can be used to identify responses inside the unit. They can be ordered as follows, from the most accurate method to the less accurate one:

— Method 1: Transient excitation of unit-plate coupled system

— **Method 2:** Base transient excitation of the unit

— **Method 3:** Modal solutions

18.2.4.2 Method 1 - Transient excitation of unit-plate coupled system

In the most general case, the shock is specified in terms of I/F acceleration SRS and no transient acceleration is available. With such limited information, the most appropriate simulation is a transient response of the unit with the supporting plate/structure, as illustrated on Figure 18-5. This is particularly important for the out of plane excitation as rocking modes of the unit on the supporting plate are taken into account. On a vertical unit, these rocking modes largely contribute to the accelerations on the boards, as illustrated by Figure 18-6.

With some experience in shock testing, the plate can be chosen to be representative of the test bench structure. The transient analysis thus simulates a qualification shock. Alternatively, the supporting structure can be chosen representative of the real satellite environment.

The various steps of the simulation method are largely discussed in [RD-0107]. The key point is that simple force models for the shock excitation, e.g. a half sine or a triangular profile, result in a

representative acceleration field at the base of the unit. Only the duration of the shock pulse needs to be tuned. Measured and predicted accelerations (SRS) at the four interfaces of the unit are plotted on Figure 18-7.

When the simulated acceleration field does not exactly meet the specification of the unit, SRS of the accelerations on the unit can be easily corrected, applying to the responses the SRS ratio identified between the specification and average base acceleration.

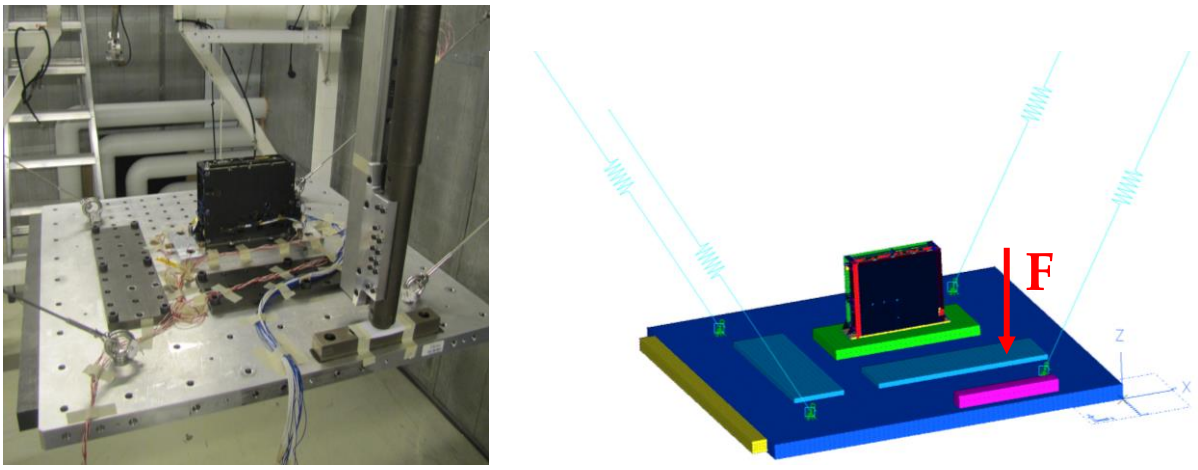

Figure 18-5: Equipment shock test and associated FE simulation

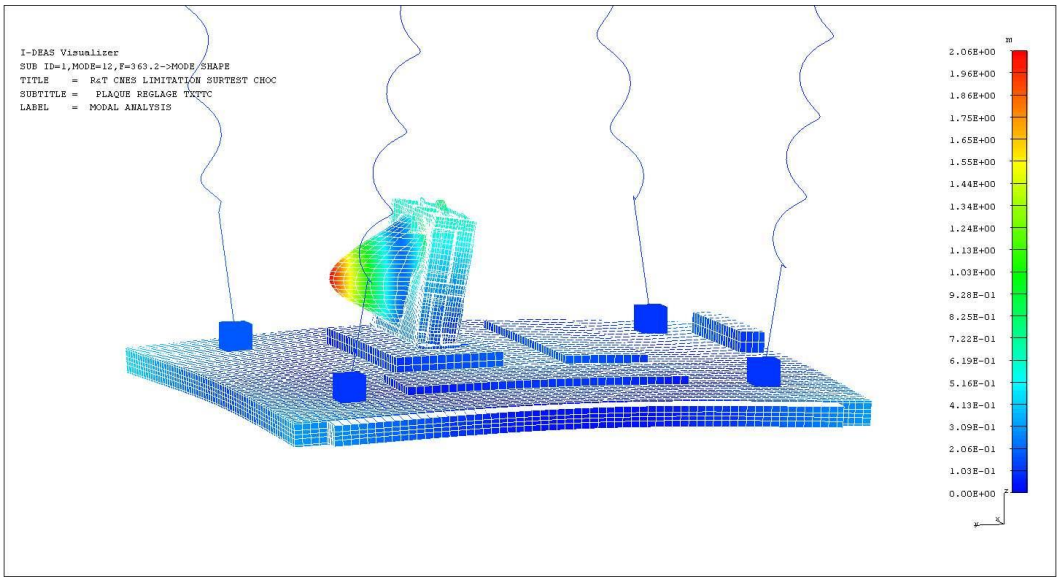

Figure 18-6: Unit rocking mode on mechanical test bench

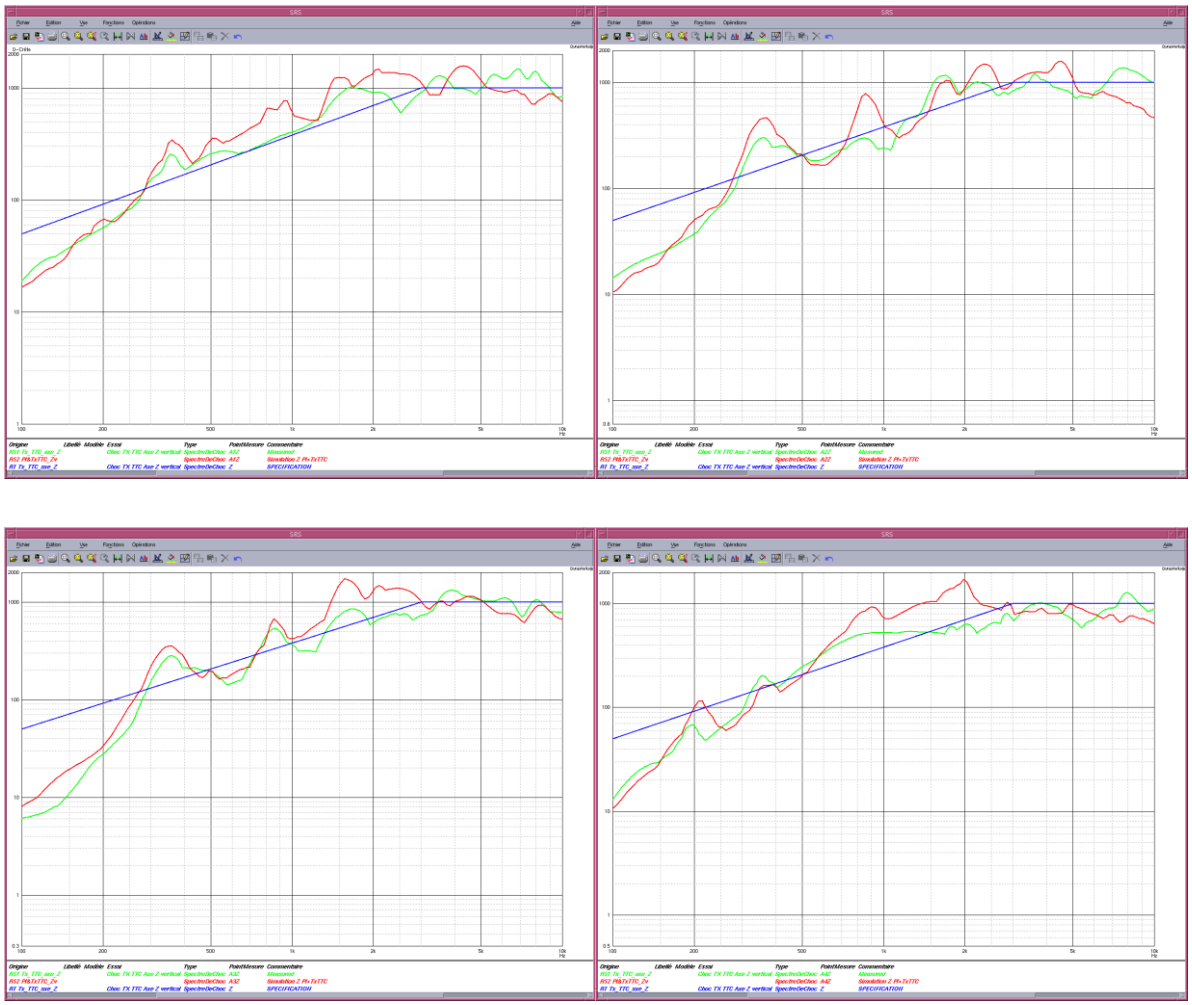

Figure 18-7: Predicted and measured accelerations (SRS) at unit I/F along Z-axis

Modelling of the contact between the unit and the plate has a large influence on calculated responses. To illustrate this influence, Figure 18-8 shows calculated and measured responses on a PCB of the unit for two different contact models, i.e. merged nodes over the entire contact surface and simple attachment at fastener locations. Even if the first mode of the unit is slightly too high, the merged solution for the contact is more representative at frequencies above 500 Hz. However, Figure 18-9 shows that such model gives an excessive response on the structure along Z-axis.

More representative contact behaviour can be obtained from non-linear solutions. In addition, this contact parameter is less important if the plate has a large flexibility (both modelling solutions tend to converge).

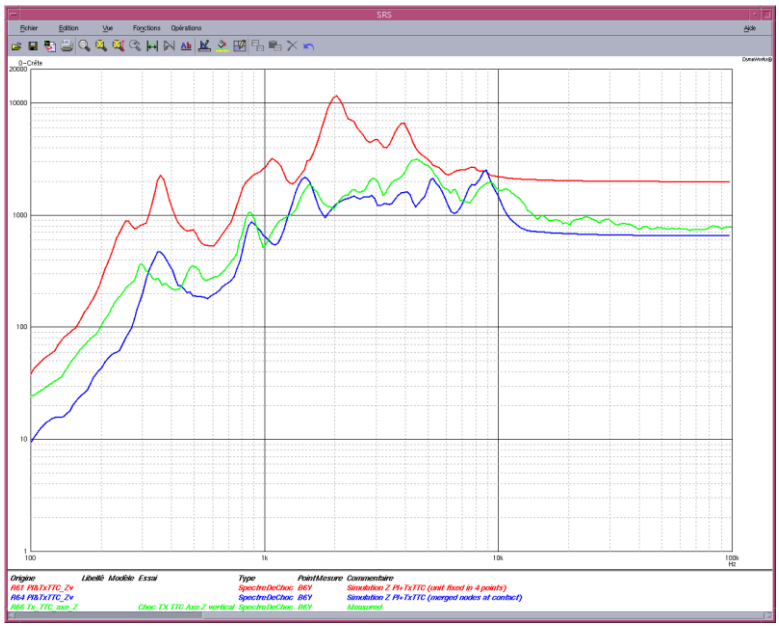

Figure 18-8: Predicted and measured acceleration on unit PCB for two different contact models (merged nodes and attachment at fastener locations)

Figure 18-9: Predicted and measured acceleration (Z axis) on unit structure for two different contact models (merged nodes and attachment at fastener locations)

Even if contact is not an issue, another limitation of the method stands in the damping simulation. Transient solutions such as Nastran SOL112 do not allow introducing several structural damping coefficients in the model. As a result, a low damping coefficient that meets the plate dynamic behaviour is underestimated for the unit response prediction.

All types of output result can be obtained with such simulation method, i.e. transient I/F force, stress or acceleration and the associated SRS. For sensitive components, the acceleration SRS can then be compared to the allowable values in chapter 17.5 or to any other database that take into account the mounting technology eventually.

18.2.4.3 Method 2 – Base transient excitation of the unit

When the acceleration field is known exactly in all three directions at each of the equipment interfaces, direct time integration yields good results up to the mid-frequency range. A transient modal solution with multiple tri-axial bases is applied. The shock is modelled by a distribution of forced accelerations, using Lagrangian Multipliers. The main assumption concerns the stiffness of the supporting structure as it is considered perfectly rigid at each interface. One single base can be used for the in-plane excitation of the unit on a rigid plate or for the out-of-plane excitation on a massive block (shock machine, Hopkinson bar). However, this simplification is inaccurate for out-of-plane excitation if the unit is mounted on a suspended thick plate and the shock is applied next to the unit, as illustrated on Figure 18-10.

The potential of this method to predict the low pass filtered transient behaviour of the electronic equipment has been demonstrated ([RD-0109], [RD-0108]). At higher frequencies, the rigid boundary conditions at the I/F of the unit are no longer valid. The inaccuracies of the finite element model (FEM), with regard to components, connectors, bolts and other details, also result in larger discrepancies.

Figure 18-11 shows predicted and measured responses on the illustrated RF unit applying multi-base (6 inputs with 4 along Z axis) transient modal excitation.

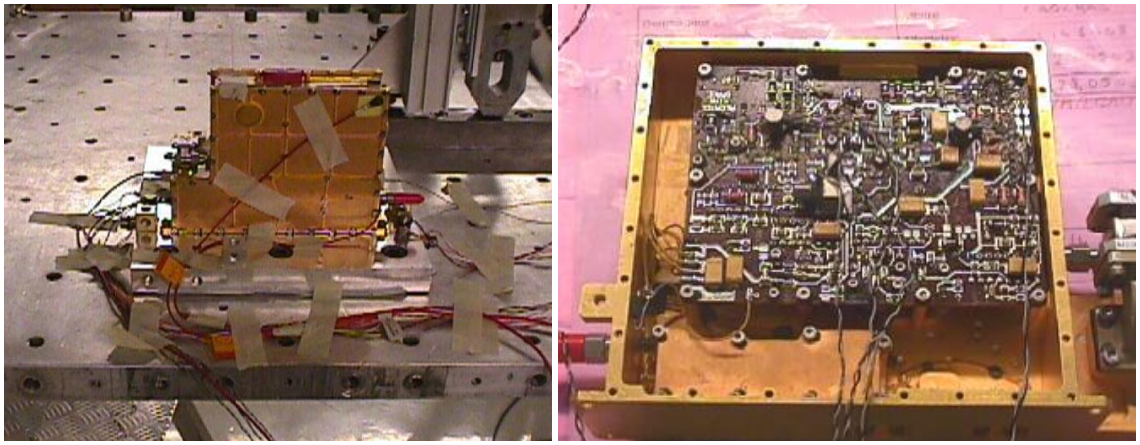

Figure 18-10: Acceleration measurements at RF unit interface and on the unit

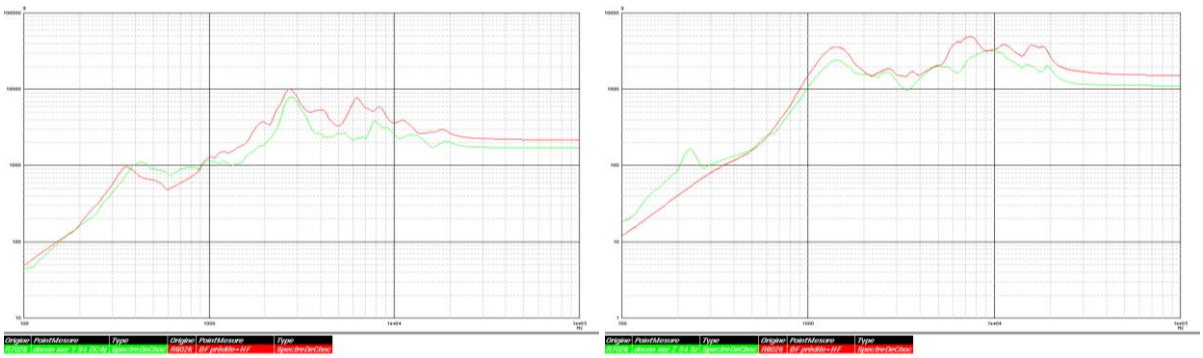

Figure 18-11: Predicted and measured accelerations (SRS) on the RF unit (from [RD-0108]) - (a) PCB along Y axis (Y excitation) - (b) Structure along Z (Z excitation)

All types of output result can be obtained with such simulation method, i.e. transient I/F force, stress or acceleration and the associated SRS. For sensitive components, the acceleration SRS can then be compared to the allowable values in chapter 17.5 or to any other database that take into account the mounting technology eventually.

18.2.4.4 Method 3 - Modal solutions

18.2.4.4.1 Method 3A – Frequency Response Function

This type of analysis allows to characterize the Frequency Response Function (FRF) between a DOF identified as the source and another identified as the unit response in the frequency domain. Usually the source DOF is a junction DOF and the corresponding FRF is the transmissibility between the clamped interface and the internal DOF.

The computed FRF depends mainly on 3 types of parameters, namely the natural frequencies, modal damping or Q factor and effective parameters (effective mass, transmissibility or flexibility). In order to be used with confidence, the FEM is compared and correlated if necessary with test data. Sine survey or tapping test are able to provide an experimental modal basis that can be further used to correlate the FEM. Once correlated, this FEM is able to provide accurate results at component interface where no measurements are available.

As explained earlier, the sine survey transmissibility corresponds to a steady state modal response and is different of the transmissibility extracted from the shock regime measurements. The shock transmissibility can be evaluated by following the same procedure described in section 18.2.2. The FEM allows computing directly the transmissibility at the right location (i.e. at the sensitive component interface – See Figure 18-12):

- Compute the transmissibility or $FRF_{sine}(f)$ between the equipment interface and the sensitive component interface.
- SRS at component I/F=SRS at unit I/F x$TF_{shock}(f)$

  Where :

  $TF_{shock}(f) = \text{shock transmissibility between unit I/F and sensor and component location}$

  $\sqrt{FRF_{sine}(f)} \le TF_{shock}(f) \le \sqrt{2xFRF_{sine}(f)}$

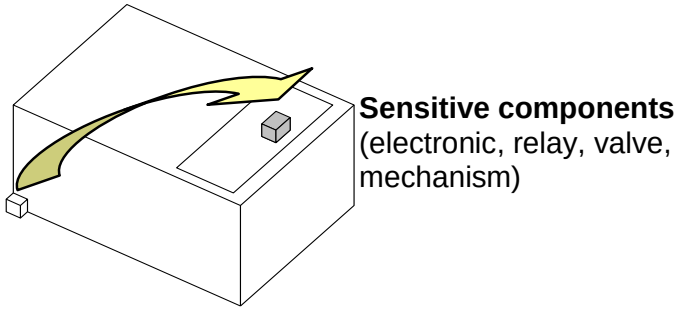

Figure 18-12: Equipment shock transmissibility

18.2.4.4.2 Cumulative modal effective transmissibility

In most cases, two distinct frequency ranges can be distinguished in the shock response spectrum of the equipment. At low frequencies, the shock excitation is eventually amplified by the modal response characteristics of the equipment. Above a certain frequency, that we call the “transition” frequency, the input is filtered. A typical response on a PCB is illustrated on Figure 18-13.

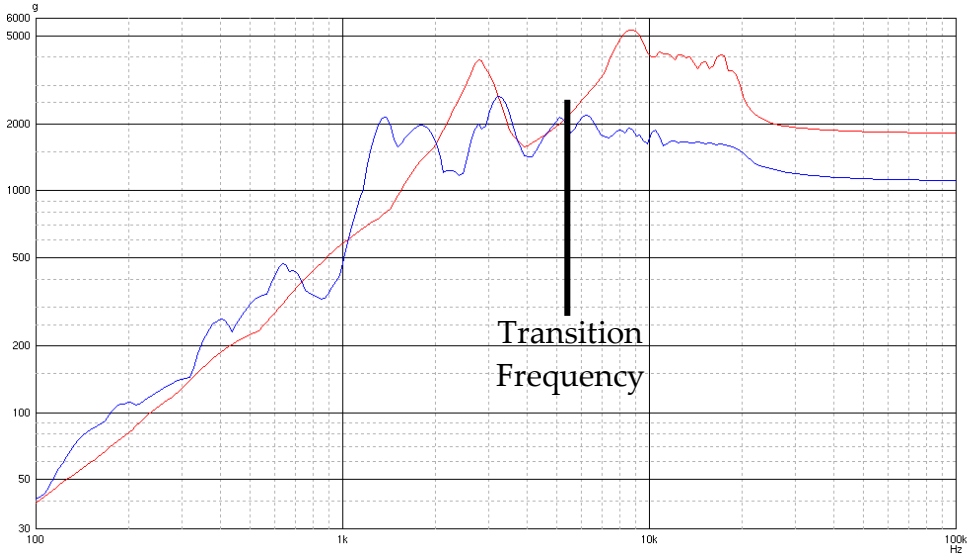

Figure 18-13: Equipment excitation level (at the I/F) and response of a PCB, in terms of SRS

The transition frequency between low and high frequency ranges can be estimated using the effective transmissibility parameter [RD-0106]. This modal parameter indicates the level of transmitted acceleration due to global modal behaviour, from a junction to any equipment point (on the PCB for instance). It can therefore be used to define the maximum frequency of the LF domain and the minimum frequency of the HF domain.

To extract this parameter, a modal analysis of the equipment finite element model (FEM) was performed. Clamped boundary conditions were applied at the interface with the fixing points. Thus, the effects of phase differences between the injected signals on the system modal behaviour are neglected. The system could then be reduced to a first sub-structure consisting of the interface degrees of freedom DOF and a second represented by a set of DOF's on the equipment model. The equation of motion leads to Eq. (1) if damping is neglected.

$$\begin{bmatrix} M_{jj} & M_{ji} \\ M_{ij} & M_{ii} \end{bmatrix} \begin{bmatrix} \ddot{u}_j \\ \ddot{u}_i \end{bmatrix} + \begin{bmatrix} K_{jj} & K_{ji} \\ K_{ij} & K_{ii} \end{bmatrix} \begin{bmatrix} u_j \\ u_i \end{bmatrix} = \begin{bmatrix} R_j \\ 0 \end{bmatrix} \qquad (1)$$

[M] and [K] are mass and stiffness matrices respectively. u_j represents the displacements imposed at the junction and u_i represents the internal displacements of the forced harmonic response. R_j represents the force reactions at the junctions. The eigenmodes of both sub-structures are introduced and transformations of Eq. (1) lead to the dynamic transmissibility matrix which links u_j and u_i:

$$\{u_i\} = \left[\tilde{T}_{ij}(\omega)\right]\{u_j\} \qquad (2)$$

$$\left[\tilde{T}_{ij}(\omega)\right] = \sum_{k=1}^{m} T_k(\omega).\tilde{T}_{ij,k} \qquad (3)$$

where $T_k(\omega)$ represents the dynamic transmissibility factor of the mode k. The effective transmissibility matrix $\tilde{T}_{ij,k}$ of the mode k is given by:

$$\tilde{T}_{ij,k} = \frac{[\Phi_{ik}][L_{kj}]}{m_k} \qquad (4)$$

where $[\Phi_{ik}]$ symbolizes the matrix of the eigenmodes for clamped interface boundary conditions and m_k represents the generalized mass of the mode k. Eq. (5) defines the participation factor L_{kj} of the mode k where $[S_{ij}] = -[K_{ii}].[K_{ij}]^{-1}$ is the junction static mode matrix.

$$L_{kj} = [\Phi_{ik}].([M_{ii}].[S_{ij}] + [M_{ij}]) \qquad (5)$$

The expression of the dynamic transmissibility matrix reveals the contribution of each mode to the equipment response. This contribution is made up of the dynamic transmissibility factor and a term which characterizes the mode. Moreover, if an infinite modal base is considered, the sum of all of the modal effective transmissibility matrices is exactly equal to the junction static mode matrix:

$$\sum_{k=1}^{+\infty} [\tilde{T}_{ij,k}] = \sum_{k=1}^{+\infty} \frac{[\Phi_{ik}].[L_{kj}]}{m_k} = [S_{ij}] \qquad (6)$$

The summation of the effective transmissibilities between an interface DOF (X, Y, Z translations) and a PCB DOF (X, Y, Z translations respectively) is presented in Figure 18-14. With this example, the parameter converges to around 95 % of the static mode transmissibility around 5,3 kHz. Thus, above this frequency, no more acceleration is transmitted to the observed point of the PCB due to global modal behaviour.

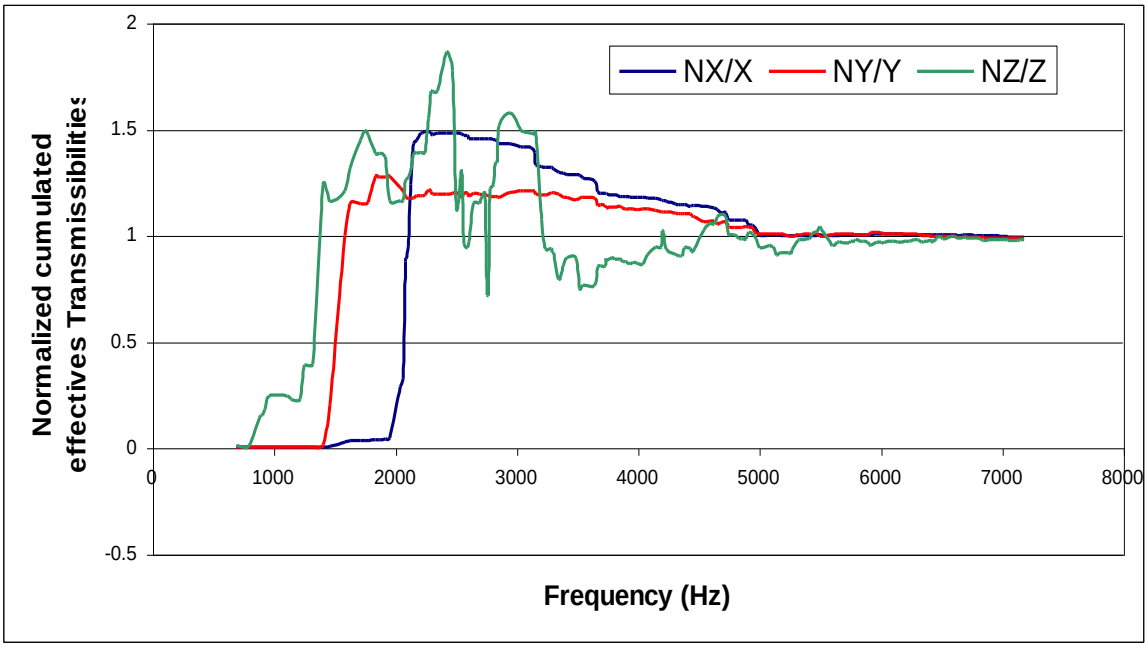

Figure 18-14: Normalized cumulated effective transmissibility of between the I/F and a PCB

Of interest is the transition frequency on the equipment printed circuit board, i.e. where critical components are most often located. An order of magnitude for this transition frequency (on the PCB) is:

- 6000 Hz for small units (mass < 1 kg, PCB area < 100 cm2)
- 4500 Hz for mid-size units (mass around 3 kg, PCB area around 400 cm2)
- 3500 Hz for large units (mass around 10 kg, standard 2E PCB size)

These frequencies can be increased if the component is located very close to the edge of the PCB.

The above mentioned transition frequencies correlate quite well qualification shock tests performed on a thick resonant plate excited by a hammer impact. The cross correlation between all interface

points is thus stronger than it would be during a pyrotechnic shock (see paragraph 13.3.4.1.2) for more explanations). As a result, the transition frequency can be lowered in the case of a pyrotechnic test. The following example corroborates this proposal. The same equipment was submitted to different shock tests:

- a resonant plate with a hammer impact
- a pyrotechnic bolt cutter and the equipment on a honeycomb panel

The results are illustrated here under (Figure 18-15). It appears that a "transition" frequency that seems to be around 2500 Hz on the resonant plate falls down to 1000 Hz when the equipment is on a representative honeycomb panel and submitted to a pyrotechnic test.

Another important remark: all the analyzed data show that, between 2000 Hz and the transition frequency, the amplification does not exceed 6 dB.

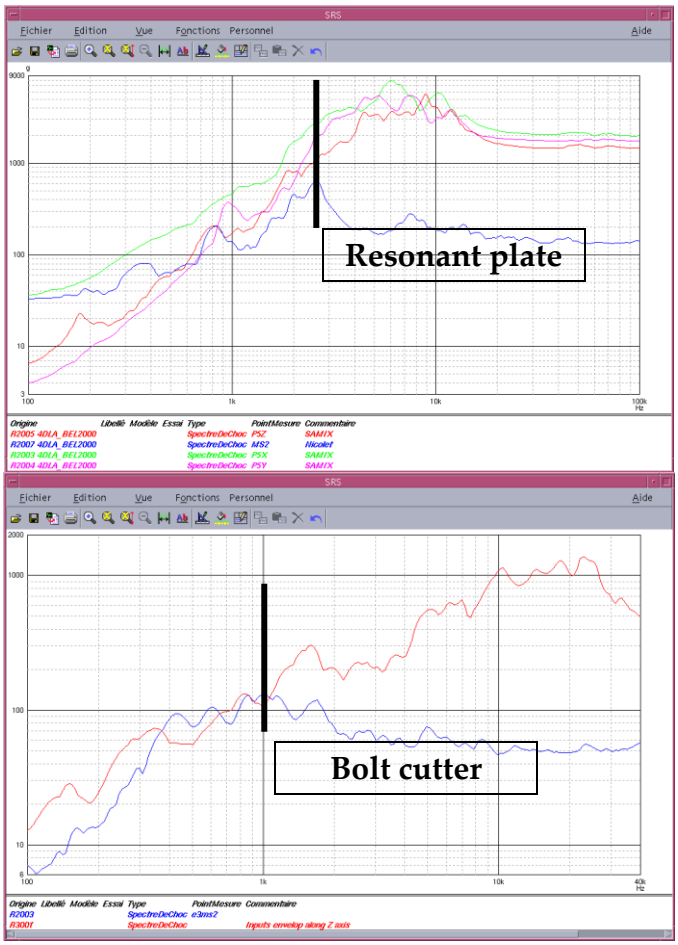

Figure 18-15: Equipment transition frequency (on a PCB) in various shock environments

18.2.4.4.3 Method 3B – Response Spectrum Analysis (RSA)

Response Spectrum Analysis (NASTRAN SOL 103) is a convenient approximate method of computing broadband peak response, based on the SRS information. The peak magnitude of the transient response can be written

$$u_k(t) = \sum_i \sum_r \phi_{ik} \psi_{ir} X_r(\omega_i, g_i, t)$$

where ψ_{ir} are the modal participation factors. The above equation may be approximated by combining the peak response values at the natural frequencies, i.e. $\bar{X}_{ri} = \max \left| X_r(\omega_i, g_i, t) \right|$, given by the specified shock response spectrum (SRS). Three methods can be used

ABS method $\quad \bar{u}_k = \sum_i \sum_r \left| \phi_{ik} \right| \left| \psi_{ir} \bar{X}_{ri} \right|$

SRSS method $\quad \bar{u}_k = \sqrt{\sum_i \left(\phi_{ik} \xi_i \right)^2}$, $\bar{\xi}_i = \sqrt{\sum_r \left(\psi_{ir} \bar{X}_{ri} \right)^2}$

NRL method $\quad \bar{u}_k = \left| \phi_{jk} \xi_j \right| + \sqrt{\sum_{i \neq j} \left(\phi_{ik} \xi_i \right)^2}$

Because it is limited to peak response calculation, RSA is generally used to compute stresses in the equipment. The results can be directly compared to material characteristics. It can also be used for I/F forces. However, the method is not so relevant in terms of component peak acceleration as most of the allowable data are defined in SRS terms. The ABS method gives the most conservative result. Positive margins with this approach bring the maximum confidence in the structural parts submitted to shocks.

The other limitation of the RSA method stands in the fact that it simulates perfectly rigid boundary conditions. This is often acceptable for in plane excitation but it is hardly true for out-of plane excitation, e.g. when the unit is fixed to a plate. To illustrate this issue, RSA has been applied to the equipment on Figure 18-5, mounted on a thick plate and submitted to shock along the three directions X, Y and Z. The RF unit was equipped with strain gauge rosettes at three different locations as illustrated on Figure 18-16. Measured and calculated maximum principal stresses are compared in the following table. As indicated above, the ABS method appears conservative at the three locations for the in-plane excitation, along X and Y axis. However, RSA is unable to predict maximum stresses for the out-of-plane excitation because they are associated to rocking modes of the unit on the plate, as explained in section 18.2.4.2, and RSA cannot simulate such dynamic behaviour.

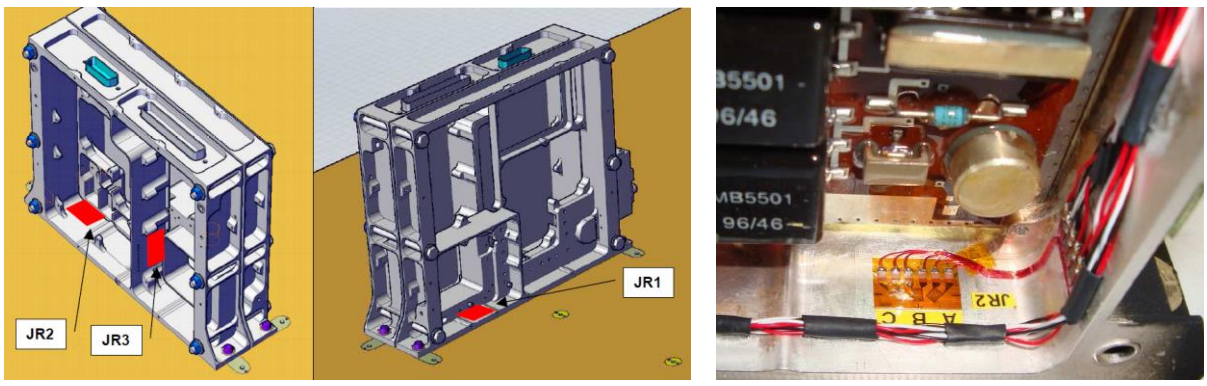

Figure 18-16: Strain gauge rosettes on the equipment

Table 18-1: Measured and RSA calculated (ABS method) stresses on equipment

	JR1		JR2		JR3	
Max principal stress (Mpa)	Test	RSA	Test	RSA	Test	RSA
X axis	**3**	**4**	**1.9**	**3.4**	**6**	**6.8**
Y axis	**3**	**3**	**2.4**	**11**	**5.5**	**12**
Z axis	**6.8**	**1.2**	**9**	**2.3**	**14**	**3.5**

18.2.4.5 Example of advanced transient (method 2) and spectrum response analyses (method 3B)

18.2.4.5.1 Industry case – anomaly of an optical assembly during QM test

This example presents the approach which has been undertaken to demonstrate the successful shock qualification of an optical assembly after an anomaly during QM-1 test has been discovered, see [RD-0112]. A brief description of the so-called Parabolic Mirror Assembly is provided in Figure 18-17, with the PMA consisting in a zerodur mirror, glued onto a mirror flange, and supported by a stable support frame.

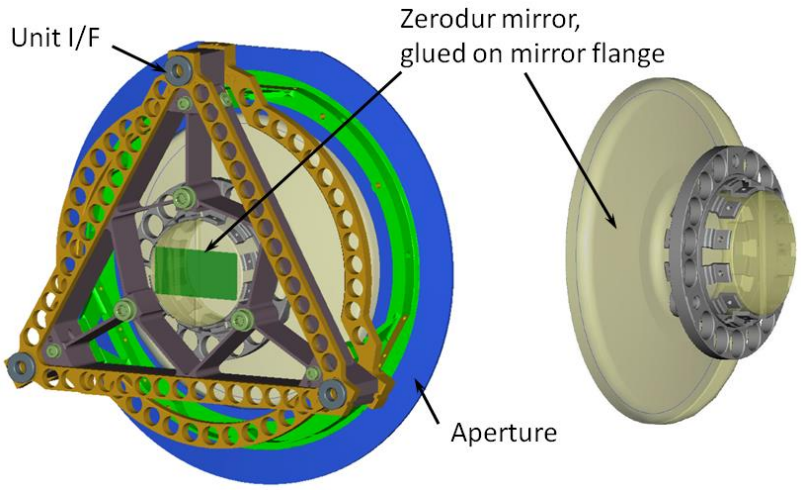

Figure 18-17: Parabolic Mirror Assembly – General layout

The unit failed the first qualification shock test in terms of shift of natural frequencies and optical alignment. Main objectives of the subsequent analyses have been:

- To correlate the finite element model with the QM-1 shock test in order to allow for an adequate shock prediction,
- To determine the root cause and assess failure criteria which could not be directly measured, so that these criteria could be checked by analysis and used as basis for successful re-performance of the QM-2 shock test,
- To identify recovery solutions, such as design modifications and/or reduced shock specification in view of QM-2 shock test.

18.2.4.5.2 Correlation of FEM shock prediction w.r.t. shock test results

The achievement of an adequate correlation of shock prediction with respect to shock test results is an essential step, in order to allow the determination of the root cause and support the identification of recovery solutions (in the case consisting in a combination between a modification of the interface design and a reduction of the shock specification).

The objectives of the correlation activity were to match the frequencies of each important modes influencing the overall response of the system, and to reproduce the tri-axial accelerations (both in time and frequency domains) at the components which are expected to be the main contributors. Therefore an adequate correlation can only be claimed if the test specimen was adequately instrumented, including control accelerometers and accelerometers measuring the response at relevant components (with time domain data available with sufficient resolution).

Details on the unit instrumentation during shock test are provided in the following figure.

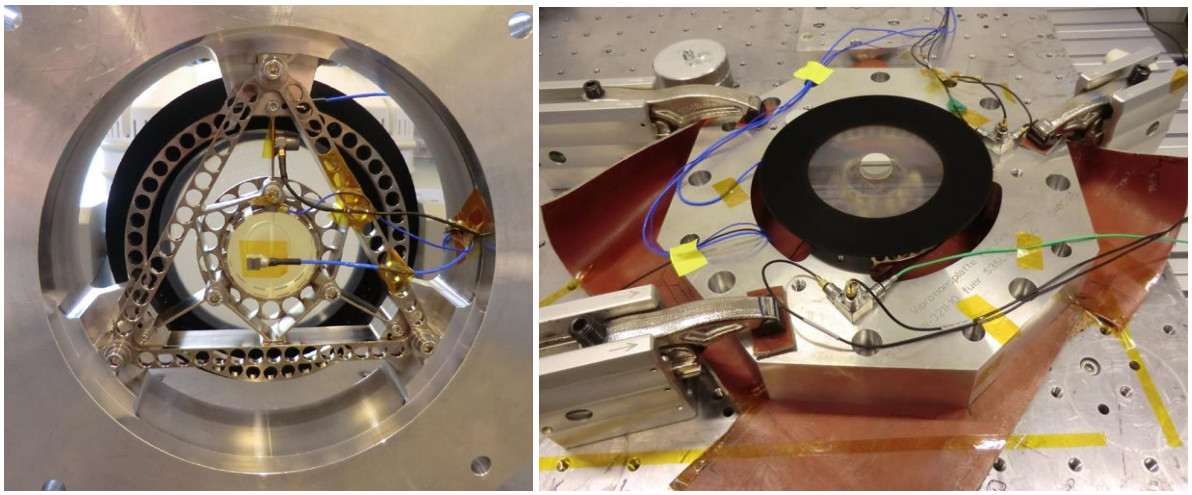

Figure 18-18: PMA instrumentation for shock test (left: sensors for internal responses – right: tri-axial control accelerometers at unit interface)

An example of achieved correlation of the mirror response, both along the main excitation axis and the cross axes , is shown in Figure 18-19. A very good correlation is achieved across the whole frequency spectrum.

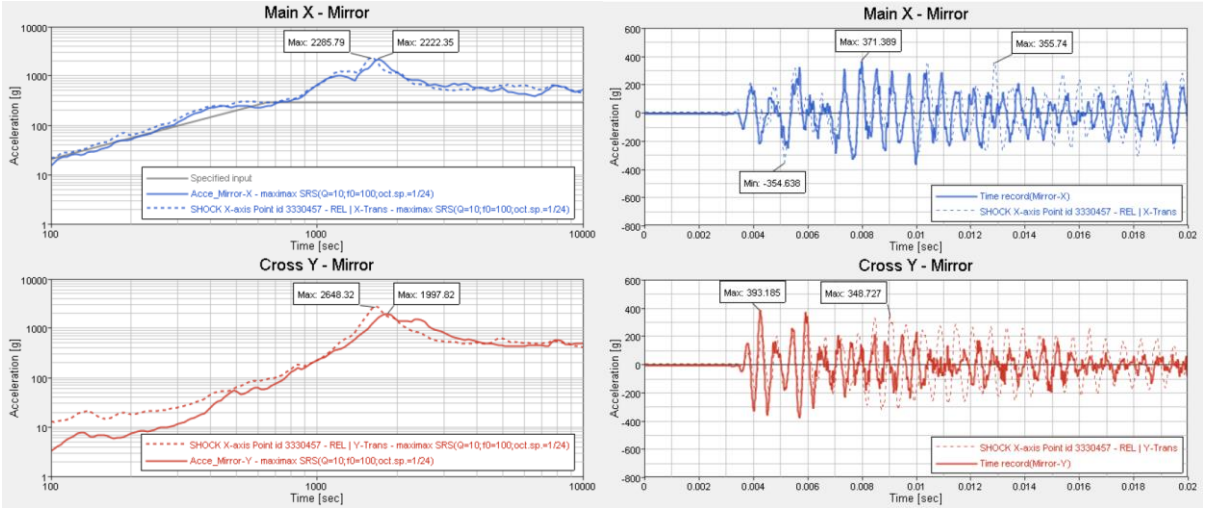

Figure 18-19: Correlation of mirror response for excitation axis along X

18.2.4.5.3 Analysis methods: transient analysis vs. response spectrum analysis

With respect to analysis methods, it is concluded from this example that transient analysis with the actual time data as basis is more straightforward for shock assessment. In general, the process is easy to apply and the results are more accurate than in response spectrum analysis (RSA). RSA is based on shock spectrum and modal characteristics of the structure which are then combined for response calculation (see paragraph 18.2.4.4.3 for details on the methodology). To account for interaction between peak responses, a statistical method is applied which usually adds too much conservatism into the analysis results. As example, the difference between transient and RSA was identified up to a factor 2.6 for axial force in bolted joints, which renders any precise assessment of the root cause and derivation of reduced shock input spectrum infeasible.

18.2.4.5.4 Identification of recovery solutions

The achieved correlated model allows assessing some failure criteria which could not be directly measured (such as margin of safety at the interface, or stress in bonded joints), as such this model can be efficiently used in support to the root cause investigation and in support to the identification of recovery solutions.

In this specific case, the recovery solutions consisted in a modification of the interface design together with a reduction of the shock specification.

For what concerns the reduction of the shock specification, some local reductions could be granted while still covering the system need (including coverage with random environment, see paragraph 12.5.3), in frequency ranges with high contribution to loads on screws and bonded joints.

Finally, prior to the re-performance of the QM-2 shock test, the confirmation of adequacy of the identified recovery solutions was gained through complementary shock analysis in association with calibration shock testing on a representative dummy.

18.2.4.5.5 Conclusion

This practical case is a good illustration of the relevance of shock analysis for the determination of the root cause and for the identification of recovery solutions. However it requires that a sufficient correlation, of FEM shock prediction with respect to shock test results, is achieved.

18.3 Verification method per type of components and/or units

18.3.1 Electronic equipment

18.3.1.1 Verification methodology

In some cases, the electronic equipment is required to withstand a stringent shock environment, which becomes a dimensioning case in the same way like any other mechanical environments. Exposure to a severe shock environment can result in structural failure of housing and interface bolts, PCB components and solder joints failure. However, **many of these failures can be avoided if the shock environment is adequately taken into consideration in the equipment design process.**

The equipment design can be supported by appropriate Finite Element Analysis, or by analytical design rules (so-called Steinberg design rules,[RD-0113]). A proper understanding of the nature of vibration and shock together with a careful evaluation of the response characteristics are two essential elements. Designing for both vibration and shock environments usually results in conflicting design requirements. An optimum design is achieved through several design iterations.

As such, SDRA for electronic equipment is a confirmation that the current equipment design is able (or not) to withstand a stringent shock environment. SDRA does not say if the current equipment design is optimum.

SDRA for electronic equipment is a complex assessment, requiring a careful screening for sensitive components, an evaluation of the transmissibility between unit interface and sensitive components, and a good knowledge of the component sensitivity thresholds.

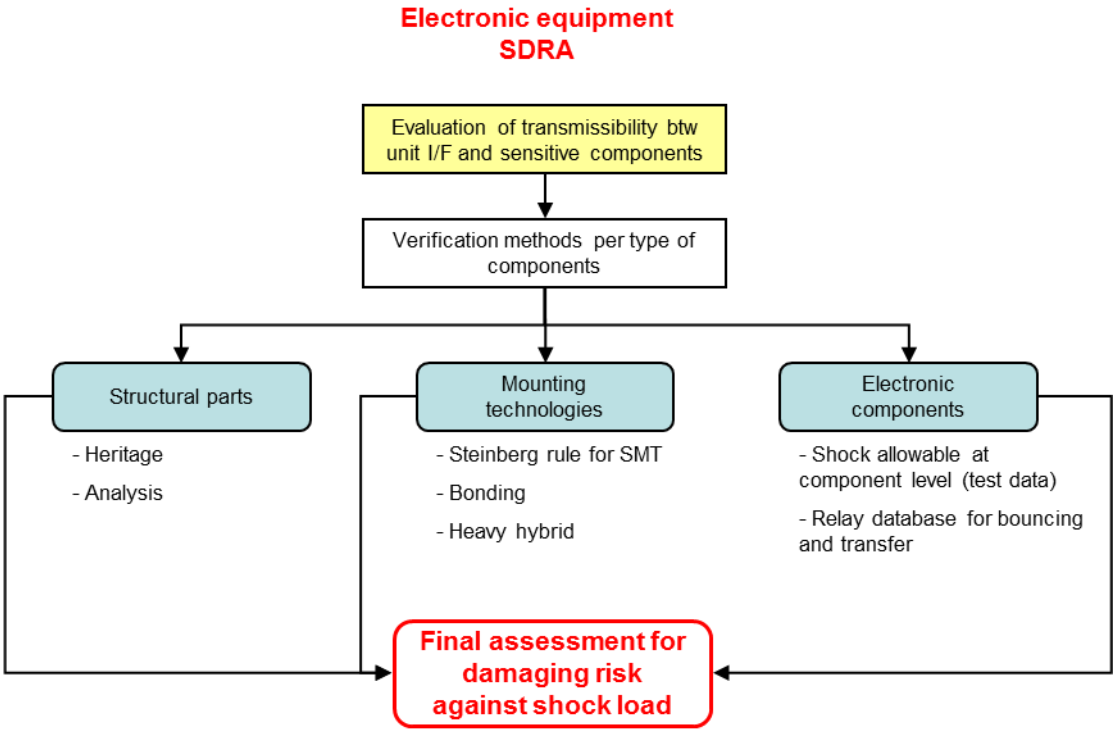

Figure 18-20: Rationale for electronic equipment SDRA

A thorough understanding of the equipment dynamic behaviour is essential, since experience has shown that shock damage is often produced by critical resonances of the electronic unit. These resonances can occur at various levels inside the equipment, at unit level (global modes) and at PCB level of course but also at component level (specific mounting conditions) and inside the component as well (e.g. quartz, relay). It is important to identify if any coupling between all these dynamics entities can occur.

The risk of a structural failure is assessed, by analysis (following heritage considerations). All component-mounting conditions (bonded joint, solder-joint or specific mounting) are validated by test or analysis (following heritage considerations). Finally, the risk of damaging a sensitive component is established, consolidating the transmissibility w.r.t. unit interface and comparing component acceleration with its sensitivity threshold.

18.3.1.2 Validation for structural parts

Structural parts can be validated applying one of the following approaches:

- Heritage exists for the unit structure. The mass distribution inside the unit is similar to the heritage as well.
- A shock analysis is performed (refer to guideline in section 18.2.4). The margin policy is adapted to the heritage on the applied method.

A specific attention should be devoted to the parts made of brittle material. As plastic deformation is inexistent within these materials, the associated degradation mode is a straight and catastrophic rupture. A conservative safety factor should be used w.r.t. the ultimate load conditions of the material.

18.3.1.3 Validation for component mounting technologies

18.3.1.3.1 Generic process

The ECSS-Q-ST-70-08C [RD-0121] defines the verification procedure to apply for soldered components. The generic process includes vibration testing (sine and random) as well as thermal cycling. The test specimen is representative of the flight configurations and the input level is established to cover the maximum deformation of the printed circuit board at part level.

18.3.1.3.2 Shock qualification of the technology

In addition to the generic process, the test vehicle can be submitted to half sine shocks whose level vary from 750 g to 1500 g (0,5 ms duration) typically. Figure 18-21 illustrates two different types of PCB (full or quarter of a double European standard size PCB) on the shock machine.

In this case, the SRS of the acceleration on the PCB resulting from the SDRA can be directly compared to the qualification status of the technology.

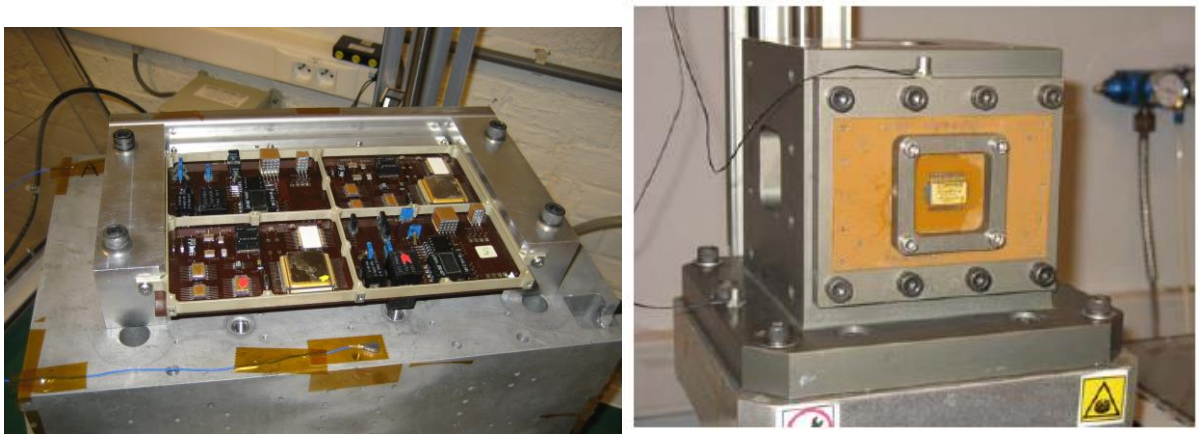

Figure 18-21: Test vehicles (PCB) for shock test qualifications of component mounting technologies

18.3.1.3.3 Equivalent SRS derived from random vibrations

When a shock test qualification has not been performed, it is possible to calculate the Random Response Spectrum (see Part 3 paragraph 12.5.3) based on the qualification to random vibrations of the generic process. As the PCB fundamental frequency is generally below 2000 Hz (max. frequency of the DSP), it can be assumed that the maximum deformation of the PCB is covered if the RRS covers the acceleration SRS resulting from the SDRA below 2000 Hz.

If the RRS does not cover the expected shock level on the PCB or if the test vehicle is not representative of the flight PCB, Steinberg rule is an alternative solution to gain in confidence.

18.3.1.3.4 Steinberg rules for lead-wire and solder-joint failures on large or heavy electronic components (See [RD-0113])

Figure 18-22 shows how the lead wires and solder joints in a large DIP/component are stressed when a PCB develops large deflections. The greatest damage occurs when the large components are mounted at the centre of a PCB, where the curvature changes and the amplification factor are the greatest.

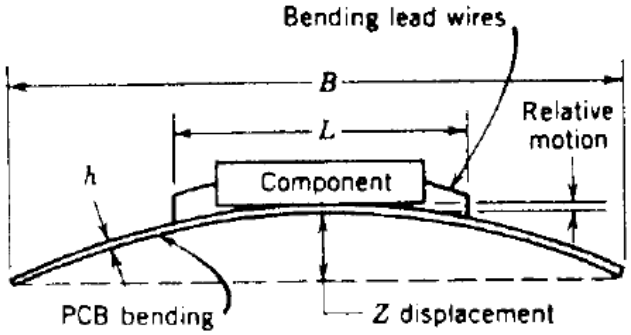

Figure 18-22: PCB resonance producing stresses in lead wires due to relative motion between the component body and the PCB

When less than a few thousand stress cycles are expected and when the structural material is expected to have a ductility of at least 5 %, then fatigue is not a major factor and stress-concentration effects are sharply reduced. Fatigue factors found in non-ferrous alloys, such as aluminium, typically are 1/3 of the ultimate tensile strength, and stress concentration typically are about 2,0 for holes and notches. Applying this correction factor to the shock environment results in the following adjusted PCB dynamic displacement:

$$Z = \frac{0.00132 \times B}{C \times h \times r \times \sqrt{L}}$$ (US unit, all dimensions in [inch])

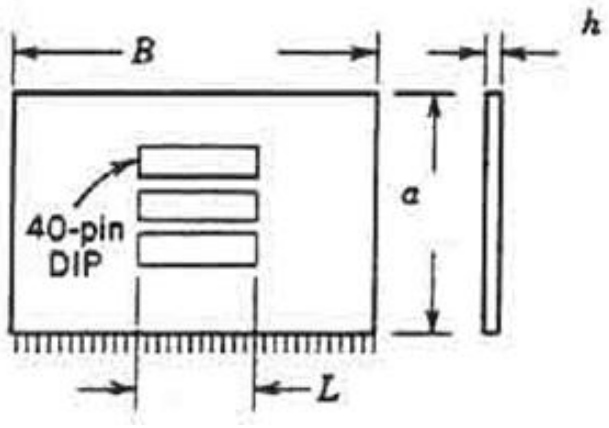

Figure 18-23: Dimensions of a typical printed-circuit board

Where:

— B = Length of PCB edge parallel to component

— L = Length of electronic component

— h = Height or thickness of PCB

— C =

1,0	for a standard dual inline package (DIP)
1,26	for a DIP with side-brazed lead wires
1,26	for a pin grid array (PGA) with two parallel rows of wires extending from the bottom surface of the PGA
1,0	for a PGA with wires around the perimeter extending from the bottom surface of the PGA
2,25	for a leadless ceramic chip carrier (LCCC)
1,0	for leaded chip carriers where the lead length is about the same as for a standard DIP
1,75	for a ball grid array (BGA)
0,75	for axial-leaded component resistors, capacitors, and fine pitch semiconductors

— r = relative position factor for component on PCB = {1, $\sqrt{2}/2$, ½}

— C =

1	When component at centre of PCB
$\sqrt{2}/2$	When component is at ½ point X and ¼ point Y on a PCB supported on 4 sides
0,5	When component is at ¼ point X and ¼ point Y on a PCB supported on 4 sides

The resonant frequency f for shock that avoids component failures due to excessive PCB deflection verifies $Z = \frac{9{,}8.A.G}{f^2}$

Where A is the shock amplification factor of a simple single-degree-of-freedom system excited by a shock pulse. **Typical values for the shock amplification range from about 0,5 to about 1,5, if the octave rule is followed.**

This yields into the following formula:

$$G = \frac{6.78E^{-4} \times B \times f^2}{A \times C \times h \times r \times \sqrt{L}}$$

SI units, all dimensions in [mm]

Where

— G = peak acceleration input to PCB, gravity units

— A = shock amplification factor

— f = resonant frequency (Hz)

NOTE In the US units, with all dimensions in [inch], the previous formula is:

$$G = \frac{1.35E^{-4} \times B \times f^2}{A \times C \times h \times r \times \sqrt{L}}$$

US units, all dimensions in [inch]

18.3.1.3.5 Finite Element Model of the PCB

A finite element model of the PCB can bring important information for the SDRA.

A modal analysis provides the PCB resonant frequencies. It can be used to simply identify the first mode and then apply Steinberg approach as described in the above chapter.

If the SRS at the base of the PCB is available, a response spectrum analysis (as described in section 18.2.4.4.3) can provide worst-case broadband information on the PCB deflection (to be compared to the allowed deflection proposed by Steinberg).

Finally, the model can be used to calculate the transient deflection of the PCB in a qualification environment, i.e. submitted to a half sine excitation for example, as explained in 18.3.1.3.2. Then, this information can be compared to the transient deflection calculated on another PCB of a FM unit submitted to a qualification time history measured during the shock test. This approach is relevant in the case of modular units for example.

18.3.1.4 Validation for acceleration sensitive components

If the SRS of the acceleration on a board can be evaluated, using the general transmissibility approach defined in section 18.2.4.4.3 for example, then it can be compared to the allowable SRS defined in Table 17-4 for various types of components.

A numerical approach is possible, as described in section 18.2.4, to get transient responses on the boards. It is relevant in the case of modular units when a new component (with respect to shock heritage) has been introduced for example. If the numerical simulation has been previously validated on the qualification test (applying time histories of the measured acceleration at the base), it is possible to compare the calculated accelerations on a board with the qualification values obtained by the component manufacturer. Table 18-2 illustrates such a summary table.

Table 18-2: Comparison between shock analysis and test at component level

Board	Analysis Results - Sensitive Point				Test results	Qualification method
	GROUP CODE	PART TYPE	CASE	G peak level	G peak level	MIL-STD-883 method 2002 Condition B
						g value/ msec
RT & STANDARD I/O	ASIC Digital	BACH-2	QFP256	700 g	610 g	1500g / 0.6 msec
	Crystal XO	QT25AC-24MHz	FP20			
	Memory EEPROM	28C010TFS-15	FP32			
AOCS & SPECIFIC I/O	ASIC Digital	Command Control	QFP208	650 g	560 g	1500g / 0.6 msec
	FPGA	RTSX32SU	QFP208			
	TL26-26V	TL26-26V	TO5			
PROCESSOR MODULE	Crystal XO	1104-Type 96MHz	FP20	520g	560 g	1500g / 0.6 msec
	ASIC Digital	TH1M242ES EPICA	352QFP			
	Memory EEPROM	28C010TFS-15	FP32			
	Memory EEPROM	79C0408	FP40			
	Memory SRAM	AT60142FT-DS17MSV	36FP			
	Memory SRAM	AT68166FT-YS20SV	68QFP			
	Microprocessor	TSC695F	QFP256			

18.3.1.5 General considerations on equipment design and verification w.r.t. shock

Before addressing the SRDA in details, it is important to recall the general process to be followed when developing a new design of electronic equipment. At least two different approaches, summarized in the Table 18-3, can be followed.

Table 18-3 Verification approaches for the design of an electronic equipment

Experimental approach	Mixed/Integrated approach (Test and Analysis)
Well suited when: • Equipment with modular concept • Heritage is available (availability of database for component allowable and mounting condition, overall equipment architecture) • Similarity between newly developed equipment and heritage is demonstrated (see Part 3 section **12.6**)	**Well suited when:** • Low heritage on components or equipment architecture • Analytical/numerical methods validated on previous equipment development
Usual design rules: • Analytical rules for adequate equipment design (e.g. octave rule from Steinberg to decouple supported elements from the equipment housing, solder joint failure on large component, number of I/F,…) • Company guidelines for PCB support (e.g. wedge lock, PCB bolted on frame) and component mounting conditions • Location of sensitive components and orientation of PCB considering severity of shock excitation.	**Usual design rules:** • Similar to experimental approach ones, supported by numerical predictions (Random/shock analysis on the complete equipment)
Development and validation plan: • Development model to validate the technologies not available in the heritage database (e.g. new type of component, mounting condition, new PCB dimension) • Development tests should be vibration AND shock (environment definition based on heritage qualification or company procedure)	**Development and validation plan:** • Development tests (vibrations and shock) to validate the technologies not available in the heritage database • Consistent shock simulation approach to be followed from early design to qualification, i.e. with step by step validated numerical models
Qualification: • Final qualification to be achieved on EQM/PFM equipment	**Qualification:** • Final qualification to be achieved on EQM/PFM equipment

In the SDRA context, the last step of the verification process, i.e. the qualification of the equipment, has not been achieved. **The SDRA thus consists in verifying the strict application of the rest of the process, i.e.**

a. Application of a verification approach (experimental or mixed) adapted to the equipment

b. Application of the usual design rules for the equipment

c. Application of the development and validation plan for the technologies

18.3.1.5.1 Experimental approach

a. Objectives

The objectives of early experimental shock tests can be:

- To minimise the risks before going shock qualification on QM unit.

  Preliminary shock tests can be performed on most critical components using mechanical architecture and mounting conditions representative of the QM.
- To increase the shock heritage on some parts to cover new shock specification if no QM is foreseen by the concerned program.

  A test vehicle is defined to bring sufficient shock heritage to components not covered by a previous shock qualification on similar unit.

A. CASE OF MODULAR EQUIPMENT - SHOCK TEST ON COMPLETE MECHANICAL MODEL

To increase shock heritage on some components not covered by a previous program, a technological module on which the concerned component families are mounted on PCB or structure is developed. Then, it is integrated in a Mechanical Model representative of the real unit: width, height, global modal behaviour, local modal behaviour on PCBs…

Example

The following figure shows a technological module with some critical components for which an increasing of the shock heritage was requested:

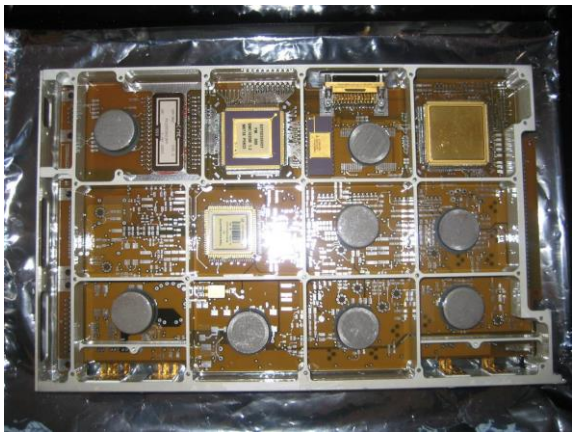

Figure 18-24: Module with critical components

Ballasts are glued on the PCB to lead to a representative global mass.

Then, this module is mounted inside a Mechanical model of the complete unit.

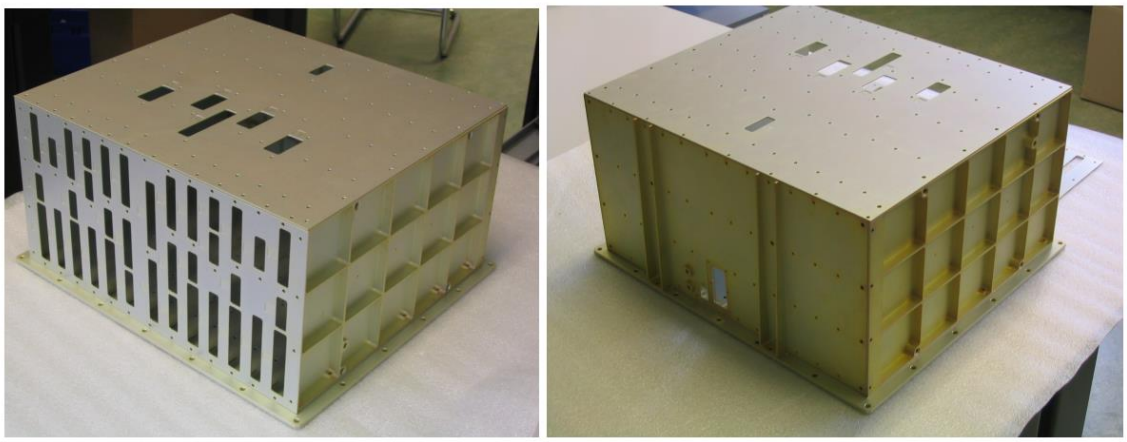

Figure 18-25: Unit Structural Model

This structural model is equipped with other dummy modules.

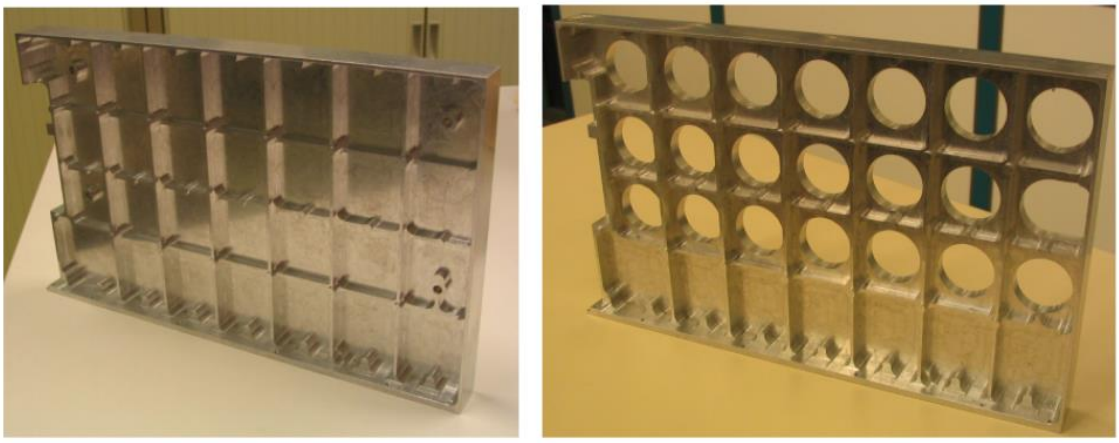

Figure 18-26: Dummy modules examples

The test sequence applied for the delta qualification (evaluation) is:

- Vibrations – 3 axes
- Shock tests

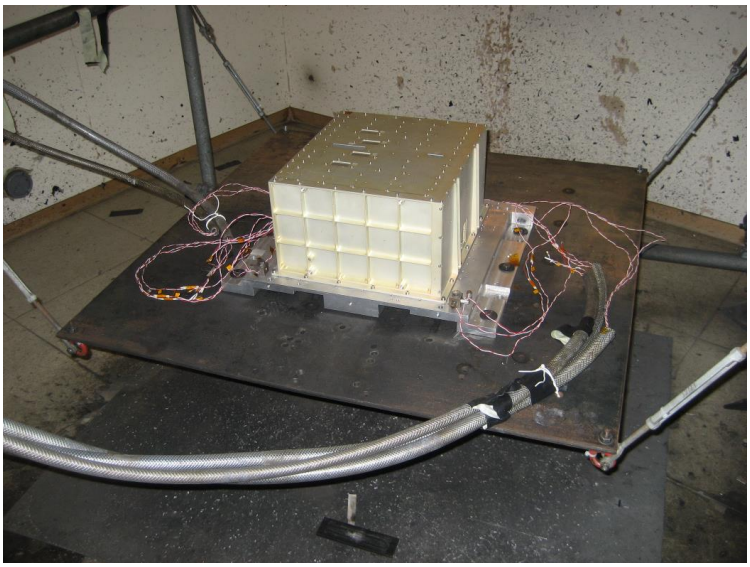

Figure 18-27: Shock test set-up - Technological module inside Structural model of the unit

B. CASE OF MODULAR EQUIPMENT - SHOCK TEST ON MODULE WITH ADAPTED MECHANICAL TOOL

To increase shock heritage on some components not covered by a previous program, a technological module on which the concerned component families are mounted on PCB or structure is developed. However, a Structural model of the complete unit is not always available. Then, it can be imagined to test a module alone (with the most critical parts) if this one is placed in an equivalent mechanical environment. For that, tools can be developed and validated to achieve a mechanical behaviour of the module identical to the one inside the global unit.

Example

The following example shows a modular unit constituted of slices, the modules, inserted in a backplane that itself constitutes the rear face of the unit.

Figure 18-28: Modular unit

The different modules are assembled together (module stacking) by use of squares directly machined in the front side of the module and by a common top cover.

Only one (EM) module was available to perform shock evaluation before going on EQM unit qualification. Thus, an additional mechanical tool has been developed to reach a global mechanical behaviour of the assembly close to the one of the complete unit.

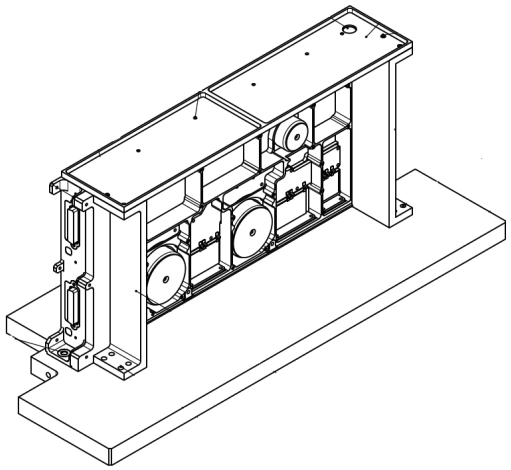

Figure 18-29: Mounting of the module to test with its shock test tool

The mechanical tool is developed to ensure the links of the module with:

- The platform
- The top plate of the complete unit
- The neighbouring module

The following mappings show the validation of the designed tool through Finite Element Models (comparison with the FEM of the complete unit).

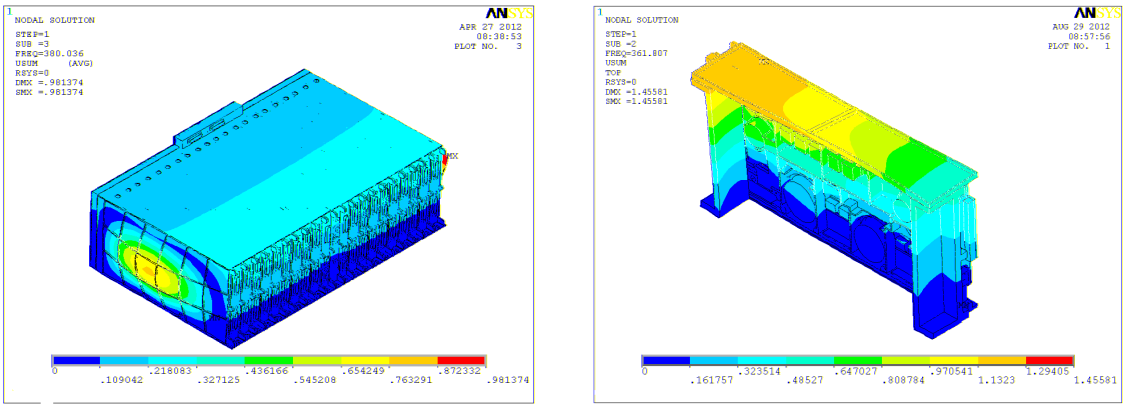

Figure 18-30: Comparison Complete unit vs. module + mechanical tool – First natural frequency

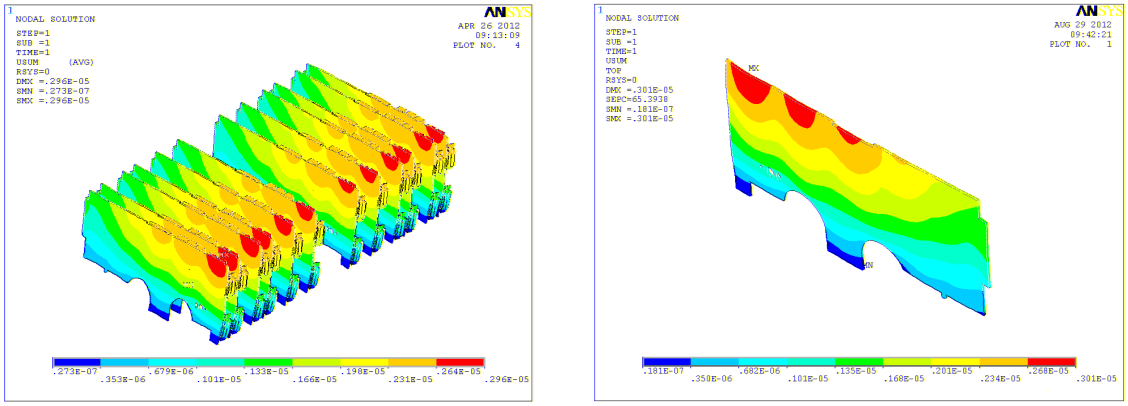

Figure 18-31: Comparison Complete unit vs. module + mechanical tool – Displacements under 1g load

The following test sequence is proposed to validate the behaviour of the technological module:

- Initial visual inspection
- Electrical test on critical components (ex: inductors and relays)
- Mounting of the mechanical tool
- Instrumentation (vibration sensors) of the module
- Sine survey to validate the mechanical tool
- Vibration tests campaign (if any)
- Instrumentation (shock sensors) of the module
- Shock tests campaign
- Final Visual inspection
- Electrical test on critical components (ex: inductors and relays)

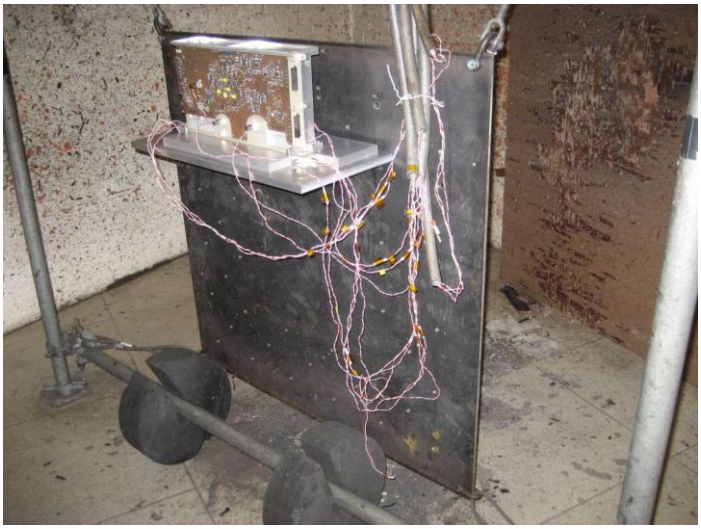

Figure 18-32: Overall view of the shock test set-up

C. CASE OF NON-MODULAR EQUIPMENT

The approach described in the previous paragraphs can be adapted to non-modular equipment. Shock evaluation (for new specification, to reduce risks on QM, etc…) can be performed on critical parts mounted in a Structural Model of the final unit. To be representative, the main mechanical parts of the unit are foreseen in the assembly. The global mass can be reached using ballasts glued on PCB or structure, with the objective to reach a global modal behaviour (for the main modes) close to the final unit. Additionally, the components are implemented with the mounting technology that is used in the nominal configuration.

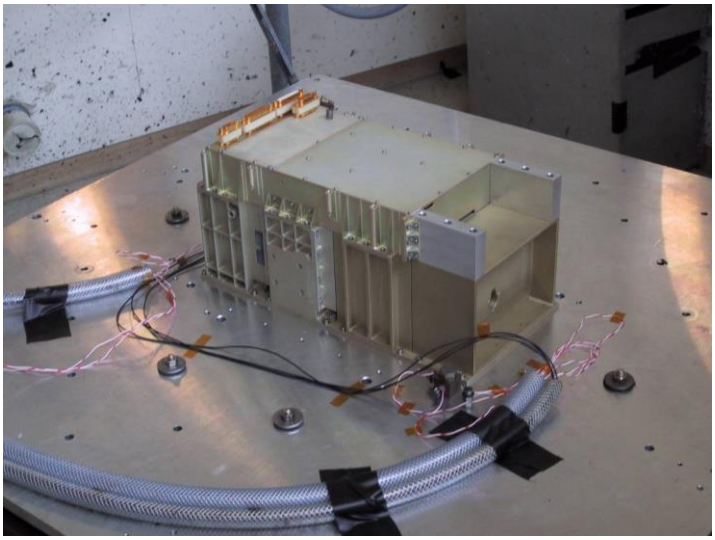

Figure 18-33: Structural Model of a Non-modular unit

18.3.1.5.2 Mixed/Integrated approach

The main difference with the previous approach stands in the fact that the development has been supported by shock simulations of the unit. The applied simulation approach should result from an heritage demonstration that the simulation gives suitable unit responses with respect to shock test measurements. Thus, among the various simulation methods discussed in Chapter 18.2.4, only the transient ones, i.e. method 1 and 2, seem relevant in this context. Method 1 is recommended in case the supporting structure is a flexible panel. Method 2 can be justified in case the supporting structure is very stiff.

Without this validation step, shock simulation results can be used to give general trends for design modification effects but they cannot be used as is in the SDRA context.

18.3.1.6 Important considerations for robust equipment design w.r.t. shock

18.3.1.6.1 Component mounting conditions

The example given in section 17.5.2.1 shows the importance of the component mounting conditions on the printed circuit board or on the structure. These mounting conditions can have different effects:

- a local resonance can be destructive if its frequency is highly excited by the shock (as in the above mentioned case), in particular if it is characterized by a low damping factor
- a low frequency local mode of the component filters the high frequency content of the shock on the component that could excite destructive internal resonances of the component
- a local dynamic behaviour can increase functional issues on relays by introducing additional degrees of freedom, rotation in particular

The following example illustrates the last point regarding functional issues on relays. Two TL relays were implemented on both side of a symmetrical board (Figure 18-34). One is directly bonded to the PCB and the other one is bonded on a column of composite material, with a few mm offset from the board. The PCB has been submitted to half sine shocks (3 axes) with levels varying from 600 g to 2200 g. Bouncing and transfers have been recorded. No transfer is observed with the relay directly bonded to the PCB (Table 18-4) but various temporary or permanent transfers have occurred with the other relay, starting at a level of 1800 g (Table 18-5).

The same issue can appear using an elastic cushion under a sensitive component. It reduces indeed the shock applied to the component but it can lead to functional issues (bouncing, transfer). **Thus, it not recommended for an electronic unit that is powered on during launch.**

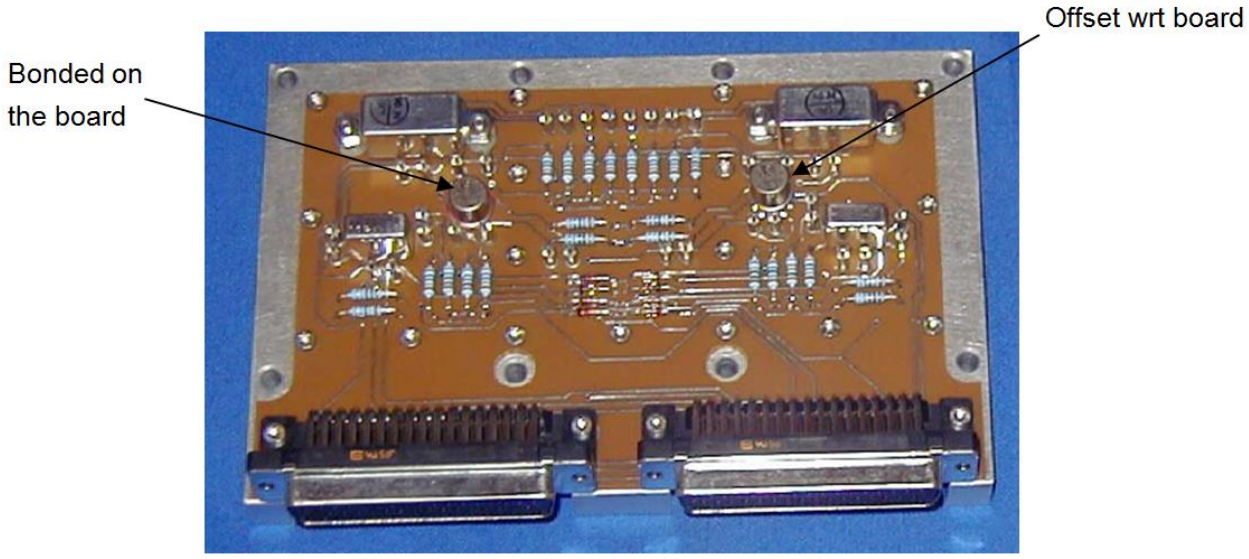

Figure 18-34: Symmetrical PCB equipped with two different TL relays

Table 18-4: Relay directly bonded to the PCB - No transfer up to 2200 g half sine

			M25					M26				
			µ coupure		Bascul. Transitoire		Bascul.	µ coupure		Bascul. Transitoire		Bascul.
			T (en ms)	t1 (en ms)	T (en ms)	t pulse (en µs)	Permanent	T (en ms)	t1 (en ms)	T (en ms)	t pulse (en µs)	Permanent
CARTE 1	600 g (0.5 ms)	axe X	-	-	-	-	-	-	-	-	-	-
		axe Y	-	-	-	-	-	-	-		-	-
		axe Z	-	-	-	-	-	0,4	0,02	-	-	-
		axe Z *	-	-	-	-	-	-	-	-	-	-
K5	1200 g (0.3 ms)											
		axe Y	-	-	-	-	-	0,3	0,02	-	-	-
TL collé	1200 g (0.5 ms)	axe X	-	-	-	-		3,4	0,1	-	-	-
		axe X #	-	-	-	-	-	1,5	0,02	-	-	-
		axe Y	-	-	-	-	-	6	0,08	-	-	-
		axe Y *	1,3	0,01	-	-	-	-	-	-	-	-
		axe Z	-	-	-	-	-	5,2	0,2	-	-	-
	1800 g (0.5 ms)	axe X	-	-	-	-	-	4,9	0,08	-	-	-
		axe Y	-	-	-	-	-	6,7	0,6	-	-	-
		axe Z	0,4	0,03	-	-	-	2	0,5	-	-	-
	2200 g (0.5 ms)	axe X	0,7	0,7	-	-	-	17	0,08	-	-	-
		axe Y	-	-	-	-	-	5	0,2	-	-	-
		axe Z	-	-	-	-	-	5	0,7	-	-	-
CARTE 2	600 g (0.3 ms)	axe X	-	-	-	-	-	-	-	-	-	-
		axe Y	-	-	-	-	-	-	-	-	-	-
		axe Z	-	-	-	-	-	0,18	0,02	-	-	-
K5	1200 g (0.3 ms)	axe X	-	-	-	-	-	5	1,5	-	-	-
		axe Y	-	-	-	-	-	0,02	0,02	-	-	-
		axe Z	-	-	-	-	-	5	0,3	-	-	-
TL collé	1800 g (0.3 ms)	axe X	-	-	-	-	-	9	0,6	-	-	-
		axe Y	-	-	-	-	-	5	0,4	-	-	-
		axe Z	-	-	-	-	-	4,7	2,4	-	-	
	2200 g (0.3 ms)	axe X	-	-	-	-	-	20 (8)	2	-	-	-
		axe Y	0,3	0,02	-	-	-	20	2,8	-	-	-
		axe Z	1	0,02	-	-	-	6	1,5	-	-	-

Table 18-5: Relay with a few mm offset w.r.t. the PCB - Various transfers starting from 1800 g half sine

			M27					M28				
			µ coupure		Bascul. Transitoire		Bascul.	µ coupure		Bascul. Transitoire		Bascul.
			T (en ms)	t1 (en ms)	T (en ms)	t pulse (en µs)	Permanent	T (en ms)	t1 (en ms)	T (en ms)	t pulse (en µs)	Permanent
CARTE 1	600 g (0.5 ms)	axe X	-	-	-	-	-	-	-	-	-	-
		axe Y	-	-	-	-	-	-	-	-	-	-
		axe Z	-	-	-	-	-	-	-	-	-	-
		axe Z *	-	-	-	-		-	-		-	
K6	1200 g (0.3 ms)											
		axe Y	-	-	-	-	-	1,4	0,25	-	-	-
TL	1200 g (0.5 ms)	axe X	-	-	-	-	-	1,6	0,2	-	-	-
		axe X #	-	-	-	-	-	1,8	0,1	-	-	-
		axe Y	-	-	-	-	-	5,2	0,06	-	-	-
		axe Y *	2	0,2	-	-	-	-	-	-	-	-
		axe Z	-	-	-	-	-	9	0,3	-	-	-
	1800 g (0.5 ms)	axe X	0,2	0,2	-	-	-	5,3	0,4	-	-	-
		axe Y	0,5	0,5	-	-	-	7	0,4	-	-	-
		axe Z	-	-	-	-	OUI	-	-	-	-	OUI
	2200 g (0.5 ms)	axe X	1	0,7	-	-	-	43	0,6	-	-	-
		axe Y	0,5	0,1	-	-	-	20	0,4	-	-	-
		axe Z	3	0,5	0,3	50	-	70	3,6	-	-	-
CARTE 2	600 g (0.3 ms)	axe X	-	-	-	-	-	-	-	-	-	-
		axe Y	-	-	-	-	-	-	-	-	-	-
		axe Z	-	-	-	-	-	1,3	0,02	-	-	-
K6	1200 g (0.3 ms)	axe X	-	-	-	-	-	3,8	0,5	-	-	-
		axe Y	-	-	-	-	-	4	0,7	-	-	-
		axe Z	-	-	-	-	-	3,6	1	-	-	-
TL	1800 g (0.3 ms)	axe X	0,3	0,1	-	-	-	7	1,5	-	-	-
		axe Y	-	-	-	-	-	6	1,5	-	-	-
		axe Z	0,8	0,1	-	-	-	9	2	-	-	-
	2200 g (0.3 ms)	axe X	0,4	0,25	-	-	-	24	1,8	-	-	-
		axe Y	-	-	-	-	-	25	1,5	-	-	-
		axe Z	-	-	-	-	OUI	26	5,8	0,03	30	-

18.3.1.6.2 PCB mounting conditions

Printed circuit boards should be fixed on rigid areas of the unit main structure.

It is not recommended to superimpose two boards maintained through spacers by the same screws on the same attachment points of the structure, as illustrated on Figure 18-35. For the out of plane shock excitation, this has resulted in a relay transfer on the top PCB but the phenomenon did not occur on the bottom one. It can be explained by the fact that the architecture emphasizes the dynamics of the top PCB. Spacers can indeed be shearing or the assembly mass and inertia can be creating an overall bending of the supporting structure.

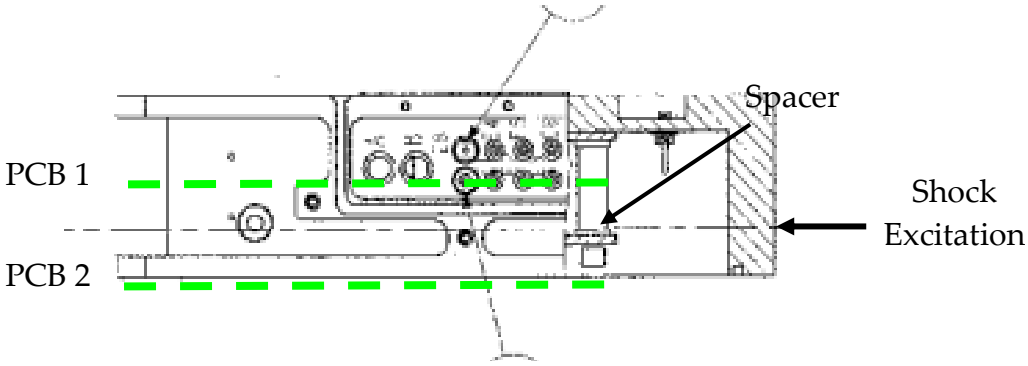

Figure 18-35: Electronic unit with 2 stacked PCBs

Large printed circuit boards (standard 2E or larger) can be attached to the unit main frame by means of wedge locks such as those illustrated on Figure 18-36.

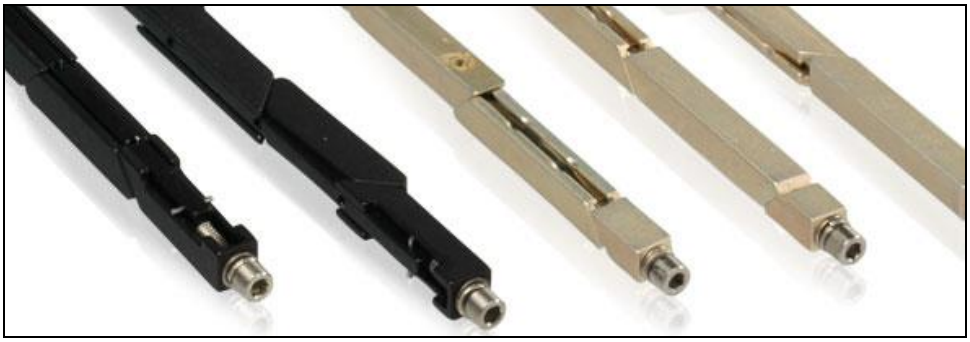

Figure 18-36: Wedge lock for PC Boards

The wedge lock is fixed to the PCB stiffener and the assembly is then inserted into a machined channel of the structure. Such attachment is compatible of a severe shock environment but it has not been demonstrated that wedge locks bring an additional filtering effect to the PCB response. Figure 18-37 shows a unit whose boards are attached with wedge locks to the top frame of the unit and screwed to the structure at the bottom. The out of plane response on the top of the boards has been measured and compared to the SRS level at the base of the unit in the same direction (Figure 18-38). It appears that the level on the PCB is filtered above 2000 Hz at one location and above 3000 Hz at another location. This is coherent with the worst-case transition frequency of 3500 Hz indicated in 18.2.4.4.2 for such units, with or without wedge locks.

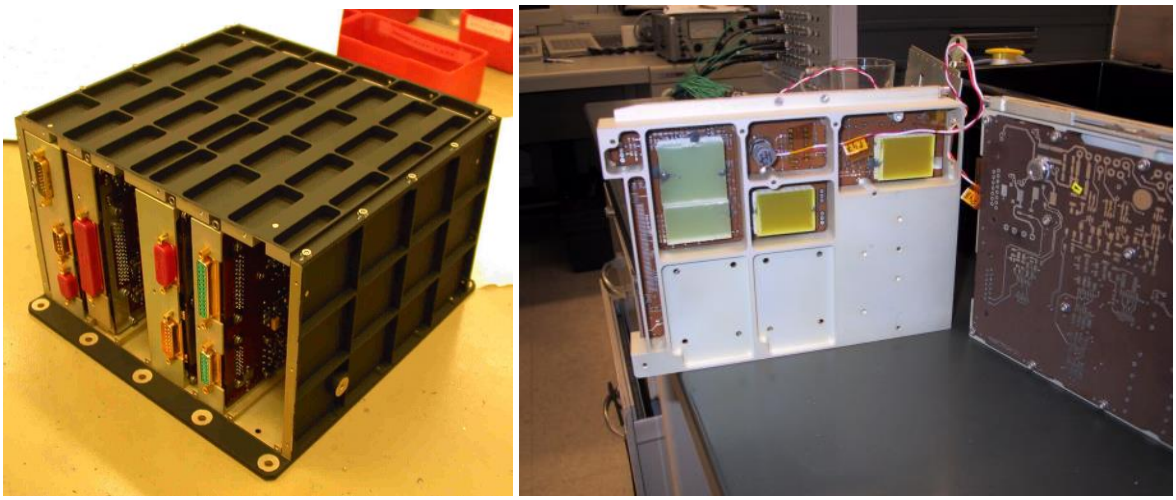

Figure 18-37: PC Boards partially fixed with wedge locks

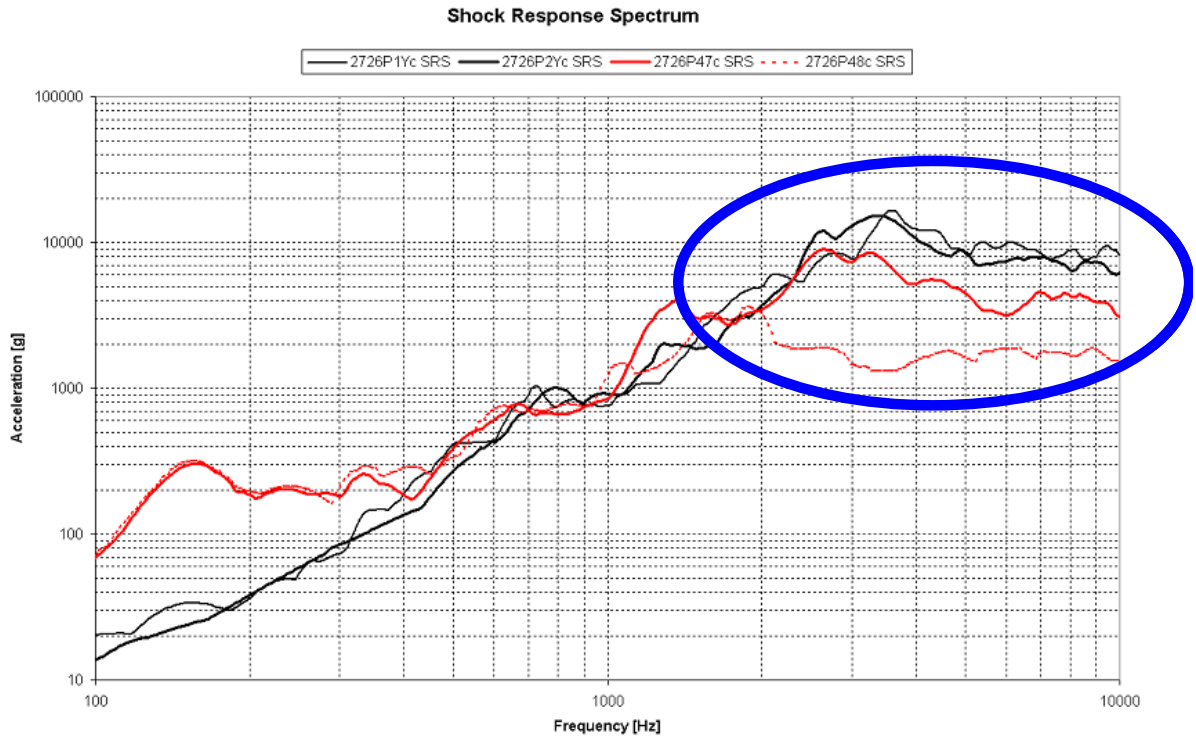

Figure 18-38: Out of plane shock response on a PCB fixed with a wedge lock compared to the SRS level at the base of the unit in the same direction

18.3.1.6.3 Shock acceleration distribution inside the equipment

The maximum value met on the acceleration time history measured on an electronic unit submitted to a pyrotechnical shock depends of the equipment area. Three different zones can be considered:

- the base plate (or basement of the equipment enclosure)
- the PCB frames (or walls of the equipment supporting the PCB)
- the PCB

The following table gives typical levels met on these 3 zones, the source of the shock being an expandable tube cutting symmetrically 2 mm x 3 mm sections of metal and located 1m from the equipment.

Table 18-6: Stacked equipment

Zone	Maximum acceleration time history
Base plate	6550 g
PCB frame	2190 g
PCB	1018 g

Table 18-7: Racked equipment

Zone	Maximum acceleration time history
Base plate	5568 g
PCB frame	5292 g
PCB	633 g

These results confirm the fact that accelerations are much higher on the base plate of the equipment than anywhere else. As a result, it **should be avoided to locate acceleration sensitive components on the base plate of the equipment.**

18.3.1.6.4 Influence of a local mass loading on PCB response

Tantalum capacitors have a very thin dielectric separation, obtained by a chemical process of oxidation; this thin dielectric layer is very sensitive to bending of the PCB support. So, it should be mounted in areas of PCB where the bending response under a shock applied to the equipment is minimized. In particular, it is not recommended to mount this type of component in an area where there is a sudden change in mass loading of the PCB, due to the presence of heavy components: the bending is growing in the intermediate area between heavy loaded and lightly loaded areas of the PCB.

18.3.1.6.5 Out of plane filtering on PCB versus position, edge/centre

The following example shows that the peak acceleration on the edge of a PCB is larger than the acceleration in the centre for a shock excitation in the perpendicular direction to board; it reaches 1500 g on the edge but only 1200 g in the middle. However the resonances of the board yield larger responses in the middle of the board for frequencies below 2000 Hz. The acceleration SRS in the middle exceeds by 10 dB the SRS on the edge of the board at 1500 Hz for example, as illustrated by Figure 18-40.

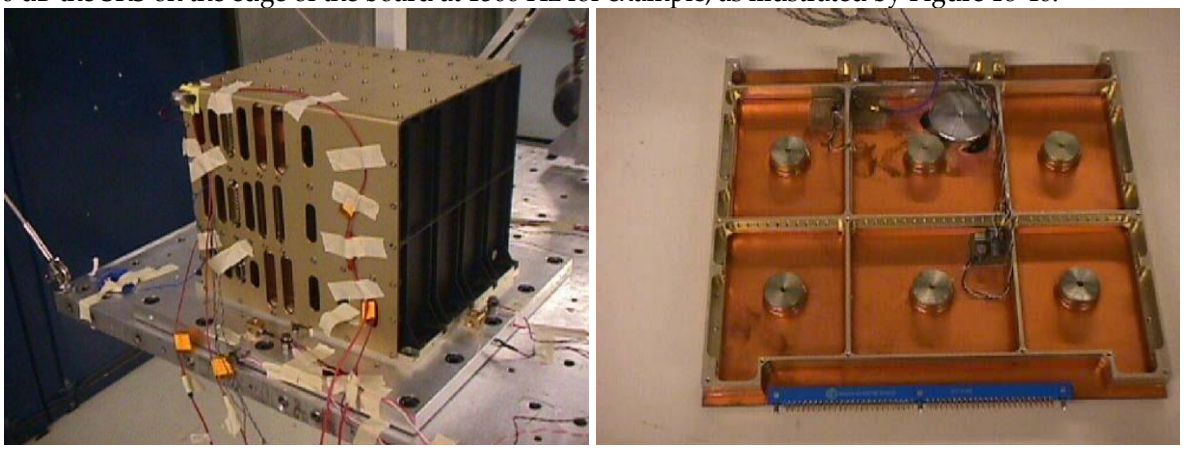

Figure 18-39: Tested equipment with instrumentation on PCB

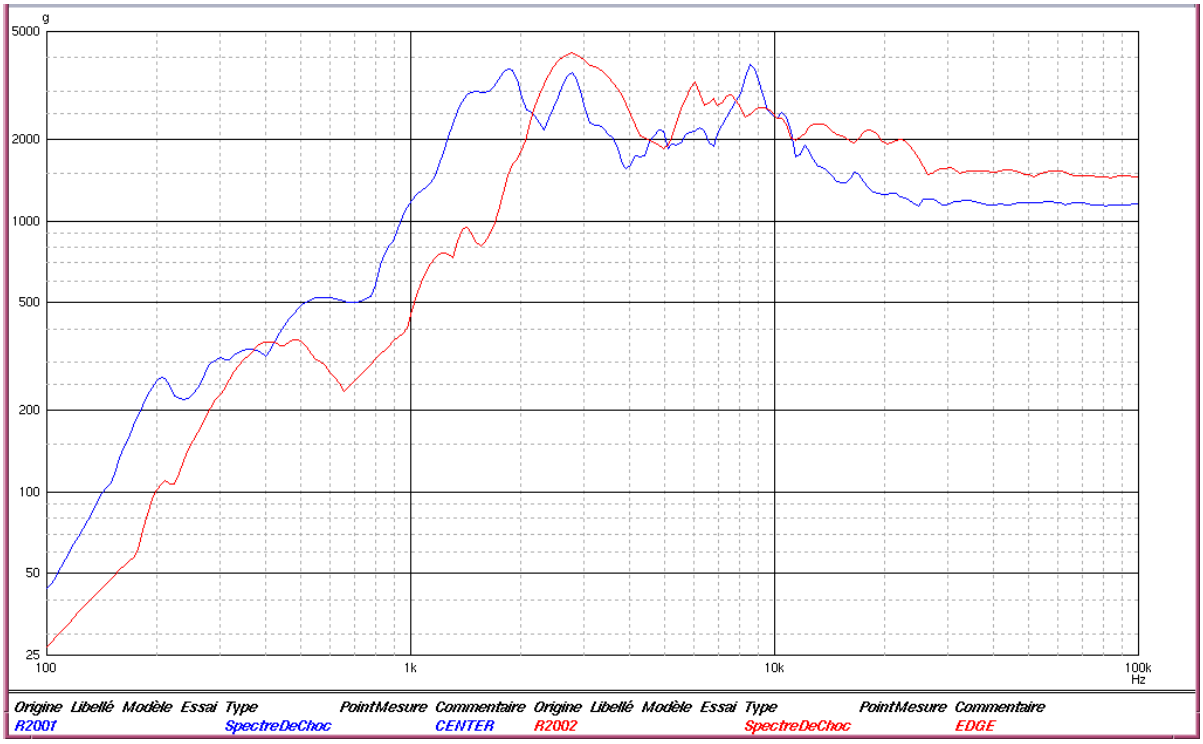

Figure 18-40: Measured SRS edge/centre on a PCB

18.3.1.6.6 Component mounting condition - Staking

See also paragraphs 18.3.1.3, 17.5.2.6, [RD-0121] and [RD-0122].

Local accelerations on printed circuit boards can be destructive for shock sensitive components. Another risk stands in bonded joints, as illustrated on Figure 18-41. If the issue is linked to an excessive deflection, it should be addressed like any other component mounting technology, referring to chapter 18.3.1.3. For heavy components, an excessive traction force can also be suspected. In this case, it is recommended to convert the local acceleration into a stress in the bonded joint simply applying Newton's law.

Figure 18-41: Pulled out component after a stringent shock test

18.3.1.6.7 Equipment mechanical design - Octave rule

In absence of relevant test data or numerical prediction, a simplified representation of the electronic system can be adopted, where chassis and PCBs are modelled as two-degree-of-freedom systems, in order to understand how dynamic coupling can occur between the chassis and the PCBs. The outer box or chassis structure is considered to be the 1st degree of freedom, after that the load path goes into the secondary members (2nd degree of freedom) such as modules and PCBs – See [RD-0113].

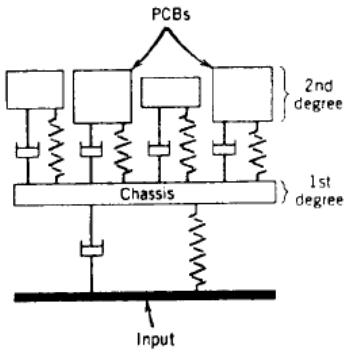

Figure 18-42: Typical representation of a chassis and PCBs as a two degree of freedom system

This type of representation, although simplified, offers the advantage to improve the physical understanding of the coupled system response. The resonant frequency of the PCB should be high enough to produce a small dynamic displacement, to avoid lead-wire and solder-joint failures. But it should also be well decoupled from the chassis resonant frequency to prevent further amplification of the PCB response.

The response to a half sine shock pulse for a two-degree-of-freedom system is shown in Figure 18-43 (lightly damped system). It evidences that the highest shock amplifications occur in areas that are between the frequency ratios R of 0,5 and 2,0, where $R = Freq_{PCB} / Freq_{box}$.

In this region, the shock amplification is only limited by the damping in the system. This quantity is usually crudely estimated, **therefore in a SDRA a high uncertainty on the shock amplification cannot be accepted, it should be verified that the octave rule is followed** (ratio R below 0,5 or above 2), to prevent coupling. The reverse octave rule (R below 0,5) is sometimes preferred since the PCB receives lower shock acceleration (PCB isolation area).

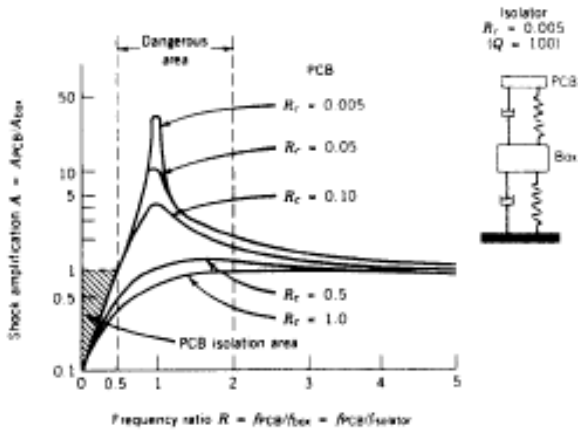

Figure 18-43: Shock response for a two-degree-of-freedom system with light damping, showing critical areas that should be avoided

18.3.1.7 SDRA example 1 – Damage assessment of a large hybrid on PCB

In the qualification process of SMART-1 and following the Shogun test, concerns have been raised that some equipment could not survive the required shock levels. Hence it has been decided to proceed to a Shock Damage Risk Analysis for the most critical units, before the equipment level testing.
In this frame, the following case has been encountered (large hybrid on PCB) and illustrates perfectly the solder overstrain aspect.

The transmissibility $F1_{sine}(f)$ between the equipment interface and this sensor has been extracted from the sine survey test ($F1_{sine}$=10 at 700 Hz, which corresponds to a shock transmissibility of around $F1_{shock}$=3). Whereas the shock transmissibility $F2_{shock}$ is already taken into account in the Steinberg's formula (through the parameter A).

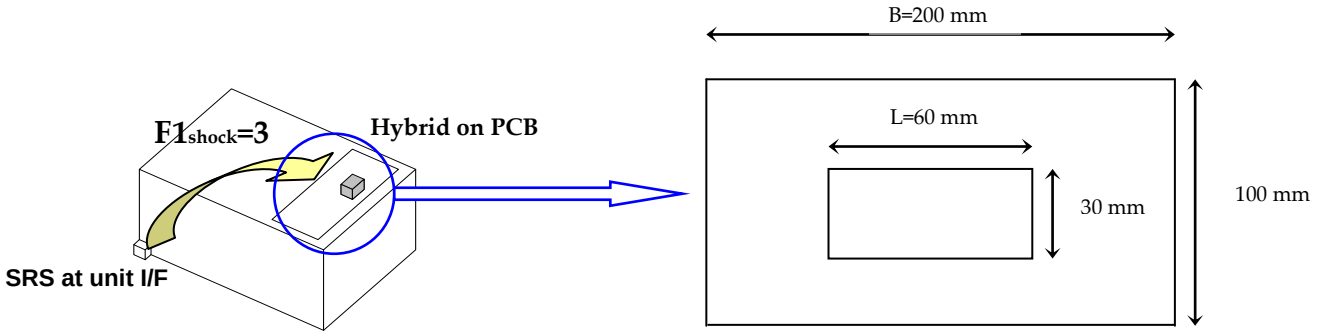

Figure 18-44: PCB dimensions and shock transmissibility characteristic

The parameters of this problem are:

- B = 200 mm
- L = 60 mm
- h = 1,45 mm
- C = 1,26 (DIP - Dual Inline Package - with side-brazed lead wires)
- r = 1 (component at the centre of PCB)
- f = 700 Hz (derived SRS level at unit interface showed high level at this frequency)
- A = 1 (the PCB mode was identified around 300 Hz (PCB development test), the reverse octave rule is satisfied in this case)

These parameters are then substituted into the Steinberg's formula (the one expressed in SI unit), to derive the maximum acceptable shock level at the PCB interface.

$$G = \frac{0.00665 \times 200 \times 700^2}{9.8 \times 1 \times 1.26 \times 1.45 \times 1 \times \sqrt{60}} = 4700g \text{ for the frequency of interest (f=700 Hz)}$$

This value is confronted to the qualification level at the PCB interface including the shock transmissibility factor.

$SRS_{PCB\ I/F} = SRS_{unit\ I/F} \times F1_{shock}$ In our case: $SRS_{PCB\ I/F}$ = 550 g x 3 = 1650 g

The resulting safety margin is positive: $\boxed{MS = \frac{4700}{1650} - 1 = 1.85}$

Considering this significant safety margin, the risk against shock is very low.

18.3.1.8 SDRA example 2 – Damage assessment of relay mounted on a PCB

The previous example could be completed to cover the case of a relay mounted on a PCB.

Let's consider that a relay GP250 is mounted on the same PCB. It should be assessed if the relay would suffer from any irreversible damage.

From Table 17-2, the maximum acceleration level supported by the relay GP250 is 1800 g (time history), which results in 3600g when converted to an SRS equivalent for frequency below 3 kHz.

It is verified that the reverse octave rule is followed; therefore the PCB receives a lower shock acceleration (PCB isolation area). An amplification factor of 1 is a conservative assumption ($F2_{shock}$ = A= 1).

The level at the relay interface is at most $SRS_{relay\ I/F}$ = 550g x 3 x 1 = 1650 g

This is compared against a maximum tolerable level of 1800 g x 2 = 3600g for the GP250.

The resulting safety margin is positive: $\boxed{MS = \frac{3600}{1650} - 1 = 1.18}$

The relay does not suffer from any irreversible damage.

In this example, the tolerance against bouncing and transfer would require a dedicated test database for the determination of an accurate threshold level (for bouncing and transfer).

18.3.2 Mechanisms – Ball bearings

18.3.2.1 Verification methodology

The SDRA process is shown schematically below. The main steps are identification of the supported bearing "payload mass", derivation of the external loads/moments and computation of the peak Hertzian ball-raceway contact stresses against which the damage risk assessment can be made.

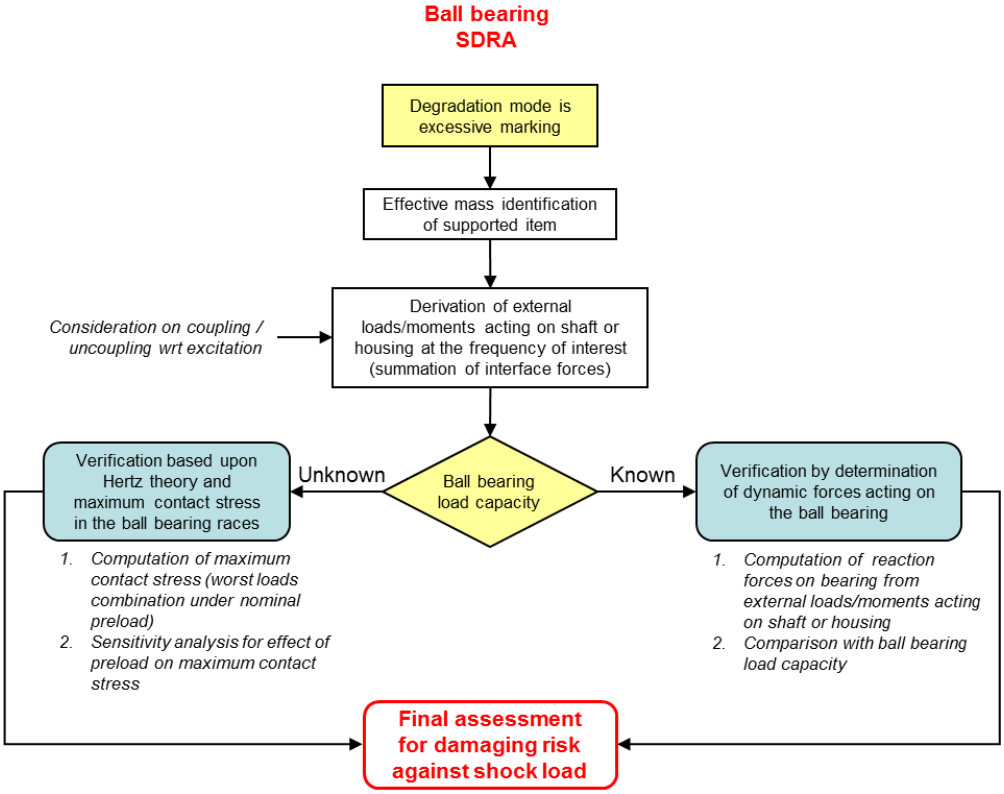

Figure 18-45: Rationale for mechanism SDRA (ball bearing)

18.3.2.2 Bearing applications

Rolling element bearings and in particular ball bearings are widely used in spacecraft applications such as scan mechanisms, reaction and momentum wheels, control moment gyros, solar array drives, deployment devices and optical pointing and tracking devices.

Rolling element bearings can be sub-divided into two classes, namely roller bearings in which the rolling elements can be of cylindrical, barrel-like or tapered form and ball bearings for which the rolling element is a truly spherical. In general roller bearings have much higher stiffness and load capacity than do ball bearings, but for space applications this advantage is offset by in general lower mechanical efficiency and less predictable and stable torque noise behaviour which they produce. Roller bearings are therefore infrequently used in spacecraft mechanisms. For this reason **the Handbook is confined to consideration of the effects of shock on ball bearings only**.

Within the ball bearing family, two types of bearing predominate, namely **Radial** (also known as **Deep Groove**) ball bearings and **Angular Contact** ball bearings. Examples of these are shown below in Figure 18-46.

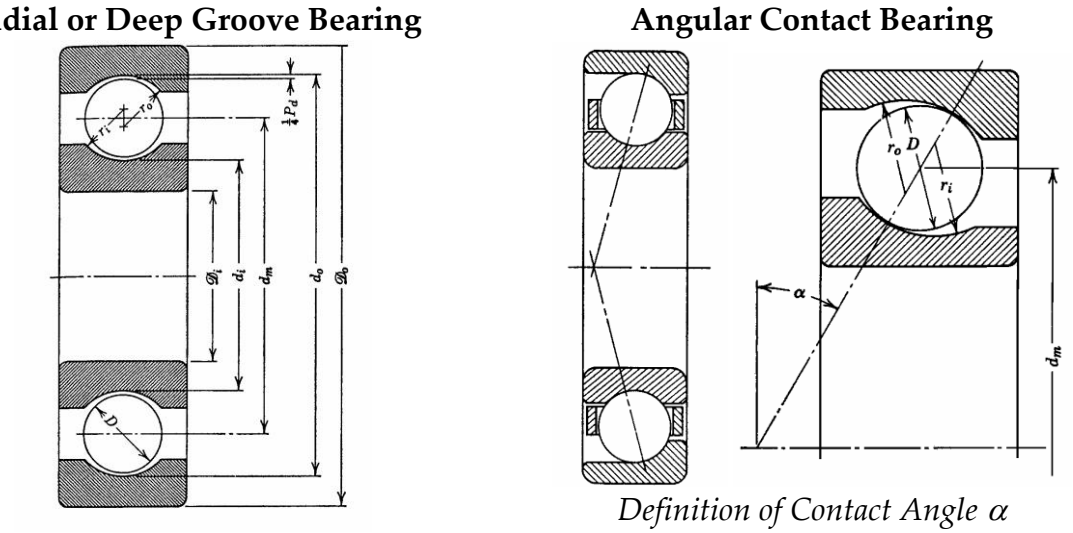

Figure 18-46: types of bearing

In both cases the detailed performance of the bearing is a function of the details of their internal geometry and material properties. A full treatment of this is beyond the scope of this Handbook, however some basic presentation of these features and a "mini-glossary" of bearing terms which can be found in manufacturers catalogues is considered appropriate.

In a radial bearing the balls are installed between essentially symmetrical grooves in the inner and outer rings. The radial bearing can be used singly or preloaded in pairs in which an axial preload is applied. If preloaded, the free (un-loaded) contact angle (line indicating the axes of the two elliptical points of contact between ball and raceway) depends on the size of the balls with respect to the so-called radial internal clearance (*Pd*) between balls and races (as shown) within the bearings. For angular contact bearings the contact angle is generated by the geometry of the bearing raceway.

In both cases the load capacity of the bearing is determined by peak Hertzian contact stresses between balls and raceway which in turn are a function of:

- Ball Size – i.e. ball diameter
- Bearing Pitch Circle Diameter (PCD) – usually taken as mean of bearing bore and outer diameters
- Ball complement – number of balls
- Contact Angle – as defined below/above * (usually in range 15° - 30°)
- Conformity – This ratio, (C) compares the raceway across track radius to ball radius. This is the most important parameter which defines contact stress within the bearing, but it is also often considered by bearing manufacturers to be proprietary data. C usually lies between around 1,035 and 1,15, with a lower value indicating a higher degree of "wrap around" between ball and raceway and so inherently better load capacity (though at the expense of some other performance parameters). Furthermore different bearing suppliers/manufacturers use different in-house terms for this parameter. Terms which can be met include:
- Osculation = 1/C (typically 0,87-0,97)
- Curvature/Transverse Race Curvature (%) = track radius/ball diameter (51,8 %-57,5 %)
- Total raceway curvature, B = C-1 (0,035-0,15)

Bearings are available in various precision grades (ABEC standard). In general higher grade bearings (ABEC 7 or ABEC 9) are fitted with better quality balls and have superior raceway surface finishes. Though not inherently more susceptible to shock damage, it is intuitively credible that higher grade

bearings would be more likely to suffer a significant change in running torque behaviour due to axial scuffing of lubricant or of raceway surface, than would a lower grade of bearing where changes to surfaces can be small compared to inherent surface features.

Other classes of bearing are shown below which are less common, but still used in space. These include, axial thrust bearings (in-essence like an angular contact bearing with zero contact angle), gothic-arch bearings (arched raceways with four points of contact per ball) and super-duplex bearings (essentially a matched pair of angular contact bearings with a common inner or outer raceway).

Axial Thrust Bearing	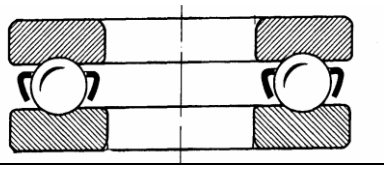
Gothic Arch (or X-type)	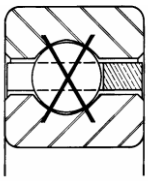
Super-Duplex (Common Outer Raceway)	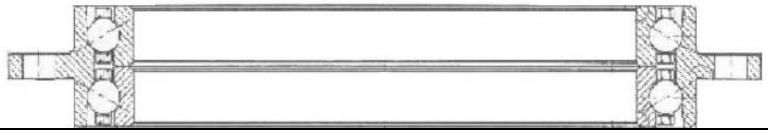

Figure 18-47: Other classes of bearing

With the exception of the axial thrust bearing, for all the remaining classes of ball bearing listed, as the preload or externally applied load is increased, the contact angle also increases. Indeed if the loading is radial or if a moment is applied the contact angle is different at each ball orbital position. For this reason, but also because of the nature of the Hertzian contacts between balls and raceways, the stiffness behaviour of ball bearings is somewhat non-linear with respect to externally applied loads (as in the case of shock loading).

The usual function of a bearing system is to locate a “bearing payload”, which can consist for example of a shaft with motor magnets and mirror attached in the case of a scan mechanism, with adequate stiffness when exposed to launch and in-flight conditions whilst providing very low or minimal and uniform resistance to rotation.

It is usual in design to use both radial and angular contact bearings in a preloaded pair configuration which provides a well-defined and repeatable stiffness and torque behaviour of the bearings both when exposed to the launch environment and in-flight. However, very rarely radial bearings are used in un-preloaded single configuration where stiffness is not important. ECSS-E-ST-33-01C requires the ball bearings to be preloaded within spacecraft mechanisms.

18.3.2.3 Methods of Bearing Preloading

There are essentially two categories of preloading technique which are classified according to the stiffness of the preloading element:

- **Soft (or Compliant) Preloading** - where the preload is locked into the bearing assembly using a relatively compliant (by comparison with bearing stiffness) spring as shown below, or by a diaphragm or other elastic means.
- **Hard Preloading** – where the preload is provided by means of a high stiffness element. Hard preloading can be achieved using a manufacturer-provided machined-in "offset", essentially a preload gap between rings which is closed by compression and locks in a manufacturer-defined preload. This configuration is known as a "matched pair" of bearings. In the case of the Gothic arch bearing an "internal" (i.e. no outer structure is required) preload is achieved by use of slightly over-size balls. In a hard-preloaded system, the lowest stiffness in the preload loop (shown in red below) can well be the bearing balls/raceway contact itself. A similar effect can be achieved if accurately machined spacers are used to separate the bearings.

Examples of typical soft (spring-preloaded) and hard preloading (matched pair) configurations are shown in Figure 18-48:

Example of Soft Preload (Back-Back Configuration) Achieved by Means of A Spring

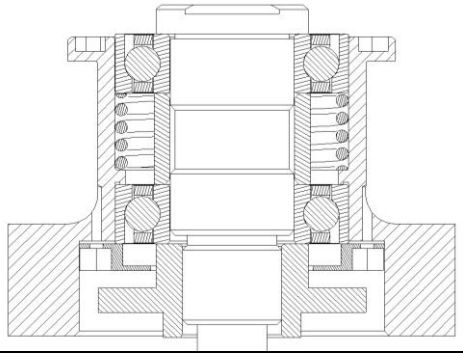

Hard Preload Achieved by Bearing Offset (preload gap) in Back-Back and Face-Face Configurations (preload load-path shown in red)

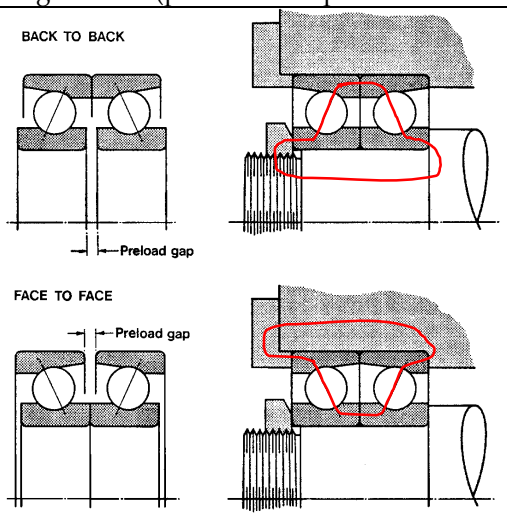

Figure 18-48: Examples of typical methods of bearing preloading

With conventional (i.e. non-variable) preload systems, it is important to identify a compromise between preload level and stiffness with respect to torque performance. High preload provides high stiffness for launch – but at the cost of possibly undesirable high torque and torque noise. Stiff preload is also preferred – but usually renders the bearing performance very sensitive to thermal gradients and generate higher torque noise than would a compliant preload system.

From the point of view of the susceptibility to the effects of shock, these two modes of preloading provide potential for quite different behaviours depending on the direction and magnitude of the external shock loading.

18.3.2.4 Bearing Damage

18.3.2.4.1 Overview

The consequences of shock-loading on bearings are believed to differ according to the amplitude, sense and orientation of the shock vector with respect to the rotational axis of the bearings.

There is also some sense in which modest loads which do not result in a gap between ball and raceway can be considered more benign than larger loads which cause "gapping". Gapping is the instantaneous off-loading of one bearing of the pair as the load on the other is increased due to external load or acceleration. Once the load on one of the bearings reaches zero, a further load opens a "gap" between nominal ball and raceway positions. When the external load or acceleration vector is reversed then balls and raceways can come into contact with large impulsive or so-called "hammering" loading which can provide increased peak stresses and therefore increased risk of damage. Furthermore for the duration of the gapping event the bearing pair ceases to behave as a pair (as only one bearing is loaded) and has much lower angular and radial stiffness behaviour and so an increased risk of bearing damage.

18.3.2.4.2 Pure Axial Loading

In this case if the shock is sufficiently large in amplitude and duration then the equivalent inertial force applied to the moving payload (usually the shaft assembly) overcomes the preload and a gap is caused instantaneously between balls and raceways of one bearing of the pair, both on the primary shock and during so-called back-lash shocks. The magnitude of the gap depends on the stiffness characteristic of the other bearing of the pair, and its preloading arrangement. For example if the bearing is compliantly (e.g. spring) preloaded, then the gap can become relatively large and there is at least the possibility of rotor/stator contact in some way.

In general the rotor/payload travel is limited by:

- contact between balls and reverse face of the raceway (radial bearing) – typically allowing of order 100 μm-200 μm travel

or

- contact between shaft and axial "snubber", usually some form of polymeric element, provided to limit travel – typically constrained to less than 100 μm

or

- contact between shaft and other static element of the mechanism (e.g. encoder read head, labyrinth seal, and end cap) – not intentionally by design and providing indeterminate and possibly variable gap size nominally identical units.

In compliantly preloaded bearings (e.g. spring or diaphragm preloaded) gapping is un-symmetric, in the sense that when the spring is in the load line there is potentially large gapping and shaft displacement, but when it is not, there could be no gapping at all provided appropriate measures permit bearing/shaft relative motion (see Figure 18-49).

Gapping can also occur in hard-preloaded bearing systems if the shock loads are sufficiently high compared to the preload (see Figure 18-50). For a hard-preloaded system with preload F_P, it can be shown that gapping does not occur if the axial load applied is < 2 x $2^{0,5}$ = ~2,83 F_P. Clearly in a hard-preloaded system, gapping is symmetrical, that is the same level of gapping is found regardless of whether the externally generated shock load is positive or negative in sense.

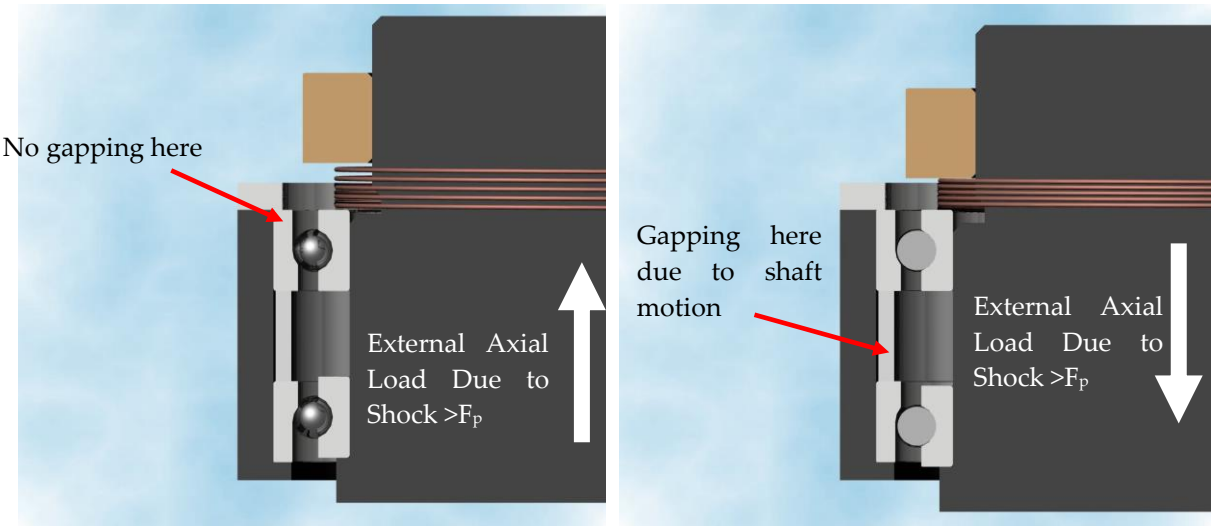

Figure 18-49: Axial Gapping in Compliantly-Preloaded Bearing System with Preload (Fp) Showing Asymmetry

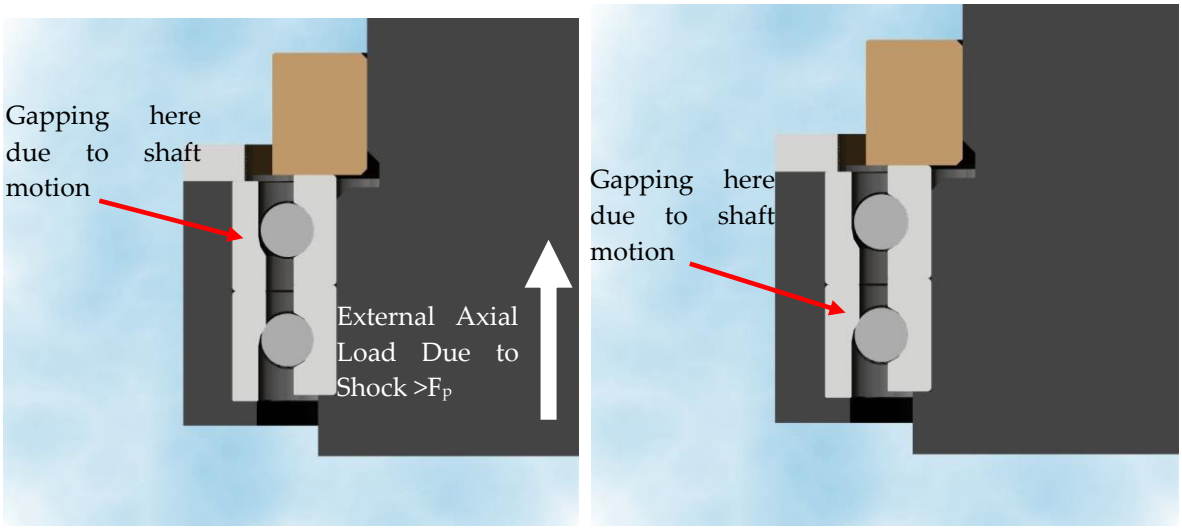

Figure 18-50: Symmetric Gapping in a Hard-Preloaded Bearing System with Preload (F_P)

Gapping is not prohibited by ECSS-E-ST-33-01C, however it is necessary to verify the adequacy of lubricant and potential consequential mechanism damage or degradation due to bearing, component or shaft motion. **This places the onus on the designer to demonstrate that IF gapping occurs, stresses remain acceptable and implications for bearing performance are demonstrated by test to be acceptable.**

18.3.2.4.3 Pure Radial and Moment Loading

When a bearing system is exposed to pure radial or moment loading – then similar behaviour can be expected, that is deflection limited by bearing system stiffness with increasing Hertzian contact stress and the possibility of gapping. Deflection is limited ultimately by contact with snubber or other mechanism element. In general it is not possible to identify whether axial or radial loading represent a worst case for stress – though the radial stiffness is often relatively high compared to axial stiffness. This means that the consequences of axial gapping phenomena are likely to be worse than radial.

18.3.2.4.4 Combined Loading

In this case, depending on the loads, both kinds of gapping can be foreseen.

18.3.2.4.5 Gapping Limits

One question which arises is the level of allowable gapping which can be safely tolerated by a given bearing application. This can be formulated in two alternative ways:

a. **How much gapping is allowable for a given bearing system under given acceleration environment?**

or

b. **With a certain fixed gapping (limited by the snubber gap setting), what is the maximum allowable external shock load such that some ball-raceway stress limit (for example the allowable ECSS peak Hertzian ball-raceway stress) is not exceeded during impact loading?**

Clearly the phenomenon of gapping is a complex one, taking into account dynamic behaviour of the bearings (essentially non-linear spring elements) under the dynamic vibration or shock environment. Given this there have been a number of "Rules of Thumb" which have been used over the years by industry in order to constrain gapping within reasonable limits, which we repeat below.

1. **Gapping Rule of Thumb 1** - Small amounts of gapping, defined as the space generated between balls and raceway – of order 20 μm (some say 30 μm) can be acceptable.
2. **Gapping Rule of Thumb 2** - IF damage results from gapping it usually occurs outside the running track of the balls (since under high axial vibration load, as in application of higher preload, the contact point between balls and raceway moves around the bearing raceway and indentation can be outside the normal running track).

Unfortunately, though often used, these Rules of Thumb are not substantiated by any traceable or systematic experimental programme. Furthermore Rule of Thumb 2 ignores the possibility of ball or lubricant damage and the requirement of ECSS that stresses should in all cases provide an appropriate margin.

The following discussion and design guidelines are applicable to axial bearing gapping only and have been developed based on an experimental programme at ESTL in which bearings supporting various masses were subjected to different levels of simulated launch vibration followed by torque testing and/or visual inspection. The intention was to provide some initial experimentally validated guidelines for designers which go beyond the industrial rules of thumb above. It is of course essential (and indeed mandatory under ECSS) to test designs produced using this approach.

18.3.2.5 Analysis of Bearing Loads, Deflections and Stresses

18.3.2.5.1 General

It is strongly recommended that for analysis of bearing loads and deflections an appropriate bearing analysis code should be used.

There are a number of proprietary codes available, built either on a Quasistatic (instantaneous force and moment balance) or a Fully Dynamic (time-stepping multi-body dynamics) methodology, including for example codes known as JONES, SHABERTH, ADORE and COBRA.

ESTL's CABARET bearing analysis code was developed under ESA funding and is strongly recommended (and available for a nominal licence administration fee for use by organisations in the ESA member states). CABARET is a Quasistatic code and many of its predictions have been validated experimentally. Comparisons have also been made between its predictions and those of a number of the proprietary codes mentioned above.

Bearing analysis codes typically enable load and deflections to be calculated, together with ball/raceway peak Hertzian stress analysis for steady state loading. If dynamic responses are calculated or estimated by other means, then such codes can also be used with some success in estimating conditions in bearings exposed to dynamic vibration and shock loading. This is the basis of the proposed approach for SDRA of bearings which compares predicted peak Hertzian stresses with allowable levels for the bearing materials and experimental data on performance with some lubricants.

However it is also necessary to understand the methodology for calculating the peak Hertzian contact stress in a single ball/raceway contact.

18.3.2.5.2 Hertzian Stress Calculation Process

The calculation of Hertzian stresses is a classical analysis much repeated in many text books. The ESTL-preferred formulation for this calculation is based on a method reported by Dowson and Higginson (see [RD-0114]) and is repeated here because it is a generalised elliptical contact analysis (suitable for all types of ball bearing contact) and is easily converted to spreadsheet form.

In calculating peak Hertzian contact stress it is normal to consider the most heavily loaded ball in the bearing (if radially loaded) or that all balls are equally loaded if axially loaded. The peak stress usually occurs at the inner raceway contact, however it is important to verify this by analysis of both contacts separately since it is sometimes the case that the bearing conformity is modified by the manufacturer to provide similar contact stresses at both raceways.

To analyse each ball-raceway contact of a bearing the procedure is as follows:

a. First of all, the bearing geometry and material setup should be defined.

   In the example below we assume a bearing with 10 balls, each of diameter 7,14mm. The bearing PCD is 31mm and as an example, we are interested in the highly stressed inner raceway contact. Assume the bearing is subjected to a uniform axial load of 100N, so that the normal load per ball is (10/sin α =) 38,6 N. The geometry is as listed below.

Ball Diameter (m)	D=0,00714
PCD (m)	d_m=0,031
Contact angle (°)	α=15
Conformity	C=1,14
Inner(I) or Outer (O)	L=I

Normal Load Per Contact Per Ball (N) P=38,6

b. We also define the material properties for the stress calculation and the reduced elastic modulus (a composite for the two materials in contact) as shown in Equation [18-1] below. In this example we define the bearing ball as "body a" and the ring as "body b".

Young's Modulus (ball) (Pa)	E_a=2,1E+11
Poisson Ratio a (ball)	ν_a=0,3
Young's Modulus (ring) (Pa)	E_b=2,1E+11
Poisson Ratio b (ring)	ν_b=0,3

c. The reduced Elastic Modulus (Pa) is then derived:

$$E_r = \frac{2E_aE_b}{\left(1-\nu_a^2\right)E_b + \left(1-\nu_b^2\right)E_a} \quad [18\text{-}1]$$

d. From the input geometry we define effective radii of curvature in the circumferential (ball orbital) x-direction and "across raceway" y-direction. Note here that the sense of the radius of curvature is by convention positive for convex and negative for concave surfaces. This means that (as shown in Equation [18-4] below) if we are interested in the inner ring/ball contact then the radius of curvature is positive in the x-direction and if the outer (i.e. L<>"I") the radius of curvature is negative, but of slightly larger magnitude.

$$r_{ax} = 0,00357 = D/2 \quad [18\text{-}2]$$

$$r_{ay} = 0,00357 = D/2 \quad [18\text{-}3]$$

$$r_{bx} = 0,01205 = \left\{ if\ L = I\ then\ \frac{d_m}{2} - \frac{D}{2}\cos(\alpha\pi/180)\ else\ -\frac{d_m}{2} + \frac{D}{2}\cos(\alpha\pi/180) \right\} \quad [18\text{-}4]$$

$$r_{by} = 0,00407 = -DC/2 \quad [18\text{-}5]$$

e. The actual geometry as defined in Equations [18-2]-[18-5] above is then transformed into a "composite geometry" with two bodies of effective radius, Rx and Ry. The Curvature Cum, R is also defined as below.

$$R_x = 2,75E-03 = \frac{1}{\frac{1}{r_{ax}} + \frac{1}{r_{bx}}} \quad [18\text{-}6]$$

$$R_y = 2,91E-02 = \frac{1}{\frac{1}{r_{ay}} + \frac{1}{r_{by}}} \quad [18\text{-}7]$$

$$R = 2,52E-03 = \frac{1}{\frac{1}{R_x} + \frac{1}{R_y}} \quad [18\text{-}8]$$

f. In order to check the correct definition of curvature sense, we confirm the check parameter C, as defined below is positive:

$$C = 328.69 = \left(1/r_{ax} + 1/r_{bx}\right) - \left(1/r_{ay} + 1/r_{by}\right) \quad [18\text{-}9]$$

g. In order to calculate the dimensions of the contact ellipse and the contact stress it is necessary to evaluate elliptic integrals. Fortunately a number of approximate algebraic expressions exist for these. Expressions from Brewe & Hamrock (see [RD-0115]) are used to approximately evaluate the necessary elliptic integrals. These expressions are defined below. The ellipticity parameter,

ζ, and elliptic integrals of first and second kinds, ϕ1 and ϕ2 are defined below (Equations [18-10]-[18-12]).

$$\varsigma = 4,6280 = 1,0339\left(\frac{R_x}{R_y}\right)^{0,636} \quad [18\text{-}10]$$

$$\phi_1 = 2,9471 = 1,5277 + 0,6023 \times \log\left(\frac{R_x}{R_y}\right) \quad [18\text{-}11]$$

$$\phi_2 = 1,0568 = 1,0003 + \frac{0,5968}{\left(\frac{R_x}{R_y}\right)} \quad [18\text{-}12]$$

h. The parameters of the Hertzian contact can now be calculated as shown below. The semi-major and semi-minor ellipse dimensions are calculated (Equations [18-13]-[18-14]) to permit the Maximum Hertzian contact stress (pressure) to be evaluated (Equation [18-16]). The normal approach within the contact (the amount by which the two loaded bodies move together under load) is also calculated (Equation [18-15]).

Semi-Major Ellipse Dimension (m)	a=2,63E-04	$\left(\frac{6\varsigma^2\phi_2 P.R}{\pi.E_r}\right)^{0.3333}$	[18-13]
Semi-Minor Ellipse Dimension (m)	b=5,69E-05	$\left(\frac{6\phi_2 P.R}{\pi.\varsigma.E_r}\right)^{0.3333}$	[18-14]
Normal Approach (m)	δ=1,79E-06	$\phi_1\left(\frac{9}{2\phi_2.R}.\frac{P^2}{(\pi.\varsigma.E_r)^2}\right)^{0.3333}$	[18-15]
Max Hertz Pressure (Pa)	σ_{max}=1,23E+09	$\frac{3P}{2\pi ab}$	[18-16]

The above methodology is easily coded by spreadsheet and has been shown to agree with bearing analysis codes (e.g. CABARET) to a very close approximation such that either the predictions of the CABARET code or of the above analysis can be used. The method is also combined with an impulsive model (described below) which yields a ball load (as input P above) to identify the effects of hammering during bearing gapping.

18.3.2.6 Consequences of dynamic behaviour

Clearly there are a number of ball bearing damage and degradation effects which can be caused by exposure to shock and the resulting displacements and contact stresses. These range from the results of excessive overloading (for example some form of plastic deformation or even fracture) at one extreme to minor local depletion of a solid lubricant film at the other which is classified more as degradation (i.e. not resulting in immediate end-of-life and possibly recoverable) than damage (which can be irrecoverable and imply end-of-life).

The effects of shock are believed to be variable depending on the type of preload (whether hard or soft), level and duration of shock, possible limitation of bearing axial travel by snubbers, magnitude of bearing payload (see later section) and lubricant in-use.

When examining bearings after exposure to shock or vibration it should be noted that in general, effects of vibration and probably of shock are less noticeable with most liquid-lubricated bearing systems (e.g. oils or greases) and more noticeable both visually and perhaps also from a performance

viewpoint in most solid lubricated bearing systems (e.g. PVD coatings of MoS_2, lead). This is because solid-lubricants are typically soft, low shear-strength materials and marks in such films are very easily detectable visually. The presence of such marks does not necessarily mean the performance of the bearings can be in any way compromised, though it can do so. This is because in many cases even the micron-level film thicknesses applied provide more than sufficient lubrication for the balls running on the bearings. Secondly when such marks are caused by extreme loading, they can be outside the normal running track and therefore have no impact on the operation of the bearings under normal operational conditions.

However scuffing of the lubricant in the ball/raceways contact zone can result in locally increased degree of ball/raceway conformance and thus an increase in the nominal running torque, perhaps also resulting in a build-up of re-adhered lubricant "debris" at the extremities of the contact zone which can contribute to torque noise.

Intuitively therefore it is believed that liquid lubricated bearings can be marginally less susceptible to performance degradation due to shock than would be an equivalent solid-lubricated bearing, because there is likely always some residual separating fluid film of lubricant present within the ball-raceway contacts and so much less likelihood that scuffing (except by generation of metallic wear debris) could occur.

In this section we list the possible deleterious effects of vibration and shock in some notional order of increasing severity.

- Local Recoverable Depletion of Solid Lubricant – having no long term adverse effect on bearing performance (see example below)
- Local Irrecoverable Depletion of Solid Lubricant – having an adverse effect on lubricant lifetime or bearing torque noise which can degrade pointing performance (for example) or reduce lifetime.
- Scuffing of Ball or Raceway Surfaces
- Settling at bearing rings/seats – potentially modifying preload after exposure
- Exceedance of ECSS Stress Design Margin at One or More Ball/Raceway Contacts
- Overloading of One or More Ball/Raceway Contacts (sub-surface yield)
- Gross Overloading of One or More Ball/Raceway Contacts (yield evident at surface) – (see example image below)
- Fracture of Balls (usually balls fracture before rings under gross overloading)

Figure 18-51 to Figure 18-53 show some examples of typical bearing features observable post-test.

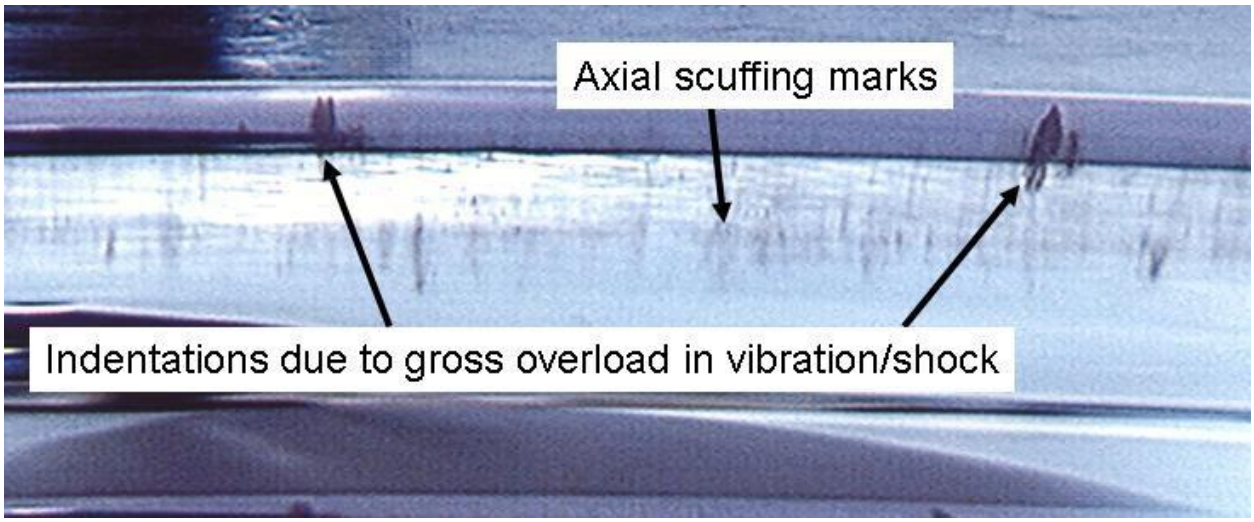

Figure 18-51: Image of raceway of grease-lubricated bearing (post cleaning) exposed to vibration, shock and gapping

After ~100 g peak response – but no post-test running

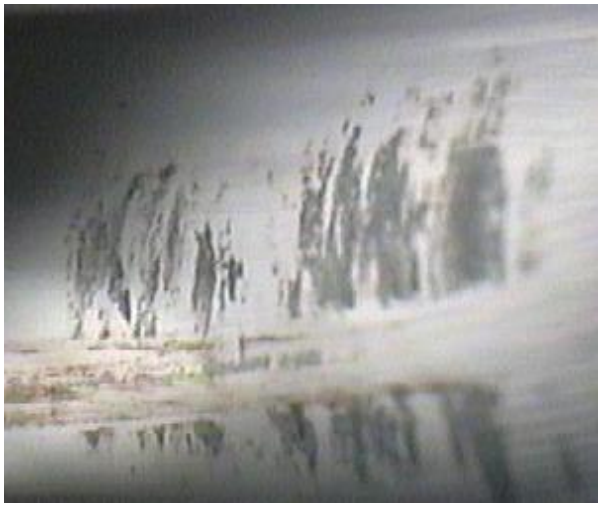

After ~ 270 g peak response but some revolutions of post-vibration running

Figure 18-52: Image of PVD lead-coated bearing exposed to vibration.

Left image shows normal running track, some free lead nodules, evidence of minor axial scuffing of the film (normal as it is very soft) and a central locally depleted zone with lead displaced at the outer edges of the elliptical contact. Right image (obliquely lit) shows a bearing raceway after exposure to higher acceleration and operation post exposure, from which it can be seen the lead is once again smeared across the elliptical contact zones by a brief period of operation providing some form of "recovery" (a view substantiated by torque measurements).

18.3.2.7 Logic for Allowable Stresses Resulting from Shock

The so-called catalogue static load capacity (or ISO 76 load capacity) of a ball bearing is related to the onset of sub-surface plastic deformation. There are two common bearing steels, 52100C and 440C which have slightly different material properties (hardness) and hence for identically designed bearings slightly different ISO 76 peak-Hertzian stress limits.

According to ECSS-E-ST-32-10C ([RD-0116]), designers should provide a margin of 25 % in stress terms against plastic deformation, hence bearings are de-rated by application of the ECSS standard by 25 % in stress terms or by around 51 % in load terms from their limitations for general industrial use. Interestingly the equivalent MIL and NASA specifications propose a derating of up to 30 % in load terms.

The de-rating process as applied to 52100C and 440C steels is shown in Figure 18-53 below.

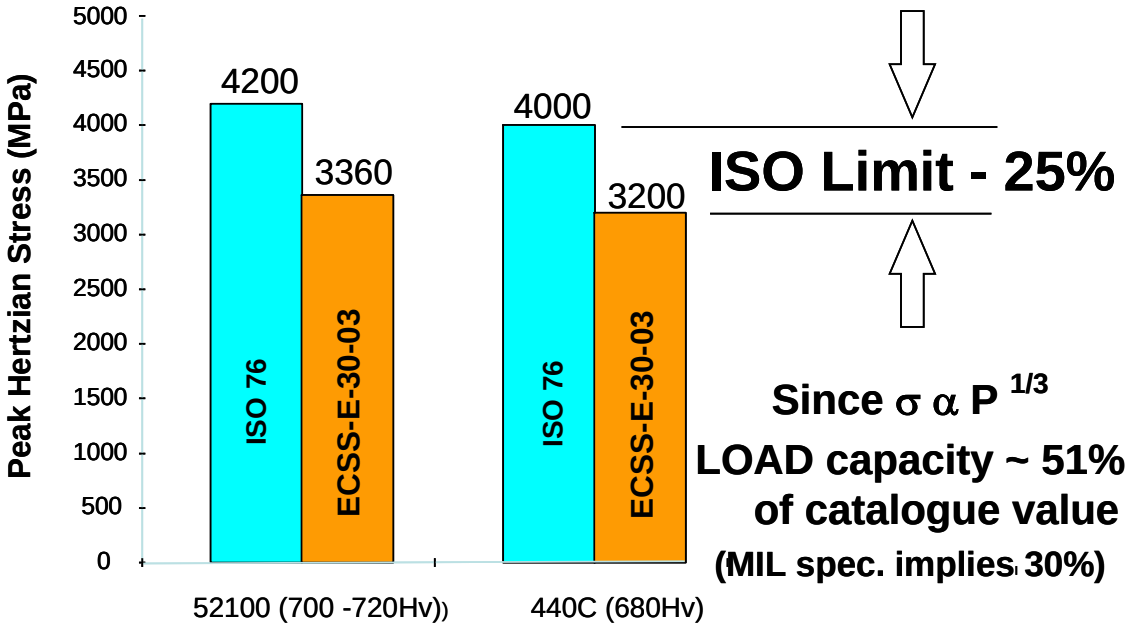

Figure 18-53: Comparison of Allowable Peak Hertzian Contact Stresses for %2100 and 440C Steels – ECSS Derating Process.

At the ISO 76 limiting stress levels, there can be sub-surface plastic deformation of the material – but this can essentially be elastically constrained by the surrounding material. There is usually no surface-visible indentation although there can be an indentation of order 0,0001 times ball diameter (0,5 μm for 5mm diameter ball) due to the strains resulting from constraining the sub-surface yield zone. In fact from experimental work carried out at ESTL, surface indentation is not "easily visible" (i.e. detectable under non-ideal lighting via microscope and with the location not precisely known beforehand) below a contact stress of ~5000MPa. Due to the relationship between peak Hertzian stress (σ) and ball load (P), $\sigma \alpha P^{1/3}$, if indentation is visible at the surface then the ball-raceway contact has been overloaded with respect to the ECSS design limits by at least a factor 3,29 as shown in the table below for 52100 steel. The appropriate US standard NASA-STD-5017 permits a slightly higher peak Hertzian stress "for bearings requiring smooth running".

Table 18-8: Peak Hertzian Stress

Peak Hertzian Stress (MPa)	**3360**	3720	4200	5000
Normalised Ball Load (Compared to ECSS Allowable)	**1**	1,35	1,93	3,29
Comment	**ECSS Allowable**	NASA Allowable	Nominal Design	Nominal Onset of "Visible" Surface Indentation

It should be noted that for hybrid ceramic bearings (usually ceramic balls and steel raceways) the steel properties (rather than the ceramic properties) prove to be the limiting factor on load capacity. For ceramic coated balls it is usual to assume that the ceramic coating is sufficiently thin to have no significant impact on the load capacity of the bearing – and so the bulk steel properties apply.

From the perspective of a shock damage risk assessment, except for the most demanding bearing applications, there is no functional degradation of the raceway at loads which induce stresses up to the ISO 76 limit and indeed there could be no degradation detectable up to peak stress levels as high as 5000 MPa. Note that this assessment ignores the role of the lubricant which can provide an over-riding logic for limiting the peak stress below the figures given in Table 18-8 above. This is discussed in 18.3.2.10.

18.3.2.8 Derivation of guidelines for SDRA of bearings

In this section the elements of a model for allowable gapping are described, prior to presentation of some examples of its use in the SDRA of bearing systems. The model was developed based [RD-0117] and has been modified for the specific case of SDRA application. The basic model is explained below.

It is well known that when a bearing ball is statically loaded against the raceway the stress increases with load and ultimately at approximately 4200 MPa (4000 MPa for 440C) there can be some local sub-surface plastic yielding. The displacement is accompanied by a certain "normal approach" movement of the centre of the ball relative to a datum on the bearing ring due to elastic deformation of the two bodies in contact. In order to estimate the impulsive loads during a dynamic collision, we have assumed that the ball is brought to rest in a distance equal to the normal approach corresponding to a certain stress.

For the SDRA, the level of stress used could be the ECSS limit (e.g. 3360 MPa), ISO 76 limit (e.g. 4200 MPa) or some more arbitrary limit – for example a peak Hertzian contact stress of 5000 MPa.

By imposing a stress limit – this effectively also limits the allowable gapping and "hammering motion" which could occur as balls and raceways return to contact.

We further assume that despite the bearing experiencing a shock of a certain duration, all of the collision energy is dissipated at the axial resonant frequency of the bearing and its payload (which can be estimated using the equation below).

$$f_n = \frac{1}{2\pi}\sqrt{k/m_2} \qquad [18\text{-}17]$$

Where:

— f_n = Axial first (natural) resonant frequency (Hz)

— k = Axial stiffness of bearing system (see NOTE) (N/m)

— m_2 `= "Payload" mass supported by the bearing system (e.g. shaft, mirror, and antenna motor rotor) (kg)

NOTE This is the tangential or local axial stiffness of the single bearing at a load which would cause off-loading of one bearing of the preloaded pair (i.e. at the preload for compliantly loaded bearings or 2,83 x preload for hard-preloaded bearings). This stiffness can in most cases be approximated using CABARET predictions.

The assumed response acceleration level at the bearing resonant frequency is generated using a shock-response spectrum technique (described earlier in the introduction of the handbook and based on a Miles equation approach).

Once gapping occurs, the bearings cease to behave as a pair until the moment of collision between balls and raceways and re-preloading. In this period one bearing of the pair is assumed to take all of the externally applied shock load and due to its stiffness characteristic, this bearing controls the gapping in the other bearing of the pair. In other words, a bearing model based on the stiffness of a single bearing in a forced 2-degree of freedom system excited at the resonant frequency of the system can be used at the onset of gapping. In this model, the bearing is treated as a linear spring with stiffness fixed at the value which causes the pair of bearings to offload (this is clearly a simplification as bearings have increasing stiffness characteristics with increasing load and hence the gapping predicted is slightly over-estimated). The bearing sits within a housing device (assumed rigid – this could be e.g. a scan mechanism or an instrument) into which the transmitted shock (derived from transmissibility method and SRS) is input and supports a payload (usually a shaft).

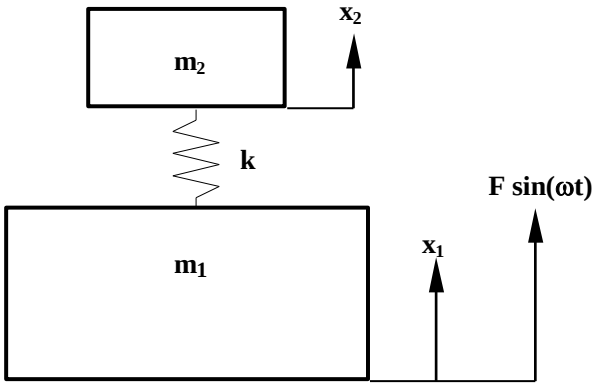

Figure 18-54: Simplified Bearing System Model

Mechanism of total mass m (= m_1 + m_2), housing device mass m_1 & bearing payload mass m_2. Bearing at moment of gapping modelled as linear spring of stiffness k and excited by an external force assumed to be sinusoidal at the bearing/payload mass natural frequency.

The equations of motion for this two-degree of freedom system can be written as,

$$m_1\ddot{x}_1 + k\left(x_1 - x_2\right) = F\sin\left(\omega t\right)$$
$$m_1\ddot{x}_2 - k\left(x_1 - x_2\right) = 0.$$

It follows that the amplitudes of oscillation of the housing device representing the static side of the bearing assembly (e.g. the instrument) A_1 and of the mass representing the bearing's payload (e.g. shaft with mirror, magnet, and antenna assembly) A_2 have the form,

$$A_1 = \frac{F\left(k - m_2\omega^2\right)}{\left(k - m_1\omega^2\right)\left(k - m_2\omega^2\right) - k^2}$$

$$A_2 = \frac{Fk}{\left(k - m_1\omega^2\right)\left(k - m_2\omega^2\right) - k^2}.$$

The relative displacement (or gapping) d of the bearing races is equal to the amplitude difference ΔA,

$$d = \Delta A = A_2 - A_1.$$

If the relative displacements are calculated at the frequency of concern, then by assuming that m_1 and m_2 move as a worst case in anti-phase and that balls and raceways collide impulsively (simplified impulse model also used) it is possible to calculate the resulting peak Hertzian contact stress level and thus the likelihood of damage due to the shock loading.

Clearly the above model elements all feature some simplifications of the complex dynamic problem which the bearings represent, however the predictions derived from this approach have been supported by experimental work in which the amounts of gapping (relative displacement) in bearings exposed to random vibration were measured non-intrusively and the torque performance of the bearings post-vibration was confirmed in-vacuum. The programme, which is reported in [RD-0117] examined two sizes of angular contact bearing which were both hard and soft-preloaded, and used a range of ball complements, payload masses, lubricants and cage types. The measured data suggests that if anything, the above approach tends to over-estimate gapping.

Furthermore absence of damage to test bearing raceways despite exposure to relatively heavy acceleration levels (up to almost $100g_{rms}$) suggests also that the experimentally experienced stresses are in-line with or perhaps slightly less than predictions.

The model from [RD-0117] has been further modified and updated in order to encompass the requirements of SDRA. This modification is mainly to the detail of the code, however an alternative formulation of the model including a Damping Factor has also been substituted in order to remove the extreme resonance behaviours if the SRS were to require analysis close to a bearing resonance. The model is also refined further by implementing a notional no-gapping rigid-body motion until the acceleration level is sufficient to generate gapping for a given bearing preload. This feature was omitted from the earlier version of the model which lead it to over-predict gapping in some cases.

18.3.2.9 Guidelines for calculating allowable shock-induced peak Hertzian contact stress levels and bearing gapping

The following methodology has been developed by ESTL in order to enable calculation of allowable shock loading and gapping levels whilst remaining within some nominal ball-raceway stress limits – whether the ECSS, ISO or other allowable stress limit.

It should be noted that whereas IN THE ABSENCE OF GAPPING the consequences of shock loading can be predicted by comparison of peak Hertzian stresses for the ECSS or ISO76 load capacities, IF predicted shock response levels are sufficiently high for gapping to occur, then there is a further reduction in the allowable loads due to the effect of hammering collisions which essentially reduces the allowable worst case shock response level.

The methodology is set down below in step-by-step format:

- Given the bearing type selected, calculate the approximate housing device mass (m1), the mass of the bearing "payload" m2 (usually the shaft, spacers, bearing inner rings, plus any shaft-mounted components (e.g. mirror and motor rotor)) and then identify the preload Fp and whether it is "hard" or "compliant"
- Compliant preload: Calculate the stiffness of a single bearing at Fp and the stiffness of the preload spring at Fp. Use the lower of the two values ask in Equation [18-17] above
  Hard preload: Calculate the stiffness of the single bearing at 2,83 Fp, use this for k in Equation [18-17] above (use CABARET for this as appropriate).
- Calculate the predicted first frequency (fn) using Equation [18-17] above. An assumed Damping Factor is used in order to limit the dynamic behaviour of the bearings to typical levels. From ESTL's test work with random vibration values of Damping Factor of 0,05-0,07 seem appropriate.
- Identify the frequency of most concern in the Shock Response Spectrum (fSRS) and the corresponding peak shock response acceleration g peak (SRS) at fSRS
- Calculate the single ball load and normal approach for the selected peak Hertzian contact stress limit based on the SDRA.

  This can be done by coding Equations [18-1] to [18-16] above into a spreadsheet, then using a "goal seek" function evaluate a load which gives in Equation [18-16] the desired peak Hertzian contact stress. Once this load is calculated reference to Equation [18-15] provides the corresponding normal approach.

  In most cases this allowable peak Hertzian contact stress can be 3360 MPa (52100 steel used) or 3200M Pa (for 440 C), however in some cases this can be increased perhaps to 4000 MPa, 4200M Pa or even 5000 MPa depending on the material in use, application and acceptable shock damage risk.

- At the frequency of interest calculate the impulsive ball-raceway collision force due to Hammering. This is done using a very simplified approach, in which the collision velocity is assumed to be the sum of outer and inner ring velocities (assumed 100 % out of phase). The loads generated are calculated on the basis that the relatively moving parts are brought to rest in a displacement equal to the normal approach at a desired stress level (for example at 3200 MPa). This provides an estimation of the impulsive load generated in the collision IF the desired stress level is not to be exceeded. With a "Hammering load" estimate made in this way the peak stresses during the collision can now be calculated.
- Using Hertzian analysis convert the Hammering force to a peak contact stress and compare this with the non-Hammering stresses generated at the same acceleration level. The larger stress is a limiting value. If this exceeds the limit from 5) above, then it can be that the shock exposure should be limited in order to remain within the criterion set.
- The above routine is for axial shock. A similar approach can be taken for radial shock provided that the radial stiffness of the bearing system is known.
- For a general case of combined axial, radial and moment shock applied simultaneously, it is proposed that the above approach be repeated for axial, radial and angular accelerations in turn.

The above approach can be taken as a first and simplified step in order to analyse any generally imposed external bearing loading. This loading can originate either from a primary or secondary shock (of from sine or random vibration loads), and indeed in general it is recommended that the analysis is carried out with both positive and negative shock loadings applied in order to avoid the possibility that the secondary/backlash shock, albeit of smaller magnitude, can result because of its sense, in excessive contact stresses above those expected in cases where a compliant preload is used.

18.3.2.10 Role of the Lubricant

The above analysis does not take into account any impact from the lubricant and is confined only to the effects of contact stress on the ball/raceway contacts alone and not the lubricant. This is deliberate since in MOST cases whether solid or liquid lubricated any disruption to performance of the bearings due to local lubricant depletion is temporary (if sometimes visually disturbing). Furthermore when SDRA is applied it is usually to a previously Qualified mechanism product/unit which has already been demonstrated capable of surviving Qualification vibration and shock levels, followed by successful bearing performance. Given this, the impact on the lubricant of additional shocks, or shocks of higher than anticipated magnitude is considered likely to be small if the allowable peak Hertzian contact stresses for the ball/raceway materials are not exceeded.

The following information has some relatively high degree of associated speculation, since there is little practical test data available. However in critical applications it can be considered advisable to ensure that **even during exposure to launch vibration and shock** the lubricant does not become exposed to peak Hertzian contact stresses which exceed a maximum allowable level defined with consideration to the lubricant lifetime rather than to the strength of its substrate. This can be the case if for example a solid-lubricant such as MoS_2 is used for which there is a well-defined peak Hertzian contact stress v lifetime curve (see Figure 18-55 below for typical lifetime data). In most cases even when exposed to stresses beyond such limits, the bearings "recover" and lifetime is likely not affected. However it can be the case that a more conservative approach is required if replenishment is not feasible and in such cases, it is important to take into account any known lubricant lifetime/contact stress relationship. In the SEVIRI example below, an allowable lubricant peak stress of 1500 MPa was imposed because of lubricant lifetime considerations (despite the bearings being manufactured from a 440 C steel which has an ECSS capability of 3200 MPa and an ultimate peak stress capability of 4000 MPa).

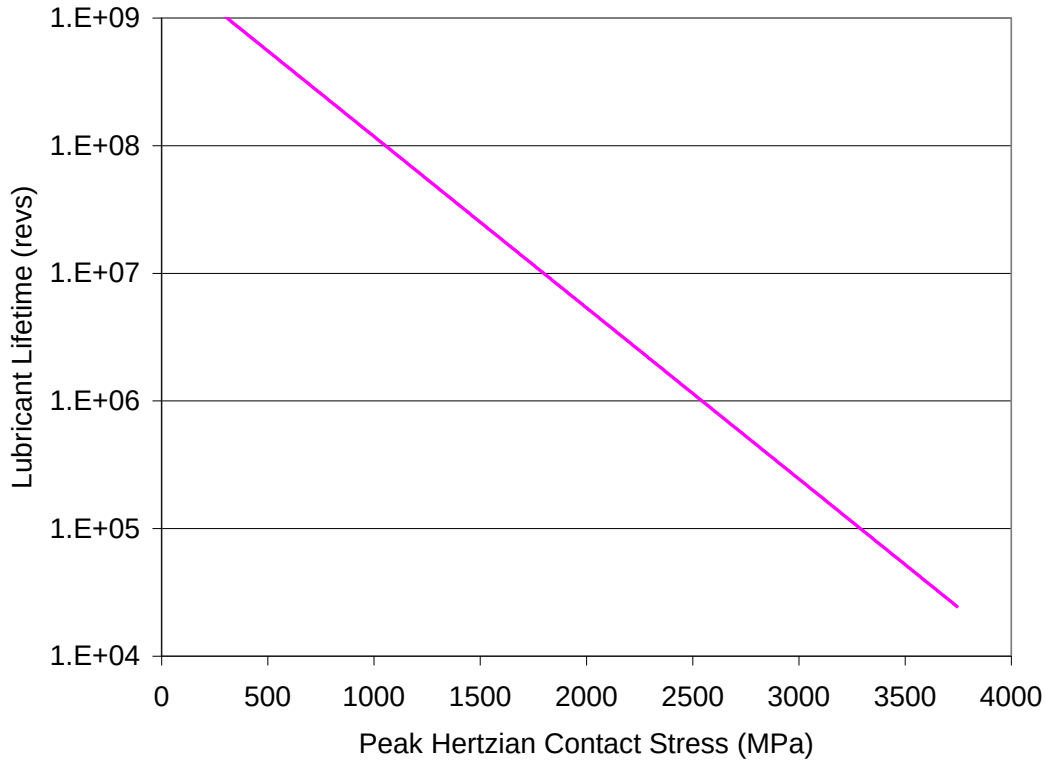

Figure 18-55: Typical lubricant lifetime v peak hertzian contact stress for PVD MoS_2 in ball bearings (life relates to rotation)

It should be noted that for liquid lubricated bearings, or for self-lubricating bearings (which effectively replenish the lubricant film during operation due to the presence of a sacrificial cage material) or for bearings lubricated by ion-plated or PVD lead, it should not normally be required to de-rate the allowable stress level, since for these lubricants there is evidence that the lubricant is either effective across a very wide range of contact stress, or self-recovering/replenishing. For most bearings lubricated by PVD MoS_2 film it can be sufficient to consider the film replenish-able (since such bearings often incorporate an MoS_2-containing cage material). However IF no possibility of replenishment exists, then the conservative approach outlined above, in which allowable stress is limited by lubricant lifetime requirements, should be taken.

We summarise in Table 18-9 below some tentative guidelines for allowable lubricant peak hertzian stress limits.

Table 18-9: Tentative Peak Hertzian Stress Limits for Lubricants Exposed to Shock (52100 Steel substrate assumed)

Lubricant	Lubricant Peak Hertzian Stress Limit (Assumes 52100 steel substrate)	Comment
Oils and Greases	4200 MPa	Possibly Higher – there is no evidence that exposure to stresses >4200 MPa during vibration/shock will deplete the lubricant performance in any way.
Ion-plated/PVD Lead	4200 MPa	Possibly Higher – presently considered to be functional up to the elastic limit of the substrate.
Self-Lubricating Bearings (e.g. PGM-HT)	4200 MPa	Since the lubricant is self-repairing and inherently torque "noisy" there is no evidence that for life considerations peak stresses in vibration or shock should be limited.
PVD MoS_2 with replenishing cage (e.g. PGM-HT)	4200 MPa	If film can be replenished, then allowable stress can be increased to the bearing capability
PVD MoS_2 alone (no replenishment possible)	Depends on Lifetime Requirement	For critical applications, limit stresses to achieve lifetime requirements for the application.

18.3.2.11 Examples and Application of Method

Based on system and subsystem dynamic responses (sine survey tests), and going back to real meaning of SRS (SRS makes sense only at responses of the subsystem), we now present some case by case analysis of the effects of shock on ball bearings.

The compatibility of the method is limited to the main modes of the subsystem (i.e. the main modes of the bearing system, taking into account possible uncertainties on the frequency).

Case by case analysis (for the main modes of the subsystem) based on summation of interface forces derived from FE analysis:

$$F \leq \sum_i M^{f_i}_{effective} . SRS(f_i)$$

$$F \approx \sum_i M^{f_{eqt1}}_{effective} . SRS(f_{eqt1}) + \underbrace{M_{residual} . SRS(f_{eqt2})}_{Covers\ QS\ dimensioning}$$

However where no FE analysis is available as an alternative approach a rigid mass is assumed (i.e. 100 % of mass participating) and this provides an over-estimate in load terms of the input at any frequency. However since for Hertzian contact stress is proportional to load ^{0,333}, then the overestimate in stress terms is less, typically around a 40 % - 70 % overestimate (assuming a typical error of a factor 3 - 5 say in the participating mass).

18.3.2.12 SDRA example 1 – MSG Scan Mirror Bearing

MSG, successfully qualified with respect to Ariane 4 shock environment, came across the problem that it did not formally fulfil the shock specification requirements imposed by Ariane 5 launcher authorities. Despite the use of attenuator devices, some concerns were raised that some equipment (and especially the SEVERI instrument) could not survive these required shock levels.

MSG being a meteorological spinning satellite, most of its instruments are scanning and rotating. This is realised by mechanisms guided by ball bearings. A special attention has been devoted to the shock verification of these shock sensitive items. In order to assess the risk of degradation/damage of bearings, detailed assessments of the contact stresses in the bearings race have been carried out with CABARET software.

The SEVERI scan mirror is mounted on a tubular frame with 2 pairs of angular contact ball bearings (in back-to-back configuration).

The geometrical/material data are the following:

- Outer diameter: OD = 120,65 mm
- Inner diameter: ID = 95,2 mm
- Ball diameter: d = 6,35 mm
- Number of balls of each row: Z = 40
- Nominal contact angle of balls: $\alpha_B = 36°$
- Osculation at outer groove radius: $\phi_o = 0,92$
- Osculation at inner groove radius: $\phi_i = 0,93$
- Material characteristics: E = 2,04 E+11 Pa, $\nu = 0,3$
- Nominal axial preload: $F_{preload} = 300$ N

The total mass of the scan mirror and the mirror frame is: M = 23,9 kg.

The investigated frequency range is (550 - 600) Hz, where slight exceedances are observed.

Considering that this frequency range is relatively high, the modes of the scan mirror (and associated effective masses) were computed using FE.

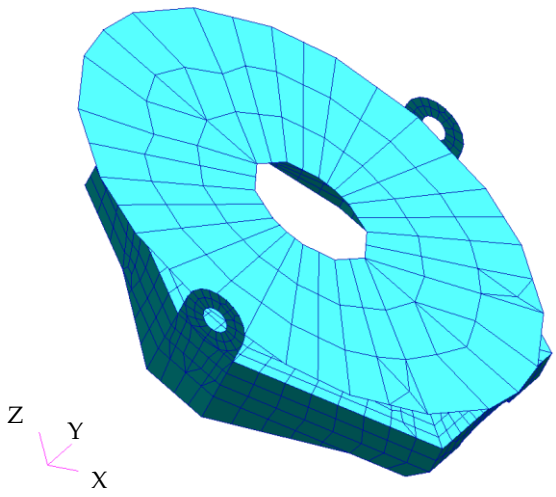

Figure 18-56: FE model of SEVERI scan mirror

The boundaries conditions used are the following:

- Clamped at Drive Unit I/F
- Supported at bearings I/F

As shown below, the most dominant modes are encountered below 300 Hz. Only small residual masses remain above.

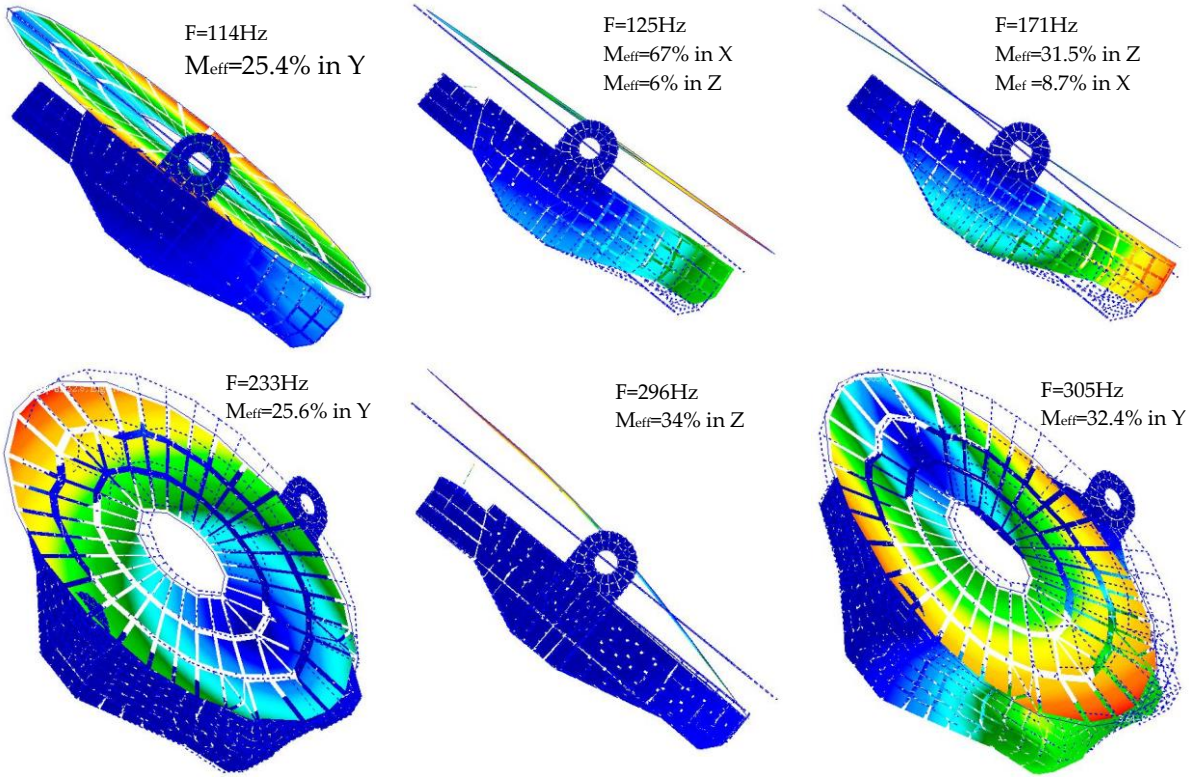

Figure 18-57: Scan mirror effective masses

Since no dominant mode exists in the frequency range of concern (around 600 Hz), no amplification is expected. Therefore, the excitation at 600 Hz can be easily derived from the SRS responses, which should be divided by a factor 3 (due to the transient (non harmonic) nature of the signal - Refer to the Introduction to the handbook):

$$\gamma_{axial} = \gamma_{radial} = \frac{60 \times 9.81}{3} = 196 m/s^2$$

a. Radial bearing direction – Load derivation

$$F_{radial} = \frac{60 \times 9.81}{3} \times \frac{24}{2} \times 0.3 = 705N \text{ (see NOTE)}$$

NOTE All residual mass is applied (30 %) at 600 Hz

b. Axial bearing direction – Load derivation

$$F_{axial} = \frac{60 \times 9.81}{3} \times \frac{24}{2} \times 0.2 = 470N \text{ (see NOTE)}$$

NOTE All residual mass is applied (2 0 %) at 600 Hz

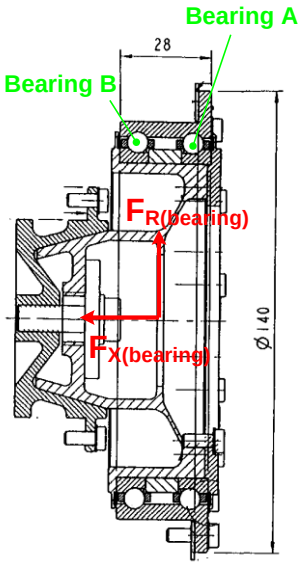

Figure 18-58: Bearings and loads terminology

The above axial load is insufficient to overcome the hard axial preload (this would require >~850 N ($300 \times 2 \times 2^{0,5}$) hence no axial gapping is predicted.

From CABARET analysis under the combined axial and radial shock loads during launch induce a maximum Hertz stress around **1150 MPa**.

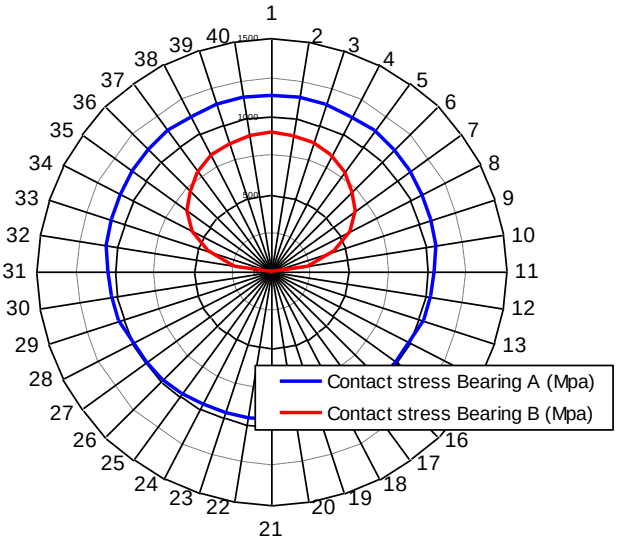

Figure 18-59: Stresses repartition in both bearing – CABARET computation

Table 18-10: Max stresses per bearing

σ_{max} - Bearing A	1141 MPa
σ_{max} - Bearing B	0 / 972 MPa

These values are well below a conservative figure of 1500 MPa selected for lubricant lifetime reasons. No damage is expected, life duration is not impacted.

Scan mirror bearings are therefore not an issue for this loading case.

18.3.2.13 SDRA example 2 – MSG Scan Mirror Bearing – Higher loads inducing gapping

For the same bearing IF an assumed axial load reached, say 850 N, then axial gapping would be predicted and thus there would be a possibility for hammering damage to the raceways.

In this section we assume the same bearing and payload conditions – however we further assume that the axial load is increased to 900 N, and then to 3000 N in order to demonstrate the role of gapping and hammering in modification of the predicted contact stresses.

Our model predicts that if the SRS dictates an input condition of 900 N at 600 Hz, then the gapping is around 50μm, but the corresponding peak Hertzian stresses is around 1300 MPa.

If on the other hand the frequency of interest were reduced (to 300 Hz) or increased (say to 1200 Hz) then using the methodology outlined above (see 18.3.2.9) reveals that for relatively low gapping, the highest stress occurs whereas for relatively high frequency of interest, peak stresses lower than the nominal combined case are generated.

This shows that the simple allowable gapping "rule of thumb" can in fact be inadequate in some circumstances.

Table 18-11: Shock induced peak hertzian contact stresses – 900N axial load

Axial Load of 900N Applied			
Frequency of interest from SRS	300 Hz	600 Hz	1200 Hz
Predicted Peak Hertzian Contact Stress	2080 MPa	1317 MPa	1036 MPa
Predicted Gapping	10 μm	50 μm	23 μm
Predicted Peak Hertzian Contact Stress From Quasistatic Analysis Ignoring Gapping/Hammering	1036 MPa		

If the axial load is increased to 3000 N as a further example, then the peak stresses and gapping as a function of frequency are also worth further consideration as shown below.

Table 18-12: Shock induced peak hertzian contact stresses – 3000N axial load

Axial Load of 3000N Applied			
Frequency of interest from SRS	300 Hz	600 Hz	1200 Hz
Predicted Peak Hertzian Contact Stress	4604 MPa	2914 MPa	1844 MPa
Predicted Gapping	38 μm	180 μm	75 μm
Predicted Peak Hertzian Contact Stress From Quasistatic Analysis Ignoring Gapping/Hammering	1541 MPa		

In this case the peak stresses exceed the bearing static load capacity at 300 Hz with a relatively modest 38 μm of gapping, whereas at other frequencies, much larger gapping levels are predicted (but stresses are lower). It is also notable that both at if gapping hammering is ignored, peak stresses predicted can be as low as 33 % of the stresses due to hammering. **Given this it is strongly recommended to identify as part of any SDRA whether the shock loads generated are sufficient to cause gapping and if so this should be identified a potential major bearing and lubricant risk factor.**

18.3.3 Valves

18.3.3.1 Verification methodology

Two types of valves should be distinguished, depending on their respective damage mode:

- Valves with mechanical "stop-end". The elastomer seal is in this case protected from degradation, and the damage mode is limited to a transient leakage due to mobile part lifting.
- Valves without mechanical "stop-end". The damage mode can go from a transient leakage to a permanent leakage (due to seal degradation).

The rationale for a valve SDRA is further developed in the following flowchart.

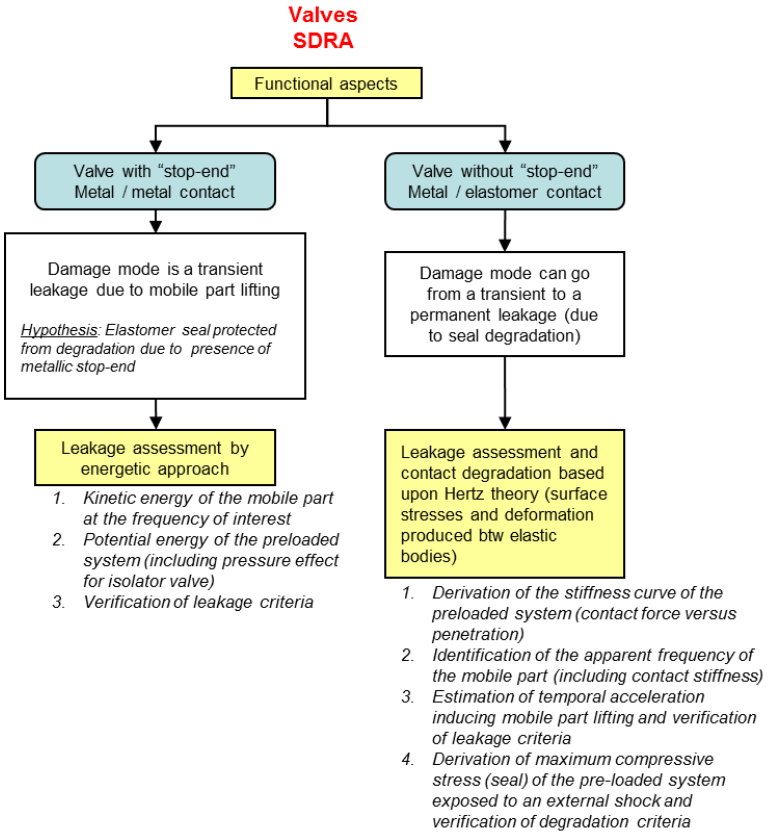

Figure 18-60: Rationale for valve SDRA

Irrespective of the type of valve, a valve is always preloaded and can be used in isolation or regulation mode. In the case of isolation mode, a back pressure (acting against the preload) is considered in the assessment. Additionally, the SDRA should be limited to the valve sensitive axis (defined by the constrained displacement of the mobile parts).

The verification methodologies are further developed in the Figure 18-61. The transient leakage assessment results from an energetic approach (comparing the total potential energy stored in the system to kinetic energy of the mobile parts), whereas the seal degradation (leading to a permanent leakage) is assessed following the Hertz theory for contact stresses and deformations produced by pressure between elastic bodies.

Valves with mechanical "stop-end"

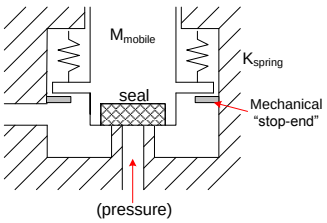

- Calculation of Kinetic Energy of mobile parts:

$$E_c = \frac{1}{2}.M_{mobile}.\left(\frac{Q_{shock}.Acc.9.81}{2\pi.freq_{acc}}\right)^2$$

Where:

Q_{shock}: amplification factor to cover eventual coupling between excitation and internal resonances (identified through sine survey or analytically considering a 1 dof system)

Acc: maximum SRS acceleration at the valve interface within critical frequency range, at a frequency $freq_{acc}$

- Computation of Potential Energy stored in the system (spring + eventually pressure):

$W_{spring} = F_{spring}.dl \quad (\text{for short stroke})$

$W_{pressure} = P_{input}.S.dl \quad (\text{for isolation valve})$

- Verification of leakage criteria:

— Isolation Valve

$$SM_{freqacc}^{opening} = \frac{W_{spring} - W_{pressure}}{E_c} - 1$$

— Regulation Valve

$$SM_{freqacc}^{opening} = \frac{W_{spring}}{E_c} - 1$$

If SM>0 ➔ no transient leakage

Valves without mechanical "stop-end"

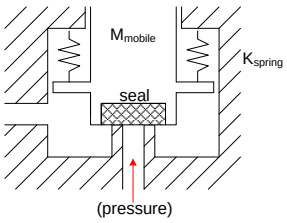

- Evaluation of the elastomer seal deformation based on Hertz theory:

The body in contact with the elastomer seal is considered to be a cylinder (developed torus) with an equivalent length of

$$L_{circ} = \pi\frac{D+d}{2} \quad [m]$$

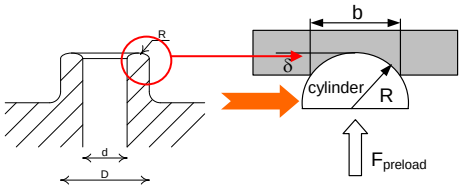

The flux applied on the elastomer is: $P = \frac{F_{spring}}{L_{circ}}$ [N/m]

The width of rectangular contact area is given by:

$$b = 1.6\sqrt{P.K_D.C_E}$$

Where P is the load per unit length (flux)

$K_d = D_{cyl} = 2.R$

$$C_E = \frac{1-v_{steel}^2}{E_{steel}} + \frac{1-v_{elastomer}^2}{E_{elastomer}}$$

The penetration δ due to the preload can be computed:

$$\delta = R.\left(1 - \cos\left(Arcsin\left(b/2.R\right)\right)\right) \quad [m]$$

- Derivation of the stiffness curve of the preloaded system:

The evolution of the contact force with respect to the penetration δ can be evaluated. Hence around the preload, the contact stiffness becomes $K_{contact} = \frac{F_{preload}}{\delta}[m]$ (valid for small δ).

Once the contact stiffness is known, the sensitive natural frequency of the valve can be determined (1dof system with 2 parallel springs). In case this natural frequency falls within the critical frequency range of the valve, it is necessary to verify the leakage criteria and to assess the degradation of the elastomer seal.

- Damage assessment of elastomer seal:

The flux applied on the elastomer is computed including the external force acting on the mobile part (at natural frequency):

$$\Rightarrow p = \frac{F_{ext} + F_{preload}}{L_{circ}}[N/m]$$

When substituting this value into the Hertz formula, the maximum compressive stress is derived (as maximum allowable, 50MPa is a generic safe limit).

Figure 18-61: Verification methodology for valves with and without "stop-end"

18.3.3.2 SDRA Example 1 – Valve with mechanical "stop-end"

In this section are reported two examples of SDRA performed in the frame of the ARTEMIS project related for:

- Isolation Valve (Preload and pressure effect)
- Regulation Valve (Preload effect)

The valve design is identical for both modes (isolation and regulation). The valve design is shown in Figure 18-62 (a). By design, the sensitive axis is the axial one.

For this application, the random test allowed to cover the maximum expected environment up to about 1500 Hz. The SDRA was therefore limited to the higher frequency range. The maximum expected environment is 800 g at 3300 Hz.

By the resonance research of the valve along the axial axis, a significant number of modes with high amplification factor was found below 1000 Hz (see Figure 18-62). Therefore it is not expected to get significant dynamic amplification at higher frequencies (Q_{shock}=1).

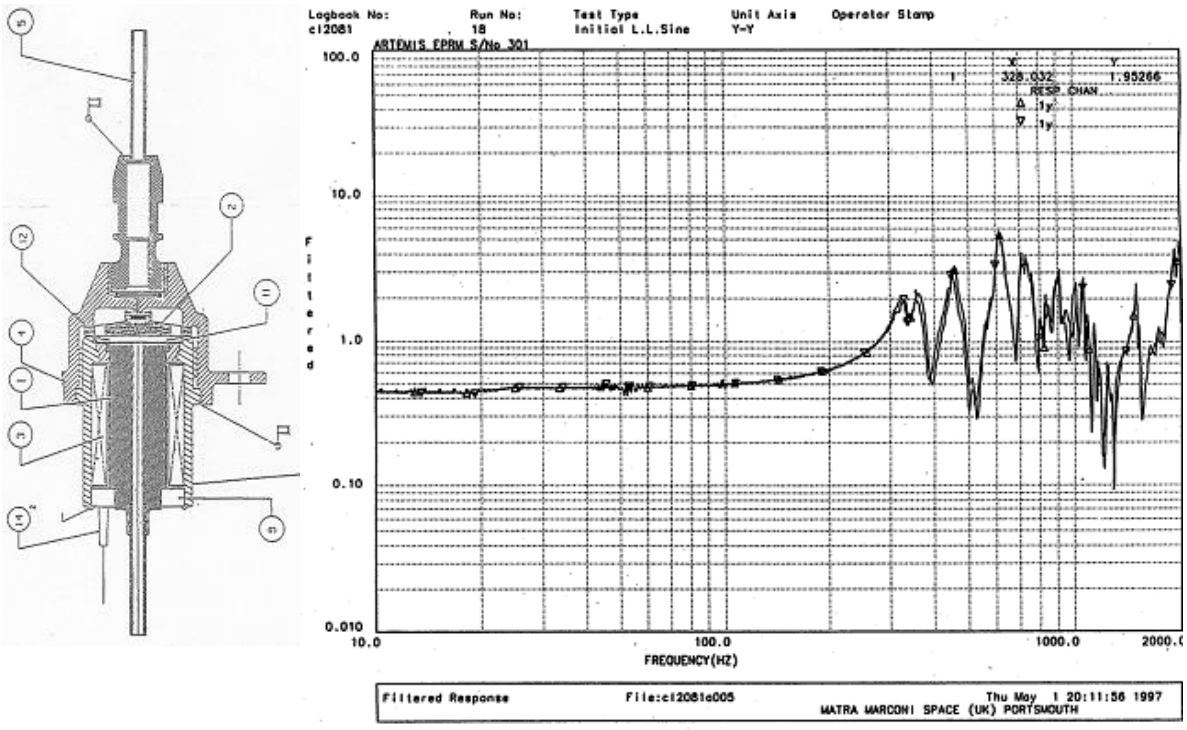

(a) **(b)**

Figure 18-62: (a) Typical RV & IV Design - (b) EPRM resonance search along Y-axis

The valves are initially closed in passive mode and due to a shock event along the valve axis a leakage can occur.

Considering:

- armature mass: 0,00716 kg
- spring force: 3,4 N
- course: 2,5 E-4 m
- Input pressure (max): 6,3 MPa
- Section:7,07 E-8 m²

Thus the kinetic energy is:

$$Ec = \frac{1}{2} x\, 0.00716 \left[\frac{800 x\, 9.81}{3300 x\, \pi x\, 2} \right]^2 = 5.13E-4\,J$$ (no amplification factor due to favourable dynamic uncoupling)

The potential energy is derived by:

- W_{spring} = 3,4 × 2,5E-4 J = 8,5 E-4 J
- $W_{pressure}$ = (6,3 E +6)(7,07 E-8)(2,5 E-4) J = 1,1 E-4 J

For the Isolator valve the safety margin with respect to the opening valve is:

$$SM_{3300Hz}^{opening} = \frac{W_{spring} - W_{pressure}}{Ec} - 1 = \frac{8.5\ 10^{-4} - 1.1\ 10^{-4}}{5.13\ 10^{-4}} - 1 = 0.44$$

Then no leakage is expected.

For the Regulator valve the safety margin is:

- W (spring)/Ec –1 = (8,5 E-4/5,13 E-4) –1 = 0,66

Hence, no opening and consequently no damage are expected.

18.3.3.3 SDRA Example 2 – Valve without mechanical “stop-end”

18.3.3.3.1 Case description

The following case has been encountered and is a perfect example, since implies the consideration of two damage criteria (leakage and damage of the elastomer seal).

Schematic drawing of the valve is shown in Figure 18-63. A close-up on the seal design is also shown.

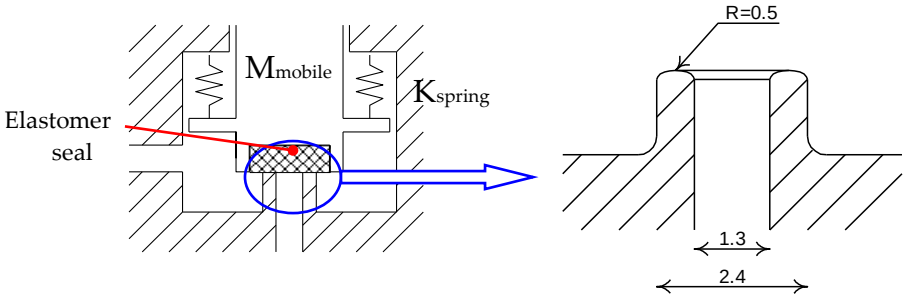

Figure 18-63: Example of valve without mechanical stop-end

This preloaded system has the following characteristics:

- Spring pre-load: $F_{preload}$ = 13,3N ± 0,3 N
- Spring stiffness: K_{spring} = 1,48E+3 N/m
- Mobile mass: M_{mobile} = 17g
- E_{steel} = 2E+11 Pa
- $E_{elastomer}$ = 1,24E+7 Pa

For this type of valve, the Shock damage risk analysis is based on the mathematical theory developed by Hertz for the surface stresses and deformations produced by pressure between elastic bodies. In [RD-0119] are given formulas for the elastic stress and deformation produced by pressure between bodies of various forms, and for the dimensions of the area of contact formed by the compressed surfaces.

In our case the contact occurs between a torus (steel) and a flat plate (elastomer seal). It is considered that Hertz's theory for the surface stresses and deformations produced by pressure between cylinder (developed torus) and flat plate is applicable.

18.3.3.3.2 Leakage assessment

Based upon Hertz's theory, the deformation of the elastomer seal due to the preload is evaluated.

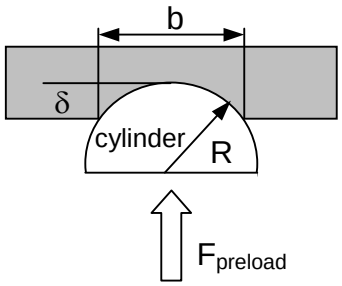

Figure 18-64: Contact conditions

The width of rectangular contact area is given by

$$b = 1.6\sqrt{p.K_D.C_E}$$

Where:

— p is the load per unit length

— $K_d = D_{cyl} = 2.R$

$$C_E = \frac{1-v_{steel}^2}{E_{steel}} + \frac{1-v_{elastomer}^2}{E_{elastomer}}$$

The length of the equivalent cylinder is equal to the length of developed torus (seal design – see figure).

$$l_{equivalentcyl} = \pi \frac{2.4+1.3}{2} x10^{-3} = 0.0058m$$

Load per unit length $\Rightarrow$ $$p = \frac{F_{preload}}{l_{equivalentcyl}} = 2288N/m$$

It comes:

— $K_D = 0{,}001\text{m}$

— $C_E = 6{,}05^E\text{-}8$

— $b = 5{,}96^E\text{-}4\text{m}$

The penetration δ due to the preload can be computed: $\delta = R.\left(1-\cos\left(\text{Arcsin}\left(\frac{b}{2R}\right)\right)\right) = 9.8510^{-5}\text{m}$

Following this method, the evolution of the contact force with respect to the penetration δ is evaluated; this corresponds to the stiffness curve of the preloaded system.

As shown in Figure 18-65, the penetration does not increase in proportion to the loading.

However, an assumption of linearity makes sense, if the penetration is small.

Hence, around the preload, the contact stiffness becomes: $K_{contact} = \frac{F_{preload}}{\delta} = 1.3510^5\ \text{N/m}$

Around the preload (13,3 N, δ = 9,85 E-5m), the leakage can occur when the displacement reaches δ. In this case, the penetration ranges from 0 to about 2δ.

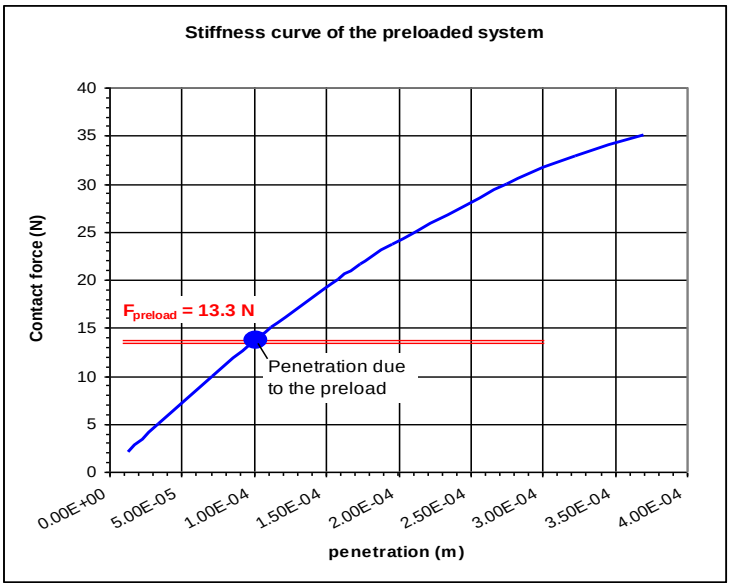

Figure 18-65: Stiffness curve of the preloaded system

The mobile mass being 17 g, thus the apparent frequency is: $\text{Freq} = \frac{1}{2\pi}\sqrt{\frac{1.3510^5 + 1.4810^3}{0.017}} = 450\text{Hz}$

As resulting from these assumptions, the temporal acceleration is: $\gamma = (2\pi \times 450)^2 . \delta = 790\ \text{m/s}^2 = 80\text{g}$.

The equivalent SRS at this frequency is about 3 times higher, that is 240 g.

The estimated shock level at the valve interface is 150 g at 450 Hz, and then the safety margin associated to the leakage is:

$$\text{MS} = \frac{240}{150} - 1 = 0.6$$ The first damage criteria is satisfied (no leakage)

18.3.3.3.3 Damage assessment of elastomer seal

Because of the fact that the stress is highly localized, the actual stress intensity can be very high. Formulas based on Hertz theory give the maximum compressive stress, which occurs at the centre of the surfaces of contact. In discussing this relationship, it is convenient to refer to the computed stress as the Hertz stress.

$$Max\,\sigma = 0,798\sqrt{\frac{p}{K_D C_E}}$$

In this relationship, p (load per unit length) is computed considering the preload force and the external force acting on the mobile part. The estimated shock level at the valve interface is 150 g at 450 Hz, and then the corresponding external force is: $F_{ext} = \frac{150 \times 9.81}{3} \times 0.017 = 8.34N$

$$\Rightarrow p = \frac{F_{ext} + F_{preload}}{l_{equivalentcyl}} = 3730N/m$$

This value is substituted into the Hertz formula, to derive the maximum compressive stress.

$$\Rightarrow \text{Max } \sigma = 6{,}26\ 10^6 \text{ Pa}$$

The loading is considered as being safe, neither excessive deformation nor degradation are expected.

18.3.4 Optical components

18.3.4.1 Verification methodology

The rationale for brittle material is further developed in the following flowchart.

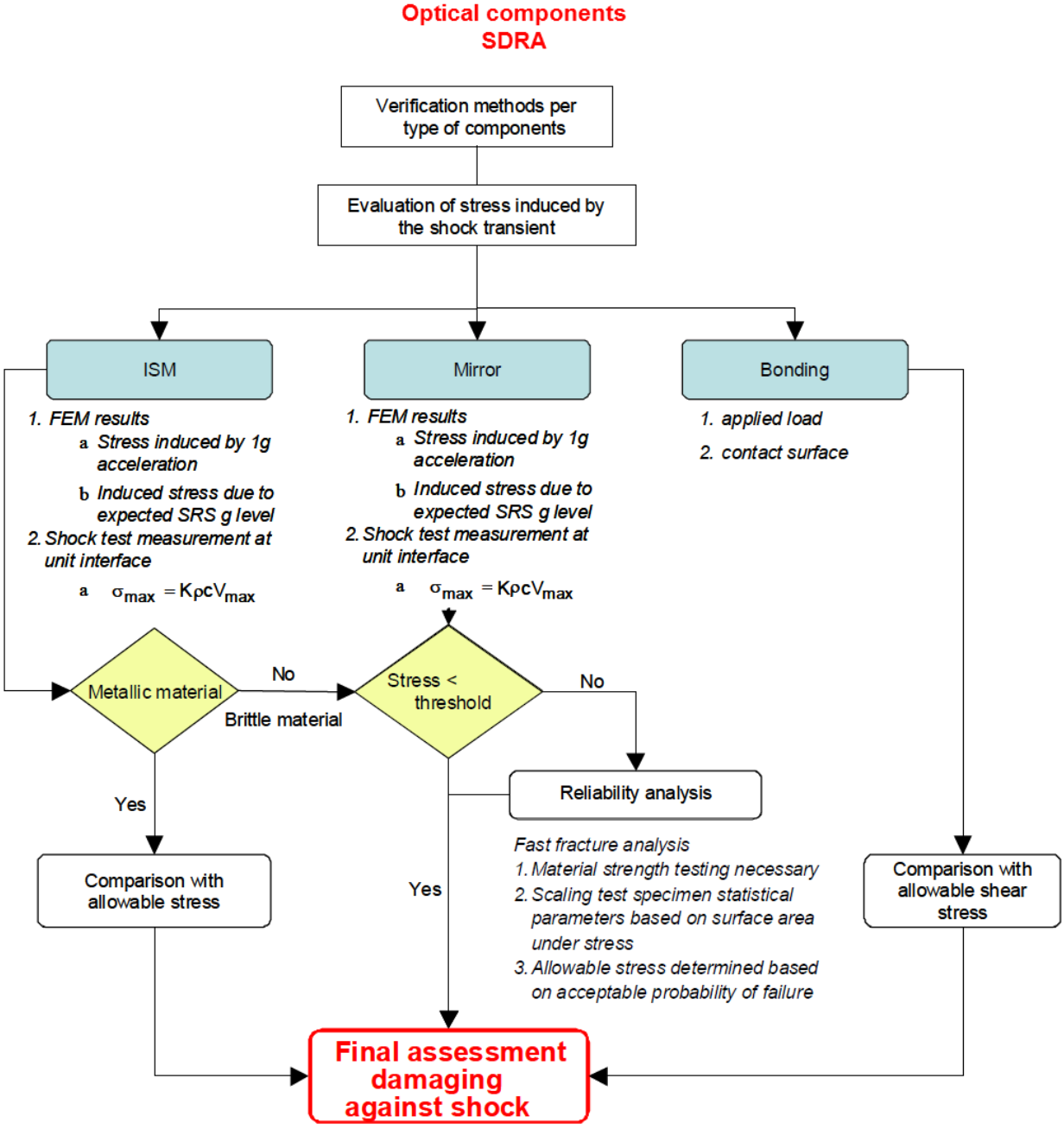

Figure 18-66: Rationale for brittle material assessment

18.3.4.2 Evaluation of stress induced by the shock transient

18.3.4.2.1 By analysis

- Classical methodology

  FEM can be used to evaluate the expected stress in the optical components. The general approach is based on:

  — Consideration of the local dynamics (Torque, Momentum Flux, Force, bending moment,…)

  — Structural analysis related to the stress induced by 1g for both the lateral and the axial direction

  — Expected induced stress due to the expected g-level for the lateral and the axial directions

  — Computation of the stress criterion (e.g. Von Mises in metals)

  — Comparison of the induced stress criteria versus the maximum allowable ones (material dependent)

- Methodology for structural ceramics and glasses

  Strength in ceramics and glasses depends upon several factors that makes the strength analysis more complex than in other materials (see 18.3.4.3).

  Concerning the FE analysis, it is necessary to make a specific post-processing of the FEM outputs, in order to compute an effective size (area or volume, depending on the type of flaws causing failure in the material). This effective size depends on the geometry of the structure and on the stress field shape.

  The maximum stress in the structure can then be compared to an allowable value deduced from adequate elementary tests and the effective size of the considered couple {structure; load case}.

18.3.4.2.2 Shock test measurement at unit interface

Shock test measurement at unit interface can be used to derive in the structural parts of the optical components an envelope of the induced stress by using the relationship $\sigma_{max} = K\rho cv_{max}$. A conservative envelope can then be deduced by considering a sufficient margin on the K factor (see Part 3, paragraph 12.4.2.3.1)

This approach is very approximate and can be insufficient for ceramics and glasses, if the estimated stress is above the threshold.

18.3.4.3 Structural brittle materials

18.3.4.3.1 Introduction and basis

Structural brittle materials include e.g. ceramic and glass.

This section is based on [RD-0102], [RD-0103] and [RD-0104].

18.3.4.3.2 Ceramics' specific mechanical behaviour

When metal components are subjected to applied loads the material has the capacity to generate dislocations that migrate through the microstructure. This property permits yielding and minor shape adjustments without catastrophic failure of the component. Structural ceramics and other brittle materials (glass) typically do not have this property and therefore their failure behaviour is brittle contrary to metals.

As a result ceramic components are highly sensitive to micro-structural inhomogeneities and surface damage from processing, which leads to an increased scatter in the strength behaviour with respect to classical materials. Also, there is no deterministic strength for brittle materials, notably because it is a function of the size of the component (see Figure 18-67).

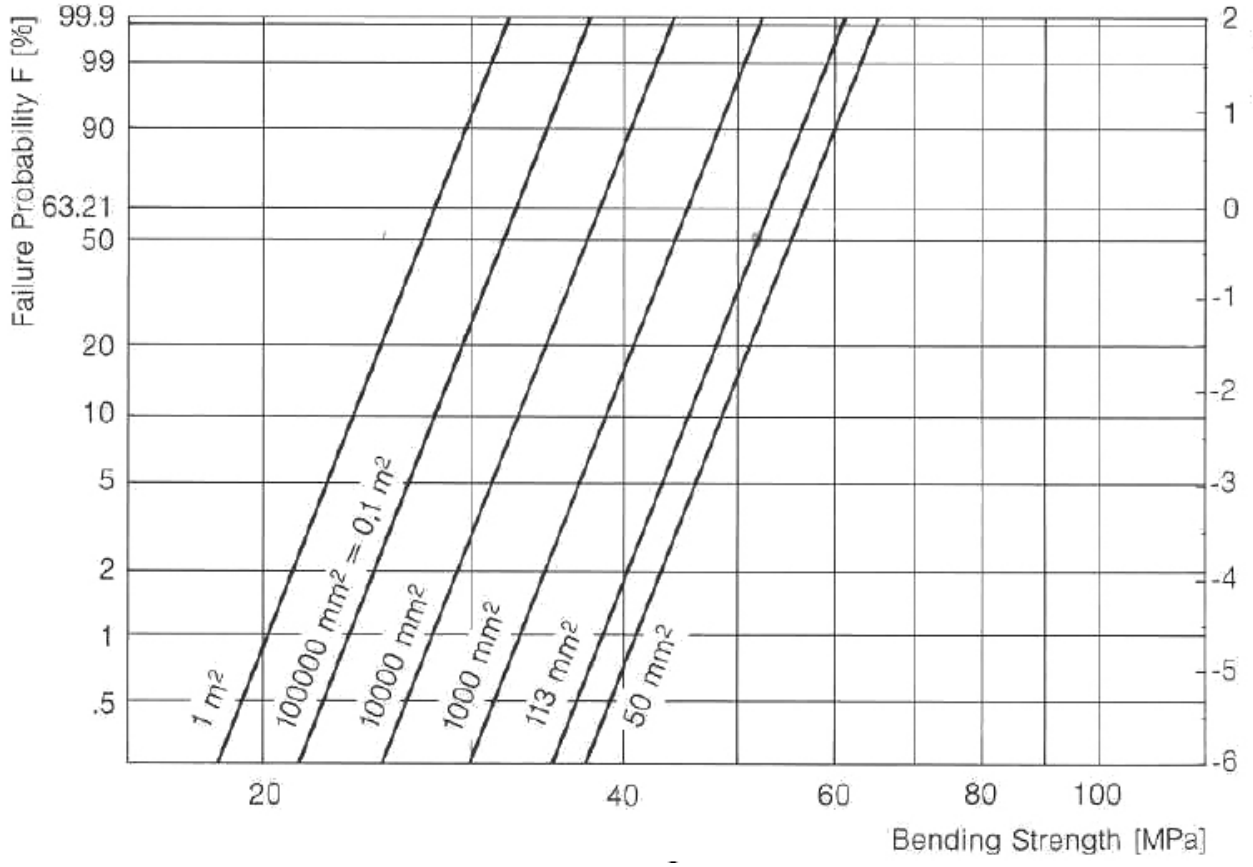

Figure 18-67: Failure probability of ZERODUR® as a function of test surface area, for a given surface finish

Additionally cracks can propagate under tensile loads associated to propitious environmental conditions to a critical value and then experience uncontrolled crack growth until the part physically fractures. This phenomenon is called Sub-Critical Crack Growth. However it can be considered as not activated during shock which is a very short event: only fast fracture is considered.

By definition, the safety factor SF for a component subjected to a single load L is given by the ratio $SF = \frac{R}{L}$, where R is the resistance (or strength) of the material from which the component is fabricated. Making use of the concept of a safety factor, the probability of failure (Pf) for the component where a single load is applied is given by the expression $P_f = Prob\left(\frac{R}{L} \le 1\right)$. For the most general case, the assumption is made that both R and L are random variables. Under this assumption P_f is the product of two finite probabilities summed over all possible outcomes: $P_f = \int_{-\infty}^{+\infty} g_{RL}(x)dx = \int_{-\infty}^{+\infty} F_R(x).f_L(x)dx$, where F_R is the cumulative distribution function (CDF) of the random variable R and f_L is the probability density function (PDF) of the random variable L. The probability of failure is the area under the composite function $g_{RL}(x)$ (see Figure 18-68).

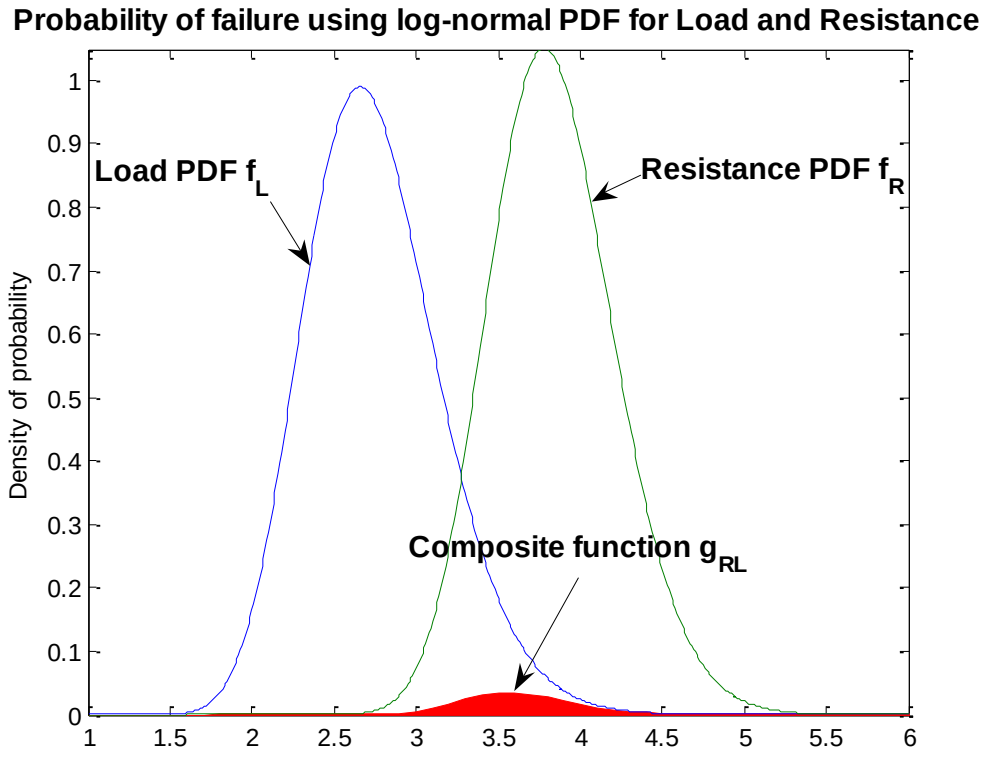

Figure 18-68: Interference Plot for Load and Resistance Random Variables

Variations of magnitude for the load L are not typical as for the strength of brittle material. Consequently a common assumption is to considerer the load as a deterministic design variable while strength is a random design variable. It can be expressed by $f_L(x) = \delta(x - \sigma)$ leading to the probability of failure $P_f = F_R(\sigma)$. Knowing that brittle material strength are generally represented by a Weibull distribution, the probability of failure of such brittle component can be expressed by the following relationship $P_f(\sigma) = 1 - e^{(\sigma/\sigma_\theta)^m}$ where σ_θ is the characteristic strength (63,2 % of the specimens fail at this level) and m is the Weibull modulus (indicator of the scatter of the data), for the given effective size of the tested sample.

The material characteristics depend on several factors (see Figure 18-69 for example of dependence on surface finish):

- material composition;
- surface finish, for materials where strength-driving flaws are spread on the surface, in particular for glasses;
- potential sub-critical crack growth;
- size of the loaded zone (depends on structure shape and loading case).

Material	Surface condition	Characteristic strength σ_0 [MPa]	Weibull factor λ
ZERODUR®	SiC 600	108.0	16.0
ZERODUR®	SiC 320	71.3	12.4
ZERODUR®	SiC 230	57.5	15.7
ZERODUR®	SiC 100	53.6	18.7
ZERODUR®	D 15 A	130.6	10.6
ZERODUR®	D 35	78.7	15.7
ZERODUR®	D 64	62.8*	11.0*
ZERODUR®	D 151	54.1*	28.2*
ZERODUR®	D 251	48.8	11.1
ZERODUR®	Opt. polish	293.8	5.3
ZERODUR®	D 64 etched	391.4*	3.0*
ZERODUR®	D 151 etched	497*	3.4*
ZERODUR®	SiC 600 at 77K	192.7	10.7
glassy ZERODUR®	SiC 320	66.6	16.7

Figure 18-69: Example of dependence on surface finish: ZERODUR® Weibull parameters for standard sample [RD-0104]

The strength of the actual component can be estimated using the test specimen strength using a ratio of the effective dimension under tensile stress.

18.3.4.3.3 Application to strength estimation

- Rule-of-thumb guidelines

  Rule-of-thumb tensile design strength is typically around **10 MPa** for nominal glass materials like ZERODUR®. This neglects the specific glass composition, subcritical crack growth, surface area under stress, and nature of the load - static or cyclic. If the stress induced by the shock transient is evaluated conservatively (by FEM or by using the Pseudo Velocity Shock Spectrum) under this value, then no damage is expected.

  This "threshold" value has been defined in glasses based on a huge past experience of the manufacturers, using several test campaigns showing that below a certain level of stress the failure probability is zero. Figure 18-70 shows that the Weibull distribution is bent for lower failure probabilities, revealing a threshold that is conservatively estimated at 10 MPa.

  On new ceramic materials, the development maturity is not enough detailed in literature to propose comparable threshold value. This becomes therefore the own know-how of the designer and manufacturer.

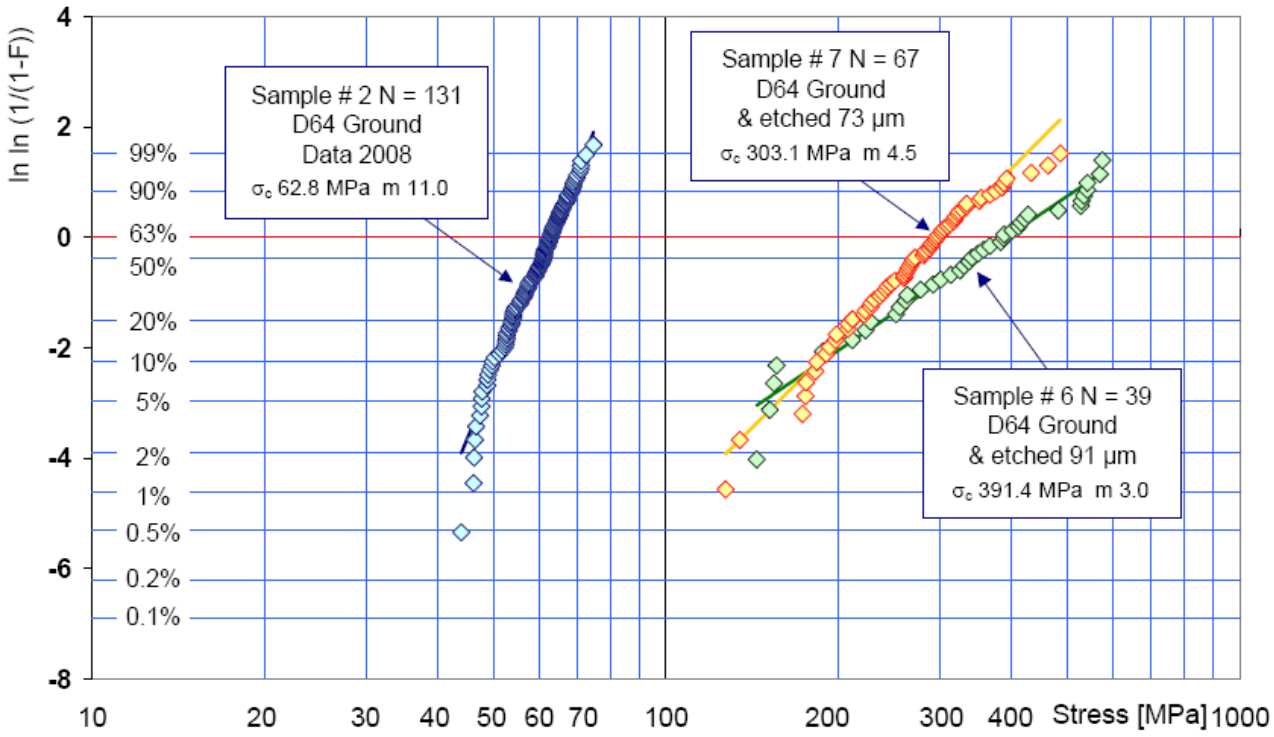

Figure 18-70: Example of threshold behaviour on ZERODUR® [RD-0105]

- Complete rules

  For glass components subject to stress levels that exceed 10 MPa, or for materials not having such a threshold, material strength testing is necessary to characterize the strength properties of the material. Material testing enables the strength to be characterized using a statistical distribution (most common is the two-parameter Weibull distribution) and determines the material-related characteristics, as well as the type of size effect (surface or volume). Then a reliability analysis is recommended using test characterized strength properties of the material [RD-0102]:

$$Pf = 1 - \exp\left(-\frac{V_{eff,s}}{V_{eff,e}}\left(\frac{\sigma_{\max}}{\sigma_\theta}\right)^m\right)$$

  Where:

  — σ_{max} is the maximum equivalent stress over the volume. The equivalent stress depends on the underlying flaw population (mainly their shape). It can be related to more or less complex theories such as Principle of Independent Actions, Batdorf's or Evans-Lamon's theories.

  — V_{eff} is called the effective volume (could be an area). It takes into account the shape of the stress field. $V_{eff,s}$ is the effective volume of the sized structure and $V_{eff,e}$ is the one of the elementary sample.

  — V_o represents the size effect (here with units of volume; could be an area, for glasses for instance)

18.3.4.3.4 Application to shock risk estimation

Brittle materials used for optical components are usually far from shock sources and relatively decoupled from the supporting structure by iso-static mount (ISM). But in particular case, like small platform where the optical payload is close to the shock source, this shock issue can be encountered.

In the SDRA process, it is necessary to estimate the shock environment, and then to see how it can be represented in a strength analysis. Two situations can then be encountered:

- The environment can be covered by a load case that is proportional to the ones that have been used in the dimensioning phase (see Part 3 paragraph 12.7.1).

  In that case, the effective volume (or area) computation is already done, and the verification can be performed by applying the equations of 18.3.4.3.3., with the scaled σ_{max}.
- The environment cannot be covered by an already studied load case.

  In that case, a specific load case covering the shock environment is defined. Then the associated effective volume (or area) is computed, and used to infer final failure probability.

In these two situations, if the material has a known threshold value that is not exceeded, it is not necessary to compute a failure probability, since it can be equal to zero for stress below this threshold.

18.3.4.4 SDRA example – Mirror mounted on "mirror cell" and ISM

18.3.4.4.1 Example description

The following example has been encountered on MSG, and illustrates the verification method for ISM/blades and bonded joints.

The so-called mirror M3 was glued onto 12 blades made of INVAR (mirror cell), and connected to the main structure via 3 iso-static mounts.

A schematic model of the M3 layout is sketched in Figure 18-71.

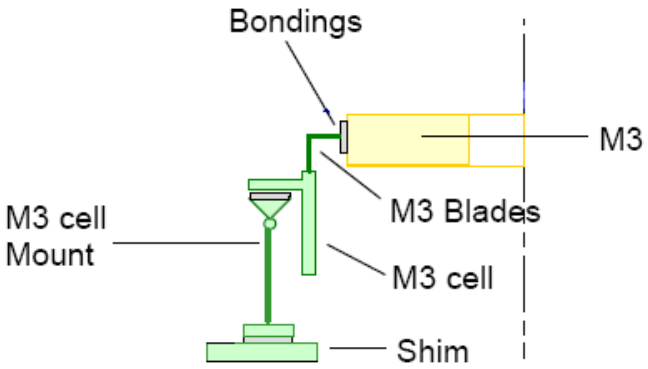

Figure 18-71: Schematic layout of MSG M3 mirror iso static mounting

Within the critical frequency range (see section 17.3), coupling between the mirror suspension modes and the shock excitation could occur, therefore a full dynamic amplification is considered. The input shock levels are directly derived from the SRS responses:

- Lateral direction: SRS = 150 g
- Axial direction: SRS = 95 g

18.3.4.4.2 Mirror blades SDRA

From structural analysis report, the Stress induced by 1-g acceleration in the INVAR supporting blades is:

- 1 g (axial) ⇨ 0,35 MPa
- 1 g (lateral) ⇨ 0,17 MPa

The scaling to the expected input levels gives:

e. For the axial direction: 95 g × 0,35 = 33 MPa tension

f. For the lateral direction: 150 g × 0,17 = 25,5 MPa Shear

g. Von Mises stress is: $\sigma_{VM} = \sqrt{\sigma^2 + 3\tau^2} = 55MPa$

The blades are made of INVAR that allows ⇨ 220 /1,1 = 200 MPa, where 1,1 is the yield safety factor.

The risk against shock is evidenced to be very low.

18.3.4.4.3 Bonded joint (blades ⇔ mirror)

The mass of the M3 = 0,06 kg. This means for the:

- ***In plane load***: 150 g x 0,06 kg [10 ms-2] = 90 N

  Considering the glued area is 5 mm x 5 mm = 25 mm²

  It is assumed that only four blades out of twelve are loaded for a lateral load, that means 25 mm² × 4 = 100 mm² is the contact surface to consider in the computation of the induced stress and this leads to 90/100 = **0,9 MPa**
- ***Out of plane load***: 95 g x 0,06 kg [10ms-2] = 57 N

  It is assumed that all the 12 mirror mounts are loaded at the same time for this direction; that means to consider 25 mm² x 12 = 300 mm². This leads to 57/300= **0,19 MPa**

The maximum shear stress in the bonded area of the ISM is then 0,92 MPa as RSS combination of the IP and OOP loads. This value is much lower than the standard adhesive allowable (around 10-15 MPa).

Furthermore no damage risk is also expected for the mirror made of ZERODUR® (10 MPa as allowable).

18.3.4.4.4 Mirror ISM SDRA

There are three blades at 120 degree supporting the M3 cell as shown in Figure 18-71 and considering 150 g acting in plane on M3 cell, the derivation of the stress on ISM is based on the followings:

- ***In-plane load:*** {[150g × 9,81(ms-2) × 0,19 (kg)]/ [2. cos (30)]} {[1/7,75]}= 20,8 MPa

  Where 0,19 kg is the M3 cell + M3 mirror mass [Kg] and 7,75 mm² is blade cross section.
- ***Out of plane load:*** For the computation of the stress at each ISM blade we consider 95 g acting in the same time on the three ISM blades and precisely: [(95 g/3) 9,81(ms-2) 019]/[7,75 (mm²)]= 7,6 MPa for each blade.

The computation of the Von misses stress is $\sigma_{VM} = \sqrt{\sigma^2 + 3\tau^2} = 37\,\text{MPa}$.

The blades are made of titanium that allows ⇨ 830 /1,1 = 750 MPa, where 1,1 is the yield safety factor.

The risk against shock is evidenced to be very low.